McGRAW-HILL PUBLICATIONS IN AERONAUTICAL SCIENCE

JEROME C. HUNSAKER, CONSULTING EDITOR

Abbott and von Doenhoff
THEORY OF WING SECTIONS

Draper, McKay, and Lees
INSTRUMENT ENGINEERING, *Vols. I, II, III*

Küchemann and Weber
AERODYNAMICS OF PROPULSION

Shaw and Macks
ANALYSIS AND LUBRICATION OF BEARINGS

Streeter
FLUID DYNAMICS

Theodorsen
THEORY OF PROPELLERS

Von Mises
THEORY OF FLIGHT

AERODYNAMICS OF PROPULSION

Dietrich Küchemann

Dietrich Küchemann
DR. RER. NAT.

Johanna Weber
DR. RER. NAT.

First Edition

NEW YORK · TORONTO · LONDON
McGRAW-HILL BOOK COMPANY, INC.
1953

AERODYNAMICS OF PROPULSION

Library of Congress Catalog Card Number: 52-6541

THE MAPLE PRESS COMPANY, YORK, PA.

PREFACE

The past decade has witnessed notable advancements in the aeronautical sciences. In particular, the greater variety of engines now in use and the requirements of high-speed flight have given rise to many new problems that have considerably widened the field of aerodynamics as applied to the production of propulsive forces. Thus a new branch of aerodynamics has been developed which we call here the *aerodynamics of propulsion*. It supplements the much older airfoil theory which is concerned with the production of lifting forces.

In this book an account is given of some of the work done in this field and problems that have arisen. Since it is a first survey, it cannot be expected to be exhaustive, and it necessarily reflects the authors' preferences. But it is hoped that the subjects selected will fill some gaps in the published material at present available and that they are treated in a way which is appropriate and profitable both to designers in aircraft and engine firms and to research workers. This does not mean, however, that detailed working charts will be provided or "recipes" given; the aim is rather to help toward an understanding of the basic processes and flow phenomena which will enable the aerodynamicist to work out problems himself and to perform his part in the design of a propulsion unit, or its installation, if called upon. It is hoped that the text will also be useful to the student of aeronautics. Just as, hitherto, no serious study of the subject could dispense with a comprehensive treatment of lifting surfaces, so a course in modern aeronautics must also provide a working knowledge of the methods and aerodynamic problems of propulsion. To assist the student and to widen the scope of the book, the treatment assumes no detailed knowledge of general aerodynamics or of higher mathematics, other than differential calculus.

The book is based on several monographs which were written at the suggestion of the British Ministry of Supply in 1945 to 1946 at the former Aerodynamische Versuchsanstalt Göttingen under the general editorship of Prof. A. Betz. We sincerely hope that the influence of our teachers, L. Prandtl and A. Betz, is still apparent. It was the persistent and friendly encouragement of the British Resident Officer at that time, Dr. R. M. Goody, that persuaded us to undertake the present revision.

We are further indebted to Sir Ben Lockspeiser, and to the Chief Scientist of the Ministry of Supply, for permission to publish the book, and in particular to W. L. Tweedie, Assistant Director of Scientific Research, for his valuable help at all times. Our warm thanks are due to our colleagues, in particular to Dr. K. Solf, of Göttingen, and to Dr. J. Seddon, G. G. Brebner, and D. E. Hartley, of Farnborough.

Most of all we should like to thank E. P. Sutton, of Bedford, who thoroughly revised the English text and made many valuable comments on the treatment. The plan of writing the book in English could never have been undertaken without his zealous cooperation.

DIETRICH KÜCHEMANN
JOHANNA WEBER

Farnborough, Hants, England
July, 1952

CONTENTS

CHAPTER 1

INTRODUCTION

1-1. Mechanism of Propulsion in Aeronautics. The general principles of the production of a propulsive force in aeronautical engineering are easily understood and can be described almost in a nutshell. Imagine a man in a vehicle which he wishes to propel forward. Without using reaction forces obtained by direct contact with the ground, he can either throw backward masses which are stored in his vehicle or seize masses from his surroundings (such as water, by means of oars) and set them in motion backward. In either case he will be utilizing as his propulsive force the force of reaction associated with the change of momentum of the masses. We shall omit the discussion of all kinds of rockets and shall concern ourselves here with practical applications of the second method: an aircraft draws air from the relative wind, supplies it with energy in the propulsion unit, and finally discharges it backward with increased velocity in a jet.

The energy at the disposal of the propulsion unit is usually stored in liquid fuel. The use of solid fuels has also been contemplated. Heat energy is made available by means of a combustion process, and it is the conversion of this heat energy into propulsive work which is the basic task of all aircraft power plants. The aerodynamic aspects of energy supply to a stream of air will therefore be the focus of our attention.

There is a great variety of ways in which heat can be converted into mechanical work usable for propulsion purposes. The simplest way of supplying energy would be the direct addition of heat to a stream tube of air by increasing its temperature at a certain cross section, which we may call the burner disk. Unfortunately, this does not generate a usable thrust force. As we shall see in Sec. 2-6, the stream tube widens both upstream and downstream in consequence of a simultaneous pressure drop and increase of velocity at the burner disk. Although the velocity of the air immediately behind the disk is higher than the free-stream velocity, the pressure is lower than the free-stream pressure; as the pressure gradually approaches atmospheric in the wake, the velocity decreases accordingly, and also approaches its free-stream value. Thus no jet is formed, and the only effect of the heat supply is that the air that passes through the burner has its temperature increased.

It will be obvious that a jet with increased velocity can be generated if the pressure at the burner disk can be increased by some means beyond what is attained with a burner in a free stream. Less air then passes through the burner, but some of the heat energy appears as kinetic energy in the flow downstream. Thermodynamically, heat supply at a higher pressure means that the working cycle which the air goes through in its changes of state from infinity upstream, through the burner, to infinity downstream, encloses a positive area in the cycle diagram, representing a finite amount of energy made available for propulsion. To achieve the increase in pressure, a fairing which surrounds the burner is the least that is necessary; it is the fairing which then experiences the actual thrust in the form of a static pressure variation along its surface. This simplest type of propulsion unit, the ram jet or Lorin duct, may be regarded as the basis of most actual aircraft engines.

The increase in pressure that can be obtained in this way from the kinetic energy of the inflow is limited by the flight speed, in that the pressure cannot rise beyond the dynamic head of the free stream. Adding a turbine-driven compressor makes possible a further increase of the combustion pressure. The limitation of the working range is overcome, and the propulsive forces are produced with a higher efficiency. Such turbojet engines are frequently used nowadays.

The expansion of the hot combustion gases in the turbine produces available energy in the form of mechanical shaft work. If this is not fully absorbed by the compressor, some of it becomes available as mechanical energy which may in turn be supplied to a separate stream of air and there converted into further propulsive work. This can be done, for instance, by a propeller. In contrast to the nonducted burner, the direct supply of mechanical energy by the propeller to an air stream does generate a usable thrust force. The stream tube containing the propeller disk contracts along its whole length, with a pressure increase at the disk from a value that is lower to a value that is higher than the free-stream pressure. Thus a jet of increased velocity is produced and a thrust force acts on the propeller blades.

Surrounding the propeller by a fairing allows the mass flow to be regulated, and more energy can be transferred to the air stream at a smaller cross-section area per unit time. A large part of the thrust may act on the fairing.

The mechanical shaft work absorbed by the propeller or ducted fan need not come from the turbine of a jet engine; any other driving unit can be used. Most widely used is the piston engine converting heat into mechanical energy by internal combustion in cylinders. Such a piston engine and propeller combination is also a two-way engine in the sense used above, since a small part of the thrust is produced directly by the heat engine in the exhaust jets and the rest by the propeller or fan in the second jet, or slip stream.

There are many possible combinations of these propulsion systems, and their development is far from complete. Another thrust-producing mechanism has recently been introduced in the form of the Argus-Schmidt tube or pulse-jet motor. A pulsating column of air in a long tube produces alternately high and low pressures at the closed forward end, and combustion takes place there about 50 times per second during the high-pressure periods. Fresh air is admitted through valves at the forward end during the low-pressure periods, assisted by the ram pressure built up while the valves are closed. With suitable tuning of the spring-operated valves and the proportions of the tube, an intermittent jet of (on the average) increased kinetic energy is discharged, and corresponding thrust forces act on the valve box and on the intake of the fairing.

The various methods described may be classified if two main types of engine are distinguished, namely, those with roughly constant horsepower and those with approximately constant thrust. Roughly speaking, the first class comprises the piston engines of the Otto or Diesel type, operating on a propeller, and the second the jet engines.

The historical development of aircraft propulsion units[1] was in exactly the opposite direction to that outlined above, beginning with the piston-engine-driven propeller and only later reaching engines which turn heat directly into propulsive work. An explanation of this is to be found in the state of development in other fields of engineering. It was the piston engine which was first available in a form suitable for application to aircraft (although the Wright brothers had to build their own when they wanted it). Propulsion by a piston engine and a propeller satisfied the needs of the designer until very recently, and only when its limitations became more and more apparent did he have to turn back to the more direct methods, which had long been known in principle.

1-2. Applicability of a Propulsion System and the Performance Requirements of Aircraft. An aircraft requires wings to produce the lifting forces which must sustain its weight in the air and a propulsion unit to provide the thrust needed to overcome the drag caused by its motion through the air. The principal aim of the propulsion unit is to do this as efficiently as possible, *i.e.*, with the least amount of fuel per unit time for a given thrust. The desirability of restricting the fuel consumption is obvious from many points of view, such as cost, weight, and space requirements; the fuel consumption is the predominant factor determining the range of flight of the aircraft.

An outstanding feature of aircraft development is the tremendous increase in flight speed which has been made possible partly by the aero-

[1] A historical survey may be found in the book by G. G. Smith, 1950, p. 34.

dynamic refinement of shape and partly by the increased power of the engines available. While the Wright brothers made their first self-propelled flight with an engine of 12 hp, a small modern aircraft requires several thousand horsepower to fly at high subsonic speeds, and tens of thousands to fly at moderate supersonic speeds.

These increasing demands on the performance of the power plant follow from the fact that the drag of different aircraft of comparable size varies roughly as the square of the flight speed for which they are designed, even if the drag rise due to compressibility of the air is ignored. The power of the engine must therefore increase at least with the cube of the design flight speed. Herein lies the importance of the distinction made between two types of engine in the previous section. To raise the speed of a given aircraft with constant-thrust engines, the thrust must be raised in proportion to the square of the speed required, and the engine weight goes up in about the same ratio. When constant-power propeller engines are used, however, the weight is roughly proportional to the power, so that a high-powered engine will become comparatively heavy because of the decreasing thrust-weight ratio.

The result is that in practice constant-horsepower engines are usually so heavy that no part of the gross weight of the aircraft remains available for fuel above some subsonic speed (around Mach number 0.8), at which the range therefore falls to zero. In general, for low speeds the range of an aircraft will be highest with a constant-horsepower type of engine; with increasing demands on speed, the range will decrease until a stage is reached at which this engine is no longer a practical proposition and the jet engine takes over.

When in addition to the engine weight the difficulties due to high flight Mach number are taken into account, such as loss of propeller efficiency and cooling problems, the constant-horsepower engine actually compares less favorably with the jet engine at high speeds.

Apart from fuel consumption and thrust per unit weight, one of the most important factors which determine the applicability of a propulsion system is the thrust per unit engine frontal area, or more generally its suitability for installation and incorporation into the aircraft. The engine itself usually adds to the aircraft drag, and its own drag and the interference drags of the installation may be high enough to make the *installed thrust* actually available for the propulsion of the aircraft appreciably less than the ideal thrust derived from measurements on the test bed. Small engines with a high thrust loading per frontal area are obviously preferable to bulky engines that are difficult to install.

A host of other special demands on the engine arises from the purpose and performance of the aircraft for which it is required, as well as those which concern its reliability and robustness, the kind of fuel that it uses,

its production costs, etc. The consequences of choosing a particular type of engine may be far-reaching in more than the obvious ways; for example, the undercarriage height and weight may be considerably reduced by the use of jet engines instead of large-diameter propellers.

In the past it has been usual to design the lifting surface and the propulsion unit of an aircraft separately—even by different people and firms—and then to fit the elements together on a fuselage containing the load to be carried. To a large extent this is still customary. It becomes less and less possible, however, as aircraft development progresses to still higher speeds and aerodynamic refinement, and there is a definite trend in modern aircraft design toward the incorporation of one into the other and unified design of the two. Installation of the comparatively large air intakes of jet engines, for instance, already necessitates this approach. Future development may lead to aircraft whose lift and propulsion elements are merged together.

There are several ways in which this can happen. An obvious one is the all-wing aircraft with propulsion units completely buried in the wing; another, less obvious but not altogether less promising, is the wingless aircraft with a large jet-driven propeller, rather like a helicopter but able to fly at high speeds with its axis of rotation nearly horizontal. Another line of development may be the extreme application of boundary-layer suction, which uses air from the boundary layer on the aircraft surfaces as working air for the engine and restores it to the full free-stream energy instead of producing a thrust force to overcome the drag associated with the boundary-layer wake.

1-3. Aims and Scope of This Book. Recent developments in aeronautics make it possible to speak of the rise of a specialized branch of aerodynamics which deals with the problems of propulsion in a more comprehensive way than before. In the last standard reference work, W. F. Durand (1935), we find alongside the fundamentals and the treatment of lift forces, stability, and control only a few items, such as propellers, which could be listed under the heading of propulsion. Most of the material that has been treated in textbooks is closely connected with ordinary airfoil theory. Even compressors and turbines are basically arrangements of airfoils moving in a particular way. But many other problems have arisen in the field of propulsion, outside the realm of airfoil theory but nevertheless of a purely aerodynamic character. It is our purpose to deal with such problems. Restricting the range of subjects by excluding propellers and turbomachines means, however, that the whole field of the aerodynamics of propulsion is not covered.

The main types of propulsion system are reviewed in a thermodynamic order in Chap. 2. This will at the same time demonstrate the character and variety of the aerodynamic problems involved. Such a treatment

cannot dispense with a certain amount of thermodynamics, and the relevant facts are briefly presented.[1] Particular types of propulsion system are discussed in more detail in Chaps. 6 to 8, beginning with the ducted propeller, to illustrate the supply of mechanical energy to the air stream, and continuing with the ram jet and the turbojet where heat is directly supplied. No attempt is made to deal fully with all the various methods of propulsion. In some cases, such as piston engines, many exhaustive textbooks are readily available; in others development is still too fluid for a satisfying account to be given.

For a better appreciation of these chapters on complete engines, some particular problems are first treated in Chaps. 3 to 5. Chapter 3 shows nonuniform flow with regions of different energies to be a common feature of a number of problems in the aerodynamics of propulsion. As may be expected, this is closely related to flows with free boundaries, which are mentioned to provide the mathematical background and the methods of calculation needed for our purpose. The method of singularities is explained, whereby bodies or surfaces of discontinuity are represented by distributions, for example, of vortices or sources. The momentum theorem is frequently used as a very convenient means of obtaining over-all results.

Chapters 4 and 5 deal with the flow about fairings and air intakes. This topic recurs again and again, since all power plants, with the exception of the propeller, are faired and air intakes are employed for all types of jet motor as well as for air scoops and for piston-engine cooler fairings.

Chapter 9 is concerned with the installation of the propulsion unit. The aerodynamic quality of the installation usually has an appreciable effect on the performance of the engine. The influence of a disturbed inflow on the thrust and fuel consumption of a jet engine is examined together with the inflow losses themselves, with the object of gaining quantitative information as to their magnitude and of seeking means of reducing them. At the same time we consider the additional external drag due to the engine. The spreading of the jet and its interference with adjacent walls or lifting surfaces are treated in Chap. 10.

As the development of propulsion systems has entered a new stage where fresh approaches are being explored, it was felt worth while to consider briefly in Chap. 11 how the flying animals have solved the problem, mainly with a view to understanding how they manage to combine the production of lift and thrust forces.

Cooling is the subject of Chap. 12. Apart from the application of heat exchangers in the further development of jet motors, coolers are of particular importance for piston engines, where about half the heat energy obtained by combustion of the fuel has to be removed without contributing directly to the purpose of the engine. Features typical of the whole book are found here again; for example, heat energy is to be added to a certain stream of air, while, in this case, mechanical energy is simultaneously removed.

[1] As is usual in modern aerodynamics, we do not distinguish between what used to be called *gas dynamics* and *thermodynamics*.

The Appendix gives tables of functions for the frequently used stream-function and velocity components due to singularities, as an aid to numerical calculations.

The reader will notice that no mention has been made of supersonic flow, which will only occasionally be touched. Although the aerodynamics of propulsion plays an even bigger part in the design of supersonic than of subsonic aircraft, it was felt that they were still too much in a state of development to allow any attempt at a comprehensive summary. The same might be said of some of the other problems treated here, and we shall more than once come to a stage where no final conclusions can be reached and where further work is needed. In such cases, the aim has been at least to indicate methods and means by which the task might be approached.

It will also be noticed that we shall not enter on a detailed discussion of the comparative merits of the various propulsion systems. The layout and performance of the whole aircraft must evidently be taken into account to do this properly, and that goes beyond the scope of this book. There are many valuable papers on this subject; a few are listed at the end of this chapter.

BIBLIOGRAPHY

General:

DURAND, W. F., "Aerodynamic Theory," Springer-Verlag, Berlin, 1935.

LICHTY, L. C., "Internal-combustion Engines," McGraw-Hill Book Company, Inc., New York, 1939.

VON MISES, R., "Theory of Flight," McGraw-Hill Book Company, Inc., New York, 1945.

ACKERET, J., Zur Theorie der Raketen, *Helv. Phys. Acta*, vol. 19, p. 103, 1946.

HUNSAKER, J. C., and B. G. RIGHTMIRE, "Engineering Applications of Fluid Mechanics," McGraw-Hill Book Company, Inc., New York, 1947.

THEODORSEN, TH., "Theory of Propellers," McGraw-Hill Book Company, Inc., New York, 1948.

KATZ, I., "Principles of Aircraft Propulsion Machinery," Pitman Publishing Corp., New York, 1949.

SMITH, G. G., "Gas Turbines and Jet Propulsion," 5th ed., Iliffe & Sons, London, 1950; Aircraft Books, Inc., New York, 1950.

MILLIKAN, C. B., "Aerodynamics of the Airplane," John Wiley & Sons, Inc., New York, 1941; Chapman & Hall, Ltd., London, 1941.

Special Subjects:

KÜCHEMANN, D., On Some Problems of the Production of Propulsion, *Brit. Min. of Supply (Völkenrode) Rept. & Trans.* 159, 1945.

REISSNER, H., Systematic Analysis of Thermal Turbojet Propulsion, *J. Aeronaut. Sci.*, vol. 14, p. 197, 1947.

KEENAN, J. H., and J. KAYE, A Survey of the Calculated Efficiencies of Jet Power Plants, *J. Aeronaut. Sci.*, vol. 14, p. 437, 1947.

SILVERSTEIN, A., Research on Aircraft Propulsion Systems, *J. Aeronaut. Sci.*, vol. 16, p. 197, 1949.

GOLLOB, G. M., Is the Propeller-driven Fighter Obsolete? *Interavia*, vol. 5, p. 639, 1950.

CASAMASSA, J. V., "Jet Aircraft Power Systems; Principles and Maintenance," McGraw-Hill Book Company, Inc., New York, 1950.

CHAPTER 2

ONE-DIMENSIONAL TREATMENT OF THE BASIC PROCESSES OF PROPULSION

To be able to deal with any problem connected with aircraft propulsion, we need a fair understanding of the thermodynamic and aerodynamic processes by which a propulsive force is produced. In this chapter the basic principles of various methods of propulsion will be described, always with the assumption that they are technically realizable. For instance, we shall discuss how the addition of a compressor affects the characteristics of an engine in which heat energy is supplied to the air without considering how a compressor works; and we shall discuss the influence of an engine fairing on the thrust-producing process, leaving for a later chapter a description of the flow around it. One aim of this presentation is to demonstrate the common characteristics of the processes employed in aircraft motors, in an attempt to make the subsequent detailed treatment with its confusing multitude of parameters more comprehensible.

A brief outline is given in Sec. 2-1 of some of the basic thermodynamic relations needed later. The close interdependence of thermodynamic and aerodynamic processes and their relation to the mechanics of propulsion make a uniform presentation desirable. This trend will also be evident in the treatment of particular subjects and details, such as the choice of mechanical units of measurement throughout. The possibility of producing mechanical work by changing the state of a gas is dealt with in Sec. 2-2. In Secs. 2-3 and 2-4 the discussion is extended to streaming gases and the available mechanical energy of the flow is related to the propulsive force. This provides a basis for the treatment of particular aircraft power units and the various ways in which they convert energy into propulsive work (Secs. 2-5 to 2-7). In Sec. 2-8, the individual types of engine are regarded as specializations of a general heat engine, and their common characteristics and their differences are briefly shown.

2-1. Fundamental Concepts of Thermodynamics. The working medium of the propulsion units of aircraft, and of jet motors in particular, is a gaseous substance; unless otherwise stated, it is assumed in this book to be a perfect gas. The thermodynamic state of a gas is usually described by its pressure p, its specific volume v or its density $\rho = 1/vg$, and by its temperature T. As is usual in engineering thermodynamics,

the specific quantities such as the specific volume are referred to unit weight of the medium and not to unit mass, as would be more correct. Specific quantities are denoted by small letters. An engineering system of units is used, with a basic length unit [meter (m) or foot (ft)], a basic weight unit [kilogram-force (kg) or pound-force (lb)], and a basic time unit [second (sec)]. Temperatures are given in degrees Kelvin (°K) and, occasionally, in degrees Rankine (°R).

The basic functions of state p, v, T are not independent of one another but, for perfect gases, obey the equation of state

$$pv = RT \qquad \text{or} \qquad p = g\rho RT \tag{2-1}$$

where g is the acceleration due to gravity and R a characteristic constant per unit weight of the gas concerned.[1]

Basic variables other than these can be introduced with the aid of the principle of the conservation of energy which, extended to thermodynamic processes, is known as the *first law of thermodynamics:* If a system changes from an initial state 1 to another state 2 and receives heat q_{12} from its surroundings and does work w_{s12} on them during the change, then the difference $(q_{12} - w_{s12})$ is independent of the way in which the change was performed. In fact,

$$q_{12} = w_{s12} + (u_2 - u_1) \tag{2-2}$$

where u is another function of state, the internal energy. In differential form,[2]

$$d'q = du + d'w_s \tag{2-2a}$$

When there is no exchange of heat between a system and its surroundings, the process is described as adiabatic. In this case,

$$u_1 - u_2 = w_{s12} \qquad \text{or} \qquad du = -d'w_s \tag{2-3}$$

Both q and u are energies per unit weight and have therefore the dimension of a length. For our purposes here there is no need to introduce a special unit for measuring q; consequently, the *mechanical equivalent of heat* does not appear in Eq. (2-2). Note that we have taken heat absorbed by the system and work done by it as positive.

If mechanical work is performed while there is equilibrium between inner and outer pressures so that $d'w_s = p\,dv$, the first law of thermodynamics can be written as

$$d'q = du + p\,dv \tag{2-4}$$

Another function of state is the enthalpy i, which is useful when processes involving streaming gases are considered. It is defined by

$$i = u + pv \qquad \text{or} \qquad di = du + p\,dv + v\,dp \tag{2-5}$$

so that Eq. (2-4) reads

$$d'q = di - v\,dp \tag{2-6}$$

The specific-heat capacity, or specific heat, c, relates the quantity of heat added to the temperature change produced in the medium:

$$d'q = c\,dT \tag{2-7}$$

The value of c depends on the conditions under which the heat $d'q$ is supplied to the system; c_p denotes the value of c for changes at constant pressure, and c_v for those at constant volume. Then, from Eqs. (2-4), (2-6), and (2-7),

$$c_v = \left(\frac{\partial u}{\partial T}\right)_{v=\text{const}} \qquad \text{and} \qquad c_p = \left(\frac{\partial i}{\partial T}\right)_{p=\text{const}}$$

For perfect gases, the internal energy and, by Eqs. (2-1) and (2-5), the enthalpy depend only on the temperature:

$$du = c_v\,dT \qquad \text{and} \qquad di = c_p\,dT \tag{2-8}$$

The values of the specific heats can in most cases be taken as constant.[1] Since $di = du + R\,dT$, it follows that

$$c_p - c_v = R \tag{2-9}$$

Denoting c_p/c_v by k,

$$c_p = \frac{k}{k-1}R \qquad \text{and} \qquad c_v = \frac{1}{k-1}R \tag{2-10}$$

Some special changes of state which are of practical importance are:

1. Isobaric processes, where p = const, so that from Eq. (2-1)

$$\frac{v_1}{v_2} = \frac{\rho_2}{\rho_1} = \frac{T_1}{T_2}$$

2. Isothermal processes, where T = const, so that, from Eq. (2-1),

$$\frac{p_1}{\rho_1} = \frac{p_2}{\rho_2}$$

[1] Standard value of g is 9.81 m/sec² = 32.2 ft/sec². For air,

$$R = 29.27 \text{ m/°K} = 53.36 \text{ ft/°R}$$

[2] The differentials $d'q$ and $d'w_s$ are primed because, in general, neither q nor w_s is a function of state. Equation (2-2a) can only be integrated if the path of integration is given, *i.e.*, if the way in which the gas changes from state 1 to state 2 is fixed.

[1] For air, c_v = 73.2 m/°K = 133.3 ft/°R and c_p = 102.5 m/°K = 186.7 ft/°R, at T = 273°K = 460°R. Then k = 1.40.

3. Adiabatic processes, where $d'q = 0$; Eqs. (2-1) and (2-6) give

$$di - v\,dp = c_p\,dT - RT\frac{dp}{p} = 0$$

Integration gives the well-known relations

$$\begin{aligned}\frac{p_1}{p_2} &= \left(\frac{T_1}{T_2}\right)^{k/(k-1)}\\ \frac{p_1}{p_2} &= \left(\frac{\rho_1}{\rho_2}\right)^{k}\\ \frac{\rho_1}{\rho_2} &= \left(\frac{T_1}{T_2}\right)^{1/(k-1)}\end{aligned} \tag{2-11}$$

Certain processes of this kind are called *isentropic* processes, as will be explained later.

The *second law of thermodynamics* relates to the availability of the energy of a system and its surroundings[1] for conversion into mechanical work. It states the impossibility of converting into work all the heat supplied to an engine operating on a periodic cycle.

The quantitative statement of the law which we shall need here defines a new function of state, the entropy, s. If s_1 is the specific entropy of a medium in state 1 and s_2 is the specific entropy in state 2, then

$$s_2 - s_1 = \int_1^2 \frac{d'q}{T} \qquad ds = \left(\frac{d'q}{T}\right)_{\text{reversible}} \tag{2-12}$$

reversible path

where the integral is taken over any reversible path by which state 2 can be reached from state 1.

A reversible change $1 \rightarrow 2$ is defined as a change such that both the system and its surroundings can somehow be restored exactly from state 2 to the original state 1. In an irreversible change, *e.g.*, a process involving friction, the increase in specific entropy of a medium exceeds the integral $\int_1^2 d'q/T$. To include both types of process, we state

$$s_2 - s_1 \geq \int_1^2 \frac{d'q}{T} \qquad ds \geq \left(\frac{d'q}{T}\right)_{\text{actual}} \tag{2-12a}$$

actual path

where the $d'q$ now refer to the actual heat received in the change of state $1 \rightarrow 2$.

Irreversibility is wasteful in the conversion of energy into mechanical work. If Σs is the sum of the total entropies of the various media of a

[1] By which we mean the system and the surroundings which influence it or are influenced by it.

system and its surroundings, then in any process

$$d(\Sigma s) \geq 0 \tag{2-13}$$

the sign "greater than" referring to irreversible processes. Reversible and irreversible changes between the same conditions of a system differ in the changes of entropy of the surroundings. All real processes are irreversible, but the idea of a reversible process is of great practical importance as a guide to perfection.

It would be out of place here to attempt to discuss these statements fully, and the reader is referred to the treatment of entropy and the second law of thermodynamics in other textbooks[1] for a proper discussion.

For a perfect gas [since a process of the type considered in deriving Eq. (2-4) is reversible], we have from Eqs. (2-4), (2-6), and (2-8),

$$\begin{aligned}ds &= \frac{du + p\,dv}{T} = c_v\frac{dT}{T} + R\frac{dv}{v}\\ &= \frac{di - v\,dp}{T} = c_p\frac{dT}{T} - R\frac{dp}{p}\end{aligned}$$

so that

$$\begin{aligned}s_2 - s_1 &= c_v \ln\frac{T_2}{T_1} + R\ln\frac{v_2}{v_1}\\ s_2 - s_1 &= c_p \ln\frac{T_2}{T_1} - R\ln\frac{p_2}{p_1}\\ s_2 - s_1 &= c_p \ln\frac{\rho_1}{\rho_2} + c_v\ln\frac{p_2}{p_1}\end{aligned} \tag{2-14}$$

The special case $s_2 = s_1$ leads to Eqs. (2-11).

The state of a gas is determined when any two functions of state are given, and can thus be represented as a point in a two-dimensional system of coordinates. A curve in such a diagram describes a change of state. Three diagrams are most frequently used: (1) The pv diagram, (2) the Ts diagram, and (3) the is diagram.

When using these diagrams, we shall follow the usual custom in aerodynamics by representing the variables in a nondimensional form. Reference values can easily be found upstream of the body considered, in the undisturbed flow. Those employed are p_0, $\rho_0 = 1/v_0 g$, T_0, and the relation (2-1)

$$p_0 v_0 = \frac{p_0}{\rho_0 g} = RT_0$$

is applied. RT_0 is used as reference unit for specific energies. A nondimensional enthalpy is thus

$$\frac{i}{RT_0} = \frac{c_p}{R}\frac{T}{T_0} = \frac{k}{k-1}\frac{T}{T_0}$$

[1] Some are listed in the Bibliography at the end of this chapter.

The entropy is made nondimensional with the gas constant R, for then the energy given by the integral

$$\int \frac{T}{T_0}\, d\left(\frac{s}{R}\right)$$

is again measured in terms of RT_0.

2-2. Conversion of Heat into Mechanical Energy in Flow Processes. In aircraft propulsion, the change of state of a working medium is of interest because of the mechanical work associated with it. The production of mechanical work out of a supply of heat is the main technical purpose of a propulsion unit. There are two possible ways in which work can be produced continuously by changing the state of a medium: (1) The same medium is made to undergo the same changes of state periodically; the medium goes through a *cycle* and always returns to the initial state. (2) Successive quantities of the medium are made to undergo the same changes one after another, as in steady-flow processes. This latter case is our main concern here.

In undergoing a change of state in an engine, the flowing air delivers to the surroundings mechanical energy which can be technically utilized. This energy we shall call the *technical work*, denoted by w. It is not the same as the w_s in Eq. (2-2), which dealt with a static, nonflow process where the mechanical energy produced by the change was all in the form of work. In an actual propulsion unit, mechanical energy may also be delivered to the air from outside. Since the system is the air, this, by our definition, is negative work.

To write down an energy balance for a flow process, we must include the work done on the medium in state 1 in delivering it to the region in which the change of state takes place and the work which it does in leaving the region in state 2, as well as its kinetic energy $e_k = V^2/2g$ in states 1 and 2, where V is the velocity of the medium. The remaining mechanical energy term is then the technical work w.

The work done on the gas in delivering it is obtained as follows. Let it be delivered in state 1 across a surface of area S. To displace the gas which is in the surface a distance dx through it, work $p_1 S\, dx$ is done; that is, work $p_1 S\, dx$ is done in delivering a weight $S\, dx/v_1$. Then the work done in delivering unit weight is $p_1 S\, dx\, v_1/S\, dx = p_1 v_1$. Similarly, work $p_2 v_2$ is done by unit weight of air leaving the region.

Thus the energy equation for a flow process is

$$u_1 + p_1 v_1 + e_{k1} + q_{12} = w_{12} + u_2 + p_2 v_2 + e_{k2}$$

or

$$i_1 + e_{k1} + q_{12} = w_{12} + i_2 + e_{k2}$$

so that

$$d'w = -di - de_k + d'q \tag{2-15}$$

This may be called the first law of thermodynamics for flowing media. It will be used frequently below. To be complete, the relation should contain also the changes in potential energy of position, which are not taken into account here.

If no technical work is done, $d'w = 0$, and

$$\frac{1}{2g}(V_2^2 - V_1^2) = q_{12} + i_1 - i_2 \tag{2-15a}$$

which, with Eqs. (2-1), (2-8), and (2-10), gives the energy equation for perfect gases:

$$\frac{k}{k-1}\frac{p_1}{\rho_1} + \frac{1}{2}V_1^2 + gq_{12} = \frac{k}{k-1}\frac{p_2}{\rho_2} + \frac{1}{2}V_2^2 \tag{2-16}$$

or, nondimensionally,

$$\frac{k}{k-1}\frac{p_1/p_0}{\rho_1/\rho_0} + \frac{k}{2}M_1^2 + \frac{q_{12}}{RT_0} = \frac{k}{k-1}\frac{p_2/p_0}{\rho_2/\rho_0} + \frac{k}{2}M_2^2 \tag{2-16a}$$

introducing the Mach number

$$M = \frac{V}{a_0} \tag{2-17}$$

where

$$a_0 = \sqrt{k\frac{p_0}{\rho_0}} \tag{2-18}$$

is the velocity of sound in the undisturbed flow.

In some cases, technical work and kinetic energy may conveniently be taken together as the *available mechanical energy* of the flow, e_a:

$$e_a = w + e_k \tag{2-19}$$

Air enters with kinetic energy e_{k1}, and $e_{a1} = e_{k1}$. Energy is added by the thermodynamic process, and the available energy of the air is then $e_{a2} = e_{k2} + w$. Introducing this into Eq. (2-15), we see that

$$d'e_a = d'q - di = -v\, dp \tag{2-20}$$

This states that the available energy depends only on the difference of the enthalpies of the two states if no heat is supplied. The actual production of mechanical work, for instance, as shaft work by a turbine or as kinetic energy by a nozzle, is usually done without heat supply. The work performed is then Δe_a, and it can readily be read off as the difference of the two enthalpies from an *is* diagram. Equation (2-20) states further that the available energy in a change of state at constant pressure remains constant. In an isothermal change of state, all the heat is transformed into available energy.

We can now reconsider the flow processes in aircraft engines in the light of Eq. (2-20). It is profitable to replace the flow process by a cycle process. In a flow process, the pressure of the air is generally the same far ahead and far behind the engine, and this presents the means of linking conditions far behind with those far ahead by adding a fictitious change of state at constant pressure. The flow process is thus completed into a cycle. The available energy of a cycle is equal to the net quantity of heat supplied, the initial and final conditions being identical. According to Eq. (2-20), the available energy remains constant in changes at constant pressure, and thus the continuous flow process and the cycle are equivalent as regards the available energy. They are also equivalent as regards the total intake and output of energy and thus have the same efficiencies. In the real process, a certain quantity of energy is removed by convection and appears as an enthalpy difference; in the equivalent cycle, the same energy is removed as a quantity of heat at constant pressure. A few processes of technical importance are described below as an illustration.

One of the most important thermodynamic processes is the hypothetical Carnot cycle (see Fig. 2-1). It is built up of an isentropic (s = const) compression $0 \rightarrow 1$, supply of heat $q_{12} = \int_1^2 T\,ds$ = area $a12ba$ at constant temperature T_1, isentropic expansion $2 \rightarrow 3$, and rejection of heat q_{03} = area $a03ba$ at the constant temperature T_0 of the surroundings. (Because of this, the Carnot cycle cannot easily be interpreted as a flow process, in which the rejection of heat takes place at constant pressure.) The available energy is given by the area 01230 and

$$\Delta e_a = q_{12}\frac{T_1 - T_0}{T_1} \qquad (2\text{-}21)$$

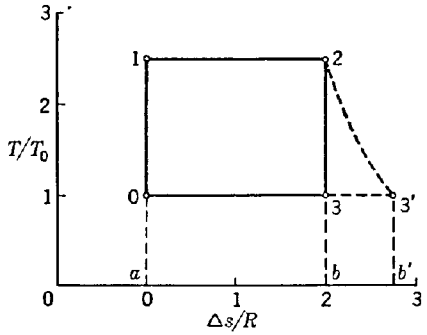

FIG. 2-1. Ts diagram of the Carnot cycle.

The heat (area $a03ba$) which is absorbed by the surroundings is the unavailable portion of the heat supplied. A thermal efficiency of the cycle can be defined by relating the available energy to the quantity of heat supplied:

$$\eta_{th} = \frac{\Delta e_a}{q_{12}} \qquad (2\text{-}22)$$

The maximum efficiency of the ideal Carnot cycle is then

$$\eta_{th} = \frac{T_1 - T_0}{T_1} \qquad (2\text{-}23)$$

If the expansion $2 \rightarrow 3$, for instance, is irreversible, the same quantity of heat (area $a12ba$) is supplied from the source at T_1 but the greater quantity of heat $a03'b'a$ is rejected to the surroundings. The available energy is thus reduced by $T_0\,\Delta s$, and the efficiency correspondingly.

Another cycle of particular interest for jet engines is the *constant-pressure process*, consisting of two isentropic and two constant-pressure changes of state. The corresponding pv and Ts diagrams are shown in Fig. 2-2. Starting from the state 0, the air is compressed isentropically to the pressure p_1, reaching the temperature T_1. From $1 \rightarrow 2$, heat q_{12} is absorbed by the working medium (in a burner) at constant pressure.

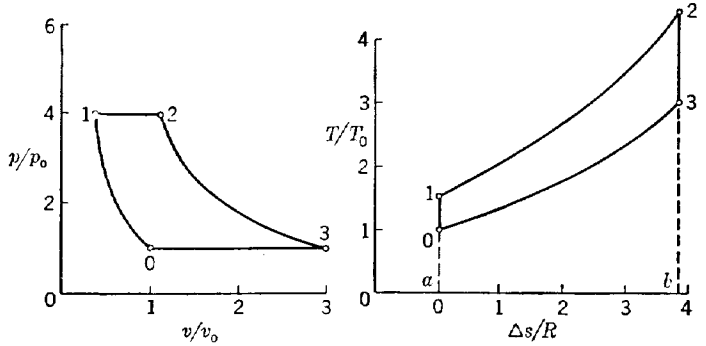

FIG. 2-2. Constant-pressure cycle.

The temperature increases to T_2 and the entropy to s_2. The heat added is $q_{12} = c_p(T_2 - T_1)$, if the kinetic energy of the stream remains constant, by Eq. (2-15). In the subsequent isentropic expansion to $p_3 = p_0$, the temperature decreases to T_3. Finally, from $3 \rightarrow 0$, heat $-q_{03}$ is removed by a "cooler," at constant pressure. The available energy, as in all cycle processes, is equal to the net heat supplied, which by Eq. (2-7) is

$$\Delta e_a = q_{12} - q_{03} = c_p(T_2 - T_1) - c_p(T_3 - T_0)$$

With part of the heat q_{12} supplied lost in the cooler, the thermal efficiency of the process becomes

$$\eta_{th} = \frac{\Delta e_a}{q_{12}} = 1 - \frac{T_3 - T_0}{T_2 - T_1} = 1 - \frac{T_0}{T_1}\frac{T_3/T_0 - 1}{T_2/T_1 - 1}$$

Now Eq. (2-14) states that the ratio of temperatures for isentropic changes between the same isobars is constant, so that

$$\frac{T_1}{T_0} = \frac{T_2}{T_3} = \left(\frac{p_1}{p_0}\right)^{(k-1)/k} \qquad \text{and} \qquad \frac{T_3}{T_0} = \frac{T_2}{T_1}$$

The efficiency of the process is therefore

$$\eta_{th} = 1 - \frac{T_0}{T_1} = 1 - \left(\frac{p_0}{p_1}\right)^{(k-1)/k} \tag{2-24}$$

The efficiency increases with increasing pressure ratio p_1/p_0 or temperature ratio T_1/T_0. This is easily seen also from the Ts diagram where the efficiency is represented by the ratio of the area 01230, for the work, to the area $a12ba$, for the heat. This ratio increases if the isobar 12 is shifted to higher pressures.

The efficiency of the constant-pressure process, Eq. (2-24), shows a formal resemblance to that of the Carnot cycle, Eq. (2-23). But T_1 is not the highest temperature attained during the process, since $T_2 > T_1$, and a Carnot cycle with T_2 as highest temperature would clearly have a higher efficiency than that given by Eq. (2-24). This is because the

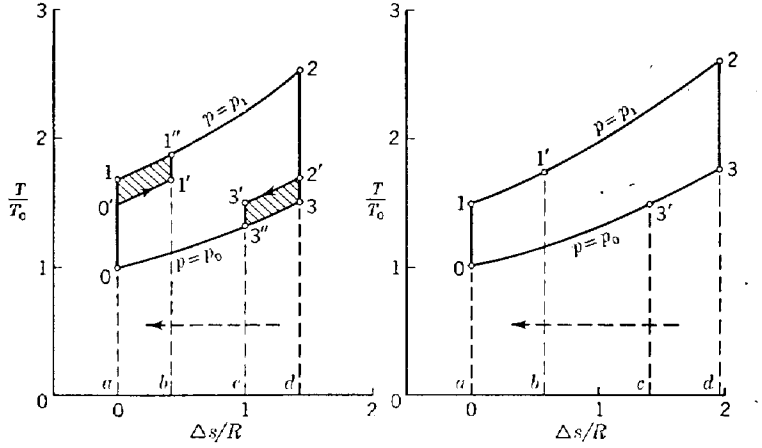

FIG. 2-3. Modifications to the constant-pressure cycle by means of heat exchangers. Left, $T_1 > T_3$. Right, $T_1 < T_3$.

constant-pressure process is irreversible during the absorption (or delivery) of heat, where finite differences of temperature between the source of heat and the working medium occur.

A problem of some practical importance is how to improve the constant-pressure process in itself without changing the pressures of the working medium and the temperatures of the heat sources. Obviously, the transfer of heat will have to be done as far as possible in a reversible way. Leaving compression and expansion isentropic, two possibilities present themselves, depending on whether $T_1 > T_3$ or $T_1 < T_3$

Let $T_1 > T_3$ (Fig. 2-3). The compression is interrupted at 0′, at temperature T_3, and at pressure p_1'; and the expansion is interrupted at 2′, at temperature T_1, and at pressure p_2'. Gas in the state 0′ is brought

into heat exchange with gas in the state 2′, resulting in an increase of temperature of the former from T_3 to T_1 and a simultaneous decrease of the latter from T_1 to T_3. The maximum amount of heat that can be exchanged (in the direction of the arrow in Fig. 2-3) is $q_{13} = c_p(T_1 - T_3)$, represented by the areas $a0'1'ba$ or $c3'2'dc$. Isentroic compression $1' \rightarrow 1''$ and expansion $3' \rightarrow 3''$ connect 1′ and 3′ with the ordinary cycle. The heat exchange causes a loss of available energy indicated by the hatched areas; but the heat to be supplied is also reduced by an amount corresponding to the area $a11''ba$. The efficiency of the process is obviously improved.

Now suppose that $T_1 < T_3$ (Fig. 2-3). Here, heat exchange between the gases at T_1 and T_3 is possible without further modification of the process. The maximum amount of heat to be transferred (in the direction of the arrow) is $q_{13} = c_p(T_3 - T_1)$, represented by the area $c3'3dc$, and the heat to be supplied from outside is reduced by the same amount. The available energy being unaltered, the efficiency of the process is thus increased to

$$\eta_{th} = 1 - \frac{T_0}{T_3} \tag{2-25}$$

This method of using heat exchangers within the process suggests that the thermal efficiency could be increased even further if compression and expansion could be isothermal instead of isentropic. The process would then become reversible and the efficiency would be

$$\eta_{th} = 1 - \frac{T_0}{T_2} \tag{2-26}$$

The technical difficulties to be overcome would be considerable, even taking into account only the heat exchangers themselves. In modern jet engines, the ordinary constant-pressure process is usually used.

2-3. Production of a Propulsive Force. Momentum Theorem. The chief purpose of all aircraft engines is the production of a propulsive force, a thrust, by changing the energy of the air which passes through the engine. Since this is true also of coolers, where a negative thrust (drag) is usually produced, these will also be included in our considerations. Out first aim is to relate the propulsive force to the available energy, dealt with in the previous section. The amount of energy which appears as the work of the propulsive force (and thus the thrust itself) cannot be found from purely thermodynamic considerations, which deal only with the production of mechanical energy in general and not with the particular forms in which it is manifested.

In the following we shall as usual consider energies and work as being referred to unit weight; when quantities per unit time are required, it

will be necessary to multiply by $g\rho VA$, the weight of air crossing the section of area A (with velocity V, density ρ) per unit time.

The thrust can be derived from the momentum theorem, which is particularly helpful in cases like that with which we have to deal here, where thermodynamic considerations have given a general knowledge of the flow, such as the kinetic energy of the air at stations far ahead and far behind. Since the momentum theorem will be used frequently below, it will be explained in more detail here.

The momentum theorem can be derived directly from Newton's second law of motion, $F = m\dot{V}$, which states that the rate of change of momentum of a body, or of a bounded mass system, is equal to the sum of the external applied forces. The momentum is the product of the mass and the velocity; it is a vector quantity and has the direction of the velocity. The theorem as stated above has still to be adapted to fluids considered as a continuum. For a steady motion of a fluid, it may be stated in the form:[1] The flow of momentum through a fixed surface bounding a definite volume of fluid is equal to the resultant of the pressure integral over the surface and the forces exerted by the fluid on bodies in it. We ignore gravitational forces in the fluid. To momentum entering the surface of integration there corresponds a force in the same direction, and to momentum leaving the surface a force in the opposite direction.

To determine the thrust of an engine, *i.e.*, the force component on it in the direction of motion, we apply the momentum theorem to the force and momentum components in that direction. Suppose that the velocity of the air which passes through the engine is V_0 far ahead (state 0), and V_3 far behind (state 3). The engine is replaced by a disk of area A_1, at which the energy of the flow is changed. The jet, or wake, formed is surrounded by air with velocity V_0. Velocity components other than those in the direction of the main flow are ignored. A coordinate system fixed in the disk is used.[2] A cylinder of infinite length and large diameter, with its axis in the direction of the undisturbed flow (Fig. 2-4), is chosen as surface of integration.[3] Mass flow $\rho_0 V_0 A_0$ per unit time enters the cylinder with velocity V_0 and entering momentum $\rho_0 V_0 A_0 V_0$. The leaving momentum of the mass $\rho_3 V_3 A_3$ in the jet is $\rho_3 V_3 A_3 V_3$, and that of the air which leaves the cylinder through the area

[1] See, for example, L. Prandtl and O. Tietjens; R. von Mises; J. C. Hunsaker and B. G. Rightmire.

[2] In this coordinate system the thrust F_x does not perform any work. This is permissible, however, since when the need arises we know that in a coordinate system fixed in space the propulsive work per unit time is $F_x V_0$.

[3] We do not choose a stream surface as part of the surface of integration, as is very often done. Although this would simplify matters, for no momentum enters or leaves this surface, an integration of pressures which are often unknown would be needed.

$(A_0 - A_3)$ is $\rho_0 V_0 (A_0 - A_3) V_0$. There is, however, a further contribution from the air which is pushed out of the side of the cylinder due to the expanding flow within (in a case like that drawn in Fig. 2-4). By continuity the mass flow per unit time which leaves in this way must be

$$\rho_0 V_0 A_0 - [\rho_0 V_0 (A_0 - A_3) + \rho_3 V_3 A_3] = (\rho_0 V_0 - \rho_3 V_3) A_3$$

We may assume the diameter of the cylinder so large that the axial component of the fluid velocity at its surface is V_0; then the third leaving momentum term is $(\rho_0 V_0 - \rho_3 V_3) A_3 V_0$.

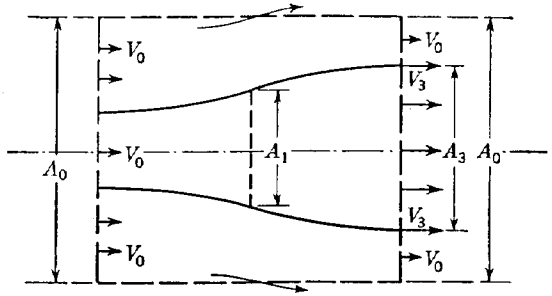

FIG. 2-4. Flow with change of energy on area A_1, with surface of integration (dotted line) for momentum theorem.

Thus the whole rate of change of momentum is

$$\delta\mathfrak{M} = \rho_0 V_0 A_0 V_0 - \rho_3 V_3 A_3 V_3 - \rho_0 V_0 (A_0 - A_3) V_0 - (\rho_0 V_0 - \rho_3 V_3) A_3 V_0$$
$$= \rho_3 V_3 A_3 (V_0 - V_3)$$

assuming that no mass is added during the change of energy. Using the equation of continuity, $\rho_3 V_3 A_3 = \rho_1 V_1 A_1$, where the subscript 1 applies to the section at which the energy is supplied, we can write this

$$\delta\mathfrak{M} = \rho_1 V_1 A_1 (V_0 - V_3) \tag{2-27}$$

The integration of the pressures along the surface is simple if we assume that the pressure far downstream in the jet is p_0, which is certainly justified. Then the forces from the pressures on the two ends of the cylinder are equal and of opposite sign ($\pm p_0 A_0$) and cancel one another. The pressures on the side walls of the cylinder, whatever their values may be, have no component in the direction of the main flow and hence do not enter the equation.

Thus the momentum theorem gives $\delta\mathfrak{M} = -F_x$, where F_x is the axial force on the disk. The minus sign occurs because we have called F_x positive (a thrust) when it is in the opposite sense to V_0. With Eq. (2-27) we obtain finally

$$F_x = \rho_1 V_1 A_1 (V_3 - V_0) \tag{2-28}$$

This states that a positive thrust is produced if a true jet with $V_3 > V_0$ is formed, and it can be put simply: The thrust is equal to the increase of momentum of the air which passes through the engine per unit time. A true jet can only occur if the kinetic energy of the jet is higher than that of the air outside it. Thus the kinetic energy of the jet provides a connection with the thermodynamic relations of the previous section, being part of the available energy.

2-4. Production of a Propulsive Force. Efficiencies. The kinetic energy of the air is increased when energy is supplied to it from the surroundings. In Sec. 2-2 we considered a supply of heat only, producing the available mechanical energy Δe_a in the form of an increase Δe_k of the kinetic energy of the air plus work w done on the surroundings. We now consider in addition an input of mechanical work $\bar{w}$ per unit weight, and shall denote it by $\bar{w}$ to distinguish it from any work w which may be taken out, for instance, work done by a windmilling propeller or shaft work taken out of a turbine. Note that we define $\bar{w}$ as of opposite sign to w for practical convenience. We shall also denote the heat input per unit weight by $\bar{q}$, in order to distinguish it from other heat energy which may be transferred during the process, for instance, heat removed by heat exchangers. The total input per unit weight is then $\bar{q} + \bar{w}$.

The thrust obtained from this energy input is given by Eq. (2-28), and the propulsive work per unit weight of the air passing through the engine, per unit time, is

$$\frac{F_x V_0}{g\rho_1 V_1 A_1} = V_0 \frac{V_3 - V_0}{g} \tag{2-29}$$

We can now define an *over-all propulsive efficiency* η by expressing the resulting propulsive work as a fraction of the energy input:[1]

$$V_0 \frac{V_3 - V_0}{g} = \eta(\bar{q} + \bar{w}) \qquad \text{or} \qquad \eta = \frac{V_0(V_3 - V_0)/g}{\bar{q} + \bar{w}} \tag{2-30}$$

It is helpful to a better understanding of the thrust-producing process to split the over-all efficiency into several component efficiencies. Producing thrust by means of a jet inevitably involves losses, since kinetic energy is left behind in the jet. Thus a purely mechanical *jet efficiency*, η_j, is obtained by relating the propulsive work to the increase in kinetic energy associated with it, which is

$$\Delta e_k = e_{k3} - e_{k0} = \frac{V_3^2 - V_0^2}{2g}$$

[1] See also the discussion on the definition of propulsive efficiencies in Letters to the Editor of the *Journal of the Aeronautical Sciences*, vol. 14, p. 564, 1947, by M. Z. Krzywoblocki, R. W. McCloy, and others.

so that

$$\eta_j = \frac{V_0(V_3 - V_0)/g}{\Delta e_k} = \frac{2}{1 + V_3/V_0} \tag{2-31}$$

This is the well-known Froude efficiency. The production of thrust is the more efficient, the less the velocity in the jet exceeds that outside it. Thus for a given thrust it is more efficient to give a small increase of kinetic energy per unit weight to a large weight of air per unit time than to generate a high-velocity jet with a small weight flow.

The over-all propulsive efficiency can now be written as the product $\eta_j\eta_k$ of the jet efficiency and the *kinetic efficiency*

$$\eta_k = \frac{\Delta e_k}{\bar{q} + \bar{w}} \tag{2-32}$$

in which we state once again that the sole purpose of the energy input, as far as propulsion is concerned, is to convert as much as possible of the energy input into kinetic energy in the jet.

We may now distinguish between the mechanical and the thermal components of the power input by splitting Δe_k into a portion $\Delta' e_k$, produced by the mechanical work $\bar{w}$, and a portion $\Delta'' e_k$, produced by the heat supplied.

Only part of the mechanical energy $\bar{w}$ supplied from outside is converted into kinetic energy $\Delta' e_k$ of the jet because of the frictional forces which are always present. Therefore an efficiency

$$\eta_{\bar{w}} = \frac{\Delta' e_k}{\bar{w}} \tag{2-33}$$

can be introduced. Considering this mechanical side of the process as one without heat supply, we obtain from Eq. (2-15), $\bar{w} - \Delta' e_k = \Delta' i$, so that

$$\eta_{\bar{w}} = \frac{\bar{w} - \Delta' i}{\bar{w}} = 1 - \frac{\Delta' i}{\bar{w}} \tag{2-33a}$$

This indicates that the energy lost by frictional forces in the engine is found as an increase of enthalpy in the jet.

Again, only part of the heat input $\bar{q}$ is converted into kinetic energy $\Delta'' e_k$, so that the efficiency is

$$\eta_{\bar{q}} = \frac{\Delta'' e_k}{\bar{q}} \tag{2-34}$$

The energy loss

$$\bar{q} - \Delta'' e_k = \bar{q}(1 - \eta_{\bar{q}})$$

adds further to the enthalpy i_3 in the jet, since, from Eq. (2-15), $\bar{q} - \Delta'' e_k = \Delta'' i$ if the thermal side of this process is considered as one

without mechanical work. With this definition of $\Delta''i$,

$$\eta_{\bar{q}} = \frac{\bar{q} - \Delta''i}{\bar{q}} = 1 - \frac{\Delta''i}{\bar{q}} \tag{2-34a}$$

If no mechanical work is taken out of the system, $\eta_{\bar{q}}$ is the same as the thermal efficiency η_{th} determined in Sec. 2-2. If, however, mechanical work is taken out, for instance, through the shaft of a turbine, then less kinetic energy $\Delta''e_k$ is produced by the given heat input $\bar{q}$. Then the increase $\Delta''e_k$ of kinetic energy is only part of the available energy $\Delta''e_a = w + \Delta''e_k$, produced by the given heat input $\bar{q}$, and the component $\eta_{\bar{q}}$ of the propulsive efficiency drops, although in terms of $\Delta''e_a$ the thermal efficiency $\eta_{th} = \Delta''e_a/\bar{q}$ may remain unaltered. In other words, the engine is then being used partly as a power station[1] to produce energy for other purposes and becomes less effective as a propulsion unit.

With these component efficiencies the over-all propulsive efficiency of Eq. (2-30) becomes

$$\eta = \eta_j \frac{\eta_{\bar{q}}\bar{q} + \eta_{\bar{w}}\bar{w}}{\bar{q} + \bar{w}} \tag{2-35}$$

since

$$\eta = \frac{F_x V_0}{g\rho_1 V_1 A_1(\bar{q} + \bar{w})} = \frac{F_x V_0}{g\rho_1 V_1 A_1 \Delta e_k} \frac{(\Delta'' e_k/\bar{q})\bar{q} + (\Delta' e_k/\bar{w})\bar{w}}{\bar{q} + \bar{w}} \tag{2-36}$$

in accordance with its definition and because $\Delta e_k = \Delta' e_k + \Delta'' e_k$.

In a comparison of the efficiencies of processes and of types of engines, it is essential to state which of the characteristic parameters is to be kept constant. An example may illustrate this point.

Let $\bar{w} = w = 0$. With the nondimensional heat input

$$C_{\bar{q}} = \frac{\bar{q}}{V_0^2/2g} \tag{2-37}$$

the propulsive efficiency becomes

$$\eta = \eta_j \eta_{th} = \frac{2}{1 + V_3/V_0} \frac{(V_3/V_0)^2 - 1}{C_{\bar{q}}} = \frac{2}{C_{\bar{q}}}\left(\frac{V_3}{V_0} - 1\right) \tag{2-38}$$

and the efficiency increases with increasing V_3 if $C_{\bar{q}}$ is constant. If, however, the total heat input is kept constant instead of the coefficient $C_{\bar{q}}$, which is related to unit weight, a different expression for η is obtained. Defining a nondimensional total heat input coefficient $C_{\bar{p}}$ by

$$C_{\bar{p}} = \frac{g\rho_1 V_1 A_1 \bar{q}}{\frac{1}{2}\rho_0 V_0^3 A_1} = C_{\bar{q}} \frac{\rho_1}{\rho_0} \frac{V_1}{V_0} \tag{2-39}$$

[1] The ordinary piston engine (excluding the propeller) is a typical example of this. The heat input is partly converted into mechanical work, taken out by the propeller shaft; a small portion of it is converted into propulsive work in the exhaust nozzles; and an appreciable part of it is usually wasted altogether in the cooler (see Chap. 12).

and introducing this into Eq. (2-38), we find

$$\eta = \frac{2}{C_{\bar{p}}} \frac{\rho_1 V_1}{\rho_0 V_0}\left(\frac{V_3}{V_0} - 1\right) \tag{2-40}$$

Since $\rho_1 V_1$ and V_3 are not independent of one another, this expression is obviously different from the one above, and indicates that, in this case, the mass-flow ratio $\rho_1 V_1/\rho_0 V_0$ plays an important part in determining the efficiency.

2-5. Power Plants Supplying Mechanical Energy to the Flow. Turning now to individual types of engines, we shall as before denote conditions far upstream by the subscript 0 and conditions ahead of and behind the device where energy is supplied from outside by 1 and 2, respectively, and far downstream in the jet by 3. Static pressures at 0 and 3 are always assumed to be equal: $p_3 = p_0$. All the variables are reduced to nondimensional form, with conditions at 0 as reference conditions.

Equation (2-15) is taken as a basis to show the various ways in which energy may be supplied or transformed. It is used in the form

$$\frac{V_3^2 - V_0^2}{2g} = -w + q + i_0 - i_3 \tag{2-41}$$

or, nondimensionally,

$$\frac{1}{2}\rho_0 \frac{V_0^2}{p_0}\left[\left(\frac{V_3}{V_0}\right)^2 - 1\right] = -\frac{w}{RT_0} + \frac{q}{RT_0} + \frac{i_0 - i_3}{RT_0} \tag{2-41a}$$

The flight velocity V_0 can be eliminated by using the Mach number of flight

$$\mathrm{M}_0 = \frac{V_0}{a_0} \qquad \text{where } a_0 = \sqrt{k\frac{p_0}{\rho_0}}$$

[see Eqs. (2-17) and (2-18)]. Equation (2-41) then reads

$$\frac{k}{2}\mathrm{M}_0^2\left[\left(\frac{V_3}{V_0}\right)^2 - 1\right] = -\frac{w}{RT_0} + \frac{q}{RT_0} + \frac{i_0 - i_3}{RT_0} \tag{2-41b}$$

In Eqs. (2-41) to (2-41*b*), w is the sum of the technical work, and it includes the energy input $\bar{w}$; similarly, q is the sum of the heat transferred, and it includes the heat input $\bar{q}$.

Let us consider the ideal propeller without friction. There is no supply of heat, $\bar{q} = 0$; but mechanical work is done by external means and transferred to the propeller through the propeller shaft, $w = -\bar{w} \neq 0$. Neither the enthalpy of the air nor the entropy in the slip stream is different from those upstream: $i_3 = i_0$ and $s_3 = s_0$. The whole of the energy supplied is transferred into kinetic energy in the jet, Eq. (2-41).

The propulsive efficiency is not unity since the kinetic energy is only partly made use of for the production of thrust. The efficiency is given by the jet efficiency of Eq. (2-31).

All the changes of state of the air follow a single isentropic curve (Fig. 2-5). Up to the propeller disk, $0 \rightarrow 1$, pressure, density, and also enthalpy decrease. In passage through the propeller disk, $1 \rightarrow 2$, each of these parameters rises suddenly. As the pressure decreases gradually to p_0 behind the propeller, $2 \rightarrow 3$, density and enthalpy too approach their initial values at 0. The diagram in Fig. 2-5 shows that no work is done

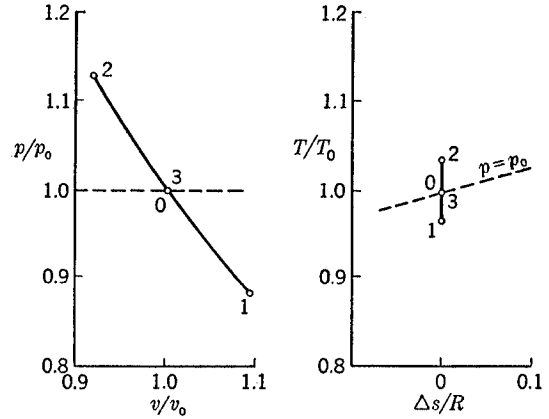

FIG. 2-5. The ideal propeller without friction.

by the flow, as the curve encloses zero area. The air only serves as a converter of the mechanical energy in the propeller shaft into kinetic energy in the slip stream.

All the mechanical work $\bar{w}$ is added between conditions 1 and 2, and therefore,

$$i_1 + \frac{V_1^2}{2g} + \bar{w} = i_2 + \frac{V_2^2}{2g} \tag{2-42}$$

This relation implies that the energy input $\bar{w}$ of a propeller can be measured by observations of the temperature ahead and behind, since $i + V^2/2g$ is the temperature indicated by a thermometer exposed in the stream.

With a real propeller some energy is lost due to frictional forces at the propeller blades. It is still true that $q = 0$, $\bar{w} \neq 0$, but now $i_3 \neq i_0$. Since the entropy cannot decrease, both entropy and enthalpy are greater in the slip stream than in the undisturbed flow: $i_3 > i_0$. Equation (2-41*b*) then reads

$$\frac{\bar{w}}{RT_0} - \frac{k}{2} M_0^2 \left[\left(\frac{V_3}{V_0} \right)^2 - 1 \right] = \frac{i_3 - i_0}{RT_0} = \frac{\Delta' i}{RT_0} > 0 \tag{2-43}$$

which indicates that only part of the work supplied is converted into kinetic energy, the rest being wasted on an increase of the enthalpy of the slip stream.

The changes of state of the air are shown in Fig. 2-6. The entropy increases when the air passes through the propeller disk, $1 \rightarrow 2$. The area $a03ba$ represents the energy lost due to friction, which appears as a temperature increase in the flow downstream. The efficiency is naturally less than that of the ideal propeller. From Eq. (2-35) we obtain $\eta = \eta_j \eta_{\bar{w}}$, where η_j is given by Eq. (2-31),[1] and

$$\eta_{\bar{w}} = 1 - \frac{\Delta' i}{\bar{w}}$$

from Eq. (2-33*a*). Keeping $\Delta' i/\bar{w}$ small is particularly difficult when the resultant velocity on the propeller blade is high so that compressibility effects increase $\Delta' i$.

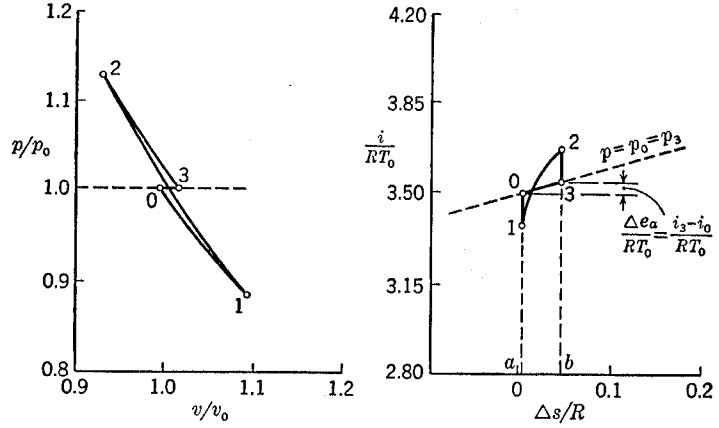

FIG. 2-6. The propeller with friction.

Another main aerodynamic problem of modern propeller design is not so apparent in these considerations. This concerns the design of propellers of large power input and high thrust, particularly at take-off, without increasing the diameter and the number of blades excessively.

One way of dealing with both problems is to surround the propeller with a fairing, thus altering the mean axial velocity at the propeller disk V_1 but not the final velocity V_3. Reducing V_1 at high flight speeds might help to overcome Mach number difficulties; increasing V_1 at low speeds results in higher thrust, Eq. (2-28), part of which will act on the fairing. A ducted and a nonducted propeller have the same jet efficiency if the

[1] This relation includes only axial losses in the slip stream and neglects tangential losses due to the kinetic energy of rotation of the slip stream.

same thrust acts on the propeller itself. The ducted propeller presents a series of aerodynamic problems beyond those of ordinary propeller theory, and will be discussed in detail in Chap. 6. For the general treatment of propellers, we refer to existing textbooks.

The case of a cold, unfaired, cooler block may be mentioned here. It is an example of a device where no energy is supplied, $\bar{q} = 0$; $\bar{w} = 0$. The sum of kinetic energy and enthalpy is therefore constant, Eq. (2-41). Due to frictional forces in the narrow tubes of the cooler block, the entropy and with it the enthalpy of the air passing through the cooler increase, and consequently the velocity falls below V_0. This causes a drag force on the nonducted cooler block, Eq. (2-28). The aerodynamic problems of cooling are dealt with in Chap. 12.

2-6. Power Plants Supplying Heat Energy to the Flow. We consider now engines which supply only heat, neither supplying nor removing mechanical energy, that is, $q = \bar{q} \neq 0$; $w = \bar{w} = 0$. This group includes the ram jet and the warm cooler block; it also includes the turbojet engine, for compressor and turbine are driven by means of the heat supplied.

There is no engine that would correspond to the ideal frictionless propeller where entropy and enthalpy remain constant; the heat cannot be transformed completely into work. But the opposite case, where all the heat is transformed into an increase of the enthalpy, is possible, that is, $\bar{q} = i_3 - i_0$, and, from Eq. (2-41), $e_{k3} - e_{k0} = 0$. Hence there is no thrust and the propulsive efficiency is zero. This is in effect an idealized heat source in a parallel stream, and may be called a *nonducted burner.*[1] Although it does not represent a practical aircraft engine, the nonducted burner will assist toward a better understanding of jet engines proper.

Figure 2-7 shows the changes of state of the air that passes through the burner. Up to the burner, $0 \rightarrow 1$, the change is isentropic, but in contrast to the case of the ideal propeller (Fig. 2-5), pressure and temperature increase. As it passes through the burner, $1 \rightarrow 2$, the temperature of the air increases further, while the pressure drops below atmospheric. The decisive factor is the increase of entropy during this stage; the process shifts to another isentropic curve, and following this from $2 \rightarrow 3$ the pressure increases again to p_0 and a further rise of temperature occurs. The quantity of heat supplied during $1 \rightarrow 2$ is represented by the area $a12ba$ in the Ts diagram. The equal area $3ba03$ corresponds to the heat $i_3 - i_0$ which is removed by the flow.

[1] The problem of the nonducted burner is quite different from that of the addition of heat to a gas flowing in a pipe (see, for example, J. V. Foa and G. Rudinger, *J. Aeronaut. Sci.*, vol. 16, p. 84, 1949; R. Weatherston, *J. Aeronaut. Sci.*, vol. 17, p. 182, 1950), the main difference being that in the latter case important modifications of the initial conditions in the flow upstream are produced by changes in the heat supply, which is clearly not the case with the nonducted burner in a free stream.

This process can be modified into one producing a usable propulsive force by purely aerodynamic means, by surrounding the burner with a fairing. The fairing of the ducted burner, or ram jet, reduces the velocity at the burner. Thus a higher pressure p_1 is obtained by the use of part of the kinetic energy e_{k0} of the inflow. This changes the whole process radically (Fig. 2-8)[1] and provides the basis of a family of aircraft propulsion units.

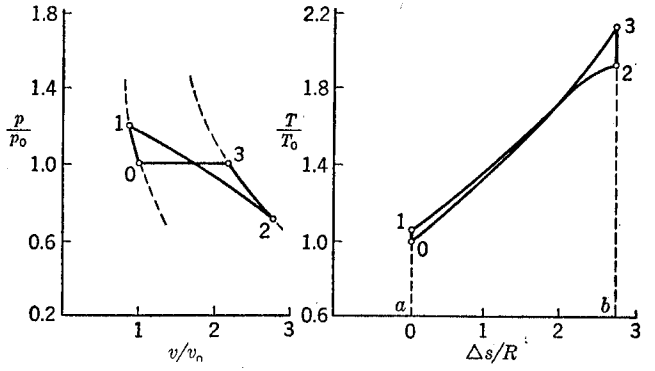

FIG. 2-7. The nonducted burner. $M_0 = 0.63$; $V_1/V_0 = 0.59$; $C_{\bar{p}} = 10$.

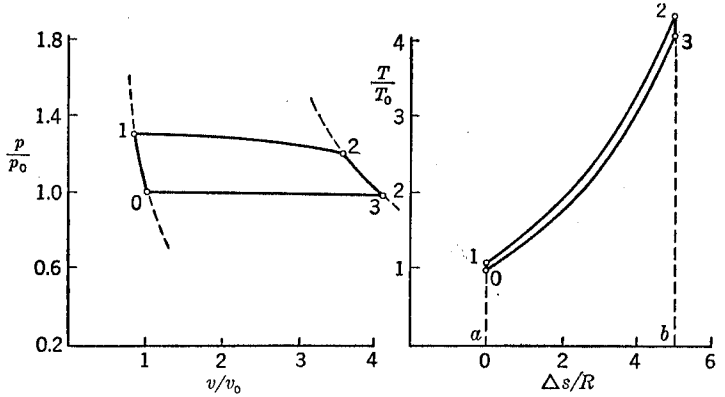

FIG. 2-8. The ducted burner (ram jet). $M_0 = 0.63$; $V_1/V_0 = 0.2$; $C_{\bar{p}} = 10$.

The heat input $\bar{q}$ is no longer equal to $i_3 - i_0$ and Eq. (2-41) gives $V_3 > V_0$, which implies that a true jet is formed and a nonzero thrust generated. The curve 01230 (Fig. 2-8) now encloses a positive area. The process is similar to the constant-pressure process treated in Sec. 2-2. In particular, the efficiency increases as the pressure ratio p_1/p_0 increases. This is well illustrated by the Ts diagram in Fig. 2-8. As the pressure reached during the change $0 \rightarrow 1$ is raised, the near isobar $1 \rightarrow 2$ moves

[1] All diagrams are drawn to scale and may thus give an idea of the efficiencies obtained.

toward higher temperature, and the ratio of the area 01230 representing the available energy to the area $a12ba$ representing the heat supplied becomes more favorable.

There are limits, however, to p_1/p_0, and the highest value is reached when the fairing reduces V_1 to zero. In that case, the efficiency depends entirely on the flight velocity or, more accurately, on the flight Mach number:

$$\eta_{\bar{q}} = \eta_{th} = 1 - \frac{1}{1 + \frac{k-1}{2} M_0^2} \tag{2-44}$$

which can be seen by eliminating p_1/p_0 or T_1/T_0 in Eq. (2-24) by means of Eq. (2-16). This is, of course, a hypothetical case, since in fact no air enters the engine. In general, the efficiency of the ram jet depends to a large extent also on the aerodynamic performance of the fairing, as will be discussed in more detail in Chap. 7.

Figure 2-9 has been prepared to illustrate the flow past the nonducted burner and ram jet and the propeller[1] and ducted propeller, showing their respective aerodynamic and thermal characteristics. The streamlines, the variation of velocity, and the thermodynamic parameters are given.

The foregoing considerations show very clearly how the thermal efficiency of engines with heat supply can be improved, namely, by adding devices to raise the combustion pressure p_1. A further possibility, the addition of heat exchangers, has already been mentioned in Sec. 2-2.

In a turbojet engine a compressor is used to raise the pressure considerably during the process $0 \rightarrow 1$. The compressor receives the necessary energy from a gas turbine, situated after the combustion chamber. Through the turbine, the high energy behind the combustion chamber is used to let the compressor raise the pressure ahead of the combustion chamber. The turbine thus transforms part of the heat supplied into mechanical energy. The turbojet engine is therefore a case where mechanical energy is taken out of the process, only to be put back in at another stage, indeed an ingenious way of raising the thermal efficiency. Since the turbine produces just as much mechanical work as the compressor consumes, no mechanical energy is exchanged with the surroundings, so that effectively $\bar{w} = 0$ (and $w = 0$) still.

Figure 2-10 gives diagrams for an ideal turbojet motor. It is assumed that the heat is supplied in the combustion chamber, $1 \rightarrow 2$, at constant pressure. This is in fact very nearly true in practice. The path $0 \rightarrow 0'$

[1] In this case, a rather large value of the power coefficient

$$C_{\bar{p}} = \frac{g\rho_1 V_1 A_1 \bar{w}}{\frac{1}{2}\rho_0 V_0^3 A_1}$$

has been assumed in order to bring out the illustration.

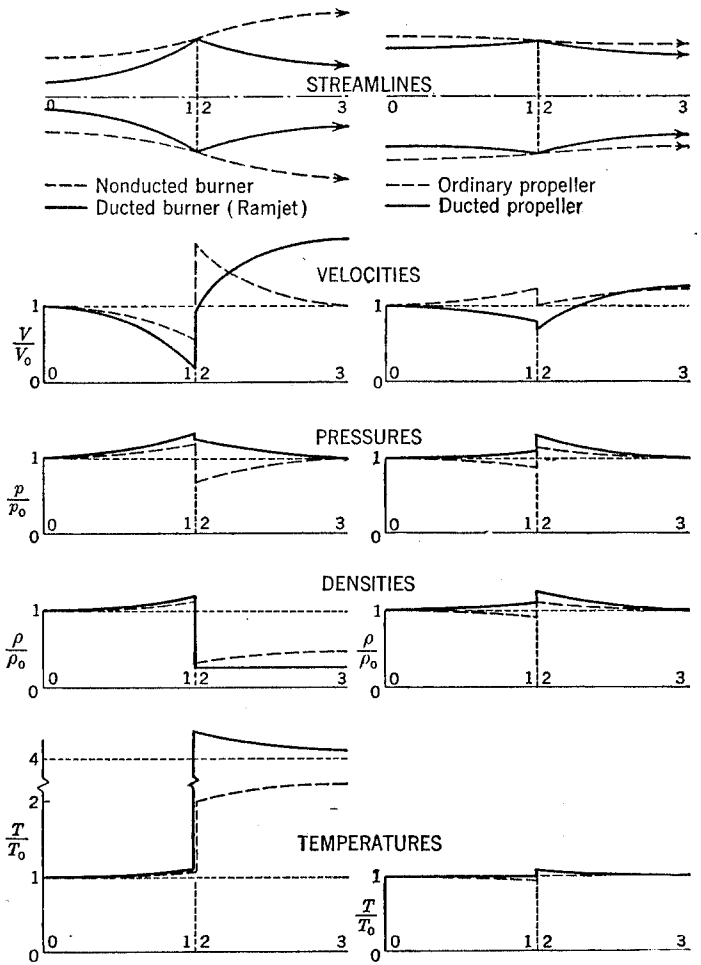

FIG. 2-9. Comparison between propulsion systems with heat supply and others with supply of mechanical energy. $M_0 = 0.63$.

		V_1/V_0	$C_{\bar{p}}$	$\frac{\text{Thrust}}{\frac{1}{2}\rho_0 V_0^2 A_1}$
Left-hand side	Nonducted burner	0.59	10	0
	Ducted burner	0.20	10	0.44
Right-hand side	Propeller	1.20	0.5	0.44
	Ducted propeller	0.80	0.5	0.44

represents the change of state ahead of the compressor. The energy consumed by the compressor is shown in the is diagram by the length $0'1$ and in the pv diagram by the area $a0'1ba$. The same quantity of work delivered by the turbine corresponds to the length $22'$ or the area $b22'cb$. The available energy, *i.e.*, the increase in kinetic energy, is given

by the areas of work or heat in the pv and Ts diagrams or by the length 2′3 in the is diagram.

In real compressors and turbines the changes $0' \rightarrow 1$ and $2 \rightarrow 2'$ are not reversible. The entropy rises in each process, and the working diagrams are modified to those in Fig. 2-11.[1] There are losses $i_1 - i_{1'}$ in the compressor, and a compressor efficiency

$$\eta_C = \frac{i_{1'} - i_0}{i_1 - i_0} \tag{2-45}$$

can be defined, comparing the real value $i_1 - i_0$ with that of a reversible process, $i_{1'} - i_0$, between the same pressures p_0 and p_1. Correspondingly,

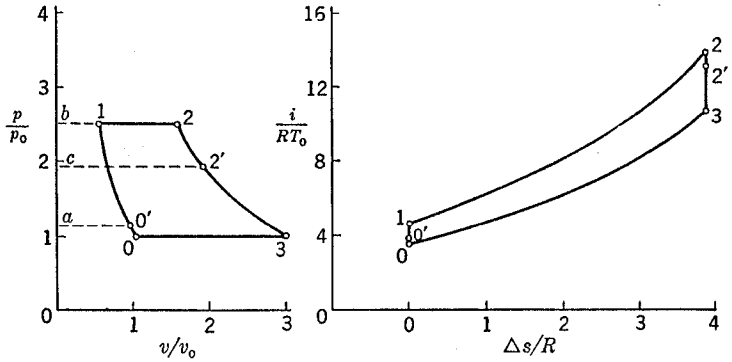

FIG. 2-10. The ideal turbojet engine.

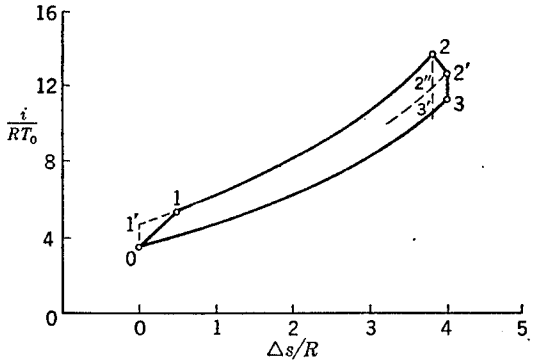

FIG. 2-11. The turbojet engine with losses in the compressor and in the turbine.

we compare the work of the turbine in the real, irreversible process between the pressures p_2 and $p_{2'}$ with that in the reversible process. In the irreversible process we arrive at point 2′ in Fig. 2-11 and in the reversible one at the point 2″. The turbine losses are therefore $i_{2'} - i_{2''}$

[1] In this diagram, the compression by ram effect is ignored. This effect in itself may be influenced a great deal by the installation of the engine, see Chap. 9.

and the efficiency

$$\eta_T = \frac{i_2 - i_{2'}}{i_2 - i_{2''}} \tag{2-46}$$

The total loss in the expansion $i_3 - i_{3'}$ is, however, smaller than the loss in the turbine $i_{2'} - i_{2''}$, since $i_{2''} - i_{3'} < i_{2'} - i_3$, which means that part of the turbine loss is regained in the nozzle or in the jet. With η_C and η_T smaller than unity the over-all propulsive efficiency is reduced, as the figure shows.

A heat exchanger alone, such as an engine cooler, presents an example where heat is added to a stream of air. The frictional forces cause a loss of energy, as they do in the cold cooler mentioned in the previous section, but the heat supplied brings a gain in kinetic energy. Thus

$$e_{k3} < e_{k0},\ e_{k3} = e_{k0},\ e_{k3} > e_{k0}$$

are each a possible case. Correspondingly, the cooler may experience either a drag, no force at all, or even a thrust. In the last case, the cooler is a propulsion unit in the true sense.

2-7. Power Plants Supplying Heat and Mechanical Energy to the Flow. While $\bar{w} = 0$ for all engines that have been discussed so far, a vast range of different kinds of engines opens up when we consider those with $\bar{w} \neq 0$; $\bar{q} \neq 0$; that is, those in which only part of the heat which is not used for driving the compressor is transformed directly into kinetic energy of the jet, while another part is used to transfer mechanical energy to the flow. In most practical cases mechanical work is transferred to another stream of air using an additional device to produce thrust there. This might be a propeller, as on the turbopropeller engine, or a ducted fan.

The thermodynamic processes are basically those of simple turbojet engines; in particular, the thermal efficiency

$$\eta_{th} = \frac{\Delta e_a}{\bar{q}}$$

the ratio of the available energy Δe_a to the heat supplied, is the same. The available energy is created in the first stream (No. I). In the *multi-stream* engine it is, however, divided between the increase in kinetic energy Δe_{kI} of a jet I and the technical work w_I. The latter is transferred as $\bar{w}_{II}$ into the second stream[1] of air (No. II) and there transformed into an increase of kinetic energy Δe_{kII} of the second jet. If the second process has the mechanical efficiency

$$\eta_{\bar{w}II} = \frac{\Delta e_{kII}}{\bar{w}_{II}}$$

[1] This assumes that mechanical work is transferred through a shaft. Matters would be different if the second system were to be fed with hot air under high pressure from the first system.

as defined in Sec. 2-4, the over-all efficiency of the compound engine is

$$\eta = \frac{\eta_{jI}\,\Delta e_{kI} + \sigma\eta_{jII}\eta_{\bar{w}II}\bar{w}_{II}}{\Delta e_{kI} + \sigma\bar{w}_{II}}\,\eta_{th} \tag{2-47}$$

where

$$\sigma = \frac{\rho_{II}V_{II}A_{II}}{\rho_I V_I A_I}$$

is the mass-flow ratio between the two streams of air. Equation (2-47) is derived from the fact that η times the power input $\bar{q}$ is equal to the sum of the propulsive work of the two component engines, which can be seen as follows

$$\eta\bar{q}g\rho_I V_I A_I = V_0(F_{xI} + F_{xII})$$

so that

$$\eta(\Delta e_{kI} + \sigma\bar{w}_{II})\,\frac{\bar{q}}{\Delta e_{kI} + \sigma\bar{w}_{II}} = \frac{F_{xI}V_0}{g\rho_I V_I A_I\,\Delta e_{kI}}\,\Delta e_{kI} + \sigma\,\frac{F_{xII}V_0}{g\rho_{II}V_{II}A_{II}\,\Delta e_{kII}}\,\frac{\Delta e_{kII}}{\bar{w}_{II}}\,\bar{w}_{II}$$

using Eq. (2-31) and $\Delta e_a = \Delta e_{kI} + \sigma\bar{w}_{II}$.

Equation (2-47) shows that the general layout of a multistream engine must be carefully planned. In the case of a turbopropeller engine, the over-all efficiency may be better than that of a pure turbojet. The jet efficiency η_{jI} is higher than that of the pure turbojet because the increase in kinetic energy is reduced ($\Delta e_{kI} < \Delta e_k$ of the turbojet for equal heat input), and therefore V_3/V_0 becomes smaller. The jet efficiency η_{jII} of the propeller will also be high, since the diameter of the propeller (and thus the mass flow through it) can be kept large enough to keep the increase in kinetic energy low. This, of course, provides the chief incentive to the design of such compound engines.

It will be more difficult, however, to keep the losses due to rotation in the slipstream of the propeller small at high speeds,[1] unless counterrotating propellers or a ducted propeller with guide vanes are provided. The value of $\eta_{\bar{w}II}$ appears on the whole to be decisive as to whether the over-all propulsive efficiency is improved or not. Being determined by the friction and other energy losses, $\eta_{\bar{w}II}$ is dependent on whether the propeller works under favorable conditions, which can be the case as long as the blade velocity is low enough for disturbing effects at the propeller blades due to compressibility to be avoided. In short, the turbopropeller engine appears more suitable for flight at moderate subsonic speeds, compared with the turbojet motor which will give the better performance at high speeds, where its jet efficiency as well as its thermal efficiency become better anyway.

[1] These do not occur in Eq. (2-47); they can be taken into account by another factor (smaller than unity) in the second term of the numerator.

The turbopropeller is, however, only one example of a multistream engine. Its present advantage is that its components, the turbojet and the propeller, are both readily available. Future applications will call for other solutions, stipulated by installation problems, since modern high-speed aircraft cannot possibly be designed for many more years by the addition of a separately designed propulsion unit to a lifting surface. The two will have to be designed as a whole.

2-8. Common Characteristics of the Various Types of Propulsion System. Our considerations in the preceding sections suggest the treatment of the various classes of engine as particular cases of a generalized power plant. We conclude this chapter with a brief summary of their common characteristics and their individual features in this light.

The air in its passage through the engine is subject in general to three distinguishable processes which change its condition: inflow, supply of energy, and outflow. In every case the purpose is to create a velocity in the outflow far behind the engine in excess of that in the inflow far ahead, so that a thrust force will be produced, Eq. (2-28). This implies that in whatever form the energy input is supplied to the engine, it is to be transformed as efficiently as possible into kinetic energy, although the kinetic energy of the jet as such is wasted according to Froude's jet efficiency relation, Eq. (2-31). When mechanical energy is supplied directly, it would ideally be possible to transform it completely into kinetic energy, but in the actual process there is always an increase of entropy due to frictional forces, and thus a reduction of the efficiency, Eq. (2-33). When heat energy is supplied, it can never be transformed completely; the maximum thermal efficiency is obtained in the Carnot cycle with reversible changes of state between two isentropes and two isotherms, Eq. (2-23). But this is the ideal to strive for, and in actual technical processes the heat is usually supplied at nearly constant pressure, Eq. (2-24). Heat exchangers are means of approaching the isothermal process, but in general attempts to improve the thermal efficiency concentrate on raising the pressure of combustion.

This is where the aerodynamic problems of the inflow come in. The inflow pressure may be increased in the free stream ahead of the inlet, in a diffuser inside the fairing, or in a specially installed compressor. For flight at subsonic speeds, any of these flow processes can theoretically be applied without energy losses, and keeping the actual losses within reasonable limits is one of the designer's main tasks. The installation of the engine in the aircraft may also influence the losses in the inflow as it passes along other surfaces.

The actual mass flow through the engine is generally determined and regulated by the conditions in the outflow, by the shape of the free jet, and by the conditions in and behind the exit opening when the engine is

faired. Apart from the lost kinetic energy of the jet, this outflow could again be free from further energy losses, even when it does mechanical work as in a turbine.

There remain the problems of the combustion itself, which mainly concern the physical chemist but will increasingly interest the aerodynamicist in so far as the combustion occurs in a flowing gas. They are basic to all aircraft engines since a heat engine of some kind is always necessary, even where we have assumed a supply of mechanical energy only. The supply of heat to a stream of air is always associated with an increase of its entropy, and it is the relative increase of the entropy for a given supply of energy that distinguishes one kind of engine from another.

Another distinguishing feature of a particular engine is the ratio between the part of the thrust that acts on the energy source itself and the total thrust. A pure heat source, for instance, is incapable of sustaining an aerodynamic load, and other parts of the engine take the thrust force. A thrust analysis of this kind is not only helpful to an understanding of the working process put will often lead the way to the satisfactory design of a particular engine.

EXERCISES

2-1. Air (to be considered as a perfect gas) changes its temperature from $T_1 = 273°\text{K}$ to $T_2 = 3T_1$ at a constant pressure. Draw the curve representing this change in a Ts and in an is diagram.

2-2. Air (to be considered as a perfect gas) expands from $p_1 = 10$ atm to $p_2 = 1$ atm at a constant temperature of $T = 273°\text{K}$. Draw the curve representing this change in a pv diagram. ($1 \text{ atm} = 1.03 \times 10^4 \text{ kg/m}^2 = 14.7 \text{ lb/in.}^2$)

2-3. Air (to be considered as a perfect gas) is compressed isentropically from $p_1 = 1$ atm to $p_2 = 3p_1$. Its initial temperature is $T_1 = 273°\text{K}$. Determine the end temperature T_2 and the change of density. Draw the curve representing this change in a pv diagram.

2-4. A Carnot cycle, with $p_1/p_2 = 10$ and $\eta_{th} = 0.5$, is modified by having compression and expansion nonisentropic with an entropy increase of $\Delta s = 0.23R$ in each of these changes of state. How much is the thermal efficiency of the cycle reduced? Determine the "compressor efficiency" from Eq. (2-45).

2-5. Draw the pv, Ts, and is diagrams of an ideal constant-pressure cycle with $p_1/p_0 = 3$ and $T_2/T_0 = 3$. Determine the thermal efficiency of the cycle graphically, and compare this with the efficiency of the corresponding Carnot cycle between the same temperatures T_0 and T_2.

BIBLIOGRAPHY

General:

KEENAN, J. H., "Thermodynamics," John Wiley & Sons, Inc., New York, 1941.

EPSTEIN, P. S., "Textbook of Thermodynamics," John Wiley & Sons, Inc., New York; Chapman & Hall, Ltd., London, 1943.

ZEMANSKY, M. W., "Heat and Thermodynamics," McGraw-Hill Book Company, Inc., New York, 1943.

BOSNJAKOVIC, F., "Technische Thermodynamik," 2d ed., T. Steinkopf, Leipzig, 1944.

SCHMIDT, E., "Einführung in die technische Thermodynamik," Springer-Verlag, Berlin, 1944; "Thermodynamics," translation by J. Kestin, Oxford University Press, London and New York, 1949.

EWING, J. A., "Thermodynamics for Engineers," 2d ed., Cambridge University Press, London and New York, 1946.

SOLF, K., Fundamental Concepts of Thermodynamics, (*AVA Monograph* J_32), *Brit. Min. of Supply* (*Völkenrode*) *Rept. & Transl.* 979, 1946.

LICHTY, L. C., "Thermodynamics," 2d ed., McGraw-Hill Book Company, Inc., New York, 1948.

OBERT, E. F., "Thermodynamics," McGraw-Hill Book Company, Inc., New York, 1948.

Tables:

KEENAN, J. H., and J. KAYE, "Gas Tables," John Wiley & Sons, Inc., New York, 1948.

KEENAN, J. H., and J. KAYE, A Table of Thermodynamic Properties of Air, *J. Applied Mechanics*, vol. 10, p. 123, 1943.

Special Subjects:

PRANDTL, L., and O. TIETJENS, "Fundamentals of Hydro- and Aeromechanics," Springer-Verlag, Berlin, 1929; translation by L. Rosenhead, McGraw-Hill Book Company, Inc., New York, 1934.

GLAUERT, H., Airplane Propellers, in "Aerodynamic Theory," W. E. Durand, editor, vol. IV, Springer-Verlag, Berlin, 1935.

WEINIG, F., "Aerodynamik der Luftschraube," Springer-Verlag, Berlin, 1940.

VON MISES, R., "Theory of Flight," McGraw-Hill Book Company, Inc., New York, 1945.

HUNSAKER, J. C., and B. G. RIGHTMIRE, "Engineering Applications of Fluid Mechanics," McGraw-Hill Book Company, Inc., New York, 1947.

THEODORSEN, TH., "Theory of Propellers," McGraw-Hill Book Company, Inc., New York, 1948.

JOST, W., "Explosion and Combustion Processes in Gases," Springer-Verlag, Berlin, 1939; translation by H. O. Croft, McGraw-Hill Book Company, Inc., New York, 1946.

CHAPTER 3

TWO-DIMENSIONAL NONHOMOGENEOUS FLOW PROBLEMS

The one-dimensional treatment in the previous chapter deals only with mean values of the flow parameters at a few fixed cross sections. In practice, detailed knowledge is often required of the nature of the changes between one cross section and the next, and of the local variation over a section. In this chapter, we shall discuss some problems of this kind that arise in practice.

Section 3-1 illustrates the general features of nonhomogeneous flow, *i.e.*, flow in different parts of which the total energy is not the same. Nonhomogeneous flows usually occur when energy is supplied from the surroundings. In some cases, and under simplifying assumptions, a homogeneous flow can be found which is equivalent to a nonhomogeneous flow with free boundaries. In Sec. 3-4 the general equations governing flows of this type are formulated. For a better understanding of the methods of calculation, we shall first remind ourselves briefly of some aspects of potential-flow theory and conformal transformations in Secs. 3-2 and 3-3. In the last two sections, two simple cases of some practical importance, the flows past a thin air intake and a nonducted cooler, are treated in more detail.

3-1. An Aerodynamic Characteristic Common to All Types of Propulsion System. The supply of energy to the flow in any aircraft engine is associated with a flow pattern which is typical in that it is nonhomogeneous, with regions of different total energy separated by the engine fairing or by free boundaries. The value of one or more of the flow parameters changes almost discontinuously at these boundaries. At a fairing the inner and outer pressures may differ; at a jet boundary there can be a discontinuity in velocity or density. Most common, of course, are differences in kinetic energy, usually associated again with discontinuities in velocity. Some typical cases are shown in Fig. 2-9, Chap. 2.

A well-known example is the ordinary propeller in the simplified treatment by the momentum theory. The mechanical energy supplied by the propeller increases the total energy in the slip stream above that of the external flow, from which it is separated by the propeller disk and the free boundary of the jet. In incompressible flow, the total energy difference may take the form either of a difference in kinetic energy, that is, in velocity, or of a pressure difference. At the propeller disk the velocity

is continuous, but there is a sudden rise in pressure and consequently a thrust force on the propeller. The free boundary cannot sustain any force, and the pressure must be the same on both sides. There must therefore be a finite difference between the velocities on the two sides.[1] The velocity field and the shape of the discontinuity surface are of great importance for the performance and the design of the propeller. Some papers on this subject are listed at the end of this chapter.

We meet a similar problem in the flow past a nonducted cooler block. The energy loss due to friction inside the block usually exceeds the gain due to the heat supply, so that the air flowing through experiences a loss of mechanical energy, usually as a pressure drop. (The flow past a windmilling propeller is similar in this respect.) There is a free boundary behind the cooler block, originating from its edges, with a discontinuity in velocity. In this case the velocity within the wake is smaller than that outside.

A characteristic of the cooler flow is that the direction at exit from the block is fixed by the direction of the tubes. When the block is normal to the main flow, the outflow and the whole wake can be taken as parallel, a convenient simplification which eliminates the need to determine a free-boundary shape.

Another related case is the flow past a nonducted burner, with its finite changes of pressure and velocity at the burner disk and discontinuities of temperature and density behind.

The nonducted-burner flow and the cooler-block flow are not of immediate practical interest, since both burner and cooler are always installed in a fairing. We shall see, however, that the streamlines of the burner (Sec. 7-7) and of the cooler (Sec. 12-3) find an application in the design of the inner shape of the fairing immediately ahead or behind the installed cooler or burner, in particular of the low-speed diffuser upstream.

Since a free boundary is a stream surface, the pattern of the flow past a nonducted cooler block will remain unaltered if the free boundary of the wake is replaced by a solid wall. If now the block is removed, then, as will be shown below, the pressure jump is transferred from the block to the wall, while the velocity field remains unchanged. The flow can be regarded as that past a thin air intake, with the wake boundary taking the part of the intake wall and the expansion occurring partly in the free stream ahead of the inlet opening and partly inside in the diffuser formed by the walls.

A problem with mixed boundary conditions is presented by the flow near the exit of a jet engine. Distinguishing between the air discharging through the nozzle and the external flow, we find we have conditions

[1] The velocity difference does not exist for long, of course; it is leveled down by turbulent mixing, ignored here (see Chap. 10).

similar to those for the thin air intake for the flow inside the nozzle and a free boundary with discontinuities in velocity, temperature, and density behind the exit. As in all problems with mixed boundary conditions, special difficulties are encountered at the junction between the wall and the free boundary. Only simple cases have as yet been investigated, mostly in connection with open-jet wind tunnels where similar problems arise.[1] For supersonic jets, see, for example, D. Pack (1948).

There are several closely related problems whose solutions could profitably be applied to the cases we discuss here. In the general drag problem, for instance, we are concerned with the flow about a body with a wake behind it. If the flow separates from the body and a *dead-water* region forms on the downstream side, the fluid is completely at rest there and the pressure is constant. A free-stream surface separates the dead-water region from the main stream; but there is a simplification in that the pressure is known to be constant along the boundary. C. W. Oseen's drag theory is an extreme application of this line of thought, which has been extended by W. Müller (1931) and F. W. Lindner (1931) among others. A general discussion of flows with free streamlines can be found in Chap. VIII of V. L. Streeter's book in this series.

The dead-water flow leads directly to the cavitation phenomena which occur when the static pressure at the surface of a body in a streaming liquid falls below the vapor pressure of the liquid. A bubble filled with gas then develops downstream of the body, bounded by a free-stream surface along which the pressure is constant. This is again simpler than the general jet problem. A summary of recent work in this field has been given by G. Birkhoff (1948); an application to our present subject can be found in Sec. 5-2.

3-2. Potential Flow. Method of Singularities. In this and the following section some of the methods of potential-flow theory, which will be needed in the rest of this chapter and elsewhere in the book, will be briefly explained.

The ideal nonviscous irrotational steady flow, or potential flow, in two dimensions can be described either by the potential function $\Phi(x,y)$, such that

$$V_x = \frac{\partial \Phi}{\partial x} \qquad V_y = \frac{\partial \Phi}{\partial y} \tag{3-1}$$

or by the stream function $\Psi(x,y)$, such that

$$V_x = \frac{\partial \Psi}{\partial y} \qquad V_y = -\frac{\partial \Psi}{\partial x} \tag{3-2}$$

where V_x and V_y are the velocity components in the x and y directions,

[1] See, for example, H. Ludwieg, 1939; D. Küchemann and F. Vandrey, 1942.

respectively.[1] Φ and Ψ are functions of position in the flow field, *i.e.*, of the two variables x and y. Both satisfy Laplace's equation

$$\nabla^2\Phi = \frac{\partial^2\Phi}{\partial x^2} + \frac{\partial^2\Phi}{\partial y^2} = 0$$
$$\nabla^2\Psi = \frac{\partial^2\Psi}{\partial x^2} + \frac{\partial^2\Psi}{\partial y^2} = 0$$

which follows from their definitions above together with the equation of continuity

$$\frac{\partial V_x}{\partial x} + \frac{\partial V_y}{\partial y} = 0$$

and the condition of no rotation in the flow

$$\frac{\partial V_x}{\partial y} - \frac{\partial V_y}{\partial x} = 0$$

The lines $\Phi = \text{const}$ are normal to the lines $\Psi = \text{const}$, which are the streamlines; and the equipotential lines and the streamlines together form the well-known orthogonal network in the plane of the flow. Also, along a streamline,

$$\frac{\partial\Psi/\partial x}{\partial\Psi/\partial y} = -\frac{dy}{dx}$$
$$\frac{dy}{dx} = \frac{V_y}{V_x} \tag{3-3}$$

This is the streamline condition, which we shall use often.

The theory of potential flow in the xy plane is greatly simplified by the introduction of the complex variable $z = x + iy$, which couples the pair of real variables x and y into a single *complex* variable, in which $i = \sqrt{-1}$. A given value of z defines a point (x,y) in the flow plane, and x is called the real part and y the imaginary part[2] of z. The introduction of the symbol i is the foundation of the algebra of complex numbers, on which the ordinary algebraic operations can be performed if i^2 is always replaced by -1. Any complex expression can be separated into its real and imaginary parts, and an equation in complex variables is true for the real parts on the two sides and the imaginary parts on the two sides separately.

Two functions of x and y, for instance, $\Phi(x,y)$ and $\Psi(x,y)$, can also be coupled together, forming a complex function

$$F(z) = \Phi(x,y) + i\Psi(x,y)$$

[1] See, for example, H. Lamb; H. Glauert; L. Prandtl and O. Tietjens; R. von Mises; V. L. Streeter.

[2] The significance of the misleading terms *real* and *imaginary* is not important, and has a historical explanation.

Complex functions, which may at this stage be thought of as mere formal expressions, are of great importance in potential flow theory, since any differentiable function of the complex variable $z = x + iy$ is a solution of Laplace's equation and can thus be used to represent the potential and stream function of a two-dimensional flow. This can be seen as follows: If $F(z)$ is differentiable,[1] then the same value of dF/dz must be obtained whether the point $z = x + iy$ is approached along a line $x = \text{const}$ or along a line $y = \text{const}$. In the first case,

$$\frac{dF}{dz} = \frac{\partial F}{\partial (iy)} = \frac{1}{i}\frac{\partial F}{\partial y}$$

and in the second

$$\frac{dF}{dz} = \frac{\partial F}{\partial x}$$

Differentiating each of these results again, we have

$$\frac{d^2F}{dz^2} = -\frac{\partial^2 F}{\partial y^2} \qquad \text{and} \qquad \frac{d^2F}{dz^2} = \frac{\partial^2 F}{\partial x^2}$$

so that

$$\nabla^2 F = \frac{\partial^2 F}{\partial x^2} + \frac{\partial^2 F}{\partial y^2} = 0$$

If $F(z) = \Phi(x,y) + i\Psi(x,y)$, we find by separating the real and imaginary parts that $\Phi(x,y)$ and $\Psi(x,y)$ each satisfy Laplace's equation.

We see further from the expressions for the first differentials of $F(z)$ above that

$$\frac{\partial F}{\partial x} = \frac{1}{i}\frac{\partial F}{\partial y} = -i\frac{\partial F}{\partial y} \qquad \text{since } \frac{1}{i} = -i$$

or, with $F = \Phi + i\Psi$,

$$\frac{\partial \Phi}{\partial x} + i\frac{\partial \Psi}{\partial x} = -i\left(\frac{\partial \Phi}{\partial y} + i\frac{\partial \Psi}{\partial y}\right) = -i\frac{\partial \Phi}{\partial y} + \frac{\partial \Psi}{\partial y}$$

Again separating the real and imaginary parts,

$$\frac{\partial \Phi}{\partial x} = \frac{\partial \Psi}{\partial y} \qquad \text{and} \qquad \frac{\partial \Phi}{\partial y} = -\frac{\partial \Psi}{\partial x} \tag{3-4}$$

It will be noted that these equations, which are called the Cauchy-Riemann differential equations, are consistent with our definitions above

[1] Complex functions which are differentiable are usually called *analytic* or *regular* functions. The condition is usually satisfied by all functions related to sensible physical problems, except at certain isolated points, where $F(z)$ may be *singular* (see below).

since

$$\frac{\partial \Phi}{\partial x} = \frac{\partial \Psi}{\partial y} = V_x \qquad \text{and} \qquad \frac{\partial \Phi}{\partial y} = -\frac{\partial \Psi}{\partial x} = V_y$$

When Φ and Ψ are thought of as the potential and stream function of a two-dimensional flow, $F(z)$ is usually called the *complex potential.*

A large number of simple analytic functions which represent standard elementary types of flow is known. These can be used to represent more complicated types of flow by superposition. Some examples are given in the following:

1. $F(z) = az$ represents a parallel flow along the x axis, if a is a real constant. From $F(z) = ax + iay$ we find $\Phi = ax$ and $\Psi = ay$, so that $V_x = \partial\Phi/\partial x = a = V_0$ and $V_y = \partial\Phi/\partial y = 0$.

2. $F(z) = (Q/2\pi) \ln z$ represents the flow out of a point *source.* This is readily seen if the complex variable is transformed into

$$z = r(\cos\vartheta + i\sin\vartheta) = re^{i\vartheta}$$

where $r = \sqrt{x^2 + y^2}$ is the radius vector from the origin to the point (x,y) and ϑ, such that $\tan\vartheta = y/x$, is the angle between this radius vector and the x axis. Then the complex potential becomes

$$F(z) = \frac{Q}{2\pi}\ln z = \frac{Q}{2\pi}\ln r + i\frac{Q}{2\pi}\vartheta$$

so that

$$\Phi = \frac{Q}{2\pi}\ln r \qquad \text{and} \qquad \Psi = \frac{Q}{2\pi}\vartheta$$

Lines $\Phi = \text{const}$ are circles ($r = \text{const}$); the streamlines $\Psi = \text{const}$ are the radii from the origin ($\vartheta = \text{const}$). (This accounts for the term *source.*) It may be noted that the quantity of fluid which flows through a section between two streamlines is given by the difference between the values of the stream function on those two streamlines. In the present case, it follows from $\Psi = Q\vartheta/2\pi$ that the flow per unit time through a complete circle (between $\vartheta = 0$ and $\vartheta = 2\pi$) is Q.

3. It is seen from the above that

$$F(z) = -i\frac{\Gamma}{2\pi}\ln z$$

represents the flow about a point *vortex,* the streamlines being concentric circles and the equipotentials radial lines, *i.e.,* interchanged from the source flow above.

4. $F(z) = M/2\pi z$ represents the flow of a *doublet.* We have

$$F(z) = \frac{M}{2\pi r}e^{-i\vartheta} = \frac{M}{2\pi r}\cos\vartheta - i\frac{M}{2\pi r}\sin\vartheta$$

so that

$$\Phi = \frac{M}{2\pi r}\cos\vartheta \qquad \text{and} \qquad \Psi = -\frac{M}{2\pi r}\sin\vartheta$$

The lines $\Psi = \text{const}$ are circles, tangential to the x axis at $x = 0$. The doublet can be obtained by letting a source and a sink of equal strength approach infinitely closely, the source strengths increasing as the distance decreases.

It is, in fact, surprising to find that a large number of practical flow problems can be solved with these few standard functions, each of which represents the flow about a *singularity*—source, vortex, doublet—so-called because in each case $z = 0$ is a point at which alone the complex potential is not differentiable. Laplace's equation is not satisfied at these singularities, although it is satisfied in the flow in a region about them.

The concept of singularities can also be applied to three-dimensional flow, although the use of the complex stream function is, of course, restricted to two dimensions. Several examples will be given below and we shall leave their discussion until we need them.

3-3. Conformal Transformations. Hodograph Method. A great help in the treatment of potential flow in two dimensions is the method of conformal transformations.[1]

One variable, z, is transformed into another, ζ, by means of a function $\zeta = f(z)$, which simply states a relation between ζ and z. Both variables may be complex:

$$z = x + iy \qquad \text{and} \qquad \zeta = \xi + i\eta$$

A point (ξ,η) in the ζ plane then corresponds to a point (x,y) in the z plane, and a network in the xy plane (formed, for instance, by lines $\Phi = \text{const}$ and $\Psi = \text{const}$) is transformed into another in the $\xi\eta$ plane. The transformation is called *conformal* if angles in the one plane are transformed into equal angles in the other, so that an orthogonal network is transformed into another orthogonal network. This means that the pattern of streamlines and potential lines in one plane is transformed into another pattern which can again represent streamlines and potential lines in the other plane, *i.e.*, a flow is transformed into another flow. For this to be so, $\zeta = f(z)$ must be an analytic function. Clearly, a conformal transformation may be used to transform a complicated flow pattern into a simpler one of which the solution, *i.e.*, the complex potential, is known.

Let us consider as a simple example the transformation

$$\zeta = z + \frac{R^2}{z}$$

[1] For closer study, we refer to A. Betz, 1948; R. V. Churchill, 1944.

where R is a real constant. Because of the term R^2/z, the point $z = 0$ in the z plane is transformed to infinity in the ζ plane. The circle

$$z = Re^{i\vartheta} = R\cos\vartheta + iR\sin\vartheta$$

in the z plane is transformed into

$$\zeta = R\cos\vartheta + iR\sin\vartheta + \frac{R^2}{R}\cos\vartheta - i\frac{R^2}{R}\sin\vartheta$$

since $e^{-i\vartheta} = \cos\vartheta - i\sin\vartheta$, so that

$$\zeta = 2R\cos\vartheta = \xi \qquad \text{where } -2R \le \xi \le +2R$$

The circle in the z plane is thus transformed into a straight line (or, as we say, a slot, since, in a flow, conditions may be different on the two sides), extending from $\xi = -2R$ to $\xi = +2R$ along the real axis in the ζ plane. A potential flow in the z plane with this circle as a streamline is transformed into a parallel flow along the ξ axis in the ζ plane. The complex potential of the parallel flow is, as we know, $F(\zeta) = \zeta$ (with $V_0 = 1$). Therefore the complex potential in the z plane is

$$F(z) = \zeta = z + \frac{R^2}{z}$$

and the potential, the stream function, and the velocity components of the flow can be derived from this.

We could have obtained the same result by superposing the complex potential $F(z) = R^2/z$ of a doublet at $z = 0$ on that of a parallel flow $F(z) = z$, since a doublet along the x axis in a parallel flow makes the circle of radius R into a streamline, as can be seen from

$$F(z) = r\cos\vartheta + ir\sin\vartheta + \frac{R^2}{r}\cos\vartheta - i\frac{R^2}{r}\sin\vartheta$$

$$= r\cos\vartheta\left(1 + \frac{R^2}{r^2}\right) + ir\sin\vartheta\left(1 - \frac{R^2}{r^2}\right)$$

in which the imaginary part is

$$\Psi = r\sin\vartheta\left(1 - \frac{R^2}{r^2}\right)$$

$\Psi = \text{const} = 0$ for $r = R$.

This example shows the equivalence of the method of conformal transformation with that of singularities. In other cases, however, one might not be able to guess the complex potential and the singularities to represent a given flow as easily, and the conformal transformation method is then most helpful. It has been extensively used in the theory of the two-

dimensional airfoil, for instance, transforming the flow around an arbitrary airfoil section first into that around a circle and then by the above transformation into a parallel flow along a slot. The method can further be used to find suitable singularities to apply to ideal flow in three dimensions where the conformal transformation fails. Such general applications are frequently made use of in this book.

The hodograph (so called by Hamilton) is a special conformal transformation.[1] It is based on the fact that

$$\frac{dF}{dz} = V_x - iV_y \tag{3-5}$$

which is readily seen from

$$\begin{aligned} dF &= \frac{\partial F}{\partial x}\,dx + \frac{\partial F}{\partial y}\,dy \\ &= \left(\frac{\partial \Phi}{\partial x} + i\,\frac{\partial \Psi}{\partial x}\right) dx + \left(\frac{\partial \Phi}{\partial y} + i\,\frac{\partial \Psi}{\partial y}\right) dy \\ &= (V_x - iV_y)\,dx + (V_y + iV_x)\,dy \\ &= (V_x - iV_y)(dx + i\,dy) \\ &= (V_x - iV_y)\,dz \end{aligned}$$

With $F(z)$ an analytic function,

$$w = f(z) = \frac{dF}{dz} = V_x - iV_y \tag{3-6}$$

is also an analytic function, and $w = f(z)$ may be considered as a conformal transformation of the z plane into the w plane, in which the real and imaginary variables are the velocity components V_x and $-V_y$ of the given flow.

This method may be applied with advantage when the flow in the hodograph plane is simple and the complex potential there can be found easily. The hodograph can be drawn if we have some knowledge of the velocity field in the given z plane (since the velocity components there are the variables in the hodograph plane). If we know, for instance, that the total velocity $\sqrt{V_x^2 + V_y^2} = V$ is constant along a certain contour in the z plane, this contour will be transformed into part of a circle in the hodograph plane, which makes the hodograph method particularly suitable for the analysis of flows with such constant-velocity free boundaries. A typical example is given in Sec. 4-5.

If the flow in the hodograph plane is known, transformation back into the z plane by means of

$$z = \int \frac{dF}{w} + \text{const} = \int \frac{dF}{dw}\frac{dw}{w} + \text{const} \tag{3-7}$$

enables the flow in the original z plane to be deduced. As may be supposed, the reverse transformation is usually the more tedious part of the method in practice.

[1] It is not necessary for our purpose to distinguish between the true hodograph and its reflection in the x axis, which is what Eq. (3-5) actually corresponds to.

3-4. Reduction of a Nonhomogeneous Flow to an Equivalent Homogeneous Flow, and the Mathematical Formulation of the Problem. Consider a nonhomogeneous flow with free boundaries, assumed for simplicity to be incompressible, nonviscous, and made up of regions with constant total energy. (It will be possible to apply our solution to a wake, in which the total energy is not constant, by superposition.) We further assume the change of energy to occur suddenly at a given surface; that is, there is a sudden change of pressure of constant amount Δp across that particular surface of discontinuity. There is of course no pressure difference across the other surface of discontinuity, the free boundary between the wake and the main flow. Then both the flow inside the wake and the flow past it are potential flows.

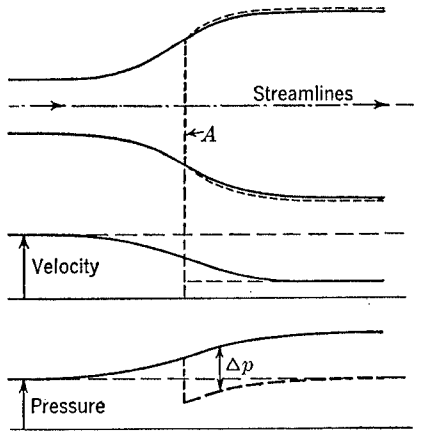

FIG. 3-1. Nonhomogeneous flow with a pressure discontinuity at A (dotted lines) and the equivalent homogeneous flow (full lines), with velocity and pressure on the line of symmetry.

Now the motion in either region at any point depends on the pressure gradients but not on the absolute value of the pressure (Euler's law), and the pressure may be altered by a constant amount over the whole region without any effect on the velocity field. Hence, by altering the static pressure inside the wake by the amount Δp, we can obtain an equivalent homogeneous flow with the same total energy everywhere. The pressure is now continuous at the former surface of energy change; but at the boundary in the equivalent flow there are discontinuities of both velocity and pressure (Fig. 3-1). To make this possible, we must assume the wake boundary to be replaced by a solid wall, which again does not alter the flow since the boundary is a stream surface. The shape of the new wall, however, is not given but has still to be determined.

The equivalent homogeneous-flow problem is then to find the stream surface (a solid wall) at which there are given discontinuities in velocity and pressure. This we can do by the methods of potential theory. If

V_i is the velocity just inside the boundary surface and V_e the velocity just outside, Bernoulli's equation applied to the two sides of the boundary gives

$$-\Delta p = \tfrac{1}{2}\rho(V_e^2 - V_i^2) = \tfrac{1}{2}\rho(V_e + V_i)(V_e - V_i) \tag{3-8}$$

This is a relation between the discontinuities in pressure and velocity. The term

$$\tfrac{1}{2}(V_e + V_i) = V_b$$

can be interpreted as the velocity in the boundary, and

$$V_i - V_e = \gamma_b$$

as the strength γ_b of a vortex sheet by which the velocity discontinuity can be replaced. If in Fig. 3-2 DF represents a short length ds of the cross section of the boundary, the total vortex strength on DF is equal to $V_i\,ds - V_e\,ds$, or $V_i - V_e$ per unit length. Then Eq. (3-8) reads

$$\Delta p = \rho V_b \gamma_b \tag{3-9}$$

determining the strength of the vortex distribution.

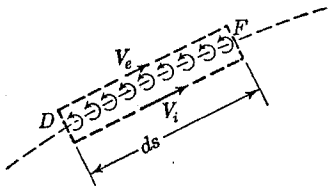

FIG. 3-2. Cross section of a boundary with a velocity discontinuity represented by a distribution of vorticity.

The force Δp per unit area acts normal to the boundary everywhere in the equivalent flow. The same relation (3-9) can, of course, be deduced from the Kutta-Joukowsky theorem, which states directly that the force acting on a vortex element is equal to the product of density, velocity, and vortex strength; and that the force is normal to the plane containing the direction of the velocity and that of the vorticity vector.

Far downstream the boundary becomes parallel to the main flow, and the external velocity at the surface is equal to the velocity V_0 of the free stream. There Eq. (3-8) gives

$$\Delta p = \tfrac{1}{2}\rho[2V_0 + (V_i - V_0)](V_i - V_0) = \tfrac{1}{2}\rho(2V_0 + \gamma_{b\infty})\gamma_{b\infty} \tag{3-10}$$

relating the final value $\gamma_{b\infty}$ of the vortex strength to the given pressure jump Δp.

In most cases, the shape of the boundary (*i.e.*, the position of the vortex distribution) is not known. It can be determined from the condition that the boundary must be a stream surface: The velocity component normal to the surface must be zero.

The velocity at any point is the resultant of the free-stream velocity and the velocity induced by the vortices. For flow in two dimensions (including flow with rotational symmetry), a coordinate system (s,σ) can be introduced, in which $s \geq 0$, $\sigma = \sigma_0 =$ constant corresponds to the boundary of the wake; and $0 \leq \sigma \leq \sigma_0$, $s = 0$ to the surface at which the original flow had a pressure jump. The velocity components normal and tangential to the boundary induced by the vortex distribution $\gamma_b(s,\sigma_0)$ can then be expressed in the form:

$$\begin{aligned} v_{bn}(s,\sigma_0) &= \int_0^\infty \gamma_b(s',\sigma_0)K_n(s,s',\sigma_0)\,ds' \\ v_{bt}(s,\sigma_0) &= \int_0^\infty \gamma_b(s',\sigma_0)K_t(s,s',\sigma_0)\,ds' \end{aligned} \tag{3-11}$$

where the functions K_n and K_t depend on the coordinates only and not on the vortex distribution. In any given case they can be determined from the geometrical conditions by the Biot-Savart law. This states that an element of length ds of a vortex filament has an influence on the velocity v at a point P given by

$$dv = \Gamma \frac{ds}{4\pi r^2} \sin\vartheta \tag{3-12}$$

where Γ is the strength of the vortex filament, r the distance from the element to P, and ϑ the angle between the radius vector from the element to P and the direction of the vortex element. dv is normal to the plane of ds and P. As is well known, this is the same relationship as that between an electric current and its associated magnetic field.

The streamline condition now reads

$$V_{bn} = V_{0n}(s,\sigma_0) + \int_0^\infty \gamma_b(s',\sigma_0)K_n(s,s',\sigma_0)\,ds' = 0 \tag{3-13}$$

where V_{0n} is the component of the free-stream velocity V_0 normal to the boundary. The boundary condition (3-9) can be written

$$\gamma_b(s,\sigma_0) = \frac{\Delta p}{\rho}\frac{1}{V_{bt}(s,\sigma_0)} = \frac{\Delta p}{\rho}\frac{1}{V_{0t}(s,\sigma_0) + \int_0^\infty \gamma_b(s',\sigma_0)K_t(s,s',\sigma_0)\,ds'} \tag{3-14}$$

Equations (3-13) and (3-14) are integral equations from which both the strength and the position of the vortex distribution are to be determined. Some special cases which illustrate the procedure will be described below. Each is simplified in some respect; the general case has not yet been treated in full.

3-5. Application to the Flow Past Thin Air Intakes. The calculation of thin air intakes is simplified by the fact that the boundary condition (3-14) need not be satisfied. The solid intake wall allows any pressure difference between the internal and external regions. (It is sometimes an advantage, however, to have the pressure constant along the surface of the intake, as will be seen in Chaps. 4 and 5.) The vortex distribution can therefore be arbitrarily chosen; the resulting shape and the pressure

distribution along its surface decide finally whether the choice was reasonable. The stream-surface condition (3-13) remains. The inverse problem, to find the vortex distribution for a given shape of the air intake, is usually a more difficult one to solve.

Let us consider for example a thin air intake extending to infinity downstream and of circular cross section, its axis, the x axis, lying in the free-stream direction. The vortex distribution to replace it can be compounded of coaxial *vortex rings*, beginning at $x = 0$ with the radius $r = R_0$. The functions K in Eq. (3-11), which are functions of the coordinates (x,r), can be calculated for axially symmetric vortex-ring distributions from the axial- and radial-velocity components v_x and v_r of an isolated vortex ring. These are given and their values tabulated in Sec. 5 of the Appendix.

For a given vortex distribution $\gamma_b(x)$, the shape $r(x)$ to satisfy the streamline condition (3-13) can be obtained by successive approximations. A suitable shape $r^{(1)}(x)$, for instance, the cylinder

$$r^{(1)}(x) = R_0 = \text{const}$$

may be taken as a first approximation, and the next approximation $r^{(2)}(x)$ obtained by determining the streamline of the first flow through the point $x = 0, r = R_0$. With the given vortex distribution arranged on $r^{(2)}(x)$, the next approximation is obtained in the same way, and so on. This process is admittedly tedious and has to be done numerically. The streamline is determined either from Eq. (3-13) or, alternatively, by finding the coordinates of the surface at which the value of the stream function $\Psi(x,r)$ is constant and equal to that at the point $x = 0, r = R_0$. For this purpose, formulas and tables for the stream function of a vortex ring are also given in the Appendix.

The stream function is not needed if Eq. (3-13) is used in the following way. If

$$\frac{dr}{dx} = \tan \vartheta$$

is the slope of the intake at any point, the normal velocity component V_n is given by

$$V_n = (V_0 + v_x) \sin \vartheta - v_r \cos \vartheta$$

so that the condition $V_n = 0$ from Eq. (3-13) reads

$$\frac{dr}{dx} = \frac{v_r}{V_0 + v_x} \tag{3-15}$$

This is Eq. (3-3) again for axially symmetrical flow. In the iteration process the shape $r(x)$ can thus be obtained by the integration of Eq. (3-15) at each stage. The convergence is often more rapid using this method.

The approximate shape obtained in the second step from a vortex distribution on a cylinder and the final, exact, stream surface differ appreciably, as the examples in Figs. 3-3 and 3-4 show. This explains why the simplified propeller theory, in which the slip stream is assumed to be a cylindrical surface, fails if the propeller is heavily loaded.

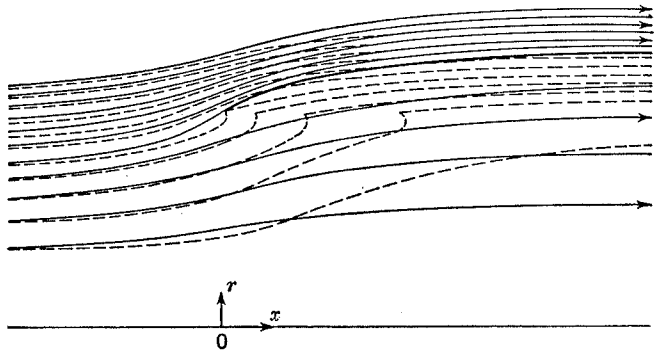

FIG. 3-3. Flow pattern for a thin air intake with axial symmetry. Broken lines, constant vortex distribution on cylinder. Full lines, constant vortex distribution on stream surface. $V_i(x = +\infty) = 0.3V_0$.

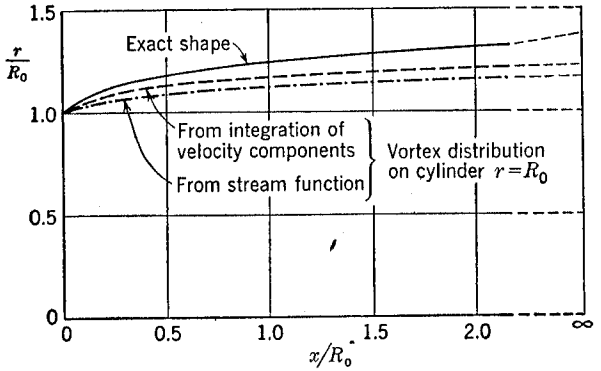

FIG. 3-4. Comparison of various methods for the calculation of a thin air intake using a constant vortex distribution.

Calculated examples for thin air intakes are given in Fig. 3-5, which shows the shapes and pressure distributions along the outer surface obtained with two different vortex distributions. Both cases have been calculated with the vortex distribution on the true stream surface. To avoid an infinitely high suction at the leading edge ($x = 0$), it is necessary to have $\gamma_b(0) = 0$.

Thin air intakes like those treated here are not of immediate practical interest in themselves. Their usefulness lies in the fact that they can be

taken as *camber lines* for practical intakes of finite thickness, as explained in Sec. 4-4. The method indicated here will be used again for the calculation of fairings of finite length in Sec. 5-4, where the inverse problem of calculating the flow about a given shape will also be treated and a more detailed explanation of the calculation process given.

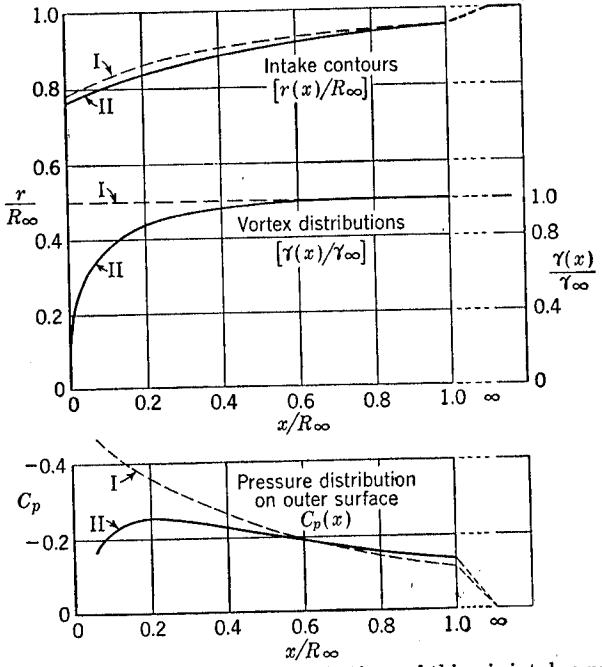

FIG. 3-5. Calculated shapes and pressure distributions of thin air intakes produced by two different vortex distributions. $V_i(x = +\infty) = 0.2V_0$.

3-6. Solution for the Flow Past a Nonducted Cooler. The general case of the flow past a nonducted cooler block is complicated by the condition that the direction of the outflow behind the block is fixed by the direction of the inner passages. This implies zero velocity component tangential to the block face. The main flow together with the induced flow of the vortices on the wake boundary may, however, have a finite component V_{Bt} in this direction, in which case it must be compensated by additional singularities on the block itself.[1] Physically, the block acts here as a *cascade* of airfoils, the circulation round its elements turning the flow into the required direction. It is natural to represent the cascade effect by a special vortex distribution on the cooler block. Ignoring the finite *chord* of the cascade elements (just as in airfoil theory the airfoil is often

[1] The method is adaptable without difficulty to the treatment of such special cooler arrangements as result in a given, nonzero, tangential velocity.

replaced by a single lifting line), we arrive at a vortex distribution γ_B on the block *surface*. At any point, the tangential velocity component from this vortex distribution is $\gamma_B/2$. The desired outflow direction is obtained if at every point of the surface

$$\frac{\gamma_B}{2} + V_{Bt} = 0 \tag{3-16}$$

and this, therefore, determines γ_B.

The stream-surface condition (3-13) and the boundary condition (3-14) for the wake will now contain additional terms for the contributions of the block vortices; both the slope of the wake boundary and the vortex distribution over it will be altered by their presence. There are now three integral equations, (3-13), (3-14), and (3-16), to determine the shape of the boundary and the two vortex distributions. A numerical solution still appears possible.

Fortunately, the problem is much simplified in some cases of practical interest. Consider the two-dimensional flow through and past a plane cooler block at right angles to the main flow. Let the flow be symmetrical about the x axis, and let the cooler be at $x = 0$; $-Y_0 \leq y \leq +Y_0$. The outflow is parallel to the main flow and the wake is assumed to be parallel too, a reasonable assumption, as experimental evidence shows. The boundary is then the two parallel lines, $y = \pm Y_0$, so that x corresponds to s and y to σ of the general case above. V_{bt} in Eq. (3-14) is then constant and equal to the mean of V_0 outside and V_B inside the wake. Hence γ_b is also constant, and, from Eq. (3-14),

$$\gamma_b = \frac{\Delta p}{\rho} \frac{2}{V_0 + V_B}$$

or

$$\frac{\gamma_b}{V_0} = -k_P \frac{(V_B/V_0)^2}{1 + V_B/V_0} \tag{3-17}$$

introducing a nondimensional pressure-drop coefficient

$$k_P = -\frac{\Delta p}{\frac{1}{2}\rho V_B^2} \tag{3-18}$$

which is a known quantity for the cooler block. k_P and V_B/V_0 are of course not independent; we find from Eqs. (3-8) and (3-18) that

$$\frac{V_B}{V_0} = \frac{1}{\sqrt{1 + k_P}} \tag{3-19}$$

The velocity components induced by the constant vortex distribution γ_b on the parallel lines $y = \pm Y_0$ can be written down explicitly with the

aid of the Biot-Savart law:

$$\frac{v_x(x,y)}{V_0} = \frac{-1}{2\pi}\frac{\gamma_b}{V_0}\left(\arctan\frac{x}{y-Y_0} - \arctan\frac{x}{y+Y_0}\right)$$
$$\frac{v_y(x,y)}{V_0} = \frac{1}{2\pi}\frac{\gamma_b}{V_0}\frac{1}{2}\ln\frac{x^2+(y-Y_0)^2}{x^2+(y+Y_0)^2} \qquad (3\text{-}20)$$

and the integration of Eq. (3-3) gives the shapes of the streamlines.

The arc-tangent functions in Eq. (3-20) are determined apart from an integer multiple of π in each case. The arbitrary constants are to be obtained from the condition that the flow has no discontinuities except at the boundary of the wake. Some particular values of the induced axial velocity are

At $x = -\infty$:	$v_x = 0$	
At $x = 0$:	$v_x = \frac{1}{2}\gamma_b = -\frac{1}{2}(V_0 - V_B)$	for $-Y_0 < y < +Y_0$
	$v_x = 0$	for $\lvert y\rvert > Y_0$
At $x = +\infty$:	$v_x = \gamma_b = -(V_0 - V_B)$	for $-Y_0 < y < +Y_0$
	$v_x = 0$	for $\lvert y\rvert > Y_0$

We note that the induced velocity is constant over the block face and over the wake far downstream. Elsewhere in the wake, $V_0 + v_x$ is not constant, contrary to the assumption of parallel flow. The reason is that the parallel boundary lines are not yet streamlines (the flow being similar to that in Fig. 3-3). The vortex distribution representing the cascade effect of the block is needed to achieve this. This distribution should induce $v_x = -(V_0 - V_B)/2$ at the block surface

$$(x = 0;\ -Y_0 < y_0 < +Y_0)$$

it should induce $v_x = 0$ far downstream; and it should also counteract the y component of the velocity induced by the boundary vortices, as given by the second of Eqs. (3-20).

A vortex distribution $\gamma_B(y)$ on the line $x = 0;\ -Y_0 < y < +Y_0$, as described above, fulfills the condition $v_x(\infty) = 0$ automatically; but it can only satisfy one of the other two conditions. However, the approximation

$$\gamma_B(y) = \gamma_0 \frac{y}{\sqrt{Y_0^2 - y^2}} \qquad (3\text{-}21)$$

fulfills both conditions sufficiently accurately for practical purposes.[1]

[1] This is the same vortex distribution as is used in Prandtl's airfoil theory in the determination of the elliptic spanwise loading, which gives constant downwash along the span and minimum induced drag. Without the boundary vortices γ_b it has been applied to the flow past a nonducted cooler block by T. Hara and Y. Nisimura, 1939. The pressure drop in the cooler is thus completely ignored in this theory.

Its induced axial velocity is constant over the block surface:

$$v_x(0,y) = +\frac{\gamma_0}{2} \qquad \text{for } -Y_0 < y < +Y_0$$

Choosing $\gamma_0 = \gamma_b$ ensures at least that the resultant velocity at the block is the same as that far downstream in the wake, since $v_x = 0$ at $x = \pm\infty$ for the distribution γ_B. The velocity component $v_y = +\gamma_B/2$ at $x = 0$ is, however, not exactly equal and of opposite sign to that induced by γ_b, Eq. (3-20). This could be achieved by the vortex distribution

$$\gamma_B(y) = \frac{V_0 - V_B}{\pi}\ln\frac{1 + y/Y_0}{1 - y/Y_0}$$

but the axial velocity increment of such a distribution is not constant over the block face. To satisfy all the conditions, the finite chord of the cooler block and vortex distributions along the chord of the cascade elements would have to be taken into account.

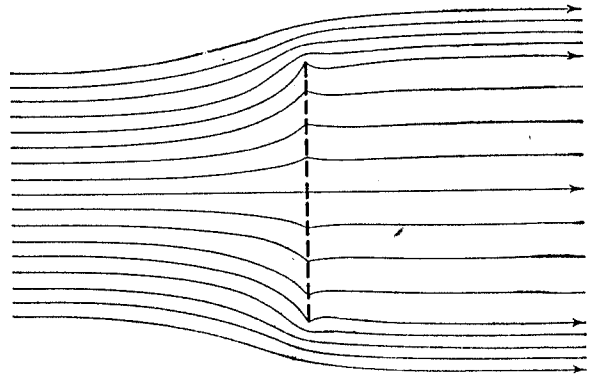

FIG. 3-6. Streamlines of the two-dimensional flow past a nonducted cooler block; one vortex distribution on the wake boundary and another on the block surface. $V_B/V_0 = 0.4$.

A streamline pattern obtained from vortex distributions combined in the way described [with γ_B from Eq. (3-21)] is shown in Fig. 3-6, where it will be seen that the essential features are reproduced. In Fig. 3-7, the calculated streamline through one edge of the block is compared with that obtained from flow observations of a full-scale cooler block in a water tunnel. The agreement between calculation and experiment is good, especially upstream of the block, which is the most interesting region in practice. A reasonable approximation to the streamlines ahead of the block is obtained even if the outflow condition is ignored and only the pressure drop considered.

It is of some importance for the actual calculation that the vortex distribution γ_b on the wake boundary can also be interpreted as a uniform

distribution of sources on the block surface. This is readily shown by a comparison of the respective complex flow potentials. For a source line at $x = 0$; $-Y_0 < y < +Y_0$, the complex potential at the point $z = x + iy$ is

$$F(z) = \Phi + i\Psi = \frac{q}{2\pi}\int_{-1}^{+1} \ln (z - iy)\, dy$$

if all coordinates are expressed as a fraction of Y_0. Integrating, and adding multiples of $2\pi i$ to the logarithm functions so as to have the discontinuity at the source disk, we obtain

$$F(z) = \frac{iq}{2\pi}\{(z - i)[\ln (z - i) - 1] - (z + i)[\ln (z + i) - 1]\}$$

The two vortex lines previously considered give the complex potential

$$F(z) = -\frac{i\gamma_b}{2\pi}\int_0^\infty [\ln (z - x - i) - \ln (z - x + i)]\, dx$$
$$= -\frac{i\gamma_b}{2\pi}\{(z - i)[\ln (z - i) - 1] - (z + i)[\ln (z + i) - 1] - 2i\}$$

The potentials found in the two ways differ only by a term $F(z) = \text{const}$, if $q = -\gamma_b$. A parallel flow, it will be seen, should be added to the wake of the source flow in order to remove the discontinuity at the cooler block surface.

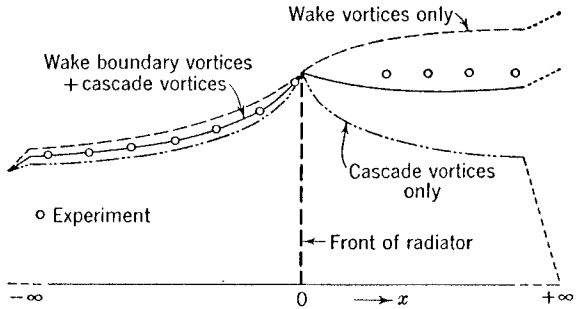

FIG. 3-7. Comparison between experiment and various methods of calculation for the flow past a nonducted cooler block. $V_B/V_0 = 0.5$; $k_P = 3$.

The equivalence between the source distribution and the vortex distribution is general: A surface covered uniformly with sources is equivalent to a vortex cylinder of semi-infinite length whose generators pass through the boundary of the surface and are normal to it. (We are familiar in electrodynamics with the equivalence of a surface covered uniformly with doublets and a vortex line forming the boundary of the surface. The vortex cylinder is therefore equivalent to the sum of

doublet disks, the sources and sinks of which balance out, leaving only a source distribution on the initial surface and a corresponding distribution of sinks at infinity.) A distribution of sources is thus an obvious substitute for a cooler block when the displacement effect of the block, caused by the pressure drop, is considered.

This relationship provides a convenient means of calculating coolers of any shape arbitrarily disposed in the flow. Using only sources means ignoring the cascade effect, but gives a reasonable approximation if only the approaching streamline is to be calculated (Fig. 3-7).[1] Actual applications will be discussed in Chap. 12.

EXERCISES

3-1. Superpose a two-dimensional source on a parallel flow. Determine the shape of the resulting body, the thickness of which is $2Y_B = 2$, and the streamlines with $\Psi/V_0Y_B = 0.2, 0.4, 0.6, 0.8, 1.0$. Solve the problem (*a*) algebraically; (*b*) by plotting Ψ/V_0Y_B for various values of x/Y_B against y/Y_B. Calculate the pressure distribution on the body and on the streamline $\Psi/V_0Y_B = 0.4$. Where is the stagnation point? (See the Appendix for formulas.)

3-2. Superpose a single three-dimensional source on a parallel flow. Determine the shape of the resulting body of revolution, the maximum diameter of which is $2R_B = 2$, and the streamlines with $\Psi/V_0R_B^2 = 0.1, 0.2, 0.3, 0.4, 0.5$. Solve the problem (*a*) by plotting $\Psi/V_0R_B^2$ for various values of x/R_B against r/R_B; (*b*) by plotting the lines $\Psi_p/V_0R_B^2 = 0, 0.05, 0.10, \ldots$, of the parallel flow and the lines $\Psi_s/V_0R_B^2 = 0, -0.05, -0.10, \ldots$, of the source flow, and by joining points where $\Psi_p + \Psi_s = \text{const}$. Calculate the pressure distribution on the surface and on the streamline

$$\Psi/V_0R_B^2 = 0.2,$$

and compare the value of the maximum velocity on the surface with that for the corresponding two-dimensional body from Exercise 3-1 above. Where is the stagnation point?

3-3. Use the momentum theorem to calculate the force in the direction of the main stream which acts on a single source of strength E in a parallel flow of velocity V_0. Note the similarity to the Kutta-Joukowsky law for the force on a vortex line, Eq. (3-9).

3-4. A two-dimensional nonducted cooler block is at right angles to the main parallel stream; it is substituted by a line of sources of constant strength. Calculate the pressure rise on the line of symmetry upstream of the block if the velocity through the block is $V_B = 0.4V_0$.

3-5. A semiporous circular disk of radius R_B is at right angles to the main parallel stream; it is substituted by a disk of uniform sources. The velocity of the flow through the disk is $V_B = 0.4V_0$. Determine the shape of the streamlines through the edge of the disk by plotting $\Psi/V_0R_B^2$ for various values of x/R_B against r/R_B, and calculate the pressure distribution on the streamlines and on the line of symmetry. Use Tables 15 to 17 of the Appendix.

BIBLIOGRAPHY

LAMB, H., "Hydrodynamics," 6th ed., Cambridge University Press, London and New York, 1932. Also Dover Publications.

[1] This method has been used by G. I. Taylor, 1944.

OSEEN, C. W., "Neuere Methoden und Ergebnisse in der Hydrodynamik," Akademische Verlagsanstalt, Leipzig, 1927.

BURGERS, J. M., On the Application of Oseen's Hydrodynamical Equations to the Problem of the Slipstream from an Ideal Propeller, *Koninl. Akad. Wetenschap, Amsterdam*, vol. 32, p. 1278, 1929.

MÜLLER, W., Zur Theorie der Kielwasserströmung um eine ebene Platte, *Ingenieur Arch.*, vol. 2, p. 20, 1931.

LINDNER, F. W., Kielwasserströmungen um eine Platte, *Ingenieur Arch.*, vol. 2, p. 169, 1931.

REISSNER, H., Axial symmetrische Flüssigkeitsstrahlen von schwacher Kontraktion, *Z. angew. Math. Mech.*, vol. 12, p. 25, 1932.

PRANDTL, L., and O. TIETJENS, "Fundamentals of Hydro- and Aeromechanics," Springer-Verlag, Berlin, 1929; translation by L. Rosenhead, McGraw-Hill Book Company, Inc., New York, 1934.

LUDWIEG, H., Über Potentialströmungen mit unstetigen Randbedingungen, Dissertation, Göttingen, 1939.

HARA, T., and Y. NISIMURA, On the Radiator Fairing, *J. Soc. Aeronaut. Sci. Nippon*, vol. 6, p. 1116, 1939.

VANDREY, F., Beitrag zur Theorie des Tragflügels in schwach inhomogener Grundströmung, *Z. angew. Math. Mech.*, vol. 20, p. 148, 1940.

KÜCHEMANN, D., and F. VANDREY, Über den Einfluss der Düse auf Widerstandsmessungen im Freistrahl, *Z. angew. Math. Mech.*, vol. 21, p. 17, 1941; vol. 22, p. 15, 1942.

TAYLOR, G. I., Air Resistance of a Flat Plate of Very Porous Material, *Brit. Aeronaut. Research Council Rept. & Mem.* 2236, 1944.

VON MISES, R., "Theory of Flight," McGraw-Hill Book Company, Inc., New York, 1945.

GLAUERT, H., "The Elements of Aerofoil and Airscrew Theory," 2d ed., Cambridge University Press, London and New York, 1948.

SQUIRE, H. B., and H. HOGG, Diffuser-Resistance Combinations in Relation to Wind-tunnel Design, *Brit. Roy. Aircraft Est. Rept. Aero.* 1933, 1944.

KÜCHEMANN, D., and J. WEBER, The Jet Problem as the Characteristic Problem of Aerodynamics of Propulsion (*AVA Monograph* $J_2$2), *Brit. Min. of Supply Rept. & Transl.* 984, 1948.

PACK, D., On the Formation of Shock-waves in Supersonic Jets (Two-dimensional Flow), *J. Mechanics and Applied Math.*, vol. 1, p. 1, 1948.

STREETER, V. L., "Fluid Dynamics," McGraw-Hill Book Company, Inc., New York, 1948.

BIRKHOFF, G., Recent Development in Free Boundary Theory, *Proc. 7th Intern. Congr. Applied Mechanics*, vol. 2, p. 1, 1948.

BETZ, A., "Konforme Abbildung," Springer-Verlag, Berlin, 1948.

CHURCHILL, R. V., "Introduction to Complex Variables and Applications," McGraw-Hill Book Company, Inc., New York, 1948.

CHAPTER 4

AIR INTAKES

In this chapter, we shall consider the flow about the part of an engine fairing which will be defined in Sec. 4-1 as the air intake. Sections 4-2 and 4-3 deal with general relations between the flow into air intakes and their pressure distribution and thrust. The idea of an optimum shape for an air intake is introduced. Sections 4-4 and 4-5 outline the principal methods which are available for the calculation of entry shapes. Section 4-5 also includes some notes on the practical design of two-dimensional air intakes. Systematic series of circular air intakes suitable for practical application are described in Secs. 4-6 and 4-7. General three-dimensional intakes are dealt with in Sec. 4-8 and, finally, Sec. 4-9 considers the internal duct and its relation to the intake flow as a whole.

4-1. Engine Fairings. Duties of an Air Intake. Since their earliest application,[1] the fairings round coolers and aircraft engines have served the obvious purpose of improving the aerodynamic shape presented to the external flow. They also fulfill a second important function, that of regulating the air flow through the duct which they enclose, taking a definite mass flow from the external stream and supplying it to some component of the power unit. The same principles still apply today to the fairings of jet engines.

Although the flow through the duct is normally regulated by control of the exit area of the fairing, the most important changes occur at the entry. The entry flow pattern may vary from a definite retardation ahead of the inlet opening in flight near the maximum speed of the aircraft (Fig. 4-1*a*) to an accelerated inflow (Fig. 4-1*b*) at climbing speed; while under static conditions air approaches the inlet from all directions (Fig. 4-1*c*). The flow about a fairing may be compared with the flow about an ordinary airfoil with circulation. The outer and inner surfaces of the fairing correspond to the upper and lower surfaces of the airfoil, the entry lip with its varying stagnation-point position taking the part of the airfoil nose. Relative variation of the internal and external velocities corresponds to variation of the circulation (lift) about the airfoil.

Like the airfoil, each section of the fairing experiences an aerodynamic force, which is inclined forward. The normal component is of little interest, affecting only the stressing, but the thrust component may make an

[1] See H. Junkers, 1921; F. E. Weick, 1929; H. Townend, 1930.

appreciable contribution to the thrust-drag balance of the complete power unit. Another purpose of the fairing, then, is to realize to the full the thrust theoretically available from this source, in the form of a definite static-pressure distribution along its surface. Any deviation from this distribution means a loss of thrust, *i.e.*, an additional external drag.

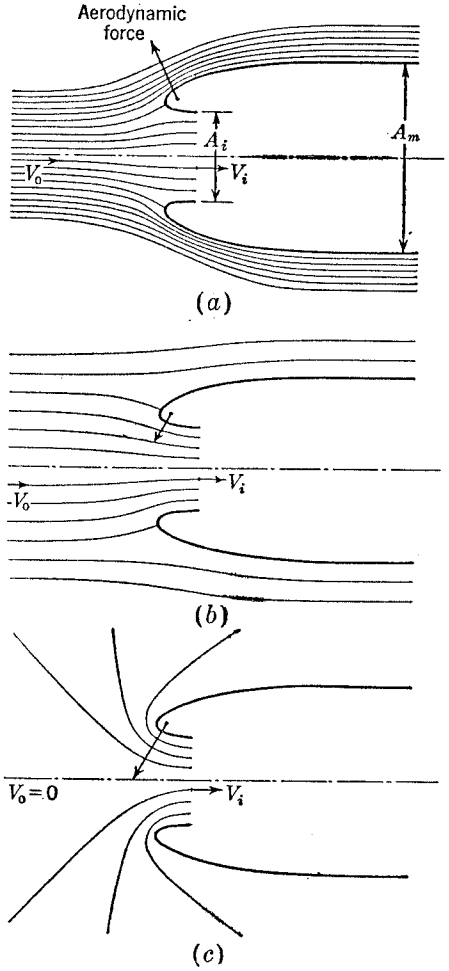

FIG. 4-1. Types of inflow. (*a*) High-speed flight. (*b*) Climbing flight. (*c*) Under static conditions.

In most cases, including the fairings of jet engines, air scoops, and nose and leading-edge intakes, the flow into the entry and round the nose of the intake can be treated separately from the flow inside. The flow ahead of the inlet is very little influenced by the particular shape of the duct behind, and the flow conditions near the exit are important only in so far as they affect the mass flow through the duct. As the experimental results in Fig. 4-2 show, the pressure distribution on the outer surface of a circular intake is scarcely changed by the presence inside of a boss, a grid, or even of a diffuser deliberately shaped to cause a heavy separation of the flow. It is only the ratio of the mean velocity V_i in the narrowest section of the inlet duct to the free-stream velocity V_0 that matters in the first instance.

In considering the inflow, therefore, we may concentrate on the part of the fairing shown in Fig. 4-1, the *intake*. Intakes with protruding spinners will be dealt with later in Chap. 9.

4-2. Basic Relation for Optimum Intake Contours. Useful relations between the inlet-duct area A_i, the maximum frontal area A_m, the inlet-duct velocity ratio V_i/V_0, and the least maximum velocity ratio V_{max}/V_0 at the outer surface of the intake can be derived from considerations of the change of momentum of the inflowing air. The idealized intake is taken as of infinite length, and cylindrical in shape from a certain distance

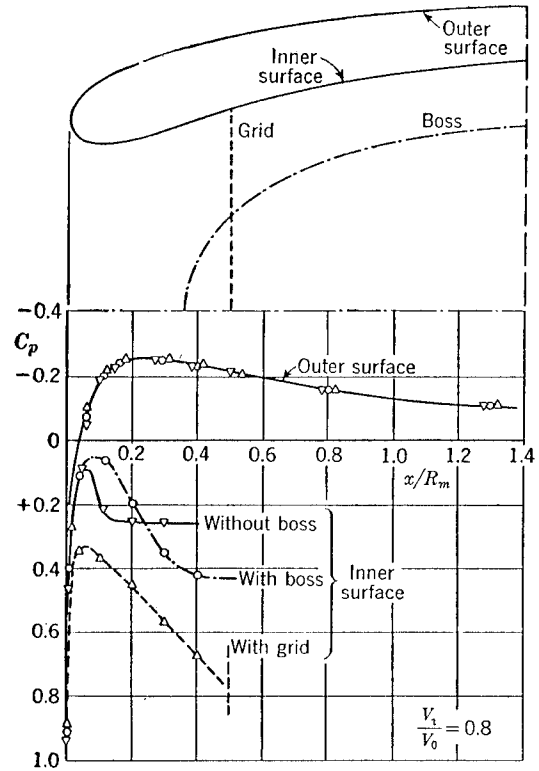

FIG. 4-2. Independence of the pressure distribution along the outer surface of conditions in the internal duct.

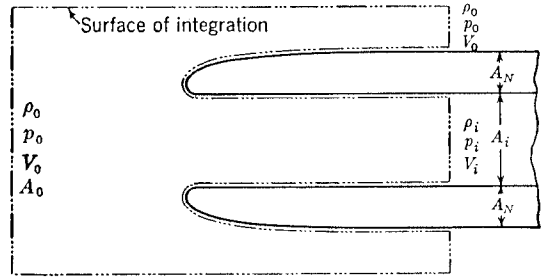

FIG. 4-3. Control surface for momentum theorem.

behind the entry. The duct is taken to be cylindrical behind the narrowest inlet cross section, as shown in Fig. 4-3. The cross sections normal to the direction of flow can be left arbitrary. We calculate the momentum in the free-stream direction of the air entering and the air leaving certain control surfaces in unit time, as explained in Sec. 2-3.

Taking the surface of integration as in Fig. 4-3, the difference between the integrals of the pressure component in the V_0 direction and the enter-

ing and leaving momentum must be zero since the control surface encloses no body which could take any forces:

$$\rho_0 V_0 A_0 V_0 + p_0 A_0 - \rho_i V_i A_i V_i - p_i A_i - \int_{A_N} p_N \, dA_N - p_0(A_0 - A_m) - (\rho_0 V_0 A_0 - \rho_i V_i A_i) V_0 = 0 \quad (4\text{-}1)$$

The first two terms in this equation represent the momentum of the mass $\rho_0 V_0 A_0$ flowing with the velocity V_0 through the forward surface A_0 of the control cylinder and the axial force which acts on that surface. The next two terms are the corresponding quantitites for the flow through the internal duct. The fifth term is the integral of the static pressure p_N over the surface of the intake; dA_N being a surface element normal to the direction of the main flow and $A_N = A_m - A_i$. The next term is the force on the part of the base of the cylinder which is outside the intake. The last term is the momentum of the air diverted through the outer part of the base of the control cylinder and through its curved surface. It is assumed that the control cylinder is large enough to ensure that the axial velocity component of this mass of air is V_0. Equation (4-1) gives

$$\int_{A_N} (p_N - p_0) \, dA_N = \rho_i V_i A_i (V_0 - V_i) - (p_i - p_0) A_i$$

Assuming incompressible flow, so that $\rho_i = \rho_0 = \rho$, and using Bernoulli's equation,

$$p_i - p_0 = \tfrac{1}{2}\rho V_0^2 - \tfrac{1}{2}\rho V_i^2 \quad (4\text{-}2)$$

a general relation for the thrust is found:

$$F_N = -\int_{A_N} (p_N - p_0) \, dA_N = \frac{1}{2} \rho V_0^2 A_i \left(1 - \frac{V_i}{V_0}\right)^2 \quad (4\text{-}3)$$

where F_N is the thrust component of the total force on the intake. This can finally be written as

$$\frac{F_N}{\frac{1}{2}\rho V_0^2 A_i} = -\frac{1}{A_i} \int_{A_N} \frac{p_N - p_0}{\frac{1}{2}\rho V_0^2} \, dA_N = \left(1 - \frac{V_i}{V_0}\right)^2 \quad (4\text{-}4)$$

There is a positive thrust force on the intake under all mass-flow conditions, independent of the outer shape and of the cross section of the entry. Figure 4-4 shows how this is borne out in practice. The points were obtained by integrating pressure distributions measured on a number of air intakes of various shapes, while the full line corresponds to Eq. (4-4) above. The points at $V_i = 0$ were obtained by blocking the internal duct by a plate, and a drag force corresponding to the full dynamic head, $\rho V_0^2 A_i/2$, acts on it. It will be seen that this drag is exactly counterbalanced by the thrust on the outer surface of the intake, as it should be for a semi-infinite body in potential flow.

Since negative pressure coefficients

$$C_p = \frac{p_N - p_0}{\frac{1}{2}\rho V_0^2} = 1 - \left(\frac{V_N}{V_0}\right)^2 \quad (4\text{-}5)$$

are necessary for there to be a positive resultant thrust, the velocity V_N at the outer surface of the intake is locally greater than the free-stream velocity. On the other hand, the local velocities should exceed the flight velocity as little as possible if disturbances at high flight Mach numbers

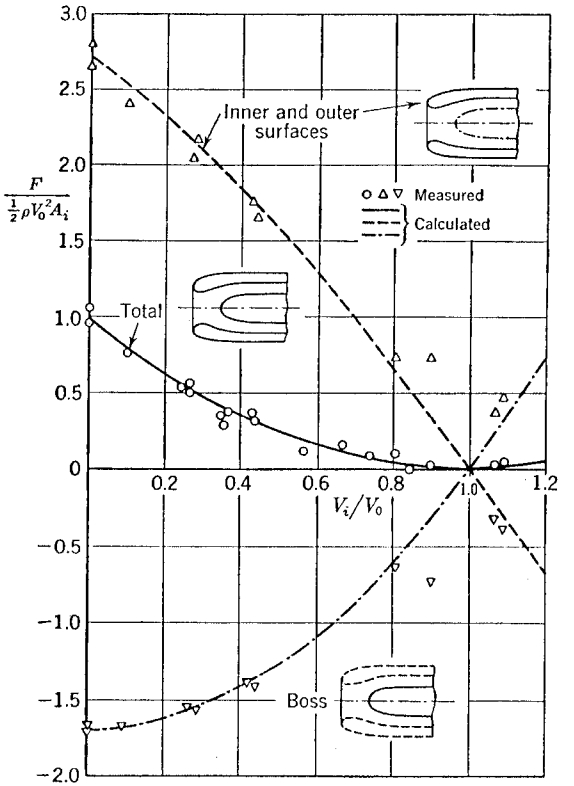

FIG. 4-4. Thrust forces acting on an air intake.

M_0 are to be avoided. Clearly, they are least, for given values of A_i and V_i/V_0, if the shape of the intake is such as to ensure that the velocity V_N is uniform over the whole outer surface, so that $V_N/V_0 = V_{max}/V_0$ is the constant velocity ratio there. Any change from the *optimum contour* which gives this result, for instance, an increase in nose radius as shown in Fig. 4-5, will necessarily lead to higher velocities; in this case positive pressures at the inner part of the nose contribute an additional drag component, which has to be compensated for by higher suction forces at the

outer surface for the total thrust to remain the same, as Eq. (4-3) says it must.

Replacing the pressure coefficient in Eq. (4-4) by the constant value corresponding to constant V_{max}/V_0 enables us to evaluate the integral in Eq. (4-4), which gives

$$\frac{F_N}{\frac{1}{2}\rho V_0^2 A_i} = -C_p\left(\frac{A_m}{A_i} - 1\right) = -\left[1 - \left(\frac{V_{max}}{V_0}\right)^2\right]\left(\frac{A_m}{A_i} - 1\right)$$

so that, in general,

$$\frac{A_m}{A_i} \geq 1 + \frac{(1 - V_i/V_0)^2}{(V_{max}/V_0)^2 - 1} \tag{4-6}$$

The intake shape for which V_{max}/V_0 is constant along the curved part of the outer surface is described as the optimum shape in respect to frontal area; the equality sign then applies in Eq. (4-6).

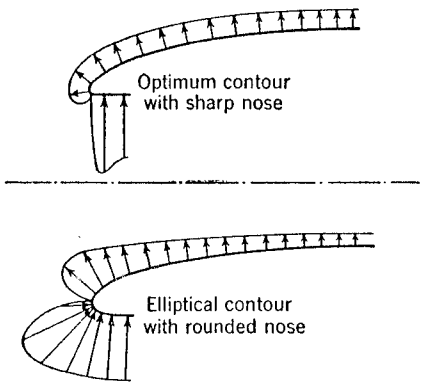

Fig. 4-5. Typical differences between the pressure distributions along the outer surface of an optimum intake and one with an elliptical contour with finite inner thickness.

The intake is said to be operating under optimum conditions when V_i/V_0 has the value for which it was designed.

Equation (4-6) shows that a certain minimum frontal area (which may be called the *thrust area*) is needed to keep the external maximum velocity within given limits. Every inlet opening, therefore, requires a surrounding fairing with a definite thickness which is greater the smaller the velocity increments are allowed to be. Since these velocity increments ultimately determine the critical Mach number at which shock waves and a drag rise can be expected, we come to the unusual conclusion that high critical Mach numbers require thick intake walls, *i.e.*, small values of A_i/A_m.

The fundamental equation (4-6) was first derived by P. Ruden (1940) for two-dimensional intakes. He also gave a method for determining the actual two-dimensional optimum shape, which will be described in Sec. 4-5. But the derivation (by the authors, 1940) given here shows that Eq. (4-6) is valid for intakes of any cross section, including circular or any three-dimensional intakes. In particular, it is true for swept leading-edge intakes, which shows that sweep gives no special benefit in this application.

Since the thrust force in Eq. (4-3) is entirely due to the change of momentum of the inflow, the thrust is the same whether all the change of

momentum takes place in the free stream, as in Fig. 4-6*a*, or part in the free stream and part in an expanding internal duct, as in Fig. 4-6*b*, or all inside the duct, as in Fig. 4-6*c*. The forces are only displaced; all the arrangements in Fig. 4-6 are equivalent in this respect, and it would be fallacious to suppose that an advantage could be gained by the use of

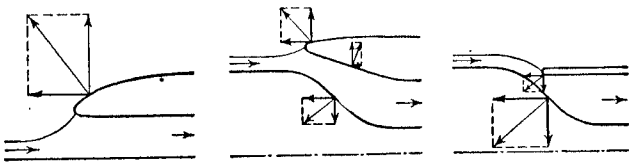

Fig. 4-6. The various places at which thrust forces may act on different types of intake.

flush air intakes as in Fig. 4-6*c*. We shall discuss this important fact more fully in Sec. 4-9 and examine relevant experimental data in Sec. 9-8.

4-3. Influence of Compressibility. Compressibility does not affect what has been said above, with the exception that the energy equation (4-2) has to be replaced by

$$\frac{k}{k-1}\frac{p_0}{\rho_0} + \frac{V_0^2}{2} = \frac{k}{k-1}\frac{p_i}{\rho_i} + \frac{V_i^2}{2} \tag{4-7}$$

This assumes isentropic inflow:

$$\frac{p_i}{p_0} = \left(\frac{\rho_i}{\rho_0}\right)^k \tag{4-8}$$

i.e., the absence of shock waves or other disturbances (see Sec. 2-1). The inlet pressure is then given by

$$\frac{p_i}{p_0} = \left\{1 + \frac{k-1}{2}\,\mathrm{M}_0^2\left[1 - \left(\frac{V_i}{V_0}\right)^2\right]\right\}^{k/(k-1)} \tag{4-9}$$

and the density ratio by

$$\frac{\rho_i}{\rho_0} = \left\{1 + \frac{k-1}{2}\,\mathrm{M}_0^2\left[1 - \left(\frac{V_i}{V_0}\right)^2\right]\right\}^{1/(k-1)} \tag{4-10}$$

in terms of the inlet velocity ratio and the free stream Mach number

$$\mathrm{M}_0 = \frac{V_0}{a_0} \qquad \text{with } a_0 = \sqrt{k\frac{p_0}{\rho_0}} \tag{4-11}$$

Then the thrust force on the intake follows from

$$\frac{F_N}{\frac{1}{2}\rho_0 V_0^2 A_i} = 2\,\frac{V_i}{V_0}\left(\frac{V_i}{V_0} - 1\right)\left\{1 + \frac{k-1}{2}\,\mathrm{M}_0^2\left[1 - \left(\frac{V_i}{V_0}\right)^2\right]\right\}^{1/(k-1)} + \frac{2}{k\mathrm{M}_0^2}\left(\left\{1 + \frac{k-1}{2}\,\mathrm{M}_0^2\left[1 - \left(\frac{V_i}{V_0}\right)^2\right]\right\}^{k/(k-1)} - 1\right) \tag{4-12}$$

For the static case, $V_0 = 0$, Eqs. (4-9) and (4-10) read

$$\frac{p_i}{p_0} = \left(1 - \frac{k-1}{2}\,\mathrm{M}_i^2\right)^{k/(k-1)} \tag{4-13}$$

$$\frac{\rho_i}{\rho_0} = \left(1 - \frac{k-1}{2}\,\mathrm{M}_i^2\right)^{1/(k-1)} \tag{4-14}$$

where $\mathrm{M}_i = V_i/a_0$ is the Mach number at the inlet. The thrust is

$$\frac{F_N}{\frac{1}{2}\rho_i V_i^2 A_i} = 2 + \frac{2}{k\mathrm{M}_i^2}\,\frac{\left(1 - \frac{k-1}{2}\,\mathrm{M}_i^2\right)^{k/(k-1)} - 1}{\left(1 - \frac{k-1}{2}\,\mathrm{M}_i^2\right)^{1/(k-1)}} \tag{4-15}$$

The thrust forces given by Eqs. (4-12) and (4-15) are not very different from those for $\mathrm{M}_0 = 0$, so that the relations obtained for incompressible flow provide a sound basis for practical calculations.

The optimum area relation (4-6) is also modified for compressible flow; Eq. (4-5) is replaced by

$$\frac{p_N}{p_0} = \left\{1 + \frac{k-1}{2}\,\mathrm{M}_0^2\left[1 - \left(\frac{V_{\max}}{V_0}\right)^2\right]\right\}^{k/(k-1)} \tag{4-16}$$

Then

$$\frac{A_m}{A_i} = 1 + \frac{F_N}{\frac{1}{2}\rho_0 V_0^2 A_i}\,\frac{1}{-C_p}$$

and

$$\frac{A_m}{A_i} = 1 + \frac{(k/2)\mathrm{M}_0^2 F_N/\frac{1}{2}\rho_0 V_0^2 A_i}{1 - \left\{1 + \frac{k-1}{2}\,\mathrm{M}_0^2\left[1 - \left(\frac{V_{\max}}{V_0}\right)^2\right]\right\}^{k/(k-1)}} \tag{4-17}$$

in which the thrust F_N is to be substituted from Eq. (4-12).

A numerical example is illustrated in Fig. 4-7, where the mass-flow ratio $\rho_i V_i/\rho_0 V_0$ has been chosen as parameter, instead of the velocity ratio V_i/V_0. The ratio of the pressure coefficient C_p of a series of intakes designed for various flight Mach numbers to the pressure coefficient C_{pi} of another series of intakes designed for incompressible flow is also shown; these intakes are compared for the same ratio $\rho_i V_i/\rho_0 V_0$. As it will be seen, compressibility does not have a large effect on the area ratio A_i/A_m necessary to maintain a given pressure coefficient at the outer surface. The simpler form (4-6) of the optimum-area theorem is therefore accurate enough for a rapid survey or a preliminary estimate.

It must be remembered, however, that Eq. (4-17) is true only for optimum intake shapes specially designed to give a uniform velocity distribution along the outer surface under given conditions, *i.e.*, at a prescribed flight Mach number and a given value of V_i/V_0. An intake

shape designed for a particular Mach number will behave differently at other Mach numbers.

It has been usual in the past to design all intake shapes, whether experimentally or theoretically, for incompressible flow only; therefore it is essential to know how the pressure coefficient C_p varies with Mach number. The well-known method of L. Prandtl and H. Glauert can be applied conveniently in the form of the streamline analogy. To a first approximation (linear perturbation theory), the pressure coefficient C_p at an intake in compressible flow is $1/\beta^2$ times the pressure coefficient C_{pa} at an *incompressible analogous intake*, obtained by increasing the longitudinal dimensions of the original intake in the ratio $1/\beta$, where $\beta = \sqrt{1 - \mathrm{M}_0^2}$.

The problem is then reduced to that of finding a relation between the pressure coefficient in incompressible flow at the given and at the analogous intake. Both have the same area ratio A_i/A_m and the same inlet velocity ratio V_i/V_0, and only a relation between C_p and the length L of the curved part of the intake is required. This length does not appear in the fundamental theorem,[1] Eq. (4-6), but experimental data from circular intakes, to be described in Sec. 5-2, show that a linear relation between D_m/L and the minimum value of C_p is a sufficiently accurate approximation, where D_m is the maximum diameter [see Eq. (5-7)]. For circular intakes, therefore,[2]

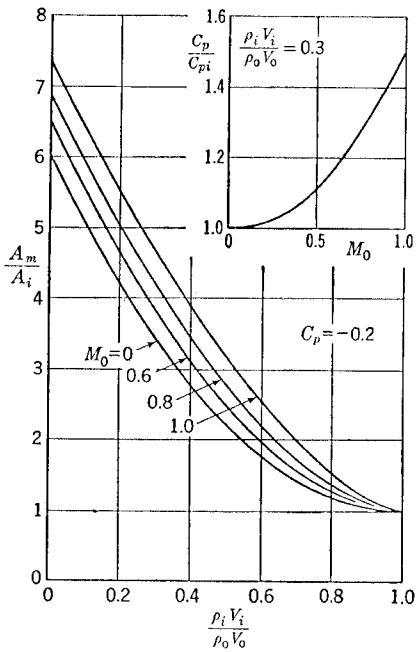

FIG. 4-7. Variation of required frontal area with free-stream Mach number and mass flow for optimum contours.

$$\frac{C_p}{C_{pi}} = \frac{1}{\beta} = \frac{1}{\sqrt{1 - \mathrm{M}_0^2}} \tag{4-18}$$

Figure 4-8 shows how well this is confirmed by experimental results. A further refinement beyond this first approximation is obviously not needed.

[1] The given intake and the analogous intake cannot both be optimum shapes for which Eq. (4-6) holds.

[2] This result is the same as the first approximation for two-dimensional airfoils, for there again a linear relation holds between the pressure coefficients at the given and at the analogous airfoil in incompressible flow.

Equation (4-18) actually applies not only to optimum shapes but also to any other intake, but then, of course, only to the neighborhood of the peak suction and not to the whole pressure distribution along the intake surface. It also does not apply to very short intakes with small values of A_i/A_m, below about 0.1, say, because there the entry only modifies the flow in the stagnation region of the body; the flow near the peak suction is essentially determined by the shape of the basic body without an entry, and the Mach number characteristics of the basic body may be quite different.

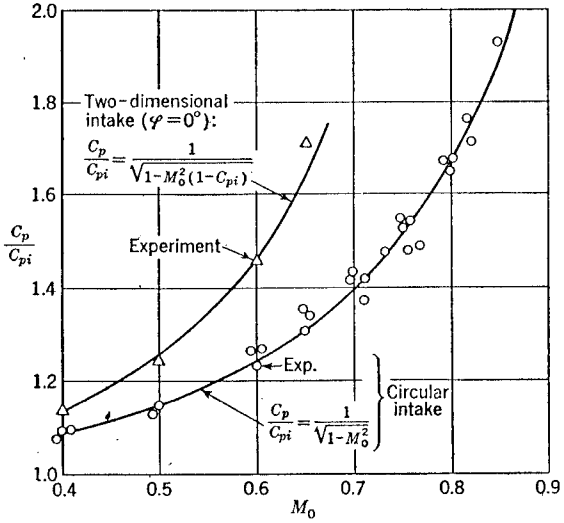

FIG. 4-8. Pressure rise with Mach number for a given intake.

Experimental evidence is too limited to establish a corresponding relation for two-dimensional or other than circular intakes. A few experimental results for two-dimensional intakes suggest, however, that the following relation might be used:

$$\frac{C_p}{C_{pi}} = \frac{1}{\sqrt{1 - M_0^2(\cos^2 \varphi - C_{pi})}} \tag{4-19}$$

This takes account of the angle of sweep φ, if any, in the case of leading-edge intakes in swept wings, for example.

It is of interest to note that the Mach number of the local velocity component normal to the peak suction line will be unity when the pressure coefficient reaches the value

$$C_p^* = \frac{2}{kM_0^2}\left[\left(\frac{2}{k+1} + \frac{k-1}{k+1} M_0^2 \cos^2 \varphi\right)^{k/(k-1)} - 1\right] \tag{4-20}$$

where φ is the angle of sweep of the peak suction line.

Both Eq. (4-20) and the preceding equation indicate that sweeping the air intake is to be expected to be beneficial. For a given design Mach number, as has been shown above, the pressure coefficient is the same for all optimum intakes and will thus not be influenced by sweep. But then the critical value C_p^* is higher for a swept intake. Although, if intakes designed for $M_0 = 0$ are compared, the pressure coefficient of an unswept two-dimensional intake rises more steeply with M_0 than that of the corresponding circular intake (Fig. 4-8), advantage can be taken of the fact that the two-dimensional leading-edge intake can be swept, which makes the rise with M_0 less steep. Given a circular intake and a swept two-dimensional intake with the same inlet area, frontal area, and inlet velocity, both of optimum shape giving uniform pressure distribution at $M_0 = 0$, it is possible to calculate an angle of sweep such that both will have the same critical Mach number (at which a local Mach number of 1 is first reached). The result of the calculation is:

Incompressible pressure coefficient C_{pi}	−0.2	−0.4	−0.6	−0.8
Angle of sweep needed	17°	26°	34°	41°

The angles of sweep required of the leading-edge intake are moderate; further sweep would make the two-dimensional intake superior to the circular intake in this respect.

4-4. Design of Intake Contours by the Method of Singularities. Two methods suggest themselves for the calculation of an intake shape:

1. The use of distributions of sources, sinks, and vortices to represent the flow about the intake. This is known as the method of singularities (see Sec. 3-2), and can be applied to both two- and three-dimensional shapes.

2. The method of conformal transformation (see Sec. 3-3), which is restricted to two-dimensional intakes. In particular, the hodograph method is very useful for the design of optimum contours with uniform pressure distribution.

Both methods have in fact been applied to the design of intake shapes in incompressible flow. The principal results of the work already done on circular intakes have been incorporated into systematic series of intake shapes (see Secs. 4-6 and 4-7), since what the designer ultimately prefers is a simple geometrical family of shapes.

We begin with circular intakes. Singularities are arranged on cylinders instead of on lines, as in two-dimensional airfoil theory. The basic unit for a thick profile without circulation is the source ring, the properties of which are described in Sec. 6 of the Appendix. By the use of a series of source and sink rings in a parallel flow, any intake shape of circular cross

section can be obtained; for all of them, however, the mean internal velocity in the semi-infinite internal duct is that of the free stream. The shape of the intake which corresponds to a given source distribution can be determined by working out the stream function Ψ over the whole xr field (x being the axial and r the radial coordinate). Lines joining points with the same value of Ψ are streamlines, and the streamline which runs through the stagnation point[1] where the total velocity

$$V = [(V_0 + v_x)^2 + v_r^2]^{\frac{1}{2}} \tag{4-21}$$

vanishes is the contour of the intake. In this equation v_x and v_r are the velocity increments induced by the source-ring distribution in the x and r direction, respectively. Calculating an intake shape in this way is naturally somewhat tedious.

The inverse problem, the determination of the source-ring distribution for a given shape, and from that the velocity distribution along the contour, is not, in general, capable of solution. It gives an integral equation of the first kind for a source-ring distribution whose strength and position are unknown.

An alternative way in which the shape and pressure distribution of an intake can be obtained depends on the surface condition that the normal velocity at the surface must vanish everywhere, so that the resultant velocity is parallel to the surface [see also Eq. (3-15)]:

$$\frac{dr}{dx} = \frac{v_r}{V_0 + v_x} \tag{4-22}$$

Since here again v_x and v_r are integrals over the source-ring distribution, the calculation of the velocity distribution is rather laborious.

In both cases, values of the stream function and the velocity components over the xr field are needed. They can be found from tables in the Appendix for the single source ring.

Rotating the two-dimensional source and sink distribution which corresponds to a two-dimensional airfoil about an axis does not give a similar ring airfoil. As an illustration of this, Fig. 4-9 shows an annular airfoil, produced by the same chordwise source-sink distribution which gives a symmetrical Joukowsky profile (dotted) in the two-dimensional case. The annular airfoil is cambered in section, in spite of the fact that the singularities used to represent it included no vortices; and the stagnation streamline is not straight but approaches the lip from the inside. This means that the convenient symmetry properties of the two-dimensional airfoil are lost. (An annular airfoil of symmetrical section can, however,

[1] This is, of course, in fact a circular stagnation line. The terms *streamline* and *stagnation point* are loosely used here in view of the two-dimensional character of the flow.

be produced by a combination of sources and vortices.) The reason for the asymmetry will be apparent if the streamline pattern of a single source ring is studied (see Fig 3 of the Appendix). The flow close to the ring is similar to that induced by a single two-dimensional source, but at large distances it behaves like that of a single three-dimensional source at the center of the ring. A stagnation point can only occur where the induced radial velocity v_r vanishes, and the line $v_r = 0$ always lies within the radius r' of the source ring (see also Sec. 6 of the Appendix).

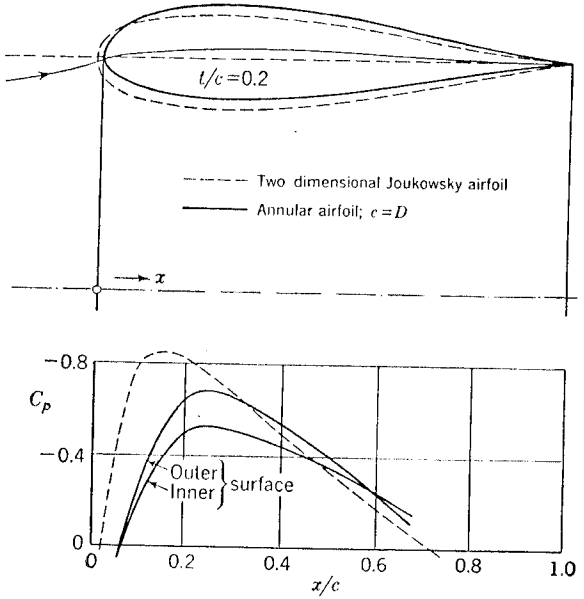

FIG. 4-9. Comparison between a two-dimensional airfoil and an annular airfoil produced by the same chordwise distribution of sources and sinks.

To make the mean internal velocity different from the free-stream velocity, distributions of vortex rings within the intake profile can be added. Values of the stream function and the velocity components for a single vortex ring can be taken from tables in the Appendix. Vortex-ring distributions starting with zero or finite strength at the nose give stagnation streamlines which approach the intake in the direction of the skeleton line, and are particularly useful for the design of intake shapes with given velocity ratios V_i/V_0. To study the flow about a given intake shape at arbitrary values of the inlet velocity ratio, it is necessary to employ vortex distributions with infinite strength at the leading edge; the stagnation point is then displaced and there is a flow round the intake nose.

Similar vortex distributions in ordinary airfoil theory represent camber and incidence, respectively.

Some care needs to be taken in the location of vortex rings used to calculate the flow past comparatively thin intake profiles. Distributions along a cylinder of constant radius have the advantage of simplicity of calculation, but may lead to unreasonable flow patterns, with some of the streamlines intersecting the cylinder. This was discussed in Sec. 3-5.

One of a systematic series of air intakes worked out by this method (described in Sec. 4-6) is shown in Fig. 4-10. It was produced by an isolated source ring, and a distribution of vortex rings of constant strength

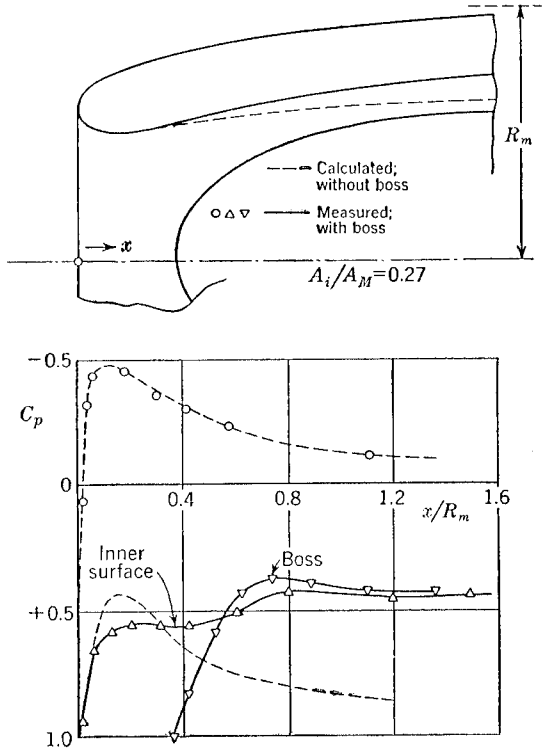

Fig. 4-10. Pressure distributions on a circular air intake with a boss inside.

extending to infinity downstream, superposed on a parallel flow. It will be seen that there is reasonable agreement between the calculated and measured pressures on the outer surface of the intake.

The design of two-dimensional air intakes is the same in principle as the design of circular intakes, by the method of singularities. Instead of source and vortex rings, pairs of sources and vortices are used. The asymmetry of the intake profiles is again a source of difficulty, and a numerical method is usually employed, beginning with given source and vortex distributions.

Two-dimensional intakes with staggered entry lips can also be represented by means of these singularities. As the example in Fig. 4-11 shows, the velocity increments are higher at the rear lip than at the forward lip. That this should be so can be deduced from the general momentum theorem of Sec. 4-2. Both lips of an unstaggered symmetrical intake experience the same thrust force; on the other hand an infinitely long protruding lip would take no thrust at all, for with the

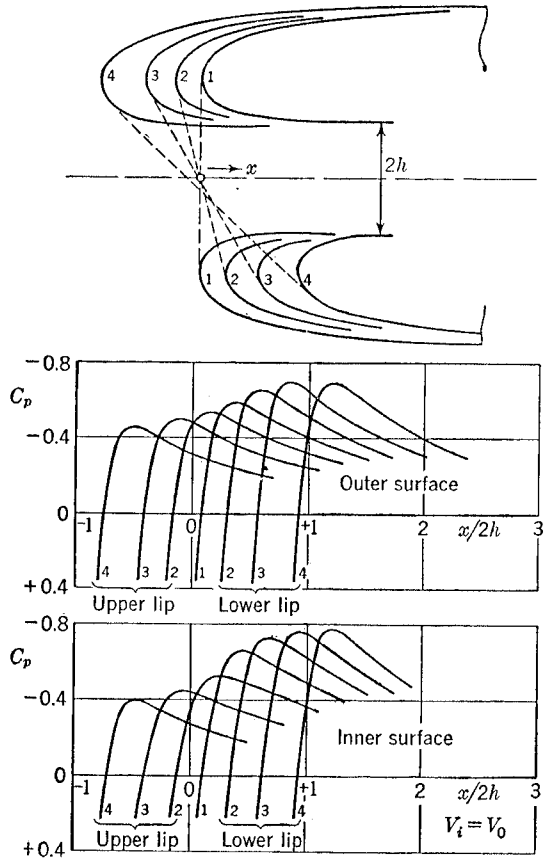

Fig. 4-11. Pressure distributions on staggered two-dimensional intakes.

retardation of the flow taking place in the region ahead of the rear lip only, the full thrust must be developed at that lip. This is a characteristic of all asymmetrical intakes with entries which are not plane and normal to the flow, such as skewed nose intakes or oval entries in the leading edge of a swept wing. The velocity increments are always higher at the rearmost part than at the leading part of the lip.

4-5. Design of Two-dimensional Intakes by Conformal Transformation. As was briefly explained in Sec. 3-3, the hodograph method pro-

vides a particularly useful tool for the calculation of optimum intake contours with constant pressure along the outer surface. It was applied to two-dimensional optimum intakes by P. Ruden (1940). The hodograph is obtained by drawing radius vectors from an origin, each having the magnitude and direction of the velocity at a point in the physical plane.

In the plane of the intake (Fig. 4-12), the stagnation streamline, starting from the point A with the velocity V_0, divides at the stagnation point B, and on the inner surface soon reaches the final velocity V_i at the point E. This is represented by the curved full line in the hodograph from A to the origin 0 and from there to E. On the outer branch of the stagnation streamline the velocity has reached the full maximum velocity V_{max} at P when it leaves the straight inner surface. Then along the whole of the curved part of the outer surface from P to C, the magnitude of the velocity remains constant, represented by half a circle in the hodograph plane. The last part of the outer surface from C to D is again parallel to the main flow, and the velocity falls to the free-stream velocity V_0. In the hodograph plane, D coincides with A.

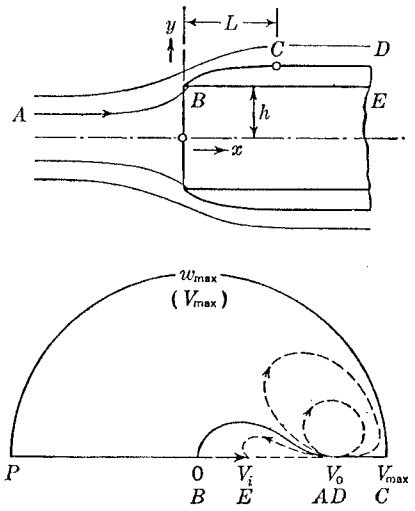

FIG. 4-12. Hodograph of a two-dimensional intake with uniform pressure distribution.

The hodograph can be completed into a full circle by reflection in the horizontal axis, and it will be seen that the flow in the hodograph plane (dotted lines in Fig. 4-12) can be represented by a source and a doublet at A plus a sink at E, the strength of the source and the sink being equal. To make the circle a streamline, their images with respect to the circle must also be taken into account.

The complex flow potential due to sources of strength Q at A (where $w = V_0 = 1$, say) and at the inverse point (where $w = V_{max}^2$, replaced by V_m^2 in the following) is, as explained in Sec. 3-2,

$$F(w) = \frac{Q}{2\pi}[\ln (w - 1) + \ln (w - V_m^2)]$$

The complex potential due to sinks at E ($w = V_i$) and at the inverse point ($w = V_m^2/V_i$) is

$$F(w) = -\frac{Q}{2\pi}\left[\ln (w - V_i) + \ln\left(w - \frac{V_m^2}{V_i}\right)\right]$$

For doublets of strength M at A ($w = 1$) and at the inverse point ($w = V_m^2$), we can find the potential from

$$F(w) = \lim_{h \to 0} \frac{Q}{2\pi}\left((\ln (w - 1) - \ln [w - (1 + h)]) + \left[\ln (w - V_m^2) - \ln\left(w - \frac{V_m^2}{1 + h}\right)\right]\right)$$

in which Qh is to be kept constant and equal to M as $h \to 0$. Taking the limit after expanding in a power series in h gives

$$F(w) = \frac{M}{2\pi}\left(\frac{1}{w - 1} - \frac{V_m^2}{w - V_m^2}\right)$$

Thus the total complex potential in the hodograph plane is

$$F(w) = \frac{Q}{2\pi}\ln\frac{(w - 1)(w - V_m^2)}{(w - V_i)(w - V_m^2/V_i)} + \frac{M}{2\pi}\left(\frac{1}{w - 1} - \frac{V_m^2}{w - V_m^2}\right) \quad (4\text{-}23)$$

If $M/Q = f$, the velocity in the hodograph plane is

$$\frac{dF}{dw} = \frac{Q}{2\pi}\left[\frac{1}{w - 1} - \frac{1}{w - V_i} + \frac{1}{w - V_m^2} - \frac{1}{w - V_m^2/V_i} - f\left(\frac{1}{(w - 1)^2} - \frac{V_m^2}{(w - V_m^2)^2}\right)\right] \quad (4\text{-}24)$$

The point $w = 0$ is a stagnation point in the hodograph flow; this determines f:

$$f = \frac{V_m^2(1/V_i - 1) - (1 - V_i)}{V_m^2 - 1} \quad (4\text{-}25)$$

From the general relation [see Eq. (3-7)]

$$z = \int \frac{dF}{dw}\frac{dw}{w} + \text{const}$$

and Eqs. (4-24) and (4-25) we get

$$z = \frac{Q}{2\pi}\left[(1 + f)\ln (w - 1) - \frac{1}{V_i}\ln (w - V_i) + \frac{1 - f}{V_m^2}\ln (w - V_m^2) - \frac{V_i}{V_m^2}\ln\left(w - \frac{V_m^2}{V_i}\right) + \frac{f}{w - 1} - \frac{f}{w - V_m^2}\right] + \text{const} \quad (4\text{-}26)$$

This equation determines the transformation from the hodograph plane back to the physical z plane, and is used to derive the streamlines in the intake plane, and in particular the shape of the intake, for given V_i and V_m from the known streamlines in the hodograph plane.

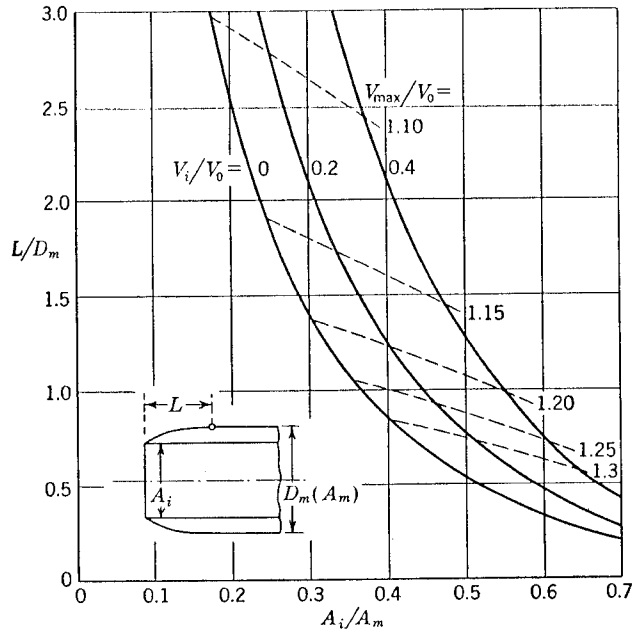

FIG. 4-13 Design chart for two-dimensional optimum intakes.

It is not possible to write down the equation of the intake contour explicitly. The following approximate formula[1] has been given by W. Brödel (1943):

$$\frac{x}{h} = \frac{V_m^2 + V_i^2}{2\pi V_m^2}(t - \ln t - 1) \tag{4-27}$$

$$\frac{y}{h} = \pm \frac{(V_m^2 + V_i^2)(V_m^2 - 1)}{2\pi V_m^2(V_m^2 + 1)} \left\{ \sqrt{(t - t_1)(t_2 - t)} + (t_1 + t_2) \arctan \sqrt{\frac{t - t_1}{t_2 - t}} - 2\sqrt{t_1 t_2} \arctan \sqrt{\frac{t_2(t - t_1)}{t_1(t_2 - t)}} \right\} \pm 1 \tag{4-28}$$

where

$$t_1 = \frac{(V_m^2 + 1)(V_m + V_i)^2}{(V_m^2 + V_i^2)(V_m + 1)^2}$$
$$t_2 = \frac{(V_m^2 + 1)(V_m - V_i)^2}{(V_m^2 + V_i^2)(V_m - 1)^2} \tag{4-29}$$

The parameter t varies between t_1 and t_2, and h is half the inlet depth. In

[1] These relations are rather complicated; a simple shape, which in most practical cases lies within the variety of shapes obtained from Brödel's relations, is that of the NACA 1-series air inlets described in Sec. 4-7.

these equations, V_m stands for V_{max}/V_0 and V_i for V_i/V_0. The length L of the curved part of the outer contour is given by

$$\frac{L}{h} = \frac{V_m^2 + V_i^2}{2\pi V_m^2}(t_2 - \ln t_2 - 1) \tag{4-30}$$

This is plotted in Fig. 4-13.

Brödel has also given an extensive theory for two-dimensional intakes based on a conformal transformation of the flow into a flow between parallel lines. His method is not limited to the design of optimum contours having given inlet velocity ratios. Other types of intake with arbitrary nose radius—and therefore of course a nonuniform velocity distribution—can also be calculated.

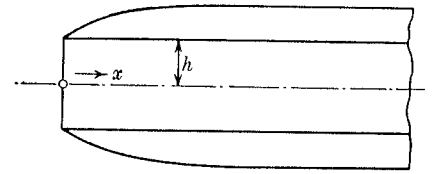

A two-dimensional optimum intake is shown in Fig. 4-14, and with it the pressure distribution on the outer surface at three different inlet velocity ratios. The full lines give the calculated and the points the experimental values. The intake was designed to give a uniform distribution with $V_{max}/V_0 = 1.2$ on the outer surface at an inlet velocity ratio $V_i/V_0 = 0.4$. The area ratio, obtained from Eq. (4-6), is thus $A_i/A_m = 0.55$. It will be seen that the uniform distribution is almost achieved at the design point. At larger inlet velocities the distribution has a flat peak well back near the point where the curved contour joins the parallel part. At smaller inlet velocities, however, a very pronounced peak is observed near the leading edge. This is due to the very small nose radius, characteristic of optimum contours.

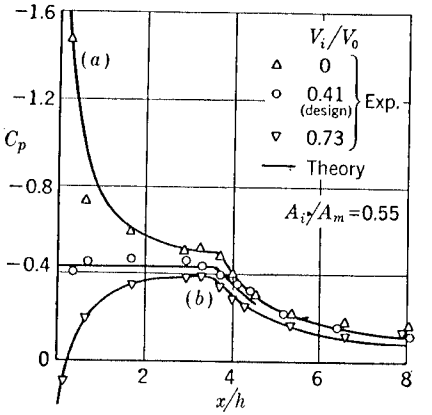

FIG. 4-14. Pressure distributions on the outer surface of a two-dimensional optimum intake.

Figure 4-15 shows the variation of the forward and rear peak velocities with the inlet velocity ratio. While the rear peak (b) does not vary much throughout the whole range, the forward peak (a) rises steeply as soon as V_i/V_0 falls below its design value. This means in practice that the flow soon breaks down at the nose. Similarly, there is a sharp peak near the nose at the inner surface when V_i/V_0 exceeds the design value by a certain amount. The working range of optimum intakes is therefore very

limited. These undesirable features, which are typical of intakes with small nose radii, will be discussed in more detail in the next section.

Figure 4-13 can be used as a design chart for two-dimensional optimum intakes. Suppose that an air intake is to be designed for given values of V_i/V_0 and V_{max}/V_0. Then Fig. 4-13 gives the area ratio and the length of the curved surface necessary. If, for safety reasons, the intake is designed for a lower inlet velocity ratio than necessary, but keeping the area ratio which was obtained before, then a higher V_{max}/V_0 but a shorter intake will result. In the same way, a longer intake with the same area ratio would give lower values of V_{max}/V_0, but the inlet velocity ratio at which there begins to be a velocity peak at the lip would be higher. Thus the curves in Fig. 4-13 will also serve to find the effect of any alteration in the length of the intake once the area ratio has been fixed.

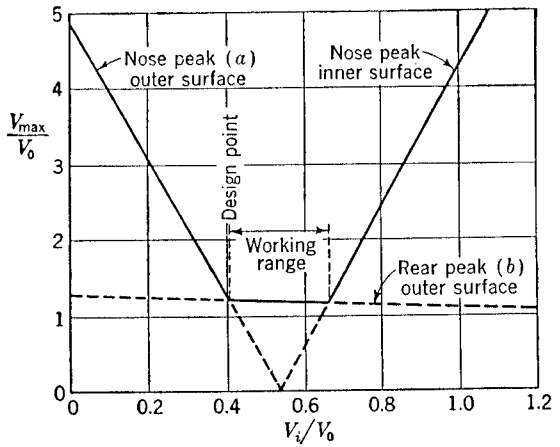

FIG. 4-15. Velocity peaks at the intake of Fig. 4-14 under varying working conditions.

4-6. A Systematic Series of Circular Air Intakes. Some calculations and experiments by the authors (1940) on circular air intakes of various shapes gave the valuable result that all which had satisfactory external pressure distributions turned out to be geometrically similar. It is possible in fact to approximate the curved part of the outer surface by a quarter ellipse or by a similar geometric curve. This important conclusion is only empirical, of course; the optimum shapes given by the methods of Sec. 4-5, for instance, are not precisely similar. However, simple geometric systems are of practical value to the designer; two series of circular air intakes are therefore described at length in this section and in Sec. 4-7.

The curved part of the outer profile of the first series of intakes is a quarter ellipse extending from the nose to the maximum diameter, and another quarter ellipse forms the inner surface as far as the minimum internal diameter. With the notation of Fig. 4-16, the outer shape is

given by

$$\frac{r}{R_m} = \frac{R_0}{R_m} + \left(1 - \frac{R_0}{R_m}\right)\sqrt{1 - \left(1 - \frac{R_m}{L}\frac{x}{R_m}\right)^2} \tag{4-31}$$

and the inner shape by

$$\frac{r}{R_m} = \frac{R_0}{R_m} - \left(\frac{R_0}{R_i} - 1\right)\frac{R_i}{R_m}\sqrt{1 - \left(1 - \frac{R_i}{L_i}\frac{x}{R_i}\right)^2} \tag{4-32}$$

The inner and outer thicknesses and the lengths of the inner and outer curved portions are given in terms of the area ratio A_i/A_m and the four constants K_1 to K_4 by

$$\frac{R_0}{R_i} = K_1 \qquad \frac{R_0}{R_m} = K_1\sqrt{\frac{A_i}{A_m}} \tag{4-33}$$

$$\frac{R_m}{L} = K_2 + K_3\left(\frac{A_i}{A_m}\right)^3 \tag{4-34}$$

$$\frac{R_i}{L_i} = \frac{1}{K_4(K_1 - 1)} \tag{4-35}$$

and the constants are given in Table 4-1.

TABLE 4-1

Class	K_1	K_2	K_3	K_4
A	1.15	0.2	12.5	1.5
B	1.10	0.2	12.5	1.3
C	1.03	0.2	7.5	1.0

The three classes A, B, and C are given to make it possible to vary the nose radius or the inner thickness. Class A has a fairly well-rounded

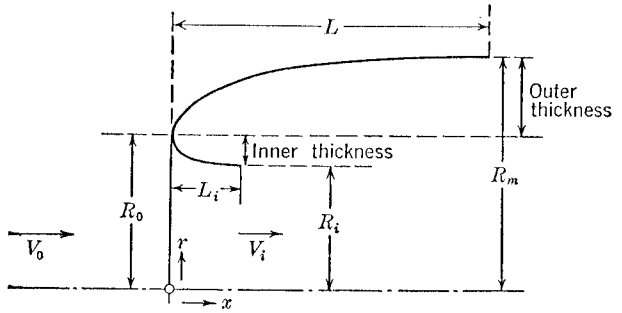

FIG. 4-16. Geometry of circular intakes.

nose, Class B a moderately rounded nose, and Class C a nose of very small radius. The length of the outer curved surface, given by Eq. (4-34) and Fig. 4-17, is the same for A and B, but greater for C. In all cases the

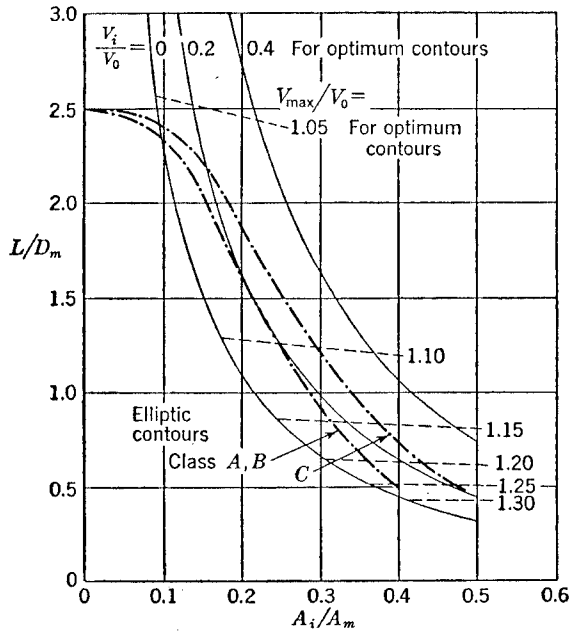

FIG. 4-17. Design chart for circular optimum intakes. Length of intake classes A, B, C.

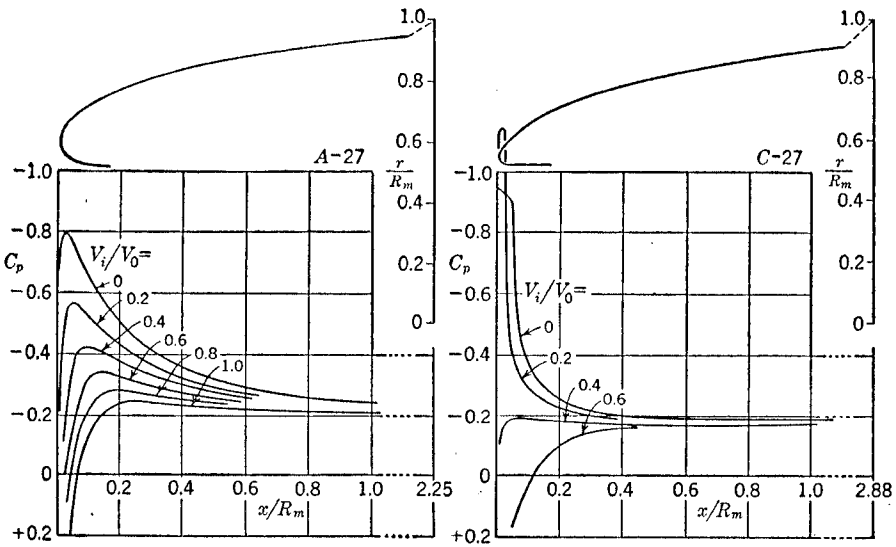

FIG. 4-18. Characteristic pressure distributions for classes A and C.

limit as A_i/A_m tends to zero is a half ellipsoid with its semiaxes in the ratio 1:5. A basic body with a better fineness ratio would be obtained by taking K_2 smaller than 0.2.

Each intake is completely defined by its class (A, B, or C) and by the value of the area ratio, and can therefore be referred to as, for instance, A-36, where the number gives the area ratio as a percentage. Other shapes can easily be obtained by interpolation, varying the constants K and taking the classes A, B, and C as a guide.

It is not essential to take quarter ellipses, of course; other geometric systems might be equally suitable. The comparatively large curvature of the ellipse near the nose tends to produce unnecessarily high velocity increments there, and a slightly flatter shape might be preferable in this respect, such as that of the NACA 1-series which is described in Sec. 4-7. But, apart from being a convenient shape for the designer, the ellipse has the definite advantage that it makes a finite inner thickness possible without any difficulty. This is not the case with flatter shapes, as will be seen in Sec. 5-2.

We now consider the aerodynamic characteristics of the series. Of all the intakes, those of Class C approximate most closely to optimum contours with uniform pressure distribution. This is illustrated in Fig. 4-18, which shows typical pressure distributions for a C-type intake, and in Fig. 4-20 (where, however, the maximum outer surface velocity is plotted as ordinate instead of the surface pressure). The pressures are fairly constant along the outer surface, but it appears that a slight improvement might be obtained by flattening the shape near the nose so as to decrease the nose radius even more. An increase in the length of the intake would also reduce the maximum velocity slightly, as the comparison in Fig. 4-17 with the curves for optimum intakes[1] suggests. This diagram also gives some indication of the useful range of lengths; a longer intake has a smaller maximum velocity in general, but on the other hand, smaller nose radii and greater lengths bring increased sensitivity to any variation in the inlet velocity ratio. In this respect Class C is a compromise, although sharp suction peaks are not avoided altogether.

In contrast to this, the intakes of Class A are much less sensitive (Fig. 4-18); the large nose thickness prevents sharp suction peaks and breakdown of the flow. However, the maximum velocity for a given inlet-velocity ratio is now much higher than that of the optimum contour, as already explained in Sec. 4-2 and Fig. 4-5. Class B is an intermediate case; the example in Fig. 4-19 might serve as a cowling for radial engines.

[1] The curves for optimum circular-intake contours are different from those in Fig. 4-13 for two-dimensional intakes, the latter generally being longer. They were obtained by a semiempirical method described below in Sec. 5-2.

Critical Mach numbers (where sonic speed is first reached on the outer surface) estimated by the use of Eqs. (4-18) and (4-20) have been plotted in Fig. 4-20, which can be used as a design chart. The region of very small area ratios (A_i/A_m smaller than about 0.1) is of course influenced by the choice of the basic body fineness ratio; the critical Mach number will be increased when the fineness ratio is greater than 1:5, the value used here.

The estimated critical Mach numbers do not always coincide with the Mach number where the measured drag begins to rise, as the examples in Fig. 4-21 show. Shapes whose pressure distributions are comparatively flat (Class C, and Class B with higher values of A_i/A_m), and which therefore have supersonic flow regions extending over a considerable part of the outer surface when the Mach number exceeds the critical, generally show a typically steep drag rise near the estimated critical Mach number. Where there is a limited local peak, however (as with Class A), which will produce only a short supersonic region close to the nose, the drag rise may be considerably delayed. This is clearly apparent in the case of the intake A-30 at $V_i = 0$ in Fig. 4-21. The two types of drag rise curve which can be distinguished in this figure suggest different underlying physical processes. This effect was first observed by H. Ludwieg (1943), and is essentially similar to what has been found with certain ordinary airfoils at incidence. The significance in the present case is that the decrease in critical Mach number which is the price of increased nose thickness, and thus insensitivity, is much less than might be supposed from the straightforward estimates in Fig. 4-20. This reduces the value of estimated critical Mach numbers as given in design charts like Fig. 4-20, although of course they always err on the safe side.

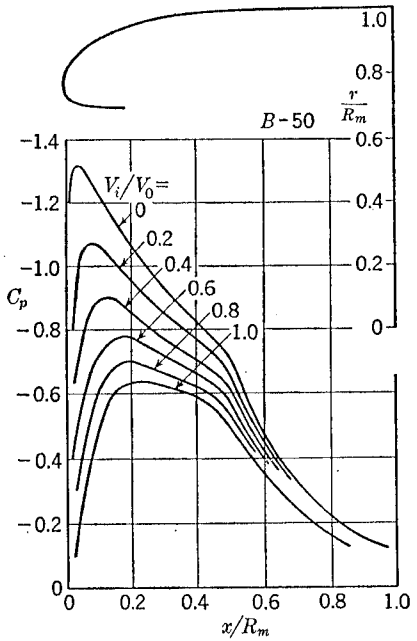

FIG. 4-19. Characteristic pressure distributions for Class B.

One of the main practical points of difference between the three types of intake is their behavior at zero forward speed. The flow may break down at the sudden bend round the nose into the inlet (Fig. 4-1c) if the nose radius is too small. As a result, there is a loss of energy which will

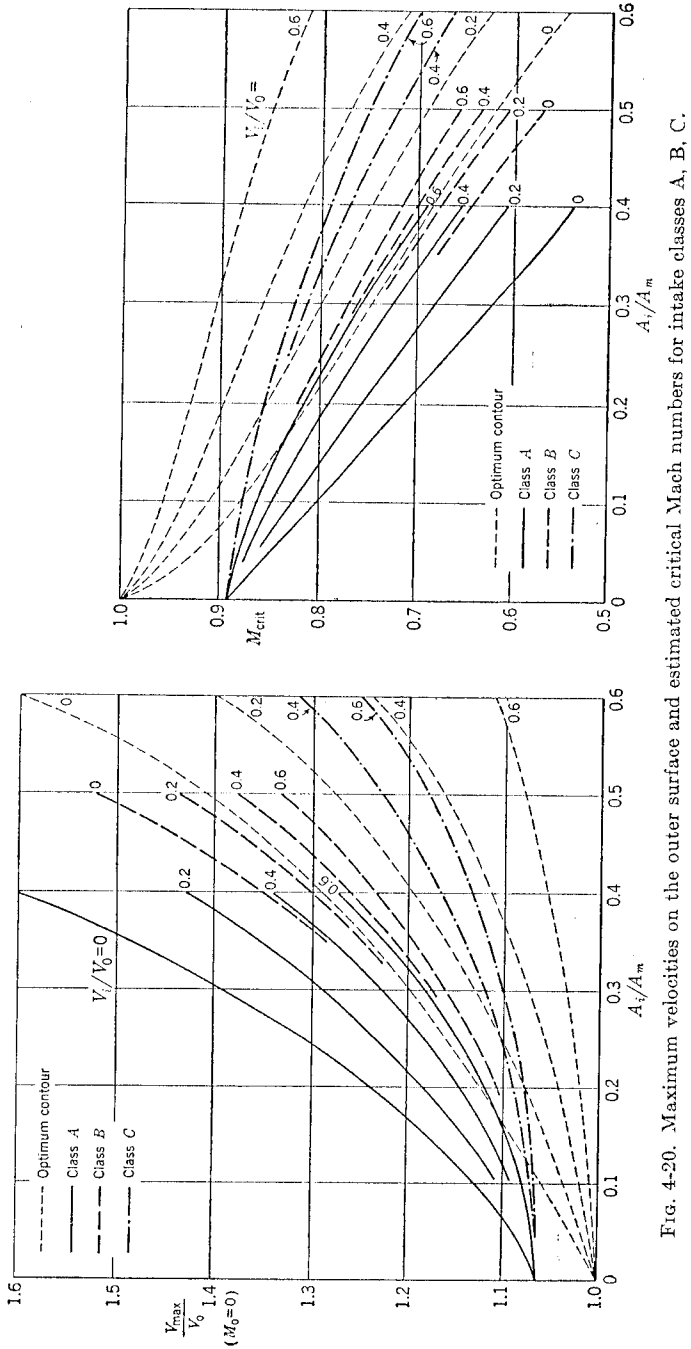

FIG. 4-20. Maximum velocities on the outer surface and estimated critical Mach numbers for intake classes A, B, C.

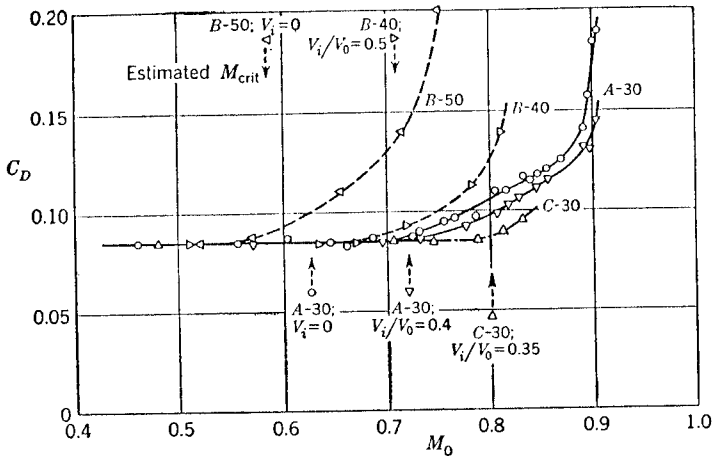

FIG. 4-21. Drag variation with Mach number for some circular intakes.

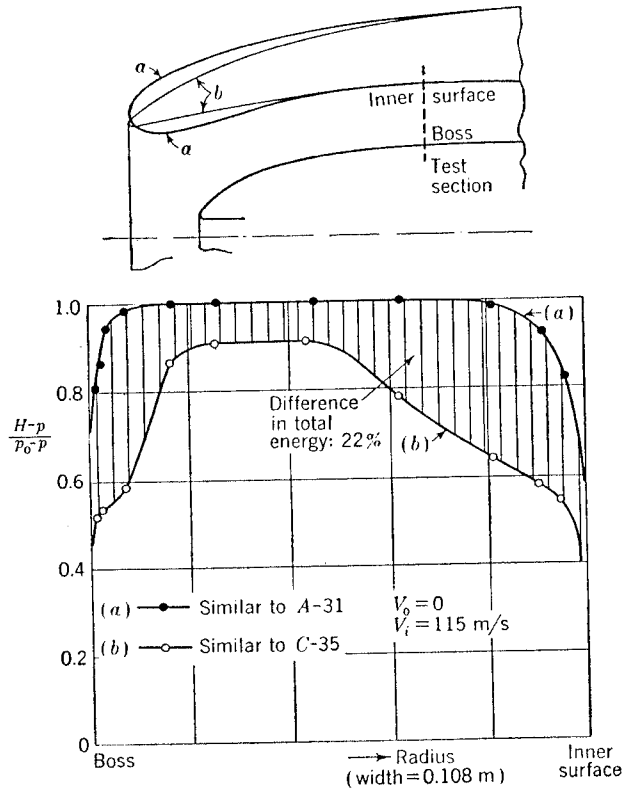

FIG. 4-22. Entry losses due to small nose thickness, from full-scale tests under static conditions.

reduce the total pressure H in the inlet, and in turn the static thrust of the jet motor (see Sec. 9-3). Measured inflow losses for incompressible flow are given in Table 4-2.

TABLE 4-2

Class	*Static Inflow Loss,* $\frac{\Delta H}{\frac{1}{2}\rho V_i^2}$
A	0.02–0.04
B	0.10–0.20
C	0.20–0.40

Figure 4-22 shows a typical example of the type of flow caused by separation at the inlet nose under static conditions, from measurements on a turbojet engine (Jumo 004). While an intake similar to A-31 suffers no inflow losses apart from what is unavoidable in the boundary layer, a heavy breakaway at the nose of an intake similar to C-35 causes a considerable loss in total energy, with a consequent reduction of the static thrust by 8 to 10 per cent.

On more modern engines, with higher mass flow and possibly relatively smaller entry areas, the effect of compressibility cannot be ignored even in the static case; the mean Mach number in the inlet might be high subsonic. Even the nose radius of an intake of Class A might not then be sufficient, as Fig. 4-23 shows. A smoother inner shape with less curvature at the nose is needed. This can be obtained by taking K_1 greater than 1.15. Finally, the detrimental effect of a sharp nose may be amplified by a subsequent expansion of the internal duct behind the inlet; a disturbance of the inflow originating at the nose would then be likely to cause much heavier duct losses than otherwise anticipated.

What has been said above is not restricted to static conditions but might also apply to the climb or flight at high altitudes. The aim should therefore be to keep the nose thickness as large as considerations of the flow at the outer surface of the intake in high-speed flight will allow.

When the axis of the intake is at an angle of incidence to the direction of the free stream, the flow becomes asymmetrical. The pressure distribution on the sides of the outer surface is not appreciably changed, but the suction is increased at the top section and reduced at the bottom section. A sufficiently accurate approximation can be made by assuming the variation from the symmetrical pressure distribution to follow a cosine law round the circumference. The peak velocity at the top section usually varies linearly with the incidence α, the rate of increase depending again on the nose radius. For inlet velocity ratios ranging between $V_i/V_0 = 0.6$ and $V_i = 0$ the slope is approximately

$$\frac{d(V_{max}/V_0)}{d\alpha} = 1.5 \text{ to } 2.5 \qquad \text{for Class A}$$

$$\frac{d(V_{max}/V_0)}{d\alpha} = 4.0 \text{ to } 5.5 \qquad \text{for Class C}$$

For intakes on which the pressure distribution has its peak well back, these slopes might be lower, down to about half the values given.

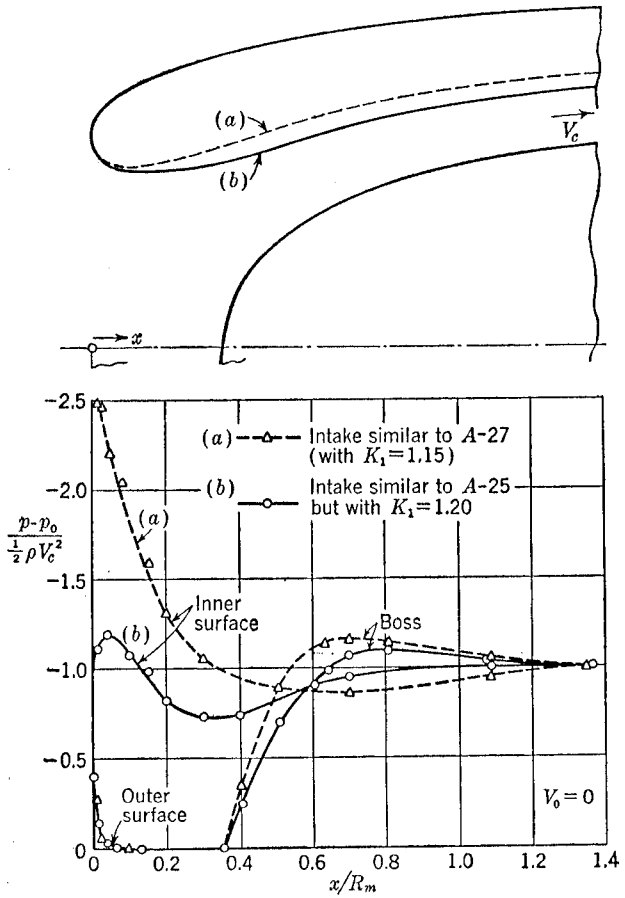

FIG. 4-23. Influence of the curvature of the inner surface near the nose on the pressure distribution round the entry lip under static conditions.

The pressure peaks due to incidence, being limited usually to a narrow region near the nose at the top, do not necessarily have any large effect on the drag characteristics of the intake at high subsonic Mach numbers. On intake A-30, in fact, the drag rise was not found to be appreciably different at $\alpha = 0°$ and $\alpha = 6°$, apart from a higher low-speed drag in the latter case.

The normal force on the intake surfaces is sometimes of interest, *e.g.*,

for stressing purposes, and it can be obtained from the pressure distributions. There is also a destabilizing pitching moment (or, in a cross flow, a yawing moment) when the intake is at incidence. The destabilizing moments of a complete nacelle will depend also on the jet. It has been found that the normal force and the destabilizing moment of an intake are influenced only little by the inlet velocity ratio. Tests on several intakes similar to those of Class A (area ratios between 0.25 and 0.40) have shown that the position of the center of pressure (on the curved part of length L), defined in the usual way, is at about $x/D_m = 0.35$ to 0.40 from the nose, over an incidence range up to about 15° and inlet velocity ratios up to 1. Both normal force and moment rise approximately linearly with incidence.

4-7. NACA 1-series Circular Air Intakes. Another series of shapes has been developed empirically from the long experience of NACA in the design of engine cowlings and air inlets by D. D. Baals, N. F. Smith, and J. B. Wright (1945) to suit the requirements of modern jet engines. It is based on the same principle of similarity as the series described in Sec. 4-6, and the external shape of the intakes from the nose ($x = 0$; $r = R_0$ in Fig. 4-16) to the cylindrical part ($x \geq L$; $r = R_m$) is represented by a single function $r(x)$. There is no mathematical expression for this function of x, and the ordinates are given in Table 4-3, in which y is the radial ordinate measured from the nose and Y is the outer thickness. Thus

$$\frac{y}{Y} = \frac{r - R_0}{R_m - R_0} = \frac{r/R_m - R_0/R_m}{1 - R_0/R_m} \tag{4-36}$$

in the notation of Fig. 4-16. The inner thickness is always the same fraction of the outer thickness,

$$R_0 - R_i = 0.025(R_m - R_0)$$

which gives

$$\frac{R_0}{R_m} = 0.0244 + 0.976\sqrt{\frac{A_i}{A_m}} \tag{4-37}$$

The inner contour of the intake is a quadrant of a circle.

There are thus two parameters, the area ratio A_i/A_m and the length L/D_m, that can be freely chosen. The intakes can therefore be designated by three digits; the first indicates the series, while the second gives the inlet diameter and the third the length as percentages of the maximum diameter $D_m = 2R_m$. Thus 1-50-150 is an intake of the 1-series of area ratio 0.25, the length of which is 1.5 times the maximum diameter.

In contrast to the intakes A, B, and C of the preceding section, whose inner thickness can be varied but whose length is fixed, the NACA 1-series leaves the length open to choice, but the inner thickness cannot be varied. The inner thickness $(R_0 - R_i)/R_i$ is the same as that of Class C for $A_i/A_m = 0.2$; for greater values of the area ratio, the thickness is

smaller than that of Class C, *i.e.*, the nose is even sharper. The external shape of the NACA 1-series is slightly flatter than a quarter ellipse.

On the whole, the properties of the NACA intakes are similar to the properties of Class C described in Sec. 4-6. This is illustrated by Fig. 4-24, where critical Mach numbers estimated from low-speed pressure measurements are given. There is a certain inlet velocity ratio for each intake at which it operates under its best condition, and at that velocity ratio the estimated critical Mach number is only between 0.02 and 0.04

TABLE 4-3. NACA 1-SERIES ORDINATES

x/L	y/Y	x/L	y/Y	x/L	y/Y	x/L	y/Y
0	0	0.13	0.4194	0.34	0.6908	0.60	0.8911
0.002	0.0480	0.14	0.4366	0.35	0.7008	0.62	0.9020
0.004	0.0663	0.15	0.4530	0.36	0.7105	0.64	0.9123
0.006	0.0812	0.16	0.4688	0.37	0.7200	0.66	0.9220
0.008	0.0933	0.17	0.4840	0.38	0.7294	0.68	0.9311
0.010	0.1038	0.18	0.4988	0.39	0.7385	0.70	0.9395
0.015	0.1272	0.19	0.5131	0.40	0.7475	0.72	0.9475
0.020	0.1472	0.20	0.5270	0.41	0.7563	0.74	0.9548
0.025	0.1657	0.21	0.5405	0.42	0.7648	0.76	0.9616
0.030	0.1831	0.22	0.5537	0.43	0.7732	0.78	0.9679
0.035	0.1994	0.23	0.5666	0.44	0.7815	0.80	0.9735
0.040	0.2148	0.24	0.5792	0.45	0.7895	0.82	0.9787
0.045	0.2296	0.25	0.5915	0.46	0.7974	0.84	0.9833
0.050	0.2436	0.26	0.6035	0.47	0.8050	0.86	0.9874
0.060	0.2701	0.27	0.6152	0.48	0.8125	0.88	0.9909
0.070	0.2947	0.28	0.6267	0.49	0.8199	0.90	0.9940
0.080	0.3181	0.29	0.6379	0.50	0.8269	0.92	0.9965
0.090	0.3403	0.30	0.6489	0.52	0.8410	0.94	0.9985
0.100	0.3613	0.31	0.6597	0.54	0.8545	0.96	0.9993
0.110	0.3815	0.32	0.6703	0.56	0.8673	0.98	0.9998
0.120	0.4009	0.33	0.6807	0.58	0.8795	1.00	1.000

below the optimum calculated from Eqs. (4-18) and (4-20). That the optimum value is not quite reached is due to the pressure distribution not being quite uniform along the whole of the outer surface. It would appear that the best shape in this respect is somewhere between the NACA shape and the elliptical shape of Class C.

The maximum velocity ratio V_{max}/V_0 and thus the estimated critical Mach number are not much increased if the value of V_i/V_0 is greater than that at the design point, because the velocity peak then occurs at the rear end of the curved part and is only little affected by a change in the inlet velocity ratio. The same comparative independence of the rear velocity peak on the inlet velocity ratio was found in the case of two-dimensional optimum intakes, as explained in connection with Fig. 4-15.

Again, when V_i/V_0 is below the design value, a sharp velocity peak occurs near the nose of the intake and the estimated critical Mach number falls steeply.

As a consequence of this, there is a definite range of practical lengths, for a given value of the area ratio A_i/A_m. It coincides roughly with the

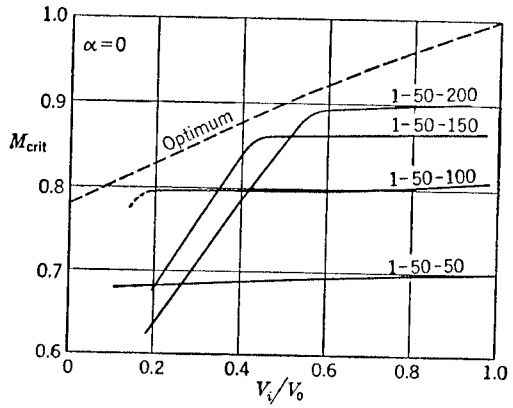

FIG. 4-24. Estimated critical Mach numbers from NACA low-speed tests on some air intakes of the NACA 1-series.

region between the lines $V_i/V_0 = 0$ and 0.4 for optimum intakes in Fig. 4-17. Outside it there is always either a forward peak (because the intake is too long) or a rear peak in the velocity distribution (because the intake is too short), and the flat optimum distribution is never reached. The fixed length of the Class C intake is practically in the middle of the range.

4-8. General Three-dimensional Intakes. In practical designs we often find air intakes which are neither bodies of revolution nor two-dimensional. It may nevertheless be possible to treat them as compounded of these basic types, and thus to make use of their known properties.

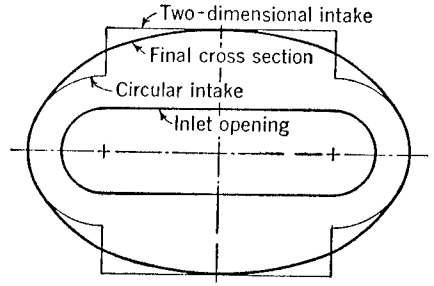

FIG. 4-25. Wall-thickness distribution round an oval inlet.

The shape of the actual inlet opening to be considered might be oval, as shown in Fig. 4-25. The ends could then be regarded as parts of a circular intake, and the flat sides as parts of a two-dimensional intake. The minimum frontal area A_m can be obtained from Eq. (4-6), which is valid for any inlet cross-section shape. The actual wall thickness should not be constant round the intake, however; the two-dimensional parts require thicker walls than the circular parts in order to keep the *local* area ratio the same all the way round.

An oval entry so designed is not likely to show any appreciable difference in its aerodynamic characteristics from those of a circular entry, as has been confirmed by drag measurements at high subsonic Mach numbers. The drag was found to rise at the same free-stream Mach number, within the accuracy of the test, for a circular intake and a flattened intake with the width of the inlet three times its height. They were still equal at an angle of yaw of 6°. When the flat sides were at incidence, on the other hand, the drag rise of the oval intake occurred earlier than in symmetrical flow, beginning in this particular case at a Mach number of about 0.65 at 6° incidence compared with about 0.80 at 0°; at $M_0 = 0.80$, the

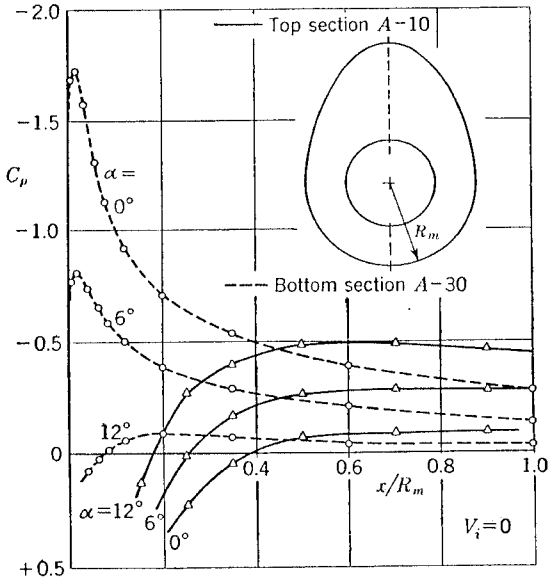

FIG. 4-26. Pressure distributions on the outer surface of an air intake of egg-shaped cross section.

drag of the oval intake inclined at 6° had risen by about 40 per cent above its low-speed value.

As another example, the maximum cross section might be egg-shaped, as illustrated in Fig. 4-26. If the shape of the inlet cross section is not already fixed, it can be so chosen as to keep the *local area ratio*, measured in terms of radii from a suitably chosen center point, constant round the intake. The result would be a similarly egg-shaped inlet cross section. If, however, both cross sections are given, as they are in Fig. 4-26, the area ratio cannot be the same all the way round. The thinner part at the bottom is worse (*i.e.*, has higher velocity increments on the outer surface) than the corresponding circular intake of the same area ratio, and the thicker part is better. Thus it is possible for the maximum velocity at

the outer surface at the top to be extremely low, as in the example shown, even at incidence.

This is obviously a consequence of asymmetry of the flow up to the entry; the outer surface velocities at the bottom may be 30 to 40 per cent higher than on the corresponding circular intake with the same (local) area ratio, in the extreme case $V_i = 0$. But this need not be detrimental in practice, since the velocity peaks disappear when the whole intake is at incidence. This type of intake is therefore very suitable for nose intakes in fuselages, providing much space inside the entry walls, sufficient in special cases even for the pilot.

Oval intakes in the leading edges of swept wings add some special problems to the ones already mentioned. These are to some extent connected with the secondary flow due to sweep of the wing which, ahead of the leading edge, has a component parallel to the wing leading edge, directed outward. Thus the inflow into an intake at the root of a sweptforward wing would be assisted by the effect of sweep; but with intakes in sweptback wings the inflow problem is aggravated, since the air at the leading edge, tending to flow parallel to the entry plane, must be induced to turn round into the inlet opening. Three main difficulties may be noted:

1. The outer surface velocities are usually higher at the rear (outboard) end of the intake, and lower at the forward (inboard) end, for sweptback wings. This is basically the same effect as has been described for staggered two-dimensional intakes in Sec. 4-4. Special care has to be taken in shaping the outboard end, possibly by thickening and rounding off the walls. This might mean that on a wing of constant thickness the actual inlet height should decrease toward the outboard end, giving an inlet opening of triangular shape with the effective local area ratio decreasing in the direction of the wing tip.

2. In high-speed flight, the retardation which in Fig. 4-1*a* took place entirely in the free stream ahead of the entry now continues along the exposed inner wall at the inboard end. We shall discuss the problems connected with retarded flows along walls in detail in Chap. 9. There is obviously a danger of flow separation from the exposed inner wall. Tests on an intake with 40° sweepback on a straight side wall gave a loss of total head in the inlet of 40 to 50 per cent of the inlet dynamic pressure when the velocity ratio was $V_i/V_0 = 0.5$. In this particular case it was possible to restore the total head in full by giving the protruding end wall a curvature to counteract the pressure rise and by contracting the internal duct slightly. It will only be possible to deal in this way with intakes with moderate angles of sweep, however; the separation effect depends mainly on the geometry of the intake, that is, on the angle of sweep, becoming increasingly severe with increasing sweep.

3. Under static conditions, the air tends to flow with a much higher

velocity into the outboard end than into the inboard end. A liberal inner thickness is therefore required at the outboard end; without it up to 30 per cent of the kinetic energy of the inflow can easily be lost.

As on all leading-edge entries, the upper and lower lips are often staggered in an attempt to keep the intake contour within the shape of the basic airfoil section (see also Secs. 4-4 and 5-3). This may mean that the protruding upper lip becomes comparatively thick and of an unsuitable shape and that the lower lip consequently becomes too thin, the more so since the thrust forces act mainly on the lower lip. The stagger should therefore not be exaggerated; the angle between the common tangent to the upper and lower lips and the vertical should not be more than about 15°. Even then, it may be necessary to thicken the lower lip, bringing it outside the basic wing contour. This does not necessarily have a detrimental effect on the flow past the wing as a whole, as is often supposed.

4-9. Internal Duct. The flow in the internal duct behind the narrowest inlet cross section is generally assumed to be independent of the flow round the outside of the intake. The variable which relates the two flows is the mean inlet velocity V_i. This fixes the flow conditions at the beginning of the internal duct; for the subsequent shape of the walls of the duct much of the extensive work and the data which have been obtained from investigations of pipe flow are applicable. There are some aspects, however, which are of special interest in connection with particular types of power plants.

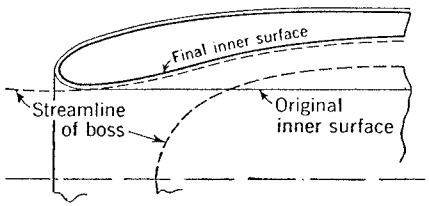

FIG. 4-27. On designing a constant-area internal duct.

It is often required, especially for turbojet engines, to design a duct which has a circular or oval cross section at the beginning and then becomes annular round an internal boss or hub. The ratio of the mean inlet velocity V_i to the velocity V_c at the end of the duct (*e.g.*, ahead of the compressor) will usually be given, and an expanding, contracting, or constant-area duct will be needed. A difficulty arises at once in the case mentioned above, where the effective cross-section area is uncertain in the region at the beginning of the boss.

Let us consider the example of Fig. 4-27, where the duct is of constant area. The plain cylindrical duct is to be replaced by another with the same constant cross section enclosing a boss beginning behind the inlet. Then the following procedure may be used to deduce a suitable shape for the inner surface of the intake: The streamlines of the flow past the boss in an unbounded stream are determined; that streamline which gives the desired cross section at the end of the duct is chosen as a first approximation. It is faired into the cylindrical intake contour near the nose.

The pressure distribution along this wall will not be uniform, however, although the velocity V_c at the end of the duct will be approximately equal to the mean velocity V_i at the beginning. But the variation of pressure along a streamline is easily determined by the usual methods,[1] and slight adjustments of the streamlines give the uniform pressure distribution desired. This involves narrowing the stream tubes ahead of the boss to counteract the stagnation effect and widening them slightly in the peak suction region of the boss to counteract the accelerated flow there. When the boss is slender in shape, the changes in pressure along the streamlines, and therefore the corrections too, should be small. The method was applied in the design of the internal duct in the example of Fig. 4-10, with satisfactory results.

This streamline method can obviously be adapted to the design of slightly expanding or contracting ducts, where the shape of a *constant-area duct* can still be used as a starting point.

Considerable thrust and drag forces[2] are experienced by the boss and the inner surface of the intake. If the inlet area A_i is equal to the area A_c at the downstream end of the duct, the forces are purely internal, and equal and opposite. Consider the boss in an unbounded free stream with velocity V_i; if it is assumed that the static pressure at the end of the duct is also p_i, the force F_B on the boss is readily found to be

$$F_B = -(p_i - p_0)A_B$$

where A_B is the cross-section area of the boss at that station. This merely states that the integral over the axial components of the pressure forces along the surface of the boss

$$\int_{A_B} (p - p_i)\, dA_B = 0$$

Assuming no energy losses,

$$\frac{F_B}{\frac{1}{2}\rho V_0^2 A_i} = -\frac{A_B}{A_i}\left[1 - \left(\frac{V_i}{V_0}\right)^2\right] \tag{4-38}$$

This is a drag force, and may be of considerable magnitude. In Fig. 4-4, experimental results obtained by integrating the measured pressure distributions[3] are compared with the estimate above, and they will be

[1] The method of singularities is again very suitable; the boss is then replaced by sources on the axis.

[2] The definition of these forces is in a sense arbitrary, depending on the static pressure assumed at the cross section at the end of the boss.

[3] In the integration of the measured pressure distributions, the same arbitrary assumption has to be made about the static pressure at A_B as in the estimate above, *i.e.*, that the pressure there is equal to p_0.

seen to agree well. We may conclude that the treatment of the boss as if it was in an unbounded free stream is justified up to inlet velocity ratios of about 0.8. Other tests have shown this to be true even if the boss begins at the entry. This is another indication that the retardation of the flow takes place ahead of the entry with this type of intake, and is a further proof of the independence of external and internal flow.

The aerodynamic load distribution on the intake changes considerably if the internal duct expands, as is generally the case with cooler installations and ram jets, and sometimes also with turbojets. The retardation

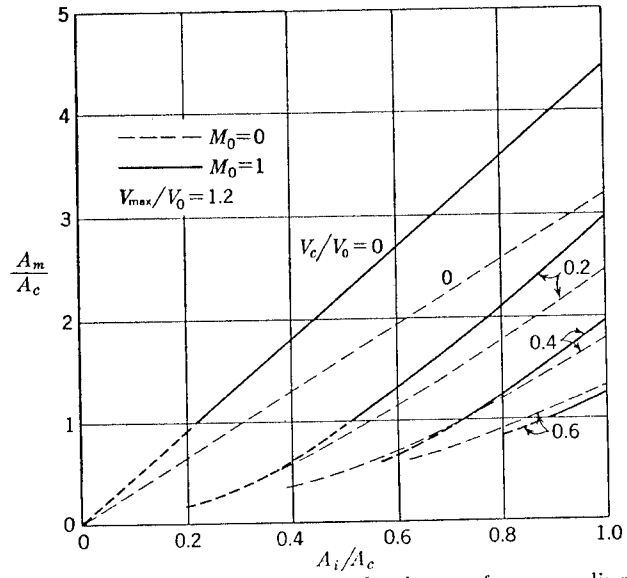

FIG. 4-28. Reduction of the required frontal area by the use of an expanding internal duct.

of the flow then takes place in two stages: (1) in the external flow, with a change in momentum which corresponds to a thrust force on the outer surface; (2) in the internal duct with a further change in momentum which produces thrust forces on the walls of the diffuser. We distinguish now between the mean velocity V_i at the narrowest cross section of the inlet and the mean velocity V_C at the downstream end of the internal duct, and between the corresponding cross-section areas. The momentum considerations of Sec. 4-2 are still applicable, and the total thrust force F is given by

$$\frac{F}{\frac{1}{2}\rho V_0^2 A_C} = \left(1 - \frac{V_C}{V_0}\right)^2 \tag{4-39}$$

On the other hand, we still have for the nose thrust F_N on the outer surface

of the intake

$$\frac{F_N}{\frac{1}{2}\rho V_0^2 A_i} = \left(1 - \frac{V_i}{V_0}\right)^2$$

that is,

$$\frac{F_N}{\frac{1}{2}\rho V_0^2 A_C} = \frac{A_i}{A_C}\left(1 - \frac{A_C}{A_i}\frac{V_C}{V_0}\right)^2 \tag{4-40}$$

The difference between the total thrust and the nose thrust gives the thrust produced by the pressure increment on the walls of the diffuser (see also Fig. 4-4).

An expanding internal duct is obviously of great advantage to the external shape of the intake, since the latter can now be designed for higher values of V_i/V_0 when V_C/V_0 is given, as is usually the case. The resulting reduction of the required frontal area is shown in Fig. 4-28, which includes the influence of compressibility, obtained in the way outlined in Sec. 4-3. The savings in frontal area and length are further illustrated by the example in Fig. 4-29, where the two fairings shown have

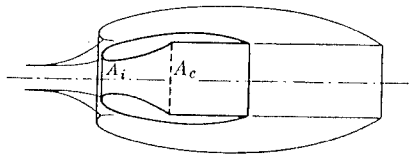

FIG. 4-29. Two circular fairings with the same aerodynamic loading (V_{max}) on their outer surfaces.

the same aerodynamic loading on their outer surfaces for the same flow through the internal duct.

These gains must, however, be paid for in the internal flow, for the boundary layer along the walls of the duct, where the second retardation of the flow takes place, is able to cope with only a limited adverse pressure gradient. On the other hand, use can be made of the retardation which the installed body (cooler block or burner) would cause upstream of itself in an unlimited flow, as explained in Sec. 3-6.

When the expanding duct precedes a compressor, no such mitigation of the adverse pressure gradient is to be expected. Here expanding or even curved ducts usually cause noticeable energy losses. These do not depend primarily on the inlet velocity ratio V_i/V_0, that is, they occur under all flight conditions. An example is shown in Fig. 4-30 from tests on a full scale turbojet motor (Jumo 004). The losses are considerable if the cross-section area in front of the compressor is more than 20 to 25 per cent larger than the inlet cross-section area, and the tested duct shapes represent favorable cases. It may be noted that the flow separation

actually occurs at the surface of the boss. The consequences of such losses will be discussed in Chap. 9.

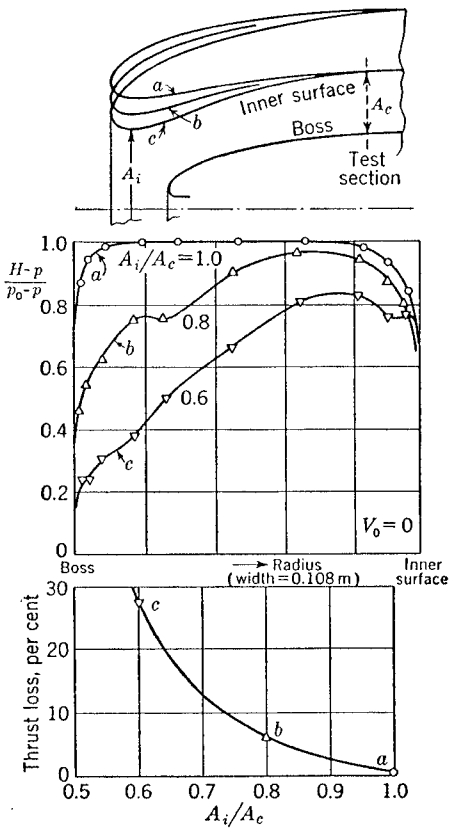

FIG. 4-30. Influence of an expansion in the internal duct on the internal total-head distribution and on the thrust of a turbojet engine, from full-scale tests under static conditions.

EXERCISES

4-1. Calculate the frontal area of optimum intakes with $A_i = 0.2\ \text{m}^2$ for $V_i/V_0 = 0.4$ which give maximum velocities on the outer surface $V_{max}/V_0 = 1.05, 1.1, 1.2, 1.3, 1.5$, assuming incompressible flow. Estimate the critical Mach numbers for these intakes from Eqs. (4-18) and (4-20).

4-2. Calculate the thrust force which acts on an air intake with $A_i = 0.2\ \text{m}^2$ and a constant inlet velocity $V_i = 150$ m/sec at flight Mach numbers between 0 and 1. Assume sea-level conditions ($\rho_0 = 0.125$ kg-sec^2/m^4; $a_0 = 340$ m/sec; $k = 1.4$).

4-3. Compare the shape of the intake C-20 with the corresponding intake of the NACA 1-series with the same length.

4-4. Find the inlet area A_i of an intake with an expanding internal duct and a given area A_C at the end of the duct ($A_C = 0.2\ \text{m}^2$) if the outer surface takes the same thrust force as the diffuser walls when $V_C/V_0 = 0.4$. Assume incompressible flow. Note that of the two possible solutions only one is significant.

4-5. Plot the line $v_r = 0$ for a single source ring by plotting v_r against r/r' for various values of x/r' from the table in the Appendix.

4-6. Superpose a source ring of radius R_0 and strength $q/2\pi R_0 V_0 = 0.1$ on a parallel flow along its axis. Draw the streamline pattern, including the shape of the resulting body, by plotting the stream function $\Psi/V_0R_0^2$ against r/R_0 for a range of x/R_0, using the table in the Appendix. Note that there are two classes of streamlines, one inside the body contour starting in the source ring and the other outside the body starting at infinity. There is always a streamline of each class with the same value of the stream function, with the exception of that which goes through the stagnation point, *i.e.*, the body contour. Remember that for the stagnation point $v_r = 0$, $v_x = -V_0$. Calculate the pressure distribution on the surface of the body and compare with those obtained in Exercises 3-1 and 3-2.

BIBLIOGRAPHY

JUNKERS, H., Kühleranordnung für Luft- und andere Fahrzeuge, Deutsches Reichs Patent 299,799–800, 1921.

WEICK, F. E., Drag and Cooling with Various Forms of Cowling for a "Whirlwind" Radial Air-cooled Engine, *NACA TR* 313, 1929.

TOWNEND, H., The Townend Ring, *J. Roy. Aeronaut. Soc.*, vol. 34, p. 813, 1930.

RUDEN, P., Two-dimensional Symmetrical Inlets with External Compression, *Deut. Luftfahrtforschung* F.B. 1209, 1940; or *Jahrbuch der deutschen Luftfahrtforschung* 1941, p. I 377. Translation, *NACA TM* 1279.

KÜCHEMANN, D., and J. WEBER, Über die Strömung an ringförmigen Verkleidungen, *Deut. Luftfahrtforschung* F.B. 1236, 1940; or *Schriften deut. Akad. Luftf.*, 1943.

BRÖDEL, W., The Theory of Two-dimensional Inlets with External Compression, *Deut. Luftfahrtforschung* U.M. 716, 1943; translation, *NACA TM* 1267.

LUDWIEG, H., Widerstandsmessungen an zwei Ringhauben bei hohen Geschwindigkeiten, *Deut. Luftfahrtforschung* U.M. 3026, 1943.

BAALS, D. D., N. F. SMITH, and J. B. WRIGHT, The Development and Application of High-critical-speed Nose Inlets, *NACA TR*, 920, 1949.

SMITH, N. F., Air Inlets, Papers presented at the NACA-University Conference for Aeronautics, June, 1948, p. 307.

KÜCHEMANN, D., and J. WEBER, Power Unit Ducts; the Inflow (*AVA Monograph* $J_2$3) *Brit. Min. of Supply* (*Völkenrode*) *Rept. Transl.* 985, 986, 987, 1948.

CHAPTER 5

FAIRINGS OF FINITE LENGTH

The preceding chapter was concerned with air intakes of semi-infinite length, extending to infinity downstream. The treatment given there could be applied to intakes long enough for the velocity on the outer surface to fall to a value not appreciably exceeding that of the free stream from a certain distance behind the inlet. There are various practical cases where such a simplification is justified. These are treated in Sec. 5-1, which will pay particular attention to the flow round the end of the fairing, the *afterbody*.

In other cases, the finite length cannot be ignored. We can easily imagine fairings over which the pressure is constant, under certain optimum conditions, over the whole of the outer surface from inlet to exit, without having a region of undisturbed pressure which separates the intake from the afterbody. Such fairings and their relation to certain cavitation bubbles are discussed in Sec. 5-2. Section 5-3 contains some further remarks on leading-edge intakes, with special reference to cases where the flow round the entry must be considered in conjunction with the flow past the basic airfoil in which it is housed. Comparatively short annular airfoils and double airfoils are dealt with in Secs. 5-4 to 5-8; Secs. 5-4 to 5-7 describe calculation methods for fairings of both these types, and Sec. 5-8 some measured aerodynamic characteristics.

5-1. Flow Near the End of the Fairing. As is shown in Secs. 4-5 to 4-7, the length of the intake part of a fairing is usually not more than two or three times the maximum diameter and sometimes considerably less. If a suitable shape of similar length can be found for the rear part of the fairing, it follows that a combination of intake and afterbody will give a shape with a fineness ratio of the order of 5:1. Figure 5-1 shows the considerable distance between the regions of essentially negative pressure coefficients near the entry and on the afterbody for a particular complete nacelle of fineness ratio 4. We can therefore survey the flow over and the design of the rear part of engine nacelles of this type as separate from the inflow. We confine ourselves in the main to bodies with circular cross sections.

The method of singularities can be applied in a way similar to that of Sec. 4-4; this has not so far been done, but the outline of the procedure will be clear. The walls of a body of semi-infinite length, extending to

infinity forward, are represented by an internal distribution of sources and sinks, mainly sinks. The essential difference between entries and exits is that the energy of the jet discharged from the exit is different from that of the surrounding flow. According to Sec. 3-4, this nonhomogeneous flow may be replaced by an equivalent homogeneous flow with a vortex distribution on the border of the jet. The vortices extend into the interior of the nacelle and their strength is determined by the ratio of the velocities inside and outside the jet.

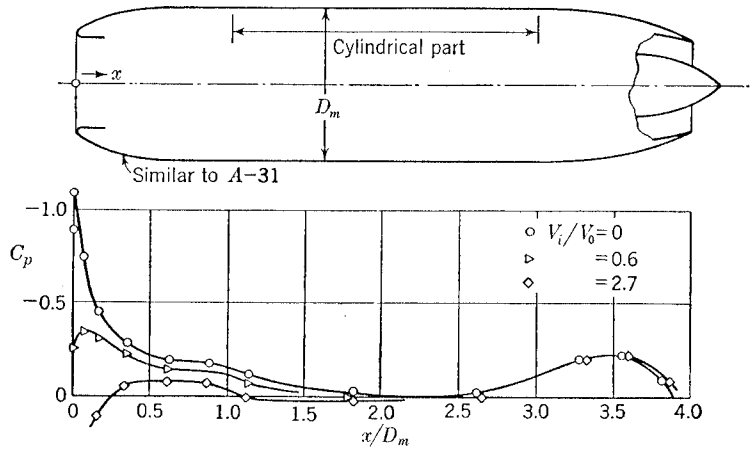

FIG. 5-1. Low-speed pressure distribution along the outer surface of a complete jet-engine nacelle.

It is not necessary to solve this problem to be able to obtain the resultant force acting on the outer surface of the afterbody. Using the momentum theorem and proceeding in much the same way as in Sec. 4-2, we find the axial force in nonviscous flow (positive in the direction of flight) to be given by

$$\frac{F_x}{\frac{1}{2}\rho V_0^2 A_m} = \frac{A_e}{A_m}\left\{-\frac{p_e - p_0}{\frac{1}{2}\rho V_0^2} + 2\left(\frac{V_e}{V_0}\right)^2\left[\sqrt{1 + \frac{p_e - p_0}{\frac{1}{2}\rho V_0^2}\frac{1}{(V_e/V_0)^2}} - 1\right]\right\}$$

$$= -\frac{1}{4}\frac{A_e}{A_m}\frac{1}{(V_e/V_0)^2}\left\{\left(\frac{p_e - p_0}{\frac{1}{2}\rho V_0^2}\right)^2 + \cdots\right\} \qquad (5\text{-}1)$$

where the symbols are defined in Fig. 5-2. Incompressible flow has been assumed. The static pressure p_e in the exit is the determining parameter. Since p_e rarely differs much from the undisturbed static pressure p_0 (except at supersonic speeds), the drag force on the afterbody will usually be small; if $p_e = p_0$ (noncontracting and nonexpanding jet), the total axial force is zero. There should be no serious difficulty, then, in designing the shape of the afterbody.

Another form of Eq. (5-1) is obtained by introducing the velocity V_j in the jet far behind the exit and assuming no losses in the jet so that Bernoulli's equation may be applied. In that case,

$$\frac{F_x}{\frac{1}{2}\rho V_0^2 A_m} = -\frac{A_e}{A_m}\left(\frac{V_j}{V_0} - \frac{V_e}{V_0}\right)^2 \qquad (5\text{-}1a)$$

These considerations are not restricted to exits of circular cross section. Further, the inner wall need not be cylindrical but can be of arbitrary shape, in which case pressures on the inner wall contribute to the total force.

The above conclusions are borne out by experiment; an example is shown in Fig. 5-3. The local suction is highest, as will be seen, at the transition from the cylindrical part of the nacelle to the curved shape of

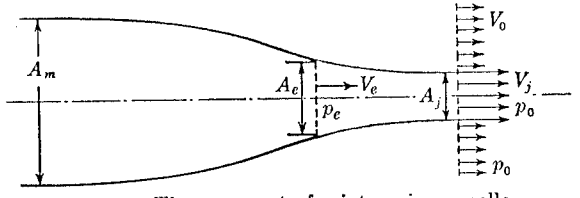

FIG. 5-2. The rear part of a jet-engine nacelle.

the beginning of the afterbody. High critical Mach numbers and consequently low velocity increments are required in this region, since any shock waves and distortion of the pressure distribution here can be expected to cause a considerable drag rise. The velocity increments can in fact be kept within reasonable limits as long as sudden changes in curvature are avoided. It appears to be sufficiently accurate to use part of an ellipsoid and to estimate the velocity increment accordingly.[1]

Turbulent mixing between the jet and the surrounding air causes an additional inflow toward the jet and can therefore modify the flow and the pressure distribution as discussed so far. The jet drags particles of air inward and gives them a radial-velocity component, reducing the pressures over the surface of the afterbody. Tests (which were made with

[1] For ellipsoids of revolution, of fineness ratio $1:\delta$, the maximum velocity increment in incompressible flow can be approximated by

$$\frac{v_{xi}}{V_0} = 0.645\delta^{\frac{2}{3}}$$

and

$$\frac{v_x}{v_{xi}} = \frac{C_p}{C_{pi}} = \frac{1}{\sqrt[4]{1 - M_0^2}}$$

for compressible subsonic flow. See D. Küchemann, *J. Aeronaut. Sci.*, vol. 18, p. 770, 1951.

a cold subsonic jet, however) have shown that the reduction of the pressure is not very large (see Fig. 5-3). The pressure decrement Δp varies approximately linearly with the exit velocity ratio and in the region of the exit is roughly given by

$$\frac{\Delta p}{\frac{1}{2}\rho V_0^2} = -0.01\left(\frac{V_e}{V_0} - 1\right) \qquad (5\text{-}2)$$

Its effect is a small increase in drag, not normally exceeding 1 to 2 per cent of the thrust in the case of a turbojet engine at subsonic speeds. It

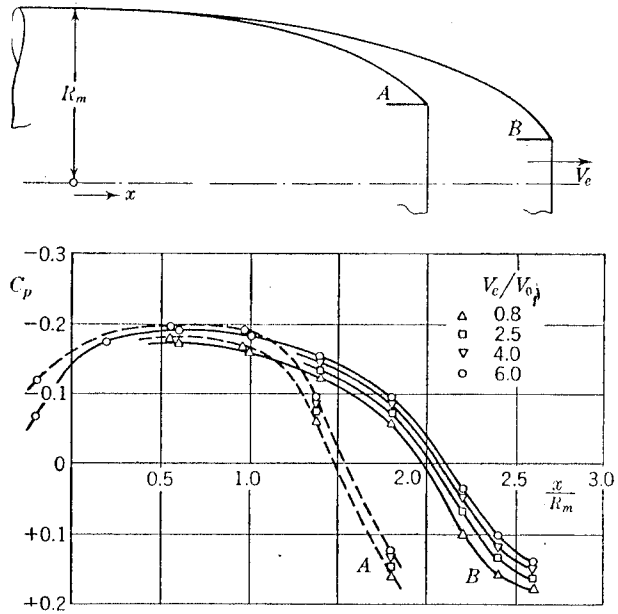

FIG. 5-3. Pressure distributions along the outer surfaces of jet-engine nacelle afterbodies of different shapes, with various jet exit velocities. (*From tests by F. Riegels and H. Eggert*, 1944.)

does not seem likely that it could be reduced by changes in the afterbody shape, nor, in the light of the present knowledge, would it really be worth while.

Attempts have been made to utilize the pressure decrement in a kind of jet pump designed to capture and accelerate a larger volume of air. This would increase the thrust and the efficiency of the engine. An annular body of diameter larger than that of the exit is situated behind the exit and is intended to experience additional thrust forces. E. N. Jacobs and J. M. Shoemaker (1932) have made experimental investigations, and a theoretical analysis has been given by A. Busemann (1939). The latter points out that the beneficial thrust increase disappears at a

certain flight speed, even if the inherent drag of the auxiliary ring is ignored. This drag will reduce the thrust still further in high-speed flight, so that the range of useful application of thrust augmentors of this type appears to be restricted to assistance at take-off, after which they would be jettisoned.

5-2. Thick Fairings with Uniform Pressure Distribution. Cavitation Method. We consider here a body of finite length which has an inlet and a duct and is symmetrical fore and aft so that its maximum thickness is at 50 per cent of its length, as in Fig. 5-4. Let the pressure distribution along the outer surface be uniform.

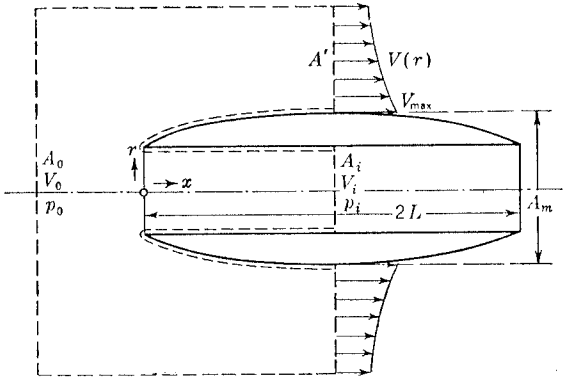

FIG. 5-4. Optimum contour of finite length with uniform pressure distribution along the outer surface.

By applying the momentum theorem as in Sec. 4-2, we get a relation between the inlet velocity ratio, the velocity on the outer surface, and the inner and outer cross-sectional areas:

$$\tfrac{1}{2}\rho(V_i - V_0)^2 A_i - \tfrac{1}{2}\rho(V_{max}^2 - V_0^2)(A_m - A_i) + \tfrac{1}{2}\rho \int_{A'} (V - V_0)^2 \, dA' = 0 \tag{5-3}$$

The surface of integration must extend a long way into the flow because the velocity on the surface of the body is nowhere equal to the undisturbed velocity, and the difficulty here lies in the evaluation of the integral involving the unknown velocity distribution away from the body in the plane of the maximum thickness.

It can be assumed that this velocity decreases from its value V_{max} at the wall according to an inverse-power law:

$$V - V_0 = \frac{V_{max} - V_0}{(r/R_m)^n} \tag{5-4}$$

where R_m is the radius corresponding to A_m. The value of n will be about 2 for long bodies of revolution and will approach 3 for short bodies. The

following relation is then obtained:

$$\frac{A_m}{A_i} \geq \frac{1 + \dfrac{(V_i/V_0 - 1)^2}{(V_{max}/V_0)^2 - 1}}{1 - \dfrac{1}{n-1}\dfrac{V_{max}/V_0 - 1}{V_{max}/V_0 + 1}} \tag{5-5}$$

The equality sign holds for optimum contours with uniform pressure distribution; if the pressure distribution is not uniform, a larger frontal area A_m is needed. This relation corresponds to Eq. (4-6), Sec. 4-2, and shows the influence of finite length.

If the area ratio for the optimum intake of infinite length is denoted by $(A_i/A_m)_0$, we see that

$$\frac{A_i/A_m}{(A_i/A_m)_0} = 1 - \frac{1}{n-1}\frac{V_{max}/V_0 - 1}{V_{max}/V_0 + 1} \tag{5-6}$$

In the practical range of V_{max}/V_0, the change in the area ratio necessary is small. With the same area ratio, the fairing of finite length has somewhat higher velocities on the outer surface than the fairing of infinite length.

The same equations are obtained for the corresponding two-dimensional flow, except that $1/(n-1)$ is replaced by $1/(2n-1)$. In this case, however, $n = 1$ for a long body and $n = 2$ for a short body.

The actual shapes of optimum fairings can be obtained experimentally by the cavitation method. Cavitation means the occurrence of *cavities* in the interior of a streaming liquid; when, in the flow past a body, for instance, the static pressure falls below the vapor pressure at some point, evaporation occurs and a bubble filled with vapor is formed. Inside the bubble the pressure must be constant and below the static pressure p_0 of the undisturbed flow. The bubble surface is a free constant-pressure boundary, and thus corresponds exactly to the case considered above.

Attempts have been made by D. P. Riabouchinsky (1920) and F. Weinig (1932) to calculate two-dimensional cavitation contours by means of the hodograph method, which lends itself to such problems. They investigated a cavitation bubble limited upstream and downstream by a flat plate. This could be taken as an approximation to represent an intake with no flow through the duct; the calculations, however, would have to be worked out in greater detail before they could be applied in practice.

An experimental method applicable to various fairing problems has been given by H. Reichardt (1944). If in a tube in a water stream with its axis in the direction of the flow the internal velocity is reduced, by the insertion of a screen for instance, a cavitation bubble is formed in the

flow outside the tube, beginning at the inlet, as shown in Fig. 5-5. In practice, the bubble is not exactly symmetrical up and down stream, as it collapses at the rear and breaks up; but the forward part up to well behind the maximum thickness gives a clear indication of the constant-pressure surface.

The method is not confined to the investigation of circular air intakes. The tube, and thus the inlet opening, may have any given cross section. Cavitation experiments are of particular value whenever theoretical information can be obtained only with great difficulty, as is the case with three-dimensional bodies of arbitrary cross section. Regions of positive pressure must be represented by solid bodies—the region near the stagnation line of a wing by a wire, the nose of a fuselage by a spherical or semi-spherical body. Wing-fuselage-intake combinations can profitably be designed in this way.

For circular air intakes of finite length, information can be gained as to the necessary area ratio and length and on the maximum velocity on the

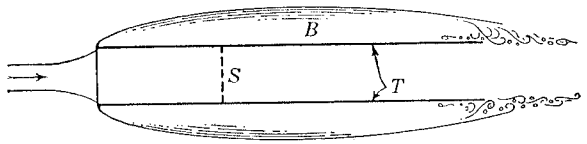

T Tube *B*: Bubble *S*: Screen

FIG. 5-5. Cavitation bubble produced by a tube with a screen inside.

outer surface. It is found that, in general, the differences between the experimental values of the area ratio and those calculated with $n = 2$ and $n = 3$ are surprisingly small and that in fact the relations derived in Sec. 4-2 for fairings of infinite length give a good approximation for practical purposes.

The length of the intake part (that is half the length of the optimum fairing as in Fig. 5-4) can be approximated, in the range of small values of V_{max}/V_0, by the empirical formula:

$$\frac{D_m}{L} = 7.8 \left\{ 1 + 0.4 \left(\frac{V_i}{V_0} \right)^2 \right\} \left(\frac{V_{max}}{V_0} - 1 \right) \qquad (5\text{-}7)$$

This expression was used to work out the curves for optimum circular-intake contours in Fig. 4-17.

The type of contour obtained by cavitation tests is illustrated in Fig. 5-6. It is markedly flatter than a half ellipse, especially near the nose. This is the reason why serious difficulties are encountered if the attempt is made to find empirically a modified entry lip with a larger nose radius, in order to avoid the undesirable qualities associated with the sharp nose. As the example in Fig. 5-6 shows, a considerable forward elongation of the

contour is necessary. Even then high values of V_{max}/V_0 cannot be avoided, so that the advantages of the *optimum contour* are easily lost in practice.

5-3. Two-dimensional Leading-edge Intakes. Air intakes in the leading edge of an airfoil usually have an inlet elongated in shape: its spanwise width is appreciably larger than its height. The flow conditions in the middle region away from the ends will approach those of a two-dimensional intake. Since an inlet of this type is an integral part of the wing, it presents not only such problems as have been considered above, but also some which concern the aerodynamic characteristics of the whole wing. While the design of an isolated intake is mainly a matter of a suitable compromise between the conflicting requirements of the inflow conditions in high-speed flight and at take-off, the design of a leading-edge inlet must also take into account the circulation round the wing, which causes an asymmetry in the flow round the nose.

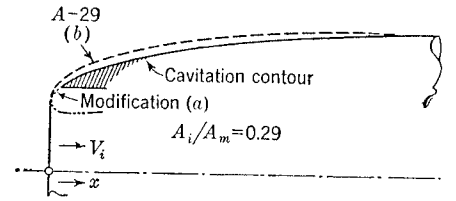

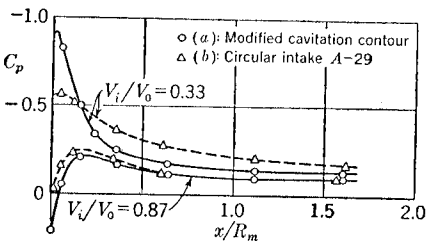

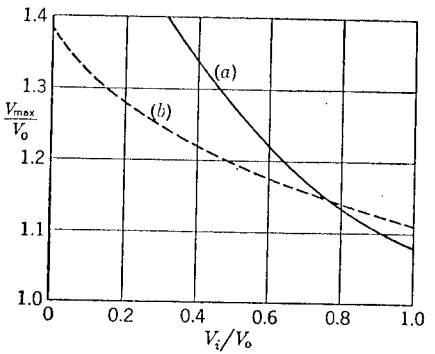

FIG. 5-6. Low-speed pressure distributions along the outer surface of a modified cavitation contour (by H. Reichardt) compared with that on a circular intake of the A-series.

Neither theoretical nor experimental investigations have progressed very far. The conformal-mapping method of W. Perl and H. E. Moses (1947), although complicated, is an extensive theory sufficiently advanced for numerical purposes. In these calculations, any object inside the duct is ignored; that is, a plain empty duct is considered but both variable inlet velocity ratio and angle of attack of the whole ducted wing can be adequately represented, the former by variation of the exit area.

Another theory for two-dimensional airfoils with ducts has been given by G. Temple and J. Yarwood (1944). Here again the special case of shapes with uniform velocity distribution is treated. Descriptions of further methods are given by H. J. S. Hughes (1944) and G. H. Peebles (1947).

For thin basic wing sections (of the order of 10 per cent or less) the results of Sec. 4-5 for two-dimensional intakes of semi-infinite length may be applied by merging the shapes deduced there into the given basic section. We find that the small nose radii of *optimum* shapes with uniform pressure distribution over the intake part are particularly undesirable in the case of leading-edge entries; in addition to their sharp pressure peaks at small inlet velocity ratios and high inflow losses at high inlet velocities, they suffer from a proneness to separation at the inner surfaces of the lower lip (with subsequent inflow losses) even at small incidences. Furthermore, the maximum lift of the airfoil section will be reduced.

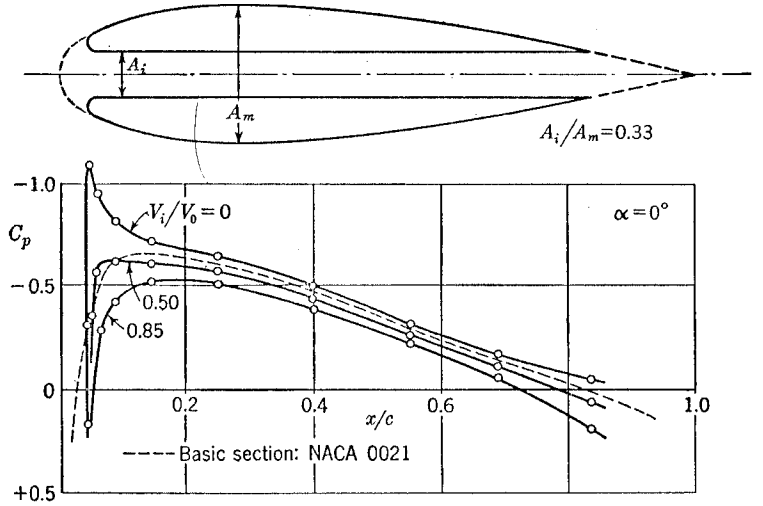

FIG. 5-7. Low speed pressure distribution along the outer surface of a wing with nose intake and duct.

This calls for nose shapes which are well rounded on the inside as well as on the outside. The use of elliptical entry shapes, similar to those of Sec. 4-6, but with their lengths adapted to the two-dimensional case (Fig. 4-13) might therefore be suggested. The calculation method of Perl and Moses mentioned above has not yet been applied to such shapes. However, it should provide a means of checking how much justification there is for the above simplification of combining isolated entry shapes of known characteristics with a basic airfoil section to form a ducted wing.

When the thickness-chord ratio is much larger than about 10 per cent, the basic airfoil has an appreciable influence on the flow round the entry. The pressure distribution of the basic section might even predominate if it is very thick, as it will be when intakes are installed in thickened wing roots. Figure 5-7 illustrates this for an example where the thickness-chord ratio of the basic section is 21 per cent. At large inlet velocity ratios ($V_i/V_0 = 0.85$), the presence of the intake reduces the effective thickness-chord ratio by the relieving effect of the mass flow through the section. At $V_i/V_0 = 0.5$, the undisturbed pressure distribution of the basic airfoil is nearly restored; but at smaller inlet velocity ratios there is a pronounced pressure peak in consequence of the thrust forces at the entry.

Swept leading-edge intakes are used for their expected favorable influence on the external flow, especially in high-speed flight. We have shown in Sec. 4-2 that the total external suction is the same whether the intake is swept or unswept.[1] Beneficial effects of sweep can, however, arise from favorable interactions between the suctions on the entry lips and the basic pressure distribution on the wing. Such favorable interactions are possible if the intake is placed near the root of a sweptback wing. Here, the pressure on the basic wing is reduced in the region ahead of the maximum thickness and increased behind, as compared with a section further out on the basic wing. The sweep of the isobars, *i.e.*, lines of constant pressure, is reduced accordingly, and the local critical Mach number, where sonic velocity is first reached, is usually lower in the central region than further outboard. The air intake can now be used to fill up the low-velocity region behind the leading edge so as to produce a smooth pressure distribution along the chord with approximately straight isobars, with the peak suction position on a continuation of the swept peak suction line further outboard on the wing. The effective sweep may even be increased. The incorporation of the air intake usually involves a shift of the maximum thickness position toward the leading edge and sometimes makes it possible to thicken the section.

Air intakes at the roots of a sweptforward wing cannot improve the flow there, on the other hand; the pressure distribution on the basic wing already has pronounced peaks near the leading edge.

With all intakes, staggering the entry lips one behind the other lowers the suction on the protruding lip and increases the suction on the rear lip (see Sec. 4-8). The effect is comparatively small, however, at inlet velocity ratios above about 0.6 if the basic airfoil is so thick that, as discussed above, its own pressure distribution predominates anyway. A drastic reduction of the pressure peak at, say, the upper lip can be achieved by giving it a greater wall thickness everywhere, making the entry asymmetric. This is the same effect as was mentioned in the discussion of egg-shaped and three-dimensional nose intakes in Sec. 4-8.

[1] This is strictly true only for optimum shapes in their design condition. For a given intake in compressible flow, there may be some further benefit from sweeping the intake in that the pressure coefficient rises more slowly with Mach number than it would do at an unswept intake, as seen from Eq. (4-19).

The maximum lift coefficient of an airfoil section with a properly designed air intake can actually exceed that of the corresponding basic airfoil. The value of $C_{L\max}$ depends on the inlet velocity ratio, as can be seen from Fig. 5-8. High inlet velocity ratios are favorable to maximum lift; but a low inlet velocity, as in landing with engines throttled, will have a detrimental effect.

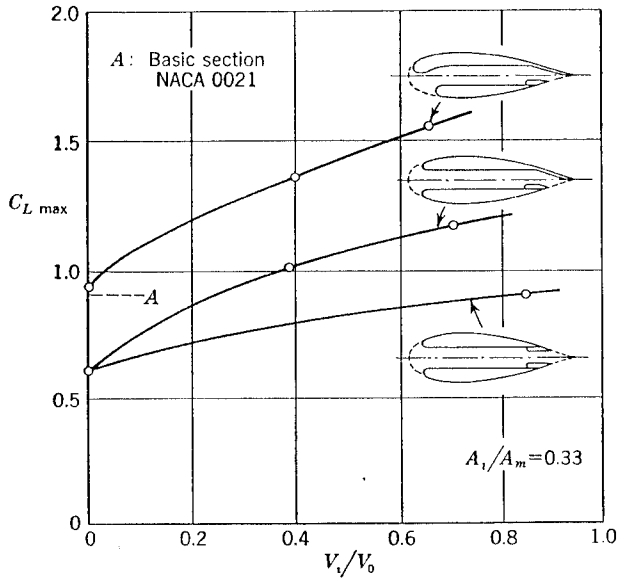

FIG. 5-8. Maximum lift coefficients of three wings with nose intakes and ducts. Aspect ratio 2.4 with end plates; effective aspect ratio 5.6; Reynolds number 1×10^6.

5-4. Theory of Thin Annular Airfoils. If the length of the fairing is not more than about two diameters (examples are cowlings of radial engines, ducted coolers, and ducted screws for ship or aircraft propulsion), the fairing must be treated as a whole. In general, the high-speed requirement that the velocity increments must be kept down is not so severe in these cases, since these cowlings are mostly employed on comparatively slow aircraft. But the problem of regulating the flow through the duct gains importance and, in many cases, it cannot be assumed that the flow is uniform across the duct. This implies that the simple one-dimensional treatment must be replaced by a more thorough investigation of the two-dimensional flow. The fairing is therefore considered as an airfoil; either an *annular* airfoil, in the case of rotational symmetry, or a *double* airfoil, in the two-dimensional case.

The rate of flow through either type of airfoil arrangement is regulated by the circulation, which becomes of primary interest; the influence of the finite thickness is less significant. In terms of the theory of ordinary single airfoils, it is not so much the thickness effect but rather the lift which is of immediate importance, since the lift, with its differences in velocity between upper and lower surfaces, is closely related to the velocity difference between the outer and inner flow. As a first step, then, thin annular or double airfoils can usefully be treated as being of zero thickness. The isolated airfoil is first considered. The method is such as to allow of extension without difficulty to airfoils in the field of flow of disturbing bodies, such as other members of the propulsion unit.

The theory of thin annular airfoils is explained more fully than might be warranted by the importance of its application to short cowlings and fairings. The reason for this is that the method employed is also applicable to any three-dimensional body which may be replaced by a distribution of vortices, as, for instance, in the design of special fuselage and nacelle shapes. We follow closely the procedure of W. Birnbaum (1923) and H. Glauert (1926), except that no use will be made of conformal transformations because we are not only considering two-dimensional airfoils.

The annular airfoil is replaced by a vortex distribution $\gamma(x)$ on its camber line, extending from $x = 0$ to $+1$, where x is measured as a fraction of the chord L. As in Sec. 3-5, the axial and radial velocity components v_x and v_r induced by this vortex distribution are related to the shape $r(x)$ of the airfoil by the streamline condition:

$$\frac{dr}{dx} = \frac{v_r(x,r)}{V_0 + v_x(x,r)} \tag{5-8}$$

Two main problems may be distinguished:

1. Given the vortex distribution, to find the corresponding shape and determine its aerodynamic characteristics.
2. Given the shape, to find the corresponding vortex distribution, from which the aerodynamic characteristics can then be determined.

In either case, by aerodynamic characteristics we mean the pressure distribution along the contour and the resultant forces, and also the velocity distribution inside the ring and the rate of flow. Special difficulties arise in each case from the fact that the vortex distribution is to be placed on the airfoil contour, and one or the other is not known. This is the same problem as was discussed in Sec. 3-5 and, in general, a solution can only be obtained by successive approximations.

As in standard airfoil theory, a first approximation is obtained by assuming the vortex distribution to be on a cylinder of radius R_0 (where R_0 is the mean distance from the axis to the chord line) and also calculating the induced velocities there only.

The induced velocity field of a single vortex ring of radius R_0 and strength Γ is treated in Sec. 5 of the Appendix and tables for the velocity

components

$$v_x\left(\frac{x}{R_0};\frac{r}{R_0}\right) = \frac{\Gamma}{2\pi R_0} v_x^*\left(\frac{x}{R_0};\frac{r}{R_0}\right)$$
$$v_r\left(\frac{x}{R_0};\frac{r}{R_0}\right) = \frac{\Gamma}{2\pi R_0} v_r^*\left(\frac{x}{R_0};\frac{r}{R_0}\right) \qquad (5\text{-}9)$$

are given there. Then the components of the velocity[1] induced by a distribution $\gamma(x)$ of vortex rings are

$$v_x(x,R_0) = \frac{1}{2\pi}\int_0^{L/R_0} \gamma(x') v_x^*\left(\frac{x-x'}{R_0/L},1\right) d\left(\frac{x'}{R_0/L}\right) \qquad (5\text{-}10)$$

$$v_r(x,R_0) = \frac{1}{2\pi}\int_0^{L/R_0} \gamma(x') v_r^*\left(\frac{x-x'}{R_0/L},1\right) d\left(\frac{x'}{R_0/L}\right) \qquad (5\text{-}11)$$

Since x is measured as a fraction of the chord L here, the parameter L/R_0 occurs in these relations. This parameter is a measure of the *curvature* of the airfoil in a transverse plane. $L/R_0 = 0$ denotes the two-dimensional case.

One way of obtaining numerical results is to approximate the distribution $\gamma(x)$ by the Birnbaum series of standard functions:

$$\gamma(x) = \sum_\nu \gamma_\nu(x) \qquad (5\text{-}12)$$

where

$$\gamma_1(x) = 2\pi V_0 c_1 \sqrt{\frac{1-x}{x}}$$

with the total circulation

$$\Gamma_1 = L\int_0^1 \gamma_1(x)\,dx = \pi^2 L V_0 c_1$$

and

$$\gamma_2(x) = 2\pi V_0 c_2 \sqrt{1-(2x-1)^2}$$

with the total circulation

$$\Gamma_2 = \frac{\pi^2}{2} L V_0 c_2$$

and

$$\gamma_3(x) = -2\pi V_0 c_3 (2x-1)\sqrt{1-(2x-1)^2}$$

with the total circulation

$$\Gamma_3 = 0$$

The c_ν are parameters which determine the strength of the vorticity. In the two-dimensional case, γ_1 gives a flat plate at incidence, γ_2 a parabolic arc, and γ_3 an S-shaped airfoil.

[1] These do not contain the contribution of the vortex ring at $x' = x$, which is, of course, $\pm\gamma(x)/2$.

The integrations in Eqs. (5-10) and (5-11) can be carried out only numerically. For convenience, the velocity components obtained from the integration,

$$v_{x\nu}^* = \frac{1}{c_\nu}\frac{v_{x\nu}}{V_0} \qquad \text{and} \qquad v_{r\nu}^* = \frac{1}{c_\nu}\frac{v_{r\nu}}{V_0}$$

are also tabulated in Sec. 9 of the Appendix for these functions and for various values of $L/2R_0$. There are marked differences from the corresponding values for two-dimensional airfoils, the most striking being that the induced velocity has nonzero axial components, since the streamlines of an isolated vortex ring are no longer circles.

The shape of the airfoil is obtained from the streamline condition (5-8) which now reads:

$$\left(\frac{dr}{dx}\right)_{x=x_\mu} = \frac{\sum_{\nu=1}^{n} c_\nu v_{r\nu}^*(x_\mu,R_0)}{1+\sum_{\nu=1}^{n} c_\nu v_{x\nu}^*(x_\mu,R_0)} \qquad (5\text{-}13)$$

n is the number of standard vortex distributions combined [here, $n = 3$, by Eq. (5-12)] and therefore determines the number of points $x = x_\mu$ where the streamline condition can be satisfied. Equation (5-13) is a system of equations from which to work out either the shape

$$r(x) = \int_0^x \frac{dr}{dx}\,dx + R_0 \qquad (5\text{-}14)$$

from given values of c_ν, or the values of c_ν for a given shape.

When the coefficients c_ν are known, the pressure distribution along the surface of the airfoil can be obtained from

$$C_p = 1 - \left[1 + \sum_\nu c_\nu\left(v_{x\nu}^* \pm \frac{\gamma_\nu}{2V_0 c_\nu}\cos\vartheta\right)\right]^2 - \left[\sum_\nu c_\nu\left(v_{r\nu}^* \pm \frac{\gamma_\nu}{2V_0 c_\nu}\sin\vartheta\right)\right]^2 \qquad (5\text{-}15)$$

where at any point $\vartheta = \arctan(dr/dx)$ is the angle between the tangent to the profile and the direction of the free stream. The negative sign within the brackets refers to the outer surface and the positive sign to the inner surface of the airfoil. Obviously, when the circulation is small (which it should be anyway) Eq. (5-15) can be simplified by the assumption that ϑ is small, so that $\cos\vartheta = 1$ and $\sin\vartheta = \vartheta$, and the term $\gamma_\nu \sin\vartheta$ can usually be neglected.

5-5. Constant-load Camber Lines. As with ordinary airfoils, camber lines which give a constant load over the whole chord are of special interest. These are included in the standard NACA series of camber lines, and for both two-dimensional and annular airfoils they are obtained from a constant distribution of vorticity, $\gamma_4(x) = \text{const} = 2\pi V_0 c_4$, to a first approximation.[1]

In this case, the integrals for the velocity components, Eqs. (5-10) and (5-11), can be solved explicitly. This is shown in Sec. 9 of the Appendix; the final result is

$$\frac{v_{x4}}{V_0} = -c_4 \left[\sqrt{1 - k^2}\, \mathsf{K}(k)\right]_{k_1}^{k_2} \tag{5-16}$$

where K is the complete elliptical integral of the first kind in Legendre's standard form (see, for example, E. Jahnke and F. Emde, 1933). The modulus k is

$$k = \frac{1}{\sqrt{1 + \left(\dfrac{x - x'}{2R_0/L}\right)^2}} \tag{5-17}$$

The limits k_1 and k_2 are the values of k for $x' = 0$ and $x' = 1$, respectively. The induced radial velocity is

$$\frac{v_{r4}}{V_0} = -c_4 [k\{\mathsf{K}(k) - 2\mathsf{D}(k)\}]_{k_1}^{k_2} \tag{5-18}$$

where $k^2\mathsf{D} = \mathsf{K} - \mathsf{E}$ and E is the complete elliptic integral of the second kind.

For the corresponding two-dimensional distribution, $v_{x4} = 0$ of course, and

$$\frac{v_{y4}}{V_0} = -c_4 \ln \frac{1 - x}{x}$$

The logarithmic infinity of v_y at $x = 0$ and $x = 1$ gives a vertical camber line tangent at both leading and trailing edges. The same singularity occurs with the annular airfoil.

It is useful to have another vortex distribution of the same family which gives an S-shaped camber line. We put

$$\gamma_5(x) = -2\pi V_0 c_5 (2x - 1) \tag{5-19}$$

The integrals for the velocity components of this linear distribution can also be solved explicitly, and we find

$$\frac{v_{x5}}{V_0} = +c_5 \left[(2x - 1)\sqrt{1 - k^2}\, \mathsf{K}(k) + \frac{2R_0}{L} 2\{k[\mathsf{K}(k) - \mathsf{D}(k)]\} \right]_{k_1}^{k_2} \tag{5-20}$$

[1] This case has also been treated by C. H. E. Warren, 1945.

$$\frac{v_{r5}}{V_0} = +c_5 \left[(2x - 1)\{k[\mathsf{K}(k) - 2\mathsf{D}(k)]\} - \frac{2R_0}{L} 2\{\sqrt{1 - k^2}\,[\mathsf{K}(k) - \mathsf{D}(k)]\} \right]_{k_1}^{k_2} \tag{5-21}$$

The radial velocity again has a logarithmic infinity at both leading and trailing edges, as in the two-dimensional case where

$$\frac{v_{y5}}{V_0} = +c_5 \left[2 + (2x - 1) \ln \frac{1 - x}{x} \right]$$

The integration of the streamline condition (5-8) to obtain the shape of the camber line has to be done numerically. The velocity components from Eqs. (5-16), (5-18), (5-20), and (5-21) are therefore also given in the tables in Sec. 9 of the Appendix.

For the corresponding two-dimensional airfoils, the following explicit expressions are obtained:

$$y_4(x) = -c_4 \left\{ (2x - 1) \ln \frac{1 - x}{x} - \ln [1 - (2x - 1)^2] \right\}$$

$$y_5(x) = +c_5 \left\{ 2x - 1 - \frac{1}{2}[1 - (2x - 1)^2] \ln \frac{1 - x}{x} \right\}$$

While this suggests that an expansion of $\gamma(x)$ in a power series might provide a general solution for thin annular airfoils, another way of simplifying the analysis is to expand the integrands in Eqs. (5-10) and (5-11) in powers of $(x - x')/R_0$ and the vortex distribution into a Fourier series. The integrals can then be solved explicitly. This method was suggested by H. E. Dickmann (1940). It is only applicable when $L/2R_0 < 1$, that is, for very short rings.

5-6. Forces on and Rate of Flow through Annular Airfoils. The aerodynamic properties of annular airfoils can be determined if the vortex distribution and the induced velocities are known.

There is a radial force F_r per unit length of the circumference, given by the Kutta-Joukowsky theorem[1] as

$$F_r = -\rho L \sum_\nu \int_0^1 \gamma_\nu(x)[V_0 + v_{x\nu}(x)]\, dx$$

with the coefficient

$$C_r = \frac{F_r}{\frac{1}{2}\rho V_0^2 L} = -2 \sum_\nu c_\nu \int_0^1 \frac{\gamma_\nu(x)}{V_0 c_\nu}\, dx - 2 \sum_\nu c_\nu^2 \int_0^1 \frac{\gamma_\nu(x)}{V_0 c_\nu} v_{x\nu}^*(x)\, dx \tag{5-22}$$

This shows that the radial force coefficient, which corresponds to the lift

[1] Mixed terms, such as $\gamma_1 v_{x2}$, are ignored here.

coefficient of ordinary airfoils, does not depend linearly on the strength of the vorticity. A theoretical maximum is reached when the circulation is so strong as to prevent any flow through the interior.

In the absence of disturbing bodies, the axial force

$$F_x = \rho \sum_\nu \int_0^1 \gamma_\nu(x) v_{r\nu}(x)\, dx - 2\pi^3 c_1^2 \tfrac{1}{2} \rho V_0^2 L \tag{5-23}$$

must vanish. The second term in this equation represents that part of F_x which is derived from the (infinitely high) suction force at the (infinitely thin) leading edge; the same term is obtained for the thin two-dimensional plate at incidence.

The method of calculation described will be used mainly to estimate the mass flow through the duct. If the vortex distribution which represents the airfoil is known, the velocity distribution across any given section of the duct can be determined. If only a mean value is wanted, the total mass flow through the interior can be deduced simply from the value of the stream function on the stagnation streamline. The ratio of Ψ_{TE}, the stream function at the trailing edge, to $R_0^2 V_0/2$, which would be the value of the stream function at that point if the airfoil were not there, gives the mass flow ratio.

In practice, it is often useful to work in terms of the mean velocity increment δ, given by

$$1 + \delta = \frac{\Psi_{TE}}{\frac{1}{2} R_0^2 V_0}$$

$$= \left(\frac{R_{TE}}{R_0}\right)^2 + \sum_\nu \frac{c_\nu}{\pi} \int_0^{L/R_0} \frac{\gamma_\nu\left(\frac{x'}{R_0}\right)}{c_\nu V_0} \Psi_\gamma{}^*\left(\frac{1 - x'}{R_0/L}; \frac{R_{TE}}{R_0/L}\right) d\left(\frac{x'}{R_0/L}\right) \tag{5-24}$$

where the nondimensional stream function of a single vortex ring

$$\Psi_\gamma{}^*\left(\frac{x - x'}{R_0}; \frac{r}{R_0}\right) = \frac{2\pi}{\Gamma R_0} \Psi\left(\frac{x - x'}{R_0}; \frac{r}{R_0}\right)$$

can be obtained from tables given in Sec. 5 of the Appendix.

The first term on the right-hand side of Eq. (5-24) is the value which would be obtained for $1 + \delta$ if the static pressure in the exit were equal to the static pressure p_0 of the undisturbed flow, as is usually assumed in a one-dimensional treatment. The second term gives the correction to this first approximation. The correction term q_ν, defined by

$$1 + \delta = \left(\frac{R_{TE}}{R_0}\right)^2 + c_\nu q_\nu \tag{5-25}$$

is given in Table 5-1 for the first two standard distributions of vortices.

TABLE 5-1. VALUES OF q_ν

$L/2R_0$ or $L/2Y_0$	Vortex distribution γ_1		Vortex distribution γ_2	
	Annular	Double	Annular	Double
0.5	2.2	1.9	1.7	1.3
1.0	1.8	1.9	1.8	1.6
1.5	1.6	1.9	1.8	1.7
2.0	1.3	1.8	1.7	1.7
3.0	...	1.5	...	1.7
4.0	...	1.2	...	1.6

The corresponding values for the two-dimensional double airfoil are also given, since the method is not confined to annular airfoils only. In evaluating the above values of q_ν, the simplification has been made that $R_{TE} = R_0$ inside the integral. The error introduced by this is usually small.

If the chord of the airfoil is of the order of one diameter or less, the velocity distribution across the duct is usually not uniform and the above corrections matter. This is shown in an example in Fig. 5-9. The

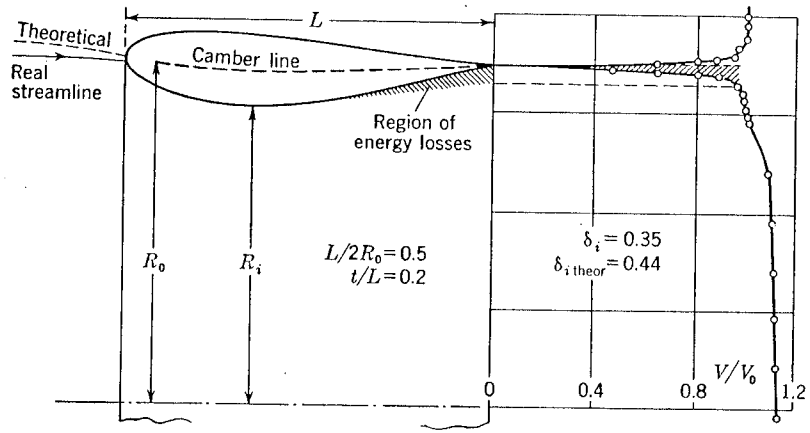

FIG. 5-9. Thick annular airfoil, with measured velocity distribution in the exit plane.

velocity distribution across the duct can be calculated directly from the vortex distribution, using Eq. (5-10) with $0 \leq r \leq R_0$.

The mass flow through an annular airfoil is also influenced by its thickness. Annular airfoils of finite thickness and comparatively small chord have as yet not been thoroughly treated. In all cases where only an estimate of the mass flow is wanted, but no detailed pressure distribution along the surface, it is permissible simply to add a suitable thickness distribution to the infinitely thin skeleton line. If the thickness is added

case in point but again only the various methods of calculation which have been used are likely to be of value to us.

5-8. Some Experimental Measurements of the Characteristics of Annular Fairings. A number of annular airfoils have been tested alone in wind tunnels, and the experimental results can be used to assess the value of the methods of the last three sections. Most of the airfoils were intended for application to ducted propellers (see Chap. 6), and this accounts for the comparatively large nose radii of most of them.

Calculated mean velocity increments δ_i for various annular airfoils are compared with measured values in Fig. 5-11.[1] The chord-diameter ratio of most of the airfoils was about 1, but some are included with $L/2R_0 = 2$

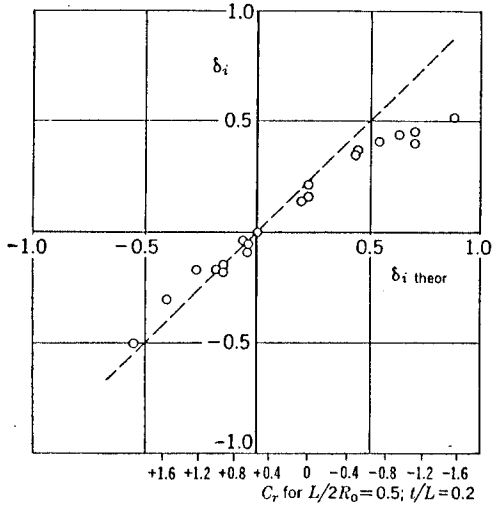

FIG. 5-11. Comparison between measured and calculated mean velocity increments for various annular airfoils.

and 0.5. The thickness-chord ratio was usually about 20 per cent, but a few were thinner, down to 10 per cent. A typical shape is shown in Fig. 5-9. It will be seen that the agreement between calculation and experiment is satisfactory. There are appreciable deviations, amounting to more than 20 per cent, when the radial-force coefficient exceeds about $C_r = -0.6$; the actual velocity increment is smaller than that predicted. This is to be expected from the pressure distribution in the diffuser (see Fig. 5-10) and as a consequence of the presence of a boundary layer (see Fig. 5-9). At positive radial-force coefficients (velocity in the duct reduced below the free-stream velocity), the range of agreement is greater, and extends up to radial-force coefficients of about 1.0 to 1.2. In general, it is easier to achieve a given mean velocity increment with an airfoil of

[1] Each point in Figs. 5-11 and 5-12 corresponds to one annular airfoil.

larger chord than with a very short airfoil, since a lower C_r, which appears to be the governing parameter, is needed for a given δ_i the larger the chord of the airfoil. The assumption that the static pressure in the exit is equal to the free-stream static pressure can only give a very rough estimate, as the exit velocity distribution in Fig. 5-9 shows.

An effective method of regulating and increasing the mass flow through an annular airfoil is by the application of flaps, or better still suction, at the trailing edge, as the shape of the pressure distribution in the diffuser suggests. Tests by B. Regenscheit (1944) have shown that δ_i can be raised from about 0.5 to about 2.0 by removing air at a volume flow rate of the order of $0.3V_0\pi R_i^2$ by suction.

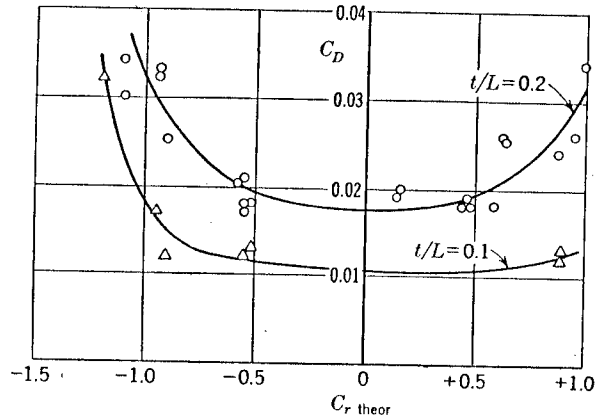

FIG. 5-12. Measured profile drag of various annular airfoils. Reynolds number about 0.5×10^6.

The drag of the airfoil is closely related to the rate of flow. It consists only of *profile drag;* there is no induced drag because there are no trailing vortices in symmetrical flow. At $C_r = 0$ and $\delta = 0$, the profile drag is about the same as that of ordinary airfoils of the same thickness-chord ratio at the same Reynolds number. This can be seen from Fig. 5-12, where a measured drag coefficient

$$C_D = \frac{\text{drag}}{\frac{1}{2}\rho V_0^2 2\pi R_i L}$$

has been plotted. The increase of C_D as C_r increases or decreases from zero appears to be slightly steeper than that observed with corresponding ordinary airfoils.

If the whole annular airfoil is at an incidence, a real lifting force occurs and, because there are now trailing vortices, an induced drag. This has been measured by H. Muttray (1941) who found that the airfoil can be compared with a biplane the *wing area* of which is $S = 2DL$ and the *span*

symmetrically on either side of the camber line, as in Fig. 5-9, the two main errors tend to cancel one another. In the first instance, the thickness of the airfoil will decrease the mass flow through the interior below that through the infinitely thin airfoil. On the other hand, a thick section symmetrical about the camber line is obtained only if a further vortex distribution is added, and that will increase the mass flow (*cf.* Sec. 4-4 and Fig. 4-9). This means that the thickness can be taken into account, to a first approximation, merely by considering the equation of continuity. The mean velocity increment at the smallest inner cross section with radius R_i is then

$$\delta_i = \frac{1 + \delta}{(R_i/R_0)^2} - 1 \tag{5-26}$$

where δ is the value for the infinitely thin airfoil.

To illustrate the method, and to show the influence of the curvature of the ring airfoil by comparing it with the straight two-dimensional airfoil, some results for conical configurations with $dr/dx = \pm 0.2$ are given in Fig. 5-10. The case of the convergent cone (decreased rate of flow through) with $L/2R_0 = 1$ is obtained by taking $c_1 = -0.0609$, $c_2 = -0.0320$, and $c_3 = -0.0106$, with Eq. (5-13) satisfied at the points $x = 0$, $x = 0.5$, and $x = 1$. Figure 5-10 shows that the surface pressure distribution is considerably different from that of the flat plate. The center of pressure is obviously no longer at the quarter-chord point; the curvature of the airfoil has the effect of moving it back. In the case of the divergent cone (increased rate of flow through) this is even more pronounced; the main aerodynamic loading is on the inner surface. This explains why a diffuser with its cone angle equal to the angle of incidence of a corresponding ordinary airfoil is far less efficient aerodynamically than the ordinary airfoil.

5-7. Theory of Thin Double Airfoils. We can employ the same method of superposing standard vortex distributions for the investigation of thin double airfoils. Consider two parallel lines of length L which are a distance $2Y_0$ apart. To the first approximation, vortex distributions $\gamma(x)$ on these lines produce infinitely thin double airfoils whose shape $y(x)$ can be calculated in exactly the same way as that described above for thin annular airfoils. The only difference is in the kernel functions in the integral equations (5-10) and (5-11), which are replaced by

$$v_x(x,Y_0) = \frac{1}{2\pi} \int_0^{L/Y_0} \gamma(x') \frac{2}{\left(\frac{x - x'}{Y_0}\right)^2 + 4} d\left(\frac{x'}{Y_0}\right) \tag{5-27}$$

$$v_y(x,Y_0) = \frac{1}{2\pi} \int_0^{L/Y_0} \gamma(x') \frac{4}{\frac{x - x'}{Y_0}\left[\left(\frac{x - x'}{Y_0}\right)^2 + 4\right]} d\left(\frac{x'}{Y_0}\right) \tag{5-28}$$

These integrals have been evaluated and are tabulated in Sec. 11 of the Appendix, for the same standard vortex distributions as above.

In Fig. 5-10, this numerical method is applied to the double airfoil which corresponds to the annular cone. It will be seen that the pressure distribution and the aerodynamic loading are distorted in the same way but not as much as was found with annular airfoils.

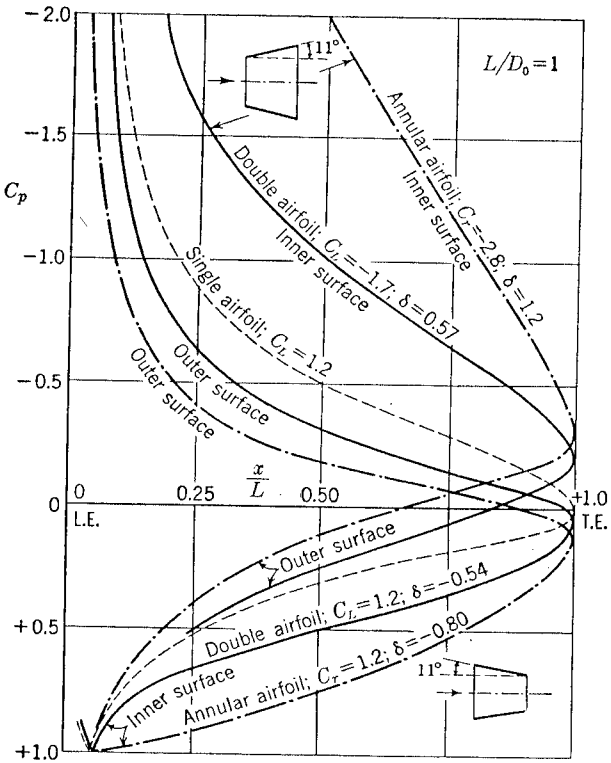

FIG. 5-10. Calculated pressure distributions for two conical annular airfoils and converging and diverging two-dimensional double airfoils, and for the corresponding two-dimensional flat plate at angle of incidence 11°.

A number of other problems with quite different practical applications are closely related to the one that we are dealing with here. One is the calculation of the characteristics of an airfoil in the proximity of the ground, treated by the method of conformal transformations by S. Tomotika and others (1935 and 1939). Few of the results are of any use here since most attention has of course been given to the influence of the ground on the lift in this case. There is reasonable agreement between the results of the exact method and those of the approximate numerical method described here, however. The biplane of infinite span is another

$b = D$. Referring the lift coefficient C_L and the induced drag coefficient C_{Di} to this area, he suggests the following relation:

$$C_{Di} = \kappa \frac{S}{\pi b^2} C_L^2 = \kappa \frac{2L}{\pi D} C_L^2 \tag{5-29}$$

where the value of κ is taken from the ordinary biplane theory as 0.55, assuming the distance between the wings to be equal to the span.

The mean velocity increment δ_i does not vary very rapidly with incidence. It can be taken as practically constant within an incidence range of about $\pm 10°$, if the nose radius is not too small. Very large chord-diameter ratios combined with a large nose radius may result in extreme insensitivity to angle of incidence. This can be made use of in the design of instruments for the measurement of velocities the direction of which is liable to change. Figure 5-13 shows an example; the tube shown was designed by W. Krüger (1942) to magnify the dynamic pressure reading, with the further special aim of making the reading independent of the angle of incidence.

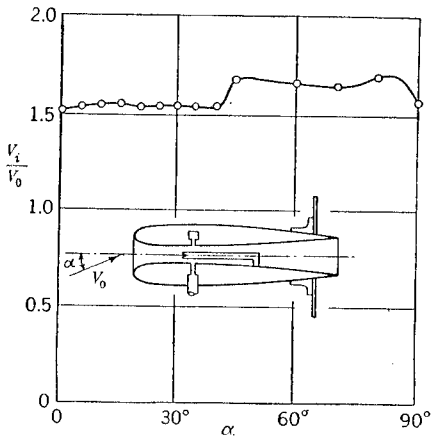

FIG. 5-13. Measured velocity over a range of angles of incidence in an annular airfoil airspeed indicator with a split flap, by W. Krüger, 1942.

5-9. Distribution of Thrust and Drag Forces on the Complete Fairing. The fairing is always an integral part of an engine nacelle and as such it takes part of the engine thrust. This is given by Eq. (2-28) as

$$T = \rho V_i A_i (V_j - V_0) = \frac{1}{2} \rho V_0^2 2 \frac{V_i}{V_0} \left(\frac{V_j}{V_0} - 1 \right) \tag{5-30}$$

(positive in the direction of flight), where V_j is the velocity far downstream in the jet. So far we have considered only the individual components of this resultant thrust, such as the suction force at the inlet (in Sec. 4-2) or the forces on the afterbody (in Sec. 5-1). We shall now illustrate by a few examples how the forces on the various surfaces can be summed and shown equal to the thrust.

There will be no over-all thrust, or drag, on a fairing alone in a nonviscous stream, and the various components must add up to zero. We have already seen in Sec. 5-6 that the axial force on thin annular airfoils vanishes. Consider now an empty fairing as shown in Fig. 5-14, assumed to be long enough to have the forces on the inlet separated from those on

the afterbody. The contraction near the end of the duct causes the velocity V_i at the inlet to be lower than the free-stream velocity V_0, and the corresponding thrust force at the nose is

$$F_N = \frac{1}{2} \rho V_0^2 A_i \left(1 - \frac{V_i}{V_0} \right)^2 \tag{5-31}$$

by Eq. (4-3). Further, there is a drag force $-F_A$ on the afterbody as given by Eq. (5-1). This is not zero if, as drawn, the flow contracts downstream of the nozzle and only reaches the final velocity value V_0 far behind the exit. We then obtain from Eq. (5-1a)

$$F_A = -\frac{1}{2} \rho V_0^2 A_e \left(1 - \frac{V_e}{V_0} \right)^2 \tag{5-32}$$

Finally, another drag force, $-F_n$, acts upon the inner walls of the nozzle as a consequence of the pressure being higher there than in the free stream.

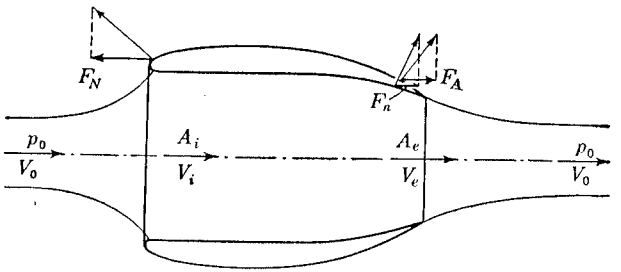

FIG. 5-14. Forces on a fairing with free flow through the interior.

A simple way of determining F_n is to apply the momentum theorem to the flow bounded by the inlet area A_i, the inner walls of the duct, and the exit area A_e. As explained in Sec. 2-3, we obtain

$$F_n = -\frac{1}{2} \rho V_0^2 A_i \left(1 - \frac{V_i}{V_0} \right)^2 + \frac{1}{2} \rho V_0^2 A_e \left(1 - \frac{V_e}{V_0} \right)^2 \tag{5-33}$$

There are no further axial forces on the fairing as the remaining walls of the fairing are assumed to be cylindrical, and we find

$$T = F_N + F_A + F_n = 0$$

that is, the thrust on the nose is compensated by a drag on the afterbody and a drag inside the nozzle.

Another simple case, in which a nonzero over-all drag is obtained, is that of a screen inserted into the cylindrical duct of a fairing of finite length (but again long enough to allow the flow around the intake to be separated from that around the afterbody), as shown in Fig. 5-15. The pressure behind the screen is assumed to be equal to the undisturbed

pressure p_0, that is, the emerging "jet" is cylindrical. The solidity of the screen may be such as to produce a velocity V_i in the duct which is smaller than V_0. The thrust force F_N on the nose of the intake is again given by Eq. (5-31), and the force F_A on the afterbody from Eq. (5-1) is zero in this case because $p_e = p_0$. There is a drag force on the screen

$$F_S = -(p_i - p_0)A_i$$

caused by the pressure drop of the flow through it. This can be rewritten by applying Bernoulli's equation to the flow upstream of the screen:

$$F_S = -\frac{1}{2}\rho V_0^2 A_i \left[1 - \left(\frac{V_i}{V_0}\right)^2\right] \tag{5-34}$$

Hence,

$$\begin{aligned} T &= F_N + F_A + F_S \\ &= \frac{1}{2}\rho V_0^2 A_i \left(1 - \frac{V_i}{V_0}\right)^2 - \frac{1}{2}\rho V_0^2 A_i \left[1 - \left(\frac{V_i}{V_0}\right)^2\right] \\ &= \frac{1}{2}\rho V_0^2 A_i 2\frac{V_i}{V_0}\left(\frac{V_i}{V_0} - 1\right) \end{aligned} \tag{5-35}$$

This is in agreement with Eq. (5-30) for the over-all force, since $V_j = V_i$ in this case.

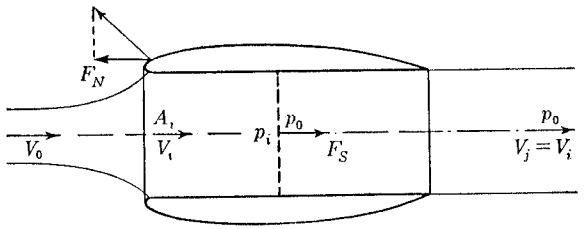

FIG. 5-15. Forces on a fairing with inserted screen.

We see from these considerations how such a thrust analysis depends on the shape of the fairing and on the type of "engine" considered. The burner of a ram-jet engine, for instance, takes no thrust so that the whole thrust force acts on the fairing. A detailed analysis of the relative contributions of the various parts of the fairing of a ram jet to the total thrust is given in Sec. 7-6. A fairing around a propeller, however, takes only part of the over-all thrust, the greater part of the thrust acting on the propeller itself, as will be seen in Chap. 6. Similarly, with a turbojet engine, the compressor bearings experience a considerable portion of the thrust and the thrust force at the nose of the intake, for instance, is relatively small at low flight speeds, rising, however, with increasing flight speed, as will be shown in Sec. 8-5.

EXERCISES

5-1. Determine the drag coefficient

$$\Delta C_D = \frac{\Delta D}{\frac{1}{2}\rho V_0^2 A_m} = -\int_{R_e/R_m}^{1} C_{pd}\left(\frac{r}{R_m}\right)^2$$

from the measured pressures on the afterbody shape B in Fig. 5-3 by graphical integration for $V_e/V_0 = 0.8$ and 6.0. Compare the results with the estimated skin-friction drag for a complete nacelle such as that in Fig. 5-1.

5-2. Confirm Eq. (5-3).

5-3. Determine the shape of the thin annular airfoil that is produced by the vortex distribution

$$\gamma(x) = -0.1[2\pi V_0 \sqrt{1 - (2x - 1)^2}]$$

on the cylinder $r = R_0$ with $L/2R_0 = 1$. Compare it with the two-dimensional airfoil produced by the same vortex distribution. Calculate the pressure distributions over the two airfoils.

5-4. Find the strength of the vortex distribution

$$\gamma(x) = c_2 2\pi V_0 \sqrt{1 - (2x - 1)^2}$$

of the two-dimensional airfoil that has the same maximum camber as the annular airfoil of Exercise 5-3. Compare the normal force coefficient C_n of the two-dimensional airfoil with the radial force coefficient C_r of the annular airfoil.

5-5. Superpose on the camber line of the annular airfoil of Exercise 5-3 a thickness distribution with 10 per cent thickness-chord ratio which has its maximum thickness at 50 per cent chord and is elliptical over the forward half and a parabolic arc over the rear half. Calculate the velocity increment δ_i, from Eq. (5-26), at $x = 0.5$.

5-6. Calculate the shape of the thin annular airfoil which has the following velocity increments at its outer surface:

$$\begin{aligned} \frac{v_x}{V_0} &= +0.10 \quad \text{at } x = 0.1 \\ &= -0.05 \quad \text{at } x = 0.5 \\ &= -0.08 \quad \text{at } x = 0.9 \end{aligned}$$

$L/2R_0 = 1$. Use the vortex distributions γ_1, γ_2, and γ_3. Put $\cos\vartheta = 1$ in Eq. (5-15).

5-7. Derive the general expressions for the velocity components of the thin two-dimensional double airfoil which belongs to the vortex distribution $\gamma(x) = 2\pi V_0 c_4$. Work out the shape of the airfoil for the numerical example $c_4 = -0.1$; $L/2Y_0 = 1$.

5-8. Confirm Eq. (5-33).

BIBLIOGRAPHY

RIABOUCHINSKY, D. P., Sur les surfaces de glissement dans les fluides, *Bull. inst. aérodynamique Koutchino*, vol. VI, p. 9, Paris, 1920.

BIRNBAUM, W., Die tragende Wirbelfläche als Hilfsmittel zur Behandlung des ebenen Problems der Tragflügeltheorie, *Z. angew. Math. Mech.*, vol. 3, p. 290, 1923.

JACOBS, E. N., and J. M. SHOEMAKER, Tests on Thrust Augmentors for Jet Propulsion, *NACA TN* 431, 1932.

WEINIG, F., Die Ausdehnung des Kavitationsgebietes, in "Hydromechanische Probleme des Schiffsantriebes," G. Kempf and E. Foerster, editors, Hamburgische Schiffbau-Versuchsanstalt, Hamburg, 1932.

TOMOTIKA, S., T. NAGAMIYA, and Y. TAKENOUTI, The Lift on a Flat Plate Placed Near a Plane Wall with Special Reference to the Effect of the Ground upon the Lift of a Monoplane Aerofoil, *Aeronaut. Research Inst., Tokyo Imp. Univ., Rept.* 8, p. 1, 1935; and Rept. 182, p. 363, 1939.

BUSEMANN, A., Schuberhöhung durch Luftbeimischung, *Lilienthal Gesellschaft der Luftfahrtforschung, Bericht* 118, 1939.

DICKMANN, H. E., Grundlagen zur Theorie ringförmiger Tragflügel (frei umströmte Düsen), *Ingenieur Arch.*, vol. 11, p. 36, 1940.

MUTTRAY, H., Über die Anwendung des Impulsverfahrens zur unmittelbaren Ermittlung des Profilwiderstandes bei Windkanaluntersuchungen, *Deut. Luftfahrtforschung* F.B. 824/3, 1941.

KRÜGER, W., Messungen an einem Staudruckmultiplikator mit grosser Anstellwinkel-Unempfindlichkeit, *Tech. Ber.*, vol. 9, p. 183, 1942.

REGENSCHEIT, B., Venturi Düse mit veränderlichem Durchfluss, *Deut. Luftfahrtforschung* F.B. 1945, 1944.

REICHARDT, H., Kavitationsmodell zur Ermittlung druckkonstanter Begrenzungsflächen für rotations-symmetrische Durchlaufgeräte, *Deut. Luftfahrtforschung* U.M. 6606, 1944.

RIEGELS, F., and H. EGGERT, Messungen am Heck von Strahlgondeln, *Deut. Luftfahrtforschung* U.M. 3201, 1944.

TEMPLE, G., and J. YARWOOD, Two-dimensional Aerofoils and Ducts with Uniform Velocity Distribution, *Brit. ARC Rept. & Mem.* 2090, 1944.

HUGHES, N. J. S., Two-dimensional Constant Velocity Ducts, *Brit. ARC Rept. & Mem.* 2089, 1944.

WARREN, C. H. E., Theory of Thin Sections Applied to Derive Surfaces of Revolution Having Specified Distributions of Pressure Differences between the Inside and Outside, *RAE TN Aero.* 1636, 1945.

PEEBLES, G. H., A Method for Calculating Airfoil Sections from Specifications of the Pressure Distribution, *J. Aeronaut. Sci.*, vol. 14, p. 451, 1947.

PERL, W., and H. E. MOSES, Velocity Distributions on Two-dimensional Wing-duct-inlets by Conformal Mapping, *NACA Rept.* 893, 1947.

GLAUERT, H., "The Elements of Aerofoil and Airscrew Theory," Cambridge University Press, London and New York, 1948.

KÜCHEMANN, D., and J. WEBER, Annular Cowlings (*AVA Monograph* J_26), *Brit. Min. of Supply (Völkenrode) Rept. Transl.* 989, 990, 1948.

JAHNKE, E., and F. EMDE, "Tables of Functions," B. G. Teubner, Leipzig, 1933.

CHAPTER 6

THE DUCTED PROPELLER

We can now proceed to the practical application of the topics of the previous chapters. The ducted propeller represents the engine with mechanical energy input in one of its simplest forms. Its ideal working process in nonviscous flow is discussed in Sec. 6-1, and the effect of viscosity in Sec. 6-2. The detailed design of the blades of the propeller itself is passed over very briefly, as methods for axial flow fans and ordinary propellers are readily applicable. The design of the annular fairing is described in Sec. 6-3, and the results of some tests on models are used in Sec. 6-4 as a practical illustration of actual ducted propeller characteristics. The chapter closes with suggestions as to possible applications of the ducted propeller, in Sec. 6-5.

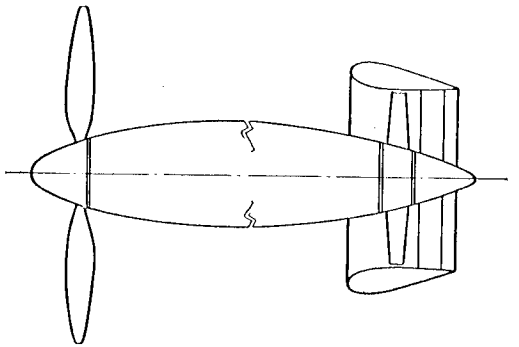

FIG. 6-1. Diagrammatic illustration of an ordinary propeller (left) and a ducted propeller (right).

6-1. Thrust and Efficiency in Ideal Flow. The ducted propeller is a development of the ordinary propeller, with the blades surrounded by a circular fairing whose cross sections along wind are of airfoil shape, as illustrated in Fig. 6-1. The diameter of the fairing is usually considerably smaller than that of the corresponding normal propeller of similar performance, and the number of blades is increased. Like the ordinary propeller, the ducted fan may be driven either by a piston engine or by a gas turbine. The possible applications will be more readily assessed when we have discussed the way in which it works, which we shall do without considering compressibility effects.

In consequence of the input of mechanical energy there is a sudden increase of pressure Δp at the propeller disk; the kinetic energy cannot change suddenly, for continuity reasons. The pressure increase is subsequently transformed into kinetic energy in the slip stream, so that whether the propeller is ducted or not the velocity V_j far behind in the jet, or slip stream, is higher than the velocity V_0 of the main stream. The total thrust force $\bar{T}$ is given by the momentum theorem, applied as in Sec. 2-3, and in nondimensional form is

$$\bar{C}_T = \frac{\bar{T}}{\frac{1}{2}\rho V_0^2 A} = 2\frac{V_A}{V_0}\left(\frac{V_j}{V_0} - 1\right) \tag{6-1}$$

where A is the propeller-disk area.

Now the axial force acting on the propeller itself is given by

$$C_T = \frac{\Delta p}{\frac{1}{2}\rho V_0^2} = \frac{p_{A2} - p_{A1}}{\frac{1}{2}\rho V_0^2} \tag{6-2}$$

which follows when the momentum theorem is applied to a surface of integration closely surrounding the disk. For the nonducted propeller, C_T and $\bar{C}_T$ are of course the same, so that applying Bernoulli's equation separately to the flow upstream and the flow downstream of the propeller,

$$\begin{aligned} p_0 + \tfrac{1}{2}\rho V_0^2 &= p_{A1} + \tfrac{1}{2}\rho V_A^2 \\ p_{A2} + \tfrac{1}{2}\rho V_A^2 &= p_j + \tfrac{1}{2}\rho V_j^2 \end{aligned} \tag{6-3}$$

we obtain the well-known equation

$$V_A = \tfrac{1}{2}(V_0 + V_j) \tag{6-4}$$

if $p_j = p_0$. This states that the average axial velocity at the propeller is the mean of the velocities far upstream and far downstream. Denoting the velocity increment $V_j - V_0$ by v_j, we can write this alternatively as

$$\frac{V_A}{V_0} = 1 + \frac{v_j}{2V_0} \tag{6-5}$$

The presence of a fairing ring, however, causes a further velocity increment at the propeller

$$v_F = \delta V_0 \tag{6-6}$$

as described in Sec. 5-6, to be superposed on the propeller flow. At large distances from the propeller, v_F disappears, but at the propeller disk,

$$\frac{V_A}{V_0} = 1 + \frac{v_j}{2V_0} + \delta \tag{6-7}$$

instead of Eq. (6-5). Thus the mass flow through a plain propeller and a ducted propeller are not the same.

Equation (6-1) now gives different values for the total thrust coefficient:

$$\begin{aligned} \bar{C}_T &= 2\left(1 + \frac{v_j}{2V_0}\right)\frac{v_j}{V_0} && \text{for the plain propeller} \\ \bar{C}_T &= 2\left(1 + \frac{v_j}{2V_0} + \delta\right)\frac{v_j}{V_0} && \text{for the ducted propeller} \end{aligned} \tag{6-8}$$

The thrust on the propeller itself is given in either case by

$$C_T = \left(\frac{V_j}{V_0}\right)^2 - 1 = 2\left(1 + \frac{v_j}{2V_0}\right)\frac{v_j}{V_0} \tag{6-9}$$

The velocity increment v_j in the slip stream may thus be expressed in terms of the thrust loading on the propeller,

$$\frac{v_j}{V_0} = \sqrt{1 + C_T} - 1 \tag{6-10}$$

and Eqs. (6-8) give the difference between the total thrust coefficients

$$\Delta\bar{C}_T = C_{T_F} = 2\delta\frac{v_j}{V_0} = 2\delta(\sqrt{1 + C_T} - 1) \tag{6-11}$$

which is equal to δC_T when C_T is very much less than 1. This force must act on the fairing. Its magnitude depends on the velocity increment δ due to the fairing and on the loading coefficient of the propeller, and the sign of δ determines whether it is a thrust or a drag force. An increase in velocity inside the fairing ($\delta > 0$) gives a thrust, and a reduction ($\delta < 0$) a drag on the fairing.

The energy input to either the plain or the ducted propeller is equal to the increase of kinetic energy in the jet far downstream where $p_j = p_0$:

$$P = \frac{1}{2}\rho V_A A[(V_0 + v_j)^2 - V_0^2] = \bar{T}\left(V_0 + \frac{v_j}{2}\right) \tag{6-12}$$

The Froude efficiency (see Sec. 2-4) is then

$$\eta_j = \frac{\bar{T}V_0}{P} = \frac{1}{1 + \frac{v_j}{2V_0}} = \frac{2}{1 + \sqrt{1 + C_T}} \tag{6-13}$$

The efficiency thus depends only on the loading on the propeller itself and not on the total thrust. This means that by the use of a fairing with $\delta > 0$, a gain in thrust can be achieved without a loss in efficiency, or the same total thrust can be obtained at a higher efficiency. This is illustrated in Fig. 6-2.

6-2. Viscosity and Other Effects. The main consequence of the viscosity of the real flow is an additional fairing drag D_F due to skin fric-

tion, etc., which has an appreciable influence on the performance of the ducted propeller.

We can define a fairing drag coefficient C_{DF}

$$C_{DF} = \frac{D_F}{\frac{1}{2}\rho V_0^2 \pi D L_F} \tag{6-14}$$

where D is the propeller diameter and L_F is the length of the ring.[1] If we also define a partial efficiency

$$\eta_F = \frac{\bar{T} - D_F}{\bar{T}} = 1 - \frac{\pi D L_F}{A} \frac{C_{DF}}{\bar{C}_T} \tag{6-15}$$

the over-all efficiency is

$$\eta = \frac{(\bar{T} - D_F)V_0}{P} = \eta_F \eta_j \tag{6-16}$$

At a given thrust coefficient, the total efficiency varies considerably with C_{DF} and L_F. The example in Fig. 6-3 shows that there is a maximum possible value for η for any given fairing drag; below the thrust coefficient at which this maximum occurs, the efficiency falls off rapidly. In

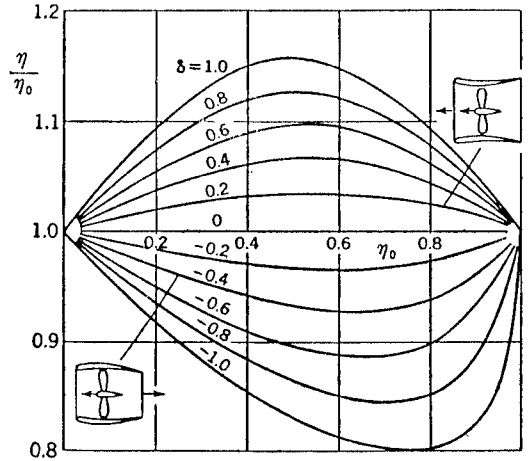

FIG. 6-2. Change of efficiency due to the velocity increments induced by the fairing, for the same total thrust.

general, therefore, there is little point in ducting a lightly loaded propeller, and it is vitally important to achieve the required value of δ with a short ring of low drag coefficient.

Some features of the ducted propeller which concern the propeller itself may be mentioned without further discussion. The fairing acts as

[1] Values of C_{DF} for various annular airfoils are given in Sec. 5-8.

an end plate to the blades and thus reduces the falling off in thrust toward their tips if the gap between blade and ring is kept small enough. This may improve the *induced efficiency* of the propeller appreciably. The blade plan-form of a ducted propeller differs therefore from that of an ordinary propeller, having much broader blades toward the tips.

The high thrust loading of the ducted propeller will make it necessary to employ some means of reducing the losses due to rotation in the slip stream. The struts which are needed anyway to mount the fairing may be made to serve also as guide vanes for this purpose; alternatively, counterrotating screws can be used.

The characteristics which have been described suggest two main spheres of application for the ducted propeller. The first is thrust augmentation at take-off and at low flight speeds, using a *thrust ring* with

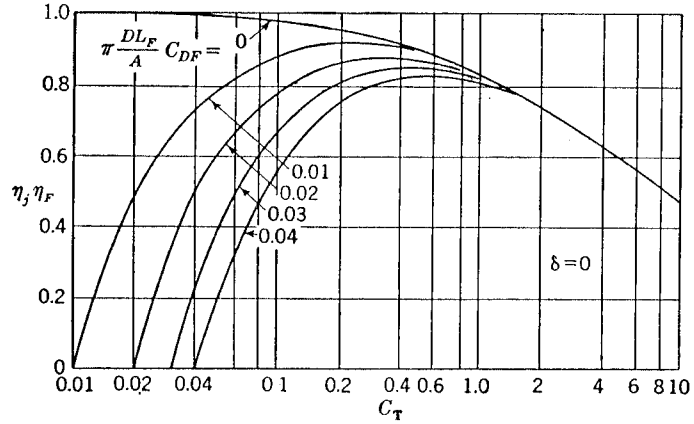

FIG. 6-3. Influence of the drag of the fairing on the over-all efficiency.

$\delta > 0$; the other is the reduction of velocity and thus of Mach number inside the fairing at the propeller blades in high-speed flight by means of a *high-speed ring* with $\delta < 0$.

6-3. Design of the Fairing. We need not discuss the design of the propeller blades here because well-known methods developed for axial flow fans and ordinary propellers are available and can be used with minor modifications. New problems arise from the flow past the fairing; the velocity field induced by the fairing must be known for the design of the blades, and a method is required for the design of a ring which will bring about a given velocity increment δ.

We have discussed the flow past isolated annular airfoils in Secs. 5-4 to 5-6 and shall now consider the mutual interference between fairing and propeller. The nature of the interference can be seen by considering a thin cylindrical ring, which presents no disturbance to a parallel flow

along its axis. But in the contracted flow past a propeller, as in Fig. 6-4, a circulation is produced even round such a ring, increasing the velocity inside the duct. We must therefore distinguish between the circulation of the isolated ring itself (in the general case of a ring of arbitrary profile), with its associated velocity increment δ_0, and the circulation induced by the propeller and other bodies which may be present, with associated velocity increment δ_1.

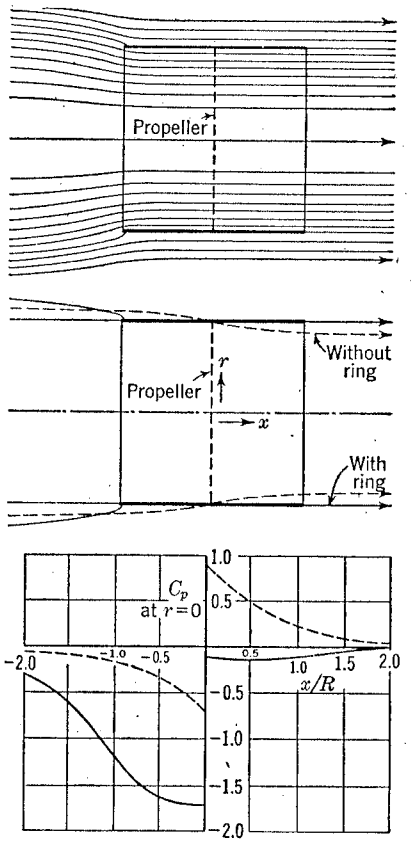

FIG. 6-4. Theoretical streamlines and pressure distributions along the axis for a propeller with and without fairing.

The method of singularities, described above in Secs. 5-4 and 5-5 for isolated airfoils, can also be used to calculate δ_1 if the propeller is also substituted by singularities. A convenient substitute is provided by a constant distribution of vortex rings on the boundary of the slip stream, which to a first approximation may be assumed to be cylindrical. This would imply an infinite number of blades, a uniform distribution of thrust along the radius, no rotation in the slip stream, and low thrust loading. These assumptions, in particular that of a cylindrical slip-stream boundary, are more likely to be fulfilled for the ducted propeller than for the ordinary propeller, and a reasonable approximation can be expected even for relatively heavily loaded propellers.

An alternative to the constant vortex-ring distribution along the cylindrical slip-stream boundary is a uniform distribution of sinks on the propeller disk. The equivalence of the two has been demonstrated in Sec. 3-6, and it is also explained there how the strength of the vortices, or sinks, is related to the velocity increment v_j in the slip stream and thus to the thrust coefficient C_T of the propeller itself, Eq. (6-9). Numerical values of the induced velocity components can readily be obtained from the tables in Sec. 10 of the Appendix. They are to be added to the velocity components v_x and v_r from Eqs. (5-10) and (5-11) in Sec. 5-4 of the vortex distribution replacing the annular airfoil. The condition that the given fairing is a streamline of the combined flow can be satisfied by

modifying the vortex distribution which represents the ring. Finally, the additional vortex distribution on the ring gives the induced axial velocity δ_1.

It will be seen from this that δ_1 is proportional to the strength of the sinks representing the propeller and thus to

$$\frac{v_j}{V_0} = \sqrt{1 + C_T} - 1 \qquad (6\text{-}16)$$

This leads to another favorable property of the ducted propeller: With a given engine to drive the propeller, the thrust coefficient increases as the flight speed decreases; hence δ_1 increases also. This influences the rate of advance, which we can define in two different ways;[1] first, we have the *external rate of advance*

$$\lambda_e = \frac{V_0}{R\omega} \qquad (6\text{-}17)$$

and second, the more significant *internal rate of advance*

$$\lambda_i = \frac{V_0(1 + \delta_0 + \delta_1)}{R\omega} = (1 + \delta)\lambda_e \qquad (6\text{-}18)$$

where R is the radius and ω the angular velocity of the propeller. The value of λ_e decreases as the flight speed is decreased; but since δ increases, λ_i varies much less with flight speed than λ_e, so that it is possible that the rate of advance actually experienced by the propeller could automatically be kept constant by the presence of the fairing. It would then be unnecessary to use variable-pitch blades.

The method described has been used to work out the simplified example in Fig. 6-4 as an illustration of the flow past a ducted propeller.[2] The induced circulation round the fairing obviously increases the mass flow through the propeller and reduces the contraction of the slip stream. As a consequence, the pressure behind the propeller is nearly constant and equal to the undisturbed pressure p_0, while the pressure ahead is very much lower than p_0.

The velocity increment δ_1 does not increase linearly with the length of the fairing, as Fig. 6-5 shows. The explanation is to be found in the shape of the slip stream; because the rate of contraction is greatest near the propeller, even a relatively short ring modifies the propeller flow considerably. The length of the ring is, however, decisive for the magnitude of the velocity increment δ_0 (see Sec. 5-6). The value of δ_1 depends to

[1] The rate of advance is often defined as V_0/nD, where D is the diameter and n the number of revolutions per unit time ($n = \omega/2\pi$). The two definitions differ by a factor π.

[2] Both here and in Fig. 6-5 the radius of the ring was taken to be 10 per cent larger than that of the disk of sinks in order to evade the singularity at the edge of the disk.

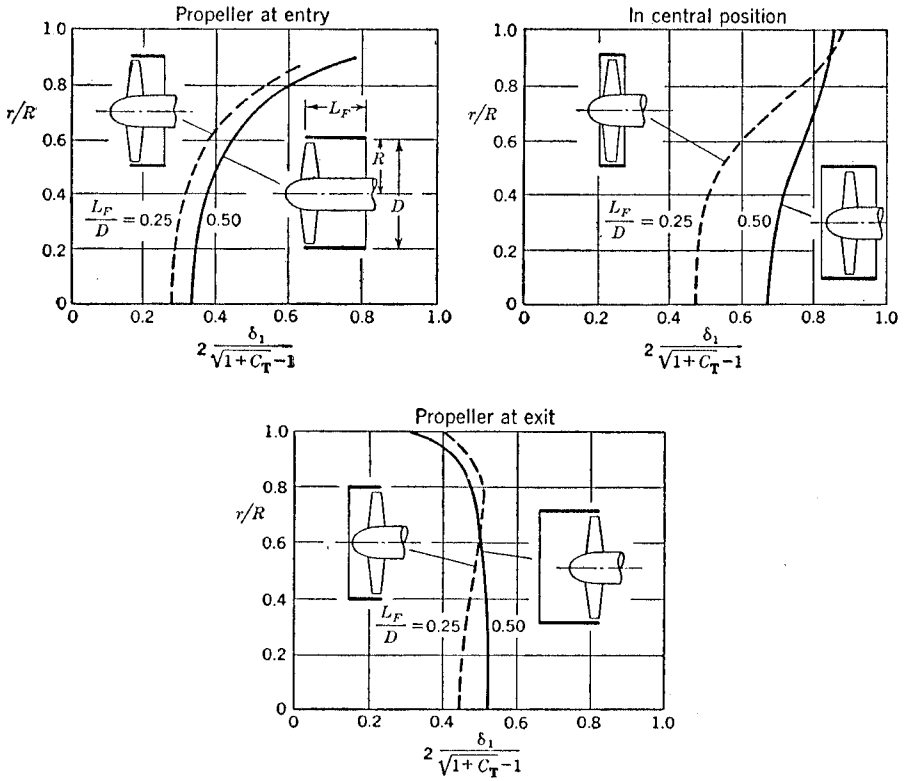

FIG. 6-5. Radial variation of the axial-velocity increment induced by a propeller at various positions inside a cylindrical ring.

some extent on the position of the propeller inside the fairing, as the examples illustrate. Further, δ_1 is by no means constant along the radius of the propeller, a fact which has to be taken into account in the design of the blades. Mean values of δ_1 across the duct are given in Table 6-1.

TABLE 6-1

L/D	$\frac{\delta_1}{\sqrt{1+C_T}-1}$	
	Screw at entry or exit	Screw in central position
0	0	0
0.25	0.24	0.33
0.50	0.25	0.39
0.75	0.25	0.43
1.00	0.25	0.46

The magnitude of the interference between propeller and ring can be measured by the aerodynamic load on the fairing, expressed in terms of

TABLE 6-2

Position of propeller	L/D of a thin cylindrical ring	C_{r1} for $C_T = 1$
Entry	0.25	−0.911
	0.50	−0.696
Central	0.25	−0.903
	0.50	−0.745
Exit	0.25	−0.952
	0.50	−0.770

the radial-force coefficient C_r. We denote by C_{r1} the part of C_r which is produced by the interference of the propeller. Its value again depends on the position of the propeller and on the fairing length; some calculated values are given in Table 6-2. For C_T not equal to 1, C_{r1} is to be multiplied by $(\sqrt{1 + C_T} - 1)/0.414$.

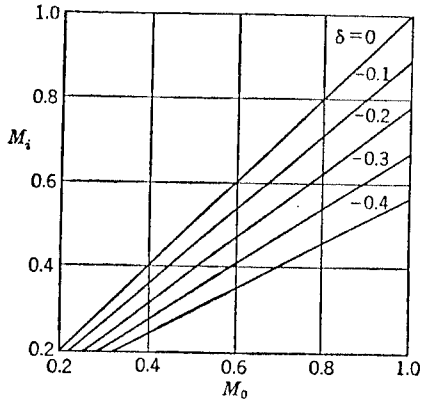

FIG. 6-6. Reduction of Mach number inside the ring for various velocity decrements, $\delta < 0$.

When a thrust ring is to be designed for low flight speeds, the thrust will be given; the required velocity increment δ and the shape of the fairing will be determined subsequently. A high-speed ring will be designed for a certain Mach number M_i of the flow through the propeller, lower than the flight Mach number M_0. Assuming isentropic inflow and taking only axial velocity components into account, we obtain

$$\frac{M_i}{M_0} = \frac{1 + \delta}{\sqrt{1 + \frac{k-1}{2} M_0^2[1 - (1 + \delta)^2]}} \tag{6-19}$$

where M_0 is referred to the free-stream velocity of sound and M_i is referred to the local velocity of sound. This ratio is plotted in Fig. 6-6, from which the required value of δ for a given ratio M_i/M_0 can be obtained.

6-4. Some Experimental Thrusts and Efficiencies. Although the models of ducted propellers which have been tested experimentally up to

the present cannot be described as satisfactory, the results obtained will at least serve to give our conclusions a practical orientation. The main fault of the designs investigated was the smallness of the loading coefficient C_T. In the case considered below, $C_T = 0.06$ at the design point $\lambda_i = 0.6$, which is far too low because of the fairing drag[1] and its influence on the over-all efficiency, as shown in Fig. 6-3. The propeller tested had four blades fixed in pitch, with finite chord at the tips. In this test, the forces and moments were measured separately; they were also calculated,

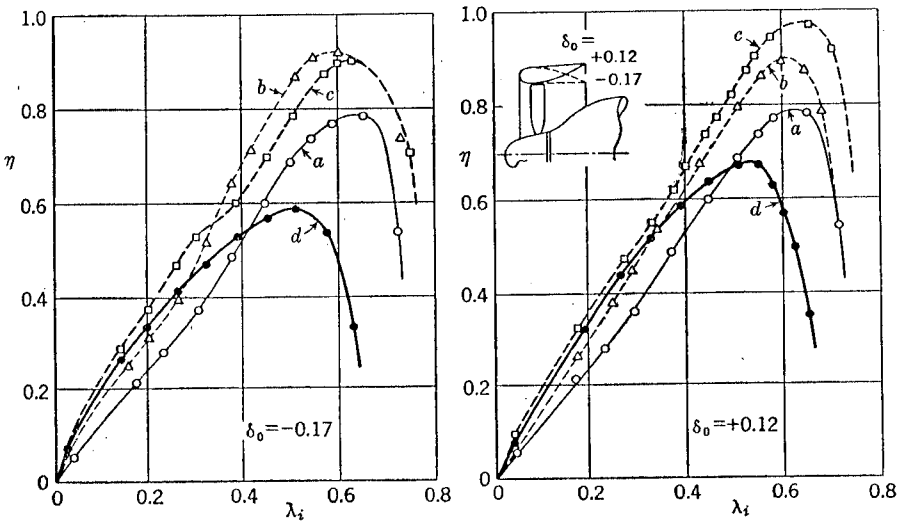

FIG. 6-7. Measured efficiencies of a ducted propeller. Curve *a*, propeller alone; curve *b*, ducted propeller, ignoring all the forces on the fairing; curve *c*, ducted propeller, ignoring only the drag of the fairing; curve *d*, over-all efficiency of the ducted propeller.

using the methods described above, and the results were found to be in good agreement.

The analysis of the efficiencies of the propeller inside two different rings in Fig. 6-7 shows clearly the various influences at work. Curve *a* in Fig. 6-7 gives the efficiency of the propeller alone, and curve *b* that of the propeller in the duct, plotted against the effective or internal rate of advance, Eq. (6-18). In curve *b* the forces on the fairing are not taken into account. The difference between the two curves measures the improvement of the flow at the propeller due to the *end-plate effect*, which is quite appreciable and about the same for the two rings. If the duct is long enough (as in the present case), the efficiency, curve *b*, can be calculated as that of a fan in a straight pipe. Curve *c* takes account of the forces on the fairing which arise from the interaction between the ring

[1] $C_{DF} = 0.015$ for the fairing with $\delta_0 = -0.17$ and $C_{DF} = 0.021$ for that with $\delta_0 = +0.12$.

and the propeller in nonviscous flow but not of the fairing drag. The efficiency for curve *c* is better than for curve *b* if $\delta = \delta_0 + \delta_1 > 0$. The value of λ_i at which curve *c* crosses curve *b* indicates where the induced circulation of the ring is equal and opposite to its circulation in a free stream, $\delta_0 + \delta_1 = 0$. This makes it possible to estimate δ_1 from the experiment if δ_0 is known. The arrangement with $\delta_0 > 0$ is slightly more efficient than that with $\delta_0 < 0$, as expected. The efficiency in either case would be very high if the drag of the fairing were less; for the reasons mentioned above it has a large influence in the present case, and the over-

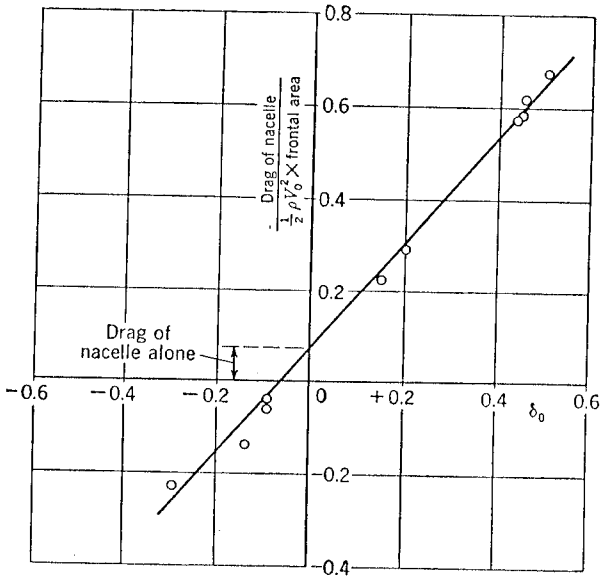

FIG. 6-8. Measured drag coefficients of a nacelle, as in Fig 6-1, in the presence of ring fairings of various shapes. The rings are not attached to the nacelle.

all efficiency, curve *d*, is less than the efficiency of the propeller alone, at the design value of λ_i in high-speed flight. It is obvious, however, that this can be improved on.

As a point of interest, it may be mentioned that there is a large interaction between the ring and the nacelle housing the driving unit. In the first instance, the velocity field of the nacelle alters the circulation round the fairing profile; second, there is an axial force on the ring and an equal and opposite axial force on the central nacelle due to the interaction between them, which can be much larger than the drag of the nacelle alone, as shown in Fig. 6-8.

6-5. Possible Applications. The results obtained so far do not give any promise of successful application of the ducted propeller to relieving the compressibility effects on the propeller blades of high-speed aircraft.

The prospect looks even less good when the increase in the drag of the fairing due to compressibility is taken into account. It would be improved if the fairing could also serve other purposes, for example as part of the tail unit. For a proper assessment of the value of the ducted propeller in this field, however, it is necessary to consider specific power units and types of aircraft, comparing the ducted propeller with other means of propulsion such as the conterrotating propeller and the jet engines. Various estimates have been made, but the conclusions are not unanimous.

The outlook for the ducted propeller is better in the low-speed range. In particular, the gain in static thrust ($V_0 = 0$) is spectacular. Applying the momentum theorem as in Sec. 6-1, we get for the total thrust coefficient (redefined for this case):

$$\bar{k}_T = \frac{\bar{T}}{\frac{1}{2}\rho(R\omega)^2 A} = \left(\frac{v_j}{R\omega}\right)^2 (1 + \delta') = k_T(1 + \delta') \qquad (6\text{-}20)$$

where δ', unfortunately not readily calculable, is the mean axial velocity induced by the fairing measured as a fraction of the velocity $v_j/2$ at the propeller disk due to the propeller alone. δ' is usually positive. The power input coefficient is then

$$\bar{k}_P = \frac{\bar{P}}{\frac{1}{2}\rho(R\omega)^3 A} = \frac{\bar{T}}{\frac{1}{2}\rho(R\omega)^2 A}\,\frac{v_j}{2R\omega}$$
$$= \frac{1}{2}\left(\frac{v_j}{R\omega}\right)^3 (1 + \delta')$$

so that

$$\bar{k}_P = \frac{1}{2}k_T^{\frac{3}{2}}(1 + \delta') = \frac{1}{2}\frac{\bar{k}_T^{\frac{3}{2}}}{\sqrt{1 + \delta'}} \qquad (6\text{-}21)$$

These relations indicate that for the same thrust k_T on the propeller itself, both the total thrust and the power coefficient are increased. This means that the physical limits to the static thrust attainable with ordinary propellers can be overcome by the ducted propeller. In most cases, the diameter of the ordinary propeller has to be much larger than would be necessary and appropriate for efficiency in high-speed flight, in order to give the required static thrust or to absorb the power available from the engine,[1] which, in the case of piston engines, could be constant and equal to the power used at top speed. The ducted propeller has the advantage here in that for the same diameter it can absorb more power and produce a higher thrust; or it can produce the same thrust with smaller diameter.

[1] See, for example, A. Betz, 1938.

Further, the ducted propeller can produce a given total thrust more efficiently. Equation (6-21) shows that the value of $\bar{k}_P$ required to give a total thrust $\bar{k}_T$ is only $1/\sqrt{1 + \delta'}$ times that for the ordinary propeller with the same value of $\bar{k}_T$. Introducing the Bendemann coefficient,

$$\zeta = \frac{\bar{k}_T}{(2\bar{k}_P)^{\frac{1}{2}}} \qquad (6\text{-}22)$$

we find $\zeta = 1$ for the ideal propeller without fairing and

$$\zeta = (1 + \delta')^{\frac{1}{2}} \qquad (6\text{-}23)$$

which can be greater than unity, for the ducted propeller.

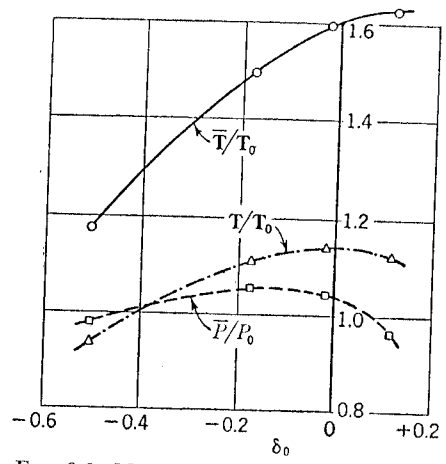

FIG. 6-9. Measured changes of thrust and power input due to fairings of different shapes, under static condition. Tractor propeller as in Fig. 6-7. T_0 and P_0 refer to the nonducted propeller.

The examples in Figs. 6-9 to 6-11 from actual experiments show that large improvements are in fact gained. The static thrust was more than doubled in certain cases (Fig. 6-10). It will be seen that the thrust increase, and thus the value of δ', depends on δ_0; and further that the fairing should have a liberal nose radius (Fig. 6-11). We also find that a constant-pitch propeller may work under much more favorable conditions when ducted (Fig. 6-9).

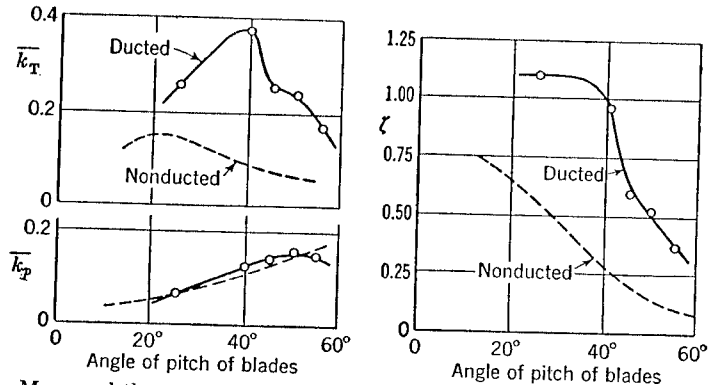

FIG. 6-10. Measured thrust and power-input coefficients, for various angles of pitch of the propeller blades; ducted propeller as in Fig. 6-1, under static conditions. From tests by W. Krüger, 1944.

All this points toward an application of the ducted propeller to aircraft in the low-speed range where the advantages would be smaller diameter; no variable pitch blades; higher rpm; and possible simplifications in con-

struction and weight, for instance, of the undercarriage. The simplified handling and increased safety due to the protection which the fairing gives from the rotating blades will be of particular value in the case of private aircraft. Ducted screws have been successfully applied to ship

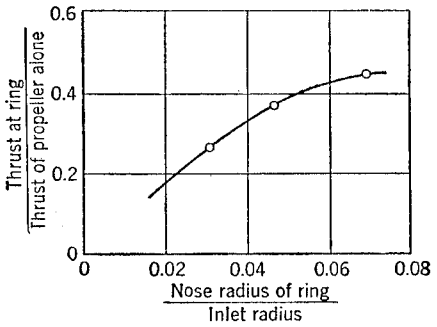

FIG. 6-11. Influence of the nose radius of the fairing on the measured thrust increment of a ducted propeller under static conditions. Tractor propeller as in Fig. 6-7.

propulsion, especially to tugboats, in the form of the Kort nozzle,[1] and similar tractor aircraft for towing purposes may also be envisaged.

EXERCISES

6-1. A ducted propeller with disk area $\frac{1}{3}m^2$ absorbs a power input

$$P = 1{,}000 \text{ hp} = 75{,}000 \text{ m-kg/sec}$$

The fairing is such as to produce at the propeller disk a velocity increment

$$\delta V_0 = (0.1 + 0.4v_j/V_0)V_0$$

Calculate the thrust acting on the screw and the over-all thrust for flight speeds between 100 m/sec and 200 m/sec, at sea level, and determine the jet efficiencies. Assume incompressible flow.

6-2. Calculate the external and the internal rates of advance for the ducted propeller of Exercise 6-1. The propeller radius is 0.5 m; $n = 3{,}000$ rpm.

6-3. Determine the over-all efficiency $\eta_j\eta_F$ of the ducted propeller of Exercise 6-1 for $C_{DF} = 0.01$ and $L_F/D = 0.5$ and 0.3 ($D = 1$ m), and find the corresponding reduction of the thrust.

6-4. A body of revolution of semi-infinite length and diameter R_0, replaced by a single source at $x/L = 0.4$, is placed inside a thin cylindrical airfoil at $0 \leq x \leq 2R_0$ of radius R_0. Replace the cylinder by a vortex distribution that cancels the radial-velocity components induced by the body on the axis at the points $x/L = 0.1, 0.5, 0.9$. Use the method of Sec. 5-4 and the tables of the Appendix (Sec. 9).

6-5. Determine the axial force which acts on the body in the arrangement of Exercise 6-4 by calculating the velocity at the position of the single source and applying the result of Exercise 3-3 (see also Sec. 12 of the Appendix).

BIBLIOGRAPHY

BETZ, A., Physikalische Grenzen des erreichbaren Standschubes, *Jahrbuch der deutschen Luftfahrtforschung* 1938, p. I 348.

[1] See, for example, F. Horn, 1940.

HORN, F., Beitrag zur Theorie der ummantelten Schiffsschraube, *Schiffbau*, vol. 12, pp. 2, 18, 1940.

KRÜGER, W., On Wind Tunnel Tests and Computations Concerning the Problem of Shrouded Propellers, *Deut. Luftfahrtforschung* F. B. 1949, 1944; translation, *NACA TM* 1202.

PABST, O., B. GÖTHERT, J. HUEBER, and W. STIESS, Die Mantelschraube, *Deut. Luftfahrtforschung* U.M. 1319, 1944.

PARISEN, R. B., J. C. ARMSTRONG, and S. C. HUNTLEY, Theoretical Evaluation of the Ducted-fan Turbo-jet Engine, *NACA TN*. 1745, 1949.

KÜCHEMANN, D., and J. WEBER, The Ducted Screw (*AVA Monograph* $J_3 4$), *Brit. Min. of Supply (Völkenrode) Rept. & Transl.* 981, 1948.

CHAPTER 7

THE RAM-JET ENGINE

As a counterpart to the ducted propeller, the ram jet is used here to demonstrate the application of the general results of the earlier chapters to a pure heat engine. Sections 7-1 to 7-5 deal with the ideal ram jet, disregarding losses.[1] The restrictions imposed on the shape of the combustion chamber by practical requirements are treated in Sec. 7-1, and the restrictions to the heat input in Sec. 7-3. Section 7-2 serves to introduce some compressible flow parameters which help to simplify the analysis. The treatment of the outflow through the nozzle in Sec. 7-4 is

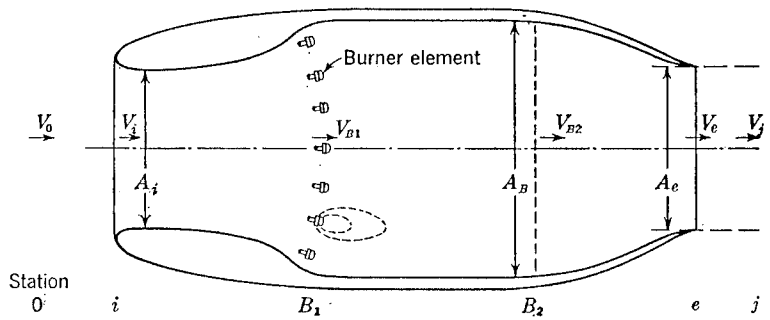

FIG. 7-1. Subsonic ram jet to burn gaseous fuel. (*From a design by O. Pabst and H. Multhopp*, 1944.)

applicable to all types of jet engine. Section 7-5 gives the thrust and efficiency in the ideal case, and the main deviations from the ideal are surveyed in Sec. 7-6. A brief reference to the results of a model test follows in Sec. 7-7. Some remarks on supersonic ram jets are made in Sec. 7-8.

7-1. Ideal Working Process. Constant-pressure and Constant-area Combustion. The ram jet, whose basic working process was summarized in Sec. 2-6, is one of the simplest of aircraft motors. Its principle was first described by the French engineer Lorin as early as 1908, but its practical application has only recently been seriously considered. A workable design[2] for subsonic speeds is shown in Fig. 7-1.

[1] We follow here, to some extent, the presentation given by H. Ludwieg and W. Mangler, 1947.

[2] The performance of this particular design, by O. Pabst and H. Multhopp, is briefly discussed in Sec. 7-7.

Design parameters and the performance of the engine can be deduced from the general equations of flow set out in Chap. 2: the equation of state (2-1), the energy equation (2-16), the equation of continuity, the entropy equation (2-11) or (2-14), and the momentum theorem. The pressure p, density ρ, temperature T, and the velocity V at any cross section are fixed by the free-stream values p_0, ρ_0, T_0, V_0, the heat input, and the geometric dimensions of the duct (in particular the ratio of the exit area to the cross-section area of the combustion chamber).

In the ideal case, there are no energy losses in either the inflow $(0 \rightarrow B_1)$ or the outflow $(B_2 \rightarrow j)$. An initial compression in the free stream $(0 \rightarrow i)$ ahead of the entry is followed by a further compression in the inlet diffuser $(i \rightarrow B_1)$ inside the fairing. Fuel supplied either as a liquid or as a gas is burned in the combustion chamber $(B_1 \rightarrow B_2)$, and a jet with increased kinetic energy is discharged through the nozzle. Since only the kinetic energy of the free stream is available to produce the necessary pressure increase ahead of the combustion chamber, the ram jet cannot generate any thrust under static conditions $(V_0 = 0)$.

The final relations obtained are clumsy, but there is no particular difficulty in deriving them. In the main, attention has been concentrated on simple design charts and graphical presentation for speedier evaluation of the results; some of the relevant papers are referred to in the Bibliography at the end of this chapter. Without going into detail, we shall use here the methods which illustrate the working process and design problems most clearly; it will be possible to demonstrate from time to time how rearrangement or expression in terms of different parameters can simplify the analysis. We shall also use the example of the ram jet to show how particular practical requirements compel the designer to deviate from the ideal process and to compromise between conflicting considerations.

We have already seen in Chap. 2 that the best thermodynamic process is the Carnot process with the addition of heat at constant temperature. This cannot easily be realized in practice, and for a ram jet type of engine the basic cycle with the best thermal efficiency, for given conditions at the beginning of the combustion chamber, is obtained when the combustion is at constant pressure. The thermal efficiency of the constant-pressure process

$$\eta_{th} = 1 - \frac{T_0}{T_{B1}} = 1 - \left(\frac{p_0}{p_{B1}}\right)^{(k-1)/k} \tag{7-1}$$

is less than that of the Carnot cycle, from Eq. (2-23). It will be shown below that even the constant-pressure process is not always the most suitable for a real ram jet because of practical limits on the geometric dimensions, in particular on the maximum cross-section area A_B of the

combustion chamber, which usually determines the frontal area of the complete engine.

With combustion at constant pressure, the cross section of the combustion chamber must increase in the direction of flow. This can be shown by application of the momentum theorem to a surface of integration formed by the areas A_{B1} and A_{B2} at the beginning and the end of the combustion chamber and its side walls. Assuming that the burner acts only as a source of heat and sustains no forces, we have for constant-pressure combustion ($p_{B1} = p_{B2} = p_B$),

$$V_{B1} = V_{B2} \tag{7-2}$$

using the equation of continuity

$$\rho_{B1} V_{B1} A_{B1} = \rho_{B2} V_{B2} A_{B2}$$

Equation (7-2) follows directly from the thermodynamic considerations in Sec. 2-2, where it was found that in a change of state at constant pressure the kinetic energy and therefore the velocity are constant, by Eqs. (2-19) and (2-20). Hence, with the assumption that the air is a perfect gas,

$$\frac{A_{B2}}{A_{B1}} = \frac{\rho_{B1}}{\rho_{B2}} = \frac{T_{B2}}{T_{B1}} \tag{7-3}$$

the cross section increases as the temperature increases, and the largest area is reached at the end of combustion.

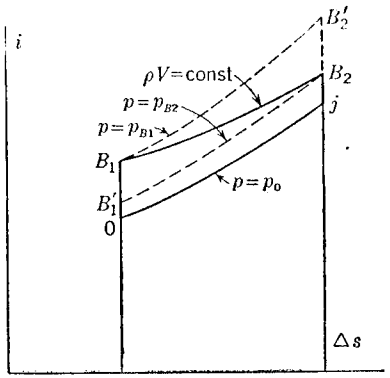

FIG. 7-2. Comparison between a process using a cylindrical combustion chamber and the constant-pressure process (schematic).

Let this maximum area A_B be the given maximum permissible frontal area, and let $0B_1'B_2j$ in Fig. 7-2 represent the constant-pressure process with this maximum area. The cross-section area at B_1' is then smaller than A_B. Now, consider the case where the cross-section area at B_1 is A_B. The constant-area line B_1B_2 (ρV = const) is found to lie above $B_1'B_2$; for a given A_B, that is, combustion at constant area obviously gives a higher thermal efficiency than combustion at constant pressure. The pressure at the beginning of combustion is increased, and it is desirable to have it as high as possible. The constant-pressure combustion $0B_1B_2'j$, with the same conditions at the beginning of combustion, still has a higher efficiency than the constant-area combustion $0B_1B_2j$, but like any other process in which the line B_1B_2 is crossed, it would require a larger cross-section area than the given $A_{B2} = A_B$. We

conclude that the best thermal efficiency given the maximum cross-section area is obtained with a cylindrical combustion chamber.[1] This example illustrates the impossibility of defining the best thermal efficiency of the ram-jet process (or, for that matter, of any other jet-engine process) in a completely general way.

The maximum temperature is also limited in a practical engine by the physical properties of the materials of which the fairing and burners are made. The highest temperature in a ram jet process is reached at the end of the combustion chamber, whether the combustion is at constant pressure or at constant area. The process with constant-area combustion again has a higher thermal efficiency than the constant-pressure process when both have the same maximum temperature.

The limitation on combustion-chamber area leads to another restriction. There is a maximum quantity of heat which can be supplied to air passing through a cylindrical combustion chamber without waste, because the pressure at the end of combustion must not fall below the free-stream pressure p_0; that is, in Fig. 7-2 the line B_1B_2 must not cross the line $p = p_0$. If it does, there is no further increase in thrust, but a decrease, although more heat has been supplied. This is what happens in the case of the nonducted burner, and it is the reason why no thrust is produced (see Sec. 2-6). There is a further limit in that the Mach number at the end of combustion cannot exceed 1, as will be shown presently.

7-2. Some Compressible-flow Parameters. We digress here to introduce some additional parameters which we shall need in the analysis which follows. In gas dynamics it is often useful to make the velocities and functions of state nondimensional in terms either of the *stagnation* or of the *critical* conditions.[2] To explain these ideas, we consider the isentropic flow of a gas in a stream tube of varying cross section. At a given section A let the velocity be V, the pressure p, the density ρ, the velocity of sound $a(= \sqrt{kp/\rho})$, the specific entropy s, etc.

Suppose the stream tube to contract in the direction of flow until a cross section is reached at which the velocity is equal to the local velocity of sound. Conditions there are described as the critical conditions for the stream tube and denoted by p^*, ρ^*, $a^*(= V^*)$, etc. Alternatively, suppose the stream tube to expand to infinite cross section and therefore zero velocity, and call the conditions there the stagnation conditions, denoting them by p_{st}, ρ_{st}, a_{st}, etc. The stagnation and critical conditions are uniquely related to the conditions at A by the equation of state, the continuity equation, the entropy equation $ds = 0$, and the energy equa-

[1] This supplies a belated justification for the concept of the *burner disk* used in Sec. 2-6.

[2] For further information, see, for example, H. W. Liepmann and A. E. Puckett, 1947.

tion. For example the energy equation in the form of eq. (2-16) gives

$$\frac{k}{k-1}\frac{p}{\rho}+\frac{1}{2}V^2=\frac{k}{k-1}\frac{p^*}{\rho^*}+\frac{1}{2}V^{*2}=\frac{a^{*2}}{k-1}+\frac{1}{2}a^{*2}$$

by Eq. (2-18), or

$$\frac{1}{k-1}a^2+\frac{1}{2}V^2=\frac{1}{2}\frac{k+1}{k-1}a^{*2} \qquad (7\text{-}4)$$

$$i+\frac{V^2}{2g}=\frac{k+1}{k-1}\frac{a^{*2}}{2g}$$

Again,

$$\frac{k}{k-1}\frac{p}{\rho}+\frac{1}{2}V^2=\frac{k}{k-1}\frac{p_{st}}{\rho_{st}}=\frac{a_{st}{}^2}{k-1}$$

or with the energy equation in the form of Eq. (2-15) and using Eq. (2-8),

$$i+\frac{V^2}{2g}=c_pT+\frac{V^2}{2g}=i_{st}=c_pT_{st}=\frac{1}{g}\frac{k}{k-1}\frac{p_{st}}{\rho_{st}} \qquad (7\text{-}5)$$

The stagnation temperature is indicated directly by a pitot-head thermometer as a means of measuring the total energy [see, for example, Eq. (2-42), Sec. 2-5]. The Mach number M*, which is used below, means V/a^*, not V^*/a^* which is of course unity by definition.

Thus the stagnation and critical conditions are properties of the flow at any point of a gas flow, defined by a hypothetical isentropic expansion or contraction from that point. In a flow which is isentropic throughout they have the same values everywhere; hence their usefulness as reference parameters. In the flow through a ram jet they have different values before and after combustion, but in any isentropic part of the working process they remain constant.

7-3. Flow in a Constant-area Combustion Chamber. Returning to the ram jet, we can now investigate the flow in the combustion chamber of constant cross-section area in more detail. If subscripts B_1 and B_2 refer to the beginning and the end of the cylindrical combustion chamber, we have, from the energy equation (2-15) or (2-16) together with Eq. (2-8),

$$\begin{aligned}\rho_{b1}V_{B1}\left(i_{B1}+\frac{V_{B1}{}^2}{2g}+q\right)&=\rho_{B1}V_{B1}\left(c_pT_{B1}+\frac{V_{B1}{}^2}{2g}+q\right)\\&=\rho_{B1}V_{B1}\left(\frac{1}{g}\frac{k}{k-1}\frac{p_{B1}}{\rho_{B1}}+\frac{V_{B1}{}^2}{2g}+q\right)\\&=\rho_{B2}V_{B2}\left(i_{B2}+\frac{V_{B2}{}^2}{2g}\right)\end{aligned} \qquad (7\text{-}6)$$

These equations can be simplified by applying the continuity equation

$$\rho_{B1}V_{B1}=\rho_{B2}V_{B2} \qquad (7\text{-}7)$$

and then applying the momentum theorem to the cylinder formed by the combustion-chamber walls and the cross sections B_1 and B_2,

$$p_{B1}-p_{B2}=\rho_{B1}V_{B1}(V_{B2}-V_{B1})$$

or

$$p_{B1}+\rho_{B1}V_{B1}{}^2=p_{B2}+\rho_{B2}V_{B2}{}^2 \qquad (7\text{-}8)$$

Further, the heat input can be measured in terms of the total energy at the beginning of the combustion chamber, and a coefficient C_q can be defined as[1]

$$C_q=\frac{q}{i_{B1}+\frac{V_{B1}{}^2}{2g}}=\frac{q}{i_0+\frac{V_0{}^2}{2g}}=\frac{q}{\frac{a_0{}^2}{(k-1)g}\left(1+\frac{k-1}{2}\mathrm{M}_0{}^2\right)} \qquad (7\text{-}9)$$

if we assume that there are no losses in the inflow from the free stream to the beginning of the combustion chamber.

With the help of Eqs. (7-4) and (7-9), we can now express the energy equation in the simple form

$$a_{B1}{}^{*2}(1+C_q)=a_{B2}{}^{*2} \qquad (7\text{-}10)$$

The continuity equation becomes

$$\rho_{B1}a_{B1}{}^*\mathrm{M}_{B1}{}^*=\rho_{B2}a_{B2}{}^*\mathrm{M}_{B2}{}^* \qquad (7\text{-}11)$$

and the momentum theorem (7-8)

$$\rho_{B1}a_{B1}{}^{*2}(1+\mathrm{M}_{B1}{}^{*2})=\rho_{B2}a_{B2}{}^{*2}(1+M_{B2}{}^{*2}) \qquad (7\text{-}12)$$

Eliminating ρ_{B1}, ρ_{B2} and $a_{B1}{}^*$, $a_{B2}{}^*$, we have

$$\frac{1+\mathrm{M}_{B1}{}^{*2}}{\mathrm{M}_{B1}{}^*}\frac{1}{\sqrt{1+C_q}}=\frac{1+\mathrm{M}_{B2}{}^{*2}}{\mathrm{M}_{B2}{}^*} \qquad (7\text{-}13)$$

and, finally,

$$\mathrm{M}_{B2}{}^*=\frac{1+\mathrm{M}_{B1}{}^{*2}\pm\sqrt{(1-\mathrm{M}_{B1}{}^{*2})^2-4C_q\mathrm{M}_{B1}{}^{*2}}}{2\mathrm{M}_{B1}{}^*\sqrt{1+C_q}} \qquad (7\text{-}14)$$

which determines the Mach number at the end of the combustion chamber. For subsonic flow, the negative sign is to be taken.

Equation (7-14) has a real solution for $\mathrm{M}_{B2}{}^*$ only if

$$C_q\le\frac{(1-\mathrm{M}_{B1}{}^{*2})^2}{4\mathrm{M}_{B1}{}^{*2}} \qquad (7\text{-}15)$$

This means that there is a limit to the amount of heat that can be put into the stream. For the maximum value of C_q given by the equality sign in

[1] This coefficient differs from the one used in Sec. 2-4 by the factor

$$(k-1)V_0{}^2/(k+1)a_0{}^{*2}$$

Eq. (7-15), we obtain $M_{B2}^* = 1$ from Eq. (7-14); *i.e.*, the velocity at the end of the combustion chamber is always below the critical velocity of sound there.

The above calculation is valid for both subsonic and supersonic flow ahead of the combustion, for Eq. (7-13) remains unaltered if M_{B1}^* is replaced by its reciprocal $1/M_{B1}^*$. Consequently, a normal shock wave, across which $M_{B1}^* = 1/M_{B1}^*$ (see below), would not affect Eq. (7-13).

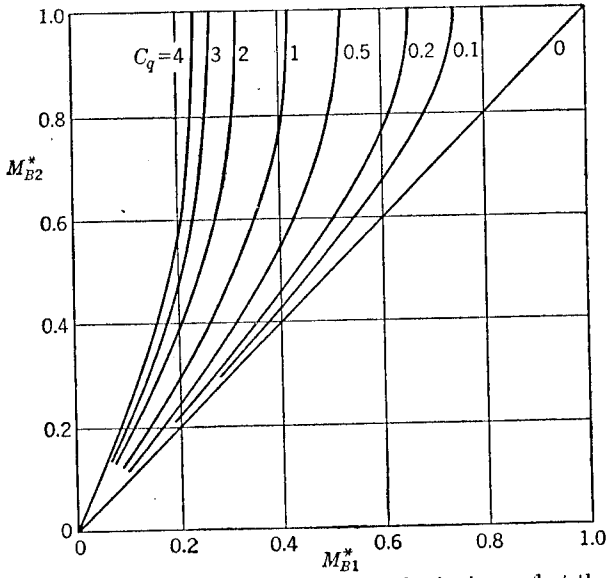

FIG. 7-3. Relation between the Mach numbers at the beginning and at the end of a cylindrical combustion chamber, for various heat-input coefficients.

Figure 7-3 shows how M_{B2}^* varies with C_q. The initial Mach number M_{B1}^* is always less than M_{B2}^*, but this does not in practice impose a severe limitation, since it is usually necessary to keep M_{B1}^* low anyway for combustion to be possible; if the speed through the combustion chamber is too high the flames will be blown out.

The changes of density, pressure, and temperature in a cylindrical combustion chamber can now be deduced in terms of M_{B1}^*, M_{B2}^*, and C_q, from Eqs. (7-8), (7-10), and (7-11),

$$\frac{\rho_{B2}}{\rho_{B1}} = \frac{M_{B1}^*}{M_{B2}^* \sqrt{1 + C_q}} \tag{7-16}$$

$$\frac{p_{B2}}{p_{B1}} = \sqrt{1 + C_q}\, \frac{M_{B1}^* \left(1 - \frac{k-1}{k+1} M_{B2}^{*2}\right)}{M_{B2}^* \left(1 - \frac{k-1}{k+1} M_{B1}^{*2}\right)} \tag{7-17}$$

$$\frac{T_{B2}}{T_{B1}} = \frac{p_{B2}}{p_{B1}} \frac{\rho_{B1}}{\rho_{B2}} = (1 + C_q) \frac{1 - \frac{k-1}{k+1} M_{B2}^{*2}}{1 - \frac{k-1}{k+1} M_{B1}^{*2}} \tag{7-18}$$

We find, for instance, that there is a substantial decrease in pressure, especially when the heat input is large, as Fig. 7-4 shows. The process has departed a long way from constant-pressure combustion

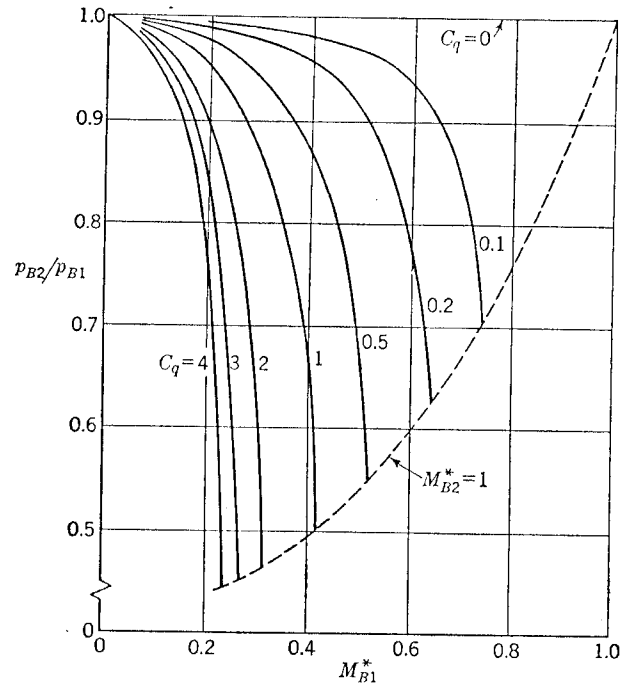

FIG. 7-4. The pressure drop in a cylindrical combustion chamber.

The restriction of the critical Mach number M_{B2}^* at the end of the combustion chamber is equivalent to a limitation of the combustion end temperature T_{B2}. From Eqs. (7-13) and (7-18), we have for $M_{B2}^* = 1$

$$\frac{T_{B2}}{T_0} = \frac{2}{k+1} \frac{1}{1 - \frac{k-1}{k+1} M_0^{*2}} \frac{(1 + M_{B1}^{*2})^2}{4 M_{B1}^{*2}}$$

$$= \frac{2}{k+1} \frac{1}{1 - \frac{k-1}{k+1} M_0^{*2}} (1 + C_q) \tag{7-19}$$

The end temperature cannot be raised beyond this value.

In the practical design of a ram jet, C_q may be given, while M_{B1}^* is to be expressed in terms of more fundamental parameters such as the flight Mach number M_0 or M_0^*. [Since

$$\frac{a_0^2}{k-1} + \frac{V_0^2}{2} = \frac{1}{2}\frac{k+1}{k-1} a_0^{*2}$$

by Eq. (7-4), $M_0 = V_0/a_0$ and $M_0^* = V_0/a_0^*$ are related by

$$M_0^{*2} = M_0^2 \frac{a_0^2}{a_0^{*2}} = \frac{(k+1)M_0^2}{2 + (k-1)M_0^2} \tag{7-20}$$

The use of M_0 or M_0^* instead of the flight speed V_0 makes the results independent of altitude and the ambient atmospheric conditions.]

Another basic parameter is the mass-flow ratio

$$m = \frac{\rho_{B1} V_{B1}}{\rho_0 V_0} \tag{7-21}$$

which in turn is dependent on the ratio of the exit area A_e of the fairing to the cross-section area A_B of the combustion chamber, as will be seen below.

The inflow up to the combustion chamber, which is assumed to be isentropic, has already been dealt with in Chap. 4, and Eqs. (4-9) and (4-10) give p_{B1}/p_0 and ρ_{B1}/ρ_0 and thus m as functions of M_0 and V_{B1}/V_0. Also,

$$M_{B1}^* = \frac{V_{B1}}{V_0} M_0 \frac{a_0}{a_0^*} = \frac{V_{B1}}{V_0} M_0^*$$

Figure 7-5 shows how the Mach number at the beginning of the combustion chamber varies with flight Mach number for various mass-flow ratios, and Fig. 7-6 shows that high flight Mach numbers and low mass-flow ratios are needed to obtain a high ram pressure. Naturally, for the subsonic ram jet, the highest pressure ratio is reached when $M_0 = 1$ and $m = 0$, for which

$$\frac{p_{B1}}{p_0} = \left(\frac{k+1}{2}\right)^{k/(k-1)} = 1.89$$

from Eq. (4-9).

7-4. Outflow through the Nozzle. The outflow from the combustion chamber through the nozzle[1] can also be regarded as an isentropic change of state during which the pressure drops until atmospheric pressure is reached, $p_j = p_0$. This usually happens at the exit of the fairing, $p_e = p_0$, unless the fairing is very short (see Sec. 5-6) or the nozzle is so shaped as

[1] See also the recent summary report by G. S. Schairer, 1951.

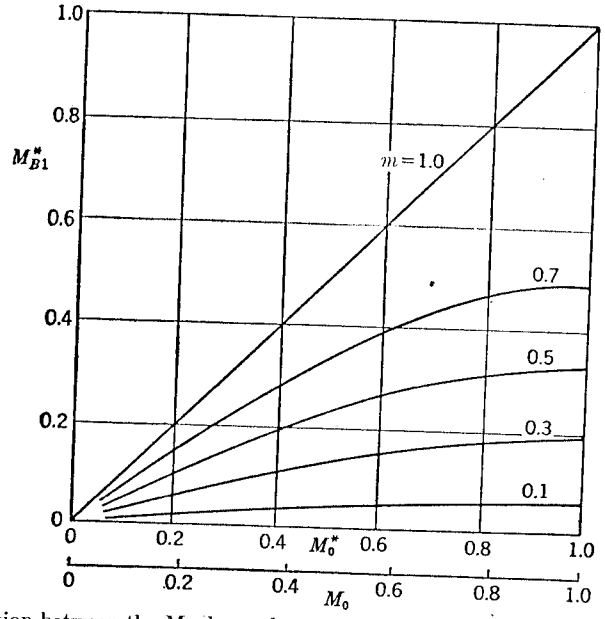

FIG. 7-5. Relation between the Mach number at the beginning of the combustion chamber and the flight Mach number, for various mass-flow ratios. Isentropic inflow.

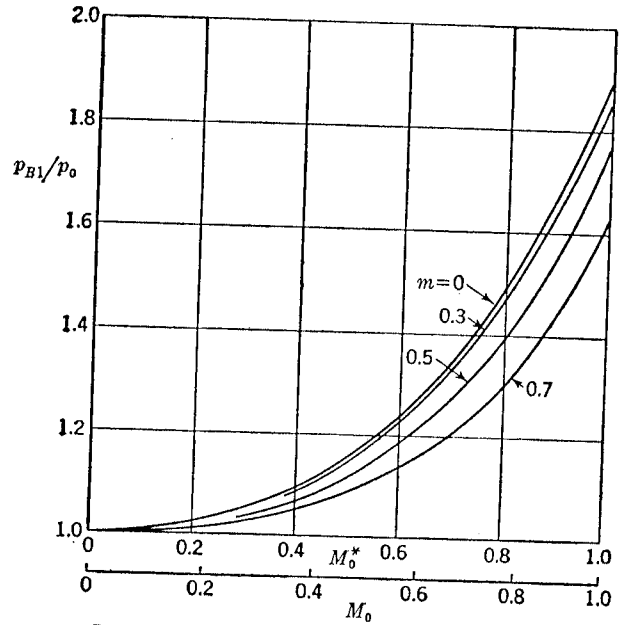

FIG. 7-6. Ram pressure for isentropic inflow.

to introduce radial-velocity components. The pressure drop is determined by

$$\frac{p_0}{p_{B2}} = \left\{1 + \frac{k-1}{2} \mathrm{M}_{B2}^2 \left[1 - \left(\frac{V_j}{V_{B2}}\right)^2\right]\right\}^{k/(k-1)} \tag{7-22}$$

which corresponds to Eq. (4-9). The velocity ratio in the nozzle can be written as

$$\begin{aligned}\frac{V_j}{V_{B2}} &= \sqrt{1 + \frac{2}{k-1}\frac{1}{\mathrm{M}_{B2}^2}\left[1 - \left(\frac{p_0}{p_{B2}}\right)^{(k-1)/k}\right]} \\ &= \sqrt{1 + \left(\frac{k+1}{k-1}\frac{1}{\mathrm{M}_{B2}^{*2}} - 1\right)\left[1 - \left(\frac{p_0}{p_{B2}}\right)^{(k-1)/k}\right]}\end{aligned} \tag{7-23}$$

and the velocity ratio V_j/V_0, which determines the thrust, is

$$\begin{aligned}\frac{V_j}{V_0} &= \frac{V_j}{V_{B2}}\frac{V_{B2}}{V_{B1}}\frac{V_{B1}}{V_0} = \frac{V_j}{V_{B2}}\frac{\rho_{B1}}{\rho_{B2}}\frac{\mathrm{M}_{B1}^*}{\mathrm{M}_0^*} \\ &= \sqrt{1 + C_q}\,\frac{1}{\mathrm{M}_0^*}\sqrt{\mathrm{M}_{B2}^{*2} + \left(\frac{k+1}{k-1} - \mathrm{M}_{B2}^{*2}\right)\left[1 - \left(\frac{p_{B2}}{p_0}\right)^{(k-1)/k}\right]}\end{aligned} \tag{7-24}$$

The sonic state is reached in the jet, $V_j = a_j^*$, if the pressure ratio in the nozzle becomes

$$\begin{aligned}\left(\frac{p_0}{p_{B2}}\right)_{\text{crit}} &= \left[1 + \frac{k-1}{2}\mathrm{M}_{B2}^2\left(1 - \frac{1}{\mathrm{M}_{B2}^{*2}}\right)\right]^{k/(k-1)} \\ &= \left[\frac{2}{k+1-(k-1)\mathrm{M}_{B2}^{*2}}\right]^{k/(k-1)}\end{aligned} \tag{7-25}$$

which follows from Eq. (7-22) and $a_{B2}^* = a_j^*$. Some numerical values are:

M_{B2}^*	0.0	0.2	0.4	0.6	0.8	0.9	1.0
$\left(\frac{p_0}{p_{B2}}\right)_{\text{crit}}$	0.528	0.541	0.581	0.656	0.784	0.878	1.000

The pressure ratio for $\mathrm{M}_{B2}^* = 0$,

$$\left(\frac{p_0}{p_{B2}}\right)_{\text{crit}} = \left(\frac{2}{k+1}\right)^{k/(k-1)} = 0.528 = \frac{1}{1.89}$$

is that given by the Saint-Venant theorem for the flow out of a large reservoir, to which the present problem is closely related. The above relations are quite general and can be applied to the flow in the nozzle of any jet engine.

At subsonic flight speeds, the sonic state can never be reached in the jet with a ram-jet type of engine, except in the trivial case $\mathrm{M}_0 = 1$, $m = 0$ where the maximum ram pressure $p_{B1}/p_0 = 1.89$ is just sufficient to produce sonic speed again in the exit; M_{B2} is then zero. For small values of m, we find, from Eq. (7-24), that

$$V_j = V_0\sqrt{1 + C_q}$$

and with $a_j^* = a_{B2}^* = \sqrt{1 + C_q}\,a_0^*$, we have $\mathrm{M}_j^* = \mathrm{M}_0^*$ [see also Eq. (7-32)]. In the practical ram jet with losses, $\mathrm{M}_j^* < \mathrm{M}_0^*$ always. If the value of m is not small, the Mach number V_j in the jet is further reduced in any case. For combustion at constant pressure, this is related to the fact that the Mach number falls in the combustion chamber (because $V_{B2} = V_{B1}$ and $a_{B2}^* = \sqrt{1 + C_q}\,a_{B1}^*$); and for the ram jet with cylindrical combustion chamber, it is a consequence of the decrease in pressure during combustion. It does not apply to the ram jet in supersonic flow or to turbojet engines in any part of the speed range.

The ratio of exit area to combustion chamber area required to make $p_e = p_0$ is

$$\frac{A_e}{A_B} = \frac{\rho_{B2}}{\rho_e}\frac{V_{B2}}{V_e} = \frac{\rho_{B2}}{\rho_j}\frac{V_{B2}}{V_j} = \left(\frac{p_{B2}}{p_0}\right)^{1/k}\frac{1}{V_j/V_{B2}} \tag{7-26}$$

and with this relation the flow conditions at any stage can be worked out as functions of M_0, C_q, and A_e/A_B.

7-5. Ideal Thrust and Efficiency. A thrust coefficient which corresponds to the loading coefficient of a propeller is obtained by relating the thrust force **T** to the dynamic pressure of the free stream and the cross-section area of the combustion chamber:

$$C_{\mathbf{T}} = \frac{\mathbf{T}}{\frac{1}{2}\rho_0 V_0^2 A_B} \tag{7-27}$$

From the momentum theorem, Eq. (2-28),

$$C_{\mathbf{T}} = \frac{\rho_{B1}V_{B1}A_B(V_j - V_0)}{\frac{1}{2}\rho_0 V_0^2 A_B} = 2m\left(\frac{V_j}{V_0} - 1\right) \tag{7-28}$$

The velocity ratio V_j/V_0 in the jet is given by Eq. (7-24). M_0 and C_q are independent parameters; the mass-flow ratio m, as well as M_{B2} and p_{B2}/p_0, can be deduced from them if the dimensions of the engine are known, *i.e.*, if the exit area ratio is given and the pressure at the exit is known.

Another convenient set of design parameters consists of the pressure at the beginning of combustion, the maximum temperature, and the flight Mach number; see, for example J. Reid and P. J. Herbert (1946).

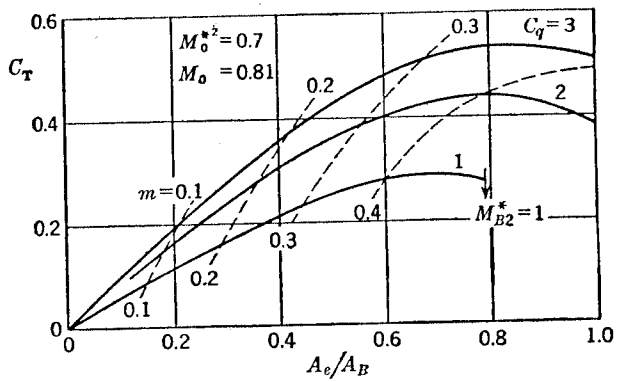

FIG. 7-7. Variation of thrust coefficient with nozzle area ratio and heat-input coefficient for an ideal ram jet at a subsonic flight speed.

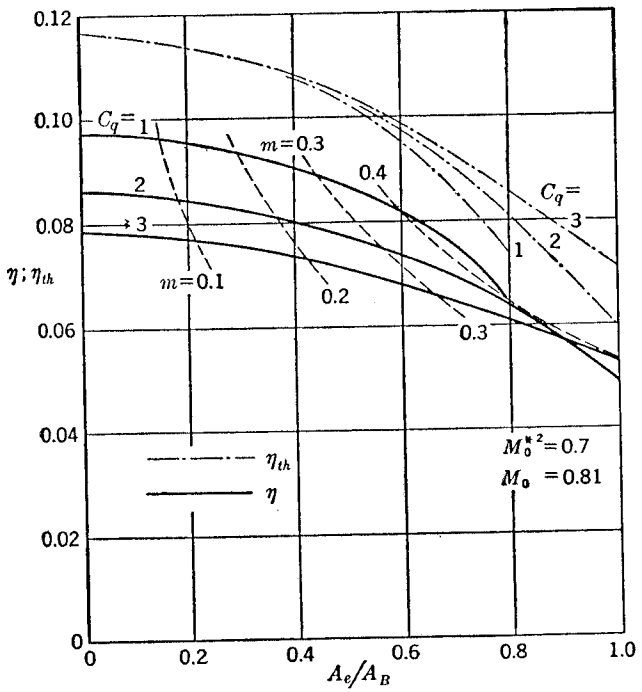

FIG. 7-8. Efficiencies corresponding to the data in Fig. 7-7.

The thrust coefficient for heat-supply coefficients $C_q = 1$, 2, and 3 is plotted in Fig. 7-7 against the exit area ratio, assuming $p_e = p_0$, at a flight Mach number of 0.81. The thrust increases at first as the nozzle is opened, because more air passes through the engine and the actual heat input is increased, C_q being constant [q in Eq. (7-9) is of course the heat input per unit weight of air]. The maximum thrust coefficient is reached

with an exit area A_e less than A_B since, as the mass flow increases, a point is reached at which the reduction of ram pressure outweighs the gain from the increased heat input. Figure 7-9 shows how the thrust coefficient at this optimum rate of flow depends on the flight Mach number.

The over-all efficiency of the ideal ram jet is

$$\eta = \frac{\mathbf{T}V_0}{q\rho_{B1}V_{B1}A_B g} = 2\frac{k-1}{k+1}\,\mathrm{M}_0^{*2}\frac{C_T}{2mC_q} = \frac{(k-1)\mathrm{M}_0^2}{2+(k-1)\mathrm{M}_0^2}\frac{C_T}{mC_q} \tag{7-29}$$

It can be split up into the thermal efficiency η_{th}, with which the heat input is converted into available mechanical energy, and the jet efficiency

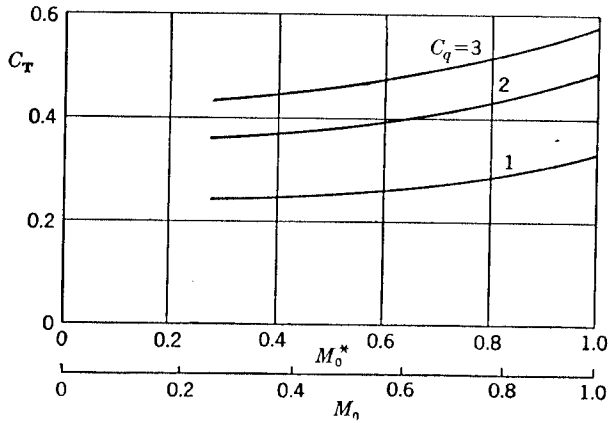

FIG. 7-9. Maximum thrust coefficients for an ideal ram jet in subsonic flow

η_j, with which the available energy is used for propulsion:

$$\eta = \eta_{th}\eta_j \tag{7-30}$$

From Eqs. (2-31) and (7-28),

$$\eta_j = \frac{2}{1+V_j/V_0} = \frac{1}{1+C_T/4m} \tag{7-31}$$

These formulas can be used to express the over-all and thermal efficiencies as functions of M_0, C_q, and m (or A_e/A_B).

The thermal efficiency falls off considerably with increase of mass flow, as the example in Fig. 7-8 shows. When the mass flow is low, the velocity in the jet [Eq. (7-24)] can be expanded in a power series in m:

$$\frac{V_j}{V_0} = \sqrt{1+C_q}\left\{1-\frac{C_q}{2}\left(1-\frac{k-1}{k+1}\,\mathrm{M}_0^{*2}\right)^{(k+1)/(k-1)} m^2 + \cdots\right\} \tag{7-32}$$

from which we see that

$$\lim_{m\to 0}\eta_j = \frac{2}{1+\sqrt{1+C_q}}$$
$$\lim_{m\to 0}\eta_{th} = \frac{k-1}{k+1}\,\mathrm{M}_0^{*2} \tag{7-33}$$

If C_q also is made very small, the over-all efficiency approaches the thermal efficiency of the constant-pressure process with the combustion

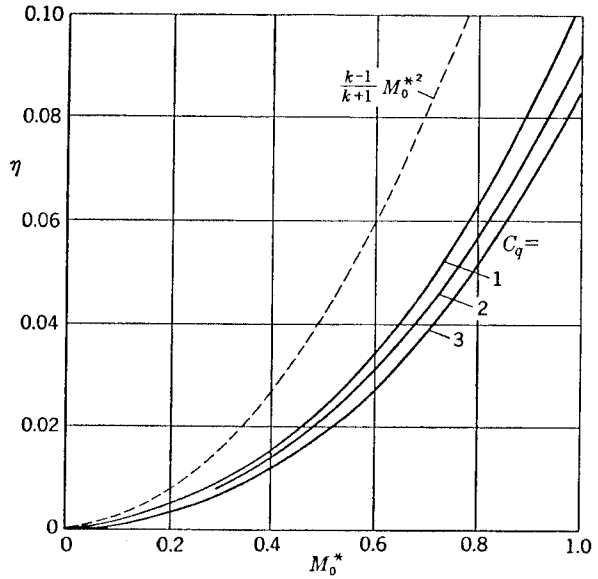

FIG. 7-10. Efficiencies corresponding to the data in Fig. 7-9.

pressure p_{B1}. Some values of the maximum thermal efficiency as given by Eq. (7-33) are:

M_0	0	0.100	0.200	0.300	0.400	0.500	0.600	0.700	0.800	0.900	1.0
M_0^*	0	0.109	0.218	0.326	0.431	0.534	0.634	0.731	0.825	0.915	1.0
$\eta_{th\max}$, %	0	0.2	0.8	1.8	3.1	4.8	6.7	8.9	11.4	13.9	16.7

These efficiencies are low compared with those of a jet engine with a compressor, as will be seen in Chap. 8.

7-6. Deviations from the Ideal Process. The ideal working process discussed so far can never be fully realized by a practical design, but the deviations are not necessarily large. Some losses are inevitable; the working air is not an ideal gas, and the flow is viscous. Other losses may be caused by unsuitably shaped components or by the nature of the engine installation in the lifting surface; the aim must be to keep these as small as possible.

Most of the more serious losses are due to the presence of the fairing, which cannot be dispensed with since without it there would be no thrust (see Sec. 2-6). Skin-friction forces on the fairing are unavoidable and their effect on the thrust and efficiency of the ram jet is similar to that discussed above in the case of the ducted propeller (Sec. 6-2). We can

again introduce a fairing drag coefficient,

$$C_{DF} = \frac{D_F}{\frac{1}{2}\rho_0 V_0^2 \pi D_B L_F}$$

where D_B is the diameter of the combustion chamber (or a corresponding length in the case of noncircular sections) and L_F the over-all length of the fairing. The net thrust is then

$$C_T = C_{T\,\text{ideal}} - 4\frac{L_F}{D_B} C_{DF} \tag{7-34}$$

where $C_{T\,\text{ideal}}$ is the thrust coefficient of the ram jet with cylindrical combustion chamber in nonviscous flow with the same m, C_q, and M_0.

The efficiency is similarly reduced,

$$\eta = \eta_{\text{ideal}}\left(1 - 4\frac{L_F}{D_B}\frac{C_{DF}}{C_{T\,\text{ideal}}}\right) \tag{7-35}$$

It is estimated that $4L_F C_{DF}/D_B$ is of the order of 0.05 to 0.1. As in the case of the ducted propeller, high thrust coefficients and short fairings are

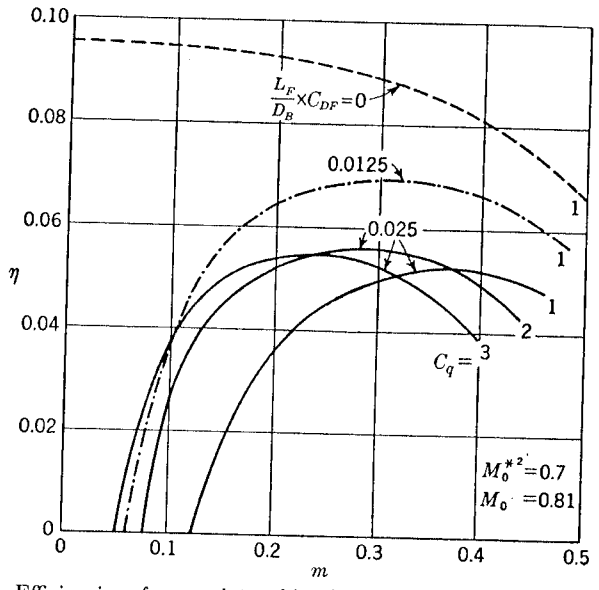

FIG. 7-11. Efficiencies of a ram jet, taking into account the drag of the fairing.

desirable to limit this reduction of efficiency. Figure 7-11 illustrates the effect of fairing drag. The greater the drag coefficient, the higher are the mass-flow and heat-input coefficients at which the optimum efficiency is reached, and the thrust coefficient can be considerably increased without much loss in efficiency.

These considerations influence the basic design of the engine. It is usually required to provide a certain thrust at a given flight speed, and

this can be done with engines of various sizes, for example, with different frontal areas. Engines of large frontal area give the required thrust at small thrust coefficients, which can be obtained with low mass-flow ratios and therefore small values of A_e/A_B or low heat-input coefficients. Engines of small frontal area can produce the same thrust by operating at high thrust coefficients. Ideally, the large engine has the better efficiency, but the smaller heavily loaded engine is preferable in viscous flow.

A further consequence of the viscosity of the flow is that the thrust forces which should act on the fairing may not be realized in full. It is therefore useful to know what the relative contributions of the various parts of the fairing to the total thrust should be, and for this we can apply the momentum theorem again. Particular flow regimes have already been studied in previous chapters—the external suction force on the intake in Sec. 4-2, the thrust in the diffuser in Sec. 4-9, and the external drag on the rear end of the fairing in Sec. 5-1. An example is given in Fig. 7-12, in which, with a particular set of values of flight Mach number, mass-flow ratio, and heat-input coefficient, the diffuser area ratio A_i/A_B is varied. As the inlet area decreases, the diffuser takes more and more of the thrust force, thus relieving the suction on the outer surface of the intake. The intake and the diffuser together sustain a higher thrust force than the net thrust of the engine, because of the drag forces at the rear of the fairing. If $p_e = p_0$, the drag on the outer surface of the fairing afterbody is zero, but the pressures inside the nozzle are higher than atmospheric and produce a resultant drag on its contracting walls. When $p_e > p_0$, the nozzle contribution is smaller, but then the drag at the outer surface of the fairing afterbody is no longer zero.

There is little likelihood of flow separation inside the nozzle because of the negative pressure gradient. On the outer surface, on the other hand, even zero afterbody drag implies a suction followed by positive pressures; this calls for careful design to avoid both shock waves and separation due to pressure gradient. The same applies to the design of the intake with its high suction, and a careful study should be made of the best distribution of thrust between intake and diffuser. Figure 7-12 shows that the diffuser can take a large share of the thrust before the mean pressure rise there becomes excessive. Moreover, the diffuser can be so shaped as to make the actual pressure rise at the walls less than the mean rise, or even zero, because of the ram effect of the burner (see Secs. 3-1 and 3-6). Diffuser shapes for practical use have as yet been designed only for cooler blocks, the requirements for which are, however, similar to those here (see Sec. 12-2).

Some further respects in which the actual process differs from the ideal may be mentioned. In practice, the heat supply is generated by burning

hydrocarbons, the weight of which is added to the air flow. The ratio μ of the weight of the fuel to the weight of air for combustion is fixed roughly by the chemical reaction. If the fuel is gasoline, the chemically correct (stoichiometric) ratio is about $\frac{1}{14}$. The actual ratio is usually

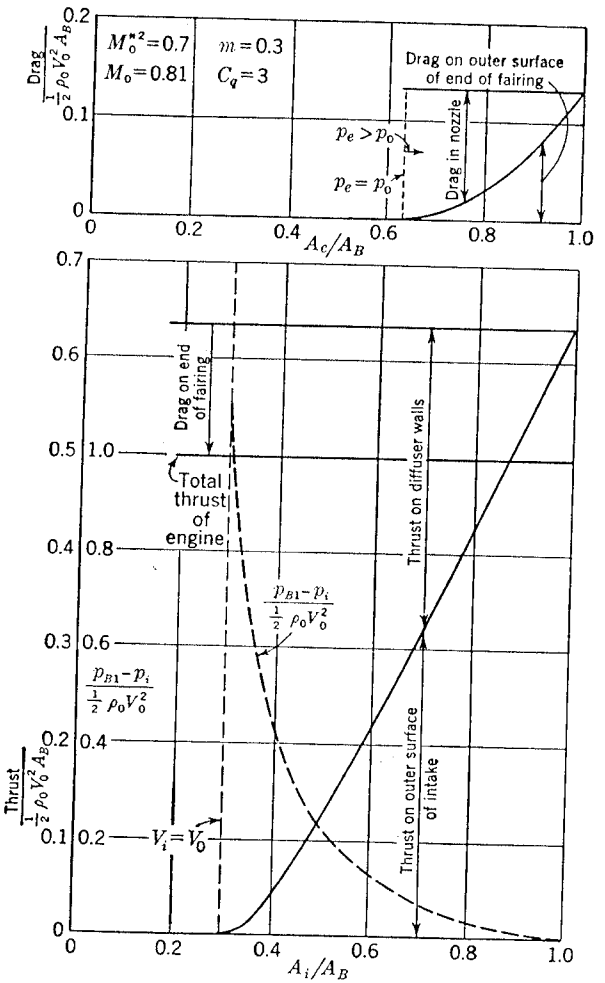

FIG. 7-12. Thrust and drag components on a ram jet and the mean pressure rise in the diffuser for various diffuser and nozzle area ratios.

lower, between 0.02 and 0.06, partly to make sure that the combustion is complete and partly so that an excess of air passes through the engine and keeps it relatively cool; the maximum temperature reached is not only limited by the material of the combustion chamber and nozzle but also by the need to avoid dissociation of the gas.

Now a constant fuel-air ratio implies a constant specific heat supply q and therefore constant C_q (at constant speed and altitude). Introducing the calorific value of the fuel, H, we obtain

$$q = \mu H$$

since the enthalpy of the fuel is small enough compared with H to be neglected. The calorific value of petrol is about $H = 4.35 \times 10^6$m-kg/kg (per kilogram of fuel used), which gives C_q values between 2 and 3 for $\mu = 0.02$ and between 4 and 5 for $\mu = 0.04$. The effect of adding the mass of the fuel can be taken into account in the energy equation (7-6) and in the continuity equation (7-7) for the combustion stage.

The fact that the working fluid is not an ideal gas makes itself apparent in that the values of c_p and k are not constant. This can be taken into account either by the use of diagrams applicable to the actual gases present or, more crudely, by treating the fluid as ideal but with different constants before and after combustion.

7-7. Experimental Efficiencies. Comparison with the Pulse Jet. Little experimental evidence is as yet available to show how far the calculated thrusts and efficiencies are realized in an actual ram-jet engine. A wind-tunnel test was actually made on a ram jet model to the design illustrated in Fig. 7-1, and some preliminary results completed.[1] The intake was the contour A-31 in the nomenclature of Sec. 4-6; the streamline diffuser was one of the series described in Sec. 12-3; and the fairing afterbody was designed using the data in Sec. 5-1. Special burners (see Sec. 8-4) which made a very short combustion chamber possible were used, with the great advantage of keeping the external drag low. Hydrogen was the fuel; thus the numerous practical difficulties associated with the evaporation and combustion of gasoline were evaded in this test.

Figure 7-13 shows the thrust and efficiency of the engine; the measured efficiency was in very good agreement with the efficiency calculated. The fairing drag allowed for in the calculation was deduced from the results given in Sec. 4-6.

As a matter of interest, the thrust and efficiency of the Argus-Schmidt intermittent jet engine (used as power plant for the V-1 missile) have been included in Fig. 7-13. They were obtained from flight measurements. The thrust of the ram jet has in fact been scaled up to the dimensions of the pulse jet ($D_{max} = 0.565$ m). The Argus-Schmidt tube works on a different principle[2] and produces a finite thrust at zero forward speed, but there is a certain amount of ram effect, partly offset by the comparatively high drag of the necessarily long fairing. With the particular thrust loadings of this comparison, the ram jet is the more efficient from about

[1] O. Pabst, 1945 (unpublished).

[2] See, for example, F. Schultz-Grunow, 1944.

$M_0 = 0.5$ onward, but the actual thrust of the pulse jet is considerably higher throughout the range shown. The thrust of the ram jet could be increased by the utilization of higher jet temperatures. Raising the jet temperature from 800 to 1000°C would increase the thrust by about 20 per cent at $M_0 = 0.8$; the efficiency would then be reduced by about 3 per cent.

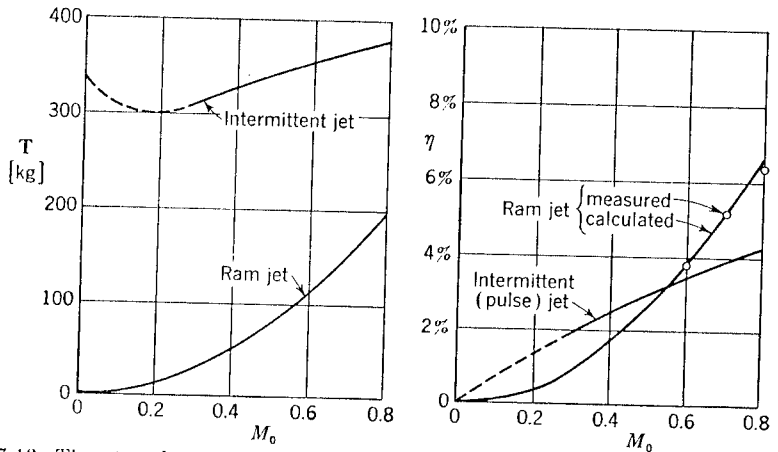

FIG. 7-13. Thrust and efficiency of the ram jet of Fig. 7-1 compared with those of the Argus-Schmidt intermittent pulse jet. (*Note:* The thrust of the ram jet has been scaled up; see text.)

7-8. Some Remarks on the Supersonic Ram Jet. It is obvious from what has been said above that the thermal efficiency of the ram jet becomes superior to that of any other available power plant at supersonic speeds. Optimum values of η_{th} from Eq. (7-1) (constant-pressure combustion and $V_{B1} = 0$) are:

η_{th}	0.05	0.17	0.44	0.64	0.76	0.83
At M_0	0.5	1	2	3	4	5

These efficiencies, together with the extreme simplicity of the engine, promise a wide range of application. The fundamental working process is the same as that described in the previous sections, and most of the relations derived there are not restricted to subsonic flow. They must be supplemented, however, by a consideration of the flow phenomena and losses which are characteristic of supersonic flow and by some new features of the practical engine. Since very few investigations of supersonic ram jets have as yet been published, we shall restrict ourselves here to a few illustrative remarks.

The layout of a ram jet designed for $M_0 = 2.9$ by K. Oswatitsch (1944) is shown in Fig. 7-14. The subsonic diffuser within the fairing, the com-

bustion chamber (this time intended to burn liquid fuel), and the subsonic nozzle are basically the same as those of a subsonic ram jet, but the duct now begins with a supersonic diffuser and ends with a supersonic nozzle.

The flow in the nozzle is of the Laval nozzle type, with a continuous transition from subsonic to supersonic speed at the narrowest cross section. New problems arise in the design of a supersonic diffuser to decelerate the flow to subsonic speed. The special type of diffuser shown in Fig. 7-14 is only one of several forms that have been suggested; it would be possible to use a duct similar to a Laval nozzle but with the flow direction reversed, or a plain Pitot intake.[1]

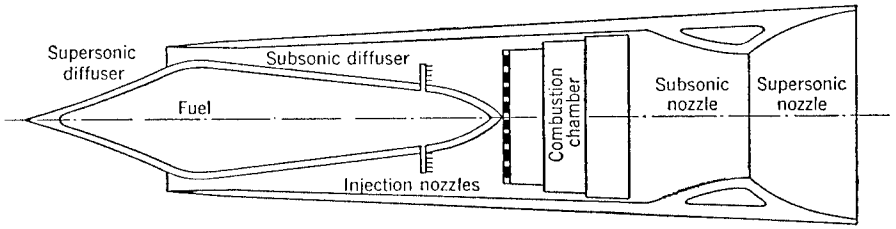

FIG. 7-14. Supersonic ram jet to burn liquid fuel, from a design by K. Oswatitsch, 1944, for $M_0 = 2.9$.

Let us consider the latter case and assume the narrowest cross section to be at the inlet opening with the subsonic diffuser immediately behind. The intake could be similar to the circular intakes of Secs. 4-6 and 4-7 (with no central body). This case might well occur in practice when an essentially subsonic intake is sometimes flown beyond the speed of sound. The supersonic diffuser might then take the simplest form of a discontinuous compression in a shock wave normal to the direction of flow, either attached to the rim of the inlet or detached upstream of the intake; the shock can be attached only with a sharp-lipped intake at one Mach number and mass-flow ratio, when the mass $\rho_0 V_0 A_i$ enters the inlet per unit time.

It will be worth while to consider briefly the changes in the flow parameters due to the shock wave and its consequences for the inflow.[2] Consider a stream tube of the inflow passing through a shock at right angles. The conditions immediately behind the shock (subscript II) are determined by those ahead (subscript I). As usual, four general equations hold: the equation of state (2-1), the continuity equation,

$$\rho_I V_I = \rho_{II} V_{II}$$

the momentum theorem applied to a surface close around the shock,

$$p_I + \rho_I V_I^2 = p_{II} + \rho_{II} V_{II}^2$$

[1] For further information, see, for example, A. Ferri, 1949.

[2] See also R. Courant and K. O. Friedrichs, 1948, for a proper discussion of these problems.

and the energy equation,

$$\frac{k}{k-1}\frac{p_I}{\rho_I} + \frac{V_I^2}{2} = \frac{k}{k-1}\frac{p_{II}}{\rho_{II}} + \frac{V_{II}^2}{2} = \frac{1}{2}\frac{k+1}{k-1}a^{*2}$$

Eliminating ρ_I, ρ_{II}, p_I, and p_{II}, we find

$$V_I V_{II} = a^{*2} \qquad \text{or} \qquad M_I^* M_{II}^* = 1 \tag{7-36}$$

which means that the flow changes from a supersonic to a subsonic state. There is a pressure rise in the shock,

$$\frac{p_{II}}{p_I} = \frac{\frac{k+1}{k-1}M_I^{*2} - 1}{\frac{k+1}{k-1} - M_I^{*2}} = 1 + \frac{2k}{k+1}(M_I^2 - 1) \tag{7-37}$$

so that

$$\frac{p_{II} - p_I}{\frac{1}{2}\rho_I V_I^2} = \frac{4}{k+1}\left(1 - \frac{1}{M_I^2}\right) \tag{7-37a}$$

Density and temperature are also increased,

$$\frac{\rho_{II}}{\rho_I} = M_I^{*2} = \frac{(k+1)M_I^2}{2 + (k-1)M_I^2} \tag{7-38}$$

$$\frac{T_{II}}{T_I} = \frac{\frac{p_{II}}{p_I}}{\frac{\rho_{II}}{\rho_I}} = \frac{\frac{k+1}{k-1}M_I^{*2} - 1}{\frac{k+1}{k-1}M_I^{*2} - M_I^{*4}} \tag{7-39}$$

Note that the compression is not isentropic.

$$\frac{s_{II} - s_I}{R} = \ln \frac{(p_{II}/p_I)^{1/(k-1)}}{(\rho_{II}/\rho_I)^{k/(k-1)}}$$

$$= \frac{k}{k-1}\ln\left[\frac{1}{M_I^{*2}}\left(\frac{\frac{k+1}{k-1}M_I^{*2} - 1}{\frac{k+1}{k-1} - M_I^{*2}}\right)^{1/k}\right]$$

$$= \frac{k}{k-1}\ln\left\{\frac{2 + (k-1)M_I^2}{(k+1)M_I^2}\left[1 + \frac{2k}{k+1}(M_I^2 - 1)\right]^{1/k}\right\} \tag{7-40}$$

An expansion or rarefaction shock is not physically possible, because the entropy change through it would be a decrease.

Applying these results to supersonic intakes, we may assume in the simplest case that all the air which passes through the engine has been subject to a normal shock in the inflow. The conditions ahead of the shock are the same as far upstream (subscript 0). Because it causes an entropy increase, the shock reduces the available energy of the inflow.

This takes the form of a reduction of the pressure that can be obtained at the beginning of the combustion chamber (subscript $B1$). When the inflow is isentropic, the compression is given by

$$\frac{p_{B1}}{p_0} = \left\{1 + \frac{k-1}{2}\,\mathrm{M}_0^2\left[1 - \left(\frac{V_{B1}}{V_0}\right)^2\right]\right\}^{k/(k-1)}$$

$$\frac{p_{B1}}{p_0} = \left\{1 + \frac{\dfrac{k-1}{k+1}\,\mathrm{M}_0^{*2}}{1 - \dfrac{k-1}{k+1}\,\mathrm{M}_0^{*2}}\left[1 - \left(\frac{V_{B1}}{V_0}\right)^2\right]\right\}^{k/(k-1)} \tag{7-41}$$

from Eq. (4-9). When the inflow is through a normal shock but otherwise isentropic, the compression is

$$\frac{\hat{p}_{B1}}{p_0} = \frac{p_{II}}{p_0}\frac{\hat{p}_{B1}}{p_{II}} = \frac{\dfrac{k+1}{k-1}\,\mathrm{M}_0^{*2} - 1}{\dfrac{k+1}{k-1} - \mathrm{M}_0^{*2}}\left\{1 + \frac{1}{\dfrac{k+1}{k-1}\,\mathrm{M}_0^{*2} - 1}\left[1 - \left(\frac{V_{B1}}{V_0}\right)^2 \mathrm{M}_0^{*4}\right]\right\}^{k/(k-1)} \tag{7-42}$$

with

$$\mathrm{M}_0^2 = \frac{2\mathrm{M}_0^{*2}}{k + 1 - (k-1)\mathrm{M}_0^{*2}}$$

by Eq. (7-20). $\hat{p}_{B1}/p_0$ is always smaller than p_{B1}/p_0. Expanding both into power series in $(\mathrm{M}_0^{*2} - 1)$, for $V_{B1} = 0$, we find, however, that the terms in $(\mathrm{M}_0^{*2} - 1)$ and $(\mathrm{M}_0^{*2} - 1)^2$ are the same for $\hat{p}_{B1}/p_0$ and p_{B1}/p_0. This means that the pressure losses are not serious for flight Mach numbers only slightly higher than 1. However, with increasing Mach number, the loss of ram pressure becomes considerable, as is shown by Table 7-1, for $V_{B1} = 0$.

TABLE 7-1

M_0	p_{B1}/p_0	$\hat{p}_{B1}/p_0$
1.0	1.89	1.89
1.5	3.7	3.4
2.0	7.8	5.6
2.5	17.1	8.6
3.0	36.7	12.1

This applies to all intakes with a normal shock in the inflow whether the shock is detached or not, provided the whole inflow is subjected to it. The reduction in pressure at the beginning of the combustion chamber results in a reduction of η_{th}, which in turn reduces the final velocity V_j in

the jet and therefore the thrust [Eq. (7-28) is still true]. The fuel consumption is also affected. The loss of available energy due to a shock is similar in its consequences to that due to flow separation in the diffuser or to frictional forces along walls ahead of the intake, discussed in detail in Chap. 9.

It still remains to be seen to what extent this type of flow can be realized and whether there are still other effects to be taken into account. Consider, for example, the flow past the outer surface of the intake. Let there be a normal shock across the stream tube entering the fairing, and let it be detached from the inlet so that there is a second (subsonic) compression behind the shock in the free stream, which may be isentropic. This subsonic retardation is associated with suction forces on the outer surface of the intake, as has been explained in Sec. 4-3.

The problem is now how to shape the intake so that such suction forces are in fact produced. It appears that this cannot be done without further complications. These begin when the main flow is still subsonic. For instance, the flow past the intake becomes supersonic locally at $\mathrm{M}_0 < 1$ as soon as the local pressure coefficient exceeds the critical value given by Eq. (4-20). Consequently, the pressure distribution along the surface will be distorted so as to give less suction; a shock wave may occur near the end of the supersonic region. The external drag is thus effectively increased and a further reduction of the over-all efficiency follows.

Further, at both subsonic and supersonic Mach numbers, the theoretical negative pressure $(p - p_0)$ at the nose of the intake which is necessary to produce the suction force may become greater than the atmospheric pressure p_0, which is of course impossible in practice since the pressure can nowhere be lower than vacuum.

Finally, at supersonic speeds there will be a stagnation line at the lip of the intake if the shock is detached, and the flow must then be accelerated along the surface until eventually it reaches the Mach number of the free stream again. It is difficult to imagine what shape of intake will give such a flow and at the same time produce the necessary thrust. Clearly, the picture of the flow presented above is incomplete, and there are further effects to be considered. These problems remain to be satisfactorily solved.

Matters are somewhat simplified if the shock wave is not detached but rests on the lip of the intake, so that no suction is required on the outer lip such as results from a subsonic compression. With the particular type of supersonic ram jet shown in Fig. 7-14 the conical body in the inlet opening is designed to produce a series of oblique shock waves running to the lip of the outer fairing at the design Mach number. The supersonic diffuser ends with a normal shock at the narrowest cross section of the

entry. The idea behind this type of supersonic diffuser is to reduce the increase of entropy compared with that in a single normal shock. In this as in any other case where the configuration of the shock waves is known, the reduction of the combustion pressure and its effect on the performance of the engine can be worked out, in the way indicated above for the simplest case of one normal shock.

Yet another fundamental difference distinguishes supersonic from subsonic air intakes. A change of flight speed or of another basic parameter does not alter the type of flow in the subsonic case, and the characteristics of a particular engine can be calculated over the whole range. In the case of supersonic air intakes, however, any deviation from the design conditions may alter the type of flow considerably. In particular, at a flight Mach number different from the design value the configuration of the shock waves will be different.

The external drag of a body with air intake in supersonic flow consists to a large extent of wave drag. This can be determined in some cases by means of known calculation methods the treatment of which goes beyond the scope of this book [see, for example, G. N. Ward (1948)]. There will be a drag component due to the pressure on the slightly conical outer surface drawn in Fig. 7-14, but in this case it is not impossible to have the outer shape cylindrical.

EXERCISES

7-1. Determine the temperature shown by a stagnation thermometer in a flow with velocity $V_0 = 300$ m/sec and temperature $T_0 = 273°K$.

7-2. Calculate the stagnation pressure in a flow at sea level with $V_0 = 300$ m/sec and $T_0 = 273°K$.

7-3. A quantity of heat $q = 2(c_pT_0 + V_0^2/2g)$ is supplied to unit weight of an air stream with an initial speed $V_0 = 300$ m/sec and initial temperature $T_0 = 273°K$. Calculate the critical velocity of sound and the stagnation temperature.

7-4. The velocity in a jet is 400 m/sec (600 m/sec; 800 m/sec). What is the temperature if the velocity is sonic?

7-5. Confirm Eq. (7-19).

7-6. Calculate the maximum-combustion end temperature T_{B2} (for $M_{B2}^* = 1$) for a ram jet flying at $V_0 = 300$ m/sec, $T_0 = 273°K$, sea level, when the velocity V_{B1} at the beginning of the combustion chamber is 50 m/sec, 100 m/sec, 150 m/sec.

7-7. Find the maximum thermal efficiency η_{th} (for $C_q \to 0$) of a ram jet flying at $V_0 = 300$ m/sec, $T_0 = 273°K$, sea level, for various values of the velocity V_{B1} at the beginning of the combustion chamber.

7-8. Calculate the maximum thermal efficiency η_{th} (for $C_q \to 0$ and $V_{B1} \to 0$) of a ram jet at supersonic speeds with $M_0 = 2, 3, 4$, when (*a*) a normal shock occurs in the inflow and (*b*) the inflow is isentropic.

BIBLIOGRAPHY

Becker, J. V., and D. D. Baals, Analysis of Heat and Compressibility Effects in the Internal Flow Systems and High-speed Tests of a Ram-jet System, *NACA TR* 773, 1943.

Schultz-Grunow, F., Gas-dynamic Investigations of the Pulse-jet Tube, translation, *NACA TM* 1131, 1947 (1944).

Pabst, O., Die Auslegung von Lorintriebwerken, *Focke-Wulf Bericht* 09041, 1944; Vorläufige Mitteilung über den Versuch an der FW-Heizdüse im Windkanal A9 der LFA Braunschweig, *Focke-Wulf Bericht* 09045, 1945.

Multhopp, Ilse, Aerodynamic Principles of the Lorin Jet-unit, *Brit. Min. of Supply (Völkenrode) Rept. & Transl.* 17, 1945.

Reid, J., and P. J. Herbert, The Gas Dynamic Theory of the Ram-jet., *Brit. ARC Rept. & Mem.* 2370, 1946.

Ludwieg, H., and W. Mangler, The Lorin Power Unit (*AVA Monograph* J_3 4.21), *Brit. Min. of Supply (Völkenrode) Rept. & Transl.* 982, 1947.

Oswatitsch, K., The Lorin Drive with Special Regard to the Range of High Supersonic Velocities (*AVA Monograph* J_3 4.22), *Brit. Min. of Supply (Völkenrode) Rept. & Transl.* 982, 1947.

Liepmann, H. W., and A. E. Puckett, "Introduction to Aerodynamics of a Compressible Fluid," John Wiley & Sons, Inc., New York, 1947.

Courant, R., and K. O. Friedrichs, "Supersonic Flow and Shock Waves," Interscience Publishers, New York, 1948.

Ferri, A., "Elements of Aerodynamics of Supersonic Flows," The Macmillan Company, New York, 1949.

Ward, G. N., The Wave Lift and Drag Forces on a Propulsive Duct (Athodyd) Moving at Supersonic Speeds, *Quart. J. Mechanics and Applied Math.*, vol. 1, No. 2, 1948.

Schairer, G. S., Performance Characteristics of Jet Nozzles, *Proc. Third Anglo-American Aeronaut. Conf.*, Brighton, 1951, Royal Aeronautical Society, London, 1951.

CHAPTER 8

THE TURBOJET ENGINE

Turbojet engines are the most widely used of present-day jet engines. We shall discuss here some of their basic principles so that a working knowledge of their chief characteristics may be acquired. Some of the properties of heat engines have already been described in Chap. 7; in this chapter, we shall have to deal only with the problems introduced by the employment of a compressor and a turbine. In Sec. 8-1, the effects of the compressor and turbine on the over-all efficiency are treated. The design of these units is not discussed here, reference being made to the existing books and papers on the subject; but Sec. 8-2 deals with the way in which the large compression ratios required influence and inevitably decrease the compressor efficiency. Some of the arguments on the subject of the relative merits of centrifugal and axial compressors are presented in Sec. 8-3. Section 8-4 consists of a brief survey of combustion chambers. The over-all performance of turbojets is discussed in Sec. 8-5. This shows to what degree the turbojet is actually a *constant-thrust* engine and what conditions must be fulfilled in order to realize the full thrust. A comparison between various propulsion systems and their performances is too wide a subject to be discussed here, and again we refer to the various existing performance charts, some of which are listed at the end of the chapter. For a description of present-day jet engines, we refer to the exhaustive book by G. G. Smith.

8-1. Influence of the Compressor and Turbine Efficiencies and of the Combustion End Temperature on the Over-all Efficiency. The main characteristic of the turbojet engine is its high combustion pressure compared with that of the ram jet. This is achieved by a turbine-driven compressor. The basic thermodynamic processes of these engines have already been discussed in Secs. 2-2 and 2-6. Diagrams of an actual turbojet engine and of the working cycle are shown in Figs. 8-1 and 8-2 together with a rough sketch of the changes in velocity, pressure, and temperature that the air undergoes on its way through the engine. Obviously, the main aerodynamic problem is how to achieve the high compression ratio needed, but there are also the problems of combustion itself and the metallurgical problems which ensue from the high air temperatures at the turbine entry. The importance of the latter and the need to limit the combustion end temperature T_{B2} will be seen when it is realized that, in the Derwent 5 engine for instance, the turbine rotor runs

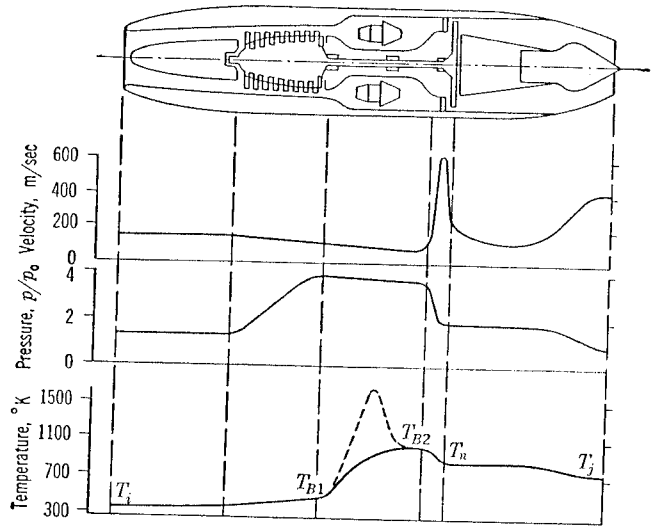

FIG. 8-1. Sketch of the Jumo 004 engine, and illustration of the variations of velocity, pressure, and temperature of the air.

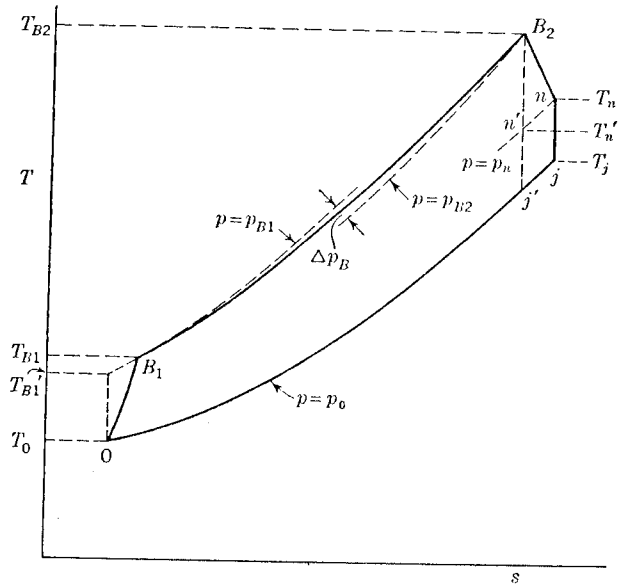

FIG. 8-2. Diagram of the working cycle of a turbojet engine, including compressor and turbine losses, but ignoring ram effect.

in gas at a temperature of about 1130°K and that the 54 individual blades, measuring about 3 in. long and 1.25 in. wide, have each to transmit about 75 hp [see G. G. Smith (1950)].

We assume that the heat is added at constant pressure. This is only an approximation, and the actual pressure drop in the combustion chamber, which is indicated in Fig. 8-2 by Δp_B, may be large enough to cause a noticeable reduction of the thermal efficiency of the cycle. However, our assumption is sufficiently accurate for our purpose. With constant combustion pressure p_B, the thermal efficiency of the ideal cycle, without losses, is, from Eq. (2-24),

$$\eta_{th}' = 1 - \frac{T_0}{T_{B1'}} = 1 - \left(\frac{p_0}{p_B}\right)^{(k-1)/k} \tag{8-1}$$

using the notation of Fig. 8-2. Ignoring for the time being the pressure rise due to ram effect, p_B/p_0 is the pressure ratio produced by the compressor, and we find that the thermal efficiency steadily improves with increasing compression ratio. In practice, however, the compression is not isentropic as has been assumed, nor is the expansion in the turbine isentropic. This radically affects the thermal efficiency.

We obtain the thermal efficiency of the working cycle, as above, by relating the available energy, which is

$$\Delta e_a = c_p(T_{B2} - T_{B1}) - c_p(T_j - T_0)$$

(see Sec. 2-2), to the energy input. The latter is $c_p(T_{B2} - T_{B1})$, if the kinetic energy does not change during the combustion. Hence,

$$\eta_{th} = \frac{\Delta e_a}{c_p(T_{B2} - T_{B1})} = 1 - \frac{T_j - T_0}{T_{B2} - T_{B1}} \tag{8-2}$$

For isentropic compression and expansion, $T_{B1}/T_0 = T_{B2}/T_j$, which gives Eq. (8-1).

Now, if the compression is not isentropic, as in Fig. 8-2, T_{B1} is higher than the isentropic value $T_{B1'}$ for the same p_B. This implies that the compressor consumes more work but also that the energy input in the combustion chamber can be slightly smaller, the air being slightly heated already by the compressor,[1] for a given value of the maximum temperature T_{B2}. The cycle efficiency, however, is reduced. If the expansion in the turbine is not isentropic, the temperature T_j in the jet is higher than the value $T_{j'}$ which is obtained if the expansions in both turbine and nozzle are isentropic. This, of course, is a definite loss.

In Sec. 2-6, we have already defined the adiabatic efficiency of the compressor as

[1] This assumes that there are no further losses, for instance, by radiation from the compressor casing.

$$\eta_C = \frac{i_{B1'} - i_0}{i_{B1} - i_0} = \frac{T_{B1'} - T_0}{T_{B1} - T_0} \tag{8-3}$$

and that of the turbine as

$$\eta_T = \frac{i_{B2} - i_n}{i_{B2} - i_{n'}} = \frac{T_{B2} - T_n}{T_{B2} - T_{n'}} \tag{8-4}$$

[see Eqs. (2-45) and (2-46)]. These relations signify that $i_{B1} - i_0$, the work absorbed by the compressor, is greater than $i_{B1'} - i_0$, the work absorbed in an isentropic compression; and that $i_{B2} - i_n$, the work delivered by the turbine, is less than $i_{B2} - i_{n'}$, the work available from an isentropic expansion. In both cases, the real and the isentropic changes of state take place between the same pressures.

It is a necessary condition that the work delivered to the shaft of the turbine is wholly consumed by the compressor. Therefore,

$$i_{B2} - i_n = i_{B1} - i_0 \qquad \text{or} \qquad \frac{T_{B2} - T_n}{T_{B1} - T_0} = 1 \tag{8-5}$$

Using relations (8-3) to (8-5), we can now determine the values of the temperatures in the equation for the thermal efficiency, Eq. (8-2). The final relation contains the parameters $T_{B1'}/T_0$, η_C, and η_T, and there remains also the maximum temperature ratio T_{B2}/T_0. With

$$\frac{T_{B1'}}{T_0} = \left(\frac{p_B}{p_0}\right)^{(k-1)/k}$$

for the comparable isentropic compression, we obtain after some algebra, observing that $T_n/T_j = T_{n'}/T_{j'}$ and $T_{B2}/T_{j'} = T_{B1'}/T_0$,

$$\eta_{th} = \frac{1 - (p_0/p_B)^{(k-1)/k}}{1 + \dfrac{1 - \eta_C}{\eta_C\eta_T \dfrac{T_{B2}}{T_0} - \left(\dfrac{p_B}{p_0}\right)^{\frac{k-1}{k}}} \left[1 + \eta_C^2 \frac{1 - \eta_T}{1 - \eta_C} \frac{T_{B2}/T_0}{\eta_C \dfrac{T_{B2}}{T_0} - \left(\dfrac{p_B}{p_0}\right)^{\frac{k-1}{k}} + 1} \right]} \tag{8-6}$$

or

$$\eta_{th} = \frac{\eta_{th}'}{1 + \dfrac{(1 - \eta_{th}')(1 - \eta_C)}{(1 - \eta_{th}')\eta_C\eta_T \dfrac{T_{B2}}{T_0} - 1} \times \left[1 + \eta_C^2 \frac{(1 - \eta_{th}')(1 - \eta_T)}{1 - \eta_C} \frac{T_{B2}/T_0}{(1 - \eta_{th}')\eta_C \dfrac{T_{B2}}{T_0} - \eta_{th}'} \right]}$$

This clumsy formula can be simplified slightly if the pressure ratio is so small that

$$1 - \left(\frac{p_B}{p_0}\right)^{(k-1)/k}$$

is negligible compared with $\eta_C T_{B2}/T_0$. In that case,

$$\eta_{th} = \frac{\eta_C\eta_T(T_{B2}/T_0) - (p_B/p_0)^{(k-1)/k}}{\eta_C\eta_T\left(\frac{T_{B2}}{T_0} - 1\right) - \left[\left(\frac{p_B}{p_0}\right)^{(k-1)/k} - 1\right]}\,\eta_{th}' \approx \frac{\eta_C\eta_T(T_{B2}/T_0) - 1}{\eta_C\eta_T(T_{B2}/T_0 - 1)}\,\eta_{th}' \qquad (8\text{-}7)$$

We find from both Eqs. (8-6) and (8-7), that the efficiency η_{th}' of the ideal cycle, from Eq. (8-1), is reduced by a factor which contains the compression ratio, the maximum temperature ratio, and, to a first approximation, the product $\eta_C\eta_T$ of the efficiencies of compressor and turbine. $\eta_{th} = 0$ for

$$\eta_C\eta_T = \frac{T_{B1'}}{T_{B2}} = \frac{(p_B/p_0)^{(k-1)/k}}{T_{B2}/T_0}$$

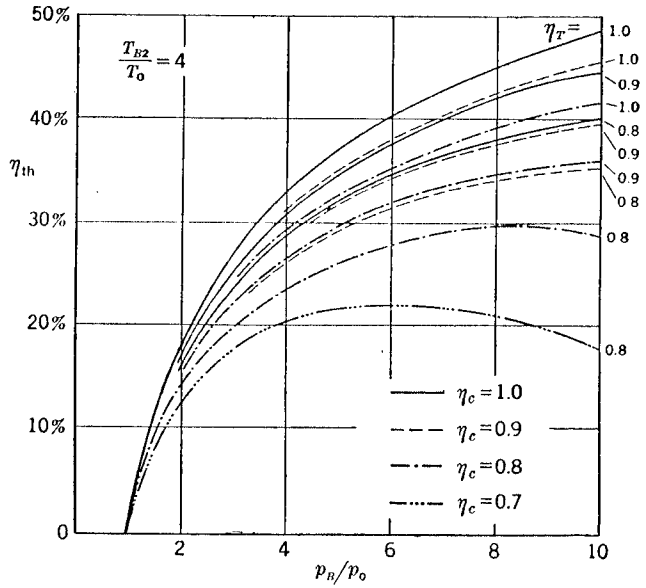

FIG. 8-3. Calculated thermal efficiencies of a turbojet engine for various compressor and turbine efficiencies.

Figure 8-3 gives some numerical values obtained from Eq. (8-6). Reduction of the thermal efficiency of the cycle due to small inefficiencies of compressor and turbine occurs mainly at high compression ratios, and a maximum value of the efficiency is obtained which limits the desirable compression ratio for given η_C and η_T. It will be seen that high compressor and turbine efficiencies are of vital importance for good engine performance.

Equally important is the maximum admissible temperature ratio

T_{B2}/T_0. Considerable improvement in the thermal efficiency can be gained if the temperature can be increased, as will be seen from the numerical example in Fig. 8-4 below. With present-day values of T_{B2} around 1100°K, there is still wide scope for improvement, especially since with higher temperatures the benefits from higher compression ratios can be realized. Raising the maximum temperature is largely a metallurgical problem, that of providing suitable heat-resisting materials for the turbine blades, which must be able to withstand the severe stresses resulting from the air forces and from the high centrifugal mass forces. The aerodynamicist can be of some assistance by providing effective means of

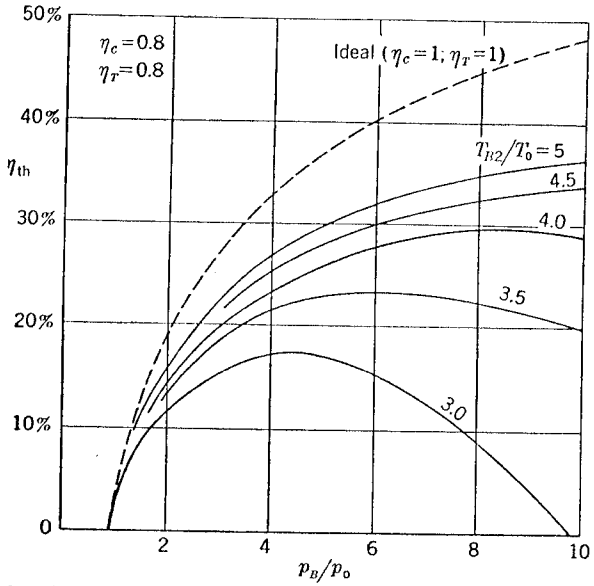

FIG. 8-4. Calculated thermal efficiencies of a turbojet engine for various maximum temperatures.

cooling the blades, for instance, by guiding cooling air through hollow blades.

We may briefly mention here the effect of the altitude of flight on the efficiency of the turbojet. Assuming roughly the same volume flow through the engine both at sea level and at a high altitude, the compressor produces the same compression ratio. The maximum temperature T_{B2} can obviously remain unchanged also. The ambient air temperature T_0, or the temperature at the compressor inlet, is smaller, however, at a high altitude,[1] which means that the maximum temperature ratio T_{B2}/T_0 increases. For instance, with $T_{B2} = 1100$°K, $T_{B2}/T_0 = 3.8$ at sea level

[1] At a height of 6 km, T_0 is about 40°K less than at sea level; above the tropopause, T_0 is about 70°K less than at sea level.

and about 5 above the tropopause. It follows from what has been said above that with higher T_{B2}/T_0 the thermal efficiency is appreciably increased (see Fig. 8-4). On the other hand, the mass flow through the engine is reduced because of the decrease in air density[1] with altitude, and this results in a corresponding decrease of thrust. The fuel consumption, however, will decrease at a greater rate with increasing altitude, as a consequence of the improved efficiency. It is therefore beneficial for long-range jet aircraft, where the fuel consumption is a decisive factor, to operate at high altitudes.

8-2. Influence of the Compression Ratio on the Compressor Efficiency. Compressors and turbines are widely used in engineering and their recent application to aircraft propulsion units did not, therefore, present any fundamental difficulties. The main consequence of their use in aircraft engines has been to impose new constructional conditions and limitations such as restriction of weight and bulk. In the analysis of axial compressors especially, all the concepts and methods of airfoil theory are readily carried over to the compressor-blade rows. For the design and the characteristics of compressors and turbines, we can therefore refer to the large number of existing textbooks and papers.

We have seen in the previous section that the compression ratio to be obtained from the compressor should be between about 4 and 10, for the maximum temperatures that are used at present. While a compression ratio of 4 may be obtainable in a single stage of a centrifugal compressor, axial compressors always require several stages, the pressure ratio per stage being about 1.2.

High compression ratios, and a large number of stages, result in a loss of efficiency. This is sometimes described by means of a *polytropic* efficiency, the idea being that the change of state follows a hypothetical polytropic law with the exponent k of the equation for adiabatic compression replaced by another, usually greater, value. In reality, the value of k does change slightly due to the addition of the fuel gases and the increase of temperature, but its value decreases (for instance, from 1.4 for the air at the inlet to about 1.3 for the exhaust gases).

We use another method here to estimate the influence of the compression ratio on the compressor efficiency, and introduce an adiabatic compressor efficiency η_s for small compression, which may be interpreted as the efficiency of a single stage of an axial compressor. In such a stage, the entropy is increased by

$$ds = \frac{c_p(1 - \eta_s)\, dT}{T}$$

[1] At an altitude of 6 km, the value of the density is about one-half of its value at sea level; at 12 km about one-fourth; and at 18 km about one-tenth.

as is illustrated in Fig. 8-5. [A hypothetical heat input $d'q = c_p(1 - \eta_s)\, dT$ is introduced here which corresponds to the increase in temperature; see also Eq. (2-12).] Integrating, we obtain for the multistage compressor of finite compression ratio:

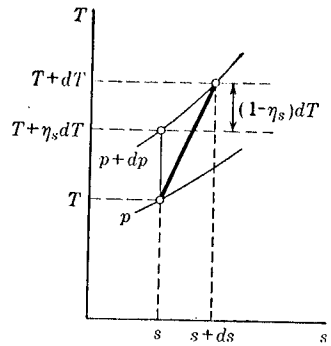

FIG. 8-5. Temperature-entropy diagram for an infinitesimal compressor stage.

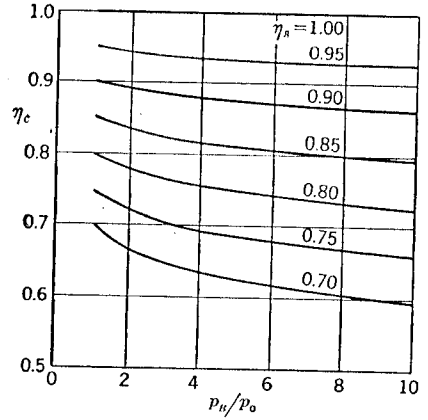

FIG. 8-6. Influence of the stage efficiency on the total compressor efficiency.

$$s_{B1} - s_0 = c_p(1 - \eta_s) \ln \frac{T_{B1}}{T_0}$$

Now, the total entropy increase at the same time is

$$s_{B1} - s_0 = c_p \ln \frac{T_{B1}}{T_{B1'}}$$

where $T_{B1'}$ is the end temperature had the compression been isentropic. The total compressor efficiency η_C then becomes, by Eq. (8-3),

$$\eta_C = \frac{T_{B1'} - T_0}{T_{B1} - T_0} = \frac{T_{B1'}/T_0 - 1}{\left(\frac{T_{B1'}}{T_0}\right)^{\frac{1}{\eta_s}} - 1} = \frac{(p_B/p_0)^{(k-1)/k} - 1}{\left(\frac{p_B}{p_0}\right)^{\frac{1}{\eta_s}\frac{k-1}{k}} - 1} \tag{8-8}$$

This relation, which was given by H. Multhopp (1940, unpublished), states that η_C decreases with increasing compression ratio, the decrease being steeper with smaller stage efficiency. Numerical values are plotted in Fig. 8-6. The deterioration is large enough to have a noticeable effect on the total thermal efficiency of the engine and to influence its layout.

8-3. Axial and Centrifugal Compressors. The stage efficiency of well-designed axial compressors is about 0.90 to 0.92, and the total compressor efficiency is well approximated by Eq. (8-8). In earlier designs, the efficiency was about 5 per cent lower. Centrifugal compressors are usually less efficient than axial compressors. It appears that the differ-

ence in efficiency is between 5 and 7 per cent for up-to-date and comparable designs.

This brings us to the still unresolved controversy between the designers who favor the axial and those who favor the centrifugal compressor. The latter commends itself by its robustness and its ease and cheapness of production. This is particularly evident in the lower compression range where one centrifugal stage is sufficient to produce the desired compression ratio compared with the four or six stages necessary in the axial compressor. The centrifugal compressor also appears to be slightly superior as regards flexibility, that is, in its ability to operate satisfactorily away from its design point so that the engine can run at reduced speed or accelerate without surging.

Generally, the design of the axial compressor demands a higher degree of aerodynamic cleanness; for instance, it is more susceptible to disturbances of the inflow. On the other hand, it provides a more uniform inflow to the combustion chamber, since it avoids changes in the general direction of the flow. Also, the matching of compressor and turbine needs great care to ensure that both are working at their highest efficiency. The development of efficient axial compressors is, however, facilitated by the fact that the individual components and their problems can be studied separately. Such an analysis of the centrifugal compressor is hardly possible as each part demands the presence of the other for even approximately correct functioning.[1]

Another essential difference between the two types is that the axial compressor passes some three or more times as much air per unit time as the centrifugal type. Since the mass flow determines the thrust of the engine if other conditions (such as maximum temperature) are the same, the frontal area of a turbojet engine with axial compressor can be proportionally smaller than that of the engine with centrifugal compressor, for a given thrust. This is not always exploited in practical designs, and often the diameter of the axial engine is still determined by large combustion chambers. Table 8-1 gives some values of the maximum static thrust per unit frontal area at sea level (from G. G. Smith, where further data may be found).

The possibility of obtaining small frontal areas is a strong argument in favor of the axial engine from the aerodynamic aspects of engine installations in high-speed aircraft. As the trend of development naturally moves toward higher compression ratios and temperatures (so that the compressor efficiency matters more) and toward installation in faster aircraft (so that small frontal areas matter more), it is understandable that the present trend concentrates more on axial compressors. It appears a possible compromise to design the first stage with *diagonal* flow,

[1] See, for example, H. Pearson, 1951.

TABLE 8-1. SOME VALUES OF THE MAXIMUM STATIC THRUST PER UNIT FRONTAL AREA AT SEA LEVEL

Manufacturer and type	Compressor type and number of stages	Thrust T, kg (or lb)	T/A_m, kg/m² (or lb/in.²)
Rolls Royce Derwent 5	Centrifugal, 1	1,600 (3,500)	1,700 (2.4)
Rolls Royce Nene	Centrifugal, 1	2,300 (5,000)	1,800 (2.6)
De Havilland Goblin 2	Centrifugal, 1	1,400 (3,100)	1,100 (1.6)
De Havilland Ghost 2	Centrifugal, 1	2,300 (5,000)	1,600 (2.3)
Allison 400 (J-33-A-23)	Centrifugal, 1	2,100 (4,600)	1,600 (2.3)
Allison 450 (J-35-A-15)	Axial, 11	1,700 (3,750)	2,400 (3.4)
Westinghouse 24c (J-34-WE)	Axial, 19	1,400 (3,000)	3,700 (5.2)
BMW 003 A	Axial, 7	800 (1,800)	2,200 (3.1)
BMW 018	Axial, 12	3,400 (7,500)	2,800 (4.0)

according to Pabst von Ohain.[1] Such a diagonal stage may give roughly the same pressure rise as three axial stages.

8-4. Combustion Chambers. A continuous stream of air is continuously heated in the combustion chamber by burning gaseous, liquid, or solid fuel. We have discussed some of the thermodynamic problems of the addition of heat energy to a stream in Sec. 7-3, and shall confine ourselves here to some of the engineering problems.

The combustion chambers of aircraft turbojet engines require the release of heat at a rate of burning far exceeding that reached in other branches of engineering, such as steam boilers or industrial furnaces. Further, there are severe limitations in respect of weight and space. The velocity of the air stream is comparatively high because of the large mass flow and small frontal area required. The danger is, therefore, that either the flames will be blown out, or quenched, or the combustion will be incomplete so that fresh air and unburnt fuel leave the nozzle, the reaction taking place in the jet. It is so vital to avoid this waste that designers usually provide for a very thorough mixing of air and fuel in the combustion chambers, even at the cost of a marked pressure drop, as shown in the example in Fig. 8-2.

A certain pressure drop (apart from that due to the addition of heat at constant cross-section area, which was mentioned in Sec. 7-3) cannot usually be avoided. This will be seen by considering the burner element sketched in Fig. 8-7 (due to O. Pabst). A circular plate is introduced into the air stream with its face normal to it, and gaseous fuel emerges radially from a slot behind the plate. The plate creates a wake behind it, limited by a "jet boundary." This decays rapidly under the influence of turbulent mixing, and it is in this mixing zone, where the velocity is still

[1] See, for example, the description of the HeS 011 engine in G. G. Smith, 1950.

fairly low, that the combustion takes place. The combustion is usually complete at some distance behind the plate, and a continuous combustion (of coal gas, for instance) can be maintained in air-stream velocities up to 150 m/sec. A practical combustion chamber would contain a number of such burner plates, as shown in the example of the ram jet in Sec. 7-7 (Fig. 7-1). The combustion is thus essentially linked to the creation of a wake, and this in turn must produce an over-all pressure drop in the combustion chamber.

A similar burner arrangement, but intended to burn liquid fuel, is illustrated in Fig. 8-8 (due to K. Wieghardt, 1945). Into a cylindrical tube a fine fuel spray is blown in the opposite direction to the air stream. After a certain mixing length which depends on the temperature of the

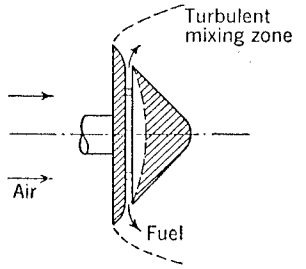

FIG. 8-7. Burner element for gaseous fuel, due to O. Pabst.

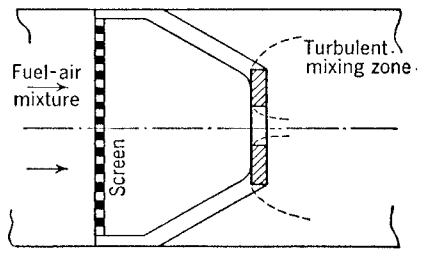

FIG. 8-8. Burner element for liquid fuel, due to K. Wieghardt.

air stream, the evaporation of the fuel spray is completed, and the actual burner (as shown) is already immersed in a stream of fuel-air mixture. A circular plate of half the tube diameter with a hole of about one-sixth the tube diameter was found to be a suitable burner. Turbulent mixing zones are again formed behind the plate and combustion takes place there. As in many similar devices, the plate acts as a baffle stabilizing the flame in the fast air stream [see, for example, P. L. Lloyd (1945)]. Increasing the turbulence of the main stream, for instance by inserting a perforated screen, naturally intensifies the combustion. Liquid hydrocarbons can thus be burnt in an excess of air up to 1:9 and velocities up to 100 m/sec, as long as the air temperature is higher than the boiling point of the fuel. Once again, the baffle and the screen are inevitable sources of pressure loss.

Present-day turbojet engines use either a single annular combustion chamber or a multiplicity of individual chambers, varying from two to sixteen in number. A typical individual chamber is shown in Fig. 8-9. The outer casing encloses a flame tube, which the air enters through a number of holes, thereby mixing thoroughly with the fuel which is sprayed into the flame tube. The outer casing thus remains comparatively cool. The flame tubes are interconnected by pipes which equalize

the pressure and also enable the flame to be propagated from one chamber to another from an initial ignition point.

A typical annular combustion chamber is shown in Fig. 8-10. There is again an inner and an outer tube and the air, entering the chamber at about 120 m/sec, divides into two parts, one of which immediately enters the flame tube, the other being guided into it through a series of slots about halfway down the combustion chamber. Again, a thorough mixing of fuel and air is achieved, at the cost of a pressure loss.

There is no room here to go into a discussion of the various thermodynamic, aerodynamic, chemical, and metallurgical problems involved in the design of combustion chambers, and we refer to the literature on the subject, a selection of which is listed below.

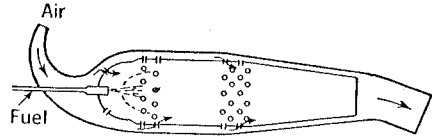

FIG. 8-9. Typical individual combustion chamber. (Lucas chamber in Rolls Royce Derwent 5.)

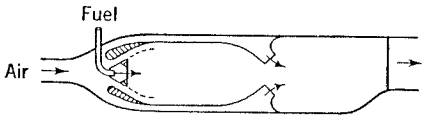

FIG. 8-10. Typical annular combustion chamber (BMW 003).

8-5. Over-all Performance of Turbojets. We have already mentioned in Sec. 1-2 that it is its property of producing constant thrust which makes the turbojet engine superior to the constant-horsepower piston engine in the higher flight speed range, from about $M_0 = 0.8$ onward. We shall now investigate whether a constant thrust is actually produced and if so, how it comes about.

The thrust is due to the change of momentum of the mass of air, $\rho_i V_i A_i$, that passes through the engine:

$$\mathbf{T} = \rho_i V_i A_i (V_j - V_0)$$

If the mass flow and the velocity V_j in the jet were kept constant at all flight speeds, V_0, then the thrust would decrease linearly with V_0 from its maximum value under static conditions ($V_0 = 0$) to zero when $V_0 = V_j$. This decrease can be avoided only if the mass flow or the jet velocity increases with flight speed.

Applying the results of Sec. 2-4, we find the velocity in the jet from the available energy Δe_a of the cycle process, which is transformed entirely into kinetic energy since no mechanical or other work is taken out of the system:

$$\Delta e_a = \frac{V_j^2 - V_0^2}{2g} \tag{8-9}$$

On the other hand, the available energy is a certain proportion of the heat

input $\bar{q}$ per unit weight of air passing through, and from Eq. (8-2)

$$\Delta e_a = \eta_{th}\bar{q} = \eta_{th}c_p(T_{B2} - T_{B1})$$

Hence,

$$V_j^2 - V_0^2 = \eta_{th}2gc_pT_0\left(\frac{T_{B2}}{T_0} - \frac{T_{B1}}{T_i}\frac{T_i}{T_0}\right) \tag{8-10}$$

where T_i is the temperature at the compressor entry. For isentropic inflow,

$$\frac{T_i}{T_0} = \left(\frac{p_i}{p_0}\right)^{(k-1)/k} = 1 + \frac{k-1}{2}\,\mathrm{M}_0^2\left[1 - \left(\frac{V_i}{V_0}\right)^2\right] \tag{8-11}$$

from Eq. (4-9). The temperature increase in the compressor can be related to the compression ratio; by Eq. (8-3),

$$\frac{T_{B1}}{T_i} = 1 + \frac{(p_B/p_i)^{(k-1)/k} - 1}{\eta_C}$$

Using

$$gc_pT_0 = \frac{1}{k-1}\,a_0^2$$

and combining all these relations, we obtain for the thrust

$$\frac{\mathbf{T}}{\frac{1}{2}\rho_0 V_0^2 A_i} = 2\frac{\rho_i}{\rho_0}\frac{V_i}{V_0} \times \left(\sqrt{1 + \frac{2}{k-1}\frac{\eta_{th}}{\mathrm{M}_0^2}\left\{\frac{T_{B2}}{T_0} - \left[1 + \frac{(p_B/p_i)^{\frac{k-1}{k}} - 1}{\eta_C}\right]\left(\frac{p_i}{p_0}\right)^{\frac{k-1}{k}}\right\}} - 1\right) \tag{8-12}$$

in which from Eq. (4-10) the density ratio ρ_i/ρ_0 for isentropic inflow is

$$\frac{\rho_i}{\rho_0} = \left\{1 + \frac{k-1}{2}\,\mathrm{M}_0^2\left[1 - \left(\frac{V_i}{V_0}\right)^2\right]\right\}^{1/(k-1)} \tag{8-13}$$

The thermal efficiency of the cycle is as determined in Sec. 8-1; for instance, for the ideal constant-pressure process, from Eq. (8-1),

$$\eta_{th} = 1 - \left(\frac{p_0}{p_i}\frac{p_i}{p_B}\right)^{(k-1)/k}$$

In the thrust equation (8-12), the maximum temperature ratio T_{B2}/T_0 and the compression ratio p_B/p_i may be regarded as properties of the heat engine, and therefore as independent of the flight speed, assuming the air flow through the engine to be suitably regulated. This means that the velocity ratio V_i/V_0 is given. For constant-volume flow, V_i = const, and V_i/V_0 decreases as the flight speed increases; hence p_i/p_0 and ρ_i/ρ_0 increase also. With rising p_i, the thermal efficiency of the cycle is improved.

To illustrate this, we choose some numerical values[1]: $p_B/p_i = 3$; $T_{B2}/T_0 = 3$; $V_i = 150$ m/sec; $A_i = 0.2$ m^2; at sea level. For simplicity, compressor and turbine efficiency are assumed to be unity. The weight of air passing through the engine per unit time is then $37\rho_i/\rho_0$ kg/sec, and the static thrust $\mathbf{T}_{\text{static}} = 1{,}640$ kg.

The resulting thrust, plotted in Fig. 8-11 against the flight Mach number, is not strictly constant. There is an initial decrease, following the

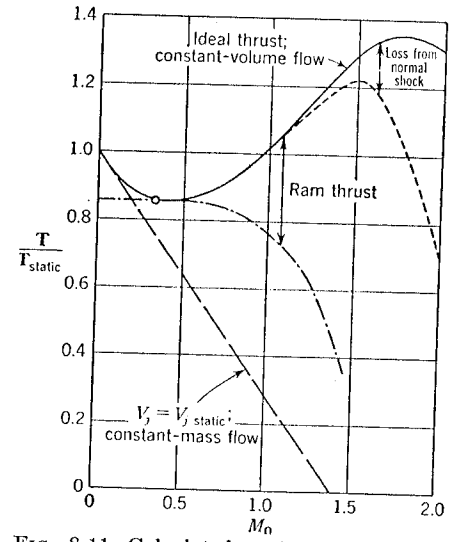

FIG. 8-11. Calculated variation with flight Mach number of the thrust of a turbojet engine. (For the normal shock loss, see Sec. 9-2.)

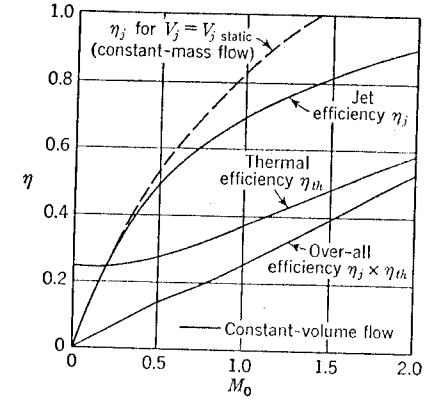

FIG. 8-12. Calculated efficiencies of the turbojet engine of Fig. 8-11.

line V_j = const; but then the ram effect causes the thrust to rise until eventually it exceeds the static thrust. This increase is caused partly by the higher thermal efficiency of the cycle due to the pressure increase, as shown in Fig. 8-12; and partly by the increased mass flow due to the higher density of the air. The higher thrust thus depends on our assumption of constant-volume flow.[2]

As the thrust increase is accompanied by a higher velocity in the jet, a point is reached at which V_j becomes the local velocity of sound, that is, when

$$V_j = \sqrt{(k-1)c_pgT_j} = a_0\sqrt{\frac{T_j}{T_0}} \tag{8-14}$$

[1] The compression ratio and the maximum temperature are rather low but, with $\eta_C = \eta_T = 1$, the final thrust and the jet velocity are of the same order as found in modern turbojet engines of the size assumed.

[2] We do not deal here with the control problems of jet engines. The paper by S. C. Himmel and R. P. Krebs, 1951, for instance, will introduce the reader to a multitude of problems concerning the dynamic behavior of the controlled engine.

In the present example, this occurs at $M_0 = 0.34$. At higher flight Mach numbers, the jet velocity is supersonic and a Laval nozzle would be required to achieve this. If a supersonic nozzle is not provided, the jet velocity will not rise beyond its sonic value, the exit being choked, and the thrust would be less than that given in Fig. 8-11.

For the ideal constant-pressure process with $\eta_C = \eta_T = 1$, the condition (8-14) for sonic speed in the jet reads

$$\left(\frac{V_j}{V_0}\right)^2 = \frac{1}{M_0^2}\frac{T_{B2}/T_0}{T_{B1}/T_0}$$

since $T_j/T_0 = T_{B2}/T_{B1}$. On the other hand, by Eq. (8-10),

$$\left(\frac{V_j}{V_0}\right)^2 = 1 + \frac{2}{k-1}\frac{1}{M_0^2}\left(1 - \frac{1}{T_{B1}/T_0}\right)\left(\frac{T_{B2}}{T_0} - \frac{T_{B1}}{T_0}\right)$$

taking $\eta_{th} = \eta_{th}'$ from Eq. (8-1). This gives a relation between T_{B2} and T_{B1} which must be fulfilled to have sonic speed in the jet:

$$\frac{T_{B2}}{T_{B1}} = M_0^2\left(\frac{V_j}{V_0}\right)^2 = \frac{\frac{2}{k-1}\left(\frac{T_{B1}}{T_0} - 1\right) - M_0^2}{\frac{2}{k-1}\left(\frac{T_{B1}}{T_0} - 1\right) - 1}$$

Hence, $T_{B2} > T_{B1}$ and thus $V_j > V_0$ only for $M_0 < 1$. This implies that, at supersonic flight Mach numbers, the velocity in the jet must be supersonic to have $T_{B2} > T_{B1}$ and thus $V_j > V_0$, which is the necessary condition for a true thrust to be produced.

The exit area can be determined from the continuity equation

$$\rho_i V_i A_i = \rho_j V_j A_j$$

$$\frac{A_j}{A_i} = \frac{\rho_i}{\rho_0}\frac{T_j}{T_0}\frac{V_i}{V_0}\frac{1}{V_j/V_0}$$

since $p_j = p_0$ and $\rho_j/\rho_0 = T_0/T_j$. These are known quantities. The exit area required does not vary very much; in the present example, assuming that $A_j = A_e$ and that the static pressure in the exit is p_0, the value of A_e/A_i varies from 0.64 at $M_0 = 0$ to about 0.62 at $M_0 = 0.6$, rising again to 0.64 at $M_0 = 1$ and 0.69 at $M_0 = 1.3$.

The thrust increase, as in Fig. 8-11, is accompanied by a higher fuel consumption. The increase over the static fuel consumption is about 10 per cent at $M_0 = 0.5$ and about 35 per cent at $M_0 = 1$, with the value $Q = 1.66 \times 10^6$ m-kg/sec at $M_0 = 0$. Since the over-all efficiency $\eta = \eta_j\eta_{th}$ rises almost linearly with the flight Mach number, at higher values of M_0, the specific fuel consumption

$$\frac{Q}{T} = \frac{V_0}{\eta_j\eta_{th}} \qquad (8\text{-}15)$$

is practically constant there. The fuel consumption can be determined directly from

$$Q = g\rho_i V_i A_i \bar{q} = g\rho_i V_i A_i c_p(T_{B2} - T_{B1})$$

which gives, with the relations used above,

$$\frac{Q}{\frac{1}{2}\rho_0 V_0^3 A_i} = \frac{2}{(k-1)M_0^2}\frac{\rho_i}{\rho_0}\frac{V_i}{V_0} \times \left\{\frac{T_{B2}}{T_0} - \left[1 + \frac{(p_B/p_i)^{(k-1)/k} - 1}{\eta_C}\right]\left(\frac{p_i}{p_0}\right)^{(k-1)/k}\right\} \qquad (8\text{-}16)$$

There is a maximum both to the thrust and the fuel consumption, reached in the present example at about $M_0 = 1.7$. This is because we limited the maximum temperature T_{B2} at the end of the combustion chamber. Since such a limitation is always necessary for turbojet engines, as explained earlier, this restricts the practical application of the turbojet, even if the ideal thrust shown in Fig. 8-11 can be realized. This then is the point at which the ram jet takes over; in the absence of a turbine, the combustion end temperature is not so severely limited.

The main conclusion is that the thrust of a turbojet in its main range of application (*i.e.*, above about $M_0 = 0.8$) depends to a very large extent on the fact that pressure and density at the compressor entry increase with flight speed as the result of ram effect. If this increase is not achieved, for some reason or other, then the velocity in the jet and the mass flow are not increased beyond their values under static conditions and the thrust falls off with flight speed as indicated by the dotted line in Fig. 8-11, just as it does with *constant-horsepower* piston engines. The turbojet then fails to be a *constant-thrust engine*, and fails to justify one of its main claims for superiority over the piston engine with propeller.

One of the tasks of the aerodynamicist is therefore to ensure, by suitable design of the air intake and engine installation, that the inflow suffers the smallest possible loss of energy. When $M_0 < 1$, the inflow can be very nearly isentropic, as has been assumed above; but when $M_0 > 1$, compression from the supersonic flow in the free stream to the normally subsonic flow in the intake duct is not possible without shock waves occurring, with subsequent energy losses. Inflow problems and the associated thrust losses will be discussed in the next chapter.

We may also remind ourselves that the rise of pressure and density at the entry is accompanied by a change of momentum of the inflow, with corresponding thrust forces. These may occur either in the form of external suction forces on the intake walls, if the compression takes place in the free stream, or as increased pressures on the walls of an expanding duct (see Sec. 4-9). Their magnitude is determined by Eq. (4-12) and is indicated in the example of Fig. 8-11 by the "ram thrust." This thrust

constitutes a vital part of the over-all thrust in the main range of application of the turbojet. If it cannot be realized, then the working range of the turbojet engine as an aircraft propulsion unit is severely curtailed.

EXERCISES

8-1. Plot an *is* diagram for a turbojet engine with $p_B = 4p_0$; $T_{B2} = 4T_0$; $\eta_C = 0.85$; $\eta_T = 0.9$. Assume sea-level conditions and ignore ram effect. Find the available energy, the energy input, and the thermal efficiency from the graph, and compare the result with Eq. (8-6).

8-2. Confirm Eq. (8-6) algebraically.

8-3. The pressure in the combustion chamber of the engine in Exercise 8-1 decreases linearly with temperature from $4p_0$ to $3p_0$. Find the resulting change of the thermal efficiency from the *is* diagram.

8-4. During a single stage of a four-stage compressor the energy $0.1c_pT_0$ is supplied to unit weight of air with an adiabatic efficiency of 0.85. Plot the Ts diagram. What is the over-all adiabatic efficiency of the compressor?

8-5. The over-all propulsive efficiency of a turbojet engine flying at a speed of 300 m/sec is given. Convert this into the value of the specific fuel consumption, measured, for instance, in kilograms (or pounds) of fuel per kilogram (or pounds) of thrust per hour, or measured in pounds of fuel per shaft horsepower per hour. Take the calorific value of the fuel as 4.35×10^6 m-kg per kilogram of fuel (or 150,000 Btu per gallon for a fuel of specific gravity 0.81).

8-6. A turbojet engine ($A_i = 0.5$ m^2; $V_i = 150$ m/sec), working on an ideal constant-pressure cycle, produces 2,000 kg thrust at $M_0 = 0.9$, at sea level, where $\rho_0 = 0.125$ kg-sec^2/m^4; $a_0 = 340$ m/sec. The engine works under choked conditions, *i.e.*, the velocity is sonic at the exit. The inflow is isentropic and $\eta_C = \eta_T = 1$. (*a*) Determine the necessary compression ratio p_B/p_i and the combustion end temperature T_{B_2}/T_0. (*b*) Determine the efficiencies η_{th} and η_j and the over-all efficiency.

BIBLIOGRAPHY

General:

Keenan, J. G., "Elementary Theory of Gas Turbines and Jet Propulsion," Oxford University Press, London and New York, 1946.

Smith, G. G., "Gas Turbines and Jet Propulsion," 5th ed., Iliffe & Sons, London, 1950; Aircraft Books, Inc., New York, 1950.

Hunsaker, J. C., and B. G. Rightmire, "Engineering Applications of Fluid Mechanics," McGraw-Hill Book Company, Inc., New York, 1947.

Buckingham, E., Jet Propulsion for Airplanes, *NACA TR* 159, 1923.

Ackeret, J., and C. Keller, Aerodynamic Heat Engine Operating on a Closed Cycle, *Z. Ver. deut. Ing.*, vol. 85, p. 491, 1941; translation, *NACA TM* 1034.

Ellis, M. C., and C. E. Brown, NACA Investigation of a Jet Propulsion System Applicable to Flight, *NACA TR* 802, 1944.

Keenan, J. H., J. Kaye, and C. A. Rieke, The Calculated Performance of a Jet Propulsion Device: Systems CHT, PCHTJ, CchtJ, CHTX, *NACA ACR* 5B02, 1945.

Pinkel, B., and I. M. Karp, Performance Charts for a Jet-propulsion System Consisting of a Compressor, a Combustion Chamber, and a Turbine, *NACA ARR* E6E14, 1946.

Cox, H. R., British Aircraft Gas Turbines. *J. Aeronaut. Sci.*, vol. 13, p. 53, 1946.

Cleveland Laboratory Staff, Performance and Ranges of Application of Various Types of Aircraft-propulsion Systems, *NACA TN* 1349, 1947.

Reissner, H., Systematic Analysis of Thermal Turbojet Propulsion, *J. Aeronaut. Sci.*, vol. 14, p. 197, 1947.

Keenan, J. H., and J. Kaye, A Survey of the Calculated Efficiencies of Jet Power Plants, *J. Aeronaut. Sci.*, vol. 14, p. 437, 1947.

Lichty, L. C., "Thermodynamics," 2d ed., McGraw-Hill Book Company, Inc., New York, 1948.

Pinkel, B., and I. M. Karp, A Thermodynamic Study of the Turbojet Engine, *NACA TR* 891, 1949.

Compressors and Turbines:

Keller, C., and L. S. Marks, "The Theory and Performance of Axial Flow Fans," McGraw-Hill Book Company, Inc., New York, 1937.

Ruden, P., Investigation of Single Stage Axial Fans, Translation, *NACA TM* 1062.

Betz, A., Axial Superchargers, *Jahrbuch der deutschen Luftfahrtforschung*, 1938, p. II 183; translation, *NACA TM* 1073.

Betz, A., and I. Flügge-Lotz, Design of Centrifugal Impeller Blades, *Ingenieur Arch.*, vol. 9, p. 486, 1938; translation, *NACA TM* 902.

Riegels, F., and J. Weber, Beitrag zur Berechnung von Kreiselrädern mit nichtstossfreiem Eintritt, *Ingenieur Arch.*, vol. 12, p. 63, 1941.

Sörensen, E., Potential Flow through Centrifugal Pumps and Turbines, translation, *NACA TM* 973.

Betz, A., W. Encke, H. Marcinowski, H. Pabst von Ohain, H. Weise, and others, Verdichter für Luftstrahltriebwerke (Report on Heidenheim Congress, 1943), *Lilienthal Gesellschaft der Luftfahrtforschung, Bericht* 171, 1943.

Perl, W., and M. Tucker, A General Representation for Axial-flow Fans and Turbines, *NACA TR* 814, 1945.

Hayne Constant, H., L. J. Cheshire, A. R. Howell, D. N. Walker, R. G. Voysey, J. Reeman, and T. A. Taylor, The Development of the Internal Combustion Turbine, *Proc. Inst. Mech. Engrs. (London)*, vol. 153, p. 409, 1945.

Encke, W., A. Föll, A. Frerichs, and H. Quentin, Turbo-machines (*AVA Monograph O*), *Brit. Min. of Supply (Völkenrode) Rept. & Transl.* 932–936, 1947.

Burtt, J. R., Investigation of Performance of Typical Inlet Stage of Multistage Axial-flow Compressor, *NACA RM* E9E 13, 1949.

Encke, W., Investigations on Experimental Impellers for Axial Blowers, translation, *NACA TM* 1123.

Moult, E. S., and H. Pearson, The Relative Merits of Centrifugal and Axial Compressors for Aircraft Gas Turbines, *J. Roy. Aeronaut. Soc.*, March, 1951.

Bogdonoff, S. M., The Performance of Axial-flow Compressors as Affected by Single-stage Characteristics, *J. Aeronaut. Sci.*, vol. 18, p. 319, 1951.

Himmel, S. C., and R. P. Krebs, The Effects of Changes in Altitude on the Controlled Behaviour of a Gas-turbine Engine, *J. Aeronaut. Sci.*, vol. 18, p. 433, 1951.

Combustion:

Lewis, B., and G. von Elbe, "Combustion, Flames, and Explosions of Gases," Harvard University Press, Cambridge, Mass., 1938.

Lloyd, P., Combustion in the Gas Turbine, *Proc. Instit. Mech. Engrs.*, vol. 153, p. 462, 1945.

Jost, W., "Explosion and Combustion Processes in Gases," McGraw-Hill Book Company, Inc., New York, 1946.

WIEGHARDT, K., Combustion Chambers (*AVA Monograph* J_3 3.3), *Brit. Min. of Supply* (*Völkenrode*) *Rept. & Transl.* 980, 1946.

HILL, F. U., and H. MARK, Performance of Experimental Turbojet-engine Combustor, *NACA RM* E7J13, 1948.

PINKEL, I. I., and H. SHAMES, Analysis of Jet-propulsion Engine Combustion-chamber Pressure Losses, *NACA Rept.* 880, 1949.

Third Symposion on Combustion, Flame, and Explosion Phenomena, The Williams & Wilkins Company, Baltimore, 1949.

CHAPTER 9

INSTALLATION OF JET ENGINES

The *installed thrust* of a propulsion unit is always less than the thrust which can be obtained on the test bed. The main reasons for the difference—ram *pressure losses in the inflow* and *external interference drags*—are discussed in Sec. 9-1. Section 9-2 gives a theoretical treatment of approach losses and duct losses. The external drag can easily be interpreted as a reduction of the available thrust; the effect of inflow losses on thrust and fuel consumption needs a special investigation, however. A general method is described in Secs. 9-3 and 9-4. Sections 9-5 to 9-7 deal with special cases of internal duct losses and the use of boundary-layer material to supply the engine. Measured inflow losses with various intake arrangements and measured interference drags are discussed in Secs. 9-8 to 9-12, and some ways of assessing the merits and disadvantages of particular types of installation are indicated.

9-1. General Survey of Installation Losses. The variety of ways in which the propulsion unit can be installed in an aircraft has been greatly multiplied by the arrival of the jet engine. Piston engines driving propellers have usually been mounted either in the nose of the fuselage or in nacelles attached to the wing; with jet engines on the other hand the whole range from completely external nacelles to totally buried engines inside the lifting surface or the body is covered. As an extreme case of integration, we may imagine a special type of ram jet (suggested by H. Multhopp) where fuel is burned in the stagnation region of the wing, eliminating aircraft drag at its source.

We are concerned here with the influence of the installation on the thrust—not on the lift. As far as the ordinary propeller is concerned, this is fully covered by existing textbooks, which deal with such matters as the influence on the propeller of the flow past the nose of the body, the forces on the propeller at incidence, and the action of the wing as a guide vane. As might be expected, jet engines present many new problems. In most cases the installation reduces the propulsive efficiency of the engine; there is a loss of thrust for a given fuel consumption compared with the isolated engine as treated in the preceding chapters.

We distinguish between two categories of installation losses:

1. Inflow and duct losses which directly affect the working process of the engine and thereby its thrust.

2. External interference drags due to the addition of the power unit, with what can be thought of as an indirect effect on the thrust available for propulsion.

Losses of the first kind are small when the engine is installed in the fuselage or in an isolated nacelle with its air intake in the nose. The inflow may then be regarded as near isentropic, except at supersonic speeds when there is a shock wave ahead of the inlet or a system of shocks. Duct losses may nevertheless occur in long pipes leading to the compressor or in long jet pipes. The inflow losses are higher if the air inlet is in or near a wall along which the air must flow with a loss of some of its available energy in a boundary layer. This may occur if the engine is partly or wholly installed in the fuselage with side intakes. Putting the air intake into the wing root away from the body wall necessitates curved ducts and subsequent duct losses, however.

On the other hand, the external drag of partly or wholly incorporated engines is generally small compared with that of engines attached externally to the fuselage or the wing, and in the latter case a further drag increase from interference between nacelle and body may have to be reckoned with. We see, in fact, that inflow losses and external drag are often complementary; as far as possible, they should be assessed on a common basis so that the installation can be designed to compromise between them.

To express the external installation drag in terms of an effective thrust loss, let

$$\Delta C_D = \frac{\Delta D}{\frac{1}{2}\rho_0 V_0^2 A_m}$$

be the external drag increment related to the dynamic head of the free stream and the maximum frontal area A_m of the isolated nacelle.[1] If

$$C_{DE} = \frac{D_{\text{engine nacelle}}}{\frac{1}{2}\rho_0 V_0^2 A_m}$$

is the drag coefficient of the isolated engine nacelle, which is generally known or can be estimated from skin friction, etc., we have for the effective loss of thrust

$$\Delta \mathbf{T} = -\frac{1}{2}\rho_0 V_0^2 A_m C_{DE}\frac{\Delta C_D}{C_{DE}}$$

and the relative thrust loss is

$$\frac{\Delta \mathbf{T}}{\mathbf{T}'} = -\frac{1}{2}kp_0\frac{C_{DE}}{\mathbf{T}'/A_m}\mathrm{M}_0^2\frac{\Delta C_D}{C_{DE}} \qquad (9\text{-}1)$$

[1] In most cases, it will be sufficient to take A_m as the frontal area of the engine.

where $\mathbf{T}'$ is the known thrust of the isolated engine without installation losses.

$$\mathrm{M}_0 = \frac{V_0}{\sqrt{kp_0/\rho_0}}$$

is the flight Mach number.

In Eq. (9-1) the factor kp_0 is a function of altitude, and for a given engine both C_{DE} and $\mathbf{T}'/A_m$ are known. The relative thrust loss depends therefore on the relative drag increment due to installation, $\Delta C_D/C_{DE}$, and increases with the square of the flight Mach number, apart from the variation of $\Delta C_D/C_{DE}$ with M_0.

The value of $\mathbf{T}'/A_m$ does not vary much between current turbojet engines; $\mathbf{T}'/A_m = 2{,}100\ \mathrm{kg/m^2} = 3\ \mathrm{lb/in.^2}$ is a mean sea-level value[1] which is exceeded by engines with axial compressors and not quite reached by engines with centrifugal compressors. It does not vary very much with flight speed. Taking a value of about 0.06 for C_{DE}, we have at sea level

$$\frac{\Delta \mathbf{T}}{\mathbf{T}'} = -0.2\mathrm{M}_0^2\frac{\Delta C_D}{C_{DE}} \qquad (9\text{-}2)$$

which may serve as a rough guide. The constant in this relation will become smaller with increasing altitude. The value of $\Delta C_D/C_{DE}$ may vary between 0 and 2 for practical installations and the subsequent loss of effective thrust can thus be considerable, especially in high-speed flight. Some experimental data will be discussed in detail below.

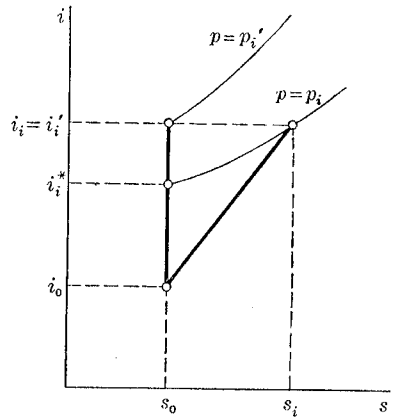

FIG. 9-1. Comparison of isentropic and nonisentropic inflow (diagrammatic).

To define the inflow losses, we compare the real flow from free-stream conditions (subscript 0) up to the inlet or to a station inside the duct ahead of the compressor (subscript i) with an isentropic inflow up to the same station (parameters marked by a dash). To determine the respective states fully, we assume the same volume flow into the inlet in the two cases, $V_i' = V_i$.

In the ideal inflow, the enthalpy would rise from i_0 to i_i' (Fig. 9-1), the entropy remaining unchanged. The entropy increases in the real inflow. Since $V_i = V_i'$, the enthalpy and temperature at the inlet are the same for the two inflows, by the energy equation (2-15a) and Eq. (2-8), assuming the air to be a perfect gas. A lower pressure is therefore

[1] See Table 8-1, page 175.

reached, $p_i < p_i'$, and

$$\frac{\rho_i}{\rho_i'} = \frac{p_i}{p_i'} = 1 - \frac{\Delta p_i}{p_i'} \tag{9-3}$$

by Eq. (2-1). The entropy increase in the real process can be expressed in terms of the pressure loss:

$$s_i - s_0 = R \ln \frac{p_i'}{p_i} = R \ln \frac{1}{1 - \Delta p_i/p_i'} > 0 \tag{9-4}$$

by Eq. (2-14), whereas, of course, $s_i' - s_0 = 0$. In this equation and in Eq. (9-3), the *pressure-loss coefficient*

$$\frac{\Delta p_i}{p_i'} = \frac{p_i' - p_i}{p_i'}$$

can be introduced; we shall find this a convenient parameter to characterize the inflow losses.

Now the pressure rise of the real inflow from p_0 to p_i could have been obtained with an increase of enthalpy from i_0 to i_i^*, had the inflow been isentropic (Fig. 9-1). We can therefore introduce a *ram efficiency*

$$\eta_{\text{ram}} = \frac{i_i^* - i_0}{i_i' - i_0} = \frac{T_i^* - T_0}{T_i' - T_0} \tag{9-5}$$

to express the $(i_i^* - i_0)$ available from the real inflow as a fraction of the $(i_i' - i_0)$ from the ideal inflow.[1] Using the relation

$$i = \frac{k}{k-1}\frac{p}{g\rho}$$

together with Eqs. (2-11) and (9-3), we can put η_{ram} in terms of the pressure-loss coefficient:

$$\eta_{\text{ram}} = \frac{\left(\frac{p_i}{p_0}\right)^{(k-1)/k} - 1}{\left(\frac{p_i'}{p_0}\right)^{(k-1)/k} - 1} = \frac{\left(\frac{p_i'}{p_0}\right)^{(k-1)/k}\left[1 - \frac{\Delta p_i}{p_i'}\right]^{(k-1)/k} - 1}{\left(\frac{p_i'}{p_0}\right)^{(k-1)/k} - 1}$$

If $\Delta p_i/p_i' \ll 1$, as is usually the case, this can be written as

$$\begin{aligned}\eta_{\text{ram}} &= 1 - \frac{k-1}{k}\frac{(p_i'/p_0)^{(k-1)/k}}{(p_i'/p_0)^{(k-1)/k} - 1}\frac{\Delta p_i}{p_i'} \\ &= 1 - \frac{1 + [(k-1)/2]\mathrm{M}_0^2[1 - (V_i/V_0)^2]}{(k/2)\mathrm{M}_0^2[1 - (V_i/V_0)^2]}\frac{\Delta p_i}{p_i'}\end{aligned} \tag{9-6}$$

by Eq. (4-9), to the first order.

[1] This definition of the ram efficiency corresponds to the compressor and turbine efficiencies of Eqs. (8-3) and (8-4).

The term in $\Delta p_i/p_i'$ in this relation depends only on the flight Mach number M_0 and the inlet velocity ratio V_i/V_0. Thus under given flight conditions, the ram efficiency is determined by the pressure-loss coefficient. It will be seen in Sec. 9-3 that the loss of efficiency of a turbojet engine due to inflow losses is also proportional to $\Delta p_i/p_i'$, to the first order, so that by Eq. (9-6) the loss of over-all efficiency is proportional to the loss of ram efficiency.

The pressure-loss coefficient $\Delta p_i/p_i'$ can easily be expressed in terms of measurable quantities, such as the stagnation pressure $p_{ist} = H_i$ in the inlet as measured by a pitot tube (in subsonic flow). From the energy equation,

$$\frac{k}{k-1}\frac{H_i}{\rho_{ist}} = \frac{k}{k-1}\frac{p_0}{\rho_0} + \frac{V_0^2}{2} \tag{9-7}$$

where ρ_{ist} is the density at the stagnation point:

$$\frac{\rho_{ist}}{\rho_i} = \left(\frac{H_i}{p_i}\right)^{1/k}$$

Since

$$\frac{\rho_i'}{\rho_0} = \left(\frac{p_i'}{p_0}\right)^{1/k}$$

we obtain, using Eq. (9-3),

$$\frac{\rho_{ist}}{\rho_0} = \left(\frac{H_i}{p_0}\right)^{1/k}\left(\frac{p_i}{p_i'}\right)^{(k-1)/k}$$

so that finally, from Eq. (9-7),

$$\frac{p_i}{p_i'} = 1 - \frac{\Delta p_i}{p_i'} = \frac{H_i/p_0}{\left(1 + \frac{k-1}{2}\mathrm{M}_0^2\right)^{k/(k-1)}} = \frac{H_i/p_0}{H_i'/p_0} \tag{9-8}$$

since

$$\frac{H_i'}{p_0} = \left(1 + \frac{k-1}{2}\mathrm{M}_0^2\right)^{k/(k-1)}$$

by Eq. (4-9) for $V_i = 0$.

In practice, and in particular in experimental investigations at low speeds, two other coefficients are frequently used, which are based on pressure differences:

$$\frac{\Delta H}{q_i} = \frac{H_i' - H_i}{\frac{1}{2}\rho_i V_i^2} \quad \text{and} \quad \frac{H_i - p_0}{H_i' - p_0} = \frac{H_i/p_0 - 1}{H_i'/p_0 - 1}$$

Neither of these bears a direct relation to the working process and the loss of engine thrust. They are related to the pressure-loss coefficient by

$$\frac{\Delta p_i}{p_i'} = 1 - \frac{1 + \left[\left(1 + \frac{k-1}{2}\,\mathrm{M}_0^2\right)^{k/(k-1)} - 1\right]\frac{H_i - p_0}{H_i' - p_0}}{\left(1 + \frac{k-1}{2}\,\mathrm{M}_0^2\right)^{k/(k-1)}} \tag{9-9}$$

and

$$\frac{\Delta p_i}{p_i'} = \frac{\frac{k}{2}\,\mathrm{M}_0^2\,\frac{\rho_i}{\rho_0}\left(\frac{V_i}{V_0}\right)^2}{\left(1 + \frac{k-1}{2}\,\mathrm{M}_0^2\right)^{k/(k-1)}}\,\frac{\Delta H_i}{q_i} \tag{9-10}$$

Here, ρ_i/ρ_0 may be replaced by ρ_i'/ρ_0, to a first approximation, and then determined from Eq. (4-10).

9-2. Approach Losses and Duct Losses in the Inflow. The major contribution to the inflow loss is that of skin friction along the walls of the duct and the surfaces ahead of the inlet which are *wetted* by the inflow. This can readily be estimated. We consider only incompressible flow.

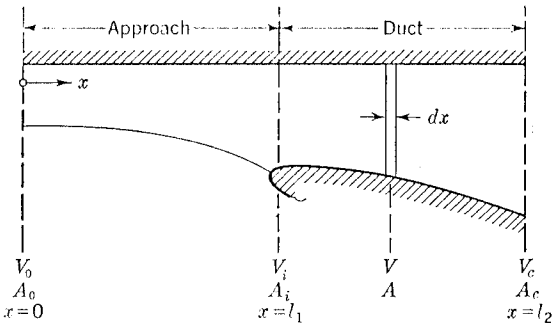

FIG. 9-2. Approach loss and duct loss (diagrammatic).

To relate the pressure-loss coefficient to the skin-friction coefficient in incompressible flow, we follow the theory of entry losses given by J. Seddon (1950). Consider an arbitrary cross section of the flow (Fig. 9-2) at a point along the x axis where the velocity is V, the dynamic head q, and the cross-section area (of the duct or of the stream tube entering the inlet, as the case may be) is A. Let B be the length of surface normal to the flow direction which is in contact with the inflow; inside the duct, B is the local perimeter. The friction force on an element of the wetted surface is

$$dF = C_F q B\,dx$$

where C_F is the skin-friction coefficient, which depends on the state of the boundary layer (laminar or turbulent), the Reynolds number, and the smoothness of the surface. If we assume complete mixing at every stage, we can transform the friction force into an equivalent mean pressure drop:

$$\frac{dF}{A} = C_F q\,\frac{B}{A}\,dx$$

The loss of total head for the whole inflow is then obtained by integrating the pressure drop over the length of the inflow:

$$\frac{\Delta H}{q_i} = \int_0^{l_2} C_F \left(\frac{V}{V_i}\right)^2 \frac{B}{A}\,dx$$

By continuity, $AV = A_iV_i$, so that

$$\frac{\Delta H}{q_i} = \int_0^{l_2} C_F \left(\frac{V}{V_i}\right)^3 \frac{B}{A_i}\,dx \tag{9-11}$$

The evaluation of this integral is simplified by the assumption that C_F is constant. Its local variations due to pressure gradients, and changes in Reynolds number, etc., are thus ignored. Let us now split the integral into two parts, corresponding to the *approach*, $0 \le x \le l_1$, and the *duct*, $l_1 \le x \le l_2$, respectively.

The duct loss is readily integrated, since we know the variation of the duct cross section.

$$\left(\frac{\Delta H}{q_i}\right)_{\text{duct}} = C_F \int_{l_1}^{l_2} \left(\frac{A_i}{A}\right)^3 \frac{B}{A_i}\,dx = C_F I \tag{9-12}$$

where I is an integral expression which depends on the shape and dimensions of the duct only. For a circular pipe of constant diameter D and length L, $I = 4L/D$, for example.

The approach loss is less simple; the velocity distribution along the approach length is not usually known. The initial and final velocities V_0 and V_i are known, however, and in the extreme case we may assume the velocity V along the approach surface to be equal to V_0 right up to the inlet, dropping suddenly to V_i there. Equation (9-11) then gives for the approach loss

$$\left(\frac{\Delta H}{q_i}\right)_{\text{approach}} = C_F \frac{S}{A_i}\,\mu^3 \tag{9-13}$$

where $\mu = V_0/V_i$ and $S = B \times l_1$ is the wetted approach area. The retardation of the real flow[1] from V_0 to V_i will have the effect of reducing the approach loss, and this can be taken into account by a retardation factor $\mathbf{k}$ so that

$$\left(\frac{\Delta H}{q_i}\right)_{\text{approach}} = C_F \frac{S}{A_i}\,\mathbf{k}\mu^3 \tag{9-14}$$

The value of $\mathbf{k}$ will be near 1.0 for very long approach walls; but $\mathbf{k}$ will be smaller than 1.0 for shorter walls. $\mathbf{k} = 0.8$ is a reasonable mean value for many practical cases.

[1] The velocity variation could of course be obtained more accurately by application of the method described in Sec. 3-6, especially from Eq. (3-20) for the velocity distribution upstream of a two-dimensional inlet.

The final expression for the total inflow loss is then[1]

$$\frac{\Delta H}{q_i} = C_F\left(\frac{S}{A_i}\,\mathbf{k}\mu^3 + I\right) \tag{9-15}$$

and Eq. (9-10) gives the pressure-loss coefficient

$$\frac{\Delta p_i}{p_i'} = \frac{\frac{k}{2}\mathrm{M}_0^2\frac{1}{\mu^2}\left[1 + \frac{k-1}{2}\mathrm{M}_0^2\left(1 - \frac{1}{\mu^2}\right)\right]^{1/(k-1)}}{\left(1 + \frac{k-1}{2}\mathrm{M}_0^2\right)^{k/(k-1)}} \times C_F\left(\frac{S}{A_i}\,\mathbf{k}\mu^3 + I\right) \tag{9-15a}$$

Since the inflow loss has been determined for incompressible flow, Eq. (9-15a) may only tentatively be used also for compressible flow[2] until more information becomes available.

These relations give the basic inflow losses under given flight conditions when the shape of the duct (I) and the wetted approach surface (S/A_i) are known. The skin-friction coefficient C_F may be varied according to the Reynolds number and the nature of the duct and approach surfaces, and this also provides a means of interpreting loss coefficients measured at low speeds in terms of full-scale values. The value of μ is nearly enough a measure of the flight speed, since V_i (which is determined by the engine) does not vary very much with flight speed and height. $\mu = 0$ under static conditions; as a rough guide $\mu = 1$ may be taken to represent climbing conditions and $\mu = 2$ high-speed level flight. Figure 9-3 shows the order of magnitude of the total-head-loss coefficient and the pressure-loss coefficient for some values of the constants which may occur in practice. Only the approach loss varies appreciably with flight speed, becoming predominant in high-speed flight.

The inflow losses according to Eq. (9-15) may be regarded as the *natural* losses which will always be present when the inflow passes along walls. Only if measures are taken to divert the boundary layer from these walls (by suction, for example) can the actual losses be smaller than is given by Eq. (9-15); this can be taken into account by reducing the value of $\mathbf{k}$. If, however, the inflow losses are found to be greater than those from Eq. (9-15) in a practical case, then this is a sign of detrimental interference effects which make the losses greater than they need be; this can be measured by increasing the value of $\mathbf{k}$. An analysis of measured inflow losses on these lines will be given below in Secs. 9-8 and 9-9.

[1] This relation may be refined by distinguishing between different values of C_F for the approach and for the duct.

[2] In compressible flow, it will be necessary to consider the variation of the density and, in particular, how the skin friction depends on the density; see, for example, H. U. Eckert, 1950; R. E. Wilson, 1950.

Unavoidable approach losses other than those discussed above occur in supersonic flow as a consequence of shock waves upstream of the inlet. These losses may be quite large compared with the inflow losses to be expected in subsonic flow, and possible interactions between shock waves and the boundary layer on approach surfaces may make them still larger.

Section 7-8 deals with the simplest case of a single normal shock, and the inlet pressures obtained with and without shock are given by Eqs. (7-41) and (7-42). The pressure-loss coefficient can also be obtained from the entropy increase $s_0 - s_0$ of the air in its passage through the

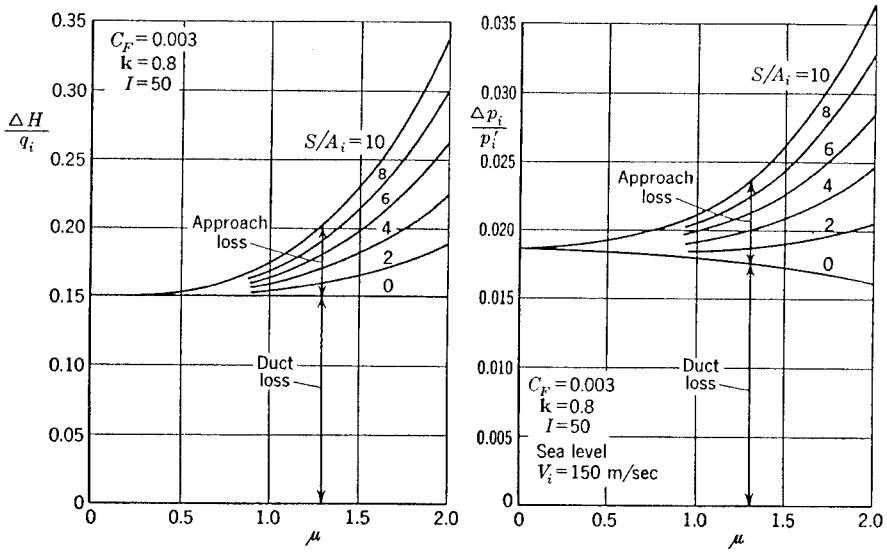

FIG. 9-3. An example showing the magnitude of the loss coefficients.

shock, which must be the same as that in the inlet given by Eq. (9-4), the inflow being otherwise isentropic. Hence, for a normal shock,

$$\frac{s_i - s_0}{R} = \frac{\hat{s}_0 - s_0}{R} = \ln\left\{\left[\frac{2 + (k-1)\mathrm{M}_0^2}{(k+1)\mathrm{M}_0^2}\right]^{k/(k-1)} \times \left[1 + \frac{2k}{k+1}(\mathrm{M}_0^2 - 1)\right]^{1/(k-1)}\right\}$$

by Eq. (7-40), so that by Eq. (9-4),

$$\frac{\Delta p_i}{p_i'} = 1 - \frac{1 + \frac{2k}{k+1}(\mathrm{M}_0^2 - 1)}{\left(1 + \frac{k-1}{2}\mathrm{M}_0^2\right)^{k/(k-1)}}\left[\frac{(k+1)\mathrm{M}_0^2}{2 + \frac{4k}{k+1}(\mathrm{M}_0^2 - 1)}\right]^{k/(k-1)} \tag{9-16}$$

This equation is true for any inlet velocity ratio V_i/V_0. Some numerical values of $\Delta p_i/p_i'$ are given in Table 9-1.

TABLE 9-1

M_0	$\Delta p_i/p_i'$	η_{ram}
1.0	0	1.000
1.2	0.007	0.992
1.5	0.07	0.93
2.0	0.28	0.80
2.5	0.50	0.69
3.0	0.67	0.58

The losses are serious at the higher supersonic Mach numbers. Their reduction by the replacement of the normal shock by an oblique shock system with lower losses is mentioned in Sec. 7-8.

9-3. Thrust and Fuel Consumption of Turbojet Engines with Inflow Losses. In this section[1] we shall compare two engines, one with ideal inflow (engine 1) and the other receiving air with reduced available energy (engine 2). It is assumed that the flight speed and altitude are the same in both cases and that both engines operate at full throttle under the same material stresses; consequently, the compressor and turbine rpm and the highest temperature—that at the turbine entry—are the same. We assume further that the exit nozzle is regulated to give the same volume flow through both engines, making the inlet velocity and the ratio between axial and tangential velocity components at the blades exactly the same and the Mach number and the Reynolds number at the compressor blades approximately the same.

The losses which occur in the inflow are measured by the pressure-loss coefficient $\Delta p_i/p_i'$, as discussed in the previous sections. Since the density at the entry to the compressor is reduced in the same ratio as the pressure, Eq. (9-3), a smaller weight of air passes through engine 2 per unit time. We exclude types of inflow which not only reduce the pressure but also have nonuniform velocity distributions at the compressor entry, reducing the efficiency of the compressor and accordingly that of the whole engine.

Figure 9-4 shows simplified working processes for the two engines. In the isentropic inflow $0 \rightarrow i'$, a certain temperature T_i' is reached. The real inflow reaches the same temperature, $T_i = T_i'$, as explained in Sec. 9-1, although there is an increase in entropy given by Eq. (9-4).

With these entry conditions, the compressor produces the same pressure ratio in both engines, so that $p_B/p_i = p_B'/p_i'$. We assume here that the compressors have the same adiabatic efficiencies. The pressure in the combustion chamber of engine 2 with inflow losses is therefore lower in the ratio $p_B/p_B' = p_i/p_i' = 1 - \Delta p_i/p_i'$. The temperature T_{B1} at the

[1] We follow here a method developed by H. Ludwieg, 1946.

beginning of the combustion chamber remains unaltered, $T_{B1} = T_{B1}'$, and the entropy difference $s_{B1} - s_{B1}'$ is still as given by Eq. (9-4).

The input of heat is assumed to take place at constant pressures, p_B and p_B', respectively. The temperature has the same maximum $T_{B2} = T_{B2}'$ at the end of the combustion chamber in both cases. With $T_{B2} - T_{B1} = T_{B2}' - T_{B1}'$, we find from Eq. (2-7) for constant-pressure processes that the heat input per unit weight of air is the same for both engines:

$$\bar{q} = c_p(T_{B2} - T_{B1}) = \bar{q}' \quad (9\text{-}17)$$

The total heat input Q, however, is less for the engine with inflow losses because of the reduced mass flow; it is lower in the same ratio as the density,

$$\frac{Q}{Q'} = \frac{\rho_i}{\rho_i'} = 1 - \frac{\Delta p_i}{p_i'} < 1$$

$$\frac{\Delta Q}{Q'} = -\frac{\Delta p_i}{p_i'} \quad (9\text{-}18)$$

which implies that engine 2 consumes less fuel than engine 1.

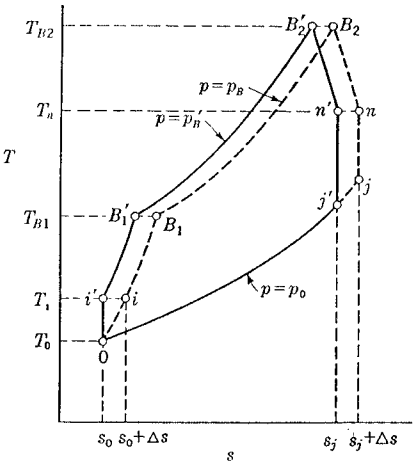

FIG. 9-4. Turbojet engine with inflow losses (diagrammatic).

The work produced in the turbine is the same as that absorbed by the compressor in each case, so that $T_n - T_{B2} = T_n' - T_{B2}'$ and thus $T_n = T_n'$. With the same turbine efficiencies, the ratio of the pressures at the beginning of the nozzle is $p_n/p_n' = p_i/p_i'$. Thus all pressures in the real engine are reduced in the same ratio. The entropy difference $s_n - s_n'$ is the same as that at the inlet, Eq. (9-4), at all stages.

In the nozzle the air expands from p_n, or p_n', to $p_e = p_j = p_0$ in the jet; but the available energy for the production of kinetic energy in the jet is now less in the case of engine 2. The available energy is equal to the enthalpy difference in the nozzle, see Eq. (2-20); for engine 2, it is $c_p(T_n - T_j)$, Eq. (2-8), which is obviously less than $c_p(T_n - T_j')$, since the temperature in the jet of engine 2 is higher (see Fig. 9-4). Consequently, engine 2 with inflow losses produces less thrust than engine 2 with isentropic inflow.

The pressure ratio p_0/p_n in the nozzle of engine 2 is greater than the ratio p_0/p_n' for engine 1. In fact,

$$\frac{p_0}{p_n} = \frac{p_0}{p_n'}\frac{p_n'}{p_n} = \frac{p_0}{p_n'}\frac{p_i'}{p_i} = \frac{p_0/p_n'}{1 - \Delta p_i/p_i'} \quad (9\text{-}19)$$

If the flow in the nozzle is subsonic, the exit area must be larger for engine

2 since the same volume of air is to be discharged, the available pressure difference $p_n - p_0$ being smaller and the temperatures T_n being equal. If the flow in the nozzle is supersonic, however, no change is required since the volume flow is then independent of the pressure ratio; the assumption of equal volume flow which we made above is fulfilled automatically.

We are now in a position to relate the thrust of the engine to the inflow loss. The thrust is equal to the increase of momentum of the air which passes through the engine per unit time,

$$\mathbf{T} = \rho_i V_i A_i (V_j - V_0) \qquad \text{and} \qquad \mathbf{T}' = \rho_i' V_i A_i (V_j' - V_0) \tag{9-20}$$

see Eq. (2-28). Thus the thrust of engine 2 is reduced in two ways: First, the mass flow is less because $\rho_i < \rho_i'$; second, the velocity V_j in the jet is smaller. The ratio of the thrust $\mathbf{T}$ of the engine with inflow losses to the ideal thrust $\mathbf{T}'$ is

$$\frac{\mathbf{T}}{\mathbf{T}'} = \left(1 - \frac{\Delta p_i}{p_i'}\right) \frac{V_j - V_0}{V_j' - V_0} = \left(1 - \frac{\Delta p_i}{p_i'}\right) \frac{V_j/V_j' - V_0/V_j'}{1 - V_0/V_j'} \tag{9-21}$$

We can replace V_0/V_j' here in terms of the jet efficiency of the ideal inflow engine,

$$\eta_j = \frac{2}{1 + V_j'/V_0}$$

so that

$$\frac{V_0}{V_j'} = \frac{\eta_j}{2 - \eta_j} \tag{9-22}$$

see Eq. (2-31). η_j is a conveniently short expression, embracing the thrust, flight speed, altitude, mass-flow ratio, and size of the engine, since, by Eq. (9-20),

$$\frac{\mathbf{T}'}{\frac{1}{2}\rho_0 V_0^2 A_i} = 2\frac{\rho_i' V_i}{\rho_0 V_0}\left(\frac{V_j'}{V_0} - 1\right) = 4\frac{\rho_i' V_i}{\rho_0 V_0}\frac{1 - \eta_j}{\eta_j}$$

It remains to find an expression for the jet velocity ratio V_j/V_j'.

The velocity in the jet is related to the pressure ratio in the nozzle by

$$V_j = \sqrt{\frac{k+1}{k-1}}\, a_n^* \sqrt{1 - \frac{2}{k+1}\frac{a_n^2}{a_n^{*2}}\left(\frac{p_0}{p_n}\right)^{(k-1)/k}}$$

This follows from the energy equation for the process described. Now $a_n^* = a_n'^*$, since pressure and density in the nozzle are reduced in the same ratio. Therefore

$$\frac{V_j}{V_j'} = \sqrt{\frac{1 - \frac{2}{k+1}\frac{a_n^2}{a_n^{*2}}\left(\frac{p_0}{p_n}\right)^{(k-1)/k}}{1 - \frac{2}{k+1}\frac{a_n^2}{a_n^{*2}}\left(\frac{p_0}{p_n'}\right)^{(k-1)/k}}}$$

which can be simplified considerably if it is assumed that the velocity at the beginning of the nozzle is low in both engines. This assumption is reasonable for purpose of the present comparison. Writing $V_n = 0$,

$$\frac{2}{k+1}\frac{a_n^2}{a_n^{*2}} = 1 - \frac{k-1}{k+1}\left(\frac{V_n}{a_n^*}\right)^2 = 1$$

Using Eq. (9-19) we then have for the jet velocity ratio

$$\frac{V_j}{V_j'} = \sqrt{\frac{1 - \left(\frac{p_0}{p_n'}\right)^{(k-1)/k} \frac{1}{(1 - \Delta p_i/p_i')^{(k-1)/k}}}{1 - (p_0/p_n')^{(k-1)/k}}} \tag{9-23}$$

Substitution of V_0/V_j' from Eq. (9-22) and V_j/V_j' from Eq. (9-23) in Eq. (9-21) for the thrust ratio gives

$$\frac{\mathbf{T}}{\mathbf{T}'} = \frac{1 - \frac{\Delta p_i}{p_i'}}{2(1 - \eta_j)}\left[(2 - \eta_j)\sqrt{\frac{1 - \left(\frac{p_0/p_n'}{1 - \Delta p_i/p_i'}\right)^{(k-1)/k}}{1 - (p_0/p_n')^{(k-1)/k}}} - \eta_j\right] \tag{9-24}$$

This can be further simplified by the assumption that the pressure loss in the inflow is small compared with the original p_i', as is justified in most practical cases. Ignoring quadratic terms of $\Delta p_i/p_i'$, we obtain

$$\frac{\Delta \mathbf{T}}{\mathbf{T}'} = \frac{\mathbf{T} - \mathbf{T}'}{\mathbf{T}'} = -L\frac{\Delta p_i}{p_i'} \tag{9-25}$$

where

$$L = 1 + \frac{1 - \frac{\eta_j}{2}}{1 - \eta_j}\frac{\frac{k-1}{2k}\left(\frac{p_0}{p_n'}\right)^{(k-1)/k}}{1 - (p_0/p_n')^{(k-1)/k}} \tag{9-26}$$

The thrust-loss factor L, which was introduced by Ludwieg, is a measure of the sensitivity of a particular engine to inflow losses. Values of L calculated using $k = 1.40$ are plotted against p_0/p_n' in Fig. 9-5 for different values of η_j. Static conditions ($V_0 = 0$) are represented by $\eta_j = 0$. It will be seen that engines in which the expansion in the nozzle is high (p_0/p_n' small) are less sensitive than those with a low expansion (p_0/p_n' large), as would be expected. For a given engine, both p_0/p_n' and η_j vary with flight speed and are to be determined from the engine data and flight conditions.

We have already seen [Eq. (9-18)] that the fuel consumption of the engine with inflow losses is less than that of the ideal-inflow engine because of the reduced mass flow. The specific fuel consumption $Q/\mathbf{T}$ is greater than $Q'/\mathbf{T}'$, however. The change in specific fuel consumption,

$$\Delta\left(\frac{Q}{\mathbf{T}}\right) = \frac{Q}{\mathbf{T}} - \frac{Q'}{\mathbf{T}'}$$

can be expressed by

$$\frac{\Delta(Q/\mathrm{T})}{Q'/\mathrm{T}'} = \frac{Q}{Q'}\frac{1}{\mathrm{T}/\mathrm{T}'} - 1$$

and to the first-order equations (9-18), (9-25), and (9-26) give

$$\frac{\Delta(Q/\mathrm{T})}{Q'/\mathrm{T}'} = (L-1)\frac{\Delta p_i}{p_i'} \tag{9-27}$$

The relative increase in specific fuel consumption is less than the relative loss of thrust; while specific fuel consumption and thrust are affected in

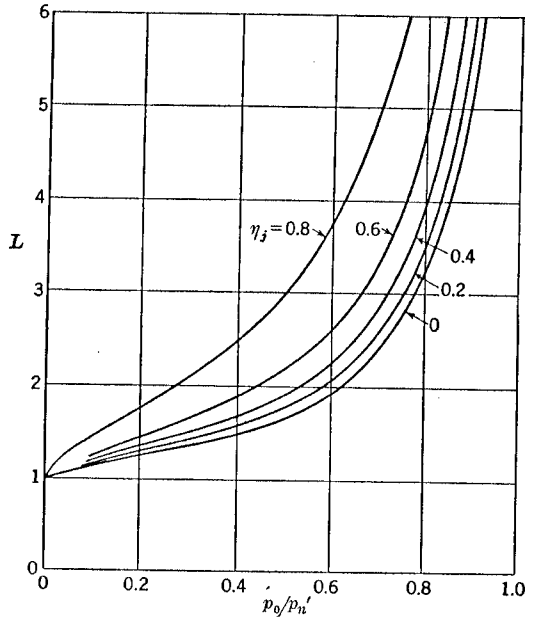

FIG. 9-5. The thrust-loss factor L of Eq. (9-26).

the same way by the reduction of mass flow, the thrust alone is further decreased by the effect on the thermal process (lower pressure in the combustion chamber) which reduces the kinetic energy in the jet and makes it hotter instead.

Consequently, the over-all propulsive efficiencies

$$\eta = \frac{\mathrm{T}V_0}{Q} \qquad \text{and} \qquad \eta' = \frac{\mathrm{T}'V_0}{Q'}$$

of the two engines are also different, with $\eta < \eta'$. At the same flight speed V_0,

$$\frac{\Delta\eta}{\eta'} = \frac{\eta - \eta'}{\eta'} = \frac{\mathrm{T}/Q - \mathrm{T}'/Q'}{\mathrm{T}'/Q'}$$

so that, from Eqs. (9-18) and (9-25), again to the first order,

$$\frac{\Delta\eta}{\eta'} = -(L-1)\frac{\Delta p_i}{p_i'} \tag{9-28}$$

The loss of over-all efficiency is less than the relative thrust loss.

In the following we shall need some numerical values for L for a representative turbojet engine. For high-speed flight with $\mathrm{M}_0 = 0.9$ at sea level, we choose $p_0/p_n' = 0.528$ (choking) and $\eta_j = 0.734$; then Fig. 9-5 gives $L = 2.7$. For static conditions, we take $p_0/p_n' = 0.6$ and $\eta_j = 0$,

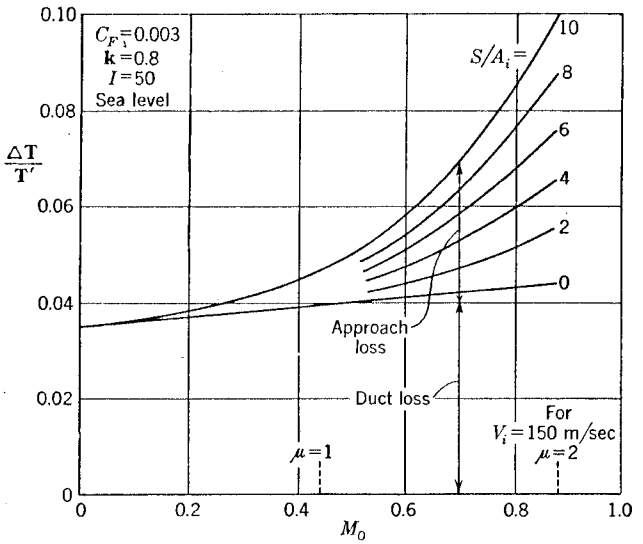

FIG. 9-6. The thrust losses which correspond to the inflow losses of Fig. 9-3 for a fictitious engine with $L = 1.9$ at $\mathrm{M}_0 = 0$ and $L = 2.7$ at $\mathrm{M}_0 = 0.9$.

and get $L = 1.9$. The pressure-loss coefficients for the example in Fig. 9-3 can now be transformed into thrust losses, Fig. 9-6.

The results obtained by this method have been compared with those from full-scale tests, referred to in Fig. 4-30, Sec. 4-9, and good agreement was found.

For the ram jet, the thrust-loss factor L can be determined from the flight Mach number M_0, the heat-input coefficient C_q, and the mass-flow ratio m. A simple formula is obtained for $m = 0$; this gives the lowest value of p_0/p_n' and thus the minimum losses.

In this case, Eq. (7-32) gives the jet efficiency

$$\eta_j = \frac{2}{1 + \sqrt{1 + C_q}}$$

and Eq. (7-21) and the relation $V_j'/V_0 = \sqrt{1 + C_q}$ give the pressure

ratio in the nozzle

$$\frac{p_0}{p_n'} = \left(1 - \frac{k-1}{k+1}\,\mathrm{M}_0^{*2}\right)^{k/(k-1)}$$

Substituting for η_j and p_0/p_n' in Eq. (9-26), we find

$$L = 1 + \frac{\sqrt{1+C_q}}{\sqrt{1+C_q}-1}\,\frac{1}{k\mathrm{M}_0^2} \tag{9-29}$$

This result shows that the subsonic ram jet is very sensitive to inflow losses. At $\mathrm{M}_0 = 0.5$, for example, $L = 10.8$ when $C_q = 1$ and $L = 5.8$ when $C_q = 5$; at $\mathrm{M}_0 = 2$, the corresponding figures are $L = 1.6$ and 1.3, respectively.

9-4. An Alternative Way of Determining the Thrust-loss Coefficient. The factor L for the relative thrust loss in Eq. (9-25) is expressed in Eq. (9-26) as a function of the jet efficiency and the pressure ratio in the nozzle. As is always the case when there is a large number of variables, there are alternative ways of proceeding, in which other sets of parameters are employed, which may be more convenient in special cases. We shall demonstrate this in the following example by expressing L in terms of the parameters[1] which we used in the treatment of turbojet engines in Chap. 8; this will at the same time illustrate the application of the general relations of Chap. 2.

Beginning with Eq. (9-21) for the thrust, we have to determine the velocity ratio V_j'/V_0 of engine 1 and the change V_j/V_j' in the jet velocity due to inflow losses.

The velocity ratio in the jet of the engine without inflow losses can be written as

$$\frac{V_j'}{V_0} = \sqrt{1 + \frac{2}{k-1}\,\frac{1}{\mathrm{M}_0^2}\,\eta_{th}\left(\frac{T_{B2}}{T_0} - \frac{T_{B1}}{T_0}\right)} \tag{9-30}$$

as explained in Eq. (8-10), Sec. 8-5. In this expression, η_{th} is the thermal efficiency of the cycle without inflow losses, which is assumed to be known, T_{B2} is the maximum temperature at the end of combustion, and T_{B1} is the temperature at the beginning of combustion. T_{B1} can be written as

$$\frac{T_{B1}}{T_0} = \frac{T_{B1}}{T_i}\,\frac{T_i}{T_0} = \left[1 + \frac{(p_B/p_i)^{(k-1)/k} - 1}{\eta_c}\right] \times \left\{1 + \frac{k-1}{2}\,\mathrm{M}_0^2\left[1 - \left(\frac{V_i}{V_0}\right)^2\right]\right\} \tag{9-31}$$

which follows from Eq. (8-11). The inlet velocity ratio V_i/V_0, the compression ratio p_B/p_i, the maximum temperature T_{B2}/T_0, and the flight Mach number M_0 are thus our basic parameters.

[1] These are suitable for calculation purposes; it may also be worth while to express L in terms of parameters which can easily be measured.

As a consequence of the difference in the working processes of engines 1 and 2 (Fig. 9-4) there is a difference in kinetic energy in the jet, resulting from the reduction of the available energy:

$$\frac{V_j'^2 - V_j^2}{2g} = c_p(T_j - T_j') \tag{9-32}$$

On the other hand, there is a constant increase of entropy throughout the process of engine 2, given by Eq. (9-4) as the entropy increase in the inflow

$$\Delta s = c_p \ln \frac{T_j}{T_j'} = R \ln \frac{p_i'}{p_i} \qquad \text{with } R = c_p\,\frac{k-1}{k}$$

Hence,

$$\frac{T_j}{T_j'} = \left(\frac{p_i'}{p_i}\right)^{(k-1)/k} \tag{9-33}$$

Combining this with Eq. (9-32), we obtain

$$V_j^2 = V_j'^2 - \frac{2}{k-1}\,a_0^2\,\frac{T_{B2}/T_0}{T_{B1}/T_0}\left[\left(\frac{p_i'}{p_i}\right)^{(k-1)/k} - 1\right] \tag{9-34}$$

because $T_j'/T_0 = T_{B2}/T_{B1}$, which is, however, strictly true only for the ideal constant-pressure process without compressor and turbine losses. The present treatment therefore underestimates the thrust reduction, although only to a small extent.

Equation (9-34) can be simplified if $V_j'^2 - V_j^2 = (V_j' - V_j)(V_j' + V_j)$ can be replaced by $(V_j' - V_j)\,2\,V_j'$, which is true if $\Delta p_i/p_i' = p_i/p_i' - 1 \ll 1$, as before. We then obtain from Eqs. (9-21) and (9-34), after some algebraic transformations,

$$\frac{\Delta \mathbf{T}}{\mathbf{T}'} = -\left\{1 + \frac{1}{k\mathrm{M}_0^2}\,\frac{T_{B2}/T_0}{T_{B1}/T_0}\,\frac{1}{\dfrac{V_j'}{V_0}\left(\dfrac{V_j'}{V_0} - 1\right)}\right\}\frac{\Delta p_i}{p_i'} = -L\,\frac{\Delta p_i}{p_i'} \tag{9-35}$$

where V_j'/V_0 and T_{B1}/T_0 are given by Eqs. (9-30) and (9-31).

This result has been used to work out the thrust loss which results from the presence of a normal shock wave in the inflow for the example in Fig. 8-11. The shock loss is as given in Sec. 9-2. We should mention that, for the particular type of engine considered, the value of L varies only slightly with flight Mach number. For example, $L = 1.81$ at $\mathrm{M}_0 = 0$; $L = 1.78$ at $\mathrm{M}_0 = 1$; and $L = 1.85$ at $\mathrm{M}_0 = 1.9$. It should be remembered that in this case supersonic jet velocities were allowed.

9-5. Influence of Duct Losses on Turbojet Engines. A turbojet engine which is completely buried inside the fuselage or wing usually needs long ducts either ahead of the compressor or in the jet pipe; there may be the choice between the two, although the engine position is often fixed by center-of-gravity requirements.

A long inflow duct has the obvious disadvantage that the velocity distribution at the compressor entry may not be uniform. Axial compressors in particular are sensitive to such disturbances and suffer a loss of efficiency. The nozzle, on the other hand, is much less sensitive.

Losses in the inflow duct and the jet pipe affect thrust and fuel consumption in different ways. The inflow-duct losses are covered by the previous section; provided that there is no breakdown of the flow, the pressure-loss coefficient can be determined from Eq. (9-12). There is also much experimental data on a variety of duct shapes. Reference may be made to the considerations in Sec. 4-9, in particular to the sometimes serious additional losses introduced by expanding ducts (see Fig. 4-30).

Using the nomenclature of Fig. 9-4, we may compare two engines: The process $0iB_1B_2nj$ includes losses in the inflow duct, like engine 2 in the previous sections. The process $0i'B_1'B_2'n'nj$ suffers losses in the jet pipe; this may be called engine 3. There is a pressure drop in the nozzle of engine 3,

$$p_n = p_n' - \Delta p_n = p_n'\left(1 - \frac{\Delta p_n}{p_n'}\right) \tag{9-36}$$

which we shall take as being the same as the loss in the inflow duct of engine 2,

$$\frac{p_n}{p_n'} = \frac{p_i}{p_i'} = 1 - \frac{\Delta p_i}{p_i'}$$

The pressure ratio p_0/p_n in the nozzle is then the same for both engines; see Eq. (9-19). Hence the velocity V_j in the jet is also the same, and by Eq. (9-20) the same thrust per unit mass flow is produced. Now, as we saw in Sec. 9-3, inflow losses reduce the mass flow because $\rho_i < \rho_i'$, Eq. (9-3). The mass flow is not reduced by jet-pipe losses since $\rho_i = \rho_i'$ (and $V_i = V_i'$ anyway). The thrust of engine 3 with jet-pipe losses is therefore higher than that of engine 2 with inflow-duct losses in the ratio

$$\frac{\rho_i'}{\rho_i} = \frac{1}{1 - \Delta p_n/p_n'}$$

so that, with L defined as in Eq. (9-26) or (9-35),

$$\frac{\Delta \mathbf{T}}{\mathbf{T}'} = -(L-1)\frac{\Delta p_n}{p_n'} \tag{9-37}$$

to the first order, for engine 3.

The total fuel consumption is higher than that of engine 2; it is the same as that of the ideal engine 1 with no losses; $Q = Q'$. The specific fuel consumption is thus the same for both engines 2 and 3:

$$\frac{\Delta(Q/\mathbf{T})}{Q'/\mathbf{T}'} = (L-1)\frac{\Delta p_n}{p_n'} \tag{9-38}$$

Where the pressure loss is produced is irrelevant to the specific fuel consumption. A long jet pipe, then, is to be preferred to a long inflow duct, if it is desirable to maintain thrust and therefore top speed as high as possible with a given engine maximum temperature. It is more difficult to construct a long jet pipe, of course, because of its high temperature.

9-6. Influence of Duct Losses on Ducted Fans. If a complete integration of the propulsion unit into the lifting surface is to be attempted, it may be profitable to consider multiway engines (see Sec. 2-7). Consider the case where a turbine engine supplies mechanical energy to a ducted fan in a second air stream, in which mechanical energy is transferred directly into propulsive work. From the general aerodynamic point of view it is best to have the intake in the leading edge and the exit at the trailing edge of the wing; the mass flow might then be varied by means of flaps, and the design could be combined with an effective high lift device. The fan or fans of such an installation again require long ducts.

We may consider the flow in the duct to be incompressible in this case because the velocity there is necessarily limited by the Mach number at the blades of the fan. The general treatment is then very similar to that of the ducted propeller in Chap. 6. The fan or compressor inside the duct produces a pressure rise

$$\Delta p_C = \psi \tfrac{1}{2}\rho U_C^2 \tag{9-39}$$

where U_C is the circumferential velocity at its blade tips. The axial velocity at the fan is

$$V_C = \varphi U_C \tag{9-40}$$

The duct losses in the form $\Delta H/q_i$ are given by Eq. (9-12). We write for convenience

$$\zeta = \frac{\Delta H}{\tfrac{1}{2}\rho V_C^2} \tag{9-41}$$

The energy balance of the flow through the duct is

$$p_0 + \frac{1}{2}\rho V_0^2 - \zeta\frac{1}{2}\rho V_C^2 + \psi\frac{1}{2}\rho\left(\frac{V_C}{\varphi}\right)^2 = p_e + \frac{1}{2}\rho V_e^2 = p_0 + \frac{1}{2}\rho V_j^2$$

From this we obtain the velocity in the jet,

$$\frac{V_j}{V_0} = \sqrt{1 + \left(\frac{\psi}{\varphi^2} - \zeta\right)\left(\frac{V_C}{V_0}\right)^2} \tag{9-42}$$

where V_C/V_0 is the velocity ratio at the fan, given by

$$\frac{V_C}{V_0} = \sqrt{\frac{1 - (p_e - p_0)/\tfrac{1}{2}\rho V_0^2}{(A_C/A_e)^2 - (\psi/\varphi^2 - \zeta)}} \tag{9-43}$$

The exit pressure p_e may well differ from p_0, especially for a wing installation.

The thrust is again given by Eq. (9-20), and the thrust coefficient is

$$C_T = \frac{T}{\frac{1}{2}\rho V_0^2 A_c} = 2\frac{V_c}{V_0}\left[\sqrt{1 + \left(\frac{\psi}{\varphi^2} - \zeta\right)\left(\frac{V_c}{V_0}\right)^2} - 1\right] \tag{9-44}$$

The over-all efficiency is the ratio of the propulsive work TV_0 to the power input P_c to the compressor,

$$\eta = \frac{TV_0}{P_c}$$

P_c can be expressed in terms of the compressor efficiency

$$\eta_c = \frac{\Delta p_c A_c V_c}{P_c} = \frac{(\psi/\varphi^2)\frac{1}{2}\rho V_c^3 A_c}{P_c} \tag{9-45}$$

by Eqs. (9-39) and (9-40). Then

$$\eta = 2\eta_c \frac{\sqrt{1 + (\psi/\varphi^2 - \zeta)(V_c/V_0)^2} - 1}{(\psi/\varphi^2)(V_c/V_0)^2} \tag{9-46}$$

For $\zeta = 0$, $\eta = \eta_c\eta_j$, since the jet efficiency is

$$\eta_j = \frac{2}{1 + V_j/V_0} = \frac{2}{1 + \sqrt{1 + (\psi/\varphi^2 - \zeta)(V_c/V_0)^2}}$$

For a given installation, ζ is known and the velocity ratio V_c/V_0 is fixed. It is then of practical importance that ψ/φ^2 has an optimum value which gives the highest efficiency; η is zero when $\psi/\varphi^2 = \zeta$, and is also low when ψ/φ^2 is large. The optimum value $(\psi/\varphi^2)_{opt}$ is obtained by putting the first derivative of η with respect to ψ/φ^2 equal to zero,

$$\left(\frac{\psi}{\varphi^2}\right)_{opt} = 2\left(\zeta + \frac{\sqrt{\zeta}}{V_c/V_0}\right) \tag{9-47}$$

The corresponding efficiency is

$$\eta_{opt} = \eta_c \frac{1}{1 + \sqrt{\zeta}\, V_c/V_0} \tag{9-48}$$

and the thrust is

$$C_{T\,opt} = 2\sqrt{\zeta}\left(\frac{V_c}{V_0}\right)^2 \tag{9-49}$$

The exit area necessary when $p_e = p_0$ is given by Eq. (9-43).

$$\left(\frac{A_e}{A_c}\right)_{opt} = \frac{V_c/V_0}{1 + \sqrt{\zeta}\, V_c/V_0} \tag{9-50}$$

Some values of the efficiencies obtained in a range of velocity ratios and thrust coefficients are shown in Fig. 9-7. There appears to be a reasonable prospect for this method of propulsion, but great care is obviously necessary in the aerodynamic design. The fan itself should be as efficient as possible, and a suitable compromise must be found between the conflicting influences of the velocity ratio and the duct-loss coefficient: Low values of V_c/V_0 suit the compressor design and make the absolute duct losses small, but the jet efficiency is then bad; if V_c/V_0 is increased to improve the jet efficiency the duct losses become important.

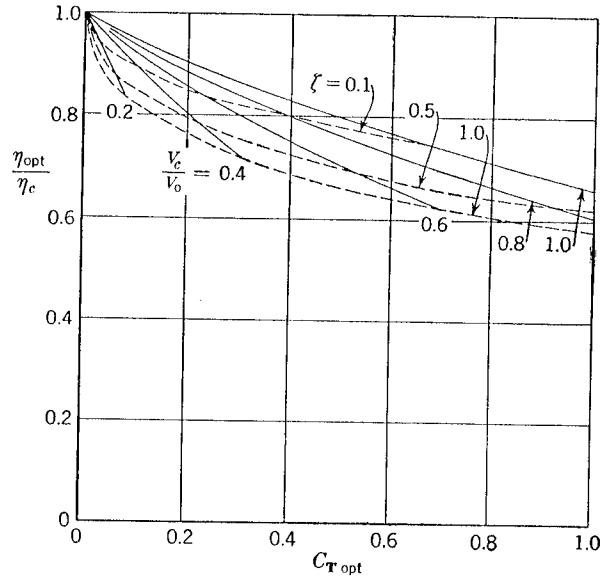

Fig. 9-7. Optimum efficiencies for ducted fans with duct losses.

9-7. Diversion of the Wing Wake into the Engine. Suppose that the wake of the wing, which contains air of reduced energy due to the effect of the boundary layer, is deliberately taken into the engine. Ideally, if the wake of the whole aircraft can be diverted into the engine no thrust is required; it is only necessary for the engine to restore the energy of the air in the wake to that in the free stream. The intake of a part of the boundary-layer material will allow a reduction of engine thrust by an amount equal to the drag which the loss of momentum of that mass of air represents. It is well known that the efficiency of propulsion of a ship by a screw propeller is improved by the use of a screw at the rear in the wake instead of a tractor screw at the bow. It will be seen below that a similar improvement is possible in aircraft propulsion.

We consider a very much simplified system by assuming the wake with reduced energy to be produced by a screen far upstream of the engine

intake. There is an isentropic compression ahead of the screen (see Fig. 9-8), followed by a pressure drop $p_{s1} - p_{s2}$ through the screen with a simultaneous increase of entropy. The flow then regains the free-stream pressure isentropically in the wake (W) and becomes parallel again. The velocity V_W in the wake is lower than V_0. It is assumed that all the air that passed through the screen flows into the inlet of the engine, and the

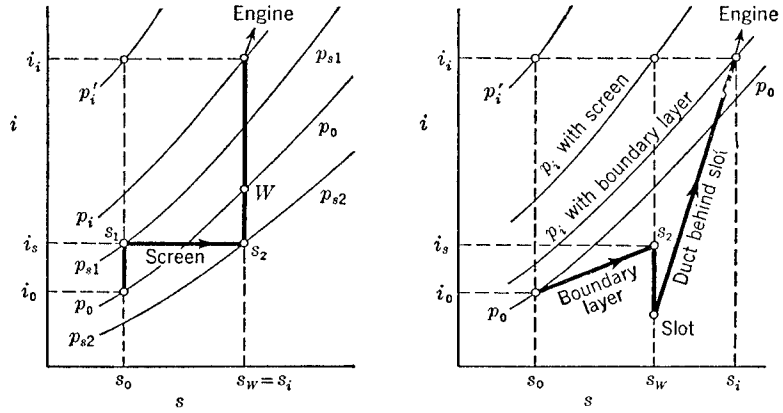

FIG. 9-8. Inflow through a screen upstream of the intake, left, and inflow of boundary-layer material through a slot, right (diagrammatic).

actual inflow from V_W to V_i is again taken as isentropic. The only pressure loss in the inflow is therefore

$$\frac{p_{s1} - p_{s2}}{p_{s1}} = \frac{\Delta p_s}{p_{s1}} \tag{9-51}$$

If we compare this with an ideal isentropic inflow with the same inlet velocity V_i (marked by a dash, as before), we find that

$$\frac{\Delta p_i}{p_i'} = \frac{\Delta p_s}{p_{s1}} \quad \text{and} \quad \frac{\rho_i}{\rho_i'} = 1 - \frac{\Delta p_i}{p_i'} = 1 - \frac{\Delta p_s}{p_{s1}} \tag{9-52}$$

using Eq. (9-3).

In practice, the boundary layer is usually sucked away through a slot, and for that to be possible the pressure in the slot must be lower than the pressure in the boundary layer (see the right-hand side of Fig. 9-8). The whole compression from the slot pressure to p_i then takes place inside the duct following the slot. It is very unlikely that this can be achieved without increase of entropy and a consequent reduction of the inlet pressure. Further, the use of boundary-layer air will often make a nonuniform velocity distribution at the compressor entry unavoidable. For these reasons, the simplified inflow through a screen represents the most favorable case.

We can consider the engine together with the screen as an entity, and compare it with another engine (2) with ordinary inflow losses as treated in Sec. 9-3. If the pressure in the inflow is the same in both cases, the actual engine thrust must also be the same. But the drag of the screen has been included with the engine losses, and thus the effective thrust of the engine in combination with the screen is higher than that of the ordinary engine by an amount that corresponds to the screen drag. In other words, the drag of the aircraft is smaller by an amount which corresponds to the screen drag, and the engine thrust can legitimately be smaller by the same amount.

The drag of the screen, or gain in thrust, is

$$\Delta \mathbf{T}_W = \rho_i V_i A_i (V_0 - V_W)$$

and, by Eq. (9-52),

$$\frac{\Delta \mathbf{T}_W}{\mathbf{T}'} = \frac{\rho_i}{\rho_i'} \frac{V_0 - V_W}{V_j' - V_0} = \left(1 - \frac{\Delta p_s}{p_{s1}}\right) \frac{1 - V_W/V_0}{V_j'/V_0 - 1}$$

V_j'/V_0 can again be replaced by the jet efficiency, from Eq. (9-22),

$$\frac{\Delta \mathbf{T}_W}{\mathbf{T}'} = \left(1 - \frac{\Delta p_s}{p_{s1}}\right) \frac{\eta_j}{2(1 - \eta_j)} \left(1 - \frac{V_W}{V_0}\right)$$

The velocity V_W in the wake of the screen remains to be determined; it is a function of $\Delta p_s/p_{s1}$ and the state in the free stream. Only the flow past the screen is involved, and V_W/V_0 can be obtained in the usual way from the energy equation. Assuming $\Delta p_s/p_{s1}$ to be small compared with unity, we find, to the first order,

$$\frac{\Delta \mathbf{T}_W}{\mathbf{T}'} = \frac{1}{kM_0^2} \frac{\eta_j}{2(1 - \eta_j)} \frac{\Delta p_s}{p_{s1}} = L_W \frac{\Delta p_s}{p_{s1}} \tag{9-53}$$

The change of engine thrust due to the inflow conditions is now

$$\frac{\Delta \mathbf{T}}{\mathbf{T}'} = \frac{\Delta \mathbf{T}_i + \Delta \mathbf{T}_W}{\mathbf{T}'} = (-L + L_W) \frac{\Delta p_s}{p_{s1}} \tag{9-54}$$

using the thrust-loss factor L from Eq. (9-26). The fuel consumption is reduced in the same ratio as the mass flow, *i.e.*, the reduction is the same for both engines, so that Eq. (9-18) still holds. The specific fuel consumption $Q/\mathbf{T}$ of the combination is less;

$$\frac{\Delta(Q/\mathbf{T})}{Q'/\mathbf{T}'} = (L - L_W - 1) \frac{\Delta p_s}{p_{s1}} \tag{9-55}$$

instead of Eq. (9-27).

Some numerical values of the wake-loss factor L_W are shown in Fig. 9-9. For a turbojet engine, L_W is smaller than L, which implies that there is a

net loss of thrust. For the fictitious engine of Sec. 9-3, with $M_0 = 0.9$ and $\eta_j = 0.734$, we have $L = 2.7$ and $L_W = 1.2$; diverting the wake into the engine reduces the thrust loss to $(2.7 - 1.2)/2.7 = 55$ per cent of that of the engine where the same inflow loss does not constitute a drag reduction, and reduces the increase in specific fuel consumption to $(2.7 - 1.2 - 1)/(2.7 - 1) = 29$ per cent of the original increase. It is possible that $L - L_W - 1$ could be negative; this would mean an actual reduction of the specific fuel consumption, and the diversion of the boundary layer would then be profitable. It must be remembered, however, that these results were based on too favorable assumptions. Extra

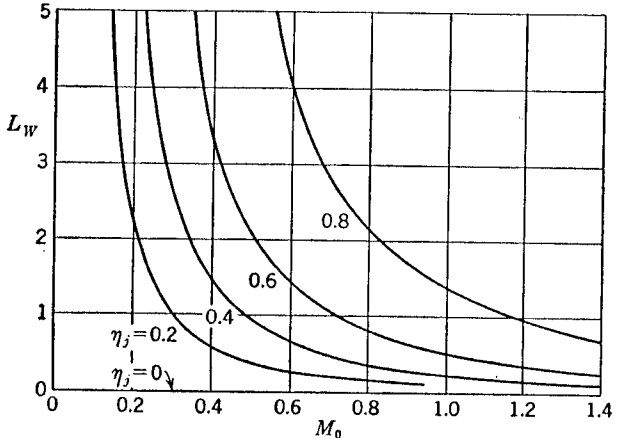

FIG. 9-9. Numerical values of the factor L_W in Eq. (9-53).

losses involved in the diversion of the boundary layer are often of major importance in deciding the practicability of boundary-layer feed schemes.

Our problem can be approached in another way with the aid of the *approach loss* introduced in Sec. 9-2. In the inflow along a wall there is a pressure loss which at the inlet is given by Eq. (9-15) with $I = 0$. At the same time, the skin-friction drag of the aircraft can be said to have been effectively reduced by the amount

$$\Delta D = -C_F S q_0$$

where S is the wetted approach area. The thrust of the engine can legitimately be lower by the same amount, and ΔD can alternatively be interpreted as a reduction $-\Delta \mathrm{T}_W$ of the thrust loss. Referred to the thrust of the engine alone,

$$\frac{\Delta \mathrm{T}_W}{\mathrm{T}'} = C_F \frac{S}{A_i} \frac{A_i}{A_m} \frac{A_m}{\mathrm{T}'} q_0 \tag{9-56}$$

Using the same values again, $\mathrm{T}'/A_m = 2{,}100$ kg/m²; $A_m/A_i = 3$; $V_i = 150$ m/sec; $\mu = 2$, that is, $V_0 = 300$ m/sec($\mathrm{M}_0 \approx 0.9$); sea level;

this gives

$$\frac{\Delta \mathrm{T}_W}{\mathrm{T}'} = +0.89 C_F \frac{S}{A_i} \tag{9-57}$$

On the other hand, the pressure loss at the inlet

$$\frac{\Delta p_i}{p_i'} = 0.69 C_F \frac{S}{A_i} \tag{9-58}$$

causes a thrust loss

$$\frac{\Delta \mathrm{T}_i}{\mathrm{T}'} = -1.86 C_F \frac{S}{A_i} \tag{9-59}$$

from Eq. (9-25), with $L = 2.7$ as before, and Eq. (9-15). Thus about half the approach thrust loss is recoverable, as was found in effect before, irrespective of the extent of the wetted approach surface. The fuel consumption from Eq. (9-18) is reduced by the amount

$$\frac{\Delta Q}{Q'} = -0.69 C_F \frac{S}{A_i} \tag{9-60}$$

Care must be taken, however, that no additional interference drag is associated with this type of inflow.

9-8. Measured Inflow Losses at Forward-facing Intakes. There is available a number of experimental measurements of the approach losses of various intake arrangements, which can be compared with Seddon's loss formula (9-15) in Sec. 9-2 to find out how far the *natural losses* are realized in practice and whether there are other interference losses of practical importance. It will be recalled that in Sec. 9-2 the pressure loss in a simplified stream tube was related to the skin friction at the approach surface only, for which the well-known skin friction of the flow along a flat plate was used.

The classic test of P. Ruden (1941), Fig. 9-10, shows the effect of a boundary layer on the inflow and the approach loss very clearly. A thin flat plate was added in the plane of symmetry of a two-dimensional intake, extending forward from the inlet. Since it replaces a stream surface, the only effect of such a plate on the inflow is that due to the boundary layer on it. The mean total head across the inlet is in fact found to be less than that of the free stream and consequently $\Delta H/q_i$ (Fig. 9-10) exceeds the ordinary duct loss $C_F I$ given by Eq. (9-12).

In the development of Eq. (9-15), only mean values of the flow properties over the cross section were involved, and before proceeding we must be more explicit as to the interpretation of such means. Of several possibilities,[1] it seems preferable to define the mean energy loss as the mean

[1] We could take the arithmetic mean of the total head loss ΔH; but it depends on the actual distribution of ΔH across the section and decreases downstream along the duct

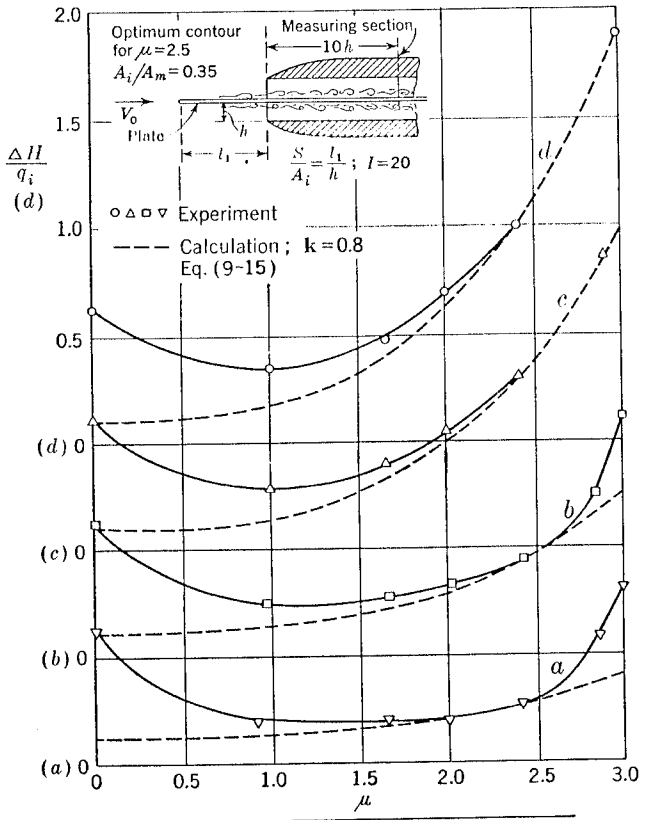

	δ/h	S/A_i	Re	c_F
a	0.10	2	0.2×10^6	0.0063
b	0.20	6	0.6×10^6	0.0050
c	0.31	15	1.5×10^6	0.0042
d	0.42	20	2.0×10^6	0.0041

FIG. 9-10. Inflow losses measured on a two-dimensional intake with a flat plate in its plane of symmetry. From tests by P. Ruden, 1941.

value of the local energy loss $\Delta H(a,b)\, dm$ of mass elements dm

$$\left(\frac{\Delta H}{q_0}\right)_{\text{mean}} = \frac{1}{A_i}\frac{1}{\bar{V}_i/V_0}\int_{A_i}\frac{V_i(a,b)}{V_0}\left[1-\frac{H(a,b)-p_0}{q_0}\right]da\,db \quad (9\text{-}61)$$

where a and b are coordinates in the inlet plane A_i, and $\bar{V}_i$ is the arithmetic mean velocity at the inlet (usually denoted simply by V_i). All the

if the distribution becomes more uniform as a result of a mixing process. This is obviously an undesirable feature. When the distribution is uniform, the arithmetic mean is identical with that of Eq. (9-61); for a nonuniform distribution it is usually higher.

quantities in Eq. (9-61) can be measured directly, $V_i(a,b)$ from additional static-pressure readings and $\bar{V}_i$ by using standard orifices.

The results in Fig. 9-10 show that for values of μ around 2.5, for which the intake was designed, the measured and calculated results agree well. Below $\mu = 2.5$, the sharp nose of the optimum intake (see Sec. 4-5 and in particular Figs. 4-15 and 4-22) causes additional losses at the inner surface of the intake lip as the stagnation point moves round to the outer

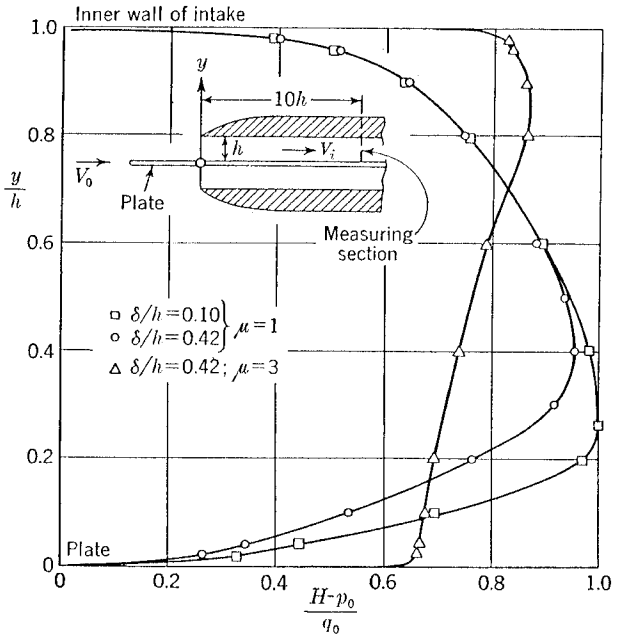

FIG. 9-11. Total-head distribution across the duct for the intake of Fig. 9-10.

surface. This effect is shown clearly by the total-head distribution across the duct in Fig. 9-11. It can easily be avoided by the use of a rounded instead of a sharp lip.

The deviation from the estimated loss curves at values of μ greater than 2.5, for small boundary-layer thicknesses,[1] is also characteristic. At this point a severe breakdown of the flow occurs near the wall as a consequence of the steep adverse pressure gradient at small inlet velocities. The energy loss in the subsequent eddies exceeds that calculated from Eq. (9-15), assuming only skin friction. In a practical design it will be necessary to try to avoid such breakdowns within the flight μ range.

It was mentioned above that the efficiency of the compressor of a

[1] The boundary-layer thickness δ is defined as that distance from the wall at which the velocity is for practical purposes equal to the undisturbed velocity. It is always determined at the inlet plane in the absence of the intake.

turbojet engine may be affected by nonuniformity of the velocity distribution at the inlet. We shall not go into a discussion of this effect here, but we may at least examine the uniformity of the measured distributions. A suitable parameter to describe it is the *dispersion* σ, introduced by Seddon, and defined by

$$\sigma^2 = \frac{1}{a}\int_a \left[\frac{V_i(a') - \bar{V}_i}{\bar{V}_i}\right]^2 da' \qquad (9\text{-}62)$$

σ is a measure of the average deviation of the local velocity $V_i(a)$ at a point a from the mean velocity $\bar{V}_i$. For uniform velocity distribution $\sigma = 0$; if $V_i = 0$ in one half of the duct and $V_i = 2\bar{V}_i$ in the other half, $\sigma = 1$; if $V_i(a)$ rises linearly from 0 to $2\bar{V}_i$ across the section, $\sigma = 0.59$. Figure 9-12 shows that the dispersion is rather high for two-dimensional inflow along a plane wall. Note, however, that the σ curves fall off when the severe flow breakdown occurs; the large eddies tend to equalize the energy losses across the duct.

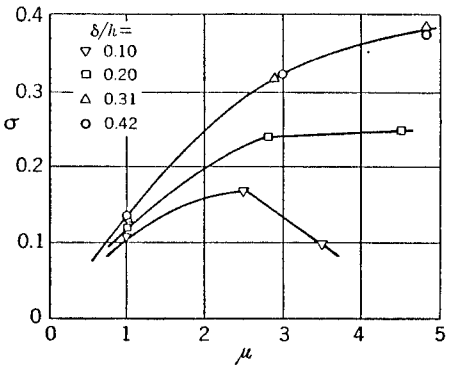

FIG. 9-12. Dispersion of the velocity across the duct for the intake of Fig. 9-10.

The approach-loss formula (9-15) is found to predict losses of annular intakes also. The results in Fig. 9-13 were obtained in tests on a circular intake with a protruding boss of ellipsoidal shape. The agreement of these results with the theory is noteworthy in that the velocity distribution along the approach surface is quite different from what was assumed in the derivation of Eq. (9-15), beginning at a stagnation point and subsequently exceeding the free-stream velocity locally. It is clear that deviations from the conditions assumed do not matter much in practice, and that the loss formula can be applied more generally than might be expected.

For a very long boss, a value 0.6 for $\mathbf{k}$ fits the measured results better than $\mathbf{k} = 0.8$, which seems a fair mean value for most practical cases. This may be connected with the fact that part of the boundary-layer material spills over the outer fairing and does not enter the inlet opening. The effect of such spilling on the external drag will be discussed in Sec. 9-10.

When the diameter D_B of a boss protruding from a circular intake is small compared with the inlet diameter D_i, the approach loss does not decrease in proportion to the wetted approach surface, according to

Eq. (9-15). An infinitely thin needle boss would still have a boundary layer, of course, and even when the approach surface is negligible, the flow breakdown in the boundary layer might initiate severe eddies and energy losses. Experiments show that such an effect does in fact occur, but that the losses can still be described by a μ^3 law, as in Eq. (9-15). The observed result can be accounted for in a simple way by varying the

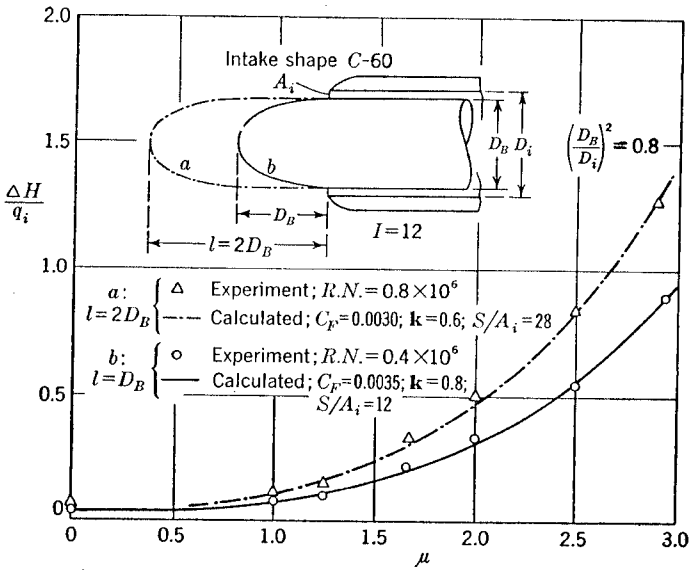

FIG. 9-13. Inflow losses measured on annular intakes.

value of $\mathbf{k}$. It is found that $\mathbf{k}$ increases gradually as the ratio D_B/D_i decreases; some values for $l/D_B = 1$ (see Fig. 9-13) are:

$(D_B/D_i)^2$	0.8	0.7	0.6	0.5	0.2
$\mathbf{k}$	0.8	1.1	1.4	1.8	10

These values may serve as a guide in similar cases. In general, $\mathbf{k} = 0.8$ signifies that there are only the natural losses from the normal boundary layer; $\mathbf{k} > 0.8$ indicates a detrimental interference on the boundary layer and possibly a flow breakdown; $\mathbf{k} < 0.8$ means that part of the normal boundary layer is diverted from the inlet.

The dispersion of the velocity distributions at the annular inlet is very similar to that in straight two-dimensional inlets. The experiments reported above give the following figures for the annular intakes with $\mu = 2$:

$(D_B/D_i)^2$	l/D_B	σ
0.5	1	0.19
	2	0.21
0.8	1	0.10
	2	0.18

The two types of intake considered so far are two-dimensional, and there is no difficulty in defining the wetted approach surface. This is slightly arbitrary, however, with three-dimensional intakes. Three-dimensional intakes may be characterized by the aspect ratio b/h of the

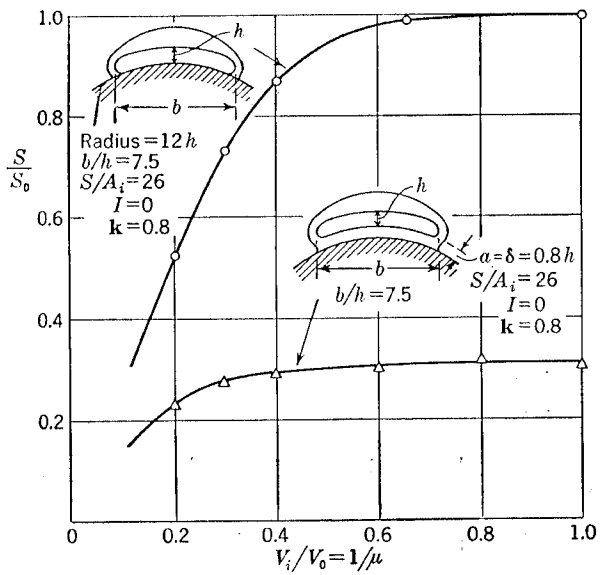

FIG. 9-14. Reduction of the effective approach surface for flat intakes on a curved wall.

inlet opening, where h is the height and b the breadth. Figure 9-14 shows an example with $b/h = 7.5$. Defining an approach surface S_0 as bl_1, where l_1 is the length of the approach wall in the streamwise direction, we find that Eq. (9-15) holds for inlet velocity ratios of about 0.5 and above ($\mu < 2$). With smaller inlet velocities it becomes apparent that part of the boundary layer is diverted sideways and does not enter the inlet; the effective approach surface S is consequently smaller than S_0.

A similar reduction of the effective approach surface due to the three-dimensional inflow will be found with all inlets of small aspect ratio. In

the practical range of μ, however, the deflection of boundary-layer air is not appreciable, and various attempts have been made to divert more by artificial means; some of these, such as suction slots, will be discussed in the next section.

A simple method of reducing the approach loss is to remove the inlet opening to a small distance a from the wall. By removing the inlet of Fig. 9-14 to a distance of about one boundary-layer thickness the effective approach surface was reduced to about $\frac{1}{3}$ of S_0. The reduction is greater, the smaller the aspect ratio of the inlet. With an inlet similar to that in Fig. 9-14 but with an aspect ratio of 2.3, the approach loss was found to be

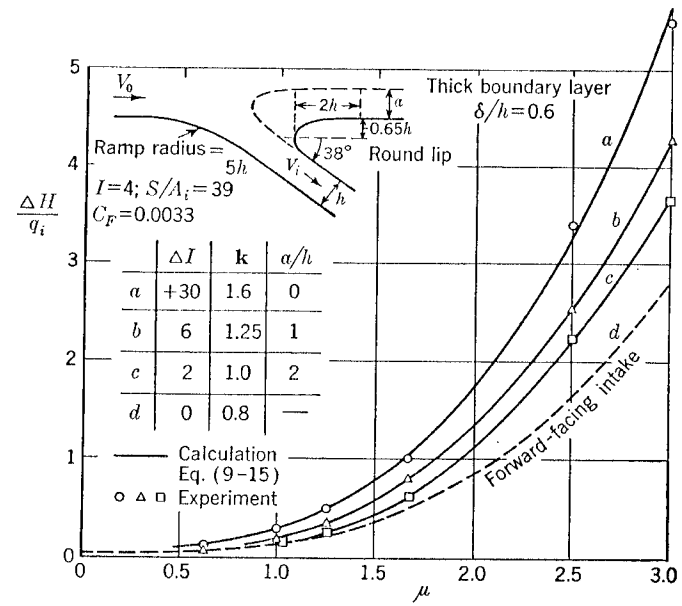

FIG. 9-15. Inflow losses measured on two-dimensional flush and semiflush intakes.

reduced to zero with $a = \delta$. The effectiveness of the method depends also on the shape of the fairing between intake and wall, in that a suitable airfoil-like shape might ease the sideways flow of the boundary layer.

Inflow losses which obey the approach-loss formula (9-15) are found also in the case of leading-edge intakes in swept wings. The retardation of the inflow is here complete only in a section normal to the free stream which is wholly enclosed in the inner duct, with part of the intake walls upstream of it, for example, the side wall at the inboard end of an intake in a sweptback wing. This surface, together with triangular areas above and below, must be regarded as wetted approach surfaces (the velocity is higher than in the duct proper), and there is a corresponding inflow loss, which obviously becomes greater as the sweep increases.

9-9. Measured Inflow Losses at Flush Intakes. Very different conditions are encountered when the intake is flush in a wall so that the flow must turn through a finite angle from the free-stream direction to enter the duct (Fig. 9-15). The advantage of inlets of this type is that they present no external frontal area. The inflow losses, however, are considerably higher than those of an ordinary forward-facing intake which stands out of the surface; as the lip is gradually moved out from the wall (semiflush intake), the loss approaches that of the forward-facing intake.

Although the loss formula (9-15) cannot be expected to cover this case, it is nevertheless found that a μ^3 law holds, and modifications need be made only to the coefficients in Eq. (9-15). The main cause of the additional inflow loss is the turning of the flow, and it depends on the direction of the duct and on the shape of the curved ramp. The turning loss can be subdivided into a term which is independent of μ and is present even when $\mu = 1$, and another which varies with μ. The first term may be added as an increment ΔI to the duct integral of Eq. (9-12), and the second accounted for as a variation of the value of **k**. The values in Table 9-2 were obtained from tests on a series of intakes illustrated in Fig. 9-15.

TABLE 9-2

a/h	ΔI		**k**	
	Lip I	Lip II	Lip I	Lip II
0	13	30	1.1	1.6
1	2	6	1.0	1.3
2	0	2	0.9	1.0

The thickness of the boundary layer at the inlet was $\delta/h = 0.6$ and the ratio of the distance a of the lip from the flush position to the duct width h was varied. The actual shape of the intake lip is also important. Both lips tested were quarter ellipses; lip I had axes of length $0.17h$ and $0.5h$, while lip II had axes $0.65h$ and $2h$ and was thus more rounded. The inflow losses were less with the thinner lip at the same value of a, probably because it guided the flow more effectively into the duct, but the thicker lip was as good with a slightly larger a.

With a thinner approaching boundary layer, $\delta/h = 0.1$, the constant term ΔI of the turning loss was reduced to zero, but there was only a very slight over-all improvement because **k** increased to about 3.5 for both lip shapes (Fig. 9-16). Obviously, the thinner boundary layer is nearly as unstable in an adverse pressure gradient as the thicker one.

The aspect ratio of the inlet opening of flush intakes has little effect. The beneficial influence of sideways diversion of the approaching bound-

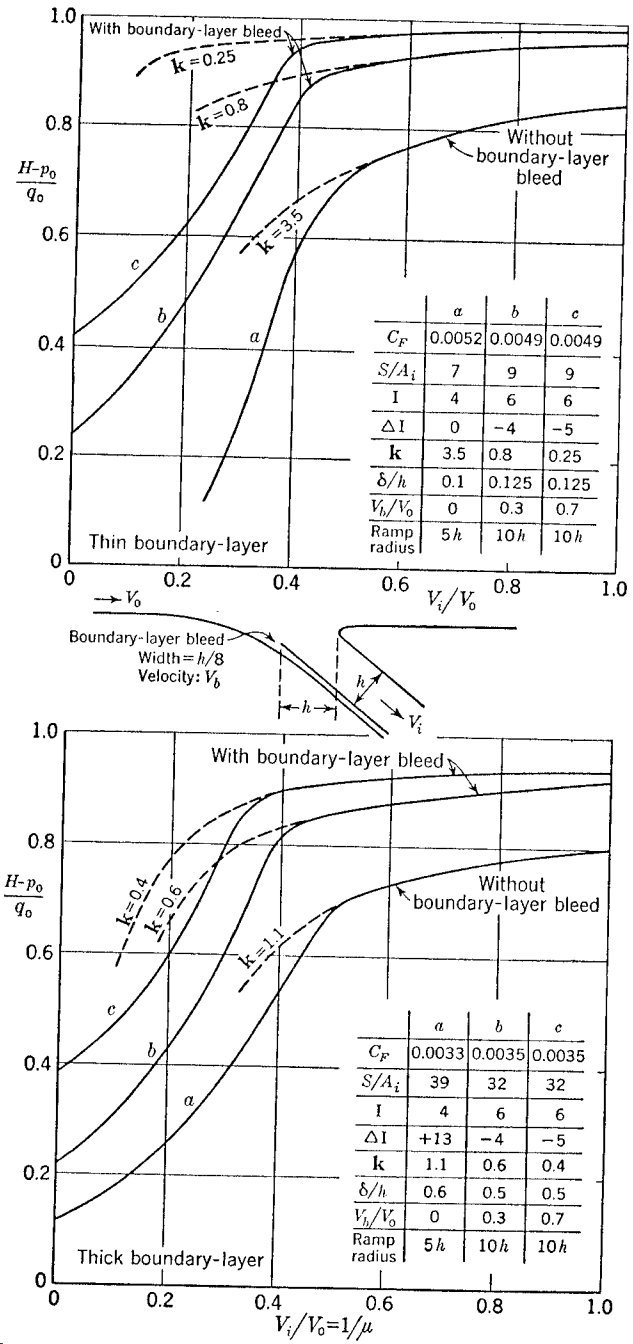

	a	b	c
C_F	0.0052	0.0049	0.0049
S/A_i	7	9	9
I	4	6	6
ΔI	0	−4	−5
k	3.5	0.8	0.25
δ/h	0.1	0.125	0.125
V_b/V_0	0	0.3	0.7
Ramp radius	5h	10h	10h

	a	b	c
C_F	0.0033	0.0035	0.0035
S/A_i	39	32	32
I	4	6	6
ΔI	+13	−4	−5
k	1.1	0.6	0.4
δ/h	0.6	0.5	0.5
V_b/V_0	0	0.3	0.7
Ramp radius	5h	10h	10h

FIG. 9-16. Influence of a boundary-layer bleed on the mean total head measured in flush intakes. From tests by H. E. Roberts and B. D. Langtry, 1950.

ary layer is largely offset and often more than counterbalanced by the increasing influence of the side walls of the inlet. Some improvement may be gained by shaping the side walls to the streamline of the approaching flow.

The additional turning loss of flush and semiflush intakes is accompanied by abnormally high values of the dispersion. In the series of tests of Fig. 9-15, σ rose almost linearly with μ; with $\mu = 2.5$ the following values were obtained:

σ	0.6	0.5	0.3
a/h	0	1	2

These should be compared with Fig. 9-12. However, as a is increased, values more typical of the forward-facing intake are approached. It appears that the flow separates seriously from the curved ramp of the flush intake and that the velocity in the duct near the inner wall is very low. Such extreme nonuniformity cannot be expected to be without serious repercussions on the working characteristics of a compressor.

The flush intake is obviously a profitable subject for the application of boundary-layer suction. The sink effect of the suction slot, or bleed, will help the flow to overcome the adverse pressure gradient behind the beginning of the curved ramp; and if a portion of the boundary layer is removed at the right place, when the flow is just about to separate, it may prevent or delay the separation.

This is clearly demonstrated by the results in Fig. 9-16 from tests by H. E. Roberts and B. D. Langtry (1950) on intake arrangements very similar to those in Fig. 9-15 but with a forward-facing boundary-layer bleed near the curved ramp. Not only does the value of ΔI become negative (this should be taken in conjunction with the basic duct integral I), but $\mathbf{k}$ is also reduced well below 0.8, depending on the suction applied (measured here by the ratio of the velocity V_b in the suction slot to V_0). Further, the severe break-down of the flow (marked by a sudden bend in the experimental curves in Fig. 9-16 away from the $\mathbf{k}$ = const curves) is delayed to lower values of V_i/V_0 by suction. The velocity distribution in the duct is also made more uniform. For a flush intake without suction, $\sigma = 0.22$ for $\mu = 1$ and $\delta/h = 0.1$, but σ is reduced to 0.06 with moderate suction ($V_b/V_0 = 0.3$) and to 0.03 with stronger suction ($V_b/V_0 = 0.7$).

Suction is often applied by the use of a boundary-layer by-pass which leads to an exit at a negative pressure region on the aircraft, for instance, near the wing root maximum thickness or a particularly bluff cabin fairing. Such a by-pass works automatically and is obviously more effective the higher the ram pressure at the inlet, or the pressure difference between

the ends of the by-pass duct, *i.e.*, the higher the value of μ. Thus a by-pass, unlike forced suction, will not reduce ΔI. The value of $\mathbf{k}$ may, however, be reduced to as little as 0.3 or 0.5 with a good design.

Another way to divert the boundary layer from flush intakes is the NACA submerged intake, as described by C. W. Frick, W. F. Davis, L. M. Randall, and E. A. Mossman (1945). As indicated in Fig. 9-17, the air enters a three-sided diffuser upstream of the inlet proper; the upper side of the diffuser is open, and the bottom wall is a straight ramp sloped by about 7°. The side walls diverge, and the air which flows along them is submerged below the external air stream which has a different velocity and direction. A vortex is formed in consequence of this, inducing a sidewash, and sweeping boundary-layer material which may have entered

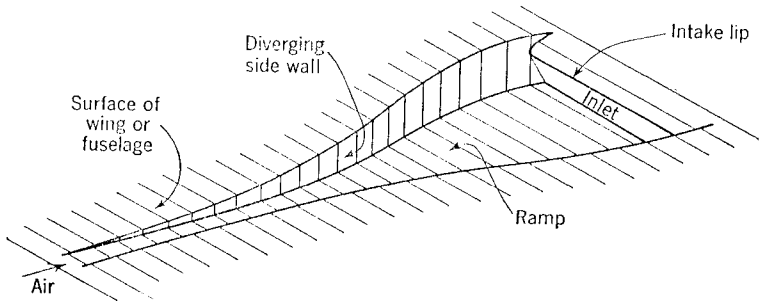

FIG. 9-17. Sketch of NACA submerged intake.

the submerged duct up into the main stream and replacing it by fresh air from outside.

It has been found that the approach loss is indeed reduced by this measure. The actual wetted approach area S is only about half the rectangle S_0 = approach length times inlet width in the design region (around $\mu = 3$). The inflow losses are higher than the ordinary losses, however, at μ values away from the design point. A theoretical study has been made of the flow in submerged air inlets by A. H. Sacks and J. R. Spreiter (1951), which includes a discussion of the boundary-layer and vortex formations.

As is often the case when particular schemes have succeeded in the reduction of the approach loss by diverting the boundary layer, the price has usually been found to be a considerable increase of the external drag, in the present case as a consequence of the sweeping vortices left behind in the main flow. The beneficial effect of a boundary-layer by-pass might easily be offset for the same reason.

For comparison purposes, the inflow losses must be expressed as a thrust reduction and as an illustration this has been done in Fig. 9-18 for some typical cases, using the same fictitious engine and other data as above.

The importance of the inflow losses in high-speed flight is clearly shown, and the excessively high thrust losses obtained with flush intakes, and the benefits of a boundary-layer bleed are emphasized. It must be remembered, of course, that a portion of this thrust loss is recovered as an effective reduction of the aircraft drag. According to the rough analysis at the end of Sec. 9-7, about half the thrust loss of case *b* in Fig. 9-18 is recovered.

Some of the curves in Fig. 9-18 show another increase in the thrust loss at the static end (near $\mu = 0$). This is mainly due to the small nose radii

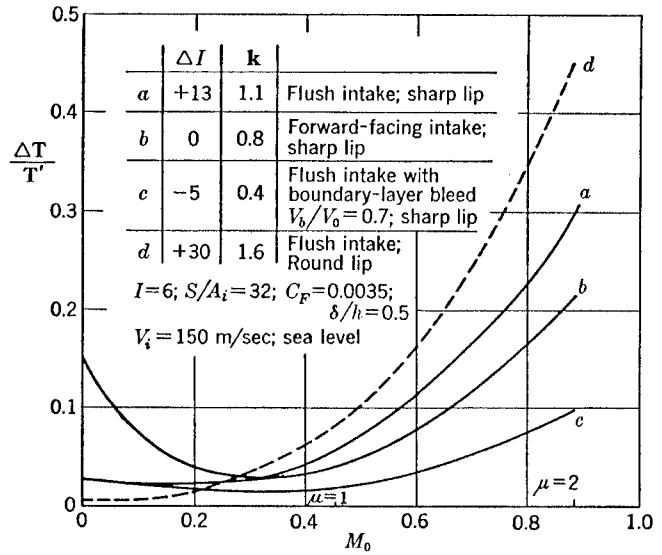

FIG. 9-18. Estimated thrust losses caused by a pressure loss at the inlet, for a fictitious turbojet engine.

of the models tested. The latter is particularly harmful in the case of forward-facing intakes because of the larger angle that the flow has to turn through at inflow under static conditions. The simplest remedy is to enlarge the nose radius of the intake lip, as was explained in Sec. 4-6.

9-10. External Interference Drag of Fuselage Installations. The external interference of air intakes and engine nacelles has not been studied very systematically. In most cases, wind-tunnel measurements of drag or pressure distribution give only incomplete information, and any assessment of the relative merits of the various installation arrangements must necessarily be inconclusive at the present stage.

Consider first an external installation of the engine in a special nacelle mounted on the fuselage. There is a low-speed interference drag which is mainly caused by modification of the flow about the body. The value of $\Delta C_D/C_{DE}$, as defined in Sec. 9-1, is about 1.25 if the frontal area of the

nacelle is one-fourth of that of the fuselage, with the arrangement shown in Fig. 9-19.

Some idea of the high-speed drag can be obtained from the pressure distributions on nacelle and fuselage. The inflow has an asymmetry which increases the velocity at the part of the intake furthest from the fuselage, compared with the isolated intake. To take the example of a circular intake, A-25 from Sec. 4-6, at $\alpha = 0$ and $V_i/V_0 = 0.4$, the velocity at the lip rises from $V_{max} = 1.18V_0$ in the isolated case to $V_{max} = 1.27V_0$ at the uppermost section when the intake is on a nacelle on top of a fuselage of

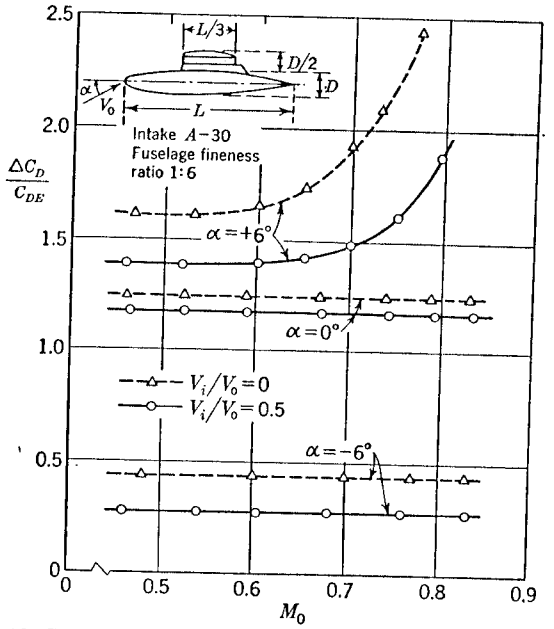

FIG. 9-19. Drag of an engine nacelle mounted on top of a fuselage.

twice the nacelle diameter. This effect is confined to a limited region, and at zero incidence does not usually cause a premature drag rise at high Mach numbers, as can be seen from the experimental results in Fig. 9-19. At positive angles of incidence, the suction peaks are higher and cause a definite increase in drag; the isolated intake would not show any drag rise within the Mach number and incidence ranges tested (see Sec. 4-6). At negative incidences (or positive incidences for an underslung nacelle), the suction peaks are reduced and the drag is considerably smaller. This is a general advantage of any nacelle installation on the lower surface of the fuselage or, of course, of the wing too.

The fairing between nacelle and fuselage should be of good airfoil shape and must be chosen with care. It has been found that symmetrical sections of the NACA four-digit series are quite suitable, even with thickness-

chord ratios as high as about 20 per cent. The thickness itself should be between 80 and 100 per cent of the maximum nacelle diameter; *i.e.*, narrow channels between nacelle and fuselage are to be avoided. With a suitably designed fairing, the velocities at the support need be no higher than elsewhere on the nacelle; this was so in the example of Fig. 9-19. There have been cases, however, where early shock waves in channels which were too narrow not only caused a drag increment but also a serious disturbance of the stability of the whole aircraft, through the interaction between the wake behind the fairing and the tailplane flow.

Similar conditions apply when the engine is removed inside the fuselage but the complete circular intake is left outside, the air being led to the engine through a curved duct (with increased internal duct losses, of course). The frontal area of the *scoop* must be at least the same as that of the nacelle intake (in contrast to the popular belief that scoops can be smaller) since the suction forces associated with the retardation of the flow to V_i at the inlet are the same in both cases (see Sec. 4-2). In fact, the velocities at the part of the scoop intake furthest from the fuselage will be further increased because of the necessarily higher curvature of the outer fairing lines. In a special case where both scoop and nacelle intake had the same circular intake shape A-25, the maximum velocity on the scoop intake was $V_{max} = 1.33V_0$, compared with $1.27V_0$ on the nacelle intake.

The low-speed drag of a scoop is usually slightly higher than that of a complete nacelle behind the same intake. In one example tested, $\Delta C_D/C_{DE} = 1.3$ instead of 1.25 for the nacelle as in Fig. 9-19. With two scoops which together had the same frontal area as the one single scoop, $\Delta C_D/C_{DE}$ was 1.6, that is, the interference was about twice as high.

The flow about the wing can appreciably affect the interference drag of an engine nacelle attached to the fuselage or a scoop intake. The available evidence indicates that the effect is never beneficial. Small engines near the wing root may give up to $\Delta C_D/C_{DE} = 2$, mainly due to the impossibility of shaping the rear end of the fairing between nacelle, wing, and fuselage satisfactorily. It is preferable in such a case to try to incorporate the nacelle or the scoop completely into the wing root. Alternatively, the nacelle may be separated from the wing, leaving a reasonably wide channel between it and the wing. The interference drag is then again between $\Delta C_D/C_{DE} = 1.2$ and 1.6.

Instead of a circular inlet for a scoop, as above, flatter shapes are often used, and in the extreme case there will be an annular intake all around the fuselage. An alternative is to have the air intake in the nose of the fuselage. In the latter case, pressure losses associated with the long ducts inside the fuselage must be accepted (see Sec. 9-5). There is no binding reason why the low-speed external drag of the fuselage should be increased

much by the nose intake; if it is assumed to rise by 10 to 15 per cent, allowance will have been made for some deterioration of the flow over the fuselage (for instance, an early transition from laminar to turbulent flow). If the diameter of the engine is about half that of the fuselage, the value of $\Delta C_D/C_{DE}$ will be about four times the drag increase; that is, $\Delta C_D/C_{DE}$ is

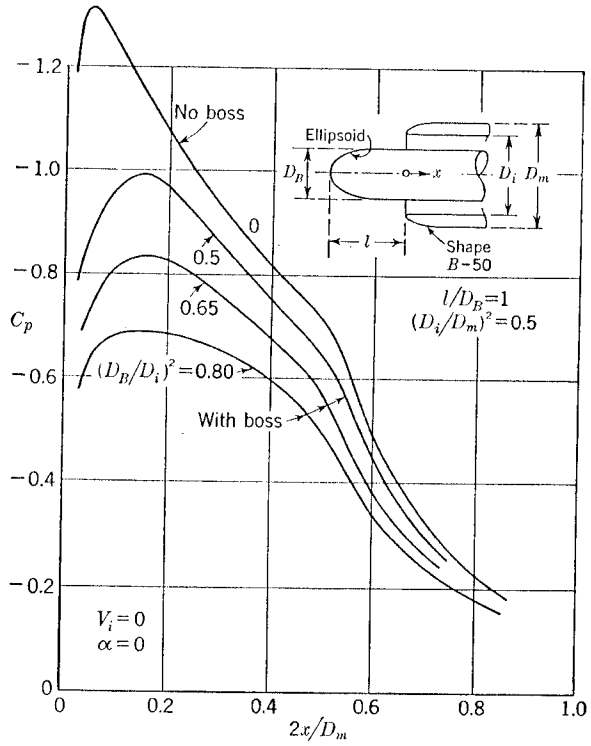

FIG. 9-20. Influence of a protruding boss on the external pressure distribution of a circular intake.

around 0.5, which is better than is usually obtained with an external installation.

A test has been made where a boss of circular cross section was put into a nose intake. Increasing the length and diameter of the boss gradually changes the nose intake into a forward-facing annular intake. At the same time, the effective area ratio of the intake is of course improved as it becomes more effectively a two-dimensional intake with

$$\frac{A_i}{A_m} = \frac{D_i - D_B}{D_m - D_B}$$

instead of $(D_i/D_m)^2$ for the nose intake (notation as in Fig. 9-20). This reduces the velocity increment on the outer surface.

There is, however, another interference effect associated with the influence of inflow losses due to boundary layer on the boss on the pressure distribution on the outer surface of the intake; the suction is reduced when the losses rise, and increasingly so as the flow separates from the boss. This is clearly shown by the experimental pressure distribution with varying boss diameter in Fig. 9-20 for the extreme case $V_i = 0$. The maximum velocity on the outer surface falls from $V_{max} = 1.52V_0$ when $D_B = 0$ to 1.30 when $(D_B/D_i)^2 = 0.8$. The reduction is less when there is flow through the inlet. For instance, V_{max}/V_0 falls from 1.38 to 1.28 when $V_i/V_0 = 0.4$.

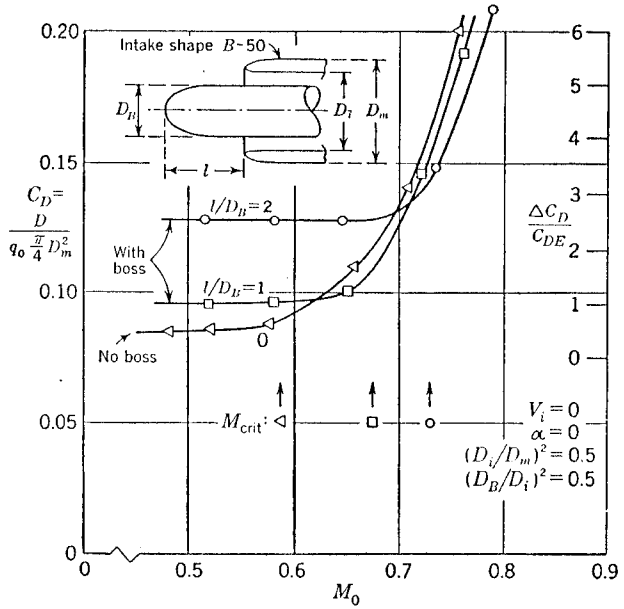

FIG. 9-21. Influence of a protruding boss on the drag of a circular intake.

The resulting drag is a combination of two opposite effects, as Fig. 9-21 demonstrates. The low-speed drag is increased with increasing boss diameter because more low-energy air reaches the external flow; the critical Mach number, as estimated from Eqs. (4-18) and (4-20), is improved. The net influence of the boss on the drag characteristics at high Mach numbers is actually relatively small.

The measured drag can be transformed into values of $\Delta C_D/C_{DE}$ if we assume, as above, $\Delta C_D/C_{DE} = 0.5$ for the nose intake without boss, and $C_D = 0.074$ for the fuselage alone; further, the fictitious engine nacelle is assumed to have the same drag coefficient as the fuselage, but $C_{DE} = 0.074/4$ if referred to the frontal area of the fuselage when the engine frontal area is only a quarter of that of the fuselage, again as

assumed above. This gives the scale for $\Delta C_D/C_{DE}$ on the right-hand side of Fig. 9-21.

However, the spilling of the boundary layer over the intake lip and thus the low-speed drag may have been exceptionally unfavorable in the case considered above. It has been found that the external drag is particularly high when the thickness of the approaching boundary layer is smaller than the height of the intake ($D_m - D_B$ in Fig. 9-21). As this is a general effect observed with any body protruding from a surface, we

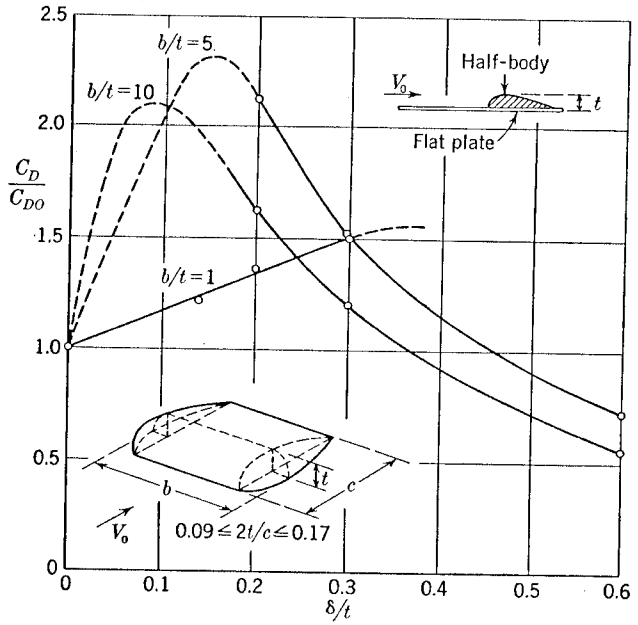

FIG. 9-22. Low-speed drag of flat half-bodies on a plane wall.

can conveniently demonstrate it by means of the results in Fig. 9-22, where half-bodies of varying span with NACA airfoil sections were attached to a plane wall. If the measured drag is compared with the drag of the body without a wall, the interference drag is found to be particularly high when the thickness δ of the approaching boundary layer is between 0.1 and 0.5 of the thickness t of the half-body. This can no doubt be explained from the fact that the adverse pressure gradient ahead of the body, to which the whole boundary layer is submitted, leads to a heavy breakdown of the flow. With increasing δ/t the body is more and more enveloped in boundary-layer air of low velocity, and the drag falls below that of the body in a free stream.

A very undesirable feature of flow separation from an approach surface (observed mainly in compressible flow) is that there may be a tendency to fluctuations of the inflow: A separation may reduce the pressure at the

inlet to such an extent that the flow reattaches; the pressure then increases and the flow separates again, and so on.

Much of what has been said above holds also for flush intakes in the side of the fuselage. Very little is known about their actual external drag. Difficulties may arise in high-speed flight, even if the low-speed interference drag is low. To illustrate this, critical Mach numbers are shown in Fig. 9-23, as estimated from pressure measurements at low speeds.[1] The critical region in high-speed flight is the ramp, and a very gentle curvature (with a radius greater than ten times the inlet width) is needed for a really fast aircraft. Otherwise, a shock wave ahead of the inlet may not only increase the external drag but also bring about a further reduction of the pressure at the inlet. Also, the lip radius should be greater than $0.1h$ (the values used in the arrangements tested) in order to relieve the high suction at the inner surface of the lip in climbing flight and under static conditions. The same is true in principle for the NACA submerged intakes, the high-speed efficiency of which is often limited by high suction peaks on the intake lip or at the beginning of the ramp.

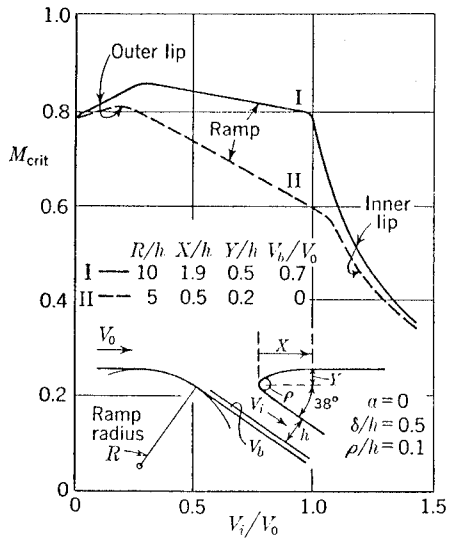

FIG. 9-23. The influence of the ramp radius on the estimated critical Mach number of flush intakes. Partly from tests by H. E. Roberts and B. D. Langtry, 1950.

The relative merits of flush and forward-facing side intakes are also affected by their influence on other parts of the aircraft. The bulges on the fuselage required by forward-facing intakes may improve the Mach number characteristics of a sweptback wing if they are located in the root leading-edge region. The result may even be an over-all saving in external drag. The same applies to wing leading-edge intakes when they are placed near the root (see Sec. 5-3).

A more conclusive comparison between the various types of installation can be made if the values of $\Delta C_D/C_{DE}$ are converted into available engine

[1] In this case, the von Karman-Tsien rule

$$C_p = \frac{C_{pi}}{\sqrt{1 - M_0^2} + (C_{pi}/2)(1 - \sqrt{1 - M_0^2})}$$

has been used together with Eq. (4-20).

thrust losses, for example, by applying Eq. (9-2). An example of such an analysis is shown in Fig. 9-24 where the nose intake of Fig. 9-21 is compared with one whose drag does not increase in the Mach number region considered (which could be achieved by using a smaller ratio of inlet area to maximum frontal area). In both cases $\Delta C_D/C_{DE} = 0.5$ at low speeds. The comparison demonstrates once again the absolute necessity of choosing a favorable inlet area ratio.

Figure 9-24 also includes a curve for a comparable engine nacelle mounted externally on the fuselage, from the results in Fig. 9-19. It

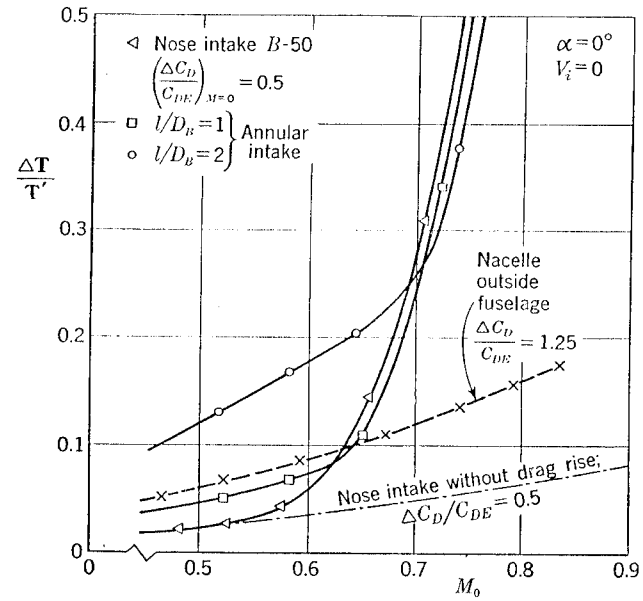

FIG. 9-24. Estimated thrust losses of a fictitious turbojet engine with various intake arrangements on a fuselage.

appears that this arrangement also is inadmissible for really fast aircraft.

Finally, the measured drags of the annular intakes in Fig. 9-21 are converted into thrust losses in Fig. 9-24. This shows that the forward-facing intake (apart from the thrust loss from the reduction of the ram pressure, curve *b* in Fig. 9-18) also has an excessively high thrust loss due to external drag. However, more evidence is needed and other values of the approaching boundary-layer thickness must be considered before any final conclusion can be drawn on this important question.

9-11. External Interference Drag of Engine Nacelles on the Wing. External wing nacelles add an interference drag (due to their location on the wing) comparable to that found for external nacelles on the fuselage. Some experimental results from low-speed tests at zero lift are shown in Fig. 9-25 for *central*, *underslung*, and *strut-mounted* nacelles. The

general tendency is for the drag to increase with increasing distance of the nacelle from the wing. The midwing position, however, involves considerable structural difficulties, and the underslung position appears to be the next best solution. With the wing at incidence, the interference drag of the underslung nacelle may fall slightly; at any rate, it usually rises less quickly than that of the central nacelle or that of the strut-mounted nacelle. With a suitable design for small lift, the underslung nacelle may actually be best, as its shape can more easily be adapted to the wing flow.

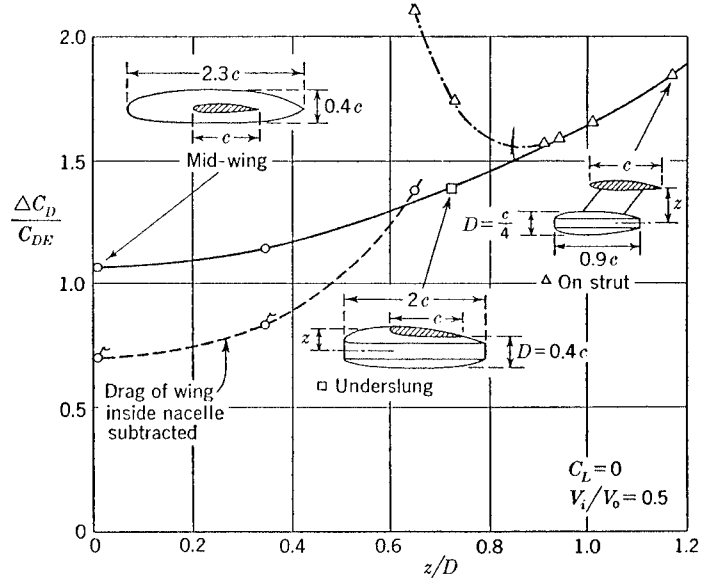

FIG. 9-25. The influence of the distance of a nacelle from the chord line of a straight wing on the low-speed drag.

To obtain a suitable fairing between the underslung nacelle and the wing, the shape of the top line from the inlet to the wing upper surface should be approximately a quarter-ellipse fairing tangentially into the wing surface, like fairing A-10 in Fig. 4-26. The spanwise width of the junction fairing should again be between 80 and 100 per cent of the nacelle diameter, to avoid narrow reentrant channels. With wing and nacelle at incidence, the cross flow around the nacelle causes an additional upwash in the wing-nacelle junction which manifests itself in pronounced velocity peaks near the leading edge of the wing. Such peaks are undesirable in high-speed flight and will also reduce the maximum lift. They can be avoided by the use of a nose fillet. In the case of the underslung nacelle of Fig. 9-25, an extension of the wing chord by 10 per cent in the junction, drooped by about 6°, was sufficient to remove them.

Struts are very rarely suitable as a means of supporting a nacelle, unless for reasons other than those considered here. If the struts are

short, there will be a high interference drag at low speeds and a large reduction of critical Mach number due to the flow in the channels between wing and nacelle. For instance, the critical Mach number on an unswept strut of 10 per cent thickness-chord ratio deduced from low-speed pressure measurements was 0.66 for a short strut ($z/D = 0.73$ in Fig. 9-25) and 0.69 for a longer strut ($z/D = 0.94$), compared with 0.77 on the wing alone (which was unswept, of 12 per cent thickness-chord ratio), at zero lift. Sweeping the strut is not likely to be very effective because its

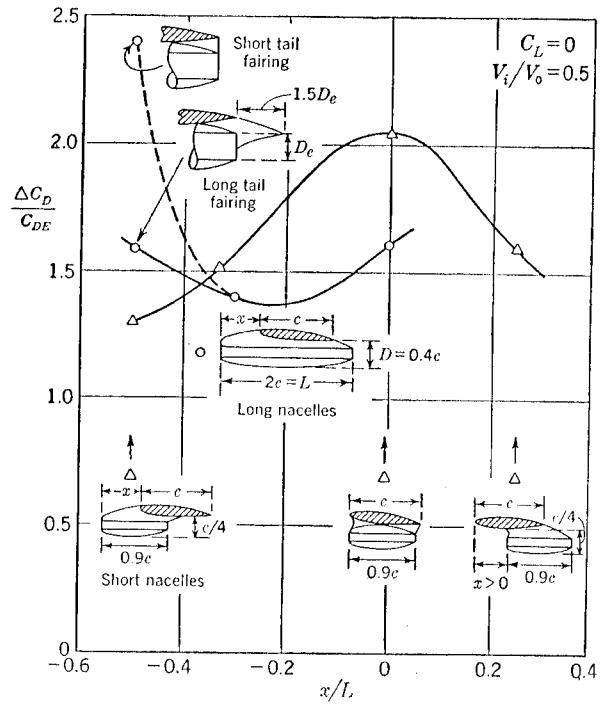

FIG. 9-26. The influence of the fore-and-aft position of an underslung nacelle on a straight wing on the low-speed drag.

aspect ratio is usually too small for any useful sweep of the isobars to be achieved.

Varying the fore-and-aft position of a nacelle relative to the wing causes less systematic change in interference than varying the height. Some experimental data in Fig. 9-26 show obvious disadvantages of having either the inlet directly beneath the leading edge of the wing or the exit beneath the trailing edge. If the nacelle length is about equal to the wing chord, both these conditions may occur at once, and the interference drag will be high. It is preferable to separate the sensitive regions of the nacelle from those of the wing (that is, to separate the suction region of the intake from the leading edge of the wing; and the exit from the trailing

edge). However, much can be gained by careful shaping. For instance, the interference drag can be considerably reduced by altering a short tail fairing (with a steep adverse pressure gradient) into a long one, even though the surface area and thus the skin friction is increased, as shown in Fig. 9-26.

When the number of engines is four or more, the question of interference between the nacelles themselves arises.[1] Experimental evidence indicates clearly that nacelles on one wing should be either at least one diameter apart or bundled together in a common fairing. If ΔC_{D0} is the sum of the drags of two nacelles far apart on a wing, then the actual ΔC_D at low speeds for two nacelles was found to vary with the clear distance, a, between them as follows:

a/D	1.0	0.5	0.25	0
$\Delta C_D/\Delta C_{D0}$	1.1	1.3	1.4	1.6

Since the interference is again mainly due to an increase of velocity in the passage between the nacelles (and a subsequent steeper adverse pressure gradient), the increase of drag is greater at high Mach numbers. For instance, with $a/D = 0.25$, high-speed tunnel tests gave the values

$\Delta C_D/\Delta C_{D0}$	3	4	5	6
M_0	0.6	0.65	0.70	0.73

Bundled nacelles, on the other hand, gave a low-speed $\Delta C_D/\Delta C_{D0}$ of about 1.1; their Mach number characteristics depend to a large extent on the shape of the fairing between the nacelles. With underslung nacelles, the fairing thickness on the underside should be at least 80 per cent of the radius of the nacelles; on the upper surface the fairing may be even thicker, running smoothly into the wing contour. It should not extend ahead of the inlet plane; if it does, there is a *wetted approach surface* as with swept leading-edge intakes and a resulting pressure loss in the inflow. Bundled nacelles usually require a very elaborate tail fairing extending beyond the jet exits and incorporating two tunnellike passages, partly enclosing the two jets.

External nacelles on swept wings present a further problem. The streamlines of a nonviscous flow across a *sheared* wing are not straight, but curved as shown in Fig. 9-27. This is true for thick wings even at zero incidence and on the upper surface the curvature increases with incidence. Obviously a straight vertical wall (for instance, the side of a straight nacelle) will distort this streamline pattern. The streamlines will

[1] A similar problem may occur, of course, when two engines are mounted on the fuselage.

widen and the velocity will be reduced near the leading edge of the part of the wing swept back from the nacelle; and they will close up toward the rear of the section, with increase in velocity. Opposite changes occur at the sweptforward wing side of the nacelle, usually resulting in a high suction peak near the leading edge.[1] This is illustrated by the experimental pressure distributions in Fig. 9-28 (case I) measured in the junctions between a 35° sweptback wing and a nacelle with a cylindrical middle part, at low speeds. The critical Mach number is reduced below that of the undisturbed wing, partly because the peak suctions are higher and partly because the sweep of the isobars is reduced to zero in the junction. By Eqs. (4-19) and (4-20) the estimated critical Mach numbers, in case I in Fig. 9-28, are $M_{crit} = 0.60$ in the sweptforward junction and 0.71 in the sweptback junction, compared with 0.85 which could have been obtained on that particular wing (of 35° sweepback and 12 per cent thickness-chord ratio) had there been no distortions. The large interference drag at high speeds due to such distortions is illustrated by the examples in Fig. 9-29.

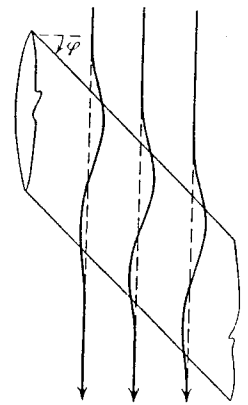

FIG. 9-27. Streamlines across a sheared wing (diagrammatic).

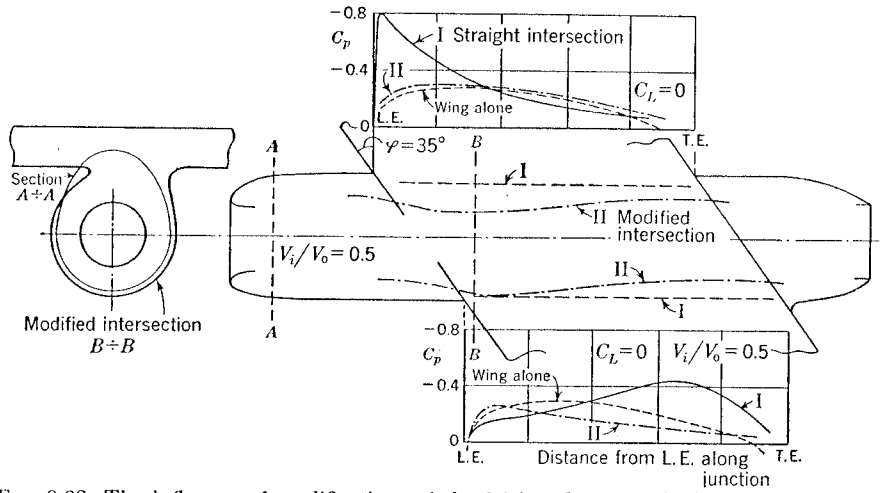

FIG. 9-28. The influence of modifications of the fairing shape on the low-speed pressure distribution in the junctions between an underslung nacelle and a 35° sweptback wing.

Attempts have been made to remedy this by modifying the *shape of the intersection.* The first solution[2] on these lines, case II in Fig. 9-28,

[1] This effect was first observed and interpreted by B. Göthert, 1942.

[2] R. Buschner, 1944; part of these tests is described in *NACA TM* 1226.

shows that the pressure distribution of the undisturbed wing has very nearly been restored, so that the estimated critical Mach numbers in the junctions are at least as high as that on the undisturbed part of the wing. These modified shapes were found empirically from observation of cavitation bubbles (as described in Sec. 5-1). The shape of the intersection lines is very similar to the shape of the streamline of the undisturbed wing at zero incidence.

9-12. Different Consequences of Inflow Losses and External Drag. We may conclude this chapter by pointing to some fundamental differ-

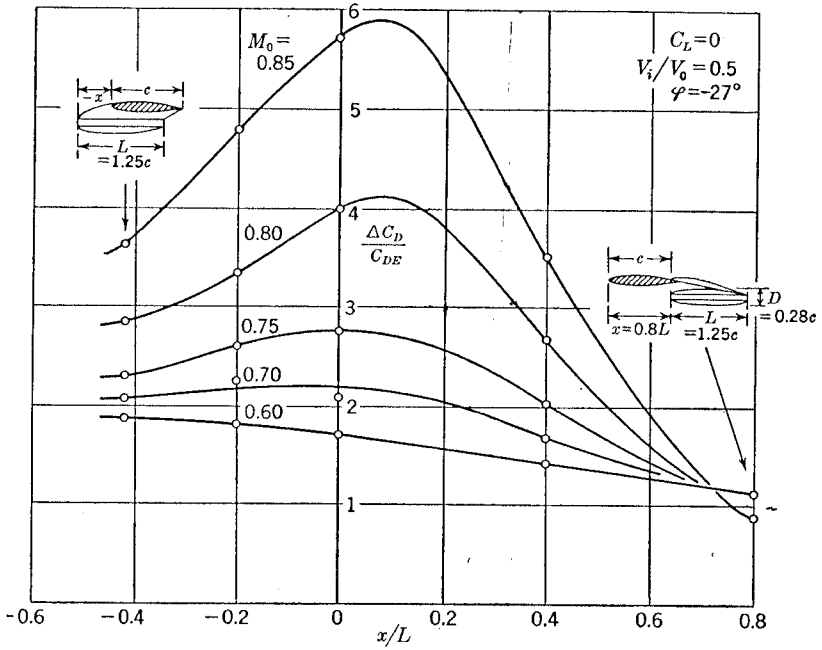

FIG. 9-29. The high-speed drag of underslung nacelles on a swept wing.

ences between external and internal installation. Consider the case where the effective thrust reduction due to the drag of an engine mounted externally[1] is the same as the thrust reduction due to inflow losses of a completely buried installation of the same engine. The total available thrust and thus the maximum flight speed are then the same in both cases; but the fuel consumption of the buried engine is lower because of the reduced mass flow, Eq. (9-18). This point should be considered in the design of an aircraft whose fuel consumption is important, such as air liners and other long-range aircraft.

The choice between external mounting and complete integration is also

[1] External mounting is here understood as an installation that causes external drag. It includes buried engines fed through forward-facing air scoops, for instance.

influenced by the flight speed for which the aircraft is designed. Suppose that the completely buried engine has only duct losses; the pressure loss $\Delta p_i/p_i'$ varies little with flight speed and the thrust loss will only rise as the factor L varies in Eq. (9-25) or (9-35). The thrust loss of the external engine, however, will usually rise more steeply, in proportion to the square of the flight speed [Eq. (9-2)], if we assume that the quality of the installation, *i.e.*, the value of $\Delta C_D/C_{DE}$, remains unchanged. Thus, the higher the flight speed for which the aircraft is designed, the more a complete integration of the engine is desirable.

The argument is also in favor of intentionally taking in an appreciable portion of the boundary layer, provided that it can be done without creating further drag.

EXERCISES

9-1. Convert the inflow losses $\Delta H/q_i$ in Fig. 9-3 into values of $(H - p_0)/q_0$ and plot these against $V_i/V_0 = 1/\mu$ for $V_i/V_0 \leq 1$. Note that a "good" value of the "efficiency" $(H - p_0)/q_0$ does not necessarily imply low actual thrust losses, by comparing with Fig. 9-6.

9-2. In a wind-tunnel test made at a Reynolds number of 0.3×10^6, the measured approach loss of an intake arrangement ($S/A_i = 8$; $\mathbf{k} = 0.8$; $\mu = 2$) was $\Delta H/q_i = 0.3$. How big will the approach loss be at a full-scale Reynolds number of 10^7?

9-3. Determine the effect of the combustion end temperature T_{B2}/T_0 on the thrust loss due to inflow losses for a turbojet engine at a flight Mach number $M_0 = 0.9$. Assume $V_i/V_0 = 0.5$ and a compression ratio $p_B/p_i = 4$ with compressor and turbine efficiencies $\eta_C = \eta_T = 0.8$. Obtain the thermal efficiency of the cycle from Fig. 8-4 for the values of T_{B2}/T_0 given there. Use Eq. (9-35) with $\Delta p_i/p_i' = 0.05$.

9-4. Determine from Eqs. (9-59) and (9-60) the percentage reduction of thrust and fuel consumption of a turbojet engine due to approach losses, with $C_F = 0.003$ and $S/A_i = 36$. What is the approximate reduction in flight speed? How would these figures be altered if the approach loss could be considered as an effective reduction of the drag of the aircraft, according to Eq. (9-57)?

9-5. A turbojet engine is mounted externally without inflow losses but with an external drag $\Delta C_D/C_{DE} = 1.23$. What is the effective reduction of the thrust at $M_0 = 0.9$ from Eq. (9-2)? Another engine (with $L = 2$) is installed internally without external drag; what inflow losses can be allowed, to give the same thrust reduction? Determine $\Delta H/q_i$ for $\mu = 2$. How much is gained in the latter case as a reduction of the fuel consumption?

BIBLIOGRAPHY

RUDEN, P., Two-dimensional Symmetrical Inlets with External Compression, *Jahrbuch der deutschen Luftfahrtforschung*, 1941, p. I 377; translation, *NACA TM* 1279.

GÖTHERT, B., Hochgeschwindigkeitsmessungen an einem Pfeilflügel, *Lilienthal Gesellschaft Luftfahrtforchung, Bericht* 156, 1942.

HENRY, J. R., Design of Power Plant Installation. Pressure Loss Characteristics of Duct Components, *NACA ARR* L4F26 (WRL-208), 1944.

BUSCHNER, R., Pressure Distribution Measurements on a Sweptback Wing with Jet Engine Nacelle, *Deut. Luftfahrtforschung* UM 3176, 1944; translation, *NACA TM* 1226.

SMITH, N. F., and D. D. BAALS, Wind Tunnel Investigation of a High-critical-speed Fuselage Scoop Including the Effects of Boundary Layer, *NACA ACR* L5B01a, 1945.

FRICK, C. W., W. F. DAVIS, L. M. RANDALL, and E. A. MOSSMAN, An Experimental Investigation of NACA Submerged-duct Entrances, *NACA ACR* 5I20, 1945.

SMITH, A. M. O., and H. E. ROBERTS, The Jet Airplane Utilising Boundary Layer for Propulsion, *J. Aeronaut. Sci.*, vol. 14, p. 97, 1947.

KÜCHEMANN, D., and J. WEBER, Disturbances of the Inflow (*AVA Monograph* J_2 3.4), *Brit. Min. of Supply (Völkenrode) Rept. & Transl.* 987, 1947.

SCHERER, A., and O. CONRAD, The Installation of Jet-propulsion Units (*AVA Monograph* K_3), *Brit. Min. of Supply (Völkenrode) Rept. & Transl.* 937–939, 1947.

SEDDON, J., Air Intakes for High-speed Aircraft, Lecture delivered to the Royal Aeronautical Society, February, 1950, *J. Roy. Aeronaut. Soc.*, October, 1952, p. 747.

ROBERTS, H. E., and B. D. LANGTRY, The Influence of Design Parameters on the Performance of Subsonic Air Inlets, *J. Aeronaut. Sci.*, vol. 17, p. 429, 1950.

LUDWIEG, H., The Effect of the Duct System on the Performance of Jet Units (*AVA Monograph* J_3 3.42), *Brit. Min. of Supply (Völkenrode) Rept. & Transl.* 980, 1947.

ECKERT, H. U., Characteristics of the Turbulent Boundary Layer on a Flat Plate in Compressible Flow from Measurements of Friction in Pipes, *J. Aeronaut. Sci.*, vol. 17, p. 573, 1950.

WILSON, R. E., Turbulent Boundary-layer Characteristics at Supersonic Speeds—Theory and Experiment, *J. Aeronaut. Sci.*, vol. 17, p. 585, 1950.

SACKS, A. H., and J. R. SPREITER, Theoretical Investigation of Submerged Inlets at Low Speeds, *NACA TN* 2323, 1951.

CHAPTER 10

JET PROBLEMS

This chapter deals with the jet and its effects on neighboring lifting surfaces and other parts of the aircraft. The spreading of a jet released into a stream of air of different speed, density, and temperature is a turbulent mixing process, and as such beyond the scope of full discussion in this book.[1] Some knowledge of the size and position of the jet is needed by the aircraft designer, however; for instance, to avoid excessive heating of parts of the structure by the jet. The spreading of the jet into still air is described in Sec. 10-1; the influence of an external stream in Secs. 10-2 and 10-3; and the effect of a neighboring wall on the spreading in Sec. 10-4. Finally, Sec. 10-5 deals with the lifting force induced on wing surfaces near the jet.

10-1. Spreading of the Jet into Still Air. Typical velocity and temperature distributions in a subsonic jet emerging with velocity V_e and temperature T_e from a circular exit into still air are given in Fig. 10-1. They show clearly the gradual mixing of the high-energy air in the jet with the air surrounding it; it will be noted that the temperature distribution spreads more rapidly than the velocity distribution.

A simplification of the geometry of the jet is adequate for the present purpose. There is a core with the full exit velocity V_e, which narrows with distance from the exit and fades out at a distance of about six exit diameters. From this point the velocity on the axis decreases. The exit temperature core is slightly shorter, ending about five exit diameters from the exit.

Up to the end of the velocity core the velocity distributions are such that on a cylinder through the exit the velocity is about half that on the axis; further downstream, the *half-velocity circles* lie approximately on a cone, of semiangle about 5°, with its apex at the center of the jet exit (Fig. 10-1). A corresponding *half-temperature cone* on which the temperature difference $T - T_0$ is equal to half that on the axis is found to have a semicone angle of about 6.5°.

The virtual boundary of the jet can be defined as the surface on which the velocity is one-tenth of that at the axis. After a slower initial expansion over the length of the core, this surface widens to a cone of semiangle

[1] Accounts of our present knowledge of free turbulence may be found in L. Prandtl, 1942; S. Goldstein, 1938; H. W. Liepmann and J. Laufer, 1947; G. K. Batchelor, 1950; S. Corrsin, 1951.

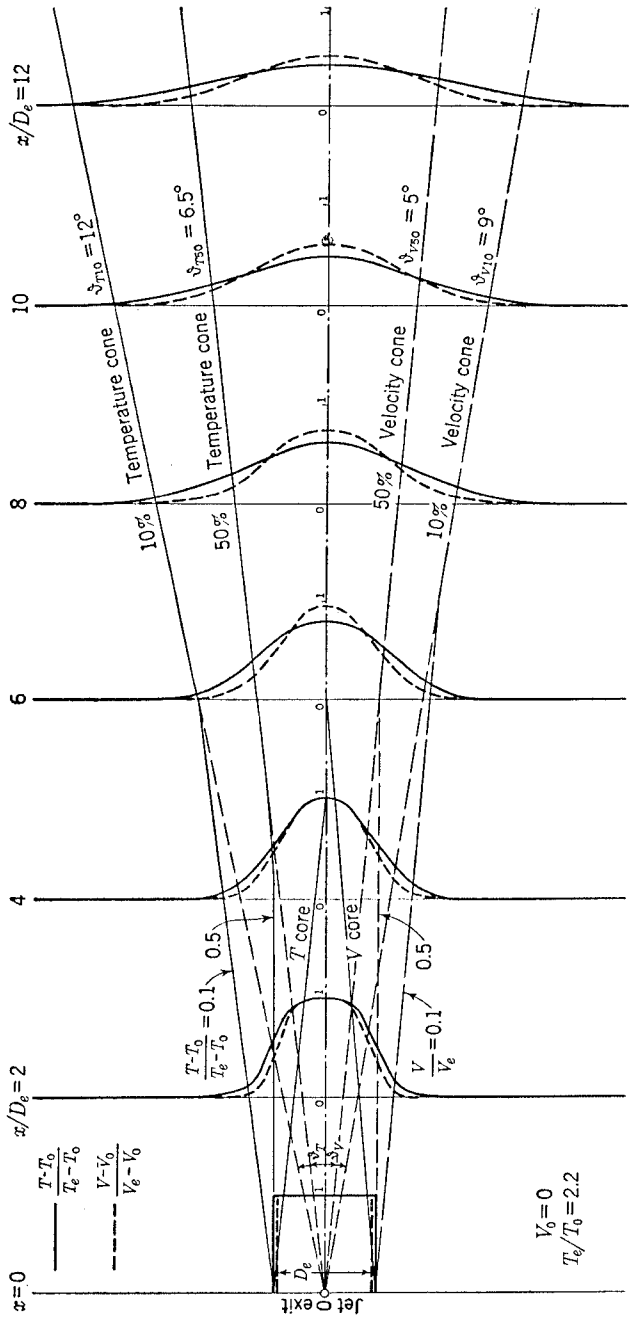

FIG. 10-1. Velocity and temperature distributions in a round jet emerging into still air. From experiments by O. Pabst, 1944.

about 9°, again with its apex at the exit. The corresponding one-tenth temperature cone has a semiangle of about 12°. These values agree approximately with the recent summary report on jet flow by H. B. Squire (1950).

The velocity and temperature on the jet axis, measured in various experiments, are plotted in Fig. 10-2. Downstream of the core, velocity

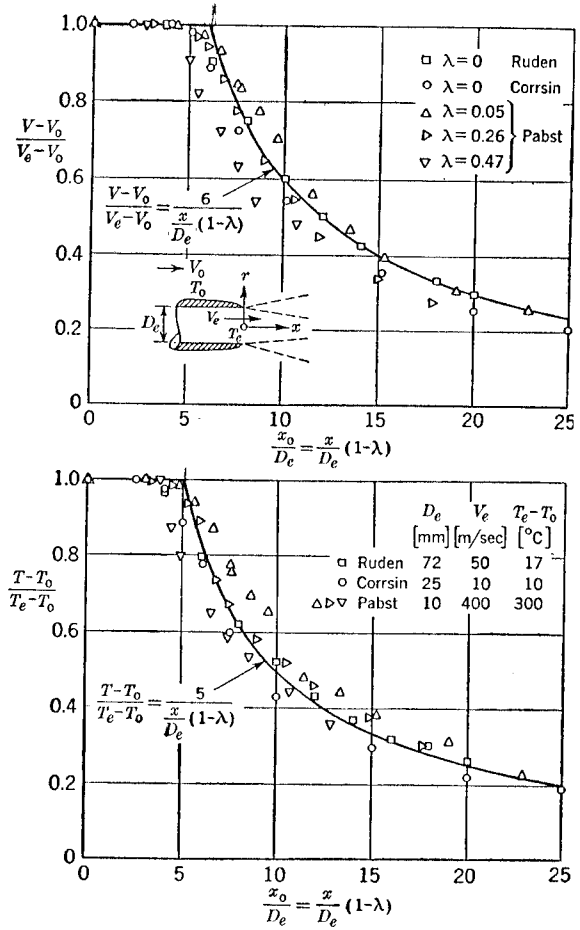

FIG. 10-2. Measured velocity and temperature distributions on the axis of a round jet.

and temperature both decrease approximately inversely as the distance from the jet exit (as predicted by theoretical analysis of the developed jet).

10-2. Spreading of the Jet in Streaming Air. To a first approximation it is permissible to superpose the external flow with velocity V_0 on the jet flow into still air. It may be assumed that for the same $(V_e - V_0)$ the mixing process is also the same; then the excess velocity $[V(x) - V_0]$ of a

particle in the jet in moving air is the same as that of a particle in the jet in still air at the same time after leaving the exit. The particle in the jet in moving air has thus traveled farther than the corresponding particle in the corresponding jet into still air.[1] For instance, a particle in the core travels to a distance

$$x_0 = V_{e0}t$$

in still surrounding air (subscript 0) during the time t, and to a distance

$$x = (V_{e0} + V_0)t$$

in moving air. With the condition $V_{e0} = V_e - V_0$, we obtain

$$x = \frac{V_e}{V_e - V_0} x_0 = \frac{1}{1 - \lambda} x_0 \qquad \text{where } \lambda = \frac{V_0}{V_e} \tag{10-1}$$

More generally,

$$dx = \frac{V(x)}{V(x) - V_0} dx_0$$

For the positions at which the velocity difference $[V(x) - V_0]$ is the same in the two cases and constant and a given fraction a of the velocity difference $(V_e - V_0)$ at the exit, we have

$$x = \frac{1 + \dfrac{1 - a}{a}\lambda}{1 - \lambda} x_0 \tag{10-2}$$

This relation can of course be regarded as a transformation from a fixed coordinate system in still air to a moving one.

For particles in the core, $a = 1$ in Eq. (10-2), and we get Eq. (10-1) again. On the half-velocity surface, $a = \frac{1}{2}$, and we have

$$x = \frac{1 + \lambda}{1 - \lambda} x_0 \tag{10-3}$$

With the help of these transformations, the data obtained for jets in still air can be generalized. Thus the length of the velocity core becomes approximately $6/(1 - \lambda)$, and that of the temperature core $5/(1 - \lambda)$. The law of the velocity decrease along the axis beyond the core may be written

$$\frac{V - V_0}{V_e - V_0} = \frac{6}{(x/D_e)(1 - \lambda)} \tag{10-4}$$

and that for the temperature,

$$\frac{T - T_0}{T_e - T_0} = \frac{5}{(x/D_e)(1 - \lambda)} \tag{10-5}$$

[1] The radial-velocity component is ignored here.

Figure 10-2 shows that these relations are accurate enough for practical purposes; there is, however, a systematic tendency in the deviations. S. Corrsin and M. S. Uberoi (1949) have attributed the more rapid rate of spread of the higher temperature jet to the reduction in density of the jet relative to the receiving medium.

The semiangle of the half-velocity cone is

$$\vartheta_{V50} = 5° \frac{1 - \lambda}{1 + \lambda} \tag{10-6}$$

to this approximation, using Eq. (10-3), and that of the half-temperature cone is

$$\vartheta_{T50} = 6.5° \frac{1 - \lambda}{1 + \lambda} \tag{10-7}$$

These relations are supported by the experimental results by O. Pabst, which also suggest the following values for the semiangles of the one-tenth velocity and temperature cones:

$$\vartheta_{V10} = 9° \frac{1 - \lambda}{1 + \lambda} \tag{10-8}$$

$$\vartheta_{T10} = 12° \frac{1 - \lambda}{1 + \lambda} \tag{10-9}$$

These formulas can be used to estimate the virtual boundary of the jet for any given exit velocity ratio $\lambda = V_0/V_e$.

In reality, of course, the flow in the jet is not homogeneous. There are turbulent fluctuations of amplitude up to 20 per cent of the exit velocity in both longitudinal and lateral directions. Irregular fluctuations of similar amplitude but of low frequency (in intermittent bursts of about 10 per second) have also been observed occasionally near the jet boundary; at full scale these may have the character of gusts and be very disturbing in practice.

Two or more parallel jets at first remain apart and can be distinguished up to a certain distance from the exit where they finally merge. It has been found that the contours of two jets still show their separate origin at a distance of about $17D_e$ when the axes are $3D_e$ apart, and at a distance of about $20D_e$ when the axes are $4D_e$ apart. The two jets coalesce completely at about $30D_e$ in both cases.

10-3. Spreading of the Jet in an Inclined Stream. So far the jet has been assumed to be in the direction of the main stream. If the main stream is at an angle α to the jet axis it tends to bend the jet gradually into its own direction. The velocity and temperature maxima are then no longer on the jet axis, but offset through a normal distance h which depends on the incidence α, the distance x from the exit, and on the exit velocity ratio λ. The velocities in a jet into still air can still be superposed

to a first order on the main stream, the vector sum of the two streams being taken. With the same procedure as above, we find

$$h = \alpha \frac{\lambda}{1 + \lambda} x \tag{10-10}$$

in the region of the core when the incidence is small. This relation has been experimentally confirmed up to $\alpha = 20°$; $\lambda = 0.5$; $x = 15D_e$.

The turbulent mixing of an inclined jet takes place more quickly, and consequently the maximum velocity and temperature at a given distance from the exit are less than would be given by Fig. 10-2. There is little experimental data available; what there is suggests the following empirical relation for the maximum velocity V_m:

$$\frac{V_m - V_0}{V_e - V_0} = \left(1 - 0.35\alpha\lambda \frac{x}{D_e}\right)\left(\frac{V_m - V_0}{V_e - V_0}\right)_{\alpha=0} \tag{10-11}$$

where the value for $\alpha = 0$ can be obtained from Eq. (10–4). In the absence of experimental data, the same factor may be applied to the temperature maxima. It is impossible, however, to define limiting cone angles, as the lines of constant velocity in a plane normal to the jet axis are no longer circles but lobed. An experimental example is shown in Fig. 10-3. Theoretical analysis of the shapes of free boundaries in a cross flow[1] lead to similar shapes.

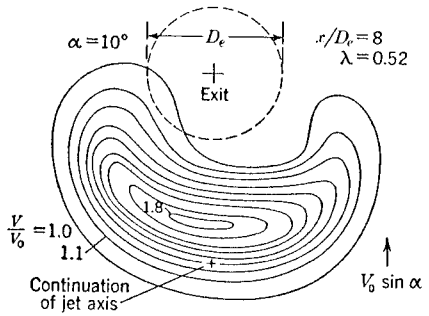

FIG. 10-3. Lines of constant velocity in a round jet at incidence to the main stream.

The deformation of the jet at incidence is very often decisively influenced by the presence of the aircraft wing. The normal deflection h of the maximum velocity line in the jet behind a midwing nacelle on a straight rectangular wing of aspect ratio 2.4, with its exit near the trailing edge, was found to be only about one-third of that given by Eq. (10-10). The maximum velocity did not fall appreciably below that of the zero-incidence case until an incidence of about 15° was reached; the shape of the jet was then still nearly circular. Obviously, the wing downwash keeps the jet down and reduces the upward bend. This interpretation may point the way to a more general treatment of the influence of the wing, namely, by adding the vector downwash velocity of the wing to those of the jet and the main stream. Since the downwash depends on the wing plan-form, the angle of sweep, and the spanwise position of the jet, it cannot be expected that simple rules will be obtained.

[1] See Hsiu-Chen Chang, 1942.

10-4. Spreading of the Jet in the Neighborhood of a Wall. What has been said above may not hold if the jet passes along a wall, such as the fuselage, or if it is near a wall so that entrainment is hindered or prevented on one side. There is a tendency to adhesion, but in many cases this can effectively be hindered by the provision of an air stream between the jet and the wall. In Fig. 10-4, the jet emerges from a nacelle attached to a plane wall, with its axis parallel to the wall. The different shapes of the jets in the two cases are due solely to differently shaped fairings between the nacelle and the wall. In the case on the left-hand side, the fairing was of airfoil shape, allowing air to flow along the wall between it and the

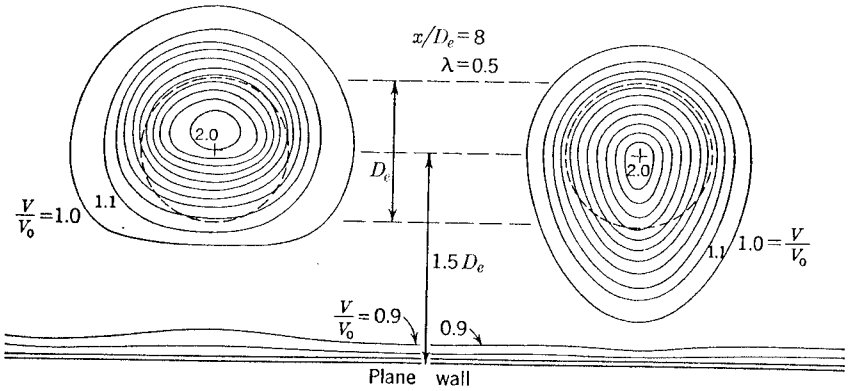

FIG. 10-4. Lines of constant velocity in a round jet parallel to a plane wall. Left-hand side, well vented; right-hand side, insufficiently vented.

jet; the fairing in the case on the right-hand side on the other hand had a bluff rear end which caused a separation of the flow. While the jet on the left was cushioned from the wall by the intervening air flow, the wake behind the bluff fairing attracted the jet to the wall. This explains why, in the example[1] shown in Fig. 10-5, the jet remains clear of the fuselage at positive incidences but sticks to it at negative incidences; the jet is effectively vented only in the first case.

It was found possible to vent a circular jet near a wall, as in Fig. 10-4, effectively even when the distance between the jet axis and the wall was only one exit diameter. The state of affairs illustrated on the right can easily be remedied by extending the fairing beyond the exit plane to allow a sufficiently small trailing-edge angle. The fairing surface facing the jet should then be shaped as part of a circular cylinder about the jet axis.

[1] These results were obtained from flow observations in a water tunnel. Such tests are very useful for the investigation of jet problems in that not only the momentum of the jet but also the density ratio can be correctly represented simply by adding air to the jet, which makes it visible at the same time.

Figure 10-6 shows a circular jet which emerges from an opening in a wall at an angle to the flow along it. It is difficult in this case to vent the jet because the venting air must first flow around the jet (which may in the first instance be regarded as a solid body) before it reaches the gap between jet and wall. The result is that the jet sticks to the wall at small exit angles; an angle of about 15° is necessary for the jet (velocity)

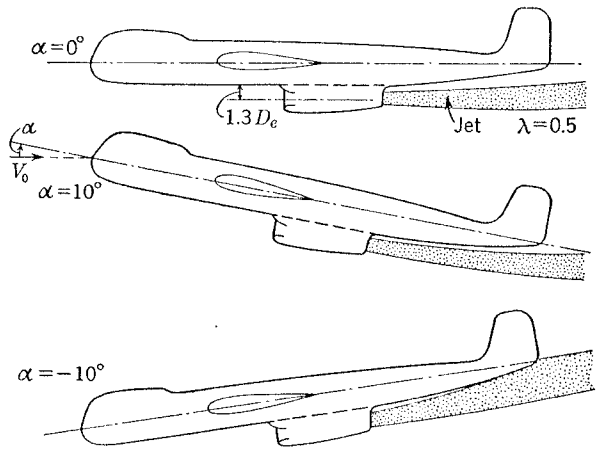

FIG. 10-5. Shape of a round jet emerging from an underslung nacelle at various incidences. From water-tunnel tests by N. Kunze, 1944.

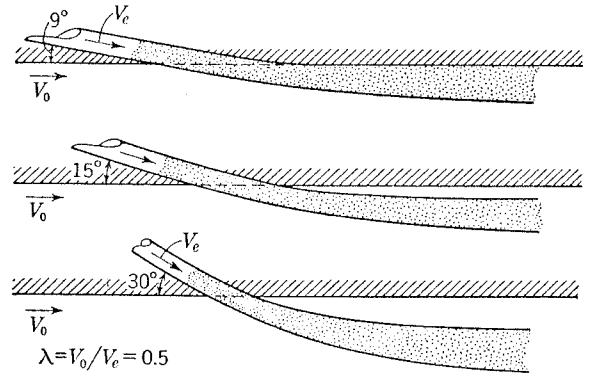

FIG. 10-6. Side elevation of a round jet emerging at an angle from a wall. From tunnel tests by H. B. Squire, 1944; and water-tunnel observations by N. Kunze, 1944.

boundary to be clear of the wall. Because of the more rapid spreading of the temperature, an angle of about 20° is recommended by H. B. Squire (1950) to prevent heating of the wall. The deflection of the line of maximum velocity in the jet is then about twice that given by Eq. (10-10).

It is naturally more difficult to induce a flow to separate a jet of flat rectangular cross section from a wall. Two-dimensional jets in particular are unlikely to detach; deflections of the jet up to 160° are possible if the

wall is suitably curved, according to H. B. Squire. This is sometimes known as the *Coanda effect.*

A round jet directed at a wall (such as the ground) is not reflected as a round jet but spreads out fanwise.[1] This occurs of course even in potential flow, and similar problems have been treated in connection with helicopters hovering near the ground. In the extreme case when the jet axis is normal to the ground, the jet spreads out radially in all directions.

10-5. Effect of the Jet on Neighboring Lifting Surfaces. The effect of the slip stream of a propeller-driven aircraft passing over the wing and tail surfaces is dealt with in a number of well-known papers and textbooks. It is seldom that the lifting surfaces of a jet aircraft lie directly in the propulsive stream; attention must, however, be paid to the forces induced on surfaces near to the very high speed jet.[2]

Consider a wing at a distance x behind the exit of a round or flat jet and a distance z above or below the jet axis, as in the sketch in Fig. 10-8. There is an induced lift force on the wing, usually directed toward the jet axis. Several effects which contribute to this force can be distinguished. Even with the wing at zero incidence, the nonuniformity of the flow causes a lift force which may be expected to be proportional to the thickness-chord ratio to a first approximation. This will readily be understood if the extreme case where the center line of the thick airfoil lies along the boundary between two regions of different velocities is considered. Second, the circulation around the wing at incidence is modified by the presence of a region of higher velocity near it; the consequent lift increment can be expected to be proportional to the incidence of the wing. Finally, there is an induced flow directed toward the jet caused by the turbulent mixing and the simultaneous slight reduction of the pressure by virtue of which the jet acts as a sink.[3] This inwash can be expressed as equivalent to a change in incidence ϵ over part of the wing area.

The total lift increment due to the influence of the jet can then be written

$$\Delta C_L = \frac{\Delta L}{\frac{1}{2}\rho V_0^2 D_e c} = f_1\alpha + f_2\frac{t}{c} + f_3\epsilon \qquad (10\text{-}12)$$

The values of the coefficients remain to be determined.

The value of f_3 depends on the lift slope of the airfoil and is thus not greater than $2\pi \cos\varphi$ (when φ = angle of sweep if any). It will usually be much less, depending on the aspect ratio of the fraction of the span which is influenced. The value of ϵ itself has been estimated on a theo-

[1] Some experimental results can be found in H. B. Squire, 1950.

[2] This problem is closely related to that of the influence of the wake of a wing on the tail plane, which has been treated by P. Ruden, 1939.

[3] The influence of this inflow on the pressure distribution along the outer surface of the jet pipe was discussed in Sec. 5-1.

retical basis by H. B. Squire and J. Trouncer (1944) and some experimental results by O. Pabst (1944) are given in Fig. 10-7. The latter were obtained under near static conditions, and the value of ϵ will be smaller at $\lambda \neq 0$. Since the maximum inflow occurs near the boundary of the jet, we may use the transformation (10-2) with $a = 0.2$; assuming that the inflow velocity is independent of λ, we obtain

$$\epsilon = \frac{1 - \lambda}{1 + 4\lambda} \epsilon_{\lambda=0} \tag{10-13}$$

This relation may be used in conjunction with the experimental data in Fig. 10-7 for estimation purposes until more evidence is available. It

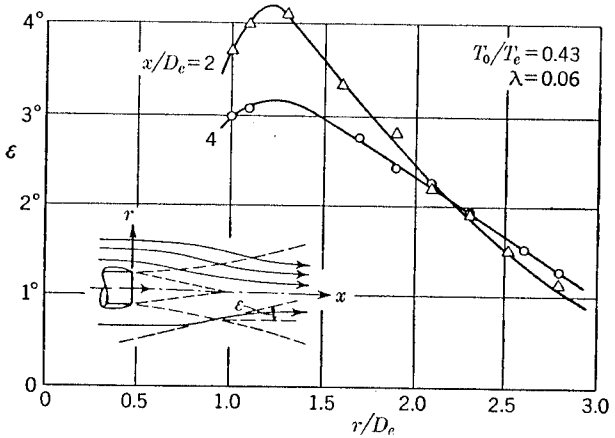

FIG. 10-7. Measured inflow angles due to turbulent mixing in a round jet. From tests by O. Pabst, 1944.

appears that the values of ϵ to be expected in high-speed flight (λ near 0.5) are very small.

The first two terms in Eq. (10-12) are usually larger than the third, so that on the whole this induced lift is of some practical importance. Information about the magnitude of f_1 and f_2 can be obtained from some low-speed tests[1] with a round jet by H. Falk (1944) summarized in Figs. 10-8 to 10-10. The wing span was large enough (at least about $7D_e$) to ensure that the total effect was measured. As will be seen, the value of f_2 depends on the geometrical position of the wing relative to the jet, on the exit velocity ratio, and on the ratio of the thickness of the wing to the diameter of the jet. This component of the lift increment was less for thicker wings in relation to the jet diameter. A maximum value of f_2 is reached near the cylinder $r = D_e/2$, and the following empirical formula agrees closely enough with the observed results:

$$f_{2\,\max} = 1.2\left(2 - \frac{t}{D_e}\right)\frac{1 - \lambda}{\lambda} \tag{10-14}$$

[1] The results of these tests include the effect of the inwash, of course.

The thickness-chord ratio of the wings tested for which this is valid varied between $t/c = 0.10$ and 0.16. Values of f_2 can be obtained from Fig. 10-8.

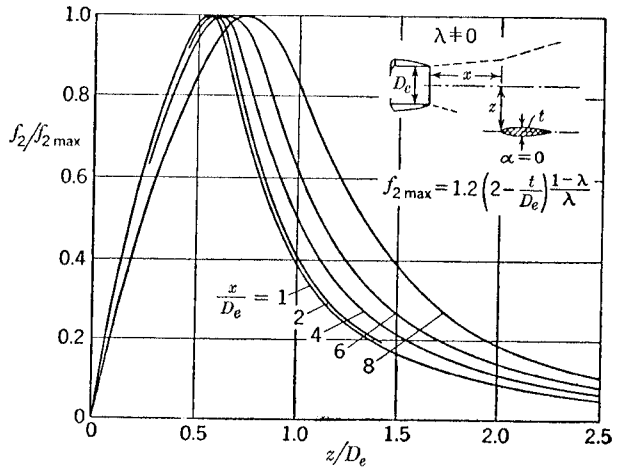

FIG. 10-8. Measured values of the coefficient f_2 in Eq. (10-12).

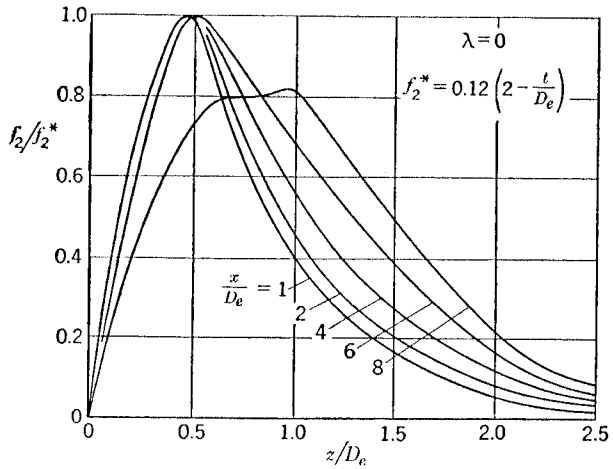

FIG. 10-9. Measured values of the coefficient f_2 in Eq. (10-15), under static conditions.

Under static conditions with $\lambda = 0$, the lift increment ΔC_L can be defined as

$$\Delta C_L = \frac{\Delta L}{\frac{1}{2}\rho V_e^2 D_e c} = f_1\alpha + f_2\frac{t}{c} + f_3\epsilon \tag{10-15}$$

and f_2 can be obtained from Fig. 10-9.

The coefficient f_1 measured on the same straight wings is plotted in Fig. 10-10. To a first order it depends only on the geometrical position of the wing and the exit velocity ratio.

If the jet is also at an incidence, the geometrical position of the wing relative to the now deformed jet should first be estimated from Eq. (10-10), taking into account, however, any straightening out of the flow by the main wing of the aircraft, as discussed in Sec. 10-3. The above results can then be used as a rough approximation in all cases where the wing is outside the jet. If the jet impinges on the wing, another direct lift force is produced and ΔC_L is no longer zero at $z = 0$, as in Fig. 10-8. Some preliminary results are reported by H. Falk (1945) but more work is needed before these effects can be fully understood and correctly predicted, as is indeed true of much of the other matter discussed in this section.

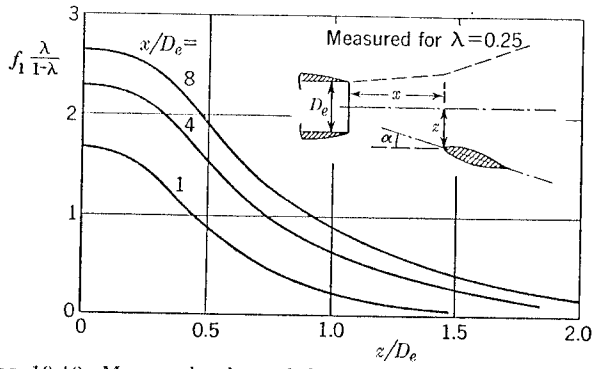

FIG. 10-10. Measured values of the coefficient f_1 in Eq. (10-12).

EXERCISES

10-1. A circular jet emerges with velocity $V_e = 500$ m/sec and temperature $T_e = 1000°$K, parallel to the main stream. Determine the velocity and temperature on the jet axis at the points $x = 8D_e$ and $x = 16D_e$ behind the exit, with flight speeds from $V_0 = 0$ to 300 m/sec ($T_0 = 300°$K).

10-2. Find the deviation of the jet of Exercise 10-1 from its axis at a distance $x = 8D_e$ behind the exit, if the jet axis is inclined to the main stream by $\alpha = 3°$ when $V_0 = 300$ m/sec, and the inclination rises with the inverse of the square of the flight speed up to $\alpha = 27°$ for $V_0 = 100$ m/sec.

10-3. Calculate the angle of inwash ϵ at the points $x = 4D_e$, $r = D_e$, $2D_e$, $3D_e$, using the data in Fig. 10-7, for the jet of Exercise 10-1.

10-4. A wing at zero incidence is situated at $z = D_e$ above the jet axis and $x = 8D_e$. Its thickness is $t = 0.1c = 0.2D_e$. Determine the induced lift coefficient ΔC_L on the wing with the jet of Exercise 10-1 at flight speeds between 100 and 300 m/sec.

BIBLIOGRAPHY

RUDEN, P., Turbulente Ausbreitungsvorgänge im Freistrahl, *Naturwissenschaften*, vol. 21, p. 375, 1933.

GOLDSTEIN, S., "Modern Developments in Fluid Dynamics," Oxford University Press, London and New York, 1938.

RUDEN, P., Windschatteneinfluss auf Rechtecktragflügel, *Jahrbuch* 1939 *der Deutschen Luftfahrtforschung*, pp. I 98, I 114; *Jahrbuch der deutschen Luftfahrtforschung* 1940, p. I 204.

PRANDTL, L., "Abriss der Strömungslehre," Friedrich Vieweg & Sohn, Brunswick, 1942.

HSIU-CHEN CHANG, Die Aufrollung eines zylindrischen Strahles durch Querwind, Dissertation, Göttingen, 1942.

CORRSIN, S., Investigation of Flow in an Axially Symmetrical Heated Jet of Air, *NACA ACR* 3L23, 1943.

KÜCHEMANN, D., Jet Diffusion in the Proximity of a Wall, *Deut. Luftfahrtforschung* U.M. 3057, 1943; translation, *NACA TM* 1214.

SQUIRE, H. B., and J. TROUNCER, Round Jets in a General Stream, *Brit. ARC Rept. & Mem.* 1974, 1944.

KUNZE, N., Strömungsaufnahmen von einem schräg aus einer ebenen Platte austretenden Strahl, *Deut. Luftfahrtforschung* U.M. 3140, 1944.

PABST, O., Die Ausbreitung heisser Gasstrahlen in bewegter Luft, *Deut. Luftfahrtforschung* UM 8004, 8007, 1944.

FALK, H., The Influence of the Jet of a Propulsion Unit on Nearby Wings, *Deut. Luftfahrtforschung* U.M. 3200; translation, *NACA TM* 1104; *AVA Ber.* 45/A/15; translation, *Brit. Min. of Supply* (*Völkenrode*) *Rept. & Transl.* 718, 1945.

KÜCHEMANN, D., and J. WEBER, Outflow and Jet Problems (*AVA Monograph* $J_2 4$ and K_3 2.5), *Brit. Min. of Supply* (*Völkenrode*) *Rept. & Transl.* 988,940, 1946.

LIEPMANN, H. W., and J. LAUFER, Investigations of Free Turbulent Mixing, *NACA TN* 1257, 1947.

PAI, S. I., Two-dimensional Jet Mixing of a Compressible Fluid, *J. Aeronaut. Sci.*, vol. 16, p. 463, 1949.

CORRSIN, S., and M. S. UBEROI, Further Experiments on the Flow and Heat Transfer in a Heated Turbulent Air Jet, *NACA TN* 1865, 1949.

SQUIRE, H. B., Jet Flow and Its Effects on Aircraft, *Aircraft Eng.*, vol. 22, p. 22, 1950.

BATCHELOR, G. K., Note on Free Turbulent Flows, with Special Reference to the Two-dimensional Wake, *J. Aeronaut. Sci.*, vol. 17, p. 44, 1950.

CORRSIN, S., The Decay of Isotropic Temperature Fluctuations in an Isotropic Turbulence, *J. Aeronaut. Sci.*, vol. 18, p. 417, 1951.

CHAPTER 11

AERODYNAMIC PROPULSION IN NATURE

Man has always been fascinated by the art of flying displayed by birds and insects, and many unsuccessful attempts have been made to imitate them. In this chapter, a very brief description will be given of the way in which they fly, as far as our present knowledge goes, if only to show that the possible methods of production of propulsive forces are not exhausted with our present-day propellers and jet engines. After a general survey in Sec. 11-1, a comparison between an oscillating wing and a propeller (both very much simplified) will be made in Sec. 11-2, providing at the same time an instructive example of an application of classical airfoil theory to propulsion problems. In Sec. 11-3, some recent model tests are discussed as an illustration, and Sec. 11-4 considers the possibility of adapting some of the principles of animal flight to aeronautical engineering.

11-1. Survey of Animal Flight. According to the zoologist, the art of flying in the animal world has been invented independently four times by different kinds of animals at different stages of evolution,[1] by the insects, the saurians, the birds, and the bats. This explains the great variety of flying organisms, and the different ways in which the same primary aim has been achieved. The insects developed plates of hard skin supported by stiffening veins; the saurians used an elastic skin spread by an enormously prolonged finger; the birds covered their arms and hands with feathers, forming a suitably shaped wing of variable plan-form and section; and the bats employ again an elastic skin which is spread by the fingers of their hands. All, however, had to adapt themselves to the laws of aerodynamics, and gradual development has taken millions of years. Those which were less successful than others paid the cost by extinction or by returning to earth.

A closer study of animal flight shows an arresting variety in the aerodynamic means in use. The methods and principles are, of course, the same as have been developed again in aeronautical engineering. A few examples will illustrate this.

For instance, large birds are apparently well able to preserve laminar flow for the sake of low drag; the first accurate drag measurements which have been made [on a buzzard in flight, by A. Raspet (1950)] have shown

[1] See, for example, E. von Holst, 1948.

that in certain flight conditions when a high forward speed is required, the flow is laminar over almost the whole surface of the bird. In contrast to this, small insects have great difficulty in achieving an effective lift-producing circulation around their wing sections because of the predominantly laminar flow at the extremely small Reynolds number of flight (of the order of 10^3, compared with about 10^5 for the larger and faster of the birds). It appears that insects may employ sharp, or saw-toothed, or hairy leading edges intentionally to induce an early transition to turbulent flow. The difference in Reynolds number explains also why the wings of the larger birds have developed efficient airfoil sections, while such shapes are of little value to insects. It is also interesting to note that to reduce their landing speed, the birds utilize all the high-lift devices which man has now devised again.

The range of ways which are available to the flying animal for producing aerodynamic lifting and propulsive forces is somewhat restricted by anatomical limitations. For instance, jet propulsion in the modern sense is beyond their means, as is any rotational movement of parts about an axis on the mechanical side. As recent study has clearly shown,[1] the flying animals usually employ the forces nearly normal to the relative wind direction which act on lifting surfaces at small incidences, and are generally known as Kutta-Joukowsky lift. Only very rarely do they make use of the drag force which is exerted by the air on a wing moved normal to its chord against the relative wind ($\alpha \approx 90°$). Most of them use their wings to generate lift and thrust simultaneously.

In principle, air forces other than pure lift always result if the wing moves relative to the general direction of flight. For instance, if a wing moves vertically downward relative to the body, which itself is moving in a horizontal direction, then the air flow relative to the wing is inclined upward; the resultant air force, being nearly normal to the wind direction, is inclined forward. Relative to the body, the resultant air force then has a vertical component, the lift, and a horizontal component, which would be a thrust in the present case. The flying animal has to perform such a movement of the wing relative to the body periodically, and many different oscillatory motions are possible. The oscillation can be transverse (flapping) or rotational (pitching), and both frequency and amplitude can be varied in either case, as well as the mean incidence of the body relative to the general direction of flight. Further, different sections along the span may have different functions. In cases with multiwing systems, the interference between the wings can be utilized to obtain optimum propulsive efficiency, or lift, or stability of flight. The special purpose which the animal pursues is the decisive factor. The air forces must invariably be produced by a flapping motion of the wing, however,

[1] See, for example, E. von Holst and D. Küchemann, 1941.

and we shall consider in the next section whether this is necessarily a disadvantage, as compared with the rotation of a propeller, or even aerodynamically superior, as is sometimes presumed.

11-2. Comparison of an Oscillating Wing and a Simplified Propeller. A good understanding of the basic flapping-wing process can be obtained by considering the flow about a plane wing which performs a translational oscillation perpendicular to the line of flight and comparing it with a similarly simplified propeller. At the same time, this will provide an instructive example of how propulsive forces can be produced.

Let a wing of elliptical plan-form move parallel to itself without any rotation[1] in a system of axes at rest relative to the main stream, according to the relations,

$$x(t) = V_0 t \qquad z(t) = a \sin 2\pi n t \tag{11-1}$$

where t denotes the time. Let the velocity V_0 of the main stream along the x axis be constant and large compared with the vertical velocity component dz/dt. This motion is equivalent to a periodic change in angle of attack about a mean value α_0:

$$\alpha(t) = \alpha_0 + \frac{dz/dt}{V_0} = \alpha_0 + \frac{1}{\lambda} \cos 2\pi n t \tag{11-2}$$

where the *rate of advance* λ is defined by

$$\lambda = \frac{V_0}{2\pi a n}$$

With the assumptions which we have made, $\lambda \gg 1$. If we add the further assumption that at any instant the motion can be treated as a steady one, which implies that the effect of the periodically separating vortices is ignored, then the distribution of the circulation γ around the airfoil can be calculated from Prandtl's airfoil equation.[2] We determine the induced downwash, in fact, of a system of trailing vortices which is taken as being a plane sheet lying in the direction of the main stream.

The spanwise distribution of the circulation at a given time t is then elliptic and given by

$$\gamma\left(\frac{y}{s}; t\right) = \frac{4}{2 + A} \sqrt{1 - \left(\frac{y}{s}\right)^2}\, \alpha(t) \tag{11-3}$$

s denoting the semispan and A the aspect ratio of the wing. The induced angle of incidence α_i is constant over the span and depends only on the time:

[1] The more complicated motion which includes a pitching oscillation is discussed by E. von Holst and D. Küchemann, 1941.

[2] Some methods and results from classical airfoil theory are used here without further explanation, and the reader is referred to the standard textbooks.

$$\alpha_i\left(\frac{y}{s}; t\right) = \alpha_i(t) = \frac{2}{2 + A}\, \alpha(t) \tag{11-4}$$

The mean lift and drag coefficients are given by the integrals

$$C_L = nA \int_0^{1/n} \int_{-1}^{+1} \gamma\left(\frac{y}{s}; t\right) d\left(\frac{y}{s}\right) dt \tag{11-5}$$

and

$$C_D = nA \int_0^{1/n} \int_{-1}^{+1} \gamma\left(\frac{y}{s}; t\right) \left[\alpha_i\left(\frac{y}{s}; t\right) - \frac{dz/dt}{V_0}\right] d\left(\frac{y}{s}\right) dt + C_{D0} \tag{11-6}$$

where C_{D0} is the profile drag of the wing (supposed constant). The second term in the C_D integral is of fundamental importance here since it represents the thrust component of the forward inclined resultant air force at a given time.[1]

The integrals in Eqs. (11-5) and (11-6) can be evaluated explicitly, as can the corresponding expression for the power input, determined as the work done by the lifting force in the vertical motion. Before writing down the results, let us consider the corresponding conditions for a similarly simplified propeller.

Consider a plane wing rolling about its axis of symmetry, which itself is inclined to the main stream (x direction) at an angle α_0. Let the rolling velocity of the tips be small compared with the main stream velocity V_0, and assume again that the sheet of trailing vortices is straight along the main stream. Such a wing may be regarded as a two-bladed propeller at a large rate of advance with blade pitch 90°, the very opposite case to that of Froude's axial propeller theory.

If Froude's flow is represented by a system of trailing vortices in the slip stream, only ring vortices are concerned; these produce an axial velocity in the slip stream, but no rotation, and this may be regarded as an approximation to the very low rate of advance case. In contrast to this, the system of trailing vortices in the slip stream behind a propeller at a very high rate of advance has the vorticity vector nearly in the direction of the main stream; the axial velocity in the slip stream is very small, but there is an appreciable loss of kinetic energy due to the rotation induced by the vortices. The efficiency based on this loss may be called the *induced efficiency*, in contrast to the *jet efficiency* as treated above (for instance, in Chap. 2). At a high rate of advance, *i.e.*, at a high flight

[1] The case treated here is the inverse of the Betz-Knoller effect:—The resultant force on an airfoil in a flow with periodic vertical fluctuations has a nonzero component directed against the main stream. See A. Betz, 1912; A. Knoller, 1913; D. Küchemann, 1945.

speed, the induced efficiency is appreciably less than unity, whereas the jet efficiency is nearly 1; in Froude's case with a low rate of advance, the induced efficiency is 1, but the jet efficiency is less than 1. The real propeller works in between these two extremes, and the trailing vortices are of helical shape, the vorticity vector having components both in the circumferential and in the axial directions. However, Froude's jet efficiency is necessarily connected with the production of propulsive forces, whereas the induced efficiency is not; for instance, the latter can be improved by means of guide vanes or counterrotating blades, without loss of thrust.

For the two-bladed propeller of radius R at a high rate of advance

$$\lambda = \frac{V_0}{2\pi R n}$$

the angle of attack is given by

$$\alpha\left(\frac{r}{R}; t\right) = \alpha_0 \cos 2\pi n t + \frac{1}{\lambda}\frac{r}{R} \tag{11-7}$$

where r is the radial coordinate along the blade. Note that the maximum angle is $\alpha_0 + 1/\lambda$ for the rotating wing as well as for the oscillating wing [Eq. (11-2)]. Applying Prandtl's airfoil equation again, we get for the circulation along the blade[1]

$$\gamma\left(\frac{r}{R}; t\right) = \frac{4}{2 + A}\sqrt{1 - \left(\frac{r}{R}\right)^2}\,\alpha_0 \cos 2\pi n t + \frac{4}{4 + A}\frac{r/R}{\lambda}\sqrt{1 - \left(\frac{r}{R}\right)^2} \tag{11-8}$$

A denotes again the aspect ratio of the whole wing. The lift and drag coefficients are then

$$C_L = nA \int_0^{1/n} \cos 2\pi n t \int_{-1}^{+1} \gamma\left(\frac{r}{R}; t\right) d\left(\frac{r}{R}\right) dt \tag{11-9}$$

and

$$C_D = nA \int_0^{1/n}\int_{-1}^{+1} \gamma\left(\frac{r}{R}; t\right)\left[\alpha_i\left(\frac{r}{R}; t\right) - \frac{r/R}{\lambda}\right] d\left(\frac{r}{R}\right) dt + C_{D0} \tag{11-10}$$

where

$$\alpha_i\left(\frac{r}{R}; t\right) = \frac{2}{2 + A}\alpha_0 \cos 2\pi n t + \frac{4}{4 + A}\frac{r/R}{\lambda} \tag{11-11}$$

The integrals in Eqs. (11-9) and (11-10) can also be solved explicitly.

The final results are:

[1] For details, see E. von Holst, D. Küchemann, and K. Solf, 1942.

For the oscillating wing

$$C_L = \frac{2\pi}{1 + 2/A}\alpha_0 = C_{L0}$$

$$C_D = \frac{C_L^2}{\pi A} - \frac{\pi}{(1 + 2/A)^2}\frac{1}{\lambda^2} + C_{D0}$$

$$C_T = \frac{\pi}{(1 + 2/A)^2}\frac{1}{\lambda^2}$$

For the propeller

$$C_L = \frac{\pi}{1 + 2/A}\alpha_0 = \frac{1}{2}C_{L0} \tag{11-12}$$

$$C_D = 2\frac{C_L^2}{\pi A} - \frac{\pi}{(1 + 4/A)^2}\frac{1}{\lambda^2} + C_{D0} \tag{11-13}$$

$$C_T = \frac{1}{2}\frac{\pi}{(1 + 4/A)^2}\frac{1}{\lambda^2} - \frac{C_L^2}{\pi A} \tag{11-14}$$

We have defined a thrust coefficient C_T here as the difference between the drag of the wing in steady flight at incidence α_0 and that given by Eq. (11-13).

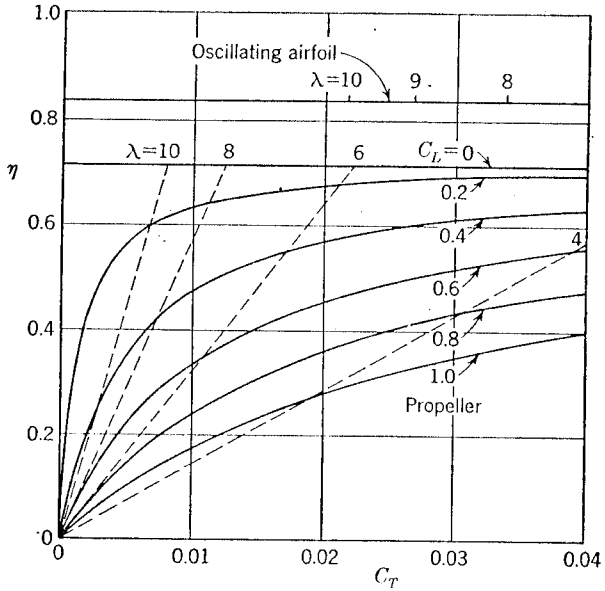

FIG. 11-1. Calculated efficiencies of an oscillating airfoil and a simplified propeller at incidence, at large advance ratios. $A = 10$.

In contrast to the oscillating wing, which has the same lift and induced drag as in the steady state, the propeller at incidence has only half the lift and twice the induced drag that it would have in the steady (nonrotating) state. Formally, we arrive at the same drag coefficient in each case if the aspect ratio of the propeller is halved in the calculation, *i.e.*, if we use the aspect ratio of one blade. To produce the same thrust at $C_L = 0$, the propeller must have a smaller rate of advance, λ_1, than the oscillating wing, λ_2:

$$\lambda_1 = 0.707\,\frac{1 + 2/A}{1 + 4/A}\,\lambda_2$$

The propulsive efficiency, which is purely an induced efficiency in the sense introduced above, is also different for the two cases:

Oscillating wing $\qquad$ Propeller

$$\eta = \frac{1}{1 + 2/A} \qquad \eta = \frac{1}{1 + 4/A}\left(1 - \frac{1}{1 + \pi A C_T/C_L{}^2}\right) \qquad (11\text{-}15)$$

The production of lifting forces does not affect the propulsive efficiency of the oscillating wing, but the efficiency of the propeller is reduced when the lift is not zero; this is illustrated by Fig. 11-1. The result indicates that at the worst the propulsive efficiency of an oscillating wing need not be below that of a propeller. Moreover, more care is needed in the aerodynamic design of a propeller to make it efficient at high speeds, since even at zero lift the efficiency of the propeller is less than that of the oscillating wing. This is obviously the consequence of a disadvantageous trailing vortex system.

11-3. Some Experimental Results from Model Tests. The examples described in the following will illustrate how lifting and propulsive forces

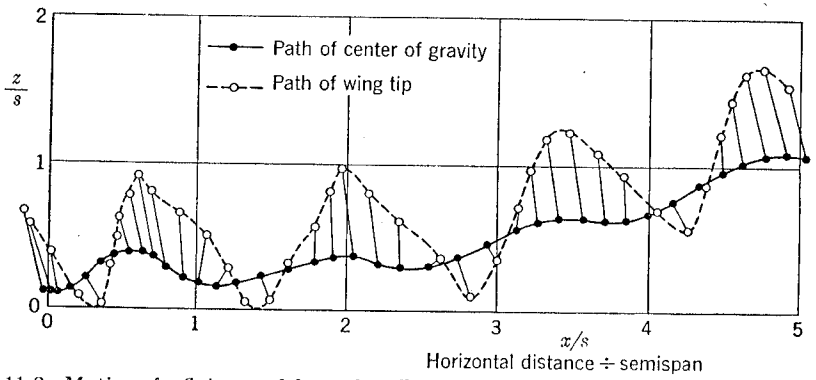

FIG. 11-2. Motion of a flying model at take-off, from a slow-motion film. Interval between consecutive points $\frac{3}{8}{}_0$ sec.

can be produced simultaneously. Most of our present knowledge of the flying characteristics of birds and insects has been gained by direct observation, sometimes aided by slow-motion cinematography or other means. This has been supplemented in recent years by model tests, either on actual flying models or on ordinary wind-tunnel models, with the obvious advantage that the significant variables can be controlled. The method has been developed by E. von Holst (1943) and a great variety of models has been built, each representing a certain type of flight.

Some results obtained from slow-motion films of such a model are given in Fig. 11-2, which shows the path of the center of gravity of the model and the path of the wing tip. While the center of gravity moves along

a steadily rising path, after an initial period, the wing tip performs an oscillation about the center-of-gravity path. The flexible wing of this model flapped in a way similar to that described in the previous section, but in addition to the transverse or plunging oscillation there was also a rotational or pitching oscillation, so that there was a further variation of the angle of incidence. The amplitude of the pitching oscillation varied over the span; at the wing root, the incidence was varied by $\pm 5°$ about a mean of 15°, and at the tip by $\pm 17°$ about a mean of only 3°. The angle described by the wing (which was hinged at its root) during the transverse oscillation was about 60°, and the pitching oscillation was not in phase with the plunging oscillation but 90° behind.[1]

The region near the wing root of this model is obviously always at a positive incidence, and the resultant force contains a positive lift throughout the whole period. This implies that the component in the flight direction will change its sign; as it moves upward, this part of the wing produces a drag. In contrast, the region near the tip changes from positive to negative incidences during a period, and the lift changes its sign periodically; there is always a thrust component, however. The tip region can therefore be regarded as the propelling part and the region near the root as the lifting part. This subdivision of the wing into regions with different functions is very common, especially among birds, and was noted as long ago as 1889 by Lilienthal. It has the disadvantage of less uniform spanwise loading distributions than in the simplified motion discussed in the previous section, and consequently higher induced drag and reduced propulsive efficiency.

These flying models were driven by small rubber motors, and the ratio of the model weight W to the horsepower P of the motor was usually very high (20 kg/hp = 44 lb/hp in the case above). The motor power might seem low compared with what an aircraft requires, but if the laws of similarity are considered it will be seen that this is not so. If the ratio of the dimensions of the model to those of a full-scale aircraft is k, then W/P is usually found to vary as $\sqrt{k}$, the larger model having the smaller value. In reality, the models are so lightly built that their weight is less than this assumes, being more nearly proportional to the fifth power of the dimensions than to the cube, which means that W/P varies as $k^{\frac{5}{2}}$. With the value of W/P quoted above for the flying model, we arrive at a figure of less than 1 kg/hp or 2 lb/hp for a small aircraft with ten times the dimensions of the model—a very powerful engine.

The available power of flying animals has not yet been investigated

[1] There is an obvious shift in phase between the gain in lift and speed and the downward movement of the wing which causes it. This is due to nonsteady motion effects, since the reduced frequency $1/2\pi\lambda$ is too high (about 0.6) to justify a quasi-stationary treatment as in the previous section.

with sufficient accuracy, but it appears that similar conditions prevail. This implies that they too are equipped with powerful "motors." We may conclude that self-powered human flight for any length of time seems to be virtually impossible, since the work that a man can perform is limited physiologically to much less than would give the necessary values of W/P.

Another series of tests by E. von Holst (1943), in which the amplitudes of both the transverse and the pitching oscillations and the angle between

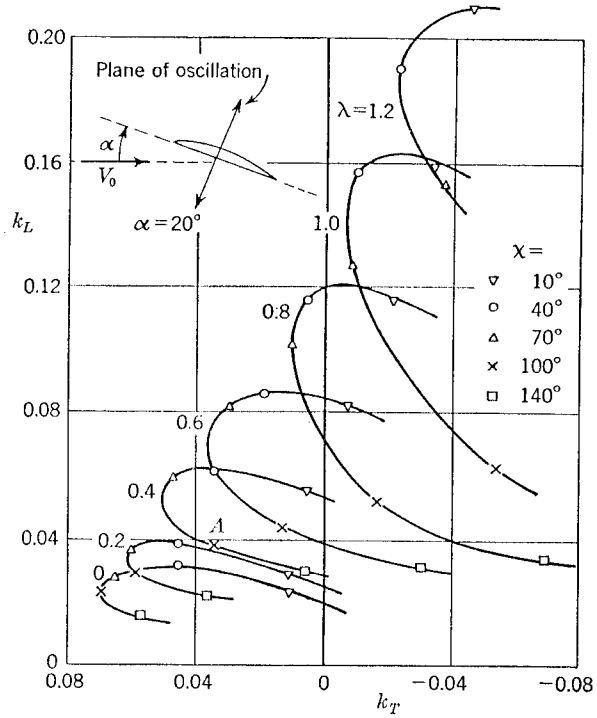

FIG. 11-3. Lift and thrust forces measured on a small oscillating wing.

the plane of the oscillation and the free-stream direction were varied, was made on a very small elliptical wing of only 32 mm semispan, in a wind tunnel. These tests were designed to show how small Reynolds numbers (below 1,000) affected the air forces obtainable and the power input required. Figures 11-3 and 11-4 show some typical results; the lift and thrust are given by the nondimensional coefficients

$$k_L = \frac{L}{\frac{1}{2}\rho u^2 S} \qquad \text{and} \qquad k_T = \frac{T}{\frac{1}{2}\rho u^2 S}$$

where u is the mean circumferential velocity and S is the sector of the circle swept by the wing in the transverse oscillation. Gravitation forces are not included. The rate of advance is defined as $\lambda = V_0/u$. In the

examples, the amplitude of the plunging oscillation was kept constant at 68°, but the amplitude χ of the pitching oscillation was varied.

Figure 11-3 shows well the wide range of possible lift[1] and thrust forces which can be obtained as a consequence of combining lifting and propelling surfaces into one organ. The vector from the origin to a point on one of the curves represents the magnitude and direction of the resultant air force. If the weight is to be supported only, the resultant force must be equal and opposite to the weight, *i.e.*, the vector from the origin is vertical. The flight path is the k_T axis (the "free-stream direction"). For

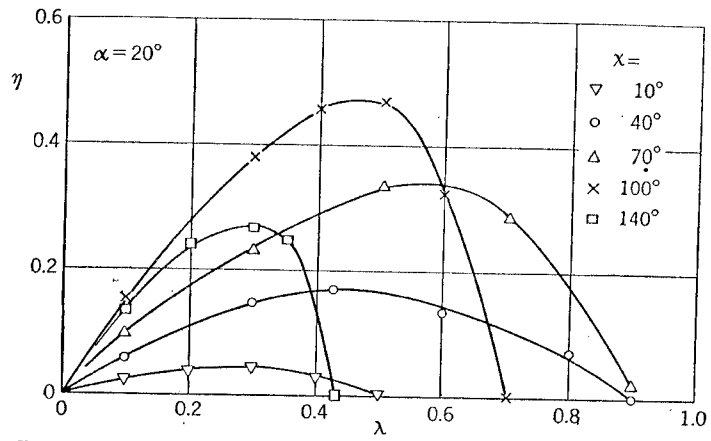

FIG. 11-4. Measured propulsive efficiency of a small oscillating wing.

instance, with $\lambda = 0.4$ and $\chi = 100°$, upward flight at an angle of climb of about 45° is possible ($0A$ in Fig. 11-3 vertical).

The corresponding propulsive efficiencies in Fig. 11-4 show that the motion is quite effective for the production of thrust, considering the low Reynolds number. Insects will probably be able to improve on it by using counteroscillating wing systems. This does not imply that a dragonfly, for instance, moves its pairs of wings strictly in opposition. Nonsteady motion effects and the finite streamwise distance between the wings may make it necessary to adopt a different phase shift between the two oscillations in order to enable the downstream wings to recover effectually the kinetic energy which would otherwise be lost in the transverse motion imparted to the air by the upstream wings. These problems have not yet been studied at all.

11-4. Adaptation of the Principles of Animal Flight to Aeronautical Engineering. The flight of the birds and insects has always been looked upon as a possible source of inspiration from which human engineering could profitably learn and copy. The fact is, however, that the cambered

[1] The ordinary lift coefficient C_L, referred to the resultant velocity of the wing tip and to the wing area, is about 0.5 (at $\lambda = 0.4$) and 0.6 (at $\lambda = 1.2$).

airfoil section with a rounded leading edge is so far the only important feature that has actually been taken over from the birds (by Lilienthal). Although there are certainly others among the methods and devices employed by the flying animal which can usefully be applied in aeronautical engineering, it must not be overlooked that in many cases, their utilization cannot be a matter of mere copying but rather of suitable adaptation to engineering needs.

For instance, it now seems clear that no striking aerodynamic benefit can be derived from the flapping motion, which is only a necessary consequence of the anatomy of the flying animal. In any engineering application therefore, it will have to be transformed into a rotation about an axis. In this light, the various forms of cyclogiro rotating-wing systems,[1] or the Voith-Schneider propeller[2] already applied successfully to ship propulsion, may be called legitimate adaptations of the principles of animal flight. And even the propeller may be regarded as a consequent development of the functions of the outer part of a bird's wing.

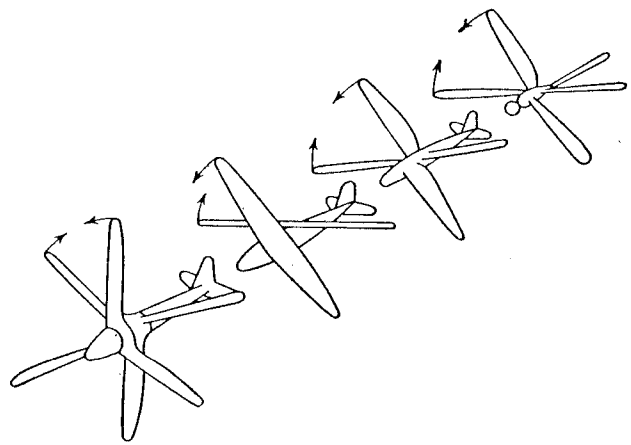

FIG. 11-5. Stages in the development of the thrust wing from the dragonfly.

There is, however, one general principle which is almost universally employed by the flying animals: Lift and thrust are generated simultaneously by the same organ; and there is no question of the addition of a propulsion unit to a lifting surface. It is possible that this principle might also be applied in the future course of aeronautical engineering. One way would be the complete integration of jet engines into the wing, mentioned in Sec. 9-6. Alternatively, at the other extreme, another way would be to dispose of the wings altogether and leave only a propeller,

[1] See, for example, J. B. Wheatley, 1933; E. Everling, 1934; J. B. Wheatley and R. Windler, 1935.

[2] See, for example, A. Betz, 1932.

which would produce the necessary lift by operating with a small inclination to the direction of flight.

Stages in the development of the latter scheme are illustrated in Fig. 11-5. Beginning with the dragonfly, the first step would be to make the wings rigid and to add a tail plane, replacing the long body, which is otherwise needed to counteract the large alternations in pitching moment caused by the periodic changes of the lift forces on the two wings. The next step indicated in Fig. 11-5 would automatically eliminate the pitching moment variations, but only the final transition to counterrotating wings (or propellers) is of real engineering significance.[1]

A further general principle of the flight of animals is always to have the plane of the transverse oscillation nearly normal to the direction of motion. This means that the axis of the *thrust wing* (Triebflügel), as the final stage in Fig. 11-5 may be called, should likewise be nearly in the direction of flight. The aircraft would take off with its axis vertical, resembling a helicopter; but unlike the helicopter, it would not keep its axis vertical but turn over gradually, until in high-speed flight it would be almost horizontal. The well-known speed limitation of the helicopter would thereby be overcome by the thrust wing.

A detailed design has been made by H. Multhopp (1944) who further suggested the use of ram jets to drive each blade individually and make it possible to dispose of the second system of blades without introducing a reaction moment about the fuselage. This is a particularly suitable application of the ram jet, since its velocity can be kept constant, and it can always work at the design point with the optimum efficiency. The rpm of the blades will thus be highest at take-off and landing, and lowest at top speed. The main flight control will be by changing the pitch of the blades.[2] The result is an aircraft which combines the high top speeds attainable by conventional modern aircraft with the maneuverability, the ability to climb in any direction, and the ability to rise into the air without a take-off run, which so far only the birds have mastered.

Speaking generally, useful adaptations of animal flight to aeronautical engineering cannot be based on observation and imitation alone, but demand a knowledge of engineering possibilities as well as an understanding of the laws of aerodynamics, which govern both animal and mechanical flight. It is not surprising that it was a mechanically minded scientist, O. Lilienthal, who was the first to give physically correct interpretations of bird flight, and who, after suitable experiments of his own,

[1] It may be mentioned that flying models of all the stages shown in Fig. 11-5 were built and found capable of normal flight by E. von Holst, who originally suggested this particular technical adaptation.

[2] For details, see E. von Holst, D. Küchemann, and K. Solf, 1942; and I. Ginzel, 1946.

became as a result the first man to leave the surface of the earth flying. The artists, from the Greeks to Leonardo da Vinci (who was, however, also an engineer) and Francesco de Goya, and the pragmatic enthusiasts of all times who made so many purposeful and courageous efforts, they all failed. Thus our own field of aeronautics provides one of the most striking examples of the *purposeless* advancement of fundamental science bringing in its trail technical achievements which had been attempted in vain for thousands of years.

BIBLIOGRAPHY

LILIENTHAL, O., "Der Vogelflug als Grundlage der Fliegekunst," 3d ed., R. Oldenbourg, Munich and Berlin, 1950.

BETZ, A., Ein Beitrag zur Erklärung des Segelfluges, *Z. Flugtech. u. Motorluftschiffahrt*, vol. 3, p. 269, 1912.

KNOLLER, R., Zur Theorie des Segelfluges, *Z. Flugtech. u. Motorluftschiffahrt*, vol. 4, p. 13, 1913.

BETZ, A., Grundsätzliches zum Voith-Schneider Propeller, in "Hydromechanische Probleme des Schiffsantriebs," G. Kempf and E. Förster, editors, Hamburgische Schiffbau-Versuchsanstalt, Hamburg, 1932.

WHEATLEY, J. B., Simplified Aerodynamic Analysis of the Cyclogiro Rotating-wing System, *NACA TN* 467, 1933.

EVERLING, E., Zur Frage des Flügelrades, *Luftwissen*, vol. 1, p. 221, 1934.

WHEATLEY, J. B., and R. WINDLER, Wind-tunnel Tests of a Cyclogiro Rotor, *NACA TN* 528, 1935.

VON HOLST, E., and D. KÜCHEMANN, Biologische und aerodynamische Probleme des Tierfluges, *Naturwissenschaften*, vol. 29, p. 348, 1941; and *Luftwissen*, vol. 8, p. 277, 1941; abridged translation in *J. Roy. Aeronaut. Soc.*, vol. 46, p. 39, 1942.

VON HOLST, E., D. KÜCHEMANN, and K. SOLF, Der Triebflügel, *Jahrbuch der Deutschen Luftfahrtforschung*, 1942, p. I 435.

VON HOLST, E., Über "künstliche Vögel" als Mittel zum Studium des Vogelflugs, *J. Ornithologie*, vol. 91, p. 406, 1943.

VON HOLST, E., Untersuchungen über Flugbiophysik, *Biol. Zentr.*, vol. 63, p. 289, 1943; *Luftwissen*, vol. 10, p. 146, 1943.

KÜCHEMANN, D., Remark on the Betz-Knoller Effect, Betz Festschrift, Göttingen, 1945; translation, *Brit. Min. of Supply (Völkenrode) Rept. & Transl.* 80, 1945.

GINZEL, I., The Thrust-wing (*AVA Monograph* K_3 4.3), *Brit. Min. of Supply (Völkenrode) Rept. & Transl.* 941, 1946.

SANDERS, J. C., and N. D. SANDERS, A Preliminary Study of a Propeller Powered by Gas Jets Issuing from the Blade Tips, *NACA TN* 1155, 1946.

VON HOLST, E., Vom Flug der Tiere und vom Menschenflug der Zukunft, *Schriften der Universität Heidelberg*, 3, 1948.

RASPET, A., Performance Measurements of a Soaring Bird, *Rept. Eng. Research Sta., Mississippi State College*, 1950.

CHAPTER 12

COOLING

The exchange of heat between part of an engine and an air stream is a common feature of aircraft propulsion. In piston engines a large portion of the heat developed by combustion of the fuel is not utilized in the working process and has to be dissipated to the free stream, mainly from the cylinders. This can be done either directly (in air-cooled engines) or indirectly, with a liquid as an intermediary *coolant* and a special heat exchanger, the *cooler block*, in which the coolant dissipates heat to the free stream. Jet engines usually require only a small cooler for the lubricating oil; if it is necessary to cool the turbine blades, it is done directly (with hollow blades, for instance). However, future turbojet engines may incorporate heat exchangers to increase the thermal efficiency, as indicated in Chap. 2.

The basic processes in a heat exchanger are well illustrated by the ordinary cooler block with liquid coolant. The dividing wall between the two media is kept at a practically constant temperature by the liquid coolant flowing on one side; on the other side, the hot wall loses heat to the air stream. As we are interested not in the isolated cooler but in practical installations in ducts, which may be of various shapes, we shall take the duct also in consideration. These matters are treated in Secs. 12-1 to 12-4. In a practical cooling-plant layout, the designer is faced with a problem which is basically simple but complicated by the multiplicity of variables at his disposal, often with conflicting influences. A complete cooler installation for a piston engine is taken as a typical example, and Secs. 12-5 to 12-7 discuss ways of achieving a satisfactory solution. The size of the cooler, the cooling power loss, and some possible installations are considered. To show how some of the simplified ideas accepted so far must be revised to meet more complicated conditions, the direct exchange of heat between two air streams is treated briefly in Sec. 12-8.

12-1. Cooler Block in a Straight Duct. Consider a cooler block such as that shown in section, in a simplified form, in Fig. 12-1. The liquid coolant flows through a number of tubes arranged transversely across the air stream. The block itself is normal to the airflow in a straight duct with cross-section area A_B, and the velocity of the air ahead of the block is V_B. The velocity in the passages between the tubes is

higher and equal to V_B/σ, where σ is the ratio of the total cross-section area of the free passages to the frontal area A_B. σ is a measure of the solidity of the cooler block and its value is always less than unity. For simplicity, we assume the temperature of the coolant to be constant and the temperature T_W of the metal walls of the tubes to be the same as that of the coolant everywhere. This is very nearly true in many practical cases (but see Sec. 12-8). Ribs are often used to increase the area of contact between the hot tubes and the air; Fig. 12-1 shows a simple type.

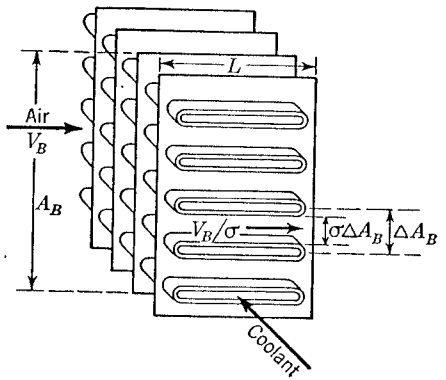

FIG. 12-1. Diagrammatic illustration of a section of a cross-flow cooler block with ribbed flat tubes for the coolant.

At a distance x from the block entry, the quantity of heat dQ dissipated to the air from a length dx of the cooler is proportional to the weight of air which passes through and to the local temperature difference; we may write

$$dQ = k_H c_p g \rho V_B A_B [T_W - T(x)] d\left(\frac{x}{L}\right) \tag{12-1}$$

where $T(x)$ is the mean air temperature in the passage at the cross section considered, and k_H is a heat-transfer coefficient. The same quantity of heat is absorbed by the air, and we find, from Sec. 2-1,

$$dQ = c_p g \rho V_B A_B \, dT(x) \tag{12-2}$$

The two expressions for dQ give a differential equation for the temperature distribution along the passage inside the block:

$$\frac{dT(x)}{T_W - T(x)} = k_H d\left(\frac{x}{L}\right)$$

This is readily solved if k_H is independent of x, which is justified by experimental evidence. The solution obtained is

$$T(x) = T_W - (T_W - T_{B1}) \exp\left(-k_H \frac{x}{L}\right) \tag{12-3}$$

The air temperature rises exponentially from T_{B1} at the block entry to

$$T_{B2} = T_W - (T_W - T_{B1}) \exp(-k_H)$$

at the block exit. We can thus express k_H in terms of easily measurable quantities:

$$k_H = \ln \frac{T_W - T_{B1}}{T_W - T_{B2}} = \ln \frac{1}{1 - \dfrac{T_{B2} - T_{B1}}{T_W - T_{B1}}} \tag{12-4}$$

The temperature ratio

$$\frac{T_{B2} - T_{B1}}{T_W - T_{B1}} = 1 - e^{-k_H} \tag{12-4a}$$

the ratio of the actual temperature increase to the maximum possible increase, depends only on the heat-transfer coefficient k_H, which should be as large as possible for the heat transferred to a given weight of air to be a maximum.

It is impossible to avoid friction at the walls in the flow of air through the narrow passages of the cooler block. This type of flow has been thoroughly investigated;[1] we may use the friction coefficient f, which is related to the shear stress F at the walls and to the pressure drop in the passages by

$$f = \frac{4F}{\frac{1}{2}\rho(V_B/\sigma)^2} = \frac{D}{L} \frac{p_{B1} - p_{B2}}{\frac{1}{2}\rho(V_B/\sigma)^2} \tag{12-5}$$

D is the hydraulic diameter of the individual passage, defined by

$$D = \frac{4 \times \text{cross-sectional area}}{\text{wetted perimeter}}$$

The friction coefficient f depends on the Reynolds number of the flow

$$\text{Re} = \frac{V_B D}{\sigma \nu}$$

on the state of the flow (laminar, turbulent); and on the surface condition (roughness, waviness, etc.). In smooth passages the regime of laminar flow is governed by the Hagen-Poiseuille law,

$$f = \frac{64}{\text{Re}} \tag{12-6}$$

and the regime of fully developed turbulent flow by the Blasius law,

$$f = \frac{0.316}{\sqrt[4]{\text{Re}}} \tag{12-7}$$

For our application to coolers we introduce the pressure-drop coefficient

$$k_P = \frac{p_{B1} - p_{B2}}{\frac{1}{2}\rho V_B^2} = \frac{1}{\sigma^2} \frac{L}{D} f(\text{Re}) \tag{12-8}$$

which can easily be measured for a cooler block in a straight duct.

[1] See, for example, J. C. Hunsaker and B. G. Rightmire, Chap. VIII and the references given there.

In an experiment to measure k_P, the pressure drop will be slightly higher than that due to skin friction because of the loss at the sudden enlargement of the cross-section area at the end of the block. This is small, however, compared with the friction loss; it depends mainly on the value of σ, and in the extreme case of square-cut ends, the mean additional pressure loss is given by the Borda-Carnot formula:[1]

$$\frac{p_{B1} - p_{B2}}{\frac{1}{2}\rho V_B^2} = \frac{(V_B/\sigma - V_B)^2}{V_B^2} = \left(\frac{1-\sigma}{\sigma}\right)^2 \tag{12-9}$$

This is to be added to the right-hand side of Eq. (12-8) to give the total value of k_P.

Heat transfer and pressure drop are not independent, and it is of practical importance to know the minimum pressure-drop coefficient needed to pay for a certain heat-transfer coefficient k_H. In order to understand this connection, we have to consider the mechanism of heat transfer.[2]

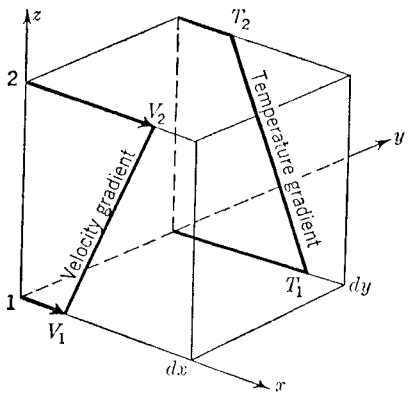

FIG. 12-2. Velocity and temperature gradient in a laminar flow region.

In aircraft coolers, heat is transferred mainly by conduction (in the metal parts and in the laminar-flow regions in the coolant and the air) and by convection (in turbulent-flow regimes). Little is transferred by radiation. In laminar flow the heat-transfer mechanism is principally molecular conduction. As explained by the kinetic theory of gases, a molecule in the airflow carries its momentum and heat from one place to another, and the quantity of heat dQ that flows through the area $dx\ dy$ per unit time is proportional to the normal temperature gradient (see Fig. 12-2):

$$dQ \propto -\frac{dT}{dz}\,dx\,dy$$

At the same time, a shear force dF proportional to the velocity gradient acts on the area element $dx\ dy$:

$$dF \propto \frac{dV}{dz}\,dx\,dy$$

Thus for the same area element $dx\ dy$, we have

$$dQ \propto -\frac{dT}{dV}\,dF$$

[1] See, for example, J. C. Hunsaker and B. G. Rightmire, paragraph 8.17.

[2] For detailed information, see the appropriate textbooks, for example, those mentioned at the end of this chapter.

or

$$dQ \propto \frac{T_1 - T_2}{V_2 - V_1}\,dF \tag{12-10}$$

for a layer of finite thickness (see Fig. 12-2), relating the transfer of heat to the friction force.

The mechanism of heat and momentum transfer in turbulent flow is not yet fully understood. According to a picture of the process due to L. Prandtl and others, lumps of air of macroscopic size move normal to the main stream; the same weight W flows from 1 to 2 per unit time as from 2 to 1, for reasons of continuity. If the full amount of heat and momentum is carried each way from one layer to the other, then the heat transferred is

$$dQ = c_p 2W(T_1 - T_2)$$

and the momentum transferred, which is equal to the shear force, is

$$dF = 2\frac{W}{g}(V_2 - V_1)$$

Thus we have

$$dQ = c_p g \frac{T_1 - T_2}{V_2 - V_1}\,dF \tag{12-11}$$

a relation of the same form as Eq. (12-10), as is to be expected, since the mechanism of convection by turbulent mixing of finite lumps of air has been assumed to be the same as the mechanism of molecular conduction. The proportionality factor[1] in Eq. (12-10) is not equal to $c_p g$, however.

Assuming heat transfer to which Eqs. (12-10) or (12-11) apply in the passages of a cooler block, the transverse velocity and temperature profiles must be similar. We may then take T_1 to be the wall temperature, T_2 the mean air temperature, $V_1 = 0$ as the air velocity at the wall, and $V_2 = V_B/\sigma$ as the mean air velocity. The shear stress may be expressed by the pressure drop:

$$dF = \frac{p_{B1} - p_{B2}}{L} A_{B\sigma}\,dx = \frac{k_p}{L}\frac{1}{2}\rho V_B^2 A_{B\sigma}\,dx$$

Using Eq. (12-1), we then obtain

$$k_H c_p g \rho V_B A_B [T_W - T(x)]\,d\left(\frac{x}{L}\right) = c_p g \frac{T_W - T(x)}{V_B/\sigma} k_P \frac{1}{2}\rho V_B^2 A_{B\sigma}\,d\left(\frac{x}{L}\right)$$

which gives

$$k_H = \frac{\sigma^2}{2} k_P \tag{12-12}$$

[1] The ratio of the factor in Eq. (12-11) to the factor in Eq. (12-10) is the Prandtl number Pr, which is about 0.7 for air. However, the laminar sublayer where Eq. (12-10) applies is usually small and thus the process of convection is generally more important.

This is basically the same as Osborne Reynolds' well-known momentum theorem of heat transfer.

We cannot expect the analogy between fluid friction and heat transfer in the cooler to follow Reynolds' law strictly; in particular, the constant may not be equal to $\sigma^2/2$. We may assume a similar law to hold, however,

$$\frac{k_H}{k_P} = k_U = \text{const} \tag{12-13}$$

The coefficient k_U is a measure of the utilization of the pressure drop for heat transfer. Experiment shows that k_U has a constant value for a given heat-exchanger system (*i.e.*, given geometry, roughness, waviness, etc.), independent of the Reynolds number, to the accuracy required. It appears that under the most favorable experimental conditions k_U can be equal to but never exceed $\sigma^2/2 (= k_{U0})$. The heat-transfer coefficient k_H is now, like k_P, a function of Reynolds number only, and with $k_U = k_{U0} = \sigma^2/2$ we have for laminar flow,

$$\begin{aligned} k_P &= \frac{1}{\sigma^2}\frac{L}{D}\frac{64}{\mathrm{Re}} \\ k_H &= \frac{1}{2}\frac{L}{D}\frac{64}{\mathrm{Re}} \end{aligned} \tag{12-14}$$

and for turbulent flow in smooth passages,

$$\begin{aligned} k_P &= \frac{1}{\sigma^2}\frac{L}{D}\frac{0.316}{\sqrt[4]{\mathrm{Re}}} \\ k_H &= \frac{1}{2}\frac{L}{D}\frac{0.316}{\sqrt[4]{\mathrm{Re}}} \end{aligned} \tag{12-15}$$

These equations show that for the heat transfer to be large the Reynolds number should be low (*i.e.*, the velocity should be low), the hydraulic diameter of the passages should be small, and the cooler block should be long.

Figure 12-3 shows some experimental results obtained from a cooler block with nominally *smooth* passages. k_H follows Eqs. (12-14) and (12-15) closely, with a transition from the laminar to the turbulent regime. k_P is higher than that given by Eqs. (12-14) and (12-15); this is typical of results obtained for rough-surfaced tubes, and indicates that the passages were not really smooth. Roughness increases the pressure drop but contributes practically nothing to the dissipation of heat. Consequently, the value of k_U (0.21) is lower than $\sigma^2/2$ (0.27 in this case). The effective roughness naturally increases as the passages become narrower, *i.e.*, as σ decreases. This is demonstrated by the results in Fig. 12-4 from a series of cooler blocks in which the passages were gradually narrowed and the number of ribs increased to reduce σ. With a given rib

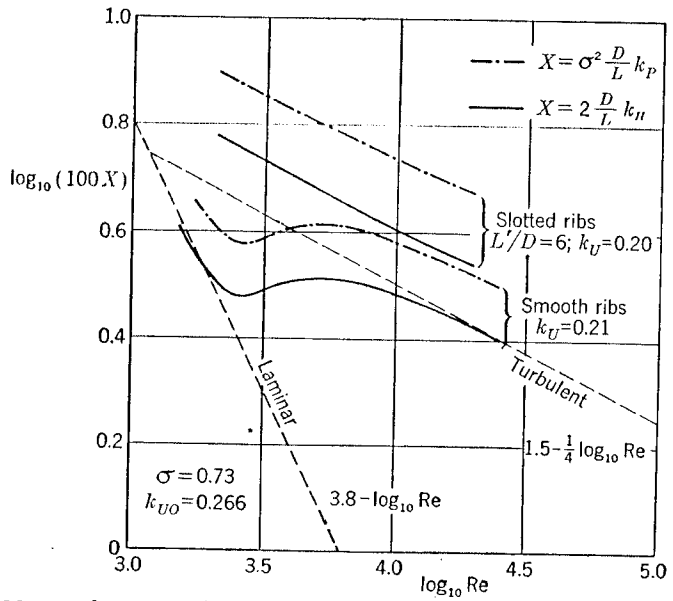

FIG. 12-3. Measured pressure drop and heat-transfer coefficients for two different heat-exchanger systems. (L' is the distance between adjacent slots.) From tests by W. Linke.

roughness, the effective roughness measured in terms of the hydraulic diameter increases as σ is reduced. This puts a practical limit to the method of increasing k_H by narrowing the passages.

The results in Fig. 12-4 were obtained from carefully made test specimens of copper; actual production blocks are usually not as good, in that roughness increases k_P even more, while k_H is slightly decreased (Fig. 12-5). This is to a small degree due to the block being made of light alloy, whose heat conductivity is less than that of copper. On the whole, it pays to avoid surface roughness, although we shall see later that the thermodynamic properties of the cooler block do not alone suffice to assess its suitability for practical use.

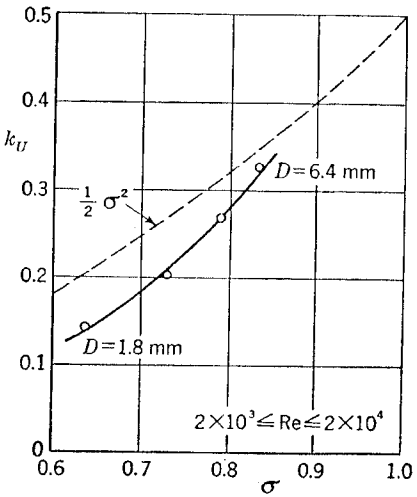

FIG. 12-4. Measured utilization coefficients for various heat-exchanger systems with *smooth* ribs.

The range of k_H can be appreciably extended beyond that which is attainable with coolers with straight

uninterrupted passages by the use of either slotted or corrugated ribs. A slot in the rib provides a new stagnation point, and a greater part of the rib will experience laminar flow, with low local Reynolds numbers. Thus k_H is increased locally, and may be higher for a complete block than that given by Eqs. (12-14) and (12-15) (see Fig. 12-3). k_P rises correspondingly but the utilization coefficient k_U is only slightly less than for a block with uninterrupted ribs (Fig. 12-5). A similar effect occurs when, in a block with several rows of tubes, the tubes are staggered. W. M. Kays and A. L. London (1950) obtained considerable improvements by such staggering.

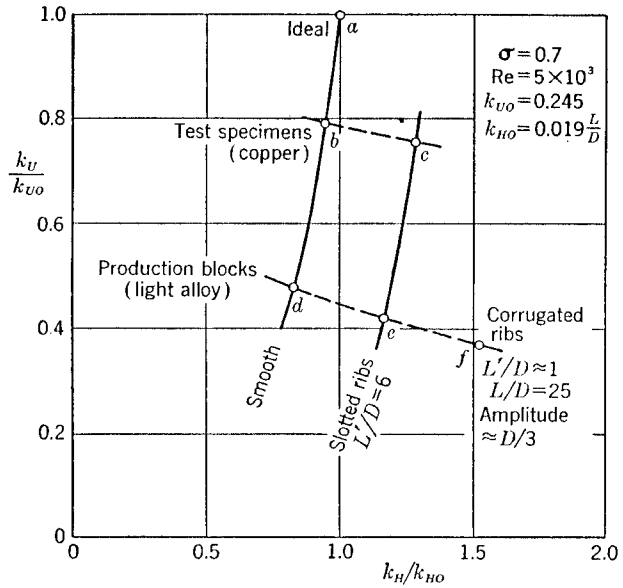

FIG. 12-5. Measured heat-transfer and utilization coefficients for various heat-exchanger systems. (L' is the distance between adjacent slots, or *wavelength* of corrugation.) From tests by W. Linke, 1944.

Corrugating the ribs produces a still greater effect on the heat transfer. The waves in the ribs (whose amplitude and length must be suitably chosen in relation to the hydraulic diameter of the tubes) increase the transverse motion in the flow and thus the heat transfer. There is again a slight reduction of k_U, but k_H is considerably higher.

There is no room here to extend this brief survey to a more detailed investigation of heat transfer or to the various special forms of heat exchangers, and the reader is referred to the textbooks on this subject. However, many technical cooling processes are essentially the same as that described here, and there will be no difficulty in applying the present methods to a more detailed treatment of the heat transfer on the coolant side, for instance. The transfer of heat in liquid coolants is much more rapid; in general, saturation is reached, that is, no more heat can be

transferred from the liquid to the walls because it cannot be dissipated on the air side. When the coolant is water, the pressure should be as high as possible so that the temperature (and thus T_W) can be raised without exceeding the boiling point.

Further problems are introduced by oil coolers. The viscosity of the oil depends on the temperature and increases so much with decreasing temperature that the oil near the cooled walls of the tubes may become viscous enough to block the flow there.

The heat transfer on the coolant side is particularly important if the *coolant* is another stream of air, as in the direct cooling of supercharger air. The wall temperature cannot then be assumed to be constant and it has to be taken into account whether the two air streams flow parallel in the same or the opposite direction or crosswise (see Sec. 12-8). The problems of heat conduction in the metal parts are usually of secondary importance.

We have not yet considered the further pressure drop caused by the supply of heat to a stream in a straight tube, in addition to that due to friction. This is essentially the same case as that treated in Sec. 7-3, where it was found that part of the heat energy is transformed into kinetic energy of the flow and that the pressure decreases accordingly. Using the same method as in Sec. 7-3 but including skin friction, assuming f to be independent of the temperature, (the Reynolds number does not vary very much because the product ρV remains constant for reasons of continuity), we obtain for the pressure drop of the *warm* heat exchanger:

$$\Delta p_w = p_{B1} - p_{B2} = \Delta p \frac{T_m}{T_{B1}} + \rho \left(\frac{V_B}{\sigma}\right)^2 \frac{T_{B2} - T_{B1}}{T_{B1}}$$

where Δp is the pressure drop of the *cold* heat exchanger, with $T_{B2} = T_m = T_{B1}$, and T_m the mean temperature of the air inside the passages. We introduce the pressure-drop coefficient k_{Pw} of the warm heat exchanger,

$$k_{Pw} = \frac{\Delta p_w}{\frac{1}{2}\rho V_B^2} = k_P \frac{T_m}{T_{B1}} + \frac{2}{\sigma^2} \frac{T_{B2} - T_{B1}}{T_{B1}} \tag{12-16}$$

and integrating $T(x)$ in Eq. (12-3) to obtain T_m, we find

$$k_{Pw} = k_P \left\{1 + \frac{T_W - T_{B1}}{T_{B1}} \left[1 - \left(1 - \frac{2k_U}{\sigma^2}\right) \frac{1 - e^{k_U k_P}}{k_U k_P}\right]\right\} \tag{12-17}$$

The term to be added to the cold value k_P has the character of a correction. It is largest if $k_U = \sigma^2/2$, in which case

$$k_{PW} = k_P \frac{T_W}{T_{B1}} \tag{12-18}$$

12-2. Cooler Block in Oblique Flow. The cooler block is very rarely installed in a flow that is everywhere normal to its face. There is usually

a diffuser upstream of the block, and the flow is at an incidence to the tubes or to the ribs, at least over part of the block. We shall consider first the simple case of parallel inflow at an angle α to the tubes, as shown in Fig. 12-6.

During the deflection from the inflow duct (of cross section A_i) to the wider cooler duct (of cross section A_B), the flow is retarded and the mean pressure should increase. In ideal flow, we obtain, from Bernoulli's equation,

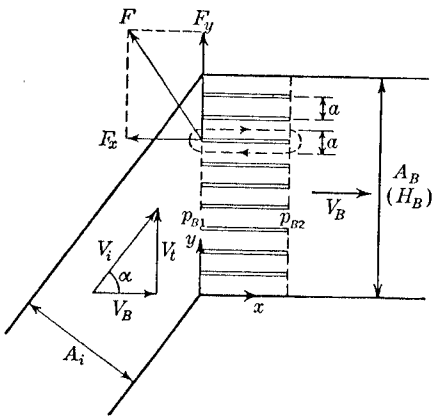

FIG. 12-6. Cooler block with inclined inflow duct.

$$\frac{p_{B1} - p_i}{\frac{1}{2}\rho V_B^2} = \tan^2\alpha = \left(\frac{V_t}{V_B}\right)^2 = \frac{1}{(A_i/A_B)^2} - 1 \qquad (12\text{-}19)$$

The pressure rise can be expressed in terms either of the angle of incidence or of the ratio of the tangential velocity V_t at the block face to the mean block velocity V_B, or of the duct-area expansion ratio.

The mechanism of the flow deflection round the corner can be interpreted in terms of a circulation round the tubes of the cooler which acts as a cascade of airfoils.[1] The circulation is such as to ensure a parallel outflow from the block in the direction of the tubes (see also Sec. 3-6). We obtain the circulation round a single element as the line integral of the velocity,

$$\Gamma = \oint V\,ds = aV_t$$

where a is the distance apart of the tubes. There is an aerodynamic force on the cascade elements. Its component parallel to the block face for an element of the spanwise extent b is given by the Kutta-Joukowsky law as

$$F_y = \rho V_B \Gamma b = \rho V_B V_t a b$$

For the mean value over the whole block, we can write the coefficient

$$C_y = \frac{\frac{H_B}{a}\int_0^a F_y\,dy}{\frac{1}{2}\rho V_B^2 A_B} = 2\frac{V_t}{V_B} = 2\tan\alpha \qquad (12\text{-}20)$$

The corresponding force component in the direction of the tubes is

$$F_x = -\rho\frac{V_t}{2}\Gamma b = -\frac{1}{2}\rho V_t^2 a b$$

[1] This property of the cooler block should be imitated also in model tests, and experiments using screens or baffles are obviously not representative.

with the coefficient

$$C_x = \frac{\frac{H_B}{a}\int_0^a F_x\,dy}{\frac{1}{2}\rho V_B^2 A_B} = -\left(\frac{V_t}{V_B}\right)^2 = -\tan^2\alpha \qquad (12\text{-}21)$$

This is a thrust force produced by local suctions at the leading edges of the block elements. It corresponds exactly to the pressure rise which results from the deflection of the flow, Eq. (12-19).

It cannot be expected that this pressure rise and the corresponding suction forces will be fully realized in practice, since present-day heat exchangers are not made with a view to sustaining suction forces. In the worst case, there is no suction at the leading edges of the elements, and the pressure loss is then higher than k_P in a straight duct by an amount given by Eq. (12-19). We distinguish, therefore, between the value k_{P0} measured in a straight duct at $\alpha = 0$ and the value

$$k_P\left(\mathrm{Re};\frac{A_i}{A_B}\right) = k_{P0}(\mathrm{Re}) + \Delta k_P\left(\mathrm{Re};\frac{A_i}{A_B}\right) \qquad (12\text{-}22)$$

when the inflow is oblique. When the whole of the suction is lost,

$$k_P^{(1)} = k_{P0} + \frac{1}{(A_i/A_B)^2} - 1 \qquad (12\text{-}23)$$

This estimate will be distinguished by the index (1) from another estimate to be derived presently.

Another estimate of the deflection loss, based on more favorable assumptions, was suggested by A. Betz (1943). It is assumed that the pressure increases without losses during the deflection as long as the pressure rise is less than the subsequent pressure drop in the block, that is, as long as no over-all pressure increase is required. It is further assumed that such an over-all increase in pressure will not occur in practice. This leads to a critical angle, or critical area ratio A_i/A_B, for which the pressure p_{B2} behind the block is equal to the pressure p_i in the inlet duct:

$$p_i = p_{B2} \quad \text{or} \quad \frac{p_{B1} - p_i}{\frac{1}{2}\rho V_B^2} = \frac{1}{(A_i/A_B)^2} - 1 = k_{P0}$$

so that

$$\left(\frac{A_i}{A_B}\right)_{\mathrm{crit}} = \frac{1}{\sqrt{1 + k_{P0}}} \qquad (12\text{-}24)$$

The over-all pressure drop is then

$$\begin{aligned} k_P^{(2)} &= k_{P0} && \text{for } \frac{A_i}{A_B} \geq \frac{1}{\sqrt{1 + k_{P0}}} \\ k_P^{(2)} &= \frac{1}{(A_i/A_B)^2} - 1 && \text{for } \frac{A_i}{A_B} \leq \frac{1}{\sqrt{1 + k_{P0}}} \end{aligned} \qquad (12\text{-}25)$$

This is denoted as estimate (2).

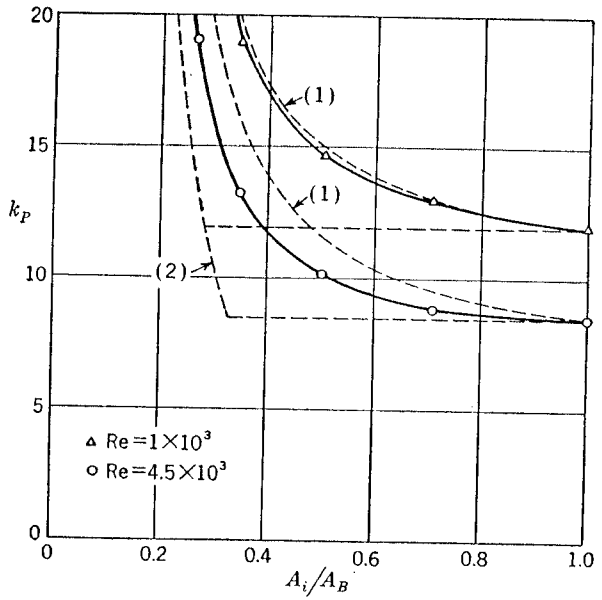

FIG. 12-7. Measured pressure-drop coefficients for a cooler block with inclined inflow duct as in Fig. 12-6.

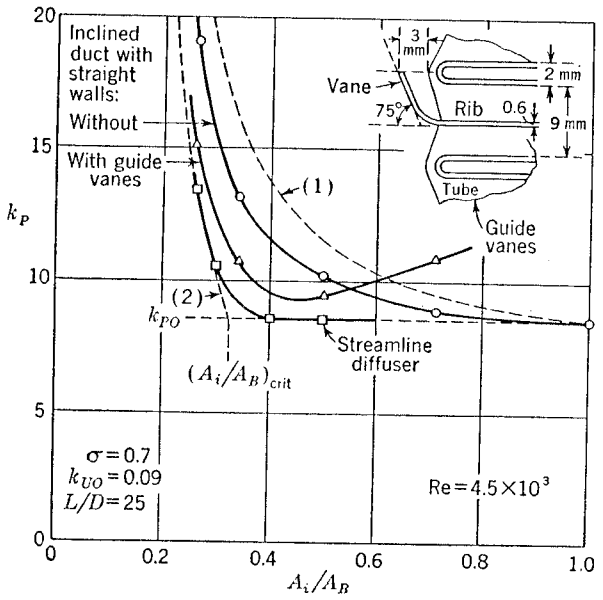

FIG. 12-8. Measured pressure-drop coefficients for a cooler block with various inflow ducts.

Figure 12-7 shows that these estimates give a useful indication of the actual losses[1]. Obviously, the deflection losses are not to be ignored. As Eq. (12-22) shows, they depend on the Reynolds number, and we find that at low Reynolds number the whole suction forces are completely lost.

The loss of the suction forces at the leading edges of the tubes implies that the flow breaks down there. Subsequent eddies improve the heat transfer, but only very slightly, and on the whole the value of k_H may be taken as that for a straight and not an inclined duct. The deflection loss Δk_P is therefore a genuine loss without any appreciable indirect compensation, and it should be kept as low as possible. Rounding off the edges and reducing the spacing of the tubes (a) are obvious means of making them more capable of sustaining suction forces. Another is the use of guide vanes; in some cases, these can easily be incorporated into the block design. Figure 12-8 gives an example; the loss curve comes fairly close to what was called estimate (2). In the case shown, the best working condition is at an angle of incidence of some 60°.

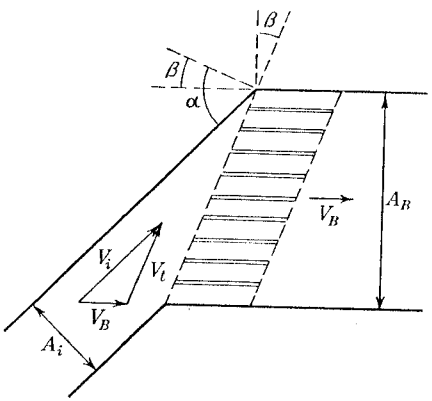

FIG. 12-9. Staggered cooler block with inclined inflow duct.

The suction forces can be slightly relieved at a given angle of incidence by staggering the block elements, as shown in Fig. 12-9. With the same method as above, we find that the suction forces are the same if

$$\tan \alpha_0 = \frac{\sin (\alpha - \beta)}{\cos \alpha}$$

where α_0 is the angle of incidence of the unstaggered block and α that of the staggered block with angle of stagger β as defined in Fig. 12-9. The corresponding relation for the area ratios is

$$\frac{A_i}{A_B} = \frac{A_{i0}/A_B}{\sqrt{2} \sin \beta (A_{i0}/A_B) \sqrt{1 - (A_{i0}/A_B)^2} + 1} \qquad (12\text{-}26)$$

according to which for the same block area A_B the inflow-duct area can be slightly smaller if the tubes are staggered. The reduction does not exceed

[1] The experimental value of k_P can easily be determined from the stagnation pressures H_i and H_{B2} in the ducts upstream and downstream of the cooler block, as measured by a pitot tube. In fact,

$$k_P = \frac{H_i - H_{B2}}{\frac{1}{2}\rho V_B^2}$$

for incompressible flow.

29 per cent, which is obtained in the extreme case $\beta = 90°$. It has been found experimentally, however, that staggering favors the realization of suction forces to a small extent, and the measured values of Δk_P approach the curve of estimate (2). This estimate, on the other hand, is not influenced by stagger as it only concerns the pressures.

12-3. Diffusers. Actual cooler installations in aircraft often have not straight but curved diffuser walls which are almost traditionally of sine-curve shape as in Fig. 12-10. The purpose of such a shape is to give the full pressure rise corresponding to the enlargement of the cross-section area upstream of the block, so that there is no pressure rise in the block entry. Experience has shown, however, that the aim is not achieved in

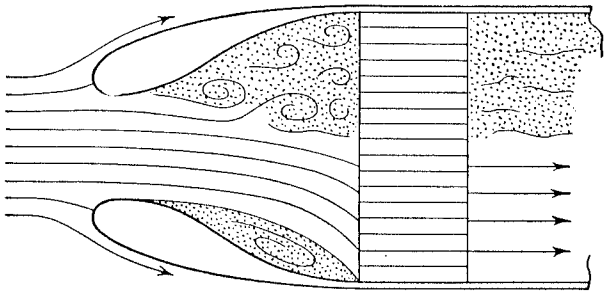

FIG. 12-10. Flow pattern in a conventional diffuser. From water-tunnel observations.

most cases because the adverse pressure gradient leads to a separation of the flow from the walls. In consequence, not only do pressure losses arise, but also the cooling effect is reduced because part of the block area is not utilized.

In contrast to this, it is possible to design diffuser walls at which there is no pressure rise. For this to be the case, the wall must be curved in such a way that the initial local pressure rise is completely balanced by centrifugal forces. The wall pressure is then constant and equal to that at the inlet cross section at the beginning of the diffuser (p_i). The pressure rise must be achieved in a sudden turn at the end of the diffuser. This implies that a constant-wall-pressure diffuser must have a cascade of airfoils behind it to turn the flow and to sustain the suction forces which correspond to the pressure rise. The angle through which the flow is turned varies across the block face; it is zero on the axis of symmetry (where the full pressure rise occurs upstream of the block) and highest at the ends (where the full pressure rise occurs during the deflection at the block entry). As the pressure rises from p_i to p_{B1} there, we find from Eq. (12-19) that the angle of maximum deflection is given by

$$\cos \alpha_{\max} = \frac{A_i}{A_B} \tag{12-27}$$

No actual worked-out example of diffuser contours with constant wall pressure is known to the authors. The hodograph method (for two-dimensional flow) or the method of singularities as explained in Chap. 3 should provide the tools needed for such a calculation.

What may be described as a compromise between a constant-wall-pressure diffuser and the conventional diffuser with inflexed walls is the

TABLE 12-1. COORDINATES OF STREAMLINE DIFFUSERS*

$\frac{x}{Y_B}$ \ $\frac{A_i}{A_B}$	Values of $\frac{y}{Y_B}$: 0.25	0.30	0.40	0.50
0.0	1.000	1.000	1.000	1.000
−0.1	0.769	0.797	0.847	0.886
−0.2	0.638	0.680	0.757	0.812
−0.3	0.561	0.608	0.694	0.761
−0.4	0.505	0.554	0.648	0.724
−0.5	0.463	0.515	0.613	0.694
−0.6	0.431	0.484	0.586	0.671
−0.7	0.405	0.459	0.563	0.651
−0.8	0.383	0.438	0.544	0.634
−0.9	0.365	0.420	0.526	0.618
−1.0	0.350	0.404	0.510	0.604
−1.2	0.328	0.384	0.489	0.585
−1.4	0.311	0.367	0.472	0.568
−1.6	0.297	0.353	0.456	0.553
−1.8	0.285	0.340	0.442	0.540
−2.0	0.275	0.329	0.430	0.529
−2.2	0.267	0.320	0.420	0.520
−2.4	0.260	0.312	0.412	0.512
−2.6	0.255	0.306	0.406	0.506
−2.8	0.252	0.302	0.402	0.502
−3.0	0.250	0.300	0.400	0.500
$\alpha_{\max}$	72°	68°	61°	54°

* See Fig. 12-11.

streamline diffuser. In Sec. 3-6 it was shown how the streamlines through the edges of a nonducted cooler block can be determined. If these streamlines are taken as the walls of the diffuser, the pressure along the wall is not constant but rises slowly though less than in the flow away from the walls. The coordinates of a systematic series of two-dimensional diffuser shapes are given in Table 12-1.[1] In tests on these shapes no flow separation could be detected. The measured wall pressures (see example

[1] The theoretical shapes have been slightly modified in order to avoid the vertical tangent at the block entry and to give a finite length.

in Fig. 12-11) show that the diffuser wall and the deflection at the block entry contribute equally to the total increase of pressure from p_i to p_{B1}. This "sharing of the burden" makes such streamline diffusers easily the best as regards efficient expansion. Figure 12-8 shows that the measured pressure losses follow the curve from estimate (2) closely.

The area ratio A_i/A_B is actually determined by the pressure-loss coefficient k_{P0} when the free streamline is chosen; it is given by Eq. (3-19),

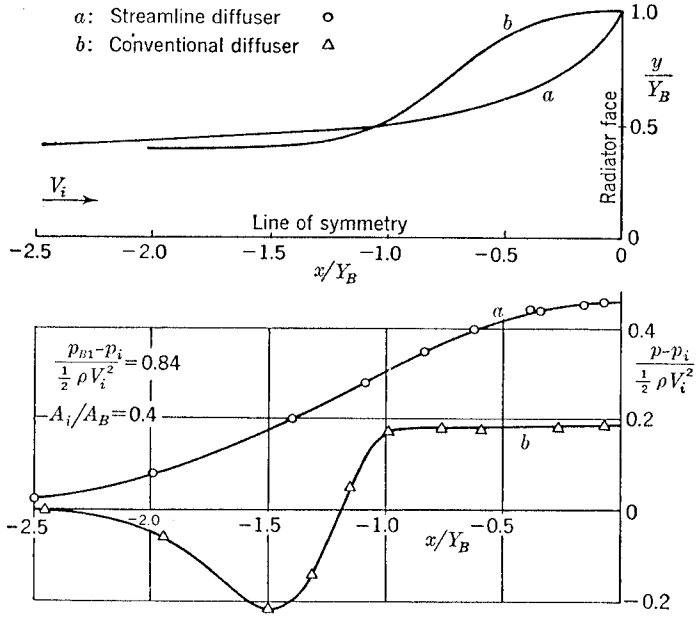

Fig. 12-11. Measured wall pressures for two different diffuser shapes.

which is the same as the critical area ratio obtained from Eq. (12-24). If A_i/A_B is smaller than this value (which is 0.32 in the case of Fig. 12-8), some additional losses Δk_P occur, due not to separation of the flow from the wall but to the angle of incidence at the outer parts of the block being too high, as a consequence of which the velocity in the outer passages is reduced and the velocity distribution across the block[1] is no longer uniform as it was when $\Delta k_P = 0$.

[1] The velocity distribution across the block, the uniformity of which is important for both heat transfer and pressure drop, is difficult to measure. The standard experimental methods (pitot-static tube, hot wire, etc.) often fail because of irregularities and fluctuations in the flow behind the block. The following method was suggested by E. von Holst, 1943, and has been found to be reliable. Small tubes of circular or square cross section are inserted into the passages at the rear end of the block (this will usually require some small part of the ribs to be cut away). Halfway along the inserted tube, whose length should be about three times its diameter, about half the cross-section area is blocked by a wall normal to the flow, for instance, diagonally. Pressure leads of hypodermic tubing end one on each side of this dividing wall, or orifice. The pressure difference between the two sides (which is conveniently large to be read accurately) can be calibrated to give the velocity by installing the block in a straight duct.

Several other types of diffuser shapes similar to these streamline diffusers but derived from simple geometric curves, such as parabolic arcs, have also been investigated experimentally. It was found that in general the pressure along the wall falls below p_i at the beginning of the curved part. An example is included in Fig. 12-11. The subsequent adverse pressure gradient must then be steeper, and the losses are usually higher than those of streamline diffusers. In the case of Fig. 12-11, $\Delta k_P = 0$ for the streamline diffuser and $\Delta k_P = 2$ for the conventional diffuser, at $k_{P0} = 8.4$.

Under favorable conditions such as may be realized in the laboratory, a flow similar to that along a streamline or constant-pressure contour may be obtained even if the wall shape is not that of a streamline. The lower part of Fig. 12-10 is an illustration of this. The flow separates from the wall but a free streamline is formed, sometimes enclosing a standing vortex. If the eddies are not carried downstream, no additional drag will result from them. A flow of this kind is supported by the stabilizing effect of the cooler block in the following way. Suppose that the flow separates from the diffuser wall and passes mainly through the middle part of the block. The velocity and therefore the pressure drop are then higher there than at the outer parts, and since the pressure behind the block is uniform, the pressure in front becomes higher in the middle. As a consequence of this, the flow tends to escape sidewise; more air flows again through the outer parts of the block, stabilizing the flow and to some extent preventing or delaying any complete breakdown. This is a general feature of the flow in ducts when, for some reason, there is a stage at which a pressure drop occurs. The natural *ram effect* of the obstacle causing the pressure drop can be used to design unconventional diffuser shapes of high efficiency.

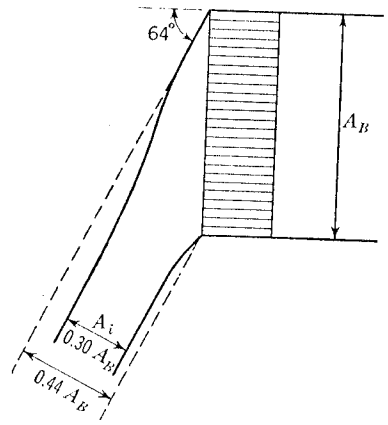

Fig. 12-12. Cooler block with straight and streamline inclined inflow ducts which give about the same losses.

The use of streamline diffusers is not limited to the symmetrical case. Any other streamline of the free flow about the nonducted cooler block may be used as a wall. Tests where the straight center line was taken as

the second diffuser wall (this has the highest pressure gradient) gave results only slightly inferior to the symmetrical diffuser. The mean direction of the flow may alternatively be inclined to the block as in Fig. 12-12. In the case shown, the upper wall has a slight inflection so that excessively high angles of deflection at the upper part of the block are avoided. It was found that the losses were again about the same as those for the symmetrical streamline diffuser in Fig. 12-8 and estimate (2). This means that nothing can be gained by inclining the diffuser unless such a geometric configuration brings about some other advantage in the layout of the installation (see Sec. 12-7).

12-4. Duct Behind the Cooler Block. In practical installations, the duct downstream of the block usually contracts as far as the exit of the

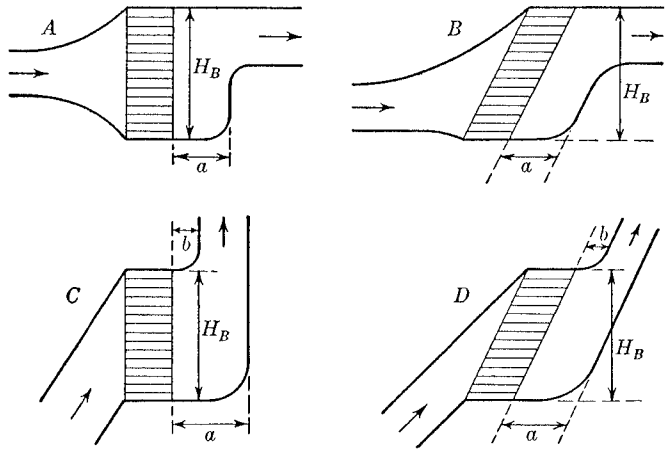

FIG. 12-13. Possible duct shapes behind the block.

fairing. Because of this, energy losses in the duct itself are generally low, unless it is curved, or unless the skin friction is unduly increased by high local velocities, or unless other obstacles such as bars or rods needed to operate an exit flap cause additional drag. There can nevertheless be a considerable reaction on the flow through the cooler block, which may increase the pressure-loss coefficient and possibly reduce the heat exchange. In the following, therefore, we shall consider the outflow duct and the cooler block together.

When the flow leaves the block, its direction is determined by the direction of the block elements. This constitutes a fundamental difference between the outflow and the inflow. Note the similarity to the flow about airfoils. In the duct the flow direction is changed. We distinguish between two cases: (1) The flow is contracted but its mean direction is unchanged (examples *A* and *B* in Fig. 12-13); (2) The flow is not only contracted but also deflected (examples *C* and *D* in Fig. 12-13). In both

cases, the natural shape of the duct is given by the boundary streamlines of the block in a free stream for a given direction of the flow far behind the block. Thus any nozzle-shaped contraction of the duct of other than streamline shape will influence the flow through the block, in particular

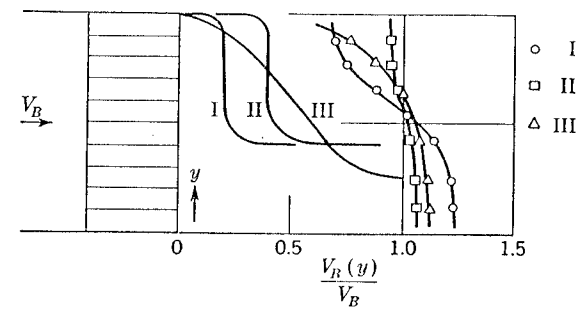

FIG. 12-14. Measured velocity distributions across a cooler block for various duct shapes behind the block.

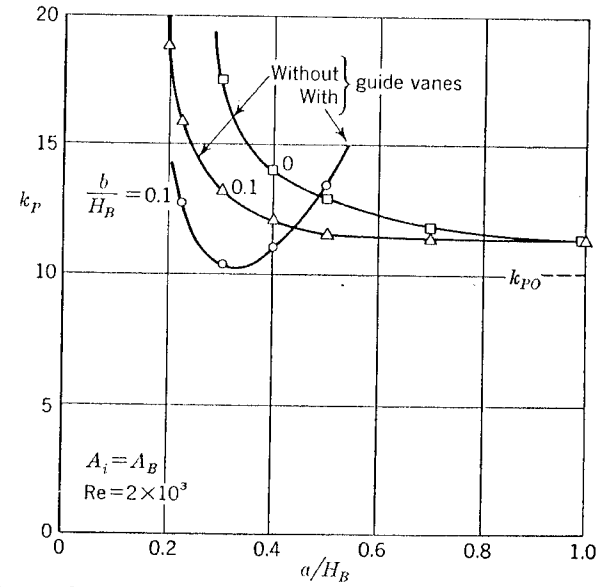

FIG. 12-15. Measured pressure-drop coefficients due to a curved duct behind the block. Guide vanes at the exit similar to those in Fig. 12-8.

the velocity distribution. Any additional deflection of the flow will add to the difficulties.

The examples in Fig. 12-14 show the extent of the effect of the outflow-duct shape on the velocity distribution across the cooler block. The pressure-loss coefficient is increased by $\Delta k_P = 6$ in case I, $\Delta k_P = 1$ in case II, and $\Delta k_P = 2$ in case III, for $k_{P0} = 8.4$. Figure 12-15 gives some experimental results for a deflecting duct similar to *C* in Fig. 12-13. A

rounded shoulder fairing on the inner bend, with height b at least 0.1 of the height of the block, is found to be essential, and guide vanes at the block exit can substantially improve the flow.

If there is also an expansion upstream of the cooler block (oblique inflow, diffuser, etc.), mutual interference between the upstream and downstream flows tends to increase the energy losses appreciably. Any nonuniformity of the flow caused by the outflow duct may upset the stabilizing effect of the block on the inflow, mentioned above, and thus

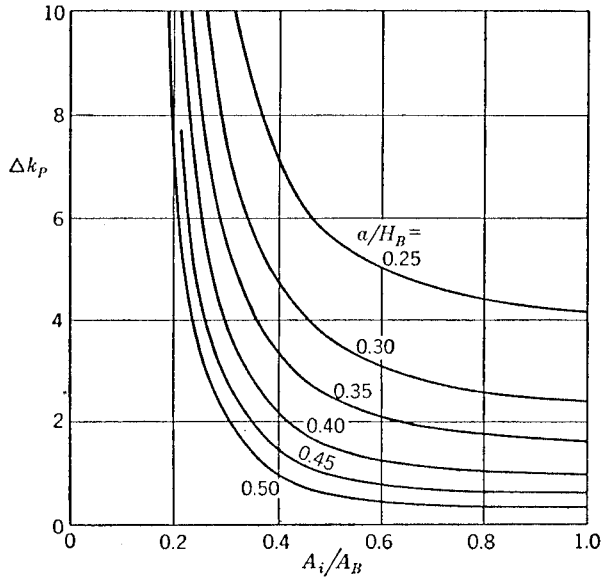

FIG. 12-16. Chart for the determination of pressure losses due to the duct behind the cooler block, for arrangements as in Fig. 12-13.

cause inflow losses in excess of those obtained with parallel outflow. Losses due to the outflow duct therefore rise steeply at small values of the area ratio A_i/A_B.

A parameter which measures one of the most important characteristics of the outflow duct is the distance a of the main deflection wall from the block exit, expressed as a fraction of the block height, in the direction of the flow through the cooler, as shown in Fig. 12-13. Approximate mean values of Δk_P from a series of tests which included all the arrangements shown in Fig. 12-13 are plotted in Fig. 12-16. Only the losses in the outflow duct and such interference losses as are caused by the outflow duct are included, and not the ordinary diffuser losses upstream of the block treated in the previous sections. To a first approximation, the Δk_P terms due to the inflow and the outflow can be added.

In a practical installation, the sum of the additional pressure losses Δk_P may be quite large compared with the k_{P0} of the block in a straight

parallel duct. It is therefore not sufficient to assess the suitability of a particular heat-exchanger system merely on a thermodynamical basis from laboratory tests on the block in a straight duct.

12-5. Determination of the Cooler Area. We now consider the installed cooler as a whole. Figure 12-17 shows the block surrounded by a fairing, with a flap or similar device to vary the exit area A_e and control the flow of air through the cooler. For the inflow up to the inlet opening and the external flow past the fairing, Chaps. 4 and 5 may be consulted; the flow phenomena inside the fairing are as described in the preceding sections.

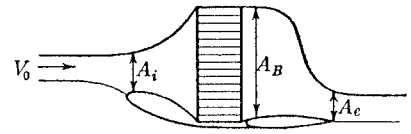

FIG. 12-17. Diagrammatic illustration of an installed cooler block.

The quantity of heat Q dissipated by the cooler depends on the weight of the air that flows through the block and on its temperature rise. By integrating dQ from Eq. (12-2) and using Eqs. (12-4) and (12-13), we obtain

$$Q = \begin{cases} c_p g \rho_B V_B A_B (T_{B2} - T_{B1}) \\ c_p g \rho_B V_B A_B (T_W - T_{B1})(1 - e^{-k_H}) \\ c_p g \rho_B V_B A_B (T_W - T_{B1})(1 - e^{-k_U k_{P0}}) \end{cases} \tag{12-28}$$

Under given flight conditions, c_p, g, ρ_B, and T_{B1} have given values (if we disregard compressibility effects for the moment), and Q, T_W, k_U, and k_{P0} are known for a given engine and a given heat-exchanger system. Then V_B and A_B remain to be determined.

The mean velocity in the cooler duct is fixed by the fact that only the kinetic energy of the main stream is available to force the air through the duct and cooler block against their various pressure losses. This is expressed by the energy equation

$$p_0 + \frac{1}{2}\rho V_0^2 - \left[(1 - \eta_i)\frac{1}{2}\rho V_0^2 + (k_{P0} + \Delta k_P)\frac{1}{2}\rho V_B^2\right] = p_e + \frac{1}{2}\rho V_B^2 \left(\frac{A_B}{A_e}\right)^2$$

in which account has been taken of possible inflow losses before the air enters the fairing, expressed by

$$\eta_i = 1 - \frac{\Delta H_i}{\frac{1}{2}\rho V_0^2} \neq 1$$

(see Sec. 9-2). It follows

$$\frac{V_B}{V_0} = \sqrt{\frac{\eta_i - \frac{p_e - p_0}{\frac{1}{2}\rho V_0^2}}{k_{P0} + \Delta k_P + (A_B/A_e)^2}} \tag{12-29}$$

This relation has been plotted in Fig. 12-18, for $\eta_i = 1$ and $p_e = p_0$. Negative pressures at the exit ($p_e < p_0$) will increase the mass flow beyond that shown in Fig. 12-18 (see Sec. 5-6). It will be seen from Fig. 12-18 that the velocity ratio V_B/V_0 is limited to a range which becomes smaller as the internal losses increase. In general, the velocity ratios V_B/V_0 are smaller than the velocity ratios that occur in jet engines, and this stronger retardation of the flow is partly responsible for the greater difficulties encountered with the installation of coolers. Further, because

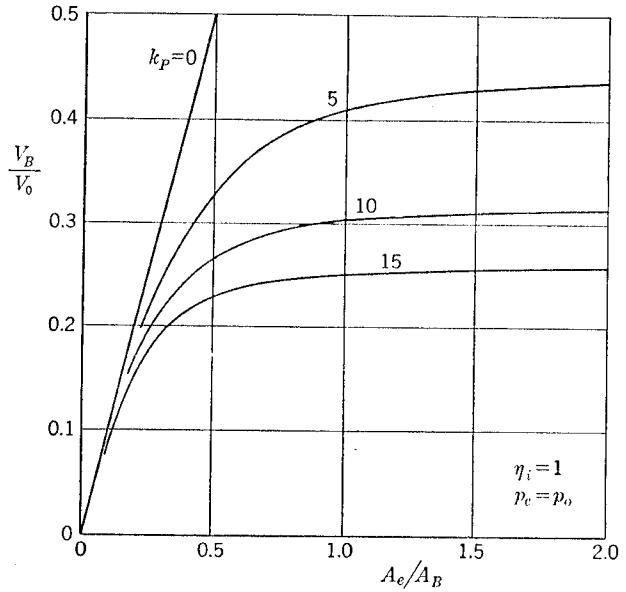

FIG. 12-18. Variation of the velocity ratio in a cooling plant with the exit area ratio and the internal pressure losses.

of the flattening of the V_B/V_0 curves as the exit area is increased, very little is gained by opening the exit beyond $A_e/A_B = 1$, say. The maximum velocity ratio is that for an infinitely large exit opening, and is equal to $1/\sqrt{k_P}$; thus V_B cannot be greater than $V_0/\sqrt{k_P}$.

Since the product $V_B A_B$ appears in Eq. (12-28), the absolute value of V_B should be as high as possible for A_B to be kept small. On the other hand, V_B is proportional to the flight speed, and the cooling plant must be laid out for the lowest flight speed $V_0{}^*$ at which effective cooling is to be guaranteed (climb conditions, for instance). The necessary frontal area of the cooler block is then, by Eqs. (12-28) and (12-29),

$$A_B = \frac{Q}{c_p g \rho (T_W - T_{B1}) V_0{}^*} \sqrt{\frac{k_{P0} + \Delta k_P + (A_B/A_e)^2}{\eta_i - \dfrac{p_e - p_0}{\frac{1}{2}\rho V_0{}^{*2}}}} \frac{1}{1 - e^{-k_U k_{P0}}} \qquad (12\text{-}30)$$

In the determination of A_B, the heat-exchanger system mainly affects the values of k_{P0} and k_U; the installation determines η_i, Δk_P, $p_e - p_0$, and A_e/A_B; the rest of the parameters depend on the engine and on the flight conditions. The characteristics of the system depend on the Reynolds number and thus on V_B; the final value of V_B from Eq. (12-29) must therefore be found by successive approximations.

Since it is the cooler-block area which is decisive in determining the size of the cooling plant, a careful consideration of all the parameters which influence A_B must be made if a satisfactory design is to be achieved. Without going into a detailed account of a design calculation, we shall discuss here how their relative importance can be assessed.

The block area is a minimum for a certain value of k_{P0} given by $\partial A_B/\partial k_{P0} = 0$,

$$1 - e^{-k_U k_{P0}} \left\{ 1 + 2k_U \left[k_{P0} + \Delta k_P + \left(\frac{A_B}{A_e} \right)^2 \right] \right\} = 0 \qquad (12\text{-}31)$$

This is a consequence of the opposing influences of thermodynamic and aerodynamic factors: Values of k_{P0} larger than the optimum increase the heat transfer ($k_H = k_U k_{P0}$) but reduce the mass flow [Eq. (12-29)], and vice versa. Again, the smallest area is obtained when $A_e/A_B \to \infty$ and $\Delta k_P = 0$, for which

$$1 - e^{-k_U k_{P0}}(1 + 2k_U k_{P0}) = 1 - e^{-k_H}(1 + 2k_H) = 0 \qquad (12\text{-}32)$$

from Eq. (12-31). This gives a fixed $k_H = 1.26$, or $k_{P0} = 1.26/k_U$. It also gives a limit to the desirable temperature increase,[1] Eq. (12-4),

$$\frac{T_{B2} - T_{B1}}{T_W - T_{B1}} = 1 - e^{-k_H} = 0.716$$

The block area in the optimum case is now

$$A_{B\,\mathrm{opt}} = \frac{Q}{c_p g \rho (T_W - T_{B1}) V_0{}^*} \frac{1.57}{\sqrt{k_U}} \qquad (12\text{-}33)$$

depending only on the utilization coefficient k_U, as far as the heat-exchanger system is concerned. In the best case, $k_U = \sigma^2/2$ [see Eqs. (12-12) and (12-13)], so that the minimum block area is

$$A_{B0} = \frac{Q}{c_p g \rho (T_W - T_{B1}) V_0{}^*} \frac{2.22}{\sigma} \qquad (12\text{-}34)$$

Figure 12-19 (case I) shows for the various systems of Fig. 12-5 how the block area must be enlarged beyond the minimum size to compensate for the shortcomings of actual heat-exchanger systems.

[1] Because this temperature ratio is less than unity, we have refrained from calling it the "efficiency" of the heat exchanger, as can be often found in the literature.

For the optimum value $k_H = 1.26$ to be obtained, a certain block length is needed. With the *ideal* values, k_{H0}, from Eqs. (12-14) and (12-15),

$$\left(\frac{L}{D}\right)_0 = 0.0393 \text{ Re} \qquad \text{for laminar flow} \qquad (12\text{-}35)$$

$$\left(\frac{L}{D}\right)_0 = 7.98 \sqrt[4]{\text{Re}} \qquad \text{for turbulent flow} \qquad (12\text{-}36)$$

The actual values of L/D can be reduced (or increased) in the same ratio

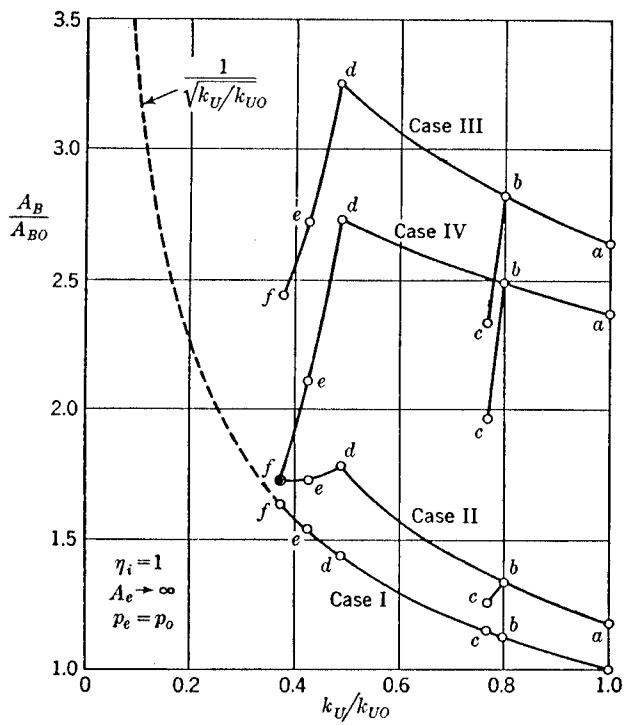

FIG. 12-19. Calculated cooler block areas for the heat-exchanger systems of Fig. 12-5. Case I, optimum length, no internal duct losses, $\Delta k_P = 0$. Case II, $L/D = 25$; $\Delta k_P = 0$. Case III, $L/D = 25$; $\Delta k_P{}^{(1)} = 7.9$ for $A_i/A_B = \frac{1}{3}$. Case IV, $L/D = 25$; $\Delta k_P{}^{(2)}$ from Eq. (12-25) for $A_i/A_B = \frac{1}{3}$.

as k_H is greater (or less) than k_{H0}. The following results are obtained for the heat-exchanger systems in Fig. 12-5:

System	*a*	*b*	*c*	*d*	*e*	*f*
L/L_0	1.00	1.05	0.78	1.21	0.86	0.66
L/D	67	71	52	81	58	44
$A_BL/A_{B0}L_0$	1.00	1.19	0.90	1.73	1.33	1.08

The table also contains optimum values of L/D obtained for fully turbulent flow at $\text{Re} = 5 \times 10^3$ with $k_{H0} = 0.0188L/D$. We find that

cooler blocks with slotted or corrugated ribs can be shorter than the ideal block. This influences the block volume and thus its weight. The volume increase beyond that of the ideal cooler is also given in the table above, again showing the benefit that can be obtained from slotted or corrugated ribs. The conception of an *ideal* smooth system thus loses in practical interest.

The optimum values of k_H and k_{P0} are different from those just given if there are internal losses Δk_P. To estimate the influence of the latter, we take the diffuser area ratio as the critical ratio given by Eq. (12-24). Diffuser and deflection losses are then either zero [for estimate (2)] or $\Delta k_P = k_{P0}$ [for estimate (1), Eq. (12-23)]. With the latter value, the optimum condition (12-31) reads, again with $A_e \to \infty$,

$$1 - e^{-k_U k_{P0}}(1 + 4k_U k_{P0}) = 1 - e^{-k_H}(1 + 4k_H) = 0$$

so that $k_H = 2.33$ and $(T_{B2} - T_{B1})/(T_W - T_{B1}) = 0.903$. The heat-transfer coefficient and also $k_{P0} = 2.33/k_U$ must be higher when there are internal losses; and the air temperature must be increased to obtain small block areas. The actual block areas

$$A_B = \frac{Q}{c_p g \rho (T_W - T_{B1}) V_0^*} \frac{2.27}{\sqrt{k_U}} = 1.44 A_B(\Delta k_P = 0) \qquad (12\text{-}37)$$

are, however, considerably higher than those for $\Delta k_P = 0$ given by Eq. (12-33). The optimum length of the block is increased by the factor $2.33/1.26 = 1.85$, and the volume and weight even more by the factor $1.44 \times 1.85 = 2.66$. These figures show that the losses in the internal duct are of at least as much importance for the size of the cooling plant as the thermodynamic properties of the heat-exchanger system.

It is not always possible to give the block the optimum length in an actual installation. For instance, ring coolers with radial flow (see Sec. 12-7) require a short block to keep the over-all diameter reasonably low. As a further example, therefore, we consider a case where L/D is fixed, say $L/D = 25$, and distinguish between the state with no internal losses (case II in Fig. 12-19), the state where the internal losses follow estimate (1), case III, and the state where they follow estimate (2), case IV. The inlet area ratio of the cowl may be fixed at $A_i/A_B = \frac{1}{3}$ throughout. We find a moderate increase in block area due to the deviation from the optimum length if there are no internal losses. With internal losses, however, a considerable increase of the block area is necessary. The advantages gained by using heat-exchanger systems with large heat transfer (slotted or corrugated ribs), even at the price of a reduction in the utilization coefficient k_U, and the gain which results from restricting internal losses to those of estimate (2), are quite apparent.

The influence of the other parameters, such as η_i, $p_e - p_0$, etc., on the size of the cooler block can easily be assessed from Eq. (12-30). The

flight altitude for which the cooling plant is designed is another important factor. The Reynolds number usually decreases slightly with increasing altitude. More important is the change in density ρ of the air which influences the block area in proportion to $1/\rho$. This would mean a considerable increase of the block area if it were not usually offset by an increase in the design speed V_0*; also, the atmospheric temperature T_0, and thus T_{B1}, is considerably lower at high altitude. On the other hand, the temperature of the coolant, and thus T_W, may be slightly reduced as the design altitude is raised, to prevent evaporation in the coolant circuit because of the lower atmospheric pressure. In an actual design, the geographical latitude in which the aircraft is likely to operate is also important, as it influences the air temperature at the block entry. Flight in the tropics obviously produces the worst conditions.

The assumption of incompressible flow which has been made so far is not always justifiable in practice. The compressible-flow relations corresponding to those of the preceding sections are clumsy but can readily be obtained by applying the methods of Sec. 4-3. It is sufficient in many cases to apply only the compressibility corrections which mainly concern the density and temperature at the block entry. For their magnitude, consider the extreme case $V_B = 0$. Assuming the air to be a perfect gas, we obtain from the energy equation [see Eqs. (2-11) and (2-16)]

$$T_{B1} - T_0 = \frac{V_0^2}{2c_p g} \tag{12-38}$$

Then the factor in Eq. (12-30) becomes

$$\frac{Q}{c_p g \rho_0 (T_W - T_{B1}) V_0} = \frac{\dfrac{k-1}{\rho_0 a_0^3} Q}{M_0 \left(\dfrac{T_W - T_0}{T_0} - \dfrac{k-1}{2} M_0^2 \right)} \tag{12-39}$$

depending on the flight Mach number. The compressibility correction may be not very large at the design speed (climb) but becomes more important in level flight; it thus concerns the mass-flow regulation and the necessary exit area rather than the block area.

12-6. Cooling Power Loss. In performing its function of dissipating heat energy from the engine to the free stream, the cooling plant produces propulsive forces by converting that energy into kinetic energy (see Sec. 2-6). Against this, energy losses due to friction in the cooler block and along the surfaces of the cowl produce a drag force in the process, and the total force D in the direction of flight may well be a drag force. Considering the cooling plant as part of the engine, we express the cooling power loss (or gain) DV_0 in terms of the heat Q to be dissipated:

$$DV_0 = KQ \tag{12-40}$$

Now the heat Q can be written as a certain fraction h of $\eta_P P$, where P is the engine power and η_P the propulsive efficiency (of the propeller, for instance). The power available for propulsion is then $\eta_P P - KQ$. Dividing this by the total energy E supplied to the engine per unit time, we obtain the over-all efficiency of the propulsion unit

$$\eta = \frac{\eta_P P - KQ}{E} = \frac{P}{E} \eta_P \left(1 - \frac{KQ}{\eta_P P} \right)$$

which can be written as

$$\eta = \eta_M \eta_P \eta_C \tag{12-41}$$

where $\eta_M = P/E$ is the efficiency of the motor itself, and η_C is the efficiency of the cooler,

$$\eta_C = 1 - hK \tag{12-42}$$

For Otto-cycle piston engines of present-day aircraft, h is of the order of $\frac{1}{2}$; the heat dissipated is about half of the propulsive power of the propeller.

To estimate the thrust due to the heat input, we simplify the actual process into a constant-pressure process (see Sec. 2-2) which has the thermal efficiency

$$\eta_{th} = 1 - \frac{T_0}{T_{B1}} \tag{12-43}$$

Ignoring other losses in the "jet," we may put

$$-DV_0 = \eta_{th} Q = Q \left(1 - \frac{T_0}{T_{B1}} \right)$$

so that

$$K = \frac{DV_0}{Q} = -\eta_{th} \tag{12-44}$$

In the extreme case $V_B = 0$, the temperature ratio in Eq. (12-43) is given by Eq. (12-38). Hence

$$K = \frac{-V_0^2}{2c_p g T_{B1}} = -\frac{\dfrac{k-1}{2} M_0^2}{1 + \dfrac{k-1}{2} M_0^2} \tag{12-45}$$

and

$$\eta_C = 1 + h \frac{\dfrac{k-1}{2} M_0^2}{1 + \dfrac{k-1}{2} M_0^2} \tag{12-46}$$

In the absence of any cooling-plant drag, the over-all efficiency of the engine would thus be increased by the factor $\eta_C = 1.034$ for $M_0 = 0.6$ and $\eta_C = 1.057$ for $M_0 = 0.8$. These values are low because the heat-input process at the low pressures available is not very efficient.

To estimate the cooling-plant drag, the factor K can be expressed as

$$K = \frac{DV_0}{Q} = C_D \frac{1}{2}\rho V_0^3 \frac{A_B}{Q} \tag{12-47}$$

where C_D is a drag coefficient based on the cooler-block area and $\frac{1}{2}\rho V_0^2$. The value of A_B/Q is given by Eq. (12-30). Using the minimum block area A_{B0} from Eq. (12-34), we have

$$K = \frac{2.22}{c_p g \rho^* (T_W - T_{B1}) V_0 {}^* \sigma} \frac{1}{2}\rho V_B^3 \frac{A_B}{A_{B0}} \frac{C_D}{(V_B/V_0)^3} \tag{12-48}$$

and

$$\eta_C = 1 - h \frac{1.11 V_B^3}{c_p g (T_W - T_{B1}) V_0 {}^* \sigma} \frac{\rho}{\rho^*} \frac{A_B}{A_{B0}} \frac{C_D}{(V_B/V_0)^3} \tag{12-49}$$

This is a convenient form from which to deduce the influence of the various parameters.

The ratio A_B/A_{B0} was discussed in the preceding section (see Fig. 12–19). It is mainly the term $C_D/(V_B/V_0)^3$ that we shall have to consider. A representative value for the factor by which it is multiplied is 0.0025, so that

$$\eta_C = 1 - 0.0025 \frac{C_D}{(V_B/V_0)^3} \tag{12-50}$$

Under unfavorable conditions (large internal losses, high altitude, etc.), this factor may be about twice as large.

The energy equation and the momentum theorem give for the (incompressible) flow through the cooler due to the pressure drop across it

$$C_D = \frac{D}{\frac{1}{2}\rho V_0^2 A_B} = 2\frac{V_B}{V_0}\left[1 - \sqrt{\eta_i - (k_{P0} + \Delta k_P)\left(\frac{V_B}{V_0}\right)^2}\right] \tag{12-51}$$

where the velocity ratio is given by Eq. (12-29). Since V_B/V_0 is small in high-speed flight, a Taylor expansion gives the following approximation, for $\eta_i = 1$:

$$C_D = (k_{P0} + \Delta k_P)\left(\frac{V_B}{V_0}\right)^3 = k_P \left(\frac{V_B}{V_0}\right)^3 \tag{12-52}$$

and Eq. (12-50) then becomes

$$\eta_C = 1 - 0.0025 k_P \tag{12-53}$$

As k_P is of the order of 10, this reduction of the cooler efficiency is only a few per cent, which is easily compensated by the increase in over-all efficiency due to the propulsive force generated by the cooler [Eq. (12-46)].

The low drag given by Eq. (12-51) is, however, the resultant of very much larger internal forces which almost balance out. These are the friction drag in the block, the thrust forces at the block entry and on the diffuser walls, the thrust force on the external surface of the air intake, and the drag force on the inner walls of the nozzle behind the block.

The friction drag in the block gives

$$\frac{C_D}{(V_B/V_0)^3} = \frac{k_{P0}}{V_B/V_0} \tag{12-54}$$

and the diffuser and cascade thrust together give

$$\frac{C_D}{(V_B/V_0)^3} = -\frac{(A_B/A_i - 1)^2}{V_B/V_0} \tag{12-55}$$

Both increase in inverse proportion to V_B/V_0. The thrust at the nose of the air intake is given by Eqs. (4-4) and (4-40) as

$$\frac{C_D}{(V_B/V_0)^3} = -\frac{A_i}{A_B}\frac{\left(\frac{V_0}{V_B} - \frac{A_B}{A_i}\right)^2}{V_B/V_0} \tag{12-56}$$

As an example, let $k_{P0} = 8$, $V_B/V_0 = 0.1$, and $A_i/A_B = \frac{1}{3}$. The cooler efficiency is then reduced by about 2 per cent in the ideal case [Eq. (12-53)]. The reduction due to the friction forces in the block is ten times as great [Eq. (12-54)]; it is compensated, however, by the diffuser thrust, which is five times as great [Eq. (12-55)], and by the intake thrust, which is twenty times as great [Eq. (12-56)]. Thus the friction drag is overcompensated, and a drag force in the nozzle of magnitude about fifteen times the total provides the balance. It is obvious that this equilibrium is seriously disturbed if one or several of the components are not realized in full. For instance, if the diffuser (or cascade) thrust is not realized, the reduction of the cooler efficiency is not 2 per cent but 10 per cent; if the suction force at the intake is not realized, the reduction of the cooler efficiency amounts to 40 per cent. This illustrates how important it is to design the block entry, diffuser, and fairing as nearly aerodynamically perfect as possible, especially for high-speed aircraft, for the terms are proportional to the flight speed.

In high-speed flight, the inflow efficiency η_i may also have a noticeable influence on the drag. With the numerical data above, a figure of $\eta_i = 0.9$ would lead to a reduction of the cooler efficiency by about 5 per cent instead of the 2 per cent for $\eta_i = 1$.

Finally, the contributions of the skin friction and form drag of the fairing must be considered. If the frontal area of the aircraft is increased by A_m by the cooler installation, the additional external drag of the cooling plant may be expressed by a drag coefficient, referred to $\frac{1}{2}\rho V_0^2$ and A_m, of the order 0.05 for aerodynamically good fairing shapes but possibly as

much as 0.1 if less care has been taken. The drag term in Eq. (12-50) is then

$$\frac{C_D}{(V_B/V_0)^3} = \frac{0.05(A_m/A_B)}{(V_B/V_0)^3} \tag{12-57}$$

As explained in Sec. 4-2, a certain minimum frontal area is needed to cope with the suction forces at the intake if the local velocity is to be low enough for adverse Mach number effects to be avoided. Equation (4-6) gives the necessary ratio of A_m to the inlet area A_i. The value of A_i/A_m should be as low as possible; from this point of view it may be advisable on high-speed aircraft to reduce the inlet area, even at the expense of further internal losses, so as to keep down the frontal area of the cowl and thus its

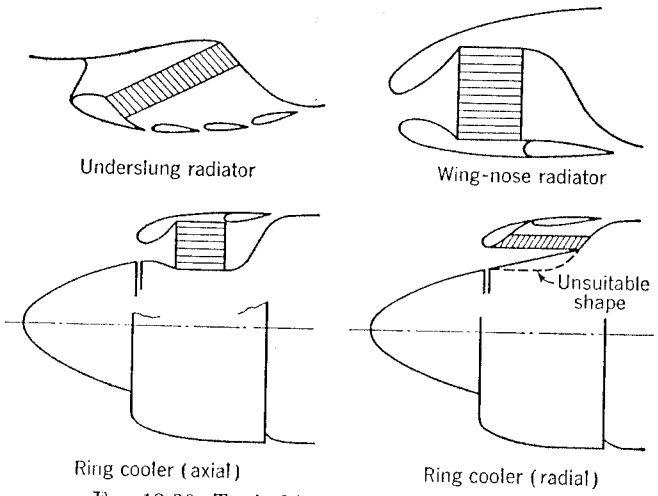

FIG. 12-20. Typical installation arrangements.

external drag. For an estimate of the external drag, let $A_i/A_B = \frac{1}{3}$ and $A_m/A_i = 3$, so that $A_m = A_B$; then the cooler efficiency is reduced by about 12 per cent for $V_B/V_0 = 0.1$. It is therefore advantageous to have the cooler buried (in the wing nose, for instance), to reduce the additional frontal area and thus A_m/A_B.

In general, we find that the cooler efficiency can reduce the over-all propulsive efficiency of a power plant considerably, by a factor of the same order as the efficiency of the propeller, especially in high-speed aircraft and at high altitudes. It may be concluded that the high cooling power loss is one of the chief pioneers of jet propulsion, since jet propulsion can do without a cooling plant!

12-7. Special Types of Installation. Although the cooling plant is an essential part of the engine, it is not always installed near the engine, and the cooler block may also be situated in the wing or underneath the

fuselage. Some typical ways of installing the cooler block are shown in Figs. 12-17 and 12-20. Only in the case of ring coolers is it possible to speak of an integration of the cooler into the propulsion unit (*power eggs*).

Underslung coolers on the fuselage or on the lower surface of the wing usually increase the frontal area of the aircraft, and their external drag is often appreciable. Being attached to a surface, the underslung cooler encounters all the difficulties associated with inflow along a wall (see Secs. 9-8 and 9-9), and it is necessary in most cases to separate the air inlet from the wall (thus increasing the frontal area again) or to use a boundary-layer by-pass. Although it improves the inflow, such a by-pass usually does very little to reduce the drag. Conventional underslung coolers, as in Fig. 12-17, often have a very uneven flow distribution through the block, with the velocity much lower near the wall than further away if a conventional reflexed diffuser wall is used (as in Fig. 12-10). This explains why the underslung type of cooler often needs to have a larger block area than aerodynamically more refined alternative installations. The cooler efficiency η_c is therefore rather low, as shown for a typical example in Fig. 12-21.

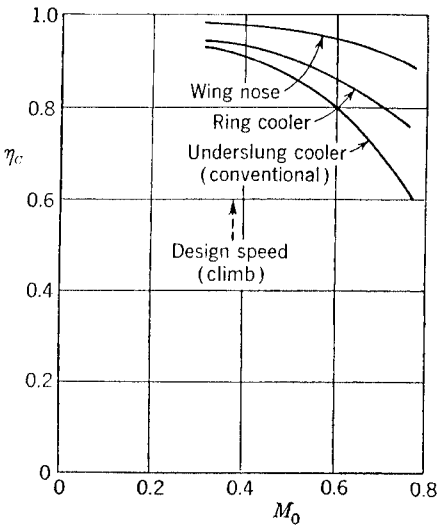

FIG. 12-21. Approximate over-all efficiencies of various cooler installations.

A more modern underslung cooler layout, by H. Voigt, is sketched in Fig. 12-20. The oblique setting of the block, together with a streamline diffuser (as in Fig. 12-12) reduces the frontal area as much as possible. Multiple flaps may provide effective regulation of the mass flow without unduly increasing the external drag, at the same time leaving a sufficiently wide duct behind the block. A cooler of this general type may be called for on high-altitude aircraft when the necessarily large block area prohibits effective burying inside the aircraft.

An aerodynamically more satisfying arrangement is the *nose cooler;* Fig. 12-20 shows a wing installation. The cooler block area required can be near the minimum, since $\eta_i = 1$ and $\Delta k_p = 0$ can be achieved by the use of a suitable diffuser area ratio together with a streamline diffuser and a sufficiently wide duct behind the block. There is usually room enough for the block to be of the optimum length. The flow through the cooler is, however, closely linked to the flow about the whole wing; for instance,

the static pressure at the exit is likely to increase as the incidence goes up, so that p_e may be greater than p_0 at the design point. Another undesirable property is the variation of the flow at the inlet caused by a change in the circulation about the wing. A slightly asymmetrical drooped diffuser and intake may suffice to ensure an inflow without losses in the main working range. The cooler efficiency of a well-designed wing-nose cooler is comparatively good up to fairly high speeds, as shown in Fig. 12-21.

Ring coolers have all the obvious advantages which result from proximity to the motor, among others short pipe lines and the possibility of rapid exchange of the whole propulsion unit. Ring coolers with axial flow may have an internal duct with low losses,[1] and the block length is not restricted as it is for ring coolers with radial or diagonal flow, where it is particularly difficult to achieve uniform flow through the block. With an unsuitably shaped wall (dotted line in Fig. 12-20), most of the air flows through the rear end of the block and the front part remains practically unused. The wall must be shaped to induce a constant radial velocity over the whole block (slightly convex for bodies of revolution); but on the other hand the block elements are then likely to be at high incidence. It may be advisable to stagger them. Radial coolers require larger flap chords than axial coolers for the duct downstream of the block to be wide enough (at least under the design conditions with flaps open). Several design studies have shown, contrary to expectations, that the radial ring cooler does not necessarily have a greater over-all diameter than the axial cooler, and that in some cases it may even be shorter than the latter. For military purposes, the radial cooler is more easily protected against bullets.

Ring coolers in general have the disadvantage that the approaching boundary layer on the spinner cannot easily be diverted and will cause inflow losses (see Sec. 9-8). There is also a mutual interference between cooler and propeller, which may, however, be beneficial if the propeller is designed (with cuffs, for instance) to increase the mass flow through the block, especially under climb conditions when it is most wanted. Ring coolers are also clearly the most suited to the application of *forced cooling* by means of an auxiliary blower.[2]

Ring coolers have much in common with the *direct cooling* of piston engines with radial cylinder arrangements. The inflow conditions and

[1] Streamline diffusers for ring coolers may be calculated by the methods described in Sec. 3-6.

[2] We refrain here from discussing forced cooling. Obviously any increase of pressure obtained by means of a blower or fan has the twofold effect of adding to the ram pressure of the free stream and forcing the air through the cooler duct (which may result in a considerable reduction of the cooler block area), and also in increasing the thermal efficiency of the conversion of heat energy into propulsive work.

the shape and the task of the cowl are the same. There is again a compression upstream of the cylinders, and the duct shape there should be similar to the streamlines of the free flow round them. The chief differences lie in the cooling process itself and in the flow behind the cylinders.

There is no intermediary liquid between the cylinders and the cooling air, but direct contact between the two. The heat-transfer coefficient is lower, and local overheating of the cylinders is not as easy to avoid as when they are surrounded by a liquid coolant, whose large latent heat of vaporization has a balancing effect. The air-cooled cylinder therefore has a more irregular temperature distribution than the liquid-cooled cylinder, and the cylinder temperature is appreciably higher. The latter is an advantage from the cooling point of view, because it makes the temperature difference higher. Ribs are used to increase the surface area of the cylinders, but their number and height are limited by the manufacturing process. Providing slots in the ribs or producing artificial turbulence has brought about some improvement in the heat transfer. Baffles round the individual cylinders to guide the air round to the back are essential since otherwise the rear surface would scarcely be cooled because of flow separation from the cylinder. One of the main sources of pressure loss inside the duct is the sudden expansion behind the cylinders or the baffles which cannot easily be avoided.

As the cooler area is fixed, the rate of dissipation of heat can only be regulated by controlling the mass flow. Forced cooling by a fan is therefore particularly attractive. Another effective means of increasing the mass flow is the NACA nose-slot cowling, where the cooling air is released from a slot at the fairing nose in a region of high negative pressure.

The relative merits of liquid- and air-cooled aircraft engines, in particular their respective cooling power losses, are the subject of a controversy of long standing; it cannot be said that it has yet been satisfactorily solved. Clearly some of the main advantages of the air-cooled engine—its simplicity, robustness, economy in space and weight, and easier maintenance—are outside aerodynamic jurisdiction.

Finally, *surface cooling*, which so far has found very little application to aircraft, may be mentioned. The most important method uses vaporization cooling. The coolant is water, which is heated beyond its boiling point under high pressure, and evaporates after leaving the engine. Heat is thus taken from the cylinders as latent heat of evaporization. The greater part of the vapor is then led along inside the surface of the aircraft (on the wing, for instance) and there condensed, the heat being delivered through the skin to the free air stream. Aerodynamically, the principal feature is the heat transfer from the surface, the treatment of which goes beyond the scope of this book, however. On the whole this method of cooling is promising, because there need be no cooling power loss. Its

main drawbacks are structural difficulties and the fact that, in the case of small aircraft (fighters, etc.), the whole wing area would not provide a large enough cooling surface, and an ordinary heat exchanger would still be needed, at least as an auxiliary.

12-8. Intercooling. The use of heat exchangers is not restricted to the liquid cooling of piston engines described in the preceding sections. We have already seen in Chap. 2 how the exchange of heat between the hot exhaust gases and the comparatively cold air ahead of the combustion chamber can improve the thermal efficiency of a turbojet engine. Another application is possible on piston engines with superchargers. The pressure of the air is increased by a compressor before it is supplied to the motor, mainly to counteract the decrease in atmospheric pressure at high altitudes, but the temperature rise in the compressor is undesirable from the point of view of engine efficiency. In each of these applications heat is exchanged between one stream of air and another.

There are several ways in which this can be done. One uses an intermediary liquid coolant: Heat is transferred from the stream of air to a liquid by means of an ordinary cooler block, and in a second block the heat is transferred to a cold stream of air. Such indirect cooling involves two blocks but has obvious advantages: The blocks can be conveniently situated; the pressure drop in the air passages can be kept comparatively low; and the pipe lines for the liquid present no particular difficulties. The actual heat-exchange process is basically as described above.

A second possibility is the use of regenerators. The hot and the cold streams of air pass side by side, and a permeable heat-collecting mass is periodically moved from one stream into the other, accumulating heat in the hot stream and delivering it to the cold stream. This is obviously a very different kind of process from what has been dealt with so far; we must refer the reader to special papers on the subject, some of which are mentioned in the Bibliography at the end of the chapter. The regenerator method of heat exchange appears particularly suitable for stationary turbine engines but will be difficult to apply to aircraft power plants because of its weight and bulk.

A third method is the direct exchange of heat between the hot and the cold air in one block. With the same medium on the two sides of the dividing metal walls, we can no longer assume that the wall temperature is constant and must now take into account the directions of the two streams, *i.e.*, whether they flow in the same direction (parallel flow), in opposite directions (counterflow), or at right angles to one another (crossflow).

Let the hot stream of air (subscript h) and the cold stream of air (subscript c) flow in the same or in opposite directions through interspersed passages of the same length L and let weights W_h and W_c pass

through the two sides per unit time. Corresponding to Eqs. (12-1) and (12-2), the heat transferred can be written as

$$dQ = k_{Hh}c_pW_h[T_h(x) - T_c(x)]d\left(\frac{x}{L}\right) = \mp c_pW_h\,dT_h(x) \quad (12\text{-}58)$$

for the hot air, and

$$dQ = k_{Hc}c_pW_c[T_h(x) - T_c(x)]d\left(\frac{x}{L}\right) = c_pW_c\,dT_c(x) \quad (12\text{-}59)$$

for the cold air, the latter absorbing the same amount as is delivered from the former. The coordinate x is measured from the block entry on the cold side, so that the upper sign in Eq. (12-58) holds for parallel flow and the lower sign for counterflow.

We see immediately that the ratio of the weights of air must be the inverse of the ratio of the heat-transfer coefficients,

$$\frac{W_h}{W_c} = \frac{k_{Hc}}{k_{Hh}} \quad (12\text{-}60)$$

If this value were exceeded on one side (for instance, because of an increase in the velocity), the excess would pass unused, the amount of heat being fixed by what the other side can take or deliver.

Equations (12-58) and (12-59) can be resolved into two differential equations for the separate temperature distributions:

$$\frac{dT_h(x)}{dx} = \mp\frac{k_{Hh}}{L}[T_h(x) - T_c(x)] \quad (12\text{-}61)$$

$$\frac{dT_c(x)}{dx} = \frac{k_{Hc}}{L}[T_h(x) - T_c(x)] \quad (12\text{-}62)$$

and another for the local temperature difference:

$$\frac{d[T_h(x) - T_c(x)]}{dx} = \left(\mp\frac{k_{Hh}}{L} - \frac{k_{Hc}}{L}\right)[T_h(x) - T_c(x)] \quad (12\text{-}63)$$

As for Eq. (12-3), the solutions are

$$T_h(x) - T_c(x) = \Delta T \exp\left(-k_{Hh} - k_{Hc}\right)\frac{x}{L} \quad (12\text{-}64)$$

for parallel flow, and

$$T_h(x) - T_c(x) = (\Delta T + T_{h2} - T_{h1}) \exp\left(k_{Hh} - k_{Hc}\right)\frac{x}{L} \quad (12\text{-}65)$$

for counterflow. These differ from one another also because of the different boundary conditions (as above, subscript 1 designates conditions at the respective entries of the streams and subscript 2 at the exits; ΔT is the given initial temperature difference $T_{h1} - T_{c1}$).

Inserting the solutions (12-64) and (12-65) into the differential equa-

tions (12-61) and (12-62) and solving gives

$$T_h(x) = T_{h1} - \frac{k_{Hh}}{k_{Hh} + k_{Hc}} \Delta T \left[1 - \exp\left(-k_{Hh} - k_{Hc}\right) \frac{x}{L}\right] \tag{12-66}$$

and

$$T_c(x) = T_{c1} + \frac{k_{Hc}}{k_{Hh} + k_{Hc}} \Delta T \left[1 - \exp\left(-k_{Hh} - k_{Hc}\right) \frac{x}{L}\right] \tag{12-67}$$

for parallel flow. In this case, the temperatures approach one another exponentially, as shown in Fig. 12-22.

For the counterflow heat exchanger in the same way we obtain, after some algebraic transformations,

$$T_h(x) = T_{h2} + \frac{k_{Hh}}{k_{Hh} - k_{Hc}} \Delta T \frac{\exp\left(k_{Hh} - k_{Hc}\right) \frac{x}{L} - 1}{1 + \frac{k_{Hh}}{k_{Hh} - k_{Hc}} \left[\exp\left(k_{Hh} - k_{Hc}\right) - 1\right]} \tag{12-68}$$

and

$$T_c(x) = T_{c1} + \frac{k_{Hc}}{k_{Hh} - k_{Hc}} \Delta T \frac{\exp\left(k_{Hh} - k_{Hc}\right) \frac{x}{L} - 1}{1 + \frac{k_{Hh}}{k_{Hh} - k_{Hc}} \left[\exp\left(k_{Hh} - k_{Hc}\right) - 1\right]} \tag{12-69}$$

The temperature distribution in a counterflow heat exchanger is thus quite different from that in a parallel-flow heat exchanger, as is illustrated by the example of Fig. 12-22.

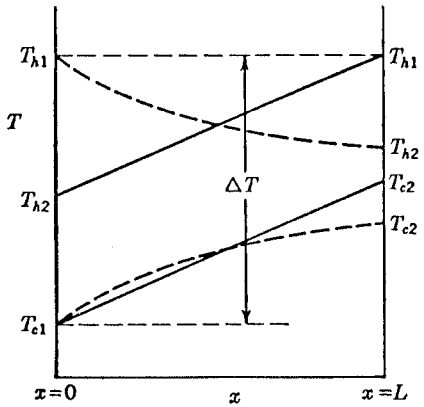

FIG. 12-22. Temperature distributions in heat exchangers. Dotted lines, parallel flow; full lines, counterflow.

A better insight may be gained by considering some special cases. First, let $W_h \gg W_c$, so that $k_{Hh} \ll k_{Hc}$ [Eq. (12-60)]. This occurs if the hot stream has a much greater density than the cold stream (for instance, if water and air are used), or if a hot air stream has a much higher velocity and if also the hot stream passages are much wider than those of the cold air so as to give very small values of k_{Hh}. In the extreme case $k_{Hh} \to 0$, we have $T_{h2} = T_{h1} = T_W = \text{const}$, that is, constant wall temperature, for both parallel flow and counterflow. Equations (12-67) and (12-69) for the temperature distribution on the cold side then both reduce to Eq. (12-3).

Similarly at the other extreme $W_c \gg W_h$ and $k_{Hc} \ll k_{Hh}$, we have a constant temperature on the cold side, and the difference between end and initial temperatures in the hot stream is the same again for both parallel flows and counterflows:

$$T_{h2} - T_{h1} = -\Delta T[1 - \exp\left(-k_H\right)] \tag{12-70}$$

Since the total amount of heat transferred is given by

$$Q = c_p W_h (T_{h2} - T_{h1}) \tag{12-71}$$

[Eq. (12-58)], this is the condition in which the maximum amount of heat is taken from the hot stream for a given weight flow W_h per unit time. For $k_H \to \infty$, we get $T_{h2} - T_{h1} = -\Delta T$ and $Q = -c_p W_h \Delta T$; that is, the full initial temperature difference is utilized.

Between these two extremes is the more likely practical case where $W_h = W_c$ and thus $k_{Hh} = k_{Hc} = k_H$. We now have different expressions for parallel-flow and counterflow heat exchangers,

$$T_{h2} - T_{h1} = -\frac{\Delta T}{2}\left[1 - \exp\left(-2k_H\right)\right] \tag{12-72}$$

and

$$T_{c2} - T_{c1} = +\frac{\Delta T}{2}\left[1 - \exp\left(-2k_H\right)\right] \tag{12-73}$$

for parallel flow; and

$$T_{h2} - T_{h1} = -\Delta T \frac{k_H}{1 + k_H} \tag{12-74}$$

and

$$T_{c2} - T_{c1} = +\Delta T \frac{k_H}{1 + k_H} \tag{12-75}$$

for counterflow, with the temperature difference between the hot and cold streams now constant everywhere. The heat exchange is larger with counterflow than with parallel flow. For instance, when $k_H = 1$, $T_{h2} - T_{h1} = -0.43\Delta T$ for parallel flow and $-0.5\Delta T$ for counterflow. The maximum values of the temperature reduction, for $k_H \to \infty$, differ by a factor of 2; $T_{h2} - T_{h1} = -\Delta T/2$ for parallel flow and $-\Delta T$ for counterflow; the counterflow heat exchanger appears superior throughout the whole range.

In practice, both types present very difficult ducting problems since curved ducts are needed at both ends of the heat-exchanger block to separate the two streams. This usually involves additional pressure losses which are not exploited for the heat transfer, and also an uneven distribution of the mass flow between the various passages. Cross-flow heat exchangers are obviously superior in this respect. They can be treated in the same way, the main difference being that two coordinates

must be used. The calculation has been carried out by W. Nusselt (1930).

The subsequent analysis of the installation of direct heat exchangers can proceed in a similar way to that described above for the simpler case of the cooler block with constant wall temperature. The problem is made particularly difficult by the fact that we have to distinguish between the values of σ on the two sides, the sum of which must necessarily be less than 1. This means that the pressure losses in one stream can only be reduced at the expense of the other [see Eq. (12-12)]. The design of such a heat exchanger must therefore always be related to the whole engine. In the case of supercharger intercooling, for instance, an excessive pressure drop on the hot air side[1] may easily offset the whole benefit of the cooling, however effective it may have been.

EXERCISES

12-1. Given two cooler blocks with the same pressure-drop coefficient $k_{P0} = 10$ and utilization coefficients $k_U = 0.1$ and 0.2, plot the temperature increase along the passages for a constant wall temperature $T_W = 380°\text{K}$ and an entry air temperature $T_{B1} = 310°\text{K}$. What are the end temperatures T_{B2} and the mean air temperatures

$$T_m = \frac{1}{L}\int_0^L T(x)\,dx$$

12-2. Calculate the correction to the pressure-drop coefficient due to heating for a cooler block in which when cold the pressure-drop coefficient $k_{P0} = 10$ and for which $k_U = 0.1$; $\sigma = 0.7$; $T_{B1} = 310°\text{K}$; $T_W = 380°\text{K}$.

12-3. Determine the force component F_x on a cooler block in the direction of the passages [Eq. (12-21)] by means of the momentum theorem, when the inflow duct is inclined by an angle α.

12-4. Determine the theoretical suction force F_x in the direction of the passages on a cooler block staggered by an angle β, in an inflow inclined at an angle α.

12-5. Given a two-dimensional, nonducted cooler block which is normal to the main stream and has a cylindrical wake, with a pressure-drop coefficient $k_{P0} = 10$, calculate the total drag and the cascade thrust. (A wind-tunnel test gave $V_B/V_0 = 0.3$ and, from the balance reading, $C_D = D/\frac{1}{2}\rho V_B^2 A_B = 4.8$.)

12-6. Compare the mean total pressure loss $p_{B2} - p_{B1}$ for various velocity distributions $V_B(y)$ over the height of a two-dimensional cooler block $-y_B \leq y \leq +y_B$, assuming the local pressure drop to be proportional to $V_B^2(y)$, for

a. $V_B(y) = V_B(1 + y/y_B)$
b. $V_B(y) = 0.5V_B$ for $-y_B \leq y < 0$
$V_B(y) = 1.5V_B$ for $0 < y \leq +y_B$
c. $V_B(y) = 0$ for $-y_B \leq y < 0$
$V_B(y) = 2V_B$ for $0 < y \leq +y_B$

12-7. Plot the ratio of the actual cooler-block area A_B to its optimum value according to Eq. (12-33) against k_{P0} for $k_U = 0.1$ and 0.2; $A_c/A_B = \infty$, $p_e = p_0$, $\eta_i = 1.0$, and $\Delta k_P = 0$.

[1] Note, however, that the decreasing temperature of the hot stream is accompanied by a rise of pressure, according to the considerations which lead to Eq. (12-16).

12-8. Determine the block areas for various installation conditions (as in Fig. 12-19), using as basic data the results from some of the heat exchanger systems investigated by W. M. Kays and A. L. London.

12-9. An air-air intercooler with $\sigma_h = \sigma_c/2$ has $k_{Hh} = 2k_{Hc} = 2$ and an initial temperature difference $\Delta T' = 100°\text{K}$. Determine the temperature distributions along the passages and the ideal pressure-drop coefficient, according to Eq. (12-12), for (*a*) parallel flow and (*b*) counterflow. Ignore the tube wall thickness.

BIBLIOGRAPHY

General:

Gröber, H., and S. Erk, "Die Grundgesetze der Wärmeübertragung," 2d ed., Springer-Verlag, Berlin, 1933.

Dryden, H. L., Aerodynamics of Cooling, in "Aerodynamic Theory," vol. 6, W. F. Durand, editor, Springer-Verlag, Berlin, 1934.

Jacob, M., "Heat Transfer," John Wiley & Sons, Inc., New York, 1949.

Eckert, E. R. G., "Introduction to the Transfer of Heat and Mass," McGraw-Hill Book Company, Inc., New York, 1950.

Kern, D. Q., "Process Heat Transfer," McGraw-Hill Book Company, Inc., New York, 1950.

Squire, H. B., Heat Transfer, in "Modern Developments in Fluid Dynamics," S. Goldstein, editor, vol. III, Oxford University Press, London and New York, 1951.

Küchemann, D., and J. Weber, *Cooling (AVA Monograph J_1), Brit. Min. of Supply (Völkenrode)* Rept. & Transl. 914–923, 1946.

Hartshorn, A. S., and L. F. Nicholson, Aerodynamics of Cooling Aircraft Reciprocating Engines, *Roy. Aircraft Est. Rept. Aero*, 2290, 1947.

Special Papers:

Meredith, F. W., Cooling of Aircraft Engines, *Aeronaut. Research Council Rept. & Mem.* 1683, 1935.

Weise, A., The Conversion of Energy in a Cooler, translation, *NACA TM* 867, 1937.

Norris, R. H., Concepts of Efficiency of Heat Transfer and Pressure Drop Relations in Heat Exchangers, *Proc. 5th Intern. Cong. Applied Mechanics*, Cambridge, Mass., 1938.

Winter, H., Theory of the Heated Ducted Cooler, translation, *NACA TM* 893, 1938.

von Karman, Th., The Analogy between Fluid Friction and Heat Transfer, *Trans. ASME*, vol. 61, p. 705, 1939.

Silverstein, A., J. N. Nielsen, and S. Katzoff, High Altitude Cooling, *NACA W. Rept.* 771–775.

Rubert, K. F., and G. S. Knopf, A Method for the Design of Cooling Systems for Aircraft Power-plant Installations, *NACA W. Rept.* L–491.

Nichols, M. R., Investigation of Flow through an Intercooler Set at Various Angles to the Supply Duct, *NACA W. Rept.* L–408.

Linke, W., Leichtmetall Systeme für Flüssigkeitskühlung, *Deut. Luftfahrtforschung* U.M. 6008, 1944.

Kays, W. M., Loss Coefficients for Abrupt Changes in Flow Cross Section with Low Reynolds Number Flow in Single and Multiple Tube Systems, *Trans. ASME*, vol. 72, p. 1067, 1950.

Kays, W. M., and A. L. London, Heat Transfer and Flow Friction Characteristics of Some Compact Heat Exchanger Surfaces, *Trans. ASME*, vol. 72, p. 1075, 1950.

Intercooling:

NUSSELT, W., Eine neue Formel für die Wärmeübertragung zwischen Kreuzströmen, *Mech. u. Thermodynamik*, vol. 1, p. 417, 1930.

REUTER, J. G., and M. F. VALERINO, Intercooler Cooling-air Weight Flow and Pressure Drop for Minimum Drag Loss, *NACA Rept.* 784, 1944.

SCHMIDT, E., The Design of Contra-flow Heat Exchangers, *Proc. Inst. Mech. Engrs. (London)*, vol. 159, p. 351, 1948.

Regenerators:

GLASER, H., and P. HENTRICH, The Constant-pressure Gas Turbine with Regenerators (*AVA Monograph P*), *Brit. Min. of Supply (Völkenrode) Rept. & Transl.* 1015–1019, 1946.

ILIFFE, C. E., Thermal Analysis of the Contra-flow Regenerative Heat Exchanger, *Proc. Inst. Mech. Engrs. (London)*, vol. 159, p. 363, 1948.

COX, M., and R. K. STEVENS, The Regenerative Heat Exchanger for Gas Turbine Power-plants, *Proc. Inst. Mech. Engrs. (London)*, vol. 163, p. 193, 1950.

APPENDIX

STREAM FUNCTION AND VELOCITY COMPONENTS FOR FREQUENTLY USED SINGULARITIES, WITH TABLES

In the course of this book the method of singularities is frequently used. Some of the singularities are of general interest, and are likely to be employed more often. Because very little information concerning their practical application is readily available, and to facilitate the actual use of their fields of flow, often described mathematically by unwieldy formulas, numerical tables are given for the properties of some of the more important distributions of sources and vortices. Those selected do not, of course, form a complete series in any way.

Since problems in the aerodynamics of propulsion are just as often axially symmetrical as two-dimensional, we treat the two cases in the same way and do not use the complex notation.

1. Three-dimensional Source. Fluid flows out of a point in all directions, and the volume that emerges in unit time is the strength of the source, denoted by E. The velocity is the same at all points on a sphere about the source as center, and thus

$$v = \frac{E}{4\pi r^2} \tag{1}$$

The velocity v has the direction of the radius vector. The streamlines are radii from the point source.

A sink is a source with negative strength; fluid flows into a point from all directions.

An arrangement of point sources along a line in the direction of the main stream gives an axially symmetrical flow. With a cylindrical coordinate system x, r, φ, a point source element at $x = a$, $r = 0$ induces the velocity components

$$v_x(x,r) = \frac{E}{4\pi} \frac{x - a}{\sqrt{(x - a)^2 + r^2}^3} \tag{2}$$

$$v_r(x,r) = \frac{E}{4\pi} \frac{r}{\sqrt{(x - a)^2 + r^2}^3} \tag{3}$$

and the stream function is

$$\Psi(x,r) = -\frac{E}{4\pi}\left(1 + \frac{x - a}{\sqrt{(x - a)^2 + r^2}}\right) = -\frac{E}{4\pi}(1 - \cos\vartheta) \tag{4}$$

where ϑ denotes the angle between the negative x axis and the radius vector from the source to the point (x,r). The concept of the stream function as used in two-dimensional potential flow is extended here to axially symmetrical flow; the quantity of fluid flowing between the stream surfaces $\Psi = 0$ and $\Psi = \Psi_0$ is $2\pi\Psi_0$.

Superposing the flow of a single source on a parallel flow,

$$V_x = V_0 \qquad V_r = 0 \qquad \Psi = \tfrac{1}{2}r^2V_0 \tag{5}$$

gives the flow about a body of revolution extending to infinity downstream. The streamline (or surface)

$$\Psi(x,r) = \frac{1}{2}r^2V_0 - \frac{E}{4\pi}\left(1 + \frac{x-a}{\sqrt{(x-a)^2 + r^2}}\right) = 0$$

represents the contour of the body, since the flow pattern remains unchanged if a stream surface is replaced by a solid boundary. The fluid from the source remains inside the body, filling it. The maximum body radius, far downstream, is given by

$$E = \pi R_B^2 V_0 \tag{6}$$

This indicates that the fluid from the source flows through the section πR_B^2 with velocity V_0. The pressure distribution along the body can be obtained by using Bernoulli's theorem, which gives for the pressure at any point (x,r)

$$\begin{aligned}\frac{p - p_0}{\frac{1}{2}\rho V_0^2} &= 1 - \left(\frac{V_x}{V_0}\right)^2 - \left(\frac{V_r}{V_0}\right)^2 \\ &= 1 - \left(1 + \frac{E}{4\pi V_0}\frac{x-a}{\sqrt{(x-a)^2 + r^2}^3}\right)^2 \\ &\quad - \left(\frac{E}{4\pi V_0}\frac{r}{\sqrt{(x-a)^2 + r^2}^3}\right)^2\end{aligned} \tag{7}$$

The velocity components and the stream function of a continuous distribution of sources of strength $q(x)$ per unit length on the axis between $x = a$ and $x = b$ can be obtained from Eqs. (2) to (4) by integration:

$$v_x(x,r) = \frac{1}{4\pi}\int_a^b q(x')\frac{x-x'}{\sqrt{(x-x')^2 + r^2}^3}\,dx' \tag{8}$$

$$v_r(x,r) = \frac{1}{4\pi}\int_a^b q(x')\frac{r}{\sqrt{(x-x')^2 + r^2}^3}\,dx' \tag{9}$$

$$\Psi(x,r) = -\frac{1}{4\pi}\int_a^b q(x')\left(1 + \frac{x-x'}{\sqrt{(x-x')^2 + r^2}}\right)dx' \tag{10}$$

M. Brand and F. Riegels (1944) have calculated velocity components and stream functions for some special source distributions (sectionally constant, linearly and quadratically increasing source strength), and given the results in diagrams.

2. Two-dimensional Source. Let sources of constant strength be distributed along an infinite straight line in the direction of the z axis, normal to the xy plane. Then the same flow conditions hold in every plane $z = \text{const}$, and the flow is two-dimensional in any such plane. The velocity is the same at all points on a circle with the source as center, and thus

$$v = \frac{Q}{2\pi r} \tag{11}$$

where Q is the volume that emerges in unit time from unit length of the source line. The velocity has again the direction of the radius vector, and the streamlines are radii from the source.

The velocity components in the x and y directions at (x,y) with a source at (a,b) are

$$v_x(x,y) = \frac{Q}{2\pi}\frac{x-a}{(x-a)^2 + (y-b)^2} \tag{12}$$

$$v_y(x,y) = \frac{Q}{2\pi}\frac{y-b}{(x-a)^2 + (y-b)^2} \tag{13}$$

and the stream function is[1]

$$\Psi(x,y) = -\frac{Q}{2\pi}\left(\pi - \arctan\frac{y-b}{x-a}\right) = -\frac{Q}{2\pi}\vartheta \tag{14}$$

where ϑ denotes the angle between the negative x axis and the radius vector from the source to the pivotal point (x,y). In this relation, the arc-tangent function is only determined apart from an integer multiple of π; this is connected with the fact that the value of the stream function changes by $Q2\pi/2\pi$ in a closed circuit about the source.

The relations (12) to (14) can of course also be obtained from the complex flow potential

$$F(z) = \frac{Q}{2\pi}\ln z$$

as explained in Sec. 3-2. The indeterminacy of the arc-tangent function here is the same as that of the logarithm function there.

The velocity field of any two- or three dimensional source distribution is continuous except at the sources themselves. If q is the strength of a continuous source distribution per unit area (or per unit length for distributions along lines in a two-dimensional field), the velocity component normal to the distribution changes discontinuously by an amount q

[1] This differs from the value given in Sec. 3-2 by the constant term $-Q\pi/2\pi$.

through the distribution, while the velocity component parallel to the distribution is continuous.

3. Vortex Element. There is no isolated "vortex" in three-dimensional flow corresponding to the isolated source, since only filaments either extending to infinity or closed can exist. The velocity field induced by any such vortex line can be determined from the Biot-Savart law, which states that an element of length ds of a vortex filament of strength Γ induces at a point P the velocity

$$dv = \frac{\Gamma}{4\pi} \frac{\sin \vartheta \, ds}{r^2} \tag{15}$$

where r is the distance from the element to P and ϑ the angle between the radius vector from the element to P and the direction of the vortex element; dv is normal to the plane which contains ds and P.

4. Two-dimensional Vortex. The flow with a straight vortex line of infinite length normal to the xy plane is the same in any plane $z = \text{const}$. Considering only the flow in such a plane, we speak of a two-dimensional vortex, or a point vortex. The Biot-Savart law gives the velocity components

$$v_x(x,y) = -\frac{\Gamma}{2\pi} \frac{y-b}{(x-a)^2 + (y-b)^2} \tag{16}$$

$$v_y(x,y) = \frac{\Gamma}{2\pi} \frac{x-a}{(x-a)^2 + (y-b)^2} \tag{17}$$

The streamlines are circles with the vortex as center. The vortex is called positive if the flow circulates about the point in the sense from the positive x axis to the positive y axis.

The stream function can be found by integrating the relations

$$v_x = \frac{\partial \Psi}{\partial y}$$

$$v_y = -\frac{\partial \Psi}{\partial x}$$

and is

$$\Psi(x,y) = -\frac{\Gamma}{4\pi} \ln [(x-a)^2 + (y-b)^2] \tag{18}$$

Formulas (16) to (18) can also be derived from the complex flow potential

$$F(z) = -i \frac{\Gamma}{2\pi} \ln z$$

as discussed in Sec. 3-2.

The velocity components and the stream function of any vortex distribution can be calculated by using either Eqs. (16) to (18) in the two-dimensional case or Eq. (15) as the contribution of an element in the

general case. The velocity field is continuous except at the position of the vortices. If γ is the vorticity per unit length of a continuous vortex distribution, the velocity tangential to the distribution changes discontinuously by an amount γ through the distribution, while the velocity component normal to it is continuous.

5. Vortex Ring. A vortex filament which forms a circle of radius r' is called a vortex ring. We use the coordinate systems x, r, φ and x, y, z, with x in the direction of the axis of the ring as in Fig. 1. The Biot-Savart law in vector notation[1] is

$$d\mathbf{v} = \frac{\Gamma}{4\pi} \frac{\mathbf{R} \times d\mathbf{s}}{R^3} \tag{19}$$

giving the velocity vector $d\mathbf{v}$ induced by an element of length $ds = r' \, d\varphi'$ of the vortex ring at the point (x,r,φ) or (x,y,z). $d\mathbf{s}/ds$ is the unit vector tangential to the vortex ring at the position of the vortex element. With the unit vectors **i, j, k** in the directions of the xyz axes, $d\mathbf{s}/ds$ can be written as

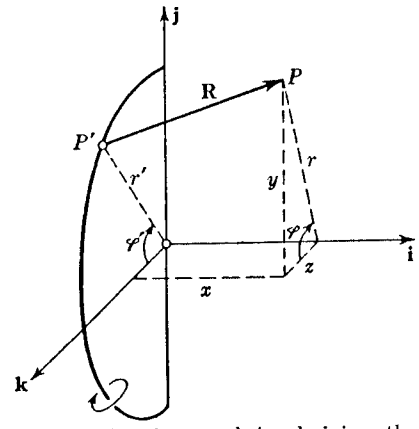

FIG. 1. Notation used in deriving the velocity components induced by a vortex ring.

$$\frac{d\mathbf{s}}{ds} = 0\mathbf{i} + \cos \varphi' \mathbf{j} - \sin \varphi' \mathbf{k} \tag{20}$$

R is the radius vector from the vortex element to the pivotal point:

$$\mathbf{R} = x\mathbf{i} + (r \sin \varphi - r' \sin \varphi')\mathbf{j} + (r \cos \varphi - r' \cos \varphi')\mathbf{k} \tag{21}$$

with

$$R = \sqrt{x^2 + r^2 + r'^2 - 2rr' \cos (\varphi - \varphi')} \tag{22}$$

Hence,

$$\begin{aligned} \mathbf{R} \times \frac{d\mathbf{s}}{ds} &= -[\cos \varphi'(r \cos \varphi - r' \cos \varphi') + \sin \varphi'(r \sin \varphi - r' \sin \varphi')]\mathbf{i} \\ &\quad + x \sin \varphi' \mathbf{j} + x \cos \varphi' \mathbf{k} \\ &= -[r \cos (\varphi - \varphi') - r']\mathbf{i} + x \sin \varphi' \mathbf{j} + x \cos \varphi' \mathbf{k} \end{aligned} \tag{23}$$

The x component of the velocity induced by the whole vortex ring is obtained from an integration round the circumference:

$$v_{\gamma x}(x,r) = -\frac{\Gamma}{4\pi r'} \int_0^{2\pi} \frac{r \cos (\varphi - \varphi') - 1}{\sqrt{x^2 + r^2 + 1 - 2r \cos (\varphi - \varphi')^3}} \, d\varphi'$$

[1] We use the same notation here as is used, for instance, by J. C. Slater and N. H. Frank, 1933.

(x/r' and r/r' have been replaced by x and r for simplicity). The integral can be expressed conveniently by writing

$$v_{\gamma x}(x,r) = -\frac{\Gamma}{4\pi r'}\frac{1}{\sqrt{x^2+(r+1)^2\,[x^2+(r-1)^2]}}\,I_1$$

where

$$I_1 = \int_0^{2\pi} \frac{r\cos(\varphi-\varphi') - 1}{\sqrt{1-\dfrac{2r\,[\cos(\varphi-\varphi')+1]}{x^2+(r+1)^2}}\left\{1+\dfrac{2r[1-\cos(\varphi-\varphi')]}{x^2+(r-1)^2}\right\}}\,d\varphi'$$

Introducing

$$k^2 = \frac{4r}{x^2+(r+1)^2} \tag{24}$$

I_1 can be written as

$$I_1 = (1-k^2)\left\{\int_0^{2\pi} \frac{r\left[2\cos^2\dfrac{\varphi-\varphi'}{2}-1\right]}{\sqrt{1-k^2\cos^2\dfrac{\varphi-\varphi'}{2}}^3}\,d\varphi' \right.$$

$$\left. \int_0^{2\pi} \frac{d\varphi'}{\sqrt{1-k^2\cos^2\dfrac{\varphi-\varphi'}{2}}^3}\right\}$$

and these integrals can be reduced to complete elliptic integrals

$$\begin{aligned}
\mathsf{K}(k) &= \int_0^{\pi/2} \frac{1}{\sqrt{1-k^2\sin^2\alpha}}\,d\alpha \\
\mathsf{E}(k) &= \int_0^{\pi/2} \sqrt{1-k^2\sin^2\alpha}\,d\alpha \\
\mathsf{D}(k) &= \int_0^{\pi/2} \frac{\sin^2\alpha}{\sqrt{1-k^2\sin^2\alpha}}\,d\alpha = \frac{\mathsf{K}-\mathsf{E}}{k^2}
\end{aligned} \tag{25}$$

Using the relations[1]

$$\int_0^{\pi/2} \frac{1}{\sqrt{1-k^2\sin^2\alpha}^3}\,d\alpha = \frac{\mathsf{E}}{1-k^2}$$

$$\int_0^{\pi/2} \frac{\sin^2\alpha}{\sqrt{1-k^2\sin^2\alpha}^3}\,d\alpha = \frac{\mathsf{K}-\mathsf{D}}{1-k^2}$$

we obtain

$$I_1 = 2r\,4(\mathsf{K}-\mathsf{D}) - 4(r+1)\mathsf{E}$$

so that

$$v_{\gamma x}(x,r) = -\frac{\Gamma}{2\pi r'}\frac{4r(\mathsf{K}-\mathsf{D})-2(r+1)\mathsf{E}}{\sqrt{x^2+(r+1)^2\,[x^2+(r-1)^2]}}$$

and finally

$$v_{\gamma x}(x,r) = \frac{\Gamma}{2\pi r'}\frac{1}{\sqrt{x^2+(r+1)^2}}\left\{\mathsf{K}(k)-\left[1+\frac{2(r-1)}{x^2+(r-1)^2}\right]\mathsf{E}(k)\right\} \tag{26}$$

[1] See, for example, H. Jahnke and F. Emde, 1938.

The axial velocity component shows singular behavior at $x = 0$, $r = r' = 1$. Near this point it can be calculated by expanding the elliptic integrals in powers of $(1-k^2)$:

$$\mathsf{K} = \Lambda + \frac{\Lambda-1}{4}(1-k^2) + \tfrac{9}{64}(\Lambda-\tfrac{7}{6})(1-k^2)^2 + \cdots$$

$$\mathsf{E} = 1 + \tfrac{1}{2}(\Lambda-\tfrac{1}{2})(1-k^2) + \tfrac{3}{16}(\Lambda-\tfrac{13}{12})(1-k^2)^2 + \cdots$$

where

$$\Lambda = \ln\frac{4}{\sqrt{1-k^2}}$$

Values of $v_{\gamma x}(x,r)$ are tabulated[1] in Table 1.

The radial velocity component induced by a vortex ring is given by Eqs. (19) and (23):

$$\begin{aligned}
v_{\gamma r}(x,r) &= \frac{\Gamma}{4\pi r'}\int_0^{2\pi}\frac{x\cos\varphi'}{\sqrt{x^2+r^2+1-2r\cos(\varphi-\varphi')}^3}\,d\varphi' \\
&= \frac{\Gamma}{4\pi r'}\frac{x}{\sqrt{x^2+(r+1)^2\,[x^2+(r-1)^2]}}\,I_2
\end{aligned}$$

where

$$I_2 = \int_0^{2\pi}\frac{\cos\varphi'\,d\varphi'}{\sqrt{1-\dfrac{2r[\cos(\varphi-\varphi')+1]}{x^2+(r+1)^2}}\left\{1+\dfrac{2r[1-\cos(\varphi-\varphi')]}{x^2+(r-1)^2}\right\}}$$

Reducing I_2 to elliptic integrals,

$$v_{\gamma r}(x,r) = \frac{\Gamma}{2\pi r'}\frac{2x(2\mathsf{K}-2\mathsf{D}-\mathsf{E})}{\sqrt{x^2+(r+1)^2\,[x^2+(r-1)^2]}}$$

or

$$v_{\gamma r}(x,r) = \frac{\Gamma}{2\pi r'}\frac{-x}{r\sqrt{x^2+(r+1)^2}}\left\{\mathsf{K}(k)-\left[1+\frac{2r}{x^2+(r-1)^2}\right]\mathsf{E}(k)\right\} \tag{27}$$

Values of $v_{\gamma r}(x,r)$ are given in Table 2.

The stream function follows from the velocity components by integration:

$$\Psi(x,r) = -r\int_0^x v_r\,dx^* + \int_0^r r^* v_x\,dr^* + \text{const} \tag{28}$$

A suitable path of integration is the part of the x axis $0 \le x^* \le x$, $r^* = 0$, followed by the radius $x^* = x$, $0 \le r^* \le r$. The first integral in Eq. (28) then disappears, and the second integral reads

$$\Psi_\gamma(x,r) = \frac{\Gamma r'}{2\pi}\int_0^r \frac{r^*}{\sqrt{x^2+(r^*+1)^2}} \times \left\{\mathsf{K}(k)-\left[1+\frac{2(r^*-1)}{x^2+(r^*-1)^2}\right]\mathsf{E}(k)\right\}dr^*$$

[1] More detailed tables have been given by D. Küchemann, 1940. They are less accurate than the tables given here, however.

TABLE 1. AXIAL VELOCITY COMPONENT OF A VORTEX RING

$$v_{\gamma x}{}^{*} = \frac{2\pi r'}{\Gamma} v_{\gamma x}\left(\frac{x}{r'}, \frac{r}{r'}\right)$$

$\frac{x}{r'}$ \ $\frac{r}{r'}$	0	0.2	0.4	0.6	0.8	1.0	1.2	1.4	1.6	1.8	2.0
0	3.142	3.240	3.586	4.432	7.091	.....	−3.345	−1.263	−0.666	−0.407	−0.271
0.2	2.962	3.033	3.263	3.695	4.081	1.336	−1.219	−0.887	−0.554	−0.363	−0.250
0.4	2.515	2.534	2.572	2.535	2.115	0.974	−0.061	−0.351	−0.331	−0.260	−0.198
0.6	1.981	1.965	1.899	1.719	1.333	0.756	0.233	−0.048	−0.141	−0.151	−0.135
0.8	1.496	1.469	1.380	1.206	0.934	0.600	0.295	0.089	−0.020	−0.065	−0.077
1.0	1.111	1.086	1.008	0.874	0.690	0.482	0.289	0.142	0.047	−0.006	−0.032
1.2	0.824	0.804	0.746	0.650	0.527	0.390	0.262	0.156	0.080	0.030	0.001
1.4	0.617	0.603	0.560	0.494	0.410	0.318	0.229	0.153	0.093	0.051	0.022
1.6	0.468	0.458	0.428	0.382	0.324	0.260	0.198	0.142	0.096	0.060	0.034
1.8	0.360	0.353	0.332	0.300	0.259	0.215	0.170	0.128	0.093	0.064	0.041
2.0	0.281	0.276	0.261	0.239	0.210	0.178	0.145	0.114	0.087	0.063	0.045

$\frac{x}{r'}$ \ $\frac{r}{r'}$	0	0.5	1.0	1.5	2.0	2.5	3.0	3.5	4.0	4.5	5.0
0	3.142	3.913	.....	−0.895	−0.271	−0.122	−0.066	−0.040	−0.026	−0.018	−0.013
0.5	2.248	2.173	0.854	−0.217	−0.167	−0.095	−0.057	−0.036	−0.024	−0.017	−0.013
1.0	1.111	0.948	0.482	0.088	−0.032	−0.043	−0.035	−0.026	−0.019	−0.014	−0.011
1.5	0.536	0.463	0.288	0.120	0.029	−0.005	−0.014	−0.014	−0.013	−0.010	−0.008
2.0	0.281	0.251	0.178	0.100	0.045	0.014	0.000	−0.005	−0.006	−0.006	−0.006
2.5	0.161	0.148	0.115	0.076	0.043	0.021	0.008	0.002	−0.001	−0.003	−0.003
3.0	0.099	0.093	0.077	0.056	0.037	0.022	0.012	0.005	0.002	0.000	−0.001
3.5	0.065	0.062	0.053	0.042	0.030	0.020	0.012	0.007	0.004	0.001	0.000
4.0	0.045	0.043	0.038	0.031	0.024	0.017	0.012	0.008	0.005	0.003	0.001
4.5	0.032	0.031	0.028	0.024	0.019	0.015	0.011	0.008	0.005	0.003	0.002
5.0	0.024	0.023	0.021	0.019	0.016	0.012	0.010	0.007	0.005	0.003	0.002

$\frac{x}{r'}$ \ $\frac{r}{r'}$	0.70	0.80	0.90	0.95	0.99	1.0	1.01	1.05	1.10	1.20	1.30
0	5.316	7.091	12.33	22.62	103.4	.....	−96.68	−17.54	−7.934	−3.345	−1.924
0.01	5.312	7.076	12.23	21.82	52.94	2.842	−47.10	−16.80	−7.842	−3.335	−1.921
0.05	5.199	6.743	10.17	12.18	5.905	2.037	−1.812	−7.948	−6.079	−3.090	−1.851
0.10	4.881	5.904	6.873	5.783	2.690	1.688	0.691	−2.315	−3.327	−2.482	−1.655
0.20	3.961	4.081	3.456	2.562	1.593	1.336	1.080	0.140	−0.687	−1.219	−1.103
0.30	3.079	2.854	2.206	1.700	1.242	1.126	1.010	0.566	0.098	−0.452	−0.612

TABLE 2. RADIAL VELOCITY COMPONENT OF A VORTEX RING

$$v_{\gamma r}{}^{*} = \frac{2\pi r'}{\Gamma} v_{\gamma r}\left(\frac{x}{r'}, \frac{r}{r'}\right)$$

$\frac{x}{r'}$ \ $\frac{r}{r'}$	0	0.2	0.4	0.6	0.8	1.0	1.2	1.4	1.6	1.8	2.0
0.0	0	0	0	0	0	.....	0	0	0	0	0
0.2	0	0.183	0.452	1.012	2.547	4.787	2.135	0.746	0.325	0.168	0.096
0.4	0	0.272	0.619	1.137	1.841	2.182	1.586	0.881	0.479	0.275	0.168
0.6	0	0.268	0.565	0.900	1.202	1.287	1.073	0.748	0.484	0.312	0.205
0.8	0	0.220	0.441	0.649	0.801	0.836	0.744	0.584	0.426	0.302	0.213
1.0	0	0.165	0.323	0.458	0.547	0.572	0.530	0.448	0.354	0.270	0.202
1.2	0	0.120	0.231	0.323	0.383	0.403	0.386	0.342	0.287	0.231	0.182
1.4	0	0.086	0.165	0.230	0.273	0.291	0.286	0.266	0.230	0.194	0.160
1.6	0	0.062	0.119	0.166	0.198	0.214	0.215	0.204	0.184	0.161	0.137
1.8	0	0.045	0.087	0.121	0.146	0.160	0.164	0.159	0.148	0.133	0.117
2.0	0	0.033	0.064	0.090	0.109	0.122	0.127	0.125	0.119	0.110	0.099

$\frac{x}{r'}$ \ $\frac{r}{r'}$	0	0.5	1.0	1.5	2.0	2.5	3.0	3.5	4.0	4.5	5.0
0.0	0	0	.....	0	0	0	0	0	0	0	0
0.5	0	0.808	1.647	0.640	0.191	0.072	0.033	0.017	0.010	0.006	0.004
1.0	0	0.394	0.572	0.400	0.202	0.099	0.052	0.029	0.017	0.011	0.007
1.5	0	0.170	0.249	0.219	0.148	0.090	0.054	0.034	0.021	0.014	0.010
2.0	0	0.078	0.122	0.123	0.099	0.071	0.048	0.033	0.022	0.015	0.011
2.5	0	0.039	0.064	0.071	0.064	0.052	0.039	0.029	0.021	0.015	0.011
3.0	0	0.021	0.036	0.043	0.042	0.037	0.030	0.024	0.018	0.014	0.011
3.5	0	0.012	0.022	0.027	0.028	0.026	0.023	0.019	0.016	0.012	0.010
4.0	0	0.008	0.014	0.018	0.019	0.019	0.017	0.015	0.013	0.011	0.009
4.5	0	0.005	0.010	0.012	0.014	0.014	0.013	0.012	0.011	0.009	0.008
5.0	0	0.003	0.006	0.009	0.010	0.010	0.010	0.009	0.009	0.008	0.007

$\frac{x}{r'}$ \ $\frac{r}{r'}$	0.70	0.80	0.90	0.95	0.99	1.00	1.01	1.05	1.10	1.20	1.30
0.00	0	0	0	0	0	.....	0	0	0	0	0
0.01	0.118	0.265	1.028	3.929	50.23	99.98	49.73	3.739	0.932	0.219	0.091
0.05	0.575	1.245	4.142	10.18	19.25	19.92	19.06	9.691	3.757	1.033	0.442
0.10	1.056	2.099	5.133	8.070	9.816	9.867	9.721	7.687	4.658	1.745	0.814
0.20	1.577	2.547	3.982	4.602	4.797	4.787	4.753	4.395	3.633	2.135	1.229
0.30	1.633	2.248	2.858	3.038	3.070	3.061	3.044	2.911	2.625	1.908	1.295

This can be integrated explicitly by parts:

$$\Psi_\gamma(x,r) = \frac{\Gamma r'}{2\pi}\sqrt{x^2+(r+1)^2}\left[\left(1-\frac{k^2}{2}\right)\mathsf{K}(k) - \mathsf{E}(k)\right] \tag{29}$$

Values of $\Psi_\gamma(x,r)$ are tabulated in Table 3. The streamline pattern of the vortex ring is shown in Fig. 2.

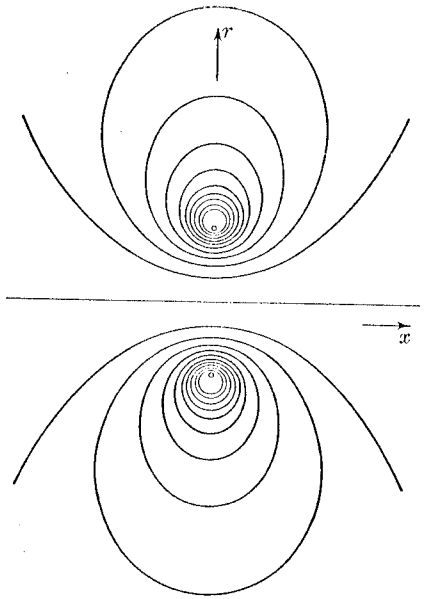

FIG. 2. Streamline pattern of a vortex ring.

6. Source Ring. A source ring is a distribution of sources of constant strength along a circle. Using the same vector notation as above, we find the velocity vector induced by an element of strength $q\ ds$ of the source ring of radius r' at the point (x,r,φ) to be

$$d\mathbf{v} = \frac{q\ ds}{4\pi R^2}\frac{\mathbf{R}}{R} \tag{30}$$

The velocity components are again obtained by integration round the circumference:

$$v_{qx}(x,r) = \frac{q}{4\pi r'}\int_0^{2\pi}\frac{x}{\sqrt{x^2+r^2+1-2r\cos(\varphi-\varphi')^3}}\,d\varphi' \tag{31}$$

$$v_{qr}(x,r) = \frac{q}{4\pi r'}\int_0^{2\pi}\frac{r-\sin\varphi'}{\sqrt{x^2+r^2+1-2r\cos(\varphi-\varphi')^3}}\,d\varphi' \tag{32}$$

with the radius r' of the ring as unit length. The integrals can be reduced to complete elliptic integrals with the modulus k of Eq. (24) in the same

TABLE 3. STREAM FUNCTION OF A VORTEX RING

$$\Psi_\gamma^* = \frac{2\pi}{\Gamma r'}\Psi_\gamma\left(\frac{x}{r'},\frac{r}{r'}\right)$$

$\frac{x}{r'}$ \ $\frac{r}{r'}$	0	0.2	0.4	0.6	0.8	1.0	1.2	1.4	1.6	1.8	2.0
0.0	0	0.064	0.268	0.665	1.438	.....	1.978	1.448	1.175	0.999	0.873
0.2	0	0.060	0.249	0.596	1.149	1.714	1.613	1.331	1.120	0.968	0.853
0.4	0	0.050	0.204	0.460	0.792	1.075	1.158	1.092	0.986	0.886	0.799
0.6	0	0.040	0.156	0.337	0.552	0.740	0.843	0.861	0.829	0.778	0.724
0.8	0	0.030	0.115	0.245	0.395	0.532	0.628	0.675	0.683	0.667	0.639
1.0	0	0.022	0.085	0.179	0.288	0.393	0.477	0.531	0.558	0.564	0.556
1.2	0	0.016	0.063	0.133	0.215	0.297	0.368	0.421	0.456	0.474	0.479
1.4	0	0.012	0.047	0.100	0.163	0.228	0.288	0.337	0.373	0.397	0.410
1.6	0	0.009	0.036	0.076	0.126	0.178	0.228	0.272	0.307	0.333	0.351
1.8	0	0.007	0.028	0.059	0.098	0.141	0.183	0.222	0.254	0.281	0.301
2.0	0	0.006	0.022	0.047	0.078	0.113	0.148	0.182	0.212	0.237	0.258

$\frac{x}{r'}$ \ $\frac{r}{r'}$	0	0.5	1.0	1.5	2.0	2.5	3.0	3.5	4.0	4.5	5.0
0.0	0	0.437	.....	1.295	0.873	0.670	0.547	0.463	0.402	0.356	0.319
0.5	0	0.278	0.885	0.943	0.763	0.622	0.521	0.448	0.392	0.349	0.314
1.0	0	0.129	0 393	0.548	0.556	0.510	0.455	0.406	0.364	0.329	0.300
1.5	0	0.062	0.201	0.322	0.380	0.389	0.374	0.350	0.325	0.300	0.278
2.0	0	0.033	0.113	0.197	0.258	0.288	0.296	0.292	0.281	0.267	0.252
2.5	0	0.019	0.068	0.127	0.177	0.212	0.231	0.238	0.238	0.232	0.225
3.0	0	0.012	0.044	0.085	0.125	0.157	0.179	0.192	0.199	0.200	0.198
3.5	0	0.008	0.029	0.059	0.090	0.118	0.140	0.155	0.164	0.170	0.171
4.0	0	0.005	0.021	0.042	0.067	0.090	0.110	0.125	0.136	0.143	0.148
4.5	0	0.004	0.015	0.031	0.050	0.069	0.087	0.102	0.113	0.122	0.128
5.0	0	0.003	0.011	0.024	0.039	0.054	0.069	0.082	0.094	0.103	0.110

$\frac{x}{r'}$ \ $\frac{r}{r'}$	0.70	0.80	0.90	0.95	0.99	1.00	1.01	1.05	1.10	1.20	1.30
0.00	0.980	1.438	2.218	2.975	4.656	.....	4.713	3.178	2.556	1.974	1.658
0.01	0.980	1.437	2.213	2.956	4.312	4.685	4.365	3.158	2.550	1.972	1.658
0.05	0.970	1.412	2.114	2.639	3.038	3.077	3.079	2.825	2.440	1.942	1.644
0.10	0.941	1.344	1.895	2.197	2.368	2.390	2.402	2.360	2.200	1.856	1.602
0.20	0.845	1.149	1.478	1.619	1.699	1.714	1.726	1.750	1.734	1.613	1.465
0.30	0.731	0.955	1.173	1.264	1.321	1.333	1.344	1.376	1.393	1.368	1.298

way as was demonstrated for the vortex ring. We obtain, finally,

$$v_{qx}(x,r) = \frac{q}{2\pi r'} \frac{2x}{\sqrt{x^2 + (r+1)^2}\,[x^2 + (r-1)^2]} \mathsf{E}(k) \tag{33}$$

$$v_{qr}(x,r) = \frac{q}{2\pi r'} \frac{1}{r\sqrt{x^2 + (r+1)^2}} \left\{ \mathsf{K}(k) - \left[1 - \frac{2r(r-1)}{x^2 + (r-1)^2} \right] \mathsf{E}(k) \right\} \tag{34}$$

Values of these velocity components are given in Tables 4 and 5.

No explicit formula can be given for the stream function of the source ring, but numerical results can be obtained from Eq. (28) by graphical integration of the velocity field. Values of $\Psi_q(x,r)$ are given in Table 6.

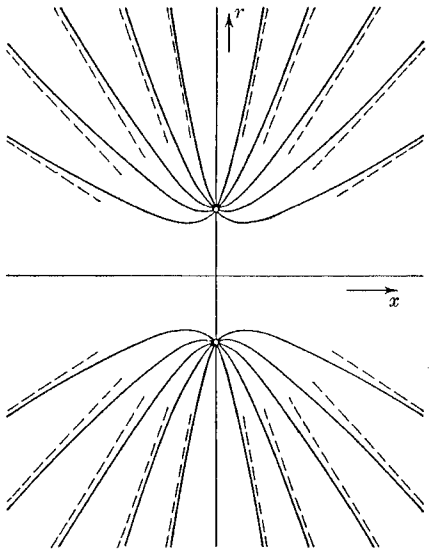

FIG. 3. Streamline pattern of a source ring.

The tables contain the velocity components and the stream function only for a quadrant of the xr plane. Values in the other quadrants are obtained from

$$\begin{aligned} v_{\gamma x}(x,r) &= v_{\gamma x}(-x,r) \\ v_{\gamma r}(x,r) &= -v_{\gamma r}(-x,r) \\ \Psi_\gamma(x,r) &= \Psi_\gamma(-x,r) \end{aligned} \tag{35}$$

and

$$\begin{aligned} v_{qx}(x,r) &= -v_{qx}(-x,r) \\ v_{qr}(x,r) &= v_{qr}(-x,r) \\ \Psi_q(x,r) &= -qr' - \Psi_q(-x,r) \end{aligned} \tag{36}$$

The streamline pattern of the source ring is shown in Fig. 3. It will be seen that near the source ring the flow is similar to that of a two-dimen-

TABLE 4. AXIAL VELOCITY COMPONENT OF A SOURCE RING

$$v_{qx}^* = \frac{2\pi r'}{q} v_{qx}\left(\frac{x}{r'}, \frac{r}{r'}\right)$$

$\frac{x}{r'}$ \ $\frac{r}{r'}$	0	0.2	0.4	0.6	0.8	1.0	1.2	1.4	1.6	1.8	2.0
0.0	0	0	0	0	0	.....	0	0	0	0	0
0.2	0.592	0.643	0.833	1.346	2.854	5.054	2.318	0.868	0.410	0.228	0.143
0.4	1.006	1.068	1.276	1.696	2.319	2.571	1.879	1.094	0.634	0.391	0.257
0.6	1.188	1.233	1.365	1.571	1.761	1.740	1.428	1.019	0.691	0.470	0.329
0.8	1.197	1.219	1.280	1.354	1.387	1.317	1.130	0.889	0.666	0.491	0.364
1.0	1.111	1.119	1.137	1.148	1.128	1.054	0.926	0.769	0.613	0.479	0.373
1.2	0.989	0.989	0.987	0.974	0.938	0.872	0.778	0.667	0.554	0.452	0.366
1.4	0.864	0.857	0.851	0.829	0.792	0.736	0.665	0.583	0.499	0.420	0.350
1.6	0.749	0.745	0.732	0.710	0.677	0.631	0.575	0.513	0.449	0.386	0.330
1.8	0.648	0.644	0.632	0.612	0.584	0.547	0.503	0.454	0.404	0.354	0.308
2.0	0.562	0.559	0.548	0.531	0.508	0.478	0.442	0.404	0.364	0.324	0.286

$\frac{x}{r'}$ \ $\frac{r}{r'}$	0	0.5	1.0	1.5	2.0	2.5	3.0	3.5	4.0	4.5	5.0
0.0	0	0	.....	0	0	0	0	0	0	0	0
0.5	1.124	1.491	2.074	0.851	0.298	0.133	0.071	0.043	0.028	0.019	0.014
1.0	1.111	1.145	1.054	0.689	0.373	0.204	0.120	0.076	0.051	0.035	0.026
1.5	0.804	0.780	0.681	0.510	0.340	0.218	0.142	0.096	0.067	0.048	0.036
2.0	0.562	0.541	0.478	0.384	0.286	0.205	0.145	0.104	0.076	0.056	0.043
2.5	0.403	0.389	0.351	0.296	0.236	0.182	0.138	0.104	0.079	0.061	0.047
3.0	0.298	0.289	0.267	0.233	0.195	0.158	0.126	0.099	0.078	0.062	0.049
3.5	0.228	0.223	0.208	0.187	0.162	0.136	0.112	0.092	0.075	0.061	0.050
4.0	0.179	0.176	0.166	0.152	0.135	0.117	0.100	0.084	0.070	0.058	0.049
4.5	0.144	0.142	0.136	0.126	0.114	0.101	0.088	0.076	0.065	0.055	0.047
5.0	0.119	0.117	0.113	0.106	0.097	0.088	0.078	0.069	0.060	0.052	0.045

$\frac{x}{r'}$ \ $\frac{r}{r'}$	0.70	0.80	0.90	0.95	0.99	1.00	1.01	1.05	1.10	1.20	1.30
0.00	0	0	0	0	0	.....	0	0	0	0	0
0.01	0.136	0.282	1.048	3.951	50.26	100.0	49.76	3.758	0.947	0.230	0.099
0.05	0.662	1.333	4.236	10.28	19.35	20.02	19.16	9.778	3.829	1.085	0.482
0.10	1.227	2.270	5.307	8.245	9.987	10.04	9.887	7.840	4.791	1.847	0.893
0.20	1.896	2.854	4.275	4.885	5.067	5.054	5.016	4.643	3.859	2.318	1.378
0.30	2.067	2.654	3.234	3.396	3.412	3.398	3.378	3.226	2.917	2.153	1.500

TABLE 5. RADIAL VELOCITY COMPONENT OF A SOURCE RING

$$v_{qr}^* = \frac{2\pi r'}{q} v_{qr}\left(\frac{x}{r'}, \frac{r}{r'}\right)$$

$\frac{x}{r'}$ \ $\frac{r}{r'}$	0	0.2	0.4	0.6	0.8	1.0	1.2	1.4	1.6	1.8	2.0
0.0	0	−0.329	−0.764	−1.550	−3.875	.....	5.659	2.803	1.800	1.287	0.978
0.2	0	−0.270	−0.593	−1.021	−1.319	1.336	3.234	2.341	1.652	1.224	0.946
0.4	0	−0.146	−0.272	−0.299	0.035	0.974	1.672	1.624	1.337	1.071	0.863
0.6	0	−0.035	−0.032	0.071	0.345	0.756	1.068	1.130	1.034	0.891	0.754
0.8	0	0.030	0.089	0.204	0.387	0.600	0.764	0.825	0.799	0.728	0.644
1.0	0	0.058	0.132	0.231	0.355	0.482	0.581	0.628	0.627	0.593	0.543
1.2	0	0.065	0.136	0.218	0.306	0.390	0.455	0.493	0.501	0.486	0.457
1.4	0	0.061	0.125	0.192	0.258	0.318	0.365	0.395	0.406	0.401	0.385
1.6	0	0.054	0.109	0.163	0.215	0.260	0.297	0.321	0.333	0.334	0.326
1.8	0	0.046	0.092	0.137	0.178	0.215	0.244	0.265	0.277	0.280	0.277
2.0	0	0.039	0.078	0.114	0.148	0.178	0.202	0.220	0.232	0.237	0.237

$\frac{x}{r'}$ \ $\frac{r}{r'}$	0	0.5	1.0	1.5	2.0	2.5	3.0	3.5	4.0	4.5	5.0
0.0	0	−1.083	.....	2.205	0.978	0.574	0.382	0.273	0.206	0.161	0.130
0.5	0	−0.126	0.854	1.274	0.810	0.522	0.360	0.263	0.200	0.158	0.128
1.0	0	0.178	0.482	0.633	0.543	0.412	0.309	0.236	0.185	0.148	0.121
1.5	0	0.147	0.288	0.363	0.354	0.304	0.248	0.201	0.163	0.135	0.112
2.0	0	0.096	0.178	0.227	0.237	0.221	0.194	0.166	0.140	0.119	0.101
2.5	0	0.062	0.115	0.149	0.163	0.161	0.150	0.133	0.118	0.103	0.090
3.0	0	0.041	0.077	0.102	0.116	0.119	0.116	0.108	0.098	0.088	0.079
3.5	0	0.028	0.053	0.072	0.084	0.090	0.090	0.086	0.081	0.075	0.068
4.0	0	0.020	0.038	0.053	0.063	0.068	0.070	0.070	0.067	0.063	0.059
4.5	0	0.015	0.028	0.039	0.048	0.053	0.056	0.056	0.055	0.053	0.051
5.0	0	0.011	0.021	0.030	0.037	0.042	0.045	0.046	0.046	0.045	0.043

$\frac{x}{r'}$ \ $\frac{r}{r'}$	0.70	0.80	0.90	0.95	0.99	1.00	1.01	1.05	1.10	1.20	1.30
0.00	−2.322	−3.875	−8.636	−18.36	−97.63	.....	102.3	21.44	11.05	5.659	3.777
0.01	−2.317	−3.862	−8.535	−17.58	−47.55	2.842	52.39	20.68	10.95	5.647	3.773
0.05	−2.225	−3.567	−6.593	−8.284	−1.815	2.037	5.831	11.52	9.093	5.378	3.692
0.10	−1.967	−2.834	−3.566	−2.374	0.710	1.688	2.652	5.448	6.122	4.700	3.465
0.20	−1.250	−1.319	−0.672	0.190	1.099	1.336	1.569	2.399	3.059	3.234	2.807
0.30	−0.621	−0.414	0.176	0.627	1.026	1.126	1.224	1.589	1.946	2.255	2.183

sional source, while at large distances from the ring it is similar to the flow from a three-dimensional source at its center.

The constant of integration can be chosen arbitrarily in the integration of Eq. (28), for example, so that the negative x axis is the line $\Psi = 0$, as in Fig. 3. The stream function is then discontinuous at $x = 0$, $r < r'$. This position of the discontinuity may be unsuitable in some applications,

TABLE 6. STREAM FUNCTION OF A SOURCE RING

$$\Psi_q^* = -\frac{2\pi}{qr'} \Psi_q\left(\frac{x}{r'}, \frac{r}{r'}\right)$$

$\frac{x}{r'}$ \ $\frac{r}{r'}$	0	0.2	0.4	0.6	0.8	1.0	1.2	1.4	1.6	1.8	2.0
0.0	0	0	0	0	0	1.57	3.14	3 14	3.14	3.14	3.14
−0.2	0	0.012	0.056	0.162	0.444	1.20	2.03	2.41	2.58	2.69	2.75
−0.4	0	0.021	0.091	0.240	0.521	0.974	1.47	1.85	2.10	2.27	2.39
−0.6	0	0.024	0.102	0.249	0.485	0.803	1.16	1.47	1.72	1.92	2.07
−0.8	0	0.024	0.099	0.231	0.424	0.669	0.939	1.20	1.43	1.63	1.79
−1.0	0	0.022	0.090	0.204	0.364	0.561	0.779	1.00	1.21	1.39	1.55
−1.2	0	0.020	0.079	0.177	0.311	0.474	0.656	0.844	1.03	1.20	1.35
−1.4	0	0.017	0.068	0.152	0.266	0.403	0.559	0.720	0.882	1.04	1.18
−1.6	0	0.015	0.058	0.131	0.228	0.345	0.479	0.621	0.764	0.905	1.04
−1.8	0	0.013	0.051	0.113	0.197	0.298	0.415	0.539	0.667	0.795	0.920
−2.0	0	0.011	0.044	0.098	0.171	0.259	0.361	0.471	0.586	0.703	0.819

$\frac{x}{r'}$ \ $\frac{r}{r'}$	0	0.5	1.0	1.5	2.0	2.5	3.0	3.5	4.0	4.5	5.0
0.0	0	0	1.57	3.14	3.14	3.14	3.14	3.14	3.14	3.14	3.14
−0.5	0	0.162	0.883	1.80	2.22	2.45	2.58	2.67	2.73	2.78	2.82
−1.0	0	0.140	0.561	1.10	1.55	1.86	2.07	2.23	2.35	2.43	2.51
−1.5	0	0.099	0.374	0.744	1.11	1.42	1.66	1.84	2.00	2.12	2.22
−2.0	0	0.069	0.260	0.527	0.819	1.09	1.33	1.53	1.70	1.83	1.95
−2.5	0	0.050	0.188	0.389	0.622	0.854	1.07	1.27	1.44	1.58	1.71
−3.0	0	0.037	0.141	0.296	0.484	0.680	0.875	1.06	1.22	1.37	1.50
−3.5	0	0.028	0.108	0.232	0.384	0.550	0.720	0.885	1.04	1.18	1.32
−4.0	0	0.022	0.086	0.185	0.311	0.452	0.600	0.749	0.892	1.03	1.16
−4.5	0	0.018	0.070	0.152	0.257	0.378	0.508	0.641	0.773	0.900	1.02
−5.0	0	0.015	0.058	0.126	0.215	0.319	0.434	0.553	0.674	0.792	0.907

$\frac{x}{r'}$ \ $\frac{r}{r'}$	0.70	0.80	0.90	0.95	0.99	1.00	1.01	1.05	1.10	1.20	1.30
0.00	0	0	0	0	0	1.57	3.14	3.14	3.14	3.14	3.14
−0.01	0.016	0.031	0.078	0.171	0.69	1.54	2.39	2.92	3.02	3.07	3.09
−0.05	0.080	0.151	0.359	0.667	1.25	1.44	1.64	2.23	2.57	2.81	2.90
−0.10	0.155	0.280	0.582	0.892	1.25	1.35	1.45	1.83	2.16	2.50	2.67
−0.20	0.268	0.444	0.745	0.958	1.15	1.20	1.25	1.45	1.68	2.03	2.26
−0.30	0.333	0 508	0.762	0.915	1.05	1.08	1.12	1.25	1.41	1.71	1.94

where

$$k^2 = \frac{4}{\left(\frac{x - x'}{R_0}\right)^2 + 4}$$

Transforming these by making k the variable,

$$\frac{x'}{R_0} = \frac{x}{R_0} - 2\sqrt{\frac{1 - k^2}{k^2}}$$

we obtain

$$v_x(x,R_0) = \frac{1}{2\pi}\int_{k_1}^{k_2} \gamma(k)\,\frac{k}{\sqrt{1-k^2}}\,\mathsf{D}(k)\,dk \tag{41}$$

$$v_r(x,R_0) = -\frac{1}{2\pi}\int_{k_1}^{k_2} \gamma(k)\left[2\mathsf{D}(k) - \frac{1}{1-k^2}\,\mathsf{E}(k)\right]dk \tag{42}$$

where the limits of the integrals are

$$k_1 = \frac{2}{\sqrt{(x/R_0)^2 + 4}}$$

$$k_2 = \frac{2}{\sqrt{\left(\frac{x}{R_0} - \frac{L}{R_0}\right)^2 + 4}} \tag{43}$$

These integrals can be evaluated by expanding the vortex distribution $\gamma(x)$ in a power series, and using the following relations from the theory of elliptic integrals:

$$\int \frac{k}{\sqrt{1-k^2}}\,\mathsf{D}(k)\,dk = -\sqrt{1-k^2}\,\mathsf{K}(k)$$

$$\int \mathsf{D}(k)\,dk = k[\mathsf{K}(k) - \mathsf{D}(k)]$$

$$\int \frac{1}{1-k^2}\,\mathsf{E}(k)\,dk = k\mathsf{K}(k)$$

$$\int \left[2\,\frac{\sqrt{1-k^2}}{k}\,\mathsf{D}(k) - \frac{1}{k\sqrt{1-k^2}}\,\mathsf{E}(k)\right]dk = \sqrt{1-k^2}\,[\mathsf{K}(k) - \mathsf{D}(k)]$$

For the constant and linear terms,

$$\gamma_4(x) = 2\pi V_0 c_4$$

$$\gamma_5(x) = 2\pi V_0 c_5\left(1 - \frac{2x}{L}\right)$$

the velocity components are

$$\frac{1}{V_0}\,v_{x4}(x,R_0) = -c_4[\sqrt{1-k^2}\,\mathsf{K}(k)]_{k_1}^{k_2} \tag{44}$$

$$\frac{1}{V_0}\,v_{r4}(x,R_0) = -c_4[k\{\mathsf{K}(k) - 2\mathsf{D}(k)\}]_{k_1}^{k_2} \tag{45}$$

$$\frac{1}{V_0}\,v_{x5}(x,R_0) = c_5\left[-\left(1 - \frac{2x}{L}\right)\sqrt{1-k^2}\,\mathsf{K}(k) + 2\,\frac{2R_0}{L}\,k\{\mathsf{K}(k) - \mathsf{D}(k)\}\right]_{k_1}^{k_2} \tag{46}$$

$$\frac{1}{V_0}\,v_{r5}(x,R_0) = -c_5\left[\left(1 - \frac{2x}{L}\right)k\{\mathsf{K}(k) - 2\mathsf{D}(k)\} + 2\,\frac{2R_0}{L}\sqrt{1-k^2}\,\{\mathsf{K}(k) - \mathsf{D}(k)\}\right]_{k_1}^{k_2} \tag{47}$$

These are given in Tables 7 to 11 for certain values of the ratio $2R_0/L$. These tables also contain the corresponding velocity components for the vortex distributions used by H. Birnbaum (1923),

$$\gamma_1(x) = 2\pi V_0 c_1\sqrt{\frac{1 - x/L}{x/L}}$$

$$\gamma_2(x) = 2\pi V_0 c_2\sqrt{1 - \left(1 - \frac{2x}{L}\right)^2}$$

$$\gamma_3(x) = 2\pi V_0 c_3\left(1 - \frac{2x}{L}\right)\sqrt{1 - \left(1 - \frac{2x}{L}\right)^2}$$

The numerical values of the latter were obtained by graphical integration. It should be noted that the velocity component v_x as given in the tables does not include the term $\pm\gamma(x)/2$. To obtain the total x component of the induced velocity add $-\gamma(x)/2$ on the outside of the vortex cylinder and $+\gamma(x)/2$ on the inside.

10. Uniform Source Distribution on a Circular Disk. It has been shown in Sec. 3-6 that the flow field of a uniform source distribution on a circular disk is the same as that of a vortex cylinder of constant strength and semi-infinite length, apart from a parallel flow in the region $x > 0$, $r < R_0$. For points on the cylinder $r = R_0$, the velocity components can be obtained explicitly by applying Eqs. (44) and (45) of the previous section to a cylinder semi-infinite in length. This only affects the limit k_2; Eq. (43) is replaced by $k_2 = 0$. Then

$$\frac{1}{V_0}\,v_x(x,R_0) = \frac{q}{2\pi V_0}\left\{\frac{\pi}{2} + \frac{x/R_0}{\sqrt{(x/R_0)^2 + 4}}\,\mathsf{K}\left(\frac{2}{\sqrt{(x/R_0)^2 + 4}}\right)\right\} \tag{48}$$

$$\frac{1}{V_0}\,v_r(x,R_0) = \frac{q}{2\pi V_0}\,\frac{2}{\sqrt{(x/R_0)^2 + 4}}\left\{\mathsf{K}\left(\frac{2}{\sqrt{(x/R_0)^2 + 4}}\right) - 2\mathsf{D}\left(\frac{2}{\sqrt{(x/R_0)^2 + 4}}\right)\right\} \tag{49}$$

No explicit formula can be given for the whole flow field. Numerical values are given in Tables 15 to 17, which were obtained by graphical integration of the results for the single source ring.

for instance, when a parallel flow along the axis is superposed on the source-ring flow in order to obtain an annular body of infinite length. In that case, it is suggested that the discontinuity be put on the cylinder $x > 0$, $r = r'$ so that

$$\begin{aligned} \Psi_q(x,r) &= -\Psi_q(-x,r) && \text{for } r < r',\ x > 0 \\ \Psi_q(x,r) &= -qr' - \Psi_q(-x,r) && \text{for } r > r',\ x > 0 \end{aligned} \tag{37}$$

7. Doublet Rings. There is a close connection between the velocity components of the source and vortex rings and the potential function and stream function of doublet rings. Superposing a source ring at $(x' + h,r')$ on a sink ring at (x',r') and taking the limit as $h \to 0$ with $m = \lim_{h\to 0} hq$ finite, we obtain a doublet ring whose axis is in the direction of the positive x axis, denoted by subscript 1. The potential function Φ_{d1} and the stream function Ψ_{d1} of the doublet ring are given by

$$\Phi_{d1} = \frac{m}{q}\frac{\partial \Phi_q}{\partial x}$$

$$\Psi_{d1} = \frac{m}{q}\frac{\partial \Psi_q}{\partial x}$$

For axially symmetrical flow,

$$v_x = -\frac{\partial \Phi}{\partial x}$$

$$v_r = -\frac{1}{r}\frac{\partial \Psi}{\partial x}$$

so that

$$\Phi_{d1} = -\frac{m}{q} v_{qx}$$

$$\Psi_{d1} = -\frac{m}{q} r v_{qr}$$

Both of these functions are tabulated.

A doublet ring with its axis pointing along the positive r axis (subscript 2) can be obtained in a similar way by superposing two vortex rings with circulations of opposite signs, their strengths increasing as the distance decreases. We find

$$\Phi_{d2} = \frac{m}{\gamma} v_{\gamma x}$$

$$\Psi_{d2} = \frac{m}{\gamma} r v_{\gamma r}$$

which again are tabulated.

8. Source Distributions of Varying Strength on a Circle. Some problems that arise when the axis of a body of revolution is inclined to the main stream can be solved by using on the surface of the body singularities composed of source rings the strength of which varies round the circumference according to $q(\varphi') = q \sin \varphi'$. The velocity components of such rings can also be given explicitly.

The calculation is similar to that for the ordinary source ring of constant strength. Replacing q in Eqs. (31) and (32) by $q \sin \varphi'$, the integration leads again to complete elliptic integrals with the modulus k from Eq. (24):

$$v_x(x,r,\varphi) = \frac{q}{2\pi r'}\frac{2x[2\mathsf{K}(k) - 2\mathsf{D}(k) - \mathsf{E}(k)]}{\sqrt{x^2 + (r+1)^2}\,[x^2 + (r-1)^2]} \sin\varphi \tag{38}$$

$$\begin{aligned} v_y(x,r,\varphi) = \frac{q}{2\pi r'}&\frac{1}{\sqrt{x^2 + (r+1)^2}\,[x^2 + (r-1)^2]} \\ &\times \left\{\left[2r\sin^2\varphi + \frac{8}{k^2}(1 - 2\sin^2\varphi)\right][2\mathsf{K}(k) - 2\mathsf{D}(k) - \mathsf{E}(k)]\right. \\ &\left. - 8(1 - 2\sin^2\varphi)[\mathsf{K}(k) - \mathsf{D}(k)] - 2\sin^2\varphi \mathsf{E}(k)\right\} \end{aligned} \tag{39}$$

$$\begin{aligned} v_z(x,r,\varphi) = \frac{q}{2\pi r'}&\frac{\sin 2\varphi}{\sqrt{x^2 + (r+1)^2}\,[x^2 + (r-1)^2]} \\ &\times \left\{\left(r - \frac{8}{k^2}\right)[2\mathsf{K}(k) - 2\mathsf{D}(k) - \mathsf{E}(k)]\right. \\ &\left. + 8[\mathsf{K}(k) - \mathsf{D}(k)] - \mathsf{E}(k)\right\} \end{aligned} \tag{40}$$

There are now of course three velocity components, in the directions of the three axes, as the axial symmetry is lost. They have not yet been tabulated.

Some functions which can be used for determining the velocity components of source rings with variable strength round the circumference have been tabulated by F. Riegels (1949).

9. Vortex Distributions on a Cylinder. The velocity components induced by a vortex distribution $\gamma(x)$ on a cylinder of radius R_0 and length L on the cylinder itself can be derived from Eqs. (26) and (27):

$$v_x(x,R_0) = \frac{1}{2\pi}\int_0^{L/R_0} \gamma\left(\frac{x'}{R_0}\right)\frac{1}{\sqrt{\left(\frac{x - x'}{R_0}\right)^2 + 4}}[\mathsf{K}(k) - \mathsf{E}(k)]\,d\left(\frac{x'}{R_0}\right)$$

$$\begin{aligned} v_r(x,R_0) = -\frac{1}{2\pi}&\int_0^{L/R_0} \gamma\left(\frac{x'}{R_0}\right)\frac{\frac{x - x'}{R_0}}{\sqrt{\left(\frac{x - x'}{R_0}\right)^2 + 4}} \\ &\times \left\{\mathsf{K}(k) - \left[1 + \frac{2}{\left(\frac{x - x'}{R_0}\right)^2}\right]\mathsf{E}(k)\right\} d\left(\frac{x'}{R_0}\right) \end{aligned}$$

TABLE 7. AXIAL AND RADIAL VELOCITY COMPONENTS INDUCED ON THE CYLINDER $0 \leq x \leq L$, $r = R_0$, BY THE VORTEX DISTRIBUTION $\gamma_1\left(\frac{x}{L}\right) = 2\pi V_0 c_1 \sqrt{\frac{1 - x/L}{x/L}}$

$$v_{x1}^* = \frac{1}{c_1}\frac{v_{x1}(x,R_0)}{V_0}$$

x/L	$L/2R_0$				
	0	0.25	0.50	1.0	2.0
0.0	0	1.63	2.70	4.29	6.52
0.1	0	1.55	2.55	3.96	5.79
0.2	0	1.47	2.39	3.63	5.07
0.3	0	1.40	2.23	3.30	4.38
0.4	0	1.32	2.07	2.97	3.74
0.5	0	1.24	1.91	2.65	3.15
0.6	0	1.16	1.75	2.33	2.61
0.7	0	1.08	1.58	2.01	2.12
0.8	0	1.00	1.42	1.70	1.67
0.9	0	0.92	1.25	1.39	1.25
1.0	0	0.85	1.08	1.09	0.85

$$v_{r1}^* = \frac{1}{c_1}\frac{v_{r1}(x,R_0)}{V_0}$$

x/L	$L/2R_0$				
	0	0.25	0.50	1.0	2.0
0.0	3.14	3.18	3.44	3.93	4.89
0.1	3.14	3.16	3.30	3.54	3.79
0.2	3.14	3.13	3.17	3.18	2.94
0.3	3.14	3.10	3.05	2.85	2.30
0.4	3.14	3.07	2.94	2.56	1.86
0.5	3.14	3.04	2.84	2.34	1.55
0.6	3.14	3.01	2.75	2.17	1.35
0.7	3.14	2.98	2.67	2.05	1.23
0.8	3.14	2.95	2.61	1.98	1.19
0.9	3.14	2.93	2.57	1.94	1.21
1.0	3.14	2.91	2.54	1.92	1.29

The tables contain values for negative x. For positive x, we find, from Eq. (36),

$$\begin{aligned} v_x(x,r) &= -v_x(-x,r) \\ v_r(x,r) &= v_r(-x,r) \\ \Psi(x,r) &= -qr^2 - \Psi(-x,r) \qquad \text{for } r < R_0 \\ \Psi(x,r) &= -qR_0^2 - \Psi(-x,r) \qquad \text{for } r > R_0 \end{aligned}$$

TABLE 8. AXIAL AND RADIAL VELOCITY COMPONENTS INDUCED ON THE CYLINDER $0 \leq x \leq L$, $r = R_0$, BY THE VORTEX DISTRIBUTION $\gamma_2\left(\frac{x}{L}\right) = 2\pi V_0 c_2 \sqrt{1 - \left(1 - \frac{2x}{L}\right)^2}$

$$v_{x2}^* = \frac{1}{c_2}\frac{v_{x2}(x,R_0)}{V_0}$$

x/L	$L/2R_0$				
	0	0.25	0.50	1.00	2.00
0.00	0	0.52	0.75	0.93	0.95
0.05	0	0.56	0.83	1.08	1.22
0.10	0	0.59	0.90	1.22	1.47
0.15	0	0.62	0.96	1.35	1.69
0.20	0	0.65	1.01	1.45	1.87
0.25	0	0.67	1.05	1.54	2.03
0.30	0	0.69	1.09	1.62	2.15
0.35	0	0.70	1.12	1.67	2.25
0.40	0	0.71	1.14	1.71	2.32
0.45	0	0.72	1.15	1.73	2.36
0.50	0	0.72	1.16	1.74	2.37

$$v_{r2}^* = \frac{1}{c_2}\frac{v_{r2}(x,R_0)}{V_0}$$

x/L	$L/2R_0$				
	0	0.25	0.50	1.00	2.00
0.00	−3.14	−3.10	−2.89	−2.54	−2.04
0.05	−2.83	−2.79	−2.59	−2.26	−1.75
0.10	−2.51	−2.48	−2.30	−1.98	−1.49
0.15	−2.20	−2.17	−2.01	−1.71	−1.25
0.20	−1.88	−1.86	−1.72	−1.46	−1.03
0.25	−1.57	−1.55	−1.43	−1.20	−0.83
0.30	−1.26	−1.24	−1.14	−0.96	−0.64
0.35	−0.94	−0.93	−0.86	−0.71	−0.46
0.40	−0.63	−0.62	−0.57	−0.47	−0.30
0.45	−0.31	−0.31	−0.28	−0.24	−0.14
0.50	0	0	0	0	0

11. Vortex Distributions on Two Parallel Lines. The two-dimensional flow which corresponds to the flow treated in the previous two sections leads us to vortex distributions on two parallel straight lines. The velocity components induced by the three standard Birnbaum distributions on such lines are given in Tables 12 to 14. They were obtained by graphical integration.

The integrals for vortex distributions which can be expanded in a power

TABLE 9. AXIAL AND RADIAL VELOCITY COMPONENTS INDUCED ON THE CYLINDER $0 \leq x \leq L$, $r = R_0$, BY THE VORTEX DISTRIBUTION

$$\gamma_3\left(\frac{x}{L}\right) = 2\pi V_0 c_3 \left(1 - \frac{2x}{L}\right)\sqrt{1 - \left(1 - \frac{2x}{L}\right)^2}$$

$$v_{x3}{}^* = \frac{1}{c_3}\frac{v_{x3}(x,R_0)}{V_0}$$

x/L	$L/2R_0$				
	0	0.25	0.50	1.00	2.00
0.00	0	0.066	0.135	0.272	0.427
0.05	0	0.081	0.168	0.342	0.578
0.10	0	0.090	0.186	0.380	0.668
0.15	0	0.092	0.191	0.390	0.703
0.20	0	0.090	0.185	0.377	0.691
0.25	0	0.082	0.170	0.344	0.638
0.30	0	0.070	0.146	0.295	0.551
0.35	0	0.055	0.115	0.233	0.437
0.40	0	0.038	0.079	0.161	0.303
0.45	0	0.019	0.040	0.082	0.155
0.50	0	0	0	0	0

$$v_{r3}{}^* = \frac{1}{c_3}\frac{v_{r3}(x,R_0)}{V_0}$$

x/L	$L/2R_0$				
	0	0.25	0.50	1.00	2.00
0.00	−1.57	−1.58	−1.60	−1.61	−1.52
0.05	−0.97	−0.99	−1.02	−1.04	−0.96
0.10	−0.44	−0.46	−0.49	−0.53	−0.49
0.15	0.03	0.01	−0.02	−0.09	−0.10
0.20	0.44	0.42	0.38	0.29	0.21
0.25	0.78	0.76	0.72	0.61	0.47
0.30	1.07	1.04	1.00	0.87	0.67
0.35	1.29	1.26	1.21	1.08	0.83
0.40	1.44	1.42	1.36	1.22	0.94
0.45	1.54	1.51	1.46	1.30	1.00
0.50	1.57	1.54	1.49	1.33	1.03

TABLE 10. AXIAL AND RADIAL VELOCITY COMPONENTS INDUCED ON THE CYLINDER $0 \leq x \leq L$, $r = R_0$, BY THE VORTEX DISTRIBUTION $\gamma_4\left(\frac{x}{L}\right) = 2\pi V_0 c_4$

$$v_{x4}{}^* = \frac{1}{c_4}\frac{v_{x4}(x,R_0)}{V_0}$$

x/L	$L/2R_0$				
	0	0.25	0.50	1.00	2.00
0.000	0	0.69	1.01	1.31	1.48
0.005	0	0.70	1.03	1.34	1.54
0.025	0	0.72	1.07	1.43	1.70
0.05	0	0.74	1.11	1.51	1.84
0.10	0	0.77	1.18	1.64	2.06
0.15	0	0.79	1.23	1.74	2.22
0.20	0	0.81	1.27	1.82	2.35
0.25	0	0.83	1.30	1.88	2.44
0.30	0	0.84	1.33	1.93	2.51
0.35	0	0.85	1.35	1.97	2.56
0.40	0	0.86	1.36	2.00	2.59
0.45	0	0.86	1.37	2.01	2.61
0.50	0	0.86	1.37	2.02	2.62

$$v_{r4}{}^* = \frac{1}{c_4}\frac{v_{r4}(x,R_0)}{V_0}$$

x/L	$L/2R_0$				
	0	0.25	0.50	1.00	2.00
0.000	$-\infty$	$-\infty$	$-\infty$	$-\infty$	$-\infty$
0.005	−5.29	−5.18	−4.98	−4.57	−3.97
0.025	−3.66	−3.55	−3.36	−2.96	−2.36
0.05	−2.94	−2.84	−2.65	−2.26	−1.69
0.10	−2.20	−2.10	−1.93	−1.57	−1.05
0.15	−1.73	−1.65	−1.50	−1.17	−0.71
0.20	−1.39	−1.31	−1.18	−0.90	−0.49
0.25	−1.10	−1.04	−0.93	−0.68	−0.35
0.30	−0.85	−0.80	−0.71	−0.51	−0.24
0.35	−0.62	−0.58	−0.51	−0.36	−0.17
0.40	−0.40	−0.38	−0.33	−0.23	−0.10
0.45	−0.20	−0.19	−0.16	−0.11	−0.05
0.50	0	0	0	0	0

TABLE 13. VELOCITY COMPONENTS INDUCED ON THE LINES $0 \leq x \leq L$, $y = \pm Y_0$, BY THE VORTEX DISTRIBUTION $\gamma_2\left(\frac{x}{L}\right) = 2\pi V_0 c_2 \sqrt{1 - \left(1 - \frac{2x}{L}\right)^2}$

$$v_{x2}^* = \frac{1}{c_2}\frac{v_{x2}(x, Y_0)}{V_0}$$

x/L	$L/2Y_0$			
	0	1	2	4
0.00	0	0.61	0.86	0.96
0.05	0	0.64	0.92	1.10
0.10	0	0.66	0.98	1.25
0.15	0	0.68	1.04	1.38
0.20	0	0.70	1.10	1.51
0.25	0	0.71	1.15	1.62
0.30	0	0.72	1.20	1.73
0.35	0	0.73	1.24	1.82
0.40	0	0.73	1.27	1.88
0.45	0	0.74	1.29	1.92
0.50	0	0.74	1.30	1.94

$$v_{y2}^* = \frac{1}{c_2}\frac{v_{y2}(x, Y_0)}{V_0}$$

x/L	$L/2Y_0$			
	0	1	2	4
0.00	−3.14	−2.86	−2.47	−1.96
0.05	−2.83	−2.57	−2.18	−1.65
0.10	−2.51	−2.28	−1.91	−1.39
0.15	−2.20	−1.98	−1.64	−1.15
0.20	−1.88	−1.69	−1.38	−0.94
0.25	−1.57	−1.41	−1.13	−0.76
0.30	−1.26	−1.12	−0.90	−0.59
0.35	−0.94	−0.84	−0.67	−0.43
0.40	−0.63	−0.57	−0.44	−0.27
0.45	−0.31	−0.28	−0.22	−0.13
0.50	0	0	0	0

TABLE 14. VELOCITY COMPONENTS INDUCED ON THE LINES $0 \leq x \leq L$, $y = \pm Y_0$, BY THE VORTEX DISTRIBUTION $\gamma_3\left(\frac{x}{L}\right) = 2\pi V_0 c_3 \left(1 - \frac{2x}{L}\right)\sqrt{1 - \left(1 - \frac{2x}{L}\right)^2}$

$$v_{x3}^* = \frac{1}{c_3}\frac{v_{x3}(x, Y_0)}{V_0}$$

x/L	$L/2Y_0$			
	0	1	2	4
0.00	0	0.055	0.177	0.348
0.05	0	0.052	0.182	0.400
0.10	0	0.049	0.185	0.439
0.15	0	0.045	0.183	0.457
0.20	0	0.040	0.174	0.452
0.25	0	0.035	0.158	0.427
0.30	0	0.029	0.134	0.377
0.35	0	0.022	0.104	0.305
0.40	0	0.015	0.071	0.215
0.45	0	0.008	0.036	0.112
0.50	0	0	0	0

$$v_{y3}^* = \frac{1}{c_3}\frac{v_{y3}(x, Y_0)}{V_0}$$

x/L	$L/2Y_0$			
	0	1	2	4
0.00	−1.57	−1.62	−1.62	−1.49
0.05	−0.97	−1.03	−1.05	−0.95
0.10	−0.44	−0.50	−0.54	−0.49
0.15	0.03	−0.03	−0.10	−0.10
0.20	0.44	0.37	0.28	0.20
0.25	0.78	0.71	0.59	0.45
0.30	1.07	0.99	0.85	0.64
0.35	1.29	1.20	1.05	0.78
0.40	1.44	1.36	1.18	0.88
0.45	1.54	1.45	1.27	0.94
0.50	1.57	1.48	1.26	0.97

TABLE 11. AXIAL AND RADIAL VELOCITY COMPONENTS INDUCED ON THE CYLINDER $0 \leq x \leq L$, $r = R_0$, BY THE VORTEX DISTRIBUTION $\gamma_5\left(\frac{x}{L}\right) = 2\pi V_0 c_5\left(1 - \frac{2x}{L}\right)$

$$v_{x5}^* = \frac{1}{c_5}\frac{v_{x5}(x,R_0)}{V_0}$$

x/L	$L/2R_0$				
	0	0.25	0.50	1.00	2.00
0.000	0	0.132	0.263	0.509	0.85
0.005	0	0.137	0.272	0.531	0.89
0.025	0	0.148	0.295	0.582	0.99
0.05	0	0.153	0.305	0.604	1.05
0.10	0	0.156	0.311	0.616	1.09
0.15	0	0.150	0.298	0.592	1.06
0.20	0	0.137	0.273	0.543	0.98
0.25	0	0.120	0.239	0.476	0.86
0.30	0	0.100	0.199	0.396	0.72
0.35	0	0.077	0.154	0.306	0.55
0.40	0	0.053	0.105	0.208	0.38
0.45	0	0.027	0.053	0.105	0.19
0.50	0	0	0	0	0

$$v_{r5}^* = \frac{1}{c_5}\frac{v_{r5}(x,R_0)}{V_0}$$

x/L	$L/2R_0$				
	0	0.25	0.50	1.00	2.00
0.000	$-\infty$	$-\infty$	$-\infty$	$-\infty$	$-\infty$
0.005	−3.24	−3.26	−3.30	−3.31	−3.20
0.025	−1.48	−1.50	−1.54	−1.57	−1.47
0.05	−0.65	−0.67	−0.72	−0.76	−0.71
0.10	0.24	0.21	0.16	0.08	0.06
0.15	0.79	0.75	0.69	0.58	0.48
0.20	1.17	1.13	1.06	0.92	0.74
0.25	1.45	1.41	1.33	1.17	0.91
0.30	1.66	1.62	1.54	1.35	1.03
0.35	1.81	1.77	1.68	1.47	1.11
0.40	1.92	1.87	1.78	1.56	1.16
0.45	1.98	1.93	1.84	1.61	1.19
0.50	2.00	1.95	1.86	1.62	1.20

TABLE 12. VELOCITY COMPONENTS INDUCED ON THE LINES $0 \leq x \leq L$, $y = \pm Y_0$, BY THE VORTEX DISTRIBUTION $\gamma_1\left(\frac{x}{L}\right) = 2\pi V_0 c_1 \sqrt{\frac{1 - x/L}{x/L}}$

$$v_{x1}^* = \frac{1}{c_1}\frac{v_{x1}(x,Y_0)}{V_0}$$

x/L	$L/2Y_0$			
	0	1	2	4
0.0	0	1.43	2.54	3.91
0.1	0	1.46	2.63	4.37
0.2	0	1.49	2.65	4.20
0.3	0	1.48	2.60	3.76
0.4	0	1.45	2.44	3.27
0.5	0	1.40	2.22	2.80
0.6	0	1.34	1.99	2.36
0.7	0	1.27	1.75	1.96
0.8	0	1.19	1.52	1.59
0.9	0	1.11	1.30	1.26
1.0	0	1.02	1.17	0.95

$$v_{y1}^* = \frac{1}{c_1}\frac{v_{y1}(x,Y_0)}{V_0}$$

x/L	$L/2Y_0$			
	0	1	2	4
0.0	3.14	3.45	4.05	5.02
0.1	3.14	3.32	3.61	3.92
0.2	3.14	3.19	3.19	2.92
0.3	3.14	3.05	2.80	2.18
0.4	3.14	2.93	2.48	1.70
0.5	3.14	2.81	2.22	1.41
0.6	3.14	2.70	2.02	1.24
0.7	3.14	2.62	1.89	1.14
0.8	3.14	2.54	1.82	1.11
0.9	3.14	2.49	1.79	1.14
1.0	3.14	2.44	1.79	1.22

TABLE 15. AXIAL VELOCITY COMPONENT $\frac{2\pi}{q} v_x\left(\frac{x}{R_0}, \frac{r}{R_0}\right)$ INDUCED BY A UNIFORM DISTRIBUTION OF SOURCES ON A CIRCULAR DISK

$\frac{x}{R_0}$ \ $\frac{r}{R_0}$	0.0	0.2	0.4	0.6	0.8	1.0	1.2	1.4	1.6	1.8	2.0
0.0	−3.14	−3.14	−3.14	−3.14	−3.14	−1.57	0	0	0	0	0
−0.2	−2.55	−2.53	−2.46	−2.31	−1.99	−1.20	−0.49	−0.23	−0.14	−0.09	−0.06
−0.4	−1.98	−1.96	−1.87	−1.68	−1.39	−0.97	−0.58	−0.34	−0.21	−0.14	−0.10
−0.6	−1.52	−1.50	−1.42	−1.27	−1.06	−0.80	−0.57	−0.38	−0.24	−0.17	−0.13
−0.8	−1.17	−1.15	−1.09	−0.98	−0.84	−0.67	−0.52	−0.38	−0.26	−0.19	−0.15
−1.0	−0.92	−0.90	−0.85	−0.78	−0.68	−0.56	−0.45	−0.35	−0.26	−0.20	−0.16
−1.2	−0.75	−0.73	−0.69	−0.64	−0.56	−0.47	−0.39	−0.32	−0.26	−0.20	−0.16
−1.4	−0.61	−0.60	−0.57	−0.53	−0.47	−0.40	−0.35	−0.29	−0.25	−0.20	−0.16
−1.6	−0.50	−0.49	−0.47	−0.44	−0.39	−0.35	−0.31	−0.27	−0.23	−0.19	−0.15
−1.8	−0.41	−0.40	−0.39	−0.36	−0.33	−0.30	−0.27	−0.24	−0.21	−0.18	−0.15
−2.0	−0.33	−0.33	−0.32	−0.30	−0.28	−0.26	−0.24	−0.21	−0.19	−0.16	−0.14

TABLE 16. RADIAL VELOCITY COMPONENT $\frac{2\pi}{q} v_r\left(\frac{x}{R_0}, \frac{r}{R_0}\right)$ INDUCED BY A UNIFORM DISTRIBUTION OF SOURCES ON A CIRCULAR DISK

$\frac{x}{R_0}$ \ $\frac{r}{R_0}$	0	0.2	0.4	0.6	0.8	1.0	1.2	1.4	1.6	1.8	2.0
0.0	0	0.315	0.670	1.110	1.795	∞	1.700	1.045	0.750	0.560	0.435
−0.2	0	0.300	0.615	0.985	1.435	1.715	1.330	0.930	0.700	0.545	0.425
−0.4	0	0.250	0.505	0.760	0.985	1.075	0.960	0.780	0.625	0.510	0.405
−0.6	0	0.200	0.390	0.560	0.695	0.740	0.710	0.620	0.530	0.450	0.375
−0.8	0	0.150	0.290	0.405	0.490	0.535	0.530	0.480	0.430	0.380	0.330
−1.0	0	0.110	0.210	0.295	0.360	0.395	0.395	0.375	0.345	0.315	0.280
−1.2	0	0.080	0.155	0.225	0.270	0.295	0.305	0.300	0.280	0.260	0.235
−1.4	0	0.060	0.115	0.170	0.210	0.230	0.240	0.240	0.230	0.215	0.200
−1.6	0	0.045	0.090	0.130	0.160	0.180	0.195	0.200	0.195	0.185	0.175
−1.8	0	0.035	0.070	0.100	0.125	0.140	0.155	0.165	0.160	0.155	0.150
−2.0	0	0.030	0.055	0.075	0.095	0.115	0.125	0.130	0.130	0.130	0.130

series can again be worked out explicitly. We give here the induced velocities and the stream function for a constant vortex distribution $\gamma(x) = \gamma_0$ on the two semi-infinite lines $x \geq 0$, $y = \pm Y_0$:

$$\frac{1}{V_0} v_x(x,y) = -\frac{1}{2\pi}\frac{\gamma_0}{V_0}\left(\arctan\frac{x}{y - Y_0} - \arctan\frac{x}{y + Y_0}\right) \tag{50}$$

$$\frac{1}{V_0} v_y(x,y) = \frac{1}{2\pi}\frac{\gamma_0}{V_0}\frac{1}{2}\ln\frac{x^2 + (y - Y_0)^2}{x^2 + (y + Y_0)^2} \tag{51}$$

$$\frac{1}{V_0 Y_0}\Psi(x,y) = -\frac{1}{2\pi}\frac{\gamma_0}{V_0}\left[\frac{1}{2}\ln\frac{x^2 + (y - Y_0)^2}{x^2 + (y + Y_0)^2} + \left(\frac{y}{Y_0} - 1\right)\arctan\frac{x}{y - Y_0} - \left(\frac{y}{Y_0} + 1\right)\arctan\frac{x}{y + Y_0}\right] \tag{52}$$

TABLE 17. STREAM FUNCTION $-\frac{2\pi}{qR_0^2}\Psi\left(\frac{x}{R_0}, \frac{r}{R_0}\right)$ OF A UNIFORM DISTRIBUTION OF SOURCES ON A CIRCULAR DISK

$\frac{x}{R_0}$ \ $\frac{r}{R_0}$	0	0.2	0.4	0.6	0.8	1.0	1.2	1.4	1.6	1.8	2.0
0.0	0	0.065	0.250	0.565	1.005	1.571	1.571	1.571	1.571	1.571	1.571
−0.2	0	0.050	0.200	0.435	0.735	1.035	1.220	1.305	1.345	1.375	1.400
−0.4	0	0.040	0.155	0.330	0.540	0.760	0.940	1.060	1.140	1.190	1.235
−0.6	0	0.030	0.120	0.250	0.410	0.580	0.730	0.855	0.955	1.025	1.080
−0.8	0	0.025	0.090	0.195	0.320	0.455	0.580	0.695	0.795	0.875	0.940
−1.0	0	0.020	0.070	0.155	0.260	0.370	0.480	0.580	0.670	0.750	0.815
−1.2	0	0.015	0.055	0.125	0.215	0.310	0.405	0.495	0.580	0.650	0.710
−1.4	0	0.010	0.045	0.100	0.175	0.260	0.345	0.425	0.500	0.570	0.625
−1.6	0	0.010	0.040	0.085	0.145	0.215	0.295	0.365	0.435	0.500	0.555
−1.8	0	0.010	0.035	0.070	0.120	0.180	0.245	0.310	0.375	0.435	0.490
−2.0	0	0.005	0.025	0.060	0.100	0.150	0.205	0.260	0.320	0.375	0.430

The arc-tangent functions are again determined apart from an integer multiple of π, which has to be chosen so that the flow is continuous everywhere except on the lines of singularities $x > 0$, $y = \pm Y_0$. This gives the following particular values:

$x = -\infty$	$v_x = 0$	$\Psi = 0$	
$x = 0$	$v_x = \frac{\gamma_0}{2}$	$\Psi = \frac{\gamma_0}{2} y$	for $\lvert y\rvert < Y_0$
	$v_x = 0$	$\Psi = \pm\frac{\gamma_0}{2} Y_0$	for $\lvert y\rvert > Y_0$
$x = +\infty$	$v_x = \gamma_0$	$\Psi = \gamma_0 y$	for $\lvert y\rvert < Y_0$
	$v_x = \frac{\gamma_0}{2}$	$\Psi = \pm\gamma_0 Y_0$	for $\lvert y\rvert = Y_0$
	$v_x = 0$	$\Psi = \pm\gamma_0 Y_0$	for $\lvert y\rvert > Y_0$

Two straight vortex lines of constant strength and semi-infinite length are equivalent to a uniform distribution of sources on the line $x = 0$, $-Y_0 \leq y \leq Y_0$ when a parallel flow is added in the region $x > 0$, $-Y_0 < y < Y_0$. In this case, the discontinuities of the arc-tangent functions must be at the position of the sources.

12. On the Numerical Evaluation of the Integrals. In many practical applications where distributions of singularities are used which differ from the few standard distributions given here, the velocity components must be obtained by graphical or numerical integration of elementary singularities. The integrand then always shows singular behavior when the pivotal point is on the line or surface over which the singularities are distributed. Difficulties usually arise only with vortex distributions,

since source distributions used are generally inside a body. The treatment of integrals which occur with two-dimensional vortex distributions has already been discussed by H. Glauert. We discuss here the case of axially symmetrical flow and indicate means of overcoming the difficulties in a graphical integration.

Let the vortex surface in the neighborhood of the singular point be given by

$$r - r' = a(x - x')$$

where a is a constant. The functions $v_{\gamma x}$, $v_{\gamma r}$, and Ψ_γ [Eqs. (26), (27), (29)] can be expanded in powers of $(x - x')$, and it will be found that

$v_{\gamma x}$ behaves like $\frac{1}{2} \ln [\sqrt{1 + a^2}\,(x - x')] + \frac{a}{1 + a^2} \frac{1}{x - x'}$

$v_{\gamma r}$ behaves like $\frac{1}{2}(x - x') \ln [\sqrt{1 + a^2}\,(x - x')] + \frac{1}{1 + a^2} \frac{1}{x - x'}$

Ψ_γ behaves like $\ln [\sqrt{1 + a^2}\,(x - x')]$

This follows from the fact that as $x - x' \to 0$, $k^2 \to 1$ and $\mathsf{E}(k) \to 1$, while $\mathsf{K}(k)$ and $\mathsf{D}(k)$ have a logarithmic infinity. We therefore have to deal with integrals in which the integrand contains a logarithmic singularity and integrals where the principal value must be taken.

As shown by F. Vandrey (1937), the logarithmic infinity can be eliminated by a suitable transformation. If in the integral

$$I = \int_0^1 f(x)\, dx$$

$f(x)$ has a logarithmic infinity at $x = 0$, then

$$I = \int_0^1 f(x)\, dx = n \int_0^1 f(x) x^{(n-1)/n} d(x^{1/n}) \tag{53}$$

where n is an integer greater than unity. The function

$$f(x)x^{(n-1)/n}$$

is not singular at $x = 0$, and graphical integration presents no difficulty.

If the integrand behaves like $1/(x - x')$ and if the singular point $x = x'$ is inside the interval of integration, we split off an interval of width δ to both sides of the singular point and combine the integrand at points symmetrical about x:

$$\int_{x-\delta}^{x+\delta} f(x')\, dx' = \int_0^\delta [f(x + h) + f(x - h)]\, dh$$

The integrand on the right-hand side is either finite or of a form that can be treated by Eq. (53).

Special care has to be taken when the singular point is at one end of the interval of integration. In general, the singularity is of the same kind as in the corresponding two-dimensional case, and it is best to subtract from the integrand the corresponding term from the two-dimensional problem and to add the solution of the two-dimensional problem to the integral.

Another type of singular integral occurs when the interval becomes infinite, as in

$$I = \int_1^\infty f(x)\, dx$$

If $f(x)$ is continuous in the whole range $1 \leq x < \infty$ and if

$$\lim_{x \to \infty} x^{(n+1)/n} f(x)$$

is finite or zero, where n is an integer, then

$$I = \int_1^\infty f(x)\, dx = n \int_0^1 f(x)\, x^{(n+1)/n} d\left(\frac{1}{x^{1/n}}\right)$$

BIBLIOGRAPHY

General:

SLATER, J. C., and N. H. FRANK, "Introduction to Theoretical Physics," McGraw-Hill Book Company, Inc., New York, 1933.

JAHNKE, H., and F. EMDE, "Tables of Functions," 3d ed., B. G. Teubner, Leipzig, 1938.

GLAUERT, H., "The Elements of Aerofoil and Airscrew Theory," 2d ed., Cambridge University Press, London and New York, 1948.

BETZ, A., "Konforme Abbildung," Springer-Verlag, Berlin, 1948.

Special Subjects:

BIRNBAUM, W., Die tragende Wirbelfläche als Hilfsmittel zur Behandlung des ebenen Problems der Tragflügeltheorie, *Z. angew. Math. Mech.*, vol. 3, p. 290, 1923.

VANDREY, F., Zur theoretischen Behandlung des gegenseitigen Einflusses von Tragflügel und Rumpf (Anhang), *Luftfahrtforschung*, vol. 14, p. 355, 1937.

KÜCHEMANN, D., Tables for the Stream Function and the Velocity Components of a Source Ring and a Vortex Ring, *Jahrbuch der deutschen Luftfahrtforschung*, p. I 547, 1940; translation, *Brit. Min. of Supply (Völkenrode) Rept. & Trans.* 710.

RIEGELS, F., and M. BRAND, Stromfunktion und Geschwindigkeitsfelder räumlicher Quellstrecken und ihr handlicher Gebrauch zur Bestimmung von Umriss und Druckverteilung rotationssymmetrischer Körper, mit Beispielen, *Deut. Luftfahrtforschung* U.M. 3106, 1944.

RIEGELS, F., Formeln und Tabellen für ein in der räumlichen Pontentialtheorie auftretendes elliptisches Integral, *Arch. Math.*, vol. 3, p. 117, 1950.

RIEGELS, F., Die Strömung um schlanke, fast drehsymmetrische Körper, *Mitt. Max-Planck-Inst. Strömungsforschung* No. 5, Göttingen, 1952.

INDEX